

# Development and Field Testing of Multiple Deployment Model Pile (MDMP)

PUBLICATION NO. FHWA-RD-99-194

JUNE 2000



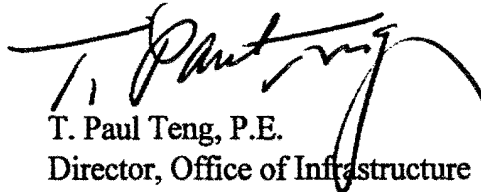
U.S. Department of Transportation  
**Federal Highway Administration**

Research, Development, and Technology  
Turner-Fairbank Highway Research Center  
6300 Georgetown Pike  
McLean, VA 22101-2296

## FOREWORD

An Instrumented Multiple deployment Model Pile (MDMP) was developed for monitoring pile/soil interaction including pile capacity gain with time. The MDMP instrumentation and field installation allows to accurately obtain parameters applicable to full scale pile design. The MDMP was successfully deployed in Newbury, MA. The obtained results demonstrate the ability to predict the time-dependent behavior of full scale piles and hence to improve the design and construction of driven piles.

This report will be of interest to geotechnical researchers and practitioners dealing with structures involving driven piles.



T. Paul Teng, P.E.  
Director, Office of Infrastructure  
Research and Development

## NOTICE

This document is disseminated under the sponsorship of the Department of Transportation in the interest of information exchange. The United States Government assumes no liability for its contents or use thereof. The report does not constitute a standard, specification, or regulation.

The United States Government does not endorse products or manufacturers. Trade and manufacturers' names appear in this report only because they are considered essential to the object of the document.

1. Report No. FHWA-RD-99-194		2. Government Accession No.		3. Recipient's Catalog No.	
4. Title and Subtitle Development and Field Testing of Multiple Deployment Model Pile (MDMP)				5. Report Date June 2000	
				6. Performing Organization Code	
7. Author(s) Samuel G. Paikowsky and Leo J. Hart				8. Performing Organization Report No.	
9. Performing Organization Name and Address Pruitt Energy Sources, Inc.      UMASS-Lowell 4307 Jefferson St., Suite 101      Geotechnical Engr. Research Laboratory Hyatssville, MD 20781              1 University Avenue Lowell, MA 01854				10. Work Unit No. (TRAVIS)	
				11. Contract or Grant No. DTFH61-95-Z-0081	
12. Sponsoring Agency Name and Address Office of Infrastructure R&D              Massachussets Highway Department 6300 Georgetown Pike                  10 Park Plaza, Suite 3510 McLean, VA 22101-2296                  Boston, MA 02116				13. Type of Report and Period Covered Final Report May 1995-March 1998	
				14. Sponsoring Agency Code	
15. Supplementary Notes Contracting Officer's Technical Representative (COTR) - Carl Ealy, HRDI-08 Technical Consultant: Jerry DiMaggio, HIBT-20					
16. Abstract A model pile is a calibrated tool equipped with instrumentation capable of monitoring the pile/soil interaction over the pile history. Monitoring includes the installation, pore pressure dissipation combined with consolidation and soil pressure equalization, and ultimately the pile behavior under loading and failure. The model pile installation and soil structure interaction simulate the actual field conditions of full-scale piles. As such, the obtained information can be utilized directly (e.g., skin friction) or extrapolated (e.g., pore pressure dissipation time) to predict the soil's response during full-scale installation. The Multiple Deployment Model Pile (MDMP) was developed as an in situ tool for site investigations. The MDMP instrumentation is capable of monitoring the pile/soil interaction throughout the life cycle of a driven pile. (1) dynamic force and acceleration readings at the pile top and along the pile during driving. (2) pore water pressure and radial stresses during equalization; and (3) skin friction, end-bearing resistance, and local (subsurface) displacement during static loading. These measurements allow the observation of pile capacity gain (a.k.a. "set-up" or "freeze") and accurately monitor the load-transfer relations. The MDMP was successfully deployed twice in Newbury, MA during March 1996. The obtained dynamic measurements allowed the evaluation of the pile's static capacity and clarified the difficulties associated with dynamic analysis of small-scale penetration. Pile capacity gain with time was examined based on normalization procedures developed by Paikowsky et al. (1995). The excess pore water pressure dissipation, variation of radial effective stresses, and pile capacity gain with time were determined for the two tests. The obtained results show that the MDMP is capable of providing accurate soil-structure interaction relations during static load testing. The measurements indicate a complex mechanism governing capacity gain that combines pore pressure dissipation and radial stress redistribution over time. These findings are used to predict the time-dependent behavior of full-scale instrumented piles and to re-evaluate the capacity gain phenomenon. The obtained results explain some unanswered questions and allow the development of procedures incorporating pile capacity gain in design and construction. Appendices to this report are on file at the Turner-Fairbank Highway Research Center, McLean, VA.					
17. Key Words Model Pile, Load Test, In Situ, Capacity Gain, Set-Up, Dynamic Measurements.			18. Distribution Statement No restrictions. This document is available to the public through the National Technical Information Service, Springfield, Virginia 22161.		
19. Security Classif. (of this report) Unclassified		20. Security Classif. (of this page) Unclassified		21. No. of Pages 284	22. Price

# SI\* (MODERN METRIC) CONVERSION FACTORS

APPROXIMATE CONVERSIONS TO SI UNITS					APPROXIMATE CONVERSIONS FROM SI UNITS				
Symbol	When You Know	Multiply By	To Find	Symbol	Symbol	When You Know	Multiply By	To Find	Symbol
<b>LENGTH</b>					<b>LENGTH</b>				
in	inches	25.4	millimeters	mm	mm	millimeters	0.039	inches	in
ft	feet	0.305	meters	m	m	meters	3.28	feet	ft
yd	yards	0.914	meters	m	m	meters	1.09	yards	yd
mi	miles	1.61	kilometers	km	km	kilometers	0.621	miles	mi
<b>AREA</b>					<b>AREA</b>				
in <sup>2</sup>	square inches	645.2	square millimeters	mm <sup>2</sup>	mm <sup>2</sup>	square millimeters	0.0016	square inches	in <sup>2</sup>
ft <sup>2</sup>	square feet	0.093	square meters	m <sup>2</sup>	m <sup>2</sup>	square meters	10.764	square feet	ft <sup>2</sup>
yd <sup>2</sup>	square yards	0.836	square meters	m <sup>2</sup>	m <sup>2</sup>	square meters	1.195	square yards	yd <sup>2</sup>
ac	acres	0.405	hectares	ha	ha	hectares	2.47	acres	ac
mi <sup>2</sup>	square miles	2.59	square kilometers	km <sup>2</sup>	km <sup>2</sup>	square kilometers	0.386	square miles	mi <sup>2</sup>
<b>VOLUME</b>					<b>VOLUME</b>				
fl oz	fluid ounces	29.57	milliliters	mL	mL	milliliters	0.034	fluid ounces	fl oz
gal	gallons	3.785	liters	L	L	liters	0.264	gallons	gal
ft <sup>3</sup>	cubic feet	0.028	cubic meters	m <sup>3</sup>	m <sup>3</sup>	cubic meters	35.71	cubic feet	ft <sup>3</sup>
yd <sup>3</sup>	cubic yards	0.765	cubic meters	m <sup>3</sup>	m <sup>3</sup>	cubic meters	1.307	cubic yards	yd <sup>3</sup>
NOTE: Volumes greater than 1000 l shall be shown in m <sup>3</sup> .									
<b>MASS</b>					<b>MASS</b>				
oz	ounces	28.35	grams	g	g	grams	0.035	ounces	oz
lb	pounds	0.454	kilograms	kg	kg	kilograms	2.202	pounds	lb
T	short tons (2000 lb)	0.907	megagrams (or "metric ton")	Mg (or "t")	Mg (or "t")	megagrams (or "metric ton")	1.103	short tons (2000 lb)	T
<b>TEMPERATURE (exact)</b>					<b>TEMPERATURE (exact)</b>				
°F	Fahrenheit temperature	5(F-32)/9 or (F-32)/1.8	Celcius temperature	°C	°C	Celcius temperature	1.8C + 32	Fahrenheit temperature	°F
<b>ILLUMINATION</b>					<b>ILLUMINATION</b>				
fc	foot-candles	10.76	lux	lx	lx	lux	0.0929	foot-candles	fc
fl	foot-Lamberts	3.426	candela/m <sup>2</sup>	cd/m <sup>2</sup>	cd/m <sup>2</sup>	candela/m <sup>2</sup>	0.2919	foot-Lamberts	fl
<b>FORCE and PRESSURE or STRESS</b>					<b>FORCE and PRESSURE or STRESS</b>				
lbf	poundforce	4.45	newtons	N	N	newtons	0.225	poundforce	lbf
lbf/in <sup>2</sup>	poundforce per square inch	6.89	kilopascals	kPa	kPa	kilopascals	0.145	poundforce per square inch	lbf/in <sup>2</sup>

\* SI is the symbol for the International System of Units. Appropriate rounding should be made to comply with Section 4 of ASTM E380.



## TABLE OF CONTENTS

1.	INTRODUCTION.....	1
1.1.	Overview .....	1
1.2.	Purpose.....	2
1.3.	Scope.....	2
1.4.	Manuscript Layout.....	3
1.5.	Contributions .....	4
2.	MODEL PILES FOR FIELD TESTING - REVIEW .....	5
2.1.	Definition and Overview .....	5
2.2.	The Cone Penetration Test (CPT) Model .....	6
2.3.	The Piezo-Lateral Stress (PLS) Cell .....	10
2.4.	The Grosch and Reese (G&R) Model Pile .....	13
2.5.	The Norwegian Geotechnical Institute (NGI) Model Pile.....	15
2.6.	The X-Probe and the 3-Inch Model Piles .....	17
2.7.	The In Situ Model Pile (IMP).....	21
2.8.	The Imperial College Pile (ICP).....	23
3.	THE MULTIPLE DEPLOYMENT MODEL PILE (MDMP).....	29
3.1.	General Description.....	29
3.2.	Requirements .....	29
3.3.	Analysis of the MDMP Loading Conditions.....	31
3.3.1.	Overview .....	31
3.3.2.	Static Capacity Analysis .....	33
3.3.3.	Dynamic Analysis .....	35
3.3.4.	Summary of Load Requirements .....	38
3.4.	Specifications for Instrumentation and Mechanical Parts.....	39
3.4.1.	General .....	39
3.4.2.	Accelerometers .....	39
3.4.3.	Load Cells.....	39
3.4.4.	Pore Pressure Transducer .....	40
3.4.5.	Total Pressure Cell.....	40
3.4.6.	Connector Housing .....	40
3.4.7.	Slip Joint.....	40
3.4.8.	Loading Frame.....	41
3.4.9.	Summary of the Instrumentation Range Requirements .....	41
3.5.	Design.....	41
3.5.1.	General .....	41
3.5.2.	N-Rod Adapter .....	42
3.5.3.	Connector Housing and Mount.....	42
3.5.4.	Upper Extension.....	42

3.5.5.	<i>Load Cells</i> .....	43
3.5.6.	<i>Couplings</i> .....	45
3.5.7.	<i>Transducer Housing</i> .....	45
3.5.8.	<i>Slip Joint</i> .....	46
3.5.9.	<i>Lower Extension</i> .....	47
3.5.10.	<i>Tip Segment</i> .....	47
3.6.	Calibration.....	48
3.6.1.	<i>Overview</i> .....	48
3.6.2.	<i>Load Cell Calibration</i> .....	48
3.6.3.	<i>Pore Pressure Transducer Calibration</i> .....	53
3.6.4.	<i>Total Pressure Cell Calibration</i> .....	54
3.6.5.	<i>Displacement Transducer Calibration</i> .....	55
3.6.6.	<i>Accelerometer Response During Dynamic Loading</i> .....	55
4.	MDMP PERIPHERAL TEST ACCESSORIES.....	59
4.1.	Overview of Peripheral Test Accessories.....	59
4.2.	Hewlett Packard Data Acquisition System.....	61
4.3.	Pile-Driving Analyzer.....	62
4.4.	Connection Box.....	64
4.4.1.	<i>General</i> .....	64
4.4.2.	<i>Power Supply Requirement</i> .....	64
4.4.3.	<i>Input</i> .....	64
4.4.4.	<i>Output</i> .....	64
4.4.5.	<i>Operation</i> .....	65
4.5.	Cables and Connections.....	66
4.5.1.	<i>General</i> .....	66
4.5.2.	<i>Input Cables</i> .....	66
4.5.3.	<i>Output Cables</i> .....	66
4.6.	Static Loading System.....	67
4.6.1.	<i>Overview</i> .....	67
4.6.2.	<i>Loading Frame</i> .....	67
4.6.3.	<i>Hydraulic Loading System</i> .....	70
4.7.	Driving System.....	70
5.	MDMP TESTS AT THE NEWBURY, MA SITE.....	71
5.1.	Site Overview and Location.....	71
5.2.	Previous Subsurface Exploration Program Studies.....	71
5.3.	UMass-Lowell Subsurface Exploration Program.....	71
5.3.1.	<i>Sampling and Field Testing</i> .....	74
5.3.2.	<i>Groundwater Monitoring</i> .....	78
5.4.	Typical Subsurface Stratigraphy.....	78
5.5.	Engineering Properties of the Clay at the Newbury Test Site.....	81
5.6.	Predicted Behavior of the Multiple Deployment Model Pile.....	85

5.6.1.	<i>Overview</i>	85
5.6.2.	<i>Estimated Increase in Pore Pressure Due to Driving</i>	85
5.6.3.	<i>Estimated Time for Excess Pore Water Pressure Dissipation</i>	87
5.6.4.	<i>Estimated Time for Capacity Gain</i>	89
5.7.	<b>MDMP Testing Procedure</b>	91
5.7.1.	<i>Overview</i>	91
5.7.2.	<i>General Test Plan</i>	93
5.7.3.	<i>Testing Procedure for the MDMP during Test NB2</i>	95
5.7.4.	<i>Testing Procedure for the MDMP during Test NB3</i>	98
6.	<b>NEWBURY SITE TEST RESULTS</b>	101
6.1.	<b>Pore Pressure Measurements</b>	101
6.1.1.	<i>Overview</i>	101
6.1.2.	<i>Pore Pressure Results for the MDMP Test NB2</i>	101
6.1.3.	<i>Pore Pressure Results for the MDMP Test NB3</i>	104
6.1.4.	<i>Common Pore Pressure Behavior of the Two Tests</i>	104
6.2.	<b>Radial Stress Measurements</b>	107
6.2.1.	<i>Total Stress</i>	107
6.2.2.	<i>Effective Stress</i>	113
6.3.	<b>Load Transfer Along the Friction Sleeve</b>	118
6.3.1.	<i>General Considerations — Initial Reading</i>	118
6.3.2.	<i>Model Pile Test NB2</i>	122
6.3.3.	<i>Model Pile Test NB3</i>	124
6.4.	<b>Surface Load Cell Measurements</b>	132
6.4.1.	<i>General</i>	132
6.4.2.	<i>Heave Measurements During Model Pile Test NB2</i>	132
6.4.3.	<i>Comparison of Surface and Internal Load Cell Measurements</i>	135
6.5.	<b>Static-Cyclic Loading</b>	135
6.5.1.	<i>Final Load Testing Sequence</i>	135
6.5.2.	<i>Model Pile Test NB2</i>	140
6.5.3.	<i>Model Pile Test NB3</i>	143
6.6.	<b>Dynamic Measurements</b>	146
6.6.1.	<i>Driving System and Dynamic Measurements</i>	146
6.6.2.	<i>Installation During Model Pile Test NB2</i>	147
6.6.3.	<i>MDMP Restrike During Model Pile Test NB2</i>	160
6.6.4.	<i>Installation During Model Pile Test NB3</i>	166
6.6.5.	<i>Restrike During Model Pile Test NB3</i>	176
6.6.6.	<i>Force Measurements</i>	182
6.6.7.	<i>Velocity Measurements</i>	183
7.	<b>ANALYSIS OF THE MDMP TEST RESULTS</b>	193
7.1.	<b>Normalized Pore Pressure Dissipation</b>	193
7.1.1.	<i>MDMP Test NB2</i>	193

7.1.2.	<i>MDMP Test NB3</i> .....	193
7.1.3.	<i>Comparison with Other Test Results</i> .....	196
7.2.	Normalized Capacity Gain .....	197
7.2.1.	<i>MDMP Test NB2</i> .....	197
7.2.2.	<i>MDMP Test NB3</i> .....	198
7.2.3.	<i>Comparison with Other Test Results</i> .....	198
7.3.	Comparison Between Predicted and Measured Values .....	200
7.3.1.	<i>Overview</i> .....	200
7.3.2.	<i>Pore Water Pressure Increase Due to Driving</i> .....	200
7.3.3.	<i>Excess Pore Pressure Dissipation and Capacity Gain</i> .....	203
7.4.	Radial Consolidation .....	203
7.5.	Time-Dependent Radial Stresses .....	206
7.6.	The Relationship Between Pore Pressure Dissipation, Frictional Capacity Gain, and Radial Stresses .....	208
7.7.	Observed Heave .....	208
7.8.	Static-Cyclic Load Tests .....	210
7.9.	Shaft Resistance and Design Parameters .....	213
7.10.	Dynamic Measurements Interpretation .....	218
7.10.1.	<i>Measured Signals and Wave Mechanics</i> .....	218
7.10.2.	<i>Capacity Based on the Energy Approach</i> .....	221
7.10.3.	<i>Capacity Based on CAPWAP Analysis</i> .....	222
7.10.4.	<i>Capacity Based on the Case Method</i> .....	235
7.11.	Comparison Between the Static Capacity and the Analyses Based on Dynamic Measurements .....	252
<b>8.</b>	<b>SUMMARY CONCLUSIONS AND RECOMMENDATIONS</b> .....	<b>257</b>
8.1.	Summary .....	257
8.1.1.	<i>The MDMP Configuration and Specifications</i> .....	257
8.1.2.	<i>The Newbury Site Testing</i> .....	257
8.1.3.	<i>Test Results</i> .....	259
8.2.	Conclusions .....	260
8.2.1.	<i>General Conclusions</i> .....	260
8.2.2.	<i>Major Conclusions</i> .....	261
8.2.3.	<i>Detailed Conclusions</i> .....	261
8.3.	Recommendations .....	262
	<b>REFERENCES</b> .....	<b>263</b>

## LIST OF FIGURES

Figure 1	The Dual Piezo Friction Cone Penetrometer (De Ruiter, 1982).....	8
Figure 2	Typical Locations of Pore Pressure Measurements for Piezocone Penetrometers.....	9
Figure 3	The Piezo-Lateral Stress (PLS) Cell (Morrison, 1984). ....	11
Figure 4	Detailed Cross-Section of the Piezo-Lateral Stress (PLS) Cell (Morrison, 1984). ....	12
Figure 5	Details of the Axial Load Cell in the Piezo-Lateral Stress (PLS) Cell (Morrison, 1984).....	14
Figure 6	The Grosch and Reese (G&R) Instrumented Model Pile (Grosch and Reese, 1980). ....	15
Figure 7	The Norwegian Geotechnical Institute (NGI) Instrumented Test Pile (after Karlsrud and Haugen, 1985).....	16
Figure 8	The 7.62-cm (3.0-in) Instrumented Model Pile (Bogard and Matlock, 1985). ....	18
Figure 9	The X-Probe (Bogard and Matlock, 1985). ....	19
Figure 10	Details of 7.62-cm (3-in) Model Pile Axial Load Cells (after Patent Number 5,259,240).....	20
Figure 11	Details of 7.62-cm (3-in) Model Pile Pressure Instruments (after Patent Number 5,259,240).....	21
Figure 12	Configuration and Instrumentation of the In Situ Model Pile (IMP) (after Lehane, 1992). ....	22
Figure 13	The Imperial College Instrumented Model Pile (Bond and Jardine, 1991).....	24
Figure 14	Typical Imperial College Model Pile Instrument Cluster (Bond et al., 1991). ....	25
Figure 15	The Surface Stress Transducer (Bond et al., 1991). ....	26
Figure 16	The Combined Axial Load Cell and Pore Pressure Unit (Bond et al., 1991). ....	27
Figure 17	Typical Configurations of the MDMP.....	30
Figure 18	Tip Configurations of the MDMP. ....	32
Figure 19	Typical Soil Profile for the Boston Area. ....	33
Figure 20	Hypothetical Soil Profile of Dense Sand. ....	34
Figure 21	Drop Hammer Configuration Modeled in the Wave Equation Analyses. ....	36
Figure 22	Photograph of the MDMP Load Cell with Sleeve.....	44
Figure 23	Photograph of the Transducer Housing With the Pore Pressure Transducer and Total Radial Stress Cell.....	45
Figure 24	Photograph of the Slip Joint with DCDT. ....	47
Figure 25	(a) Schematic of the Calibration Frame for the MDMP. ....	50
	(b) Photograph of the Calibration Frame for the MDMP .....	51
Figure 26	Pressure Instrumentation Calibration Setup .....	54
Figure 27	(a) Photograph of the Dynamic Instrumentation Testing Setup .....	56
	(b) Schematic of the Dynamic Instrumentation Testing Setup .....	57
Figure 28	Schematic of the MDMP Data Acquisition System .....	60
Figure 29	Hewlett Packard Data Acquisition System (HP DAS) .....	61

Figure 30	Pile-Driving Analyzer (PDA) Data Acquisition System .....	63
Figure 31	Connection Box, Back Faceplate .....	65
Figure 32	Connection Box, Front Faceplate .....	66
Figure 33	(a) Schematic of the MDMP Static Load Frame .....	68
	(b) Photograph of the MDMP Static Load Frame .....	69
Figure 34	Newbury Site Locus Plan .....	72
Figure 35	Newbury MDMP Site Plan .....	73
Figure 36	Representative Soil Stratigraphy at the Newbury MDMP Test Site (Chen, 1997) .....	79
Figure 37	Soil Profile of the Newbury Test Site (North-South) .....	80
Figure 38	Groundwater Elevations at the Newbury Test Site .....	81
Figure 39	Profiles of Vertical Effective Stress, Maximum Past Pressure, and OCR at the Newbury Site (Chen, 1997). .....	83
Figure 40	Profiles of Vertical Effective Stress, and Calculated and Measured Undrained Shear Strength at the Newbury Site (Chen, 1997) .....	84
Figure 41	Initial Excess Pore Pressure Distribution (only reading for $1 < \text{OCR} < 10$ included) (Paikowsky et al., 1995) .....	86
Figure 42	Effects of OCR on $\Delta u/\sigma'_v$ Along the Shaft ( $h/r \geq 17$ ) for $r/R=1$ (Paikowsky et al., 1995) .....	88
Figure 43	Predicted Pore Pressure Dissipation and Capacity Gain for the MDMP at the Newbury Site .....	90
Figure 44	Site Layout During MDMP Tests at the Newbury Site: (a) Initial Setup, (b) During Snowstorm, and (c) Static Load Test .....	92
Figure 45	Steps for Installation and Testing of the MDMP at the Newbury Site .....	94
Figure 46	(a) MDMP Being Driven and (b) Static Load Frame Assembled .....	96
Figure 47	Pore Pressure Build-Up and Dissipation With Time for Model Pile Test NB2 .....	102
Figure 48	Pore Pressure Build-Up and Dissipation With Time for Model Pile Test NB2 .....	103
Figure 49	Pore Pressure Build-Up and Dissipation With Time for Model Pile Test NB3 .....	105
Figure 50	Pore Pressure Build-Up and Dissipation With Time for Model Pile Test NB3 .....	106
Figure 51	(a) Total Radial Stress, $\sigma_r$ With Time, MDMP Test NB2 .....	109
	(b) Total Radial Stress, $\sigma_r$ With Time, MDMP Test NB2 (including a possible adjustment) .....	110
Figure 52	(a) Total Radial Stress, $\sigma_r$ With Time, MDMP Test NB2 .....	111
	(b) Total Radial Stress, $\sigma_r$ With Time, MDMP Test NB2 (including a possible adjustment) .....	112
Figure 53	(a) Effective Radial Stress, $\sigma'_r$ With Time, MDMP Test NB2 .....	114
	(b) Effective Radial Stress, $\sigma'_r$ With Time, MDMP Test NB2 (including radial stress measurement adjustment) .....	115
Figure 54	(a) Effective Radial Stress, $\sigma'_r$ With Time, MDMP Test NB2 .....	116
	(b) Effective Radial Stress, $\sigma'_r$ With Time, MDMP Test NB2 (including radial stress measurement adjustment) .....	117

Figure 55	Force Measurements in Top and Middle MDMP Load Cells for Test NB2: (a) Unadjusted records based on initial readings before driving and (b) Adjusted records based on zero loads assumed prior to the initial load test.....	120
Figure 56	Internal Load Measurements, MDMP Test NB2 .....	123
Figure 57	Adjustments to Internal Load Measurements, MDMP Test NB2 .....	125
Figure 58	Frictional Forces Along the Friction Sleeve for MDMP Test NB2.....	126
Figure 59	Shear Transfer Along the Friction Sleeve for MDMP Test NB2 .....	127
Figure 60	Internal Load Measurements, MDMP Test NB3 .....	129
Figure 61	Frictional Forces Along the Friction Sleeve for MDMP Test NB3.....	130
Figure 62	Shear Transfer Along the Friction Sleeve for MDMP Test NB3 .....	131
Figure 63	Force and Displacement Measurements Following the MDMP Installation of Test NB2, Including Heave Effect and Initial Load Test.....	133
Figure 64	Force and Displacement Measurements Following the MDMP Installation of Test NB2, Adjusted for Heave prior to the Initial Load Test.....	134
Figure 65	Comparison Between the Surface and the Internal Load Cell Measurements for MDMP Test NB2.....	136
Figure 66	Comparison Between the Surface and the Internal Load Cell Measurements for MDMP Test NB3.....	137
Figure 67	Static-Cyclic Load Test Results for MDMP Test NB2: (a) Load cell measurements versus time, (b) Displacement measurements versus time, and (c) Pore pressure measurements versus time .....	138
Figure 68	Static-Cyclic Load Test Results for MDMP Test NB3: (a) Load cell measurements versus time, (b) Displacement measurements versus time, and (c) Pore pressure measurements versus time .....	139
Figure 69	(a) Load-Displacement Relationship for Static-Cyclic Final Load Test for MDMP Test NB2.....	141
	(b) Shear Resistance-Displacement Relationship Along the Friction Sleeve During Static-Cyclic Final Load Test for MDMP Test NB2.....	142
Figure 70	(a) Load-Displacement Relationship for Static-Cyclic Final Load Test for MDMP Test NB3.....	144
	(b) Shear Resistance-Displacement Relationship Along the Friction Sleeve During Static-Cyclic Final Load Test for MDMP Test NB3.....	145
Figure 71	Blow Count and Energy Delivered Versus Penetration Depth for the Installation of MDMP Test NB2 .....	148
Figure 72	(a) PDA Dynamic Measurements During the Installation of MDMP Test NB2: Surface Force and Velocity Records Over 25 ms. ....	150
	(b) PDA Dynamic Measurements During the Installation of MDMP Test NB2: Surface Force and Velocity Records Over 5 ms. ....	151
	(c) PDA Dynamic Measurements During the Installation of MDMP Test NB2: Internal Force and Velocity Records Over 25 ms. ....	152
	(d) PDA Dynamic Measurements During the Installation of MDMP Test NB2: Internal Force and Velocity Records Over 5 ms. ....	153
Figure 73	(a) PDA Dynamic Measurements During the Installation of MDMP Test NB2: Surface Force and Velocity Records Over 25 ms. ....	154

	(b) PDA Dynamic Measurements During the Installation of MDMP Test NB2: Surface Force and Velocity Records Over 5 ms. ....	155
	(c) PDA Dynamic Measurements During the Installation of MDMP Test NB2: Internal Force and Velocity Records Over 25 ms. ....	156
	(d) PDA Dynamic Measurements During the Installation of MDMP Test NB2: Internal Force and Velocity Records Over 5 ms. ....	157
Figure 74	Blow Count and Energy Delivered Versus Penetration Depth for the Restrike of MDMP Test NB2 .....	161
Figure 75	(a) PDA Dynamic Measurements During the Restrike of MDMP Test NB2: Surface Force and Velocity Records Over 50 ms. ....	162
	(b) PDA Dynamic Measurements During the Restrike of MDMP Test NB2: Surface Force and Velocity Records Over 20 ms. ....	163
	(c) PDA Dynamic Measurements During the Restrike of MDMP Test NB2: Internal Force and Velocity Records Over 50 ms. ....	164
	(d) PDA Dynamic Measurements During the Restrike of MDMP Test NB2: Internal Force and Velocity Records Over 20 ms. ....	165
Figure 76	Blow Count and Energy Delivered Versus Penetration Depth for the Installation of MDMP Test NB3 .....	167
Figure 77	(a) PDA Dynamic Measurements During the Installation of MDMP Test NB3: Surface Force and Velocity Records Over 25 ms (at the upper location).....	169
	(b) PDA Dynamic Measurements During the Installation of MDMP Test NB3: Surface Force and Velocity Records Over 5 ms (at upper location).....	170
	(c) PDA Dynamic Measurements During the Installation of MDMP Test NB3: Surface Force and Velocity Records Over 25 ms (at the lower location).....	171
	(d) PDA Dynamic Measurements During the Installation of MDMP Test NB3: Surface Force and Velocity Records Over 5 ms (at the lower location).....	172
	(e) PDA Dynamic Measurements During the Installation of MDMP Test NB3: Internal Force and Velocity Records Over 25 ms .....	173
	(f) PDA Dynamic Measurements During the Installation of MDMP Test NB3: Internal Force and Velocity Records Over 5 ms .....	174
Figure 78	Blow Count and Energy Delivered Versus Penetration Depth for the Restrike of MDMP Test NB3 .....	177
Figure 79	(a) PDA Dynamic Measurements During the Restrike of MDMP Test NB3: Surface Force and Velocity Records Over 50 ms. ....	178
	(b) PDA Dynamic Measurements During the Restrike of MDMP Test NB3: Surface Force and Velocity Records Over 12 ms .....	179
	(c) PDA Dynamic Measurements During the Restrike of MDMP Test NB3: Internal Force and Velocity Records Over 50 ms .....	180
	(d) PDA Dynamic Measurements During the Restrike of MDMP Test NB3: Internal Force and Velocity Records Over 12 ms .....	181
Figure 80	Maximum Dynamic Forces Measured During Installation of MDMP Test NB2.....	184



Figure 81	Maximum Dynamic Forces Measured During Restrike of the MDMP Test NB2.....	185
Figure 82	Maximum Dynamic Forces Measured During Installation of MDMP Test NB3.....	186
Figure 83	Maximum Dynamic Forces Measured During Restrike of MDMP Test NB3.....	187
Figure 84	Maximum Dynamic Velocities Measured During Installation of MDMP Test NB2.....	188
Figure 85	Maximum Dynamic Velocities Measured During Restrike of MDMP Test NB2.....	189
Figure 86	Maximum Dynamic Velocities Measured During Installation of MDMP Test NB3.....	190
Figure 87	Maximum Dynamic Velocities Measured During Restrike of MDMP Test NB3.....	191
Figure 88	Normalized Excess Pore Pressure and Shear Transfer Gain, Model Pile Test NB2.....	194
Figure 89	Normalized Excess Pore Pressure and Shear Transfer Gain, Model Pile Test NB3.....	195
Figure 90	Initial excess pore pressure distribution for soils with $1 < OCR < 10$ including the MDMP data (based on Paikowsky et al., 1995).....	201
Figure 91	Effects of OCR on $\Delta u/\sigma'_v$ along the shaft ( $h/r \geq 17$ ) for $r/R=1$ with MDMP data included (based on Paikowsky et al., 1995).....	202
Figure 92	Measured Pore Pressure Dissipation and Capacity Gain for MDMP Tests at the Newbury Site With Predicted Ranges.....	204
Figure 93	Effects of Pile Radius on $t_{50}$ (Time for 50% Excess Pore Pressure Dissipation) for NC Clays ( $OCR=1-2$ ), Including MDMP Data (based on Paikowsky et al., 1995).....	205
Figure 94	Changes in Pore Pressure, and Total and Effective Radial Stresses: (a) Log Time Scale and (b) Linear Time Scale.....	207
Figure 95	Relationships between Shaft Friction, Radial Stress, and Vertical Stress for MDMP Test NB2.....	209
Figure 96	Final Load Test for MDMP Test NB2.....	211
Figure 97	Final Load Test for MDMP Test NB3.....	212
Figure 98	Shear Transfer Along the Friction Sleeve for MDMP Test NB2.....	214
Figure 99	Shear Transfer Along the Friction Sleeve for MDMP Test NB3.....	215
Figure 100	Shear Transfer Along the Friction Sleeve as a Function of the Degree Consolidation for MDMP Test NB2.....	216
Figure 101	Shear Transfer Along the Friction Sleeve as a Function of the Degree Consolidation for MDMP Test NB3.....	216
Figure 102	Undrained Shear Strength of the BBC at the Newbury Test Site: (a) Variation With Depth Along With Results of Different Testing and (b) Details of CPT and SHANSEP Parameters Between the Depths of 6.1 and 13.7 m (20 to 45 ft) (based on Paikowsky and Chen, 1998).....	217
Figure 103	Details of the Various Segments that Made Up the MDMP (from the point of surface measurements to the upper inner load cell).....	219

Figure 104	The Relationship Between the Pile Impedance and Measured Signals (modified after Rausche, 1981). .....	220
Figure 105	Surface Force and Velocity Records of the MDMP Test NB2 Restrike, Blow 1.....	224
Figure 106	Test NB2 Restrike CAPWAP Modeling of MDMP Case (1): (a) Best Match Between Measured and Calculated Force at Top and (b) Drill Rods and Pile Geometry Modeling.....	225
Figure 107	Test NB2 Restrike CAPWAP Modeling of MDMP Case (2): (a) Best Match Between Measured and Calculated Force at Top and (b) Drill Rods and Pile Geometry Modeling.....	227
Figure 108	Test NB2 Restrike CAPWAP Modeling of MDMP Case (3): (a) Best Match Between Measured and Calculated Force at Top and (b) Drill Rods and Pile Geometry Modeling.....	229
Figure 109	Modeling of Case (1), Calculated and Measured Forces at the Internal Load Cell Locations for the MDMP Test NB2 Restrike Blow 1 (analysis based on a force match at the surface measurement location only).....	231
Figure 110	Modeling of Case (2), Calculated and Measured Forces at the Internal Load Cell Locations for the MDMP Test NB2 Restrike Blow 1 (analysis based on a force match at the surface measurement location only).....	232
Figure 111	Modeling of Case (3), Calculated and Measured Forces at the Internal Load Cell Locations for the MDMP Test NB2 Restrike Blow 1 (analysis based on a force match at the surface measurement location only).....	233
Figure 112	Surface Force and Velocity Records for MDMP Test NB3 Restrike, Blow 2 .....	234
Figure 113	Test NB3 Restrike CAPWAP Modeling of MDMP, Case (1): (a) Best Match Between Measured and Calculated Force at Top and (b) Drill Rods and Pile Geometry Modeling.....	236
Figure 114	Test NB3 Restrike CAPWAP Modeling of MDMP, Case (2): (a) Best Match Between Measured and Calculated Force at Top and (b) Drill Rods and Pile Geometry Modeling.....	238
Figure 115	Modeling of Case (1), Calculated and Measured Forces at the Internal Load Cell Locations for the MDMP Test NB3 Restrike Blow 2 (analysis based on a force match at the surface measurement location only).....	240
Figure 116	Modeling of Case (2), Calculated and Measured Forces at the Internal Load Cell Locations for the MDMP Test NB3 Restrike Blow 2 (analysis based on a force match at the surface measurement location only).....	241
Figure 117	Predicted Pile Capacity for the Installation of MDMP Test NB2 (Cases 1 and 2) Based on the Energy Approach Method and the Case Method With Varying $J_c$ Values (assuming pile length is 9.88 m (32.4 ft))......	244
Figure 118	Predicted Pile Capacity for the Restrike of MDMP Test NB2 (Cases 1 and 2) Based on the Energy Approach Method and the Case Method With Varying $J_c$ Values (assuming pile length is 9.88 m (32.4 ft))......	245
Figure 119	Predicted Pile Capacity for the Installation of MDMP Test NB2 (Case 3) Based on the Energy Approach Method and the Case Method With Varying $J_c$ Values (assuming pile length is 8.72 m (28.6 ft))......	246

Figure 120	Predicted Pile Capacity for the Restrike of MDMP Test NB2 (Case 3) Based on the Energy Approach Method and the Case Method With Varying $J_c$ Values (assuming pile length is 8.72 m (28.6 ft)).....	247
Figure 121	Predicted Pile Capacity for the Installation of MDMP Test NB3 (Case 1) Based on the Energy Approach Method and the Case Method With Varying $J_c$ Values (assuming pile length is 13.84 m (45.4 ft)).....	248
Figure 122	Predicted Pile Capacity for the Restrike of MDMP Test NB3 (Case 1) Based on the Energy Approach Method and the Case Method With Varying $J_c$ Values (assuming pile length is 13.84 m (45.4 ft)).....	249
Figure 123	Predicted Pile Capacity for the Installation of MDMP Test NB3 (Case 2) Based on the Energy Approach Method and the Case Method With Varying $J_c$ Values (assuming pile length is 12.68 m (41.6 ft)).....	250
Figure 124	Predicted Pile Capacity for the Restrike of MDMP Test NB3 (Case 2) Based on the Energy Approach Method and the Case Method With Varying $J_c$ Values (assuming pile length is 12.68 m (41.6 ft)).....	251
Figure 125	Comparison Between the Measured Static Capacity for MDMP Test NB2 and Predictions Based on the Dynamic Measurements Utilizing Various Methods of Analysis .....	254
Figure 126	Comparison Between the Measured Static Capacity for MDMP Test NB3 and Predictions Based on the Dynamic Measurements Utilizing Various Methods of Analysis .....	255
Figure 127	Typical Configuration of the Modular MDMP.....	258

## LIST OF TABLES

Table 1	Comparison of Various Instrumented Model Piles.....	7
Table 2	MDMP Static Load Resistance in Soft BBC (Lower Limiting Case) .....	34
Table 3	MDMP Static Load Resistance in Dense Sand (Upper Limiting Case) .....	35
Table 4	Dynamic Loads and Accelerations in the MDMP during Easy or Hard Driving .....	37
Table 5	Summary of Load Cell Capacity Requirements.....	39
Table 6	Summary of the MDMP Required Instrumentation Ranges .....	41
Table 7	MDMP Component List .....	43
Table 8	Top Load Cell Calibration Results .....	49
Table 9	Middle Load Cell Calibration Results .....	52
Table 10	Bottom Load Cell Calibration Results.....	52
Table 11	Dynamic Calibration Results of the MDMP Load Cells .....	53
Table 12	Pore Pressure Transducer Calibration Results.....	55
Table 13	Total Pressure Cell Calibration Results .....	55
Table 14	List of Components as Shown in Figure 28.....	59
Table 15	MDMP Data Acquisition and Instrumentation Configuration .....	62
Table 16	Sampling Performed at Boring NB1.....	75
Table 17	Sampling Performed at Boring NB4.....	76
Table 18	Sampling Performed at Boring NB5.....	77
Table 19	Sampling Performed at Boring NB2.....	77
Table 20	Summary of Soil Properties at the Newbury Site (based on the preliminary test results of Y.L. Chen) .....	82
Table 21	The MDMP Static Load Tests During Test NB2 .....	97
Table 22	The MDMP Final Loading Sequence During Test NB2 .....	97
Table 23	The MDMP Static Load Tests During Test NB3 .....	99
Table 24	The MDMP Final Loading Sequence During Test NB3 .....	99
Table 25	Legend of Events for Pore Pressure Build-Up and Dissipation With Time for Model Pile Test NB2 (see Table 21 for a time schedule).....	101
Table 26	Legend of Events for Pore Pressure Build-Up and Dissipation With Time for Model Pile Test NB3 (see Table 23 for a time schedule).....	104
Table 27	Initial Adjustments to Internal Load Cell Measurements.....	121
Table 28	Average Peak Forces Measured at Three Locations in the MDMP .....	183
Table 29	Average Peak Velocity Measured at Three Locations in the MDMP .....	192
Table 30	Summary of Excess Pore Pressure Dissipation Parameters and their Comparison to a Large Data Set.....	196
Table 31	Evaluated Pore Pressure Dissipation Time (Adjusted to the PLS Diameter) Based on the Newbury Test Results Compared With a Large Data Set.....	197
Table 32	Summary of Gain of Capacity Parameters and Their Comparison to a Large Data Set.....	198
Table 33	Evaluated Gain of Capacity (Adjusted to 152.4-mm Radius Pile) Based on the Newbury Test Results Compared With a Large Data Set.....	200
Table 34	Shear Transfer Recorded During NB2 Final Load Test .....	210
Table 35	Average Shear Transfer Recorded During NB2 Final Load Test.....	213
Table 36	Shear Transfer Recorded During NB3 Final Load Test .....	213

Table 37	Average Shear Transfer Recorded During NB3 Final Load Test.....	213
Table 38	Variations in the Cross-Section / Impedance Between the Drilling Rods and the MDMP .....	218
Table 39	Energy Approach Capacity Predictions for the MDMP .....	222
Table 40	Cross-Sectional Areas for CAPWAP Modeling of the MDMP .....	223
Table 41	CAPWAP Results of Test NB2 Restrike, Case (1), Assuming a 9.88-m (32.4- ft) Model Pile Without a Slip Joint.....	226
Table 42	CAPWAP Results of Test NB2 Restrike, Case (2), Assuming a 9.88-m (32.4- ft) Model Pile With Slip Joint Modeling .....	228
Table 43	CAPWAP Results of Test NB2 Restrike, Case (3), Assuming a 8.72-m (28.6- ft) Model Pile With Pile Ending at Slip Joint .....	230
Table 44	CAPWAP Results of Test NB3 Restrike, Case (1), Assuming a 13.84-m (45.4- ft) Model Pile With Slip Joint Modeling .....	237
Table 45	CAPWAP Results of Test NB3 Restrike, Case (2), Assuming a 12.68-m (41.6- ft) Model Pile With Pile Ending at the Slip Joint .....	239
Table 46	Summary of the MDMP Final Static Capacities During the Tension (Pull-Out) and Compression Load Tests.....	253
Table 47	Summary of the MDMP Instrumentation Ranges .....	257



## CHAPTER 1. INTRODUCTION

### 1.1 Overview

Piles are common foundation members enabling the transfer of large superstructure loads into weak compressible layers or through them to strong bearing strata. Pile foundations are traditionally designed either as end-bearing or friction piles. End-bearing piles are assumed to support the entire load at the pile's tip, while friction piles rely on load transfer along the pile shaft to develop their capacity.

The displacement required to activate the shaft resistance at a point (displacement to yield = skin quake) is estimated to be 2.5 mm (0.1 in); for example, see quake values proposed by Smith (1960) and the interfacial friction test results by Paikowsky et al. (1995b). In contrast, about 0.1B of displacement (where B is the pile tip width/diameter) is necessary to activate the tip resistance (Bowles, 1988). In reality, all piles are friction piles until some or all of their shaft resistance is mobilized (along the entire pile's length), allowing the pile end to develop resistance. As a result, piles often carry the service load in friction, even if designed as end-bearing piles. The need to accurately analyze the shaft resistance component is, therefore, important for an economical design of pile foundations. For this purpose, testing methods are required that measure and evaluate the shaft friction and its variation during the service life of the pile. The obtained information enables one to improve the understanding of the underlying mechanics and hence to develop better soil-structure interaction theoretical tools. Theories of this kind can include, for example, the consideration of capacity changes with time, thus leading to better design procedures than those currently utilized in common practice.

The installation and testing of full-scale test piles is both an expensive and an inconvenient method of obtaining information for the design of pile foundations. As an alternative method, model piles, which can be used to simulate the behavior of full-scale piles, are used to obtain this information. A model pile is a scaled-down calibrated pile equipped with instrumentation, having the capacity to monitor the pile-soil interaction over the pile history. The pile history includes the three main stages of the pile's life: the initial driving, the consolidation or pore pressure/surrounding soil equalization, and finally, the loading during service. Model piles utilize electronic sensors to measure load transfer, radial stresses, pore pressure, displacement, acceleration, temperature, and inclination. Such monitoring can include: (1) during installation -- the dynamic pile response as well as the soil and water pressures; (2) during equilibrium - the excess pore pressure dissipation, variation of the soil pressure with time, and along with its influence on the pile's performance; and (3) during service -- the load displacement relations and its distribution along the pile.

The acquired data can either be applied directly in the design process (e.g., measurement of skin resistance) or extrapolated to a full-scale pile behavior (e.g., radial consolidation process) or used to develop and/or calibrate theoretical models and their parameters (e.g., bearing-capacity factors, interfacial load-displacement relations, etc.).

The presented work deals with the development, calibration, and testing of a model pile, known as the MDMP, Multiple Deployment Model Pile and its evaluation as an in situ testing tool for design and construction.

## **1.2 Purpose**

The following goals were set for the presented research:

- Design and build a model pile capable of:
  - (1) Monitoring (while withstanding) dynamic measurements of stresses and accelerations during driving.
  - (2) Monitoring the pore pressure and radial soil stresses with time.
  - (3) Measuring the pile/soil interaction.
  - (4) Multiple deployment at various sites using standard drilling rig operation.
  - (5) Independent static load testing (without the need of a drill rig).
  
- Gather data to expand the database compiled at the UMass-Lowell concerning:
  - (1) Pore pressure dissipation and capacity gain with time.
  - (2) Static pile capacity predictions based on dynamic measurements.
  - (3) Pile behavior under the static cyclic load-testing procedure.
  
- Investigate the ability to obtain design parameters using a model pile under field conditions to be applied to full-scale pile analysis and design.

## **1.3 Scope**

1. A literature search of existing model piles was conducted, allowing a review and determination of the most appropriate features of each model pile. Some of the important requirements were: robust design for impact driving and multiple deployments, ability to model open- and closed-ended pile conditions, monitoring pore pressure and total stresses, and versatility of use in different deposits.
2. Considering the aforementioned review, a model pile was developed to measure skin and tip resistance, pore pressure, radial pressure, local displacement, and dynamic response during driving. The MDMP was designed to meet the demanding requirement of an in situ tool used during site investigation to estimate the pile performance.
3. The model pile was calibrated at UMass-Lowell to verify the performance of the instrumentation. A data acquisition system was designed to be operator-friendly and flexible to monitor the pile's instrumentation throughout the entire pile history (dynamic and quasi-static).
4. A site was selected in Newbury, Massachusetts. The subsurface conditions at the site consist of a cohesive soil layer with a depth of about 3 to 15 m (10 to 50 ft) below ground surface. The Multiple Deployment Model Pile (MDMP) was installed at the same location at two



- different depths, 9.27 and 12.31 m (30.4 and 40.4 ft) to the pile tip. Data were collected continuously until the excess pore pressure developed during driving dissipated.
5. Based on the tests at Newbury, the MDMP proved to be an effective in situ tool even in the harsh New England winter environment. The entire test was completed with the use of a standard drill rig typically used for site investigations. The drill rig can be used elsewhere after the pile installation and only needs to be returned to the test location at the completion of the testing sequence in order to remove the pile and the casing.
  6. The data recovered were analyzed to determine: (a) the quality, significance, and predictive capabilities of the dynamic measurements; (b) pore pressure dissipation and capacity gain and their relationship; and (c) radial stress variations and their relationship to pore pressure dissipation and capacity gain.

#### **1.4 Manuscript Layout**

The following are short descriptions for each of the upcoming chapters:

- Chapter 2 - Review of existing model piles used for field testing.
- Chapter 3 - Description of the requirements, specifications, design, and calibration of the Multiple Deployment Model Pile (MDMP).
- Chapter 4 - Design and capabilities of the peripheral accessories required to perform the MDMP field testing.
- Chapter 5 - Overview of the subsurface investigation and testing at the Newbury Massachusetts Model Pile Test Site.
- Chapter 6 - Presentation of the results of the model pile tests at the Newbury site.
- Chapter 7 - Analysis and discussion of the model pile test results at the Newbury site.
- Chapter 8 - Conclusions and recommendations.

The following Appendices are being referred to in the manuscript. These Appendices stand alone and are not required for the continuity and clarity of the report. A copy of the Appendices can be obtained by contacting the Contracting Officer's Technical Representative.

- Appendix A. Static Capacity Analysis of MDMP
- Appendix B. Dynamic Analysis of MDMP
- Appendix C. Machine Drawing of MDMP and Load Frame
- Appendix D. Calibration Plots of MDMP Instrumentation
- Appendix E. Reaction Frame Analysis
- Appendix F. Wire Diagrams and Pinouts for DAS
- Appendix G. Static Load Test Results for the MDMP Test NB2
- Appendix H. Static Load Test Results for the MDMP Test NB3
- Appendix I. Dynamic Measurements

## **1.5 Contributions**

This research has been carried out in cooperation with the Massachusetts Highway Department (MHD) and the University of Massachusetts-Lowell (UMass-Lowell).

The support of the MHD and the collaboration and assistance of Nabil Hourani, the head of the geotechnical section, and John Pettis, geotechnical engineer, are greatly appreciated.

The Federal Highway Administration (FHWA) supported the development and testing of the MDMP, along with other related work performed at the Newbury site. Thanks are extended to Al DiMillio and Carl Ealy, research engineers of the FHWA, for their help, interest, and advice, and for providing the additional Pile Driving Analyzer (PDA) required for the multiple-source dynamic measurements.

The help provided by the laboratory director of the Civil Engineering Department at UMass-Lowell, Gary Howe, and the College of Engineering machine shop director, David Rondequ, is greatly appreciated. Mr. Howe developed the control boxes, allowing both dynamic and static measurements, and helped in all stages of laboratory calibration of the field testing.

Special thanks go to John Chen and Edward Hajduk, graduate research assistants in the Geotechnical Research Laboratory at UMass-Lowell, which was associated with this research project. Their help and collaboration during the field and laboratory testing was appreciated.

George Saliby, a graduate student in the Geotechnical Research Laboratory, assisted during the field testing and his help is acknowledged.

Les Chernauskas of Geosciences Testing and Research (GTR) assisted with the preliminary WEAP analysis, dynamic measurements, and field testing.

Ron Boggess of Geocognetics Inc. of Houston, Texas was in charge of the construction of the MDMP based on an early version of the 76.2-mm (3-in) model pile and required modifications. Final adaptation, calibration, and changes were carried out at UMass-Lowell, Geotechnical Engineering Research Laboratory.

## CHAPTER 2. MODEL PILES FOR FIELD TESTING - REVIEW

### 2.1 Definition and Overview

A model pile is a calibrated tool equipped with instrumentation capable of monitoring the pile/soil interaction over the pile history. Monitoring includes the installation, pore pressure dissipation combined with consolidation and soil pressure equalization, and ultimately, the pile behavior under loading up to failure.

The model pile installation and soil-structure interaction simulate the actual field conditions of full-scale piles in a better way than any other possible laboratory or in situ testing. As such, the obtained information can be utilized directly (e.g., skin friction) or extrapolated (e.g., pore pressure dissipation time) to predict the soil's response during full-scale pile installation.

Model piles utilize multiple electronic sensors, including, but not limited to, load cells, pressure transducers, total stress cells, accelerometers, and displacement transducers. These sensors can measure pile stresses, pore pressures, radial soil stresses, accelerations, and displacements. The data collected from the model pile can be used to determine load transfer, pile forces, soil friction values, and time-dependent capacity.

Limited numbers of model piles have been developed and their use is not common in daily practice. This view excludes the cone penetration test (CPT) that partially fulfills the "model pile" concept, though it was developed and widely used for the determination of soil parameters and site investigation. The available model piles consist of different geometries and are used for different purposes. Some model piles simulate open- and closed-ended pipe piles by varying the tip configurations. Other model piles have been used for cyclic loading simulating the conditions experienced by piles for offshore structures under wave action.

Many technical details are associated with the use and implementation of model piles. Their installation can vary between jacking and driving. While jacking advances the model pile at a constant rate of penetration (pseudo-static), driving is a quick dynamic process similar to the most common full-scale pile installation. The average rate in both cases can, however, be very similar (Paikowsky et al., 1989). Drill rods are usually used to advance the model pile. Their limited length requires frequent interruption of the installation process. This arrangement is different from that associated with common pile installation in two ways: (1) it affects the pore pressure dissipation process and (2) the stress wave propagation during driving is affected by the drill rod connections and variable cross-sections.

Pore water pressure measurements are an important aspect of model piles, especially if the effective stress theory is used as the basis for the pile/soil model. Porous stones are used to separate the water in contact with the pressure transducer from the soil and maintain saturation prior to installation. To record accurate pore pressures, the geometry of the porous stones should conform with the model pile shaft, and the porous stone material needs to ensure fast response time of the pressure transducers. The permeability of the porous stone has to be properly balanced between very high permeability that allows a quick response time and low permeability to maintain saturation when the model pile is

exposed to air and/or advancing through unsaturated soil. The porous stones and the measuring system need to be properly de-aired since air may fill some of the voids, resulting in decreased permeability and a slower response time. In addition, air can penetrate the duct pipes connecting the pressure transducers and thus affect the accuracy of the measurement.

The following sections review model piles that have been previously developed. These model piles were designed for use in the field and to test the in situ pile/soil interaction. There are other types of pile models (usually small in size) that are used in 1-g laboratory pressure chamber and centrifuge testing (Kurup, 1993). These model piles are not discussed in this chapter as their size, type of instrumentation, and conditions of testing differ substantially from that of the field model piles. Table 1 presents a summary of the reviewed model piles following a literature search performed by Peter J. Connors as presented by Ravindra Mynampaty in his Master's Thesis (Mynampaty, 1993). The table was updated with additional literature and with the features of the model pile developed for the current research and presented in Chapter 3.

## **2.2 The Cone Penetration Test (CPT) Model**

The cone penetrometer has been used to identify soil type, stratigraphy, and variability for more than 60 years. The cone penetrometer has evolved from an original mechanical cone to an electric cone and a piezocone that are currently used for in situ testing (see Figure 1). Electric cones are capable of continuously monitoring tip resistance and skin resistance. When equipped with a piezometric element, they can monitor pore pressure (DeRuiter, 1982; Schaap and Zuiberg, 1982; and Chen and Mayne, 1994).

The cone penetrometer has been standardized throughout the many years of use. The ASTM Standard Test Method for Deep, Quasi-Static, Cone, and Friction-Cone Penetration Tests of Soil (ASTM D 3441-86) states that the standard cone has a 60° point angle and a base diameter of 35.7 mm (1.406 in) resulting in a projected area of 10 cm<sup>2</sup> (1.55 in<sup>2</sup>). The standard friction sleeve has the same diameter as the cone and has a surface area of 150 cm<sup>2</sup> (23.2 in<sup>2</sup>). Non-standard cones have been developed with projected areas varying from 5 to 15 cm<sup>2</sup> as well as different size friction sleeves.

The instrumentation of the penetrometer consists of one or more axial load cells and, often, pore pressure transducers. All cone penetrometers have a load cell to measure the resistance at the tip, while new versions that are capable of measuring skin friction have an additional load measurement. A common method to measure skin resistance is the subtraction method, which requires an additional axial load cell that measures the combined load at the tip and friction sleeve. The skin resistance is then determined by subtracting the tip resistance as measured by the axial load cell at the tip from the combined resistance as measured by the axial load cell located in the shaft. Pore pressure measurements are measured with pressure transducers mounted in the tool.

TABLE 1. Comparison of Various Instrumented Model Piles.

	Cone Penetrometer	PLS	G&R Test Pile	NGI Test Pile	3.0-inch Model Pile	"X"- Probe	IMP	Imperial College	MDMP
Diameter (mm)	35.7	38.4	25.4	152.4	76.2	43.7	80.0	102	76.2
Length (cm)	varies	26.8 + Tip	88.9	500.4	245 + 245 Shoe	143.5	113.5	700	286.5
Tip Configuration	Cone	Cone	Closed	Closed End	Interchangeable	Solid Cone	Open/Closed	Solid Cone	Interchangeable
Load Cells	2	1	None	1	2	1	3	4	3
Position	Cone/Sleeve	Behind Tip	None	Top	Sleeve	Sleeve	Sleeve	Behind/Tip/Top/Sleeve	Tip/Sleeve
Strain Gauges	None	None	4	6	None	None	4	None	None
Position			Sleeve	Bottom/Sleeve			Sleeve		
Pore Pressure Transducer	up to 3	1	1	4	1	1	3	3	1
Position	Cone/Sleeve	Behind Tip	Middle of Sleeve	Bottom/Sleeve	Middle of Sleeve	Sleeve	Tip/Sleeve	Behind/Tip/Top	Middle of Sleeve
Lateral Pressure Transducer Type	None	1	None	4	1	1	4	3	1
Position		Cylindrical Lat Stress Cell Behind Tip		Bottom/Sleeve	Total Pressure Cell Middle of Sleeve	1-Middle	Total Radial Stress Sleeve	Behind/Tip/Sleeve	Total Pressure Cell Middle of Sleeve
Displacement Transducer	None	None	None	1	LVDT	1	None	3	LVDT
Position				Top	Behind Cut Shoe	Behind Tip		Top	Behind Cut Shoe
Accelerometer	None	None	None	None	4	None	None	None	3
Temp. Sensor	Special	Behind Tip	None	None	None	None	None	3	None
Slope Sensor	Special	None	None	None	None	None	None	None	None
Pile Type	Probe	Probe	6061 AL Tube	Steel Pipe	Steel Pipe	Probe	Steel Pipe	Steel Pipe	Steel Pipe
Testing Sites	Numerous Locations	Saugus, MA Empire, LA	Sabine, Texas	Oslo, Norway	CA, TX, LA B.C.	CA, TX, LA B.C.	England	Several sites in England	Newbury, MA
References	De Ruiter, 1982 Van Den Berg 1982 ASTM 3441-86 Chen & Mayne, 1994	Wissa et al., 1975 Morrison, 1984 Azzouz, 1985 Azzouz & Lutz, 1986	Grosch & Reese, 1980	Karlsrud and Haugen, 1981, 85a, 85b	Bogard & Matlock, 1985, 1990a, 1990b, 1990c	Bogard & Matlock, 1985, 1990a, 1990b, 1990c	Coop & Wroth, 1989 Lehane, 1992	Bond & Jardine, 1991, 1995 Bond et al., 1991 Jardine et al., 1992 Lehane & Jardine, 1994	Current Work

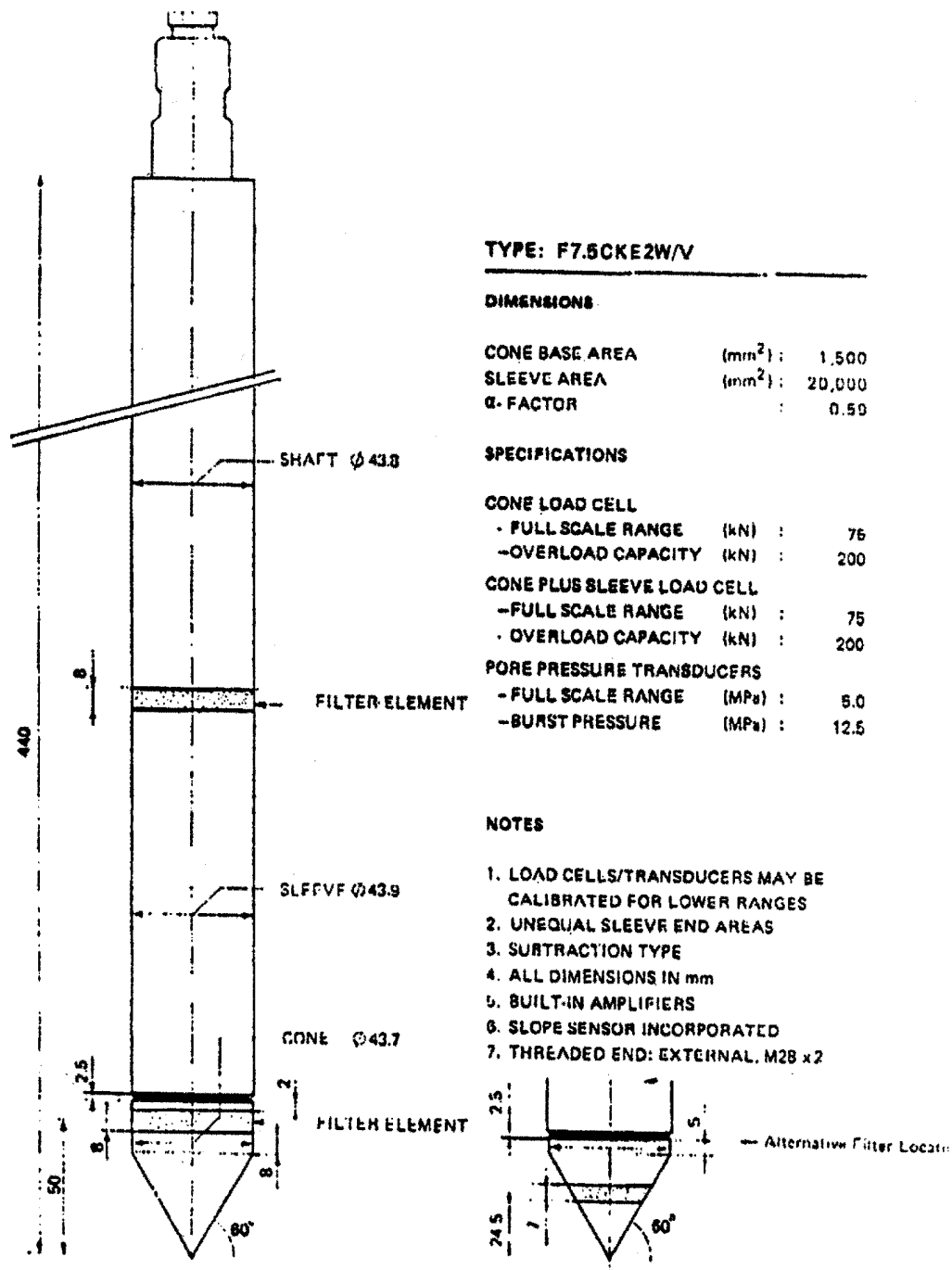
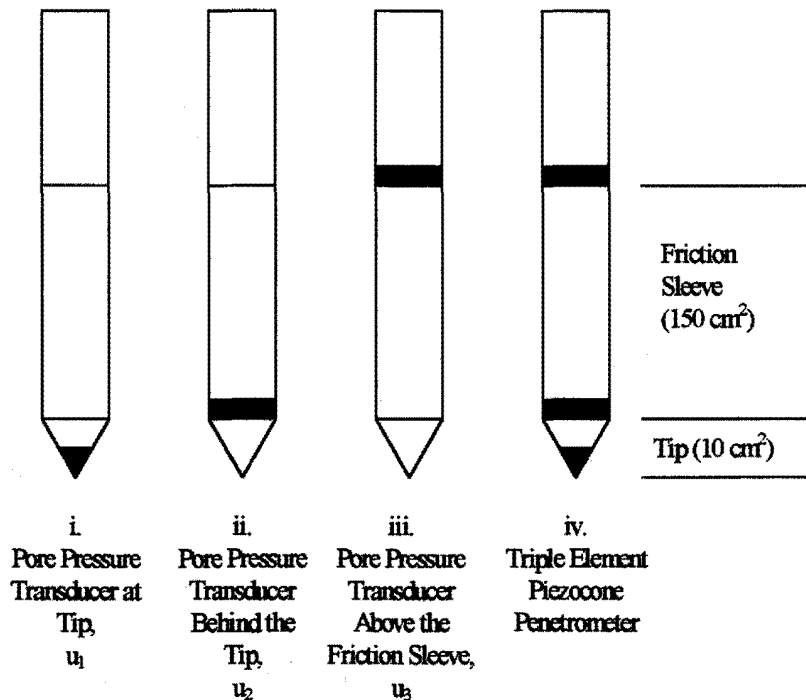


Figure 1. The Dual Piezo Friction Cone Penetrometer (De Ruiter, 1982).

The location of the pore pressure transducer is not yet standardized and is often in one or more of the following locations: at the tip, behind the tip, and/or above the friction sleeve (Figure 2). For an effective tool to investigate pile/soil interaction, pore pressure needs to be measured on the shaft, well above the friction sleeve (Paikowsky et al., 1995). Pore pressure measures at positions  $u_1$  and  $u_2$  are useful when determining soil stratigraphy. Cone penetrometer with pore pressure measurements are referred to as piezocone penetrometers.

Some variations of the cone may include other sensors such as an omni-directional inclinometer (a slope-sensing device), nuclear density probe, and acoustic probe. Nuclear density probes are able to detect changes in density of the soil by emitting and receiving radioactive isotope rays. The inclinometer can detect if the cone penetrates in the vertical direction. This verifies the depth of the model and is useful for the recovery of probes before they deviate too far off course.



**Figure 2. Typical Locations of Pore Pressure Measurements for Piezocone Penetrometers.**

The loading system for penetrometers is often contained in a portable vehicle that can be ballasted to provide the full reaction for the testing. The system includes either a hydraulic ram or a hydraulic clamping system to insert the model. The clamping system is very useful because it enables the addition of drilling rods without interrupting the advancement of the model. The cone is advanced at a constant rate of 20 mm/s.

Disadvantages that may hinder the ability of the cone to simulate pile installation are: (1) the device requires the use of drill rods to advance the cone into the soil (this delay, caused by the addition of drill

rods, enables the soil surrounding the pile to set up and pore pressure to dissipate), (2) the friction sleeve is behind the tip, hence it does not represent typical shaft conditions, and (3) the non-standardized placement of the pore pressure filter along the surface of the cone and/or at its base where the measured pore pressure is not representative of the pile shaft conditions.

### 2.3 The Piezo-Lateral Stress (PLS) Cell

The 38.4-mm- (1.51-in-) diameter Piezo-Lateral Stress Cell (PLS) (see Figure 3) was originally developed by Wissa et al. (1975). The device was introduced in 1978 to provide essential fundamental data on pile behavior in clay in order to expand the knowledge of long piles behavior, especially the skin friction component of long piles total capacity (Azzouz, 1985b; Azzouz and Lutz, 1986; and Azzouz and Morrison, 1988). In addition, the device can be utilized as an exploratory tool to directly estimate the shaft resistance of cylindrical piles (Morrison, 1984). The PLS cell has been used successfully in cohesive soils at three Boston Clay sites and at the Empire, Louisiana clay site. At the Empire site, a direct comparison could be made with full-scale piles that were previously tested at the site.

The PLS cell has three components that provide a simultaneous measurement of total lateral stress, pore pressure, and axial load throughout the various stages of the life of the model pile. The total lateral (horizontal) stress and pore pressure measurements are used to determine the horizontal effective stress acting on the pile, a dominant parameter for calculating skin friction when evaluating pile behavior in cohesive soils based on effective shear strength theory.

The lateral stress cell is made of a thin steel shell that covers a thin water-filled pressure chamber (Figure 4). The lateral stress experienced by the shell is transferred to the water in the pressure chamber where the water pressure is measured with a pressure transducer. The ideal lateral stress cell would have an infinitely thin, long steel shell with a large diameter and a minute amount of water in the pressure chamber while being insensitive to axial load. The final design incorporated these ideas as well as practical concerns such as durability and machineability. Sensitivity of the lateral stress cell is expressed as a ratio of the internal water pressure to the external horizontal stress. The constructed element has a sensitivity of 93.5%, with the steel shell being 0.038 cm (0.015 in) thick, 4.70 cm (1.85 in) long, diameter of 3.84 cm (1.51 in), and pressure chamber volume of 2.13 cm<sup>3</sup> (0.13 in<sup>3</sup>). The rated range of the lateral stress cell is 0 to 689.5 kPa (0 to 100 psi). The PLS cell also includes a thermoresistor monitoring temperature. This measurement is essential for achieving a high degree of accuracy in horizontal stress readings when using very stiff, temperature-sensitive devices such as the PLS's lateral cell. Improvement of such devices can be made when using liquid in the pressure chamber with an expansion coefficient more compatible to steel than water (for example, mercury).

A high-entry, stainless-steel porous disk allows the pore water pressure to be measured by an internal pressure transducer. The rated range of the pore pressure transducers is 0 to 1379 kPa (0 to 200 psi). Improper de-airing of the porous disk causes the system to have a slow response time to externally applied changes in pressure and is a common cause of misleading data.



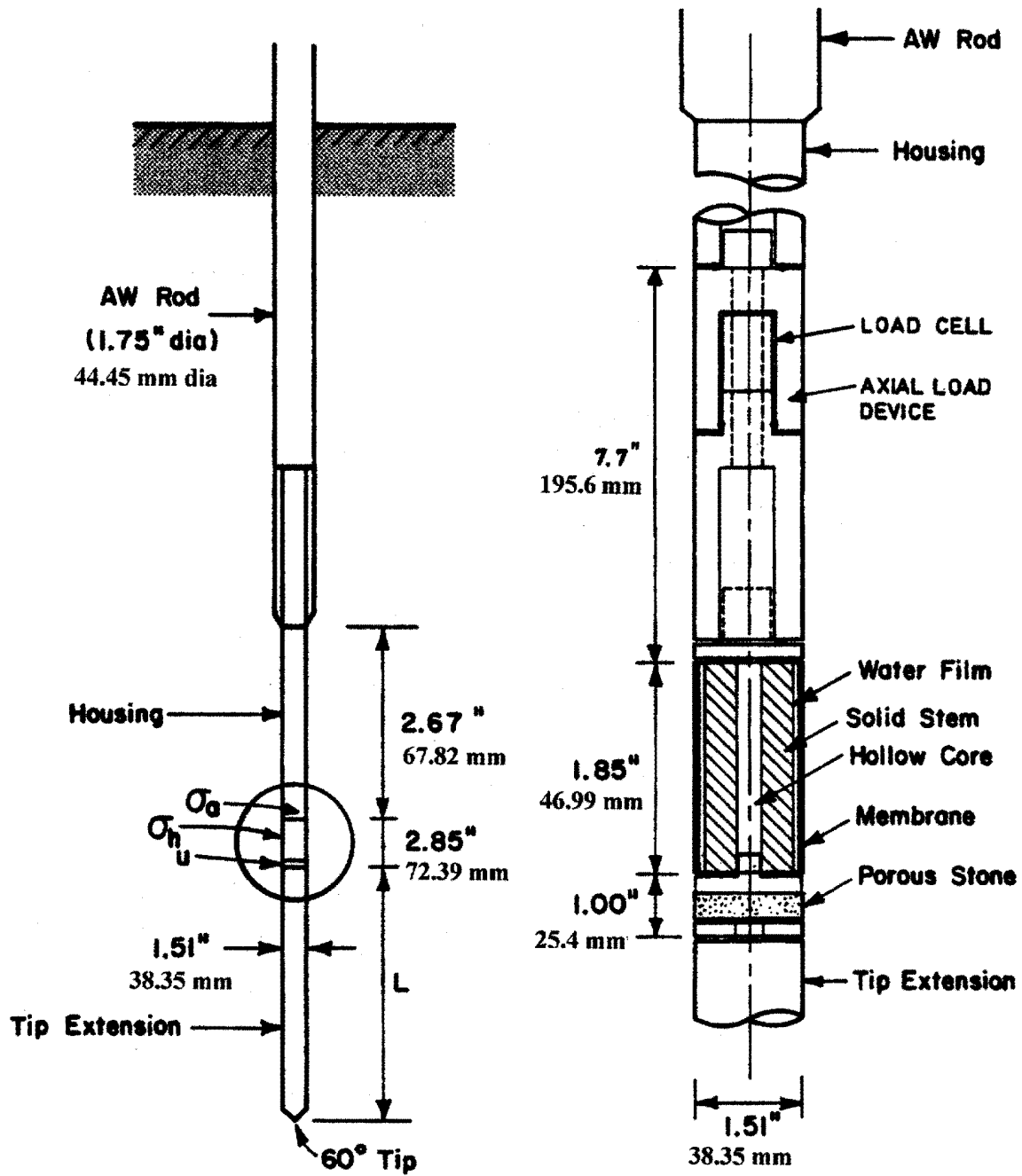


Figure 3. The Piezo-Lateral Stress (PLS) Cell (Morrison, 1984)

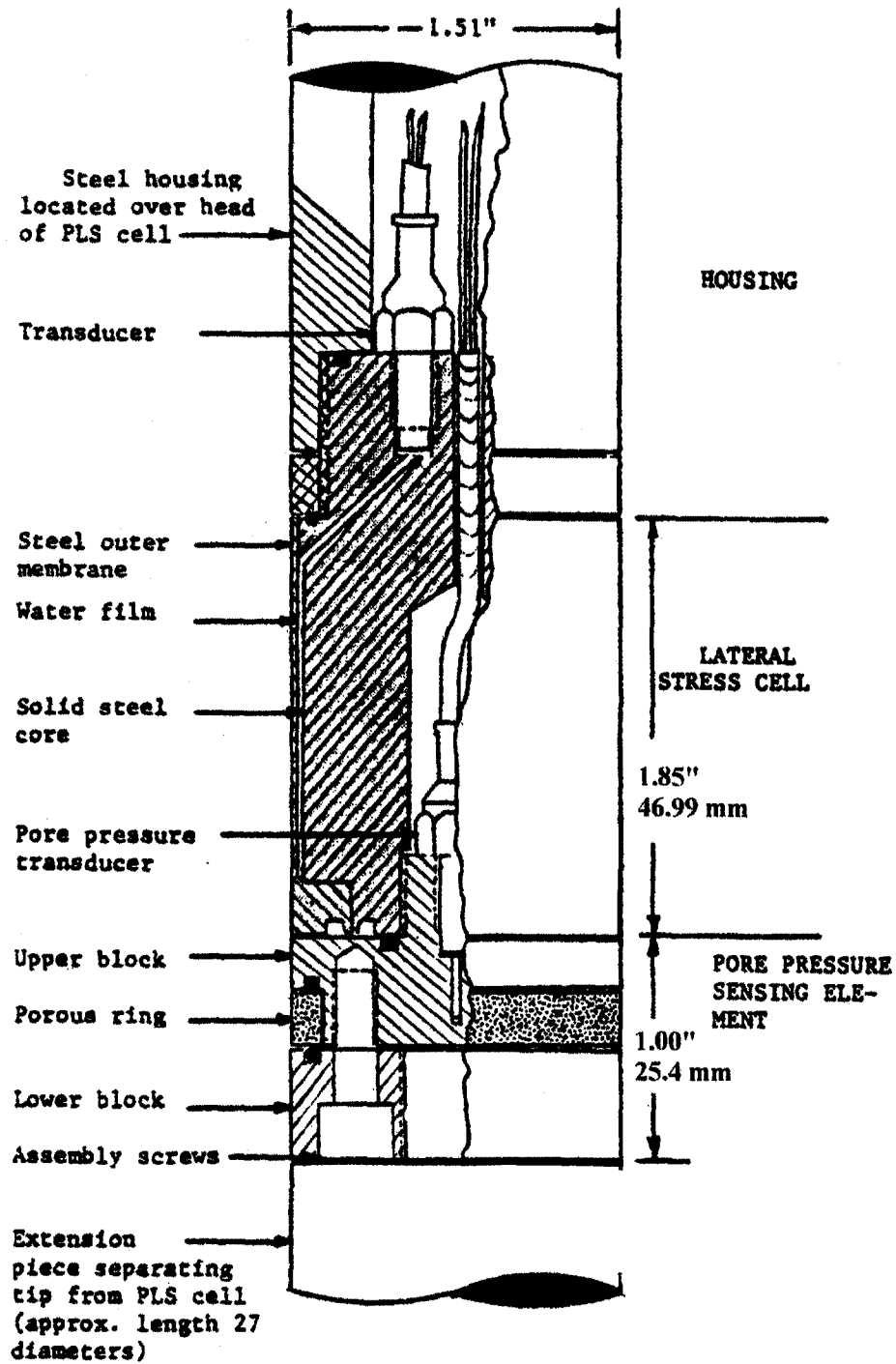


Figure 4. Detailed Cross-Section of the Piezo-Lateral Stress (PLS) Cell (Morrison, 1984).

The load cell measures the axial load required to overcome the tip resistance and shear stresses acting on the length of the shaft bounded by the load cell. Figure 5 provides a detail of the load cell assembly. The PLS has only one axial load cell and utilizes the measurement of tip resistance from an additional piezocone test to determine the skin resistance along the tip extension.

The PLS is pushed at a constant rate of 20 mm/s. Like the piezocone and CPT, the data collected with the PLS cell can be analyzed to identify soil stratigraphy. The PLS is comparable in size with AW drill rods; therefore, the cell may be pushed to significant depths without the need for casing the borehole. A disadvantage of the PLS cell is the drilling rods used need to be added at intervals of 1.524 m (5 ft) of advancement. The time needed to add a new rod allows excess pore pressure dissipation, and this must be taken into account when analyzing the pore pressure data. Care must be taken to identify virgin penetration or non-virgin penetration. The non-virgin records are significantly affected by the degree of consolidation.

An advantage of the PLS is the ability to vary the length of the tip extension. The length of the tip extension may be changed to minimize the tip effects in a particular soil. This enables a more sensitive measurement of the sleeve resistance and allows the model to simulate the shaft of a long flexible pile.

#### **2.4 The Grosch and Reese (G&R) Model Pile**

The Grosch and Reese (G&R) model pile (see Figure 6) was developed at the University of Texas for the American Petroleum Institute. The model was developed to provide insight into the mechanics of cyclic reduction in load transfer of long flexible piles utilized for offshore platforms (Grosch and Reese, 1980). The model pile is a 2.54-cm- (1.0-in-) diameter closed-ended tube, 88.9 cm (35 in) in length. The model pile is made of 6061 aluminum and is connected to a 5.08-cm- (2-in-) diameter galvanized pipe to advance the instrumented section to the desired test depth.

The G&R model pile measures the load transfer over a 25.4-cm (10-in) section with four strain gauges arranged in a Wheatstone bridge formation. This formation cancels any bending forces and measures only the axial load. A pore pressure transducer was located at the mid-point of the section that measures the load transfer. The instrumentation wires are routed through a flexible hose that was pressurized with 82.7 kPa (12 psi) of nitrogen to prevent moisture from entering the system.

The system was designed for simulating cyclic environmental loading often experienced by offshore structures. The loading system consists of a screw jack with a reversible variable-speed motor connected to the model via the 5.08-cm (2-in) galvanized steel pipe. The screw jack enabled the simulation of the environmental loading by cyclic penetration in the bottom of the shallow borehole in a soft, normally consolidated clay deposit in Sabine, Texas. The G&R model pile does not require pre-drilling to insert it to the testing depth. The compactness of the model makes the device relatively mobile.

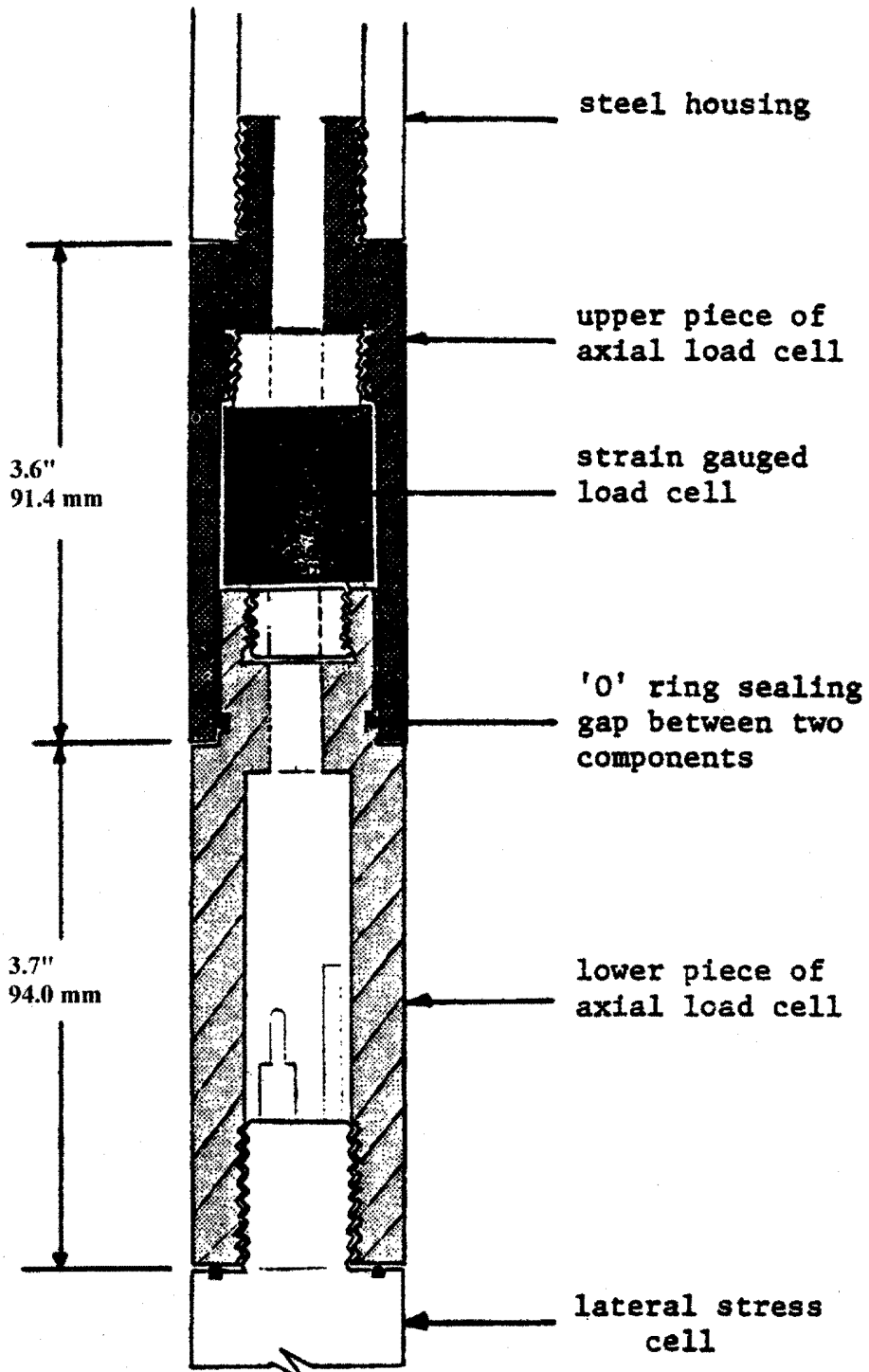


**Figure 5. Details of the Axial Load Cell in the Piezo-Lateral Stress (PLS) Cell (Morrison, 1984).**

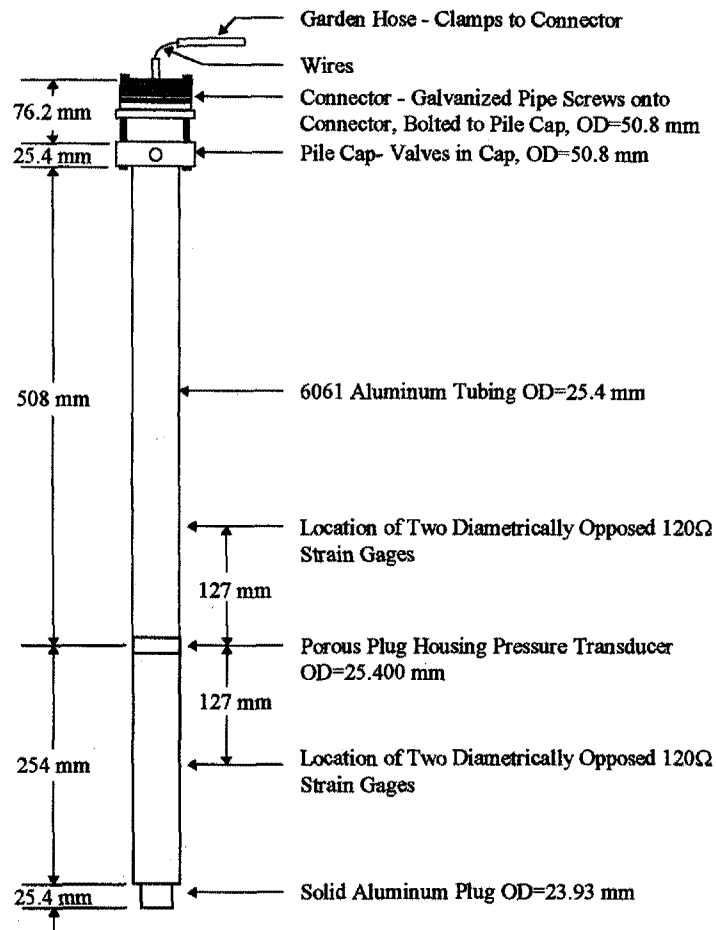


**Figure 6. The Grosch and Reese (G&R) Instrumented Model Pile**  
(Grosch and Reese, 1980).

The model pile is not designed to measure tip resistance observed by the pile. It appears that G&R's model would be less accurate than others due to its small surface area, along which load transfer is measured, and its unsophisticated monitoring capabilities. Other model pile designs allow for redundant measurement of skin resistance, while the G&R model pile does not. Also, the drill rods used to advance the model are not compatible with its diameter. This difference in size would require more force to push the model down, a force different from what the model might experience.

## 2.5 The Norwegian Geotechnical Institute (NGI) Model Pile

The Norwegian Geotechnical Institute (NGI) developed a testing instrument to investigate the effects of tension loading on pile anchors used for tension-leg type offshore platforms. The NGI model pile is not capable of measuring tip resistance and, therefore, represents model segments of long flexible piles used in practice. The 15.24-cm- (6-in-) diameter pile is about 5.0 m (16.4 ft) long as shown in Figure 7. The model pile is closed-ended to model large displacement piles (Karlsrud and Haugen, 1981, 1985a, and 1985b).

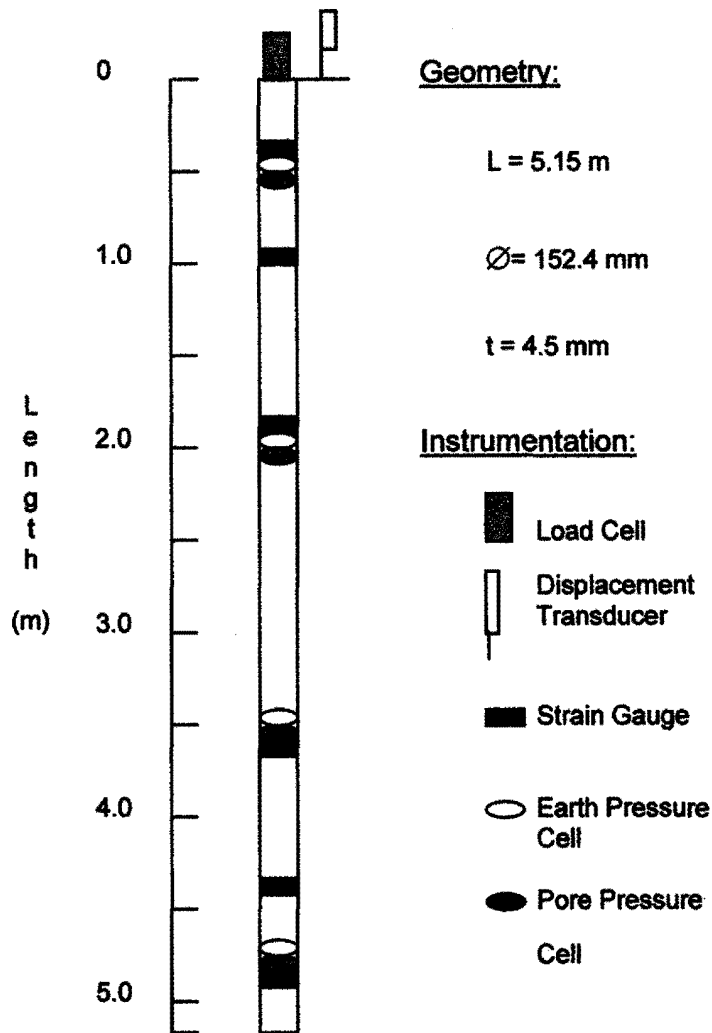


**Figure 7. The Norwegian Geotechnical Institute (NGI) Instrumented Test Pile**  
(after Karlsrud and Haugen, 1985).

The model pile has six groups of vibrating wire strain gauges distributed at different levels along the length of the pile. These strain gauges are used to determine the skin friction that develops along the pile. The effective stresses can be calculated at four different locations using measurements of earth and pore pressure cells. A displacement transducer and a load cell are positioned on top of the model pile. The instrumentation enables the measurement of the effective stresses and skin resistance during pile installation and consolidation.

The NGI model pile has been field tested extensively under a variety of loadings in overconsolidated clay at a site in Haga, outside of Oslo, Norway. Sixteen installations of the model pile were successfully conducted in the overconsolidated clay. An additional section (dummy pile) was attached to the top to advance the model pile to the testing depth. A 6.0-m-diameter concrete ring beam enabled multiple installations of the pile. A jack was used to push the model pile at a rate of 4 to 15 cm/min any place along the ring. Approximately 30 kN (3.37 tons) of force was required to advance the NGI model pile 5 m into the overconsolidated clay. Once inserted, static, rapid, and

cyclic loading tests may be performed by a loading rig that travels around the ring beam used for the installations.

The disadvantage of the NGI model pile when compared to other similar models is its large diameter and length. As a result, the model pile and its installation and loading rigs cannot be transported easily, making it inappropriate as a standard multiple deployment in situ device.

## **2.6 The X-Probe And The 3-Inch Model Piles**

The Earth Technology Corporation developed two in situ testing tools (the 7.62 cm (3.0 in) and the X-probe) to improve the understanding of axial soil/pile load-transfer behavior for long flexible piles of offshore platforms (Bogard et al., 1985; and Bogard and Matlock, 1990a, 1990b, and 1990c). Both the tools simulate a short pile segment and yield a direct in situ measurement of load transfer along the pile segment. The 7.62-cm (3.0-in) model pile (see Figure 8) has successfully been driven and jacked into a variety of soil types. The X-probe model pile segment tool was designed and built to be used on more routine site investigations. Unfortunately, the X-probe (see Figure 9) did not prove to be rugged enough for repeated testing.

The 7.62-cm (3-in) model pile is an in situ testing device with dimensions of 7.62 cm (3 in) diameter and a total tool length of approximately 4.9 m (16 ft). Different cutting shoes, with any wall thickness, can be used to model an open-ended pile, or a closed-ended configuration can be used. Test depths have been as deep as 75 m (250 ft), utilizing N-rods to advance the tool to the desired depth. The 7.62-cm (3-in) model pile is equipped with two load cells that are used to calculate the shear transfer over a section of the pile. Strain gauges (Figure 10) are mounted in a Wheatstone bridge formation to measure only axial loads. In Figure 10, a load cell cover slides over the instrumented section of the load cell to protect the strain gauges and prevent soil and moisture intrusion. Also, mounted in the load cell are two accelerometers (Figure 10). In Figure 11, a total pressure transducer and a pore pressure transducer are located between the two load cells that provide continuous measures of effective stresses at the location where the load transfer is measured. A direct current, linear variable displacement transducer (DC-LVDT) is used to measure local displacement between the cutting shoe and the instrumented portion of the pile. During tension and compression load tests, the cutting shoe acts as an anchor to allow for accurate displacement measurements.

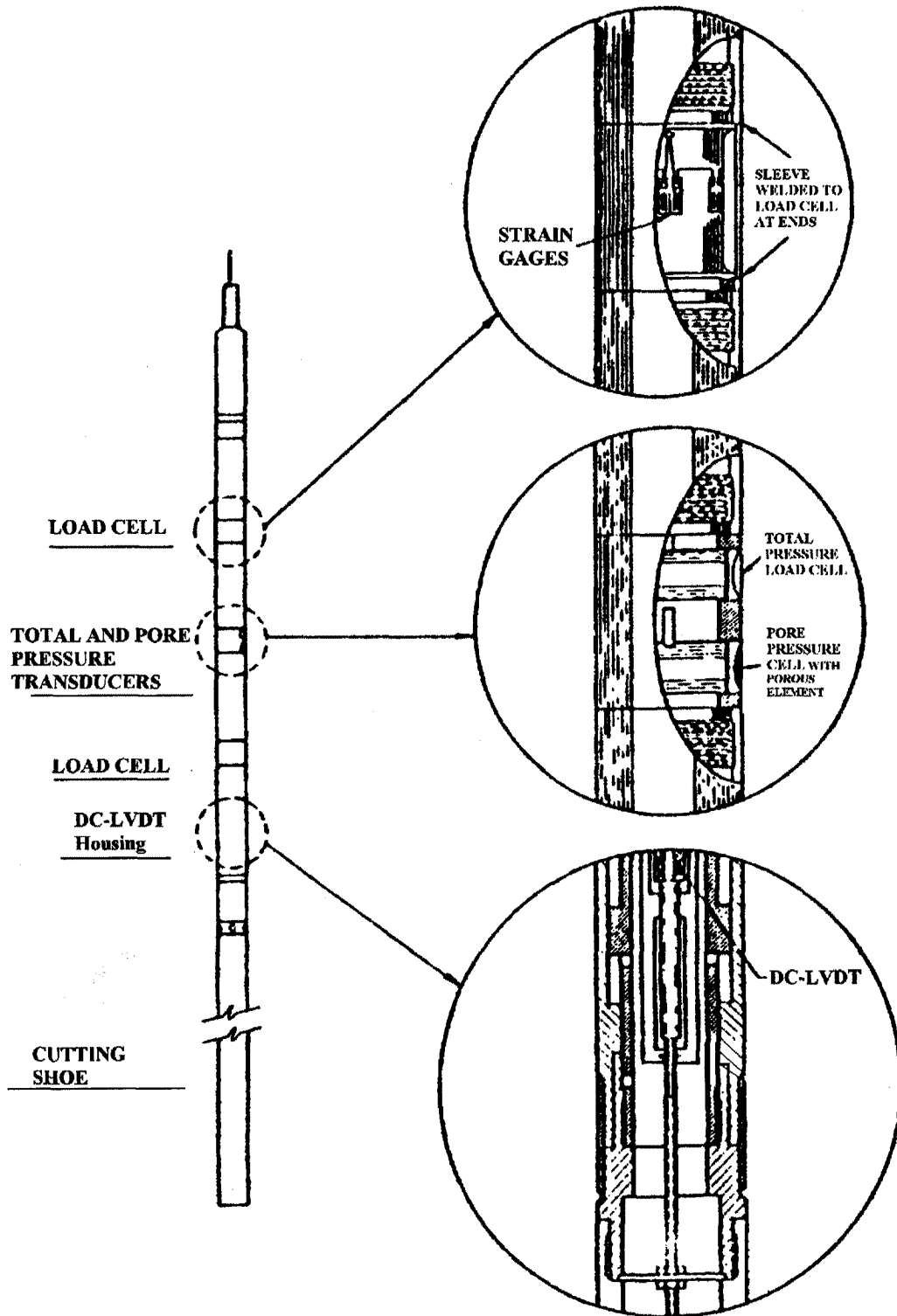
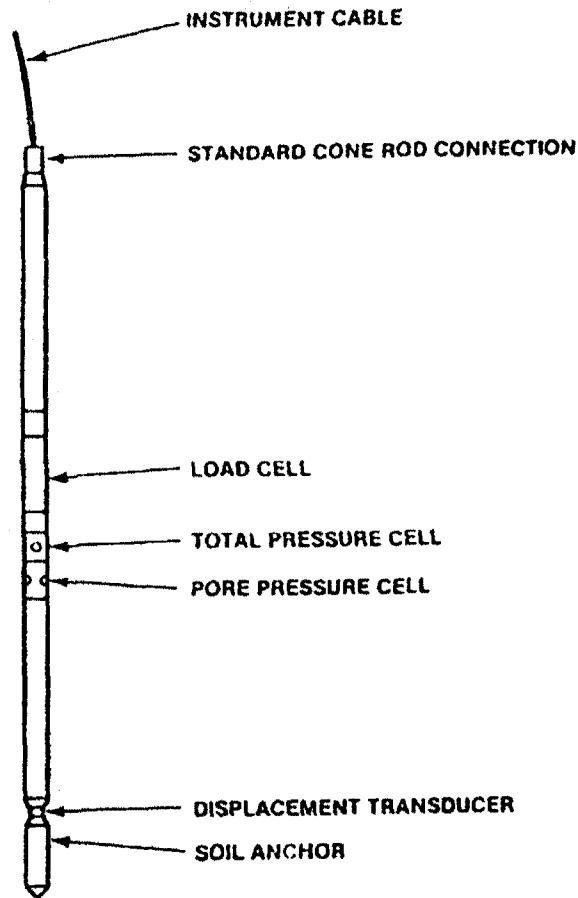


Figure 8 The 7.62-cm (3.0-in) Instrumented Model Pile (Bogard and Matlock, 1985).





**Figure 9 The X-Probe (Bogard and Matlock, 1985).**

The X-probe with a diameter of 4.37 cm (1.72 in) and 143.5 cm (56.5 in) long was designed and built to be used on routine site investigations. The X-probe simulates a plugged pile and has instrumentation that enables the measurement of pile/soil interaction behavior. The pile has a load cell that measures the shear transfer over a 200-cm<sup>2</sup> (31-in<sup>2</sup>) shaft area. Below the load cell are the total lateral pressure transducer and a pore pressure transducer that measure the effective stresses during all stages of pile history. The tip of the pile has a cone with a similar geometry to that of a cone penetrometer. The tip section acts as the reference anchor for local displacement measurements by a displacement transducer. The main advantage of the model is its compatibility with the standard CPT and, therefore, it can be deployed with conventional cone penetrometer equipment. However, the X-probe does not have the capability to measure tip responses.

The models have been extensively tested at six onshore sites along the U.S. Gulf coast, West coast, and Canada; a site offshore Louisiana from a fixed platform; and in the laboratory in a pressurized soil drum. The soil types at these locations are composed of stiff silty clay, silts, soft clay, overconsolidated Beaumont clay, and calcareous soil. At some of the sites, full-scale pile static load tests were carried out as well, which enables the comparison of axial behavior between full-scale pile load test results and model pile segment tool results.

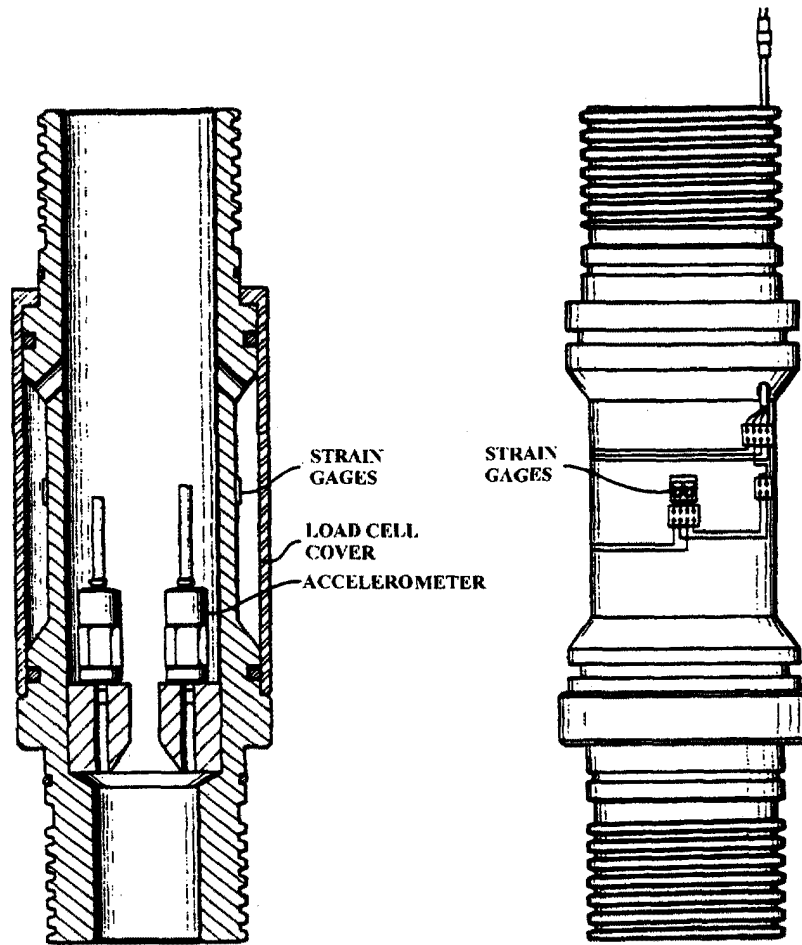


**Figure 10. Details of 7.62-cm (3-in) Model Pile Axial Load Cells**  
(after Patent Number 5,259,240).

The model piles are driven or pushed using N-rods to advance the pile to the desired depth. The instrumentation is monitored during installation and through the duration of the test. Upon the completion of installation and consolidation, a variety of load tests were performed. These loading tests included static monotonic, one-way cyclic (compression or tension only) with or without load bias, and two-way cyclic loading under tension and compression. The loading system consisted of a hydraulic ram, with a 30.48-cm (12-in) stroke, that was able to apply tension or compression loading to the models. Screw anchors are used as a reaction for compressive loadings when testing was conducted onshore.

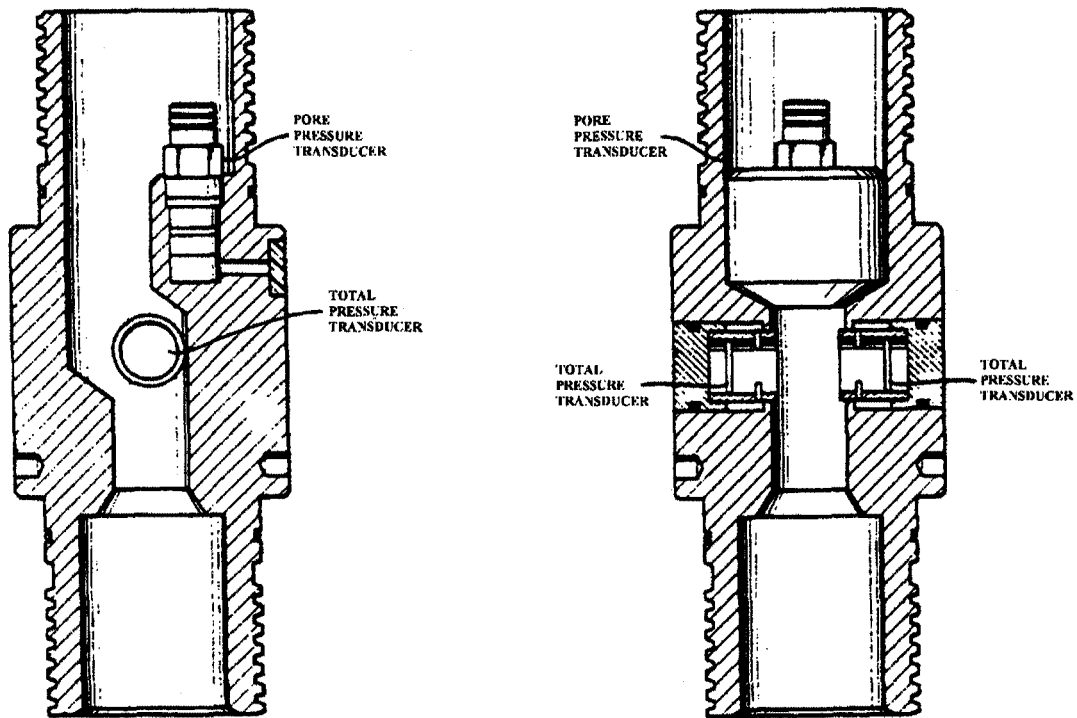
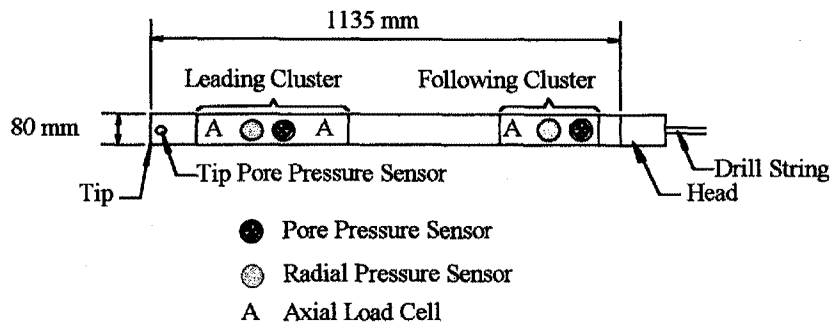


**Figure 11. Details of 7.62-cm (3-in) Model Pile Pressure Instruments**  
(after Patent Number 5,259,240).

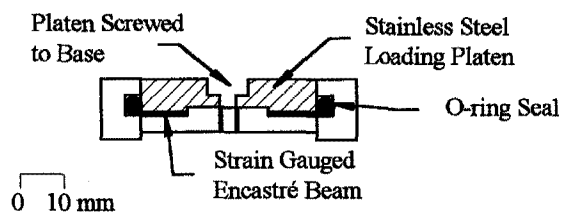
## 2.7 The In Situ Model Pile (IMP)

The IMP or In Situ Model Pile (see Figure 12) was developed at Oxford University (Coop and Wroth, 1989; and Lehane, 1992) to explore the fundamental behavior of piles in clay. Both stiff overconsolidated and normally consolidated estuarine clays were successfully tested. The model is 80 mm (3.15 in) in diameter and 1135 mm (44.7 in) long. The model pile consists of two concentric cylinders attached to a common pile head, with the inner cylinder rigidly connected to the tip assembly and the outer brass cylinder comprised of a combination of interchangeable instrumented sections. The rigid connection allows for a more sensitive measurement of shaft friction. End bearing forces are transmitted directly to the pile head through the inner cylinder and are not measured.

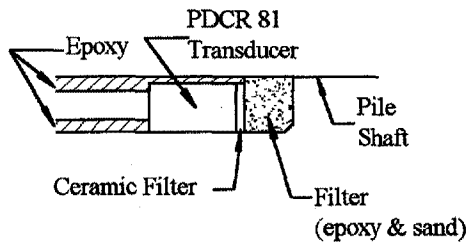
The IMP has two instrumentation clusters, with each section having two pore pressure transducers, two radial stress transducers, and a load cell. There is an additional pore pressure transducer located at the tip of the pile and a third load cell located in the leading cluster. Figure 12 presents the location of the sensors, as well as diagrams of two types of pore pressure sensors and radial stress sensor. The Druck semi-conductor transducer is a brand name pressure transducer that was installed into the IMP while the strain-gauged diaphragm was constructed specifically for the IMP. The three load cells measure axial load, enabling the skin friction to be calculated as the difference in axial load between any two load cells. In each instrumented section, two total radial stress and pore pressure transducers were installed opposite of each other to check for variation in stresses around the IMP shaft.



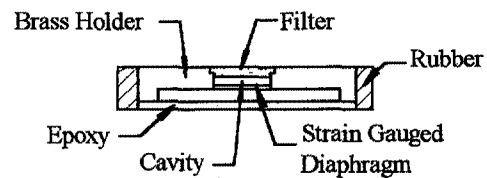
### Configuration of IMP



### Radial Stress Sensor



Pore Pressure Sensor  
with Druck Semi-Conductor Transducer



Pore Pressure Sensor  
with Strain Gauged Diaphragm

**Figure 12. Configuration and Instrumentation of the In Situ Model Pile (IMP)**  
(after Lehane, 1992).

A plunger that may be held in position or allowed to move is located within the inner cylinder. This facilitates both closed-ended and open-ended installation. The jacking system for the IMP consists of hydraulic jacking rig powered by a portable gasoline engine. The reaction for the system is provided by screw pickets. Due to the size of the loading system, NWY drill rods are used to advance the model into the soil. The NWY rods have a smaller diameter than the model pile. No load due to friction along the sides of the rods is developed and, therefore, less force is required to advance the model pile into the soil.

The IMP has been successfully employed in various sites in England. The four sites located at Madingley included two sites having normally consolidated estuarine clays and two having heavily overconsolidated clays. An additional site at Huntspill contained soft silty, normally consolidated clay. Most of the experiments were carried out closed-ended, and the jack stroke length was approximately 350 mm (13.78 in), with a jacking rate of 230 mm/min (9.06 in/min). In several tests, the progression of the model pile was halted to measure pore pressure dissipation and to conduct undrained load tests.

The entire system, inclusive of the model pile and the monitoring and jacking system, is self-contained and facilitates transportation by a typical off-road vehicle, enabling installation in inaccessible places with only a two-person crew.

## **2.8 The Imperial College Pile (ICP)**

The Imperial College instrumented model pile (see Figure 13) is a closed-ended steel model pile designed to investigate the following (Bond and Jardine, 1995; Bond et al., 1991; Bond and Jardine, 1991; Jardine et al., 1992; and Lehane and Jardine, 1994):

- Effective stresses acting at the pile/soil interface during the three main stages of the pile's history.
- Difference between tension and compression loading.
- Influence of pile end condition.
- Effect of changing the direction of loading.
- Variation in first-time load capacity with time.
- Effects of variable equalization periods.
- Effects of installation jacking rate.
- Significance of jacking as opposed to driving piles.

By studying the above effects, the objective of ICP model pile tests is to develop a theory to explain the behavior of displacement piles that is based on effective stresses.

The model pile is 10.2 cm (4.02 in) in diameter and 7 m (22.97 ft) long, with a solid 60° cone fitted at the pile tip. The model pile has three clusters of sensors spaced 1 m apart. Each cluster (see Figure 14) contains a high-capacity axial load cell, a surface stress transducer (SST), a pore pressure unit, and a temperature sensor inside the stress transducer. In addition, three displacement transducers and another axial load cell are positioned at the top of the model pile during testing. The load cell at the top verifies the measurements of the SSTs. The SSTs (Figure 15) are capable of

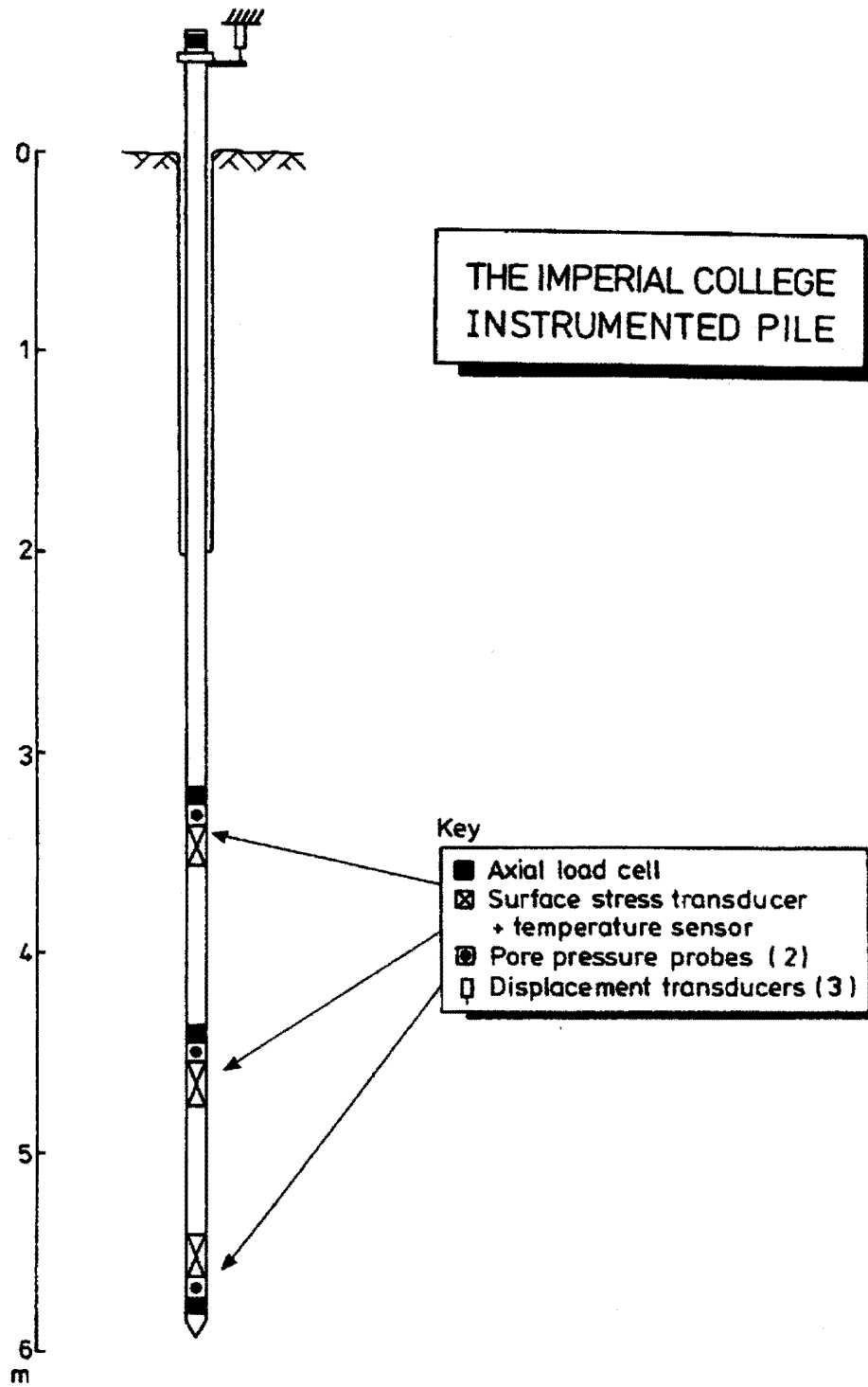
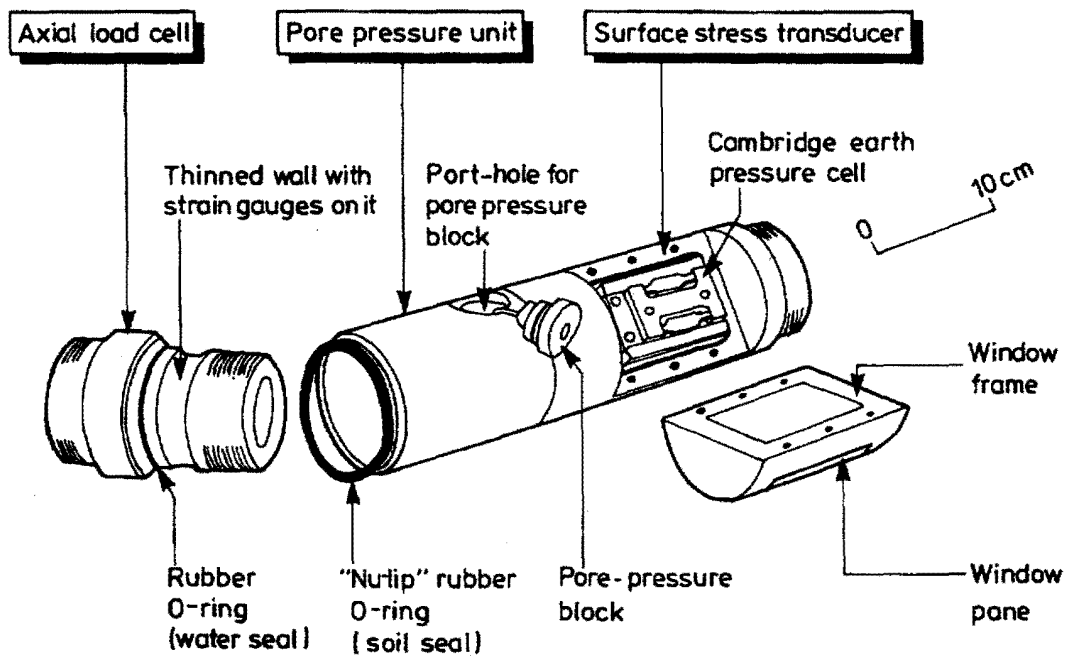
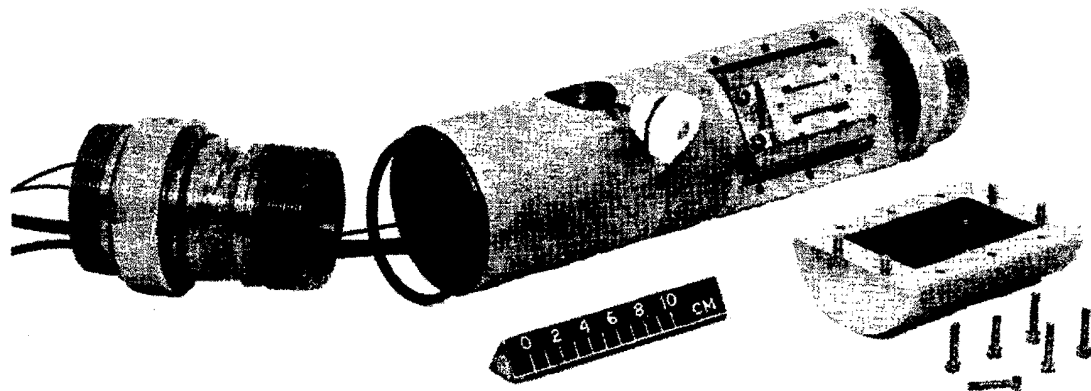
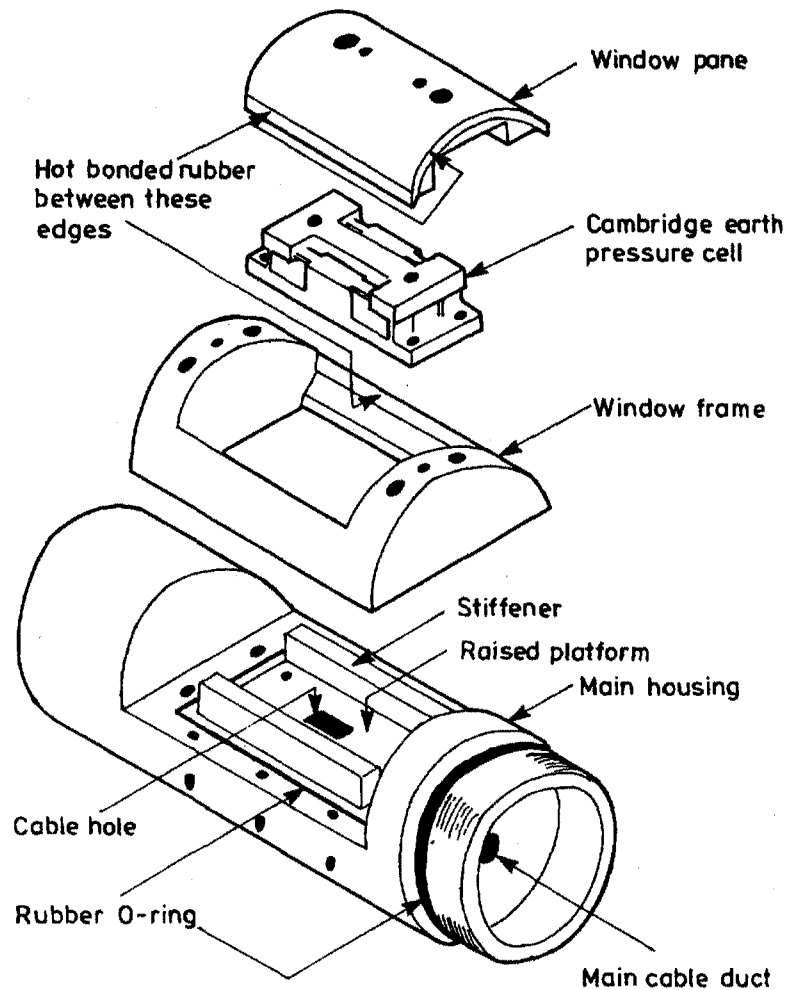


Figure 13. The Imperial College Instrumented Model Pile (Bond and Jardine, 1991).



**Figure 14. Typical Imperial College Model Pile Instrument Cluster**  
(Bond et al., 1991).

measuring the radial total stress and shear stress acting on the pile. For an axial web strain of 0.2%, the radial and shear stress capacities of the SSTs are 870 kPa (126.2 psi) and 262 kPa (38.0 psi), respectively. The pore pressure unit consists of two quick-response pore pressure probes that enable the model pile to monitor pore pressure and the effective stresses to be calculated. The temperature sensor located in each SST is required to achieve the necessary accuracy of measuring the radial stress acting on the pile. The high-capacity axial load cell (Figure 16) located in each cluster consists of a short, thin-walled section where strain gauges are mounted in a Poisson bridge to measure axial loads acting on the pile. This thin-walled section is designed so that it will yield rather than buckle, and at 0.2% axial strain, the nominal capacity is 209 kN (23.5 tons).



**Figure 15. The Surface Stress Transducer (Bond et al., 1991).**

The ICP model pile has been used in a variety of soil types, including heavily overconsolidated London clays, medium dense sand, stiff glacial till, and sensitive soft clays. Some of the sites tested included soft, sensitive marine clay at Bothkennar, Scotland; highly overconsolidated London Clay at Cannons Park, north London; and sub-rounded dune sand at Labenne, France. The model has been proven to yield highly consistent and repeatable data in all soil types that were tested. The test procedure the model underwent entailed jacking the model through a cased borehole in a series of pushes, approximately 226 mm, at variable penetration rates. There were short pauses when the jack was reset. The piles were jacked rather than driven to prevent damage to the instrumentation.

The Imperial model pile's main advantage is the incorporation of duplicate sensors at each instrument cluster to provide redundancy of measurements. Some disadvantages of the Imperial Model Pile are no instrumentation at the pile tip to monitor point resistance and a large size that might present difficulty in transportation.



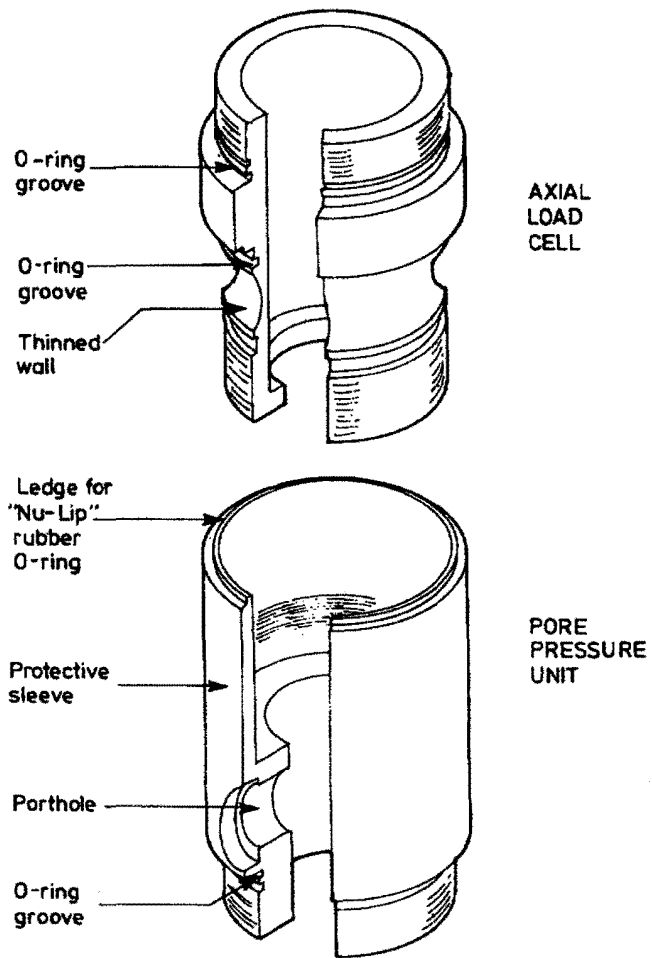


**Figure 16. The Combined Axial Load Cell and Pore Pressure Unit**  
(Bond et al., 1991).



## CHAPTER 3. THE MULTIPLE DEPLOYMENT MODEL PILE (MDMP)

### 3.1 General Description

The Multiple Deployment Model Pile (MDMP) is an in situ soil testing device very similar to the 7.26-cm (3-in) model pile previously described in section 2.6. The MDMP is composed of a series of modular sensors that are screwed together in any desired configuration. The model pile is capable of measuring axial loads, pore water pressure, total radial stresses, local displacement, and pile acceleration. A typical configuration of the modular MDMP is shown in Figure 17. In summary, the MDMP instrumentation includes three load cells, three accelerometers, a displacement transducer, a pore pressure transducer, and a total pressure cell.

Two load cells are positioned in a series with a total stress cell and pore pressure cell (located in transducer housing) centered between the load cells. The friction sleeve between the two load cells has a surface area of  $2000 \text{ cm}^2$  ( $310 \text{ in}^2$ ). By subtracting the measured loads of each load cell and using the surface area, the friction along the friction sleeve can be calculated. An additional load cell is located near the tip of the pile. This additional load cell offers another measurement of friction along a greater length of the pile, as well as a measurement of tip resistance. A slip joint is located 16.7 radii from the total stress cell and pore pressure cell. The slip joint utilizes a direct current-linear variable displacement transducer (DC-LVDT) to measure up to 5 cm (2 in) of local displacement. During load tests, the local displacement measured by the DC-LVDT and the load cells should yield a load-displacement curve that is independent of any slack and compression of the drill rods. The friction sleeve can be made of different materials of various surface finishes (different roughness), allowing the examination of surface roughness effects on the frictional pile resistance. Pile acceleration is measured in the model pile utilizing high-impact accelerometers. The accelerometers are mounted inside the model pile at the load cell locations, thereby allowing for force and velocity records at the same location and minimizing uncertainties in the acceleration records due to drill rod connections. Two sets of load cells of different capacities were designed for use with the MDMP in a variety of subsurface conditions. The MDMP can be used to model large displacement piles by using a closed-ended tip. Also, small displacement piles can be modeled by using an open-ended tip.

### 3.2 Requirements

The Multiple Deployment Model Pile (MDMP) must be able to record the following measurements during driving, static load testing, and restrikes:

- Axial loads at multiple locations along the pile (static and dynamic).
- Pore pressures (static and dynamic).
- Tip resistance (static and dynamic).
- Total radial stresses (static).
- Local displacement (static).
- Accelerations (dynamic).

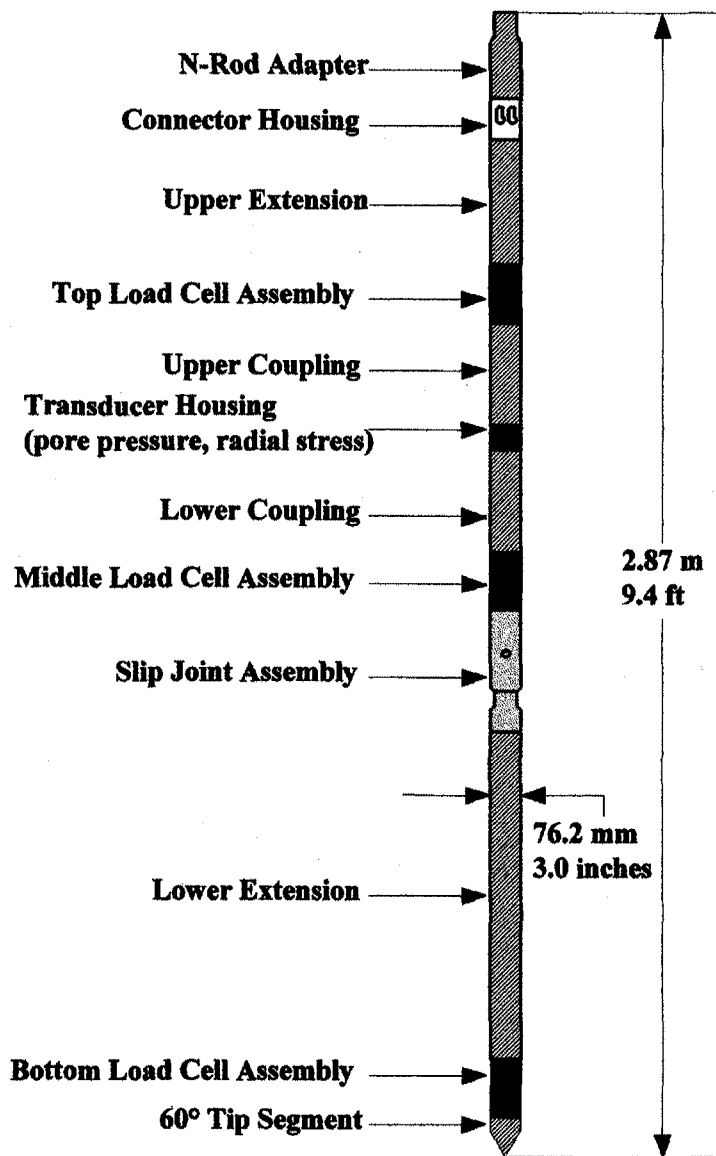


**Figure 17. Typical Configuration of the Modular MDMP.**

Total capacity, load transfer, and time-dependent information can be determined from these measurements. Initially, the MDMP tests were planned to be conducted in medium to soft Boston Blue clay deposits in the eastern Massachusetts area. Additional requirements were included so that the MDMP could be deployed in stiffer Boston Blue clay, glacial till, and/or dense sands.

The major objective of the MDMP is to simulate the installation and stress history that full-scale piles experience. To achieve this, the MDMP must be designed and constructed rugged enough to withstand driving stresses and, more importantly, the instrumentation must maintain the required standard of accuracy throughout the testing sequence. Measurements need to be

recorded during the three stages of pile history — installation, stabilization (equilibration), and static loading conditions. Total radial pressures and pore pressures are planned to be continuously monitored during all stages. Axial strains and accelerations need to be monitored during driving to provide for the dynamic prediction of the pile capacity. The MDMP can therefore be restruck to assess the gain of capacity with time. Axial strains need also to be recorded during static load testing. The MDMP has several different tip configurations (see Figure 18), including an open-ended and a closed-ended cutting shoe that simulate small displacement and large displacement piles, respectively. The cutting shoe acts as an anchor during load tests by providing a reference point for local displacement measurements in the slip joint.

To determine the required ranges of measurements for the various instrumentation, a “typical” soil profile was established (see Figure 19). This typical soil profile is based on subsurface conditions found in the Boston area and consists of the following layers (from the surface downward):

- 6 to 9 m (20 to 30 ft) of fill, organic material, silty sand, sand and gravel, and stiff clay (OCR  $\approx 8$ ).
- 9 to 12 m (30 to 40 ft) of medium Boston Blue clay (BBC) (OCR 1.5 to 7, decreasing with depth), with an  $S_u$  of about 0.4 to 0.6 tsf.
- 15 to 38 m (50 to 125 ft) of normally consolidated soft BBC (OCR  $\approx 1$  to 1.5), with an  $S_u \approx 0.22 \sigma'_{vo}$ .

This subsurface profile was used to calculate the expected conditions that the model pile will be subjected to during installation and testing. In addition, the MDMP was designed to allow for testing in stiff BBC, glacial till, and dense sand. A soil profile consisting of dense sand as shown in Figure 20 was used to represent these more difficult driving conditions.

### **3.3 Analysis of the MDMP Loading Conditions**

#### **3.3.1 Overview**

The loads (soil resistance) that the MDMP is expected to be subjected to will vary depending on the installation mode, soil type, and pile geometry. Both dynamic (driving conditions) and static (static load test conditions) analyses were conducted to evaluate the MDMP's condition under the expected loads. The MDMP load cells will be subjected to a large range of axial loads due to testing in a variety of soil profiles. Soft BBC was used to represent the lower soil resistance to be measured by the load cells. Dense sand and/or glacial till was selected to represent the upper load measurements. These two limiting cases were used in both the dynamic and static analyses outlined in the following sections. Appendices A and B detail the calculations carried out for the static and dynamic analyses, respectively.

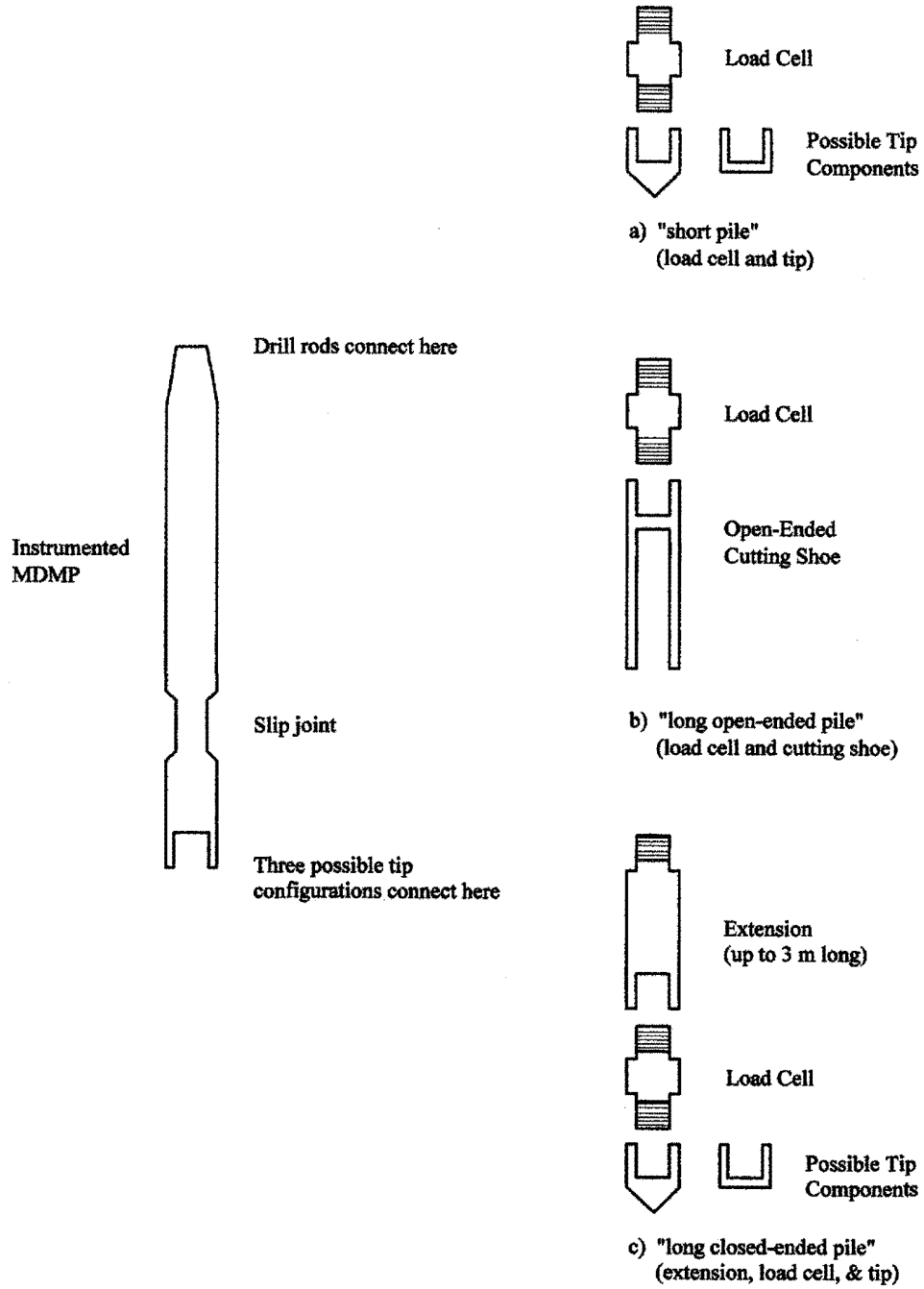


**Figure 18. Tip Configurations of the MDMP.**

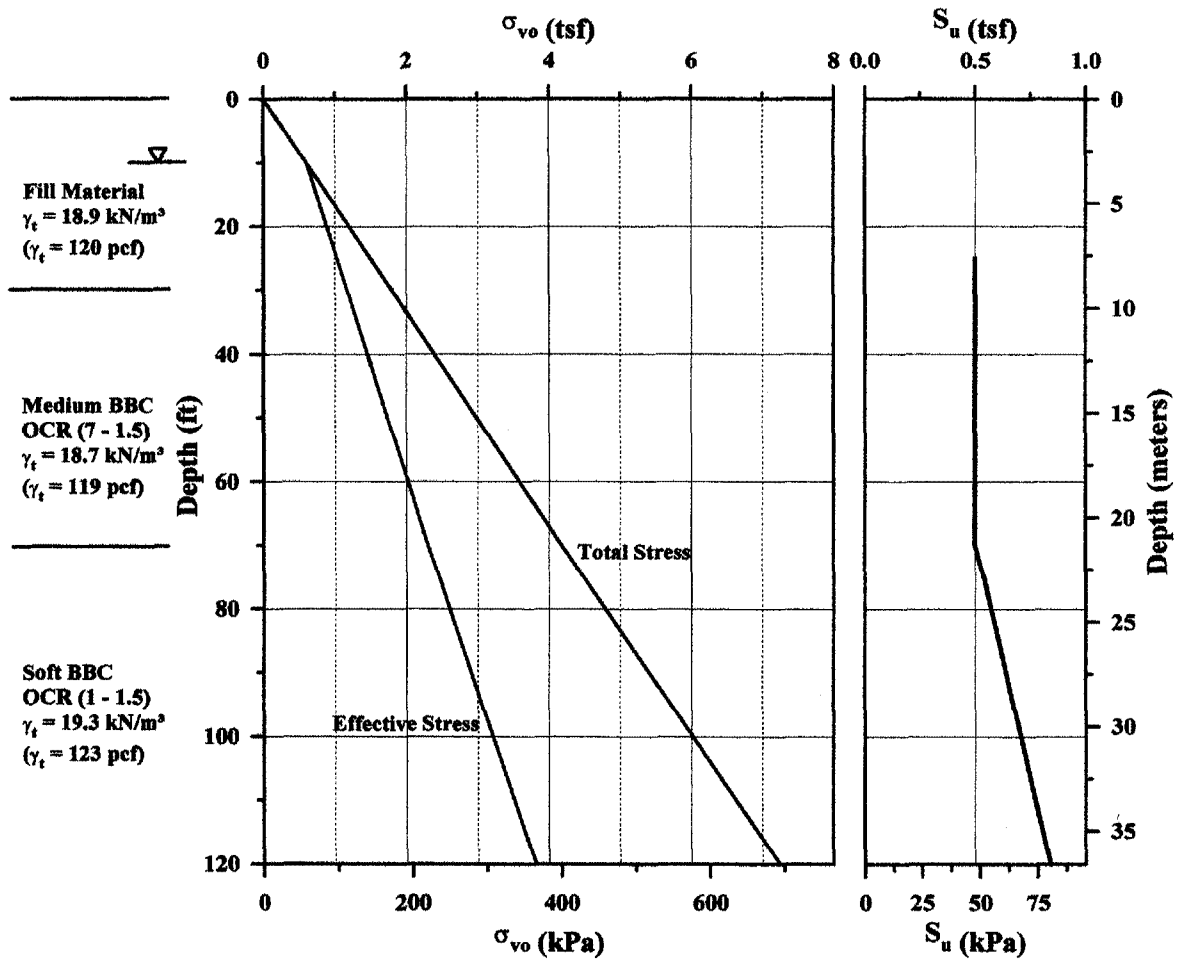


Figure 19. Typical Soil Profile for the Boston Area.

### 3.3.2 Static Capacity Analysis

Based on the review of existing model piles in Chapter 2, the MDMP was assumed to be 76.2 mm (3 in) in diameter (O.D.), with a 9.525-mm (3/8-in) wall thickness. The total length was assumed to be 4.88 m (16 ft), with a closed-ended configuration. Several empirical methods were employed to evaluate the loads under static conditions for both the soft BBC and dense sand cases. These loads were calculated at depths ranging from 12.2 to 33.5 m (40 to 110 ft).

The typical profile presented in Figure 19 was chosen to represent the soft BBC profile. The  $\alpha$  (Tomlinson, 1971) and  $\lambda$  (Vijayvergiya, 1972) methods were used for the determination of the skin friction, while traditional and CPT (de Ruiter, 1975; Toolan and Fox, 1977; and de Ruiter and Beringen, 1979) methods were used for the tip resistance. Appendix A outlines the details of the static analyses. Table 2 summarizes the calculated skin resistance, tip resistance, and total resistance for the range of depths indicated. The values presented in Table 2 are the average values from the various methods used. The total resistance acting on the 4.88-m (16-ft) MDMP section ranges from approximately 56 to 82 kN (12.6 to 18.4 kips). Therefore, the MDMP is expected to experience loads of around 45 to 90 kN (5 to 10 tons) in the soft BBC.

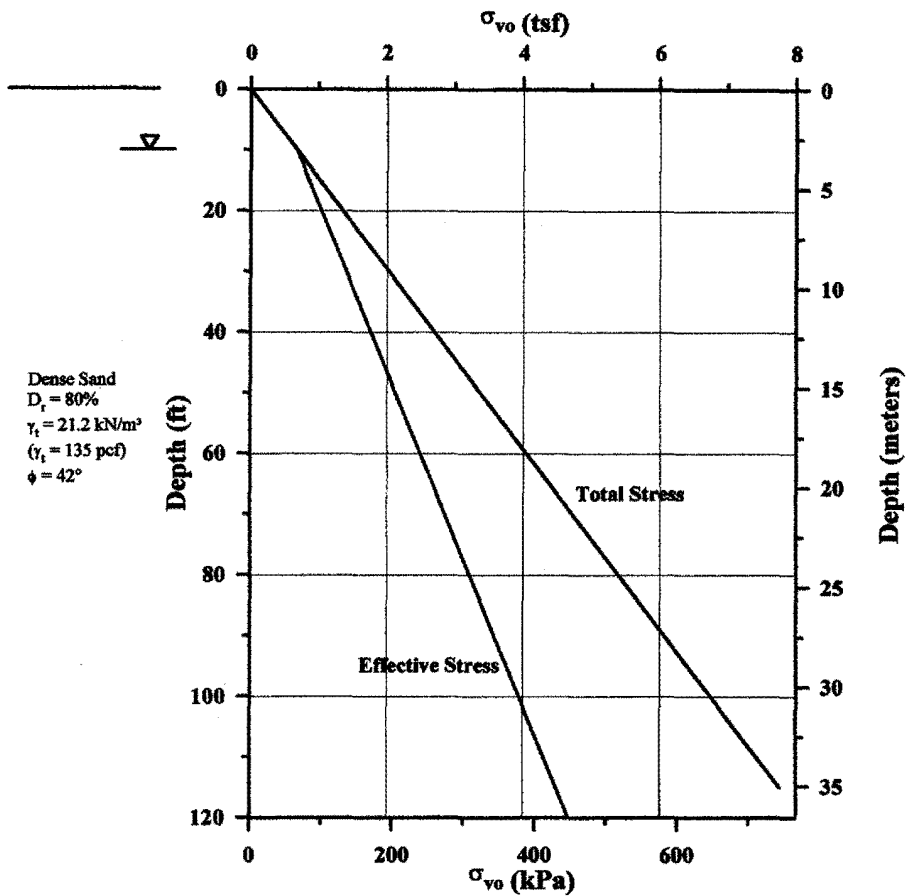


Figure 20. Hypothetical Soil Profile of Dense Sand.

Table 2. MDMP Static Load Resistance in Soft BBC (Lower Limiting Case).

Depth @ Tip (m)	Skin Resistance (kN)	Point Resistance (kN)	Total Resistance (kN)
12.2	53.7	2.6	56.3
15.2	55.2	2.6	57.7
18.3	57.7	2.6	60.3
21.3	59.2	2.6	61.8
24.4	60.5	2.9	63.4
27.4	64.8	3.2	68.0
30.5	72.1	3.6	75.6
33.5	78.3	3.9	82.2



Figure 20 presents the dense sand profile for the evaluation of the upper soil resistance limit. Meyerhof's (1951, 1976), Vesic's simplified (1975), Vesic's advanced (1977), and the American Petroleum Institute (API) (1984) methods were used for the determination of the tip resistance. The traditional, McClelland (1972), and Bhushun (1982) methods were used for the determination of skin friction. Appendix A outlines the details of the static analyses for this case. Table 3 summarizes the calculated skin resistance, tip resistance, and total resistance for the range of depths indicated. The values presented in Table 3 are the average values from the various methods used. The total resistance acting on the 4.88-m (16-ft) MDMP section ranges from approximately 186 to 465 kN (38 to 95 kips). Note that these values are conservative (for the purpose of the upper load evaluation) because they do not employ the critical depth adjustment for both resistance components — tip and skin. Based on these results, the MDMP may be expected to experience loads of around 185 to 465 kN (20 to 50 tons) in dense sands.

### 3.3.3 Dynamic Analysis

To evaluate the dynamic loads and accelerations during driving, wave equation analyses using the software program GRLWEAP (Goble, et al., 1995) were performed. The use of several hammers was investigated, including 0.62-kN, 1.33-kN, and 2.22-kN (140-lb, 300-lb, and 500-lb) drop hammers and a Delmag D-5 diesel hammer. A 0.762-m (2.5-ft) stroke was used for the drop hammers. The 2.22-kN (500-lb) drop hammer and the diesel hammer were included because they represent the most difficult possible driving conditions. It is more likely, however, that the 0.62- and 1.33-kN (140- and 300-lb) hammers will actually be used.

The drop hammer driving system used in the wave equation analyses is illustrated in Figure 21. Appendix B presents the details of the dynamic analysis related to this system. Since the MDMP will be advanced using conventional wash and drive drilling methods, N-rods with a 60.325-mm (2.375-in) O.D. and 4.763-mm (3/16-in) wall thickness were modeled to connect with the MDMP. No hammer cushion is shown, which is typically for the standard penetration test (SPT). The MDMP was assumed to be 4.57 m (15 ft) long and 76.2 mm (3 in) in diameter (O.D.), with a 9.525-mm (3/8-in) wall thickness. The tip configuration was assumed to be closed-ended.

**Table 3. MDMP Static Load Resistance in Dense Sand (Upper Limiting Case).**

Depth @ Tip (m)	Skin Resistance (kN)	Point Resistance (kN)	Total Resistance (kN)
12.2	127.2	59.6	186.8
15.2	159.2	59.6	218.8
18.3	190.4	68.5	258.9
21.3	221.5	78.3	299.8
24.4	253.5	88.1	341.6
27.4	284.7	97.9	382.5
30.5	315.8	107.6	423.4
33.5	346.9	118.3	465.3

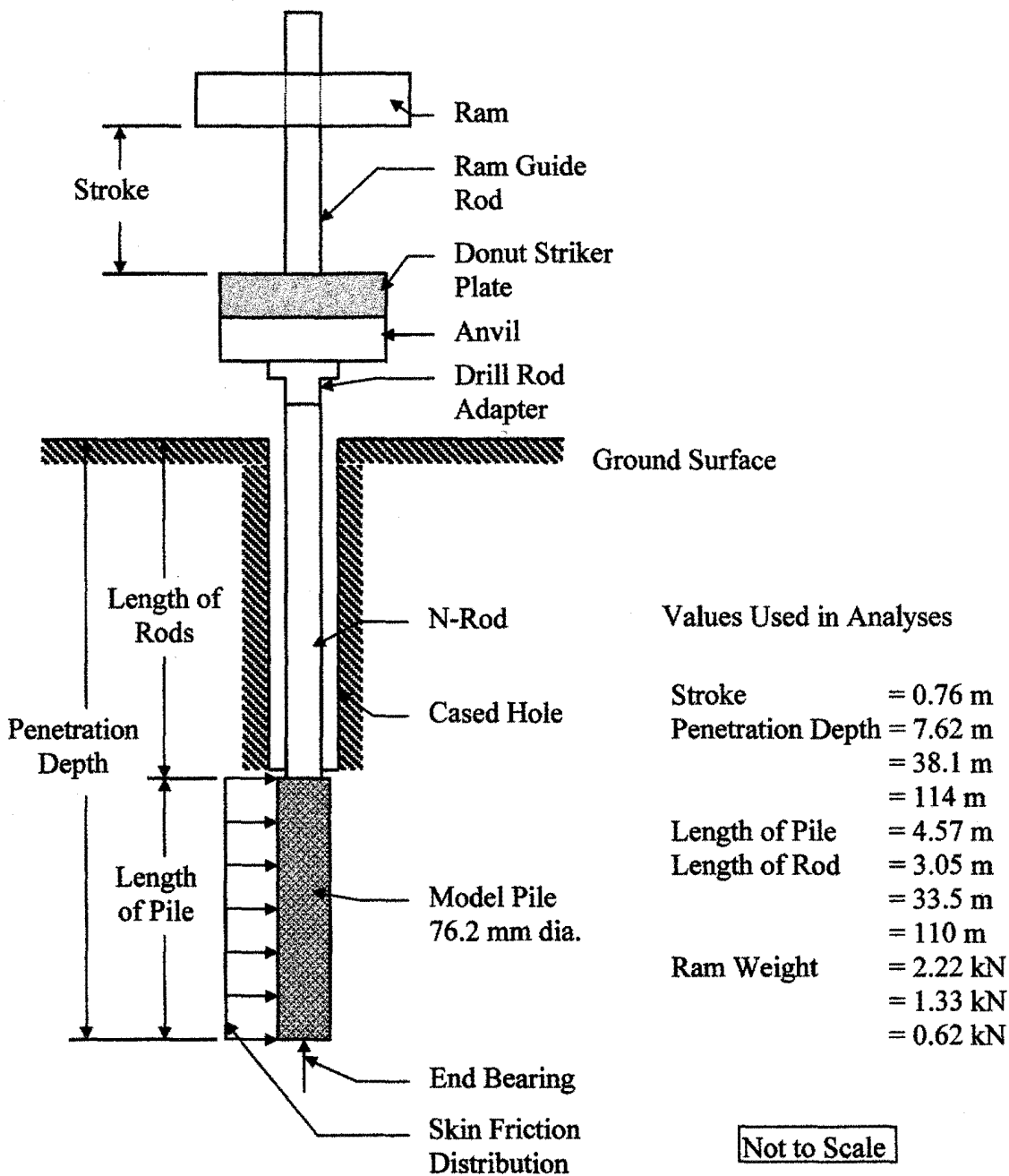


**Figure 21. Drop Hammer Configuration Modeled in the Wave Equation Analyses.**

The minimum and maximum driving stresses that the N-rods and the MDMP are expected to be subjected to were determined based on the static soil resistances presented in section 3.3.2. The lower soil resistance of 0.44 kN (0.1 kips) was used to represent easy driving conditions in soft clay, and the higher soil resistance, which varied between 44.5 and 445 kN (10 and 100 kips), was used to represent hard driving conditions in dense sand. Table 4 summarizes the maximum and minimum driving stresses in the N rods and the MDMP for each hammer type. These stresses were evaluated using three penetration lengths for each of the soil conditions. Since the MDMP

will be installed at the bottom of a cased hole, soil resistance was modeled only along the shaft and tip of the model pile. The maximum static soil resistance that could be overcome during driving varied with the hammer size and pile length. The static soil resistance increased as the hammer size increased (i.e., increase in energy) and/or the pile length decreased. Static soil resistances developed for blow counts greater than 79 blows per 10 cm (240 blows per foot) were considered unrealistic and were not included.

**Table 4. Dynamic Loads and Accelerations in the MDMP During Easy or Hard Driving.**

Hammer Type	Pile Penetration (meter)	Relative Driving Resist.	Total Static Soil Resist. (kN)	Blow Count (blows/10cm)	Max. Compr. Stress (MPa)	Max. Tensile Stress (MPa)	Max. MDMP Acceleration (g's)
					N Rods/MDMP	N Rods/MDMP	
0.623 kN Drop 0.762 m Stroke	7.6	Easy	0.4	1.0	175.1/72.4	84.1/46.9	1200
	7.6	Hard	53.4*	39*	175.8*/72.4*	53.8*/44.1*	1100
	38.1	Easy	0.4	2.0	174.4/71.7	95.8/40.0	1000
	38.1	Hard	44.5	43.0	175.1/72.4	68.3/31.0	900
	114.3	Easy	0.4	2.0	167.5/69.0	89.6/33.8	500
	114.3	Hard	44.5	43.3	168.2/69.6	57.2/23.4	500
1.334 kN Drop 0.762 m Stroke	7.6	Easy	0.4	0.7	224.1/92.4	95.8/58.6	1600
	7.6	Hard	137.9	52.8	224.8/92.4	44.8/23.4	1400
	38.1	Easy	0.4	1.3	225.5/93.1	106.9/53.1	1300
	38.1	Hard	120.1	>79	226.8/93.8	104.8/42.7	1100
	114.3	Easy	0.4	2.0	211.7/87.6	102.0/42.7	700
	114.3	Hard	120.1	>79	214.4/88.9	46.2/15.9	500
2.224 kN Drop 0.762 m Stroke	7.6	Easy	0.4	0.7	243.4/100.0	145.5/81.4	1900
	7.6	Hard	222.4	>79	318.5/135.8	30.3/17.2	1600
	38.1	Easy	0.4	1.0	244.8/100.7	91.7/57.2	1400
	38.1	Hard	124.5	40.0	246.2/101.4	125.5/51.7	1200
	114.3	Easy	0.4	1.6	232.4/95.8	112.4/46.9	800
	114.3	Hard	124.5	42.7	235.8/102.0	51.0/13.8	600
D-5 Diesel	7.6	Easy	44.5	1.0	151.0/57.2	0/0	100
	7.6	Hard	444.8	23.6	653.6/268.2	37.9/15.9	200
	38.1	Easy	44.5	1.0	153.8/47.6	0/0	100
	38.1	Hard	231.3	44.0	319.9/131.7	0/0	100

\* Interpolated from the dynamic analyses graphical results.

The allowable driving stresses (tensile and compressive) for steel are  $0.9f_y$ , which equals 223.4 MPa (32.4 ksi) based on grade 36 steel. As expected, the worst compressive stresses (653.6 MPa) and tensile stresses (145.5 MPa) were created by the D-5 diesel and 2.22-kN (500-lb) drop hammers, respectively. These stresses were calculated in the drill rods at the connection with the MDMP, where the change in cross-section (increased impedance) creates larger compressive stresses as a result of reflections in the stress wave. Based on the 2.22-kN (500-lb) hammer and, especially, the D-5 hammer simulations, the smaller cross-sectional area of the N-rods is expected to be damaged before the MDMP. If the larger hammers are used, the cross-sectional area of the drill rods may have to be increased to a larger size in order to accommodate the higher driving stresses. Alternatively, the use of cushions and a reduction of the stroke can be employed.

Discounting the D-5 diesel hammer driving simulation, the maximum compressive stress that occurred in the MDMP was 135.8 MPa (19.7 ksi) using the 2.22-kN (500-lb) drop hammer. The maximum tensile stress that occurred in the MDMP was 81.4 MPa (11.8 ksi) using the 2.22-kN (500-lb) drop hammer. The compressive stresses typically occurred at the connection of the MDMP with the drill rods (at the top of the MDMP). In general, the maximum tensile stresses were encountered toward the middle of the MDMP, although under the harder driving conditions and longer pile lengths, they were observed at the top of the MDMP. It is highly unlikely that the D-5 diesel hammer will be used (especially together with N-rods) and, therefore, excluding the D-5 simulation results, all driving stresses in the MDMP remain within the allowable stress level.

The accelerations presented in Table 4 were determined using 152.4-mm (6-in) segment lengths, except for the 114.3-m (375-ft) pile length, which was modeled using 304.8-mm (12-in) segment lengths. Based on Rausche (1995), smaller increments are required to properly analyze SPT driving systems. By increasing the number of pile segments, the stress wave can be more clearly defined as it propagates down the pile. This is especially important for uncushioned steel on steel impacts, where the impact stress signal is a high peak of short duration.

The maximum range of accelerations expected in the MDMP vary between 1500 g's and 2000 g's for shorter pile lengths (7.6 m) driven with the 1.334- and 2.224-kN (300- and 500-lb) drop hammers. The lower accelerations may be around 500 g's for the longer pile lengths (114.3 m) driven with the 0.623-kN (140-lb) drop hammer. These accelerations are approximately two to five times higher than accelerations observed during the driving of full-scale piles. Lower accelerations (100 g's to 200 g's) are obtained for the diesel hammer analysis due to the different mode in which the hammer impacts the pile.

### ***3.3.4 Summary of Load Requirements***

Table 5 summarizes the maximum loads in the MDMP obtained from the static and dynamic analyses. The indicated loads are based on a cross-sectional area of 19.94 cm<sup>2</sup> (3.09 in<sup>2</sup>). Both analyses are based on conservative assumptions to ensure that the upper limits have been identified. The different values of static capacity, 89 kN to 463 kN (20 kips to 100 kips), suggest that two separate load cell systems may be required in the MDMP so that accurate measurements can be obtained under the two soil conditions. The dynamic capacity was determined from the product of the stress and the area of the MDMP. Based on the 1.334-kN (300-lb) drop hammer in the soft to medium clay, the dynamic capacity in tension and compression are 117 kN and 186 kN (24 kips and 51 kips), respectively. The dynamic load cell requirements for the soft to medium clays, therefore, can be rounded to those indicated under "Design Requirements for MDMP" in Table 5. The dynamic capacity values for soft to medium clay (162 kN tension and 201 kN compression) are within the load cell overload range of 2.5 times the static capacity. The dynamic design requirements for the dense sand (225 kN tension and 550 kN compression) are well within the 250% overload range, even with the use of the larger hammers.

**Table 5. Summary of Load Cell Capacity Requirements.**

Soil Condition	Static Capacity (kN)	Dynamic Capacity		Design Requirements for MDMP	
		Maximum Tensile (kN)	Maximum Compressive (kN)	Static (kN)	Dynamic Tensile/Compressive (kN)
Soft to Medium Clay	89	162	201	89	225 / 225
Dense Sand/Hard Clay	463	103	535	445	225 / 550

### 3.4 Specifications for Instrumentation and Mechanical Parts

#### 3.4.1 General

The MDMP was based on a modification of the 7.62-cm (3-in) Model Pile originally developed by Bogess et al., 1983. The specifications for the load cells, accelerometers, pore pressure transducer, total pressure cell, connector housing, slip joint, tip segment, and loading frame are described below. The description of these components and other MDMP components is provided in section 3.5.

#### 3.4.2 Accelerometers

Accelerometers are mounted in the model pile to provide accurate records of pile acceleration that are independent of drill rods and hammer. The accelerometers must be capable of measuring accelerations up to 2000 g's. The accelerometers are installed at the load cell locations in the interior of the model pile and are securely attached to the pile. The accelerometers will be monitored using the PDA (Pile-Driving Analyzer). The PDA is capable of monitoring up to four accelerometers (two piezoelectric and two piezoresistive). As such, two of the MDMP accelerometers (top and bottom load cells) will be piezoelectric and one will be piezoresistive (middle load cell), with the fourth accelerometer being mounted at the top of the drill rods.

#### 3.4.3 Load Cells

##### (a) Top and Middle Load Cells

Two load cells are required to measure the friction along a section of the pile. Since a variety of soil profiles will be tested, two sets of load cells are required to measure the skin friction. Refer to section 3.3.4 for the required load ranges in the soft to medium BBC clay and dense sand. There is 2000 cm<sup>2</sup> (310 in<sup>2</sup>) of surface area between the two load cells to measure skin friction and load transfer.

##### (b) Tip Load Cell

The load cell at the tip was included to measure end-bearing capacity during compression tests and evaluate the friction along the lower pile segment. The tip load cell may be used to correlate MDMP results to the more conventional CPT. The load at the tip also provides a performance check of the slip joint, ensuring that no load is being transferred through the slip joint during

tension load tests. During compression load testing, the tip load cell must be able to measure the tip resistance when the slip joint is fully compressed. During installation, the tip load cell will continuously measure the tip resistance.

#### ***3.4.4 Pore Pressure Transducer***

The pore pressure transducer must be able to measure pore water pressure during initial driving, restrike, and static load tests. The pore pressure transducer must be able to measure the excess pore pressure dissipation continuously for several days after driving. When driving in dense overconsolidated clays or silts, the pore pressure transducer must also be able to measure negative excess pore pressures. Most importantly, the pressure transducer must physically be able to withstand stresses during driving. The increase in pore pressure due to driving can be expected to be 2.29 times the vertical effective stress (Paikowsky et al., 1995). Based on the typical soil profile in the Boston area (maximum test depth at 33.5 m (110 ft)), the predicted pore pressure immediately after driving is 1070 kPa (155 psi).

Two porous filters must be located 180° apart and mounted flush to the pile wall, maintaining the radius of the MDMP so that no local discontinuities are present. The porous filters must be permeable to enable quick response to pressure changes, but must also be of sufficiently low permeability to maintain saturation while the model pile is driven through unsaturated material. In addition, the porous filters must be durable for use in hard driving conditions, easily replaceable, and compatible with other materials utilized in the model pile to prevent corrosive effects. Lastly, a method to saturate and de-air the porous filters is required.

#### ***3.4.5 Total Pressure Cell***

The total pressure cell must be able to measure total pressure during the entire duration of the MDMP test sequence. The total pressure cell, like the pore pressure transducer, must be able to physically withstand the stresses during driving. The loading caps of the total pressure cell must also maintain the radius of the MDMP so that no local discontinuities are present. Considering the typical soil profile in the Boston area (maximum test depth at 33.5 m (110 ft)), the predicted total pressure is 1214 kPa (176 psi) (assuming  $\sigma_h$  after driving is two times  $\sigma_{vo}$ ).

#### ***3.4.6 Connector Housing***

The connector housing gathers all the wires from up to 10 MDMP sensors and connects them to a main cable that extends through the drill rods to the surface. The connector housing must also be watertight to prevent water from entering the MDMP. The cable needs to be at least 45 m (150 ft) long.

#### ***3.4.7 Slip Joint***

The slip joint is used to measure local displacements. The slip joint needs to be extended immediately after driving to allow measurements of displacement during subsequent compression load tests. The slip joint needs to be able to measure a total displacement of up to 5 cm (2 in),

allowing for four load tests to be performed with 1.25 cm (0.5 in) of displacement for each test. The displacement of 1.25 cm (0.5 in) is assumed to be enough to accommodate the soil quake (approximately 0.1 in along the shaft) and provide adequate information of the post-peak and residual soil resistance. Wires for the bottom load cell below the slip joint must be able to pass through the slip joint without affecting the slip joint or bottom load cell.

### 3.4.8 Loading Frame

Following installation, several tension and compression static load tests need to be performed over time. The static load frame needs to be attached to the drill rods, which are connected to the MDMP. The frame must be easy to assemble and position over the drill rod string and must be capable of conducting both extension and compression load tests of up to 445 kN (50 tons). The load application system must be capable of performing the tests by displacement or load control techniques. The loading system also requires sufficient throw to be connected to the drill rods and to conduct several 1.25-cm (0.5-in) load tests in succession.

### 3.4.9 Summary of the Instrumentation Range Requirements

Table 6 presents a summary of the required instrumentation as outlined in section 3.4.

**Table 6. Summary of the MDMP Required Instrumentation Ranges.**

Component	Location	Type	Installation Condition	Range
Accelerometers	Top of Rods	Piezoresistive	N/A	0-2000 g's
	Top Load Cell	Piezoelectric	N/A	0-2000 g's
	Middle Load Cell	Piezoresistive	N/A	0-2000 g's
	Bottom Load Cell	Piezoelectric	N/A	0-2000 g's
Load Cells	Top, Middle, and Bottom Load Cells	Electric Strain Gauges	Soft/Medium Soil	89 kN
			Hard/Stiff Soil	445 kN
			Dynamic	2.5 times static cap.
Pore Pressure Transducer	Transducer Housing	Electric Strain Gauges	All	1070 kPa
Total Pressure Cell	Transducer Housing	Electric Strain Gauges	All	1214 kPa
Slip Joint	Slip Joint	DC-LVDT	All	5 cm
Loading Frame	N/A	N/A	All	445 kN

## 3.5 Design

### 3.5.1 General

The MDMP is composed of several components that are screwed together (Figure 17). All of the major components are made of stainless steel to inhibit oxidation and other possible chemical reactions. Rubber O-rings are used to seal all components in order to create a watertight

environment in the interior of the pile. The outside diameter of all components remains constant (76.2 mm) throughout the entire MDMP length, except at the lower slip joint, where it is 57.15 mm (2.25 in). The overall length of the closed-ended MDMP with tip extension is 2.87 m (9.42 ft). The major components of the MDMP (referring to Figure 17) include: N-rod adapter, connector housing, upper extension, load cells, couplings, transducer housing, slip joint, lower extension, and interchangeable tip segment. Table 7 lists the different components, their description, length (when applicable to the total length), material, and related detail. The following sections provide details of the different components presented in Figure 17 and listed in Table 7. Appendix C presents the shop drawings and details of the individual components.

### ***3.5.2 N-Rod Adapter***

The N-Rod adapter is 21.59 cm (8.5 in) long and attaches the MDMP (76.2 mm diameter) to N drill rods (60.3 mm diameter) that are used to advance the model pile to the desired test depth. Type 316 stainless steel is used to machine the component. The end that is connected to the drill rod is a female modified Box thread (three threads per inch). The opposite end is a female 2.50-5 Stud ACME thread that is attached to the connector housing.

### ***3.5.3 Connector Housing and Mount***

The connector housing is 10.24 cm (4.03 in) long and is machined from Type 316 stainless steel. The end that connects to the N-rod adapter is a male 2.50-5 Stud ACME thread. The opposite end is a female 2.500-12-2 thread. Six slots that are evenly spaced about the circumference allow water to enter and/or drain from the drill rods.

The connector mount is made of 17-4PH @H1050 stainless steel. The connector mount has two functions: (1) providing a watertight seal to protect the instrumentation within the MDMP from water intrusion and (2) providing a waterproof cable connection enabling the instrumentation wiring within the MDMP to be connected to the data acquisition cable. A set screw is used to attach the connector mount to the upper extension to ensure that the mount does not rotate and the sensor wires do not shear.

### ***3.5.4 Upper Extension***

The upper extension is 31.27 cm (12.31 in) long and ensures that the instrumentation is in a zone of radial dissipation and is an adequate distance below the drill rods so that the sensors are not affected by the change in cross-sectional area from the rods to the pile. The lead wires from the various MDMP sensors are gathered together and combined in the interior of the upper extension. The component has a male and female 2.500-12-2 thread on either end and is machined from Type 316 stainless steel.



**Table 7. MDMP Component List.**

Component	Part	Length (cm)	Material	See Figure
N-Rod Adapter	N-Rod Adapter	21.59	Type 316 Stainless Steel	Appendix C
Connector Housing	Connector Housing	10.24	Type 316 Stainless Steel	Appendix C
	Connector Mount	N/A	Type 17-4PH @H1050 Stainless Steel	Appendix C
Upper Extension	Upper Extension	31.27	Type 316 Stainless Steel	Appendix C
Load Cell	Load Cell	14.60 assembled	Type 17-4PH @H1050 Stainless Steel	Appendix C
	Load Cell Cover	N/A	Type 316 Stainless Steel	Appendix C
	Accelerometer Mount	N/A	Type 6160 Aluminum	Appendix C
Coupling	Coupling	25.74	Type 316 Stainless Steel	Appendix C
Transducer Housing	Transducer Housing	5.99	Type 17-4PH @H1050 Stainless Steel	Appendix C
	Retainer	N/A	Brass	Appendix C
Slip Joint	Upper Slip Joint	20.40	Type 17-4PH @H1050 Stainless Steel	Appendix C
	Lower Slip Joint	10.21	Type 17-4PH @H1050 Stainless Steel	Appendix C
	LVDT Mount	N/A	Type 17-4PH @H1050 Stainless Steel	Appendix C
	LVDT Pad	N/A	Type 17-4PH @H1050 Stainless Steel	Appendix C
Lower Extension	Lower Extension Adapter, Male	82.04 assembled	Cold-Rolled Type 1018 Round	Appendix C
	Lower Extension Adapter, Female	N/A	Cold-Rolled Type 1018 Round	Appendix C
	Lower Extension Tubing	N/A	Mechanical Tubing	Appendix C
Open-Ended Cutting Shoe	varies	varies	varies	Appendix C
60° Tip	60° Tip	10.08	Type 316 Stainless Steel	Appendix C

N/A — not applicable

### 3.5.5 Load Cells

Three load cells are installed in the MDMP. Figure 22 is a photograph of a load cell with a sleeve. Each load cell utilizes four foil strain gauges arranged in a full Wheatstone bridge formation. The total nominal bridge resistance is 350 ohms. This formation of strain gauges cancels the effects of bending and measures only axial loads. The strain gauges are attached to

the center section of the load cell, which has a uniform cross-section of either 4.75 cm<sup>2</sup> (0.7363 in<sup>2</sup>) or 13.06 cm<sup>2</sup> (2.0249 in<sup>2</sup>) for the 89- and 445-kN (10- and 50-ton) load cells, respectively. The dynamic to static overload ratio (dynamic loading/static loading) for these load cells is 2.5, which is sufficient to accommodate the maximum anticipated driving stresses. The load cell is made from Type 17-4PH @H1050 stainless steel. There are two O-rings that maintain a watertight seal between the adjacent modular parts. Four holes allow air to flow to both sides of the uniform cross-section, thereby avoiding temperature and pressure variations that might affect the sensitivity of the load cells. Both ends are male ends with 2.500-12-2 threads. At one end, the inside circumference is threaded with a 1.820-20-2 thread to attach the LVDT mount.



**Figure 22. Photograph of the MDMP Load Cell With Sleeve.**

Each load cell is protected by a load cell cover. The load cell cover slides over the load cell and provides a watertight seal using three additional O-rings. When screwing the adjacent components to the load cell, they exert compression on the flange of the load cell cover, holding it in place. The load cell cover is 13.03 cm (5.130 in) long, with an outside diameter of 7.62 cm (3 in). There is a small gap at one end of the load cell cover to allow the load cell to strain. The load cell cover is made from Type 316 stainless steel. The assembled load cell with cover has a combined length of 14.60 cm (5.75 in).

Each load cell is fitted with an accelerometer, which is mounted in the interior of the load cell. The maximum accelerations (in terms of gravity "g") that the accelerometers will be subjected to range between approximately 500 g's to 2,000 g's. To maintain compatibility with the Pile-Driving Analyzer (to be used for monitoring the accelerometers), two types of accelerometers

(piezoelectric and piezoresistive) are employed. A piezoresistive accelerometer was selected for the middle load cell due to space constraints dictated by the DC-LVDT. The upper and lower MDMP load cell accelerometers are of the piezoelectric type.

### 3.5.6 Couplings

There are two couplings in the MDMP. These couplings are used to center the transducer housing between the two load cells and provide a known surface area for measuring the skin resistance along the friction sleeve. Both ends of each coupling are female 2.500-12-2 threads. Type 316 stainless steel is used to form the couplings, which are 25.74 cm (10.134 in) long and have a cross-sectional area of 22.83 cm<sup>2</sup> (3.54 in<sup>2</sup>).

### 3.5.7 Transducer Housing

The total stress cell and pore pressure transducer are located in the transducer housing. Figure 23 is a photograph of the transducer housing with pore pressure transducer and total radial stress cell. The transducer housing has an outside diameter of 7.62 cm (3 in) and is machined from Type 17-4PH @H1050 stainless steel. Both ends are male 2.500-12-2 threads. Two O-rings at either end form a watertight seal with adjacent components. Two holes 2.54 cm (1 in) in diameter and 0.953 cm (0.375 in) deep are aligned 180° apart. The holes are fitted with porous aluminum oxide stones. Behind each stone is a duct that allows the free flow of pore water from the porous stones to the pore pressure transducer located in the center of the transducer housing. A 2.54-cm (1-in) through-hole, located 90° from the porous stones, houses the total stress transducer.

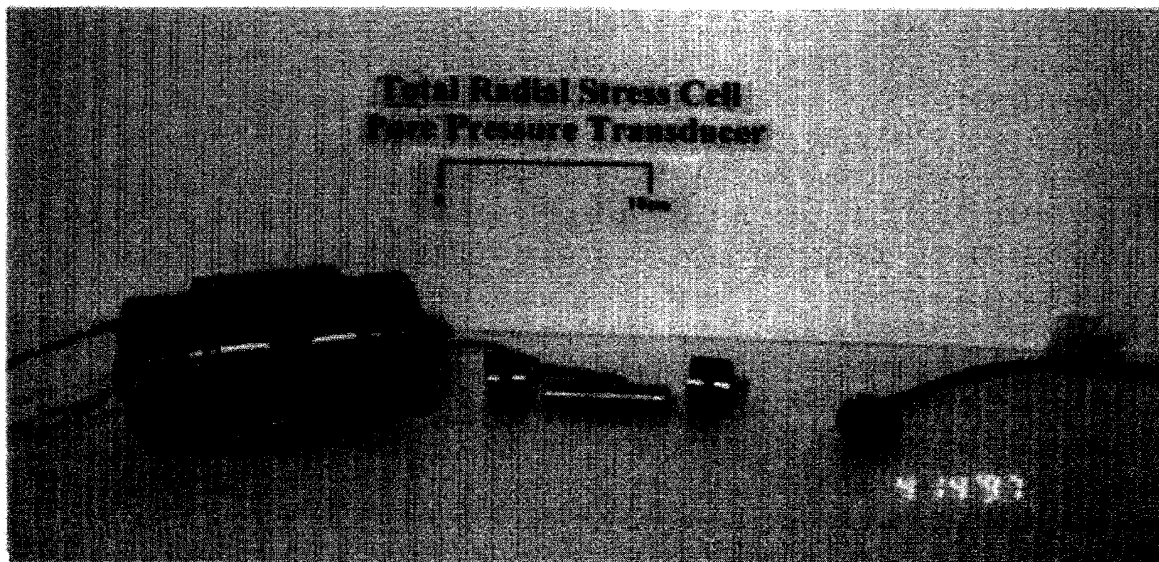


**Figure 23. Photograph of the Transducer Housing With the Pore Pressure Transducer and the Total Radial Stress Cell.**

The porous stones for the pore pressure transducer are pressed into place. The outer surface is shaped to the same curvature as the model pile so that no discontinuities will exist around the stone. The pore water flows through the pores in the stone to the transducer so that only fluid pressures are recorded. Since below-freezing temperatures were anticipated during field testing, a mixture of glycerin and water was examined for use in the transducer housing water ducts and stones. Following laboratory tests, a solution consisting of 30% glycerin and 70% water was used to saturate the stones. This solution would not freeze up to a temperature of approximately  $-7^{\circ}\text{C}$  ( $20^{\circ}\text{F}$ ) and did not appear to separate when the temperature increased back to room temperature. An added benefit to the use of a glycerin solution is that due to the increased viscosity of the solution, the porous stones will remain saturated even if exposed to air for a limited time. A Kistler Model 4140A20 pressure transducer is used to measure the pore fluid pressure. The nominal transducer output is 29.99 mV/bar using an excitation current of 4 mA and its range is 0 to 2000 kPa (0 to 290 psi). A Kistler Model 4670V signal conditioner was installed to supply the current excitation and amplify the output. This signal conditioner was incorporated into the connection box (to be described in Chapter 4).

The total stress transducer principle of measurement is similar to the load cells. Four foil strain gauges are mounted to a "dog bone"-shaped piece of aluminum (Type 2024-T4), the ends of which have a circular cross-section. The foil strain gauges are arranged in a 350-ohm full Wheatstone bridge formation to measure only axial load. Two end plugs fit over the circular ends of the aluminum "dog bone" and are fitted with O-rings to ensure watertightness. The outer surfaces of the end plugs have the same curvature as the model pile so that they are flush with the pile wall. The nominal transducer output is 0.35 mV/bar using an excitation voltage of 10 V.

### ***3.5.8 Slip Joint***

The slip joint consists of upper and lower components and is 30.61 cm (12.05 in) long when fully compressed. Figure 24 is a photograph of the components of the slip joint. The upper slip joint (20.40 cm long) is made of Type 17-4PH @1050 stainless steel with a female 2.500-12-2 threaded end. Four holes  $90^{\circ}$  apart with counterbores are used to insert guides that slide in the slots on the lower slip joint. The lower slip joint (10.21 cm long) is also made of Type 17-4PH @1050 stainless steel. The lower slip joint has four slots that the guides from the upper slip joint slide in. The lower end of the lower slip joint is threaded with 2.500-12-2 female thread as well.

The DC-LVDT that measures the local displacement of the slip joint is held in place with the LVDT mount. The LVDT mount screws into the middle load cell and a set screw securely holds the LVDT in place, providing a reference point for the top portion of the model pile. The LVDT pad is attached to the lower slip joint utilizing two #8-32 screws. The LVDT pad provides the reference point for the lower slip joint.

The DC-LVDT is manufactured by Macro Sensors and is model no. GHSD 7500-1000. The transducer measures up to 4.9 cm (2 in) of movement. The excitation voltage required is  $\pm 15$  V DC and the output range is  $\pm 10$  V DC. Specifications indicate the transducer has a shock survival of 1000 g's over 11 ms.

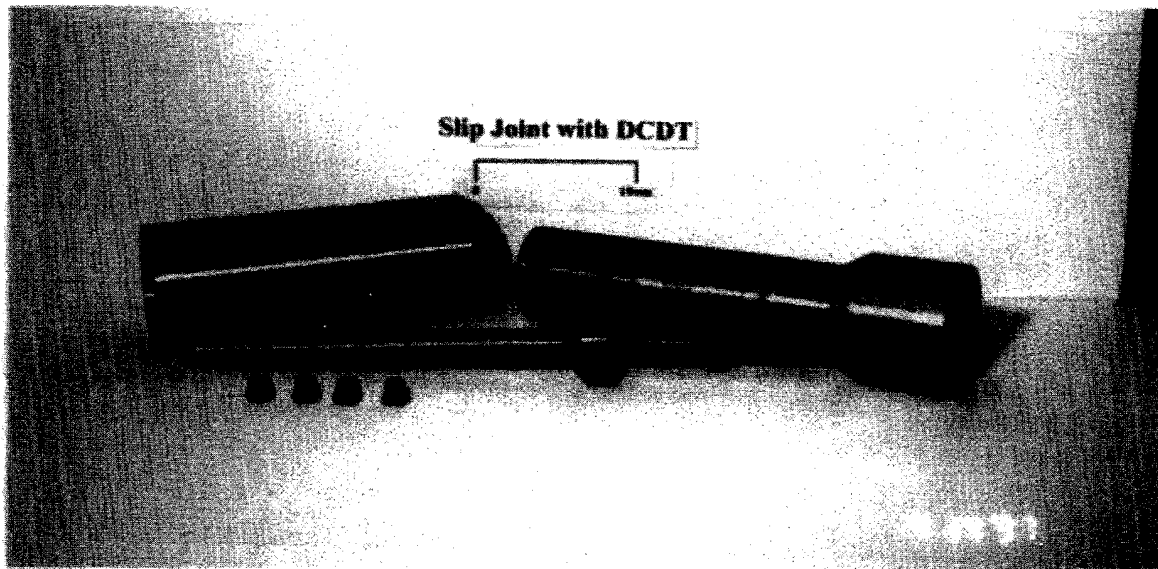


**Figure 24. Photograph of the Slip Joint With DCDT.**

### ***3.5.9 Lower Extension***

The lower extension connects the lower slip joint to the lower load cell for “long” piles. The lower slip joint screws directly into the bottom load cell for “shorter” piles. Male and female adapters are used to attach the lower extension to the lower slip joint and lower load cell. The length of the lower extension and adapters is 82.04 cm (32.3 in). This length is based on the following two criteria: (1) the additional length required to reduce end effects near the slip joint and (2) the provision of a larger frictional area for the “anchored” portion of the pile below the slip joint. The lower extension consists of male and female 2.500-12-2 threaded end pieces that are welded to a 6.35-mm- ( $\frac{1}{4}$ -in) thick mechanical tubing.

### ***3.5.10 Tip Segment***

An interchangeable tip segment 10.2 cm (4.0 in) long for a conical tip screws into the lower load cell. Various tip attachments can be fabricated so that different driving modes (such as open-ended and closed-ended penetration) could be investigated. Figure 18 presents three different possible extensions for the MDMP based on the following tip segment configurations:

- “Short” closed-ended pile, where the tip segment (angled or flat tip) screws directly into the lower load cell.
- Open-ended pile, where a threaded open-tip segment cutting shoe screws directly into the slip joint.

- “Long” closed-ended pile, where an 82.0-cm (32.3-in) extension connects the lower slip joint to the lower load cell. The tip segment (angled or flat tip) screws directly into the lower load cell.

### **3.6 Calibration**

#### **3.6.1 Overview**

The components of the MDMP were tested and calibrated before and after the testing program. To ensure that system errors did not affect the calibration process, the MDMP was completely assembled utilizing the required cables, connection box (section 4.3), and data acquisition system (section 4.2). The three load cells, pore pressure cell, total pressure cell, and slip joint DC-LVDT were all calibrated in the Geotechnical Laboratory at UMass-Lowell. The calibration process included testing the load cells, the pore pressure transducer, total pressure cell, and slip joint DC-LVDT under static loading conditions. The accelerometers were tested to ensure that they were wired correctly and the drill rods were examined to ensure that the discontinuities at the joints would not inhibit the measurement of dynamic response during driving. A 222.4-kN (25-ton) load cell and two DC-LVDTs were tested in the laboratory to be used in the static testing program. Additional instrumentation, including a strain gauge and accelerometer attached to the drill rod, was also checked in the laboratory.

#### **3.6.2 Load Cell Calibration**

The three MDMP load cells that were used in the Newbury, MA test program were calibrated five times. Refer to Appendix D for calibration plots describing the relationship between output voltage and load. The initial factory calibrations were performed by Technology & Calibration, Inc. (TechCal) before the assembly of the MDMP. Each load cell was calibrated under compression loading in 11.12-kN (2,500-lb) increments to a maximum compressive load of 111.2 kN (25,000 lb). During the calibration process by TechCal, the outer sleeve was not in position over the load cell. At the conclusion of the Newbury testing program, the load cell calibrations were rechecked at the UMass-Lowell Geotechnical Laboratory with the pile disassembled and the outer sleeves removed.

Before and after the Newbury testing program, the load cells were also calibrated at the UMass-Lowell Geotechnical Laboratory with the model pile fully assembled (the bottom load cell was not recalibrated after the testing program). The procedure for calibrating the load cells when the model pile was assembled consisted of placing the MDMP in a reaction frame and applying a compressive load with a hydraulic jack. Figures 25a and b are a schematic and a photograph of the system used for the load cell calibration. The reaction frame was constructed of two vertical W sections, 152.4 mm in depth (W6x15), and one horizontally oriented W section with the web aligned vertically, 152.4 mm in depth (W6x15), with steel members with reinforced welded joints. Appendix E provides details about the frame analysis and construction. A 222.4-kN (50,000-lb) Lebow load cell was placed in line with the model pile to record the applied compressive load. A ball connection was placed between the jack and the bottom of the model pile to eliminate movements during calibration (see Figure 25). The jacking system was comprised of an hydraulic

of an hydraulic ram and a hand-operated pump. A compressive load of 53.4 to 57.8 kN (12,000 to 13,000 lb) was applied gradually at a near constant rate and was then allowed to return instantaneously to zero. This loading procedure was repeated four times and the data were used to develop the calibration factors.

The calibrations for each of the three MDMP load cells at the different times are listed in Tables 8 through 10. The obtained calibration factors suggest that the calibration results vary depending on the timing of the calibration process with respect to testing. This can be explained in a number of ways. The factory calibration was done before the load cells were exercised and the outer sleeve was not in place. In a perfect design, the O-rings used to develop a watertight seal around the load cell instrumentation would not transfer any load. Practically, however, the O-rings are compressed to form the watertight seal and some load transfer does occur. Another reason for different factory calibrations and assembled calibrations is the voltage drop that occurs through the 60-m (200-ft) length of cable and connections.

The recalibration of the load cells at the end of the testing program was not completely linear, as the curve appeared to be bi-linear with a change in slope at 20.91 kN (4,700 lb) (Appendix D). This bi-linear behavior may be due to dried soil in the gap that allows for the load cell and O-ring expansion. The difference between the two calibrations with the outer sleeve removed (Appendix D, Factory Calibration and Recalibration) may be due to a physical change in the load cell, possibly caused by the dynamic forces or residual forces that the pile was subjected to during installation and removal.

**Table 8. Top Load Cell Calibration Results.**

Test	Calibration $\frac{V_{out}}{V_{in}}$ lb	Coefficient of Determination	Remarks
Factory Calibration	$5.0720 \times 10^{-8}$	0.99752	Without outer sleeve
Calibration Before Test	$5.1127 \times 10^{-8}$	0.99969	Model Pile Assembled
Recalibration After Test Trial #1	$6.1317 \times 10^{-8}$	0.98933	Model Pile Assembled 0-53.4 kN
Recalibration After Test Trial #1	$4.9085 \times 10^{-8}$	0.9941	Model Pile Assembled 0-20.9 kN
Recalibration After Test Trial #2	$6.4326 \times 10^{-8}$	0.98800	Model Pile Assembled 0-53.4 kN
Recalibration After Test Trial #2	$5.4595 \times 10^{-8}$	0.97649	Model Pile Assembled 0-20.9 kN
Recalibration After Test	$5.332 \times 10^{-8}$	0.9988	Without outer sleeve



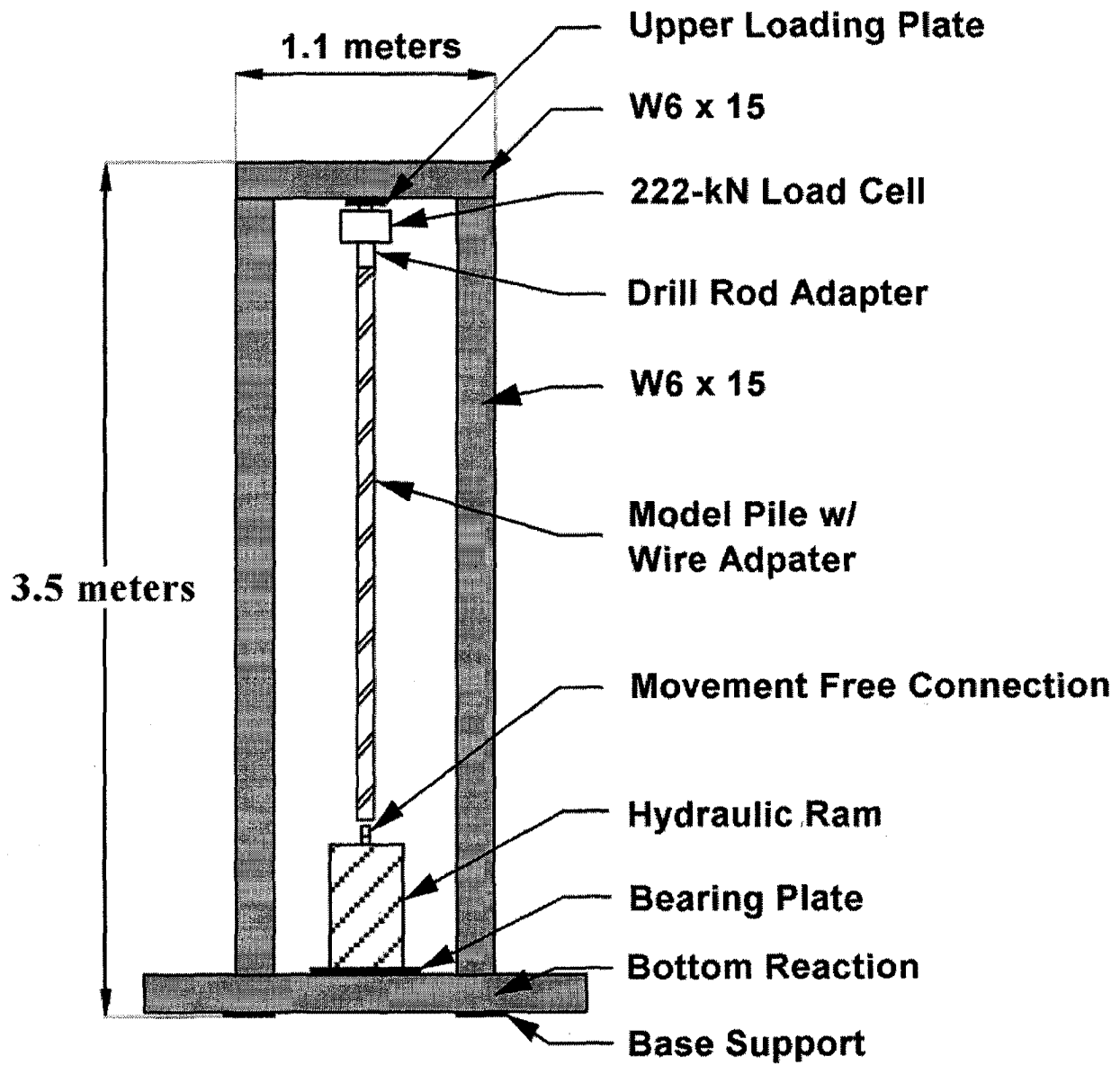
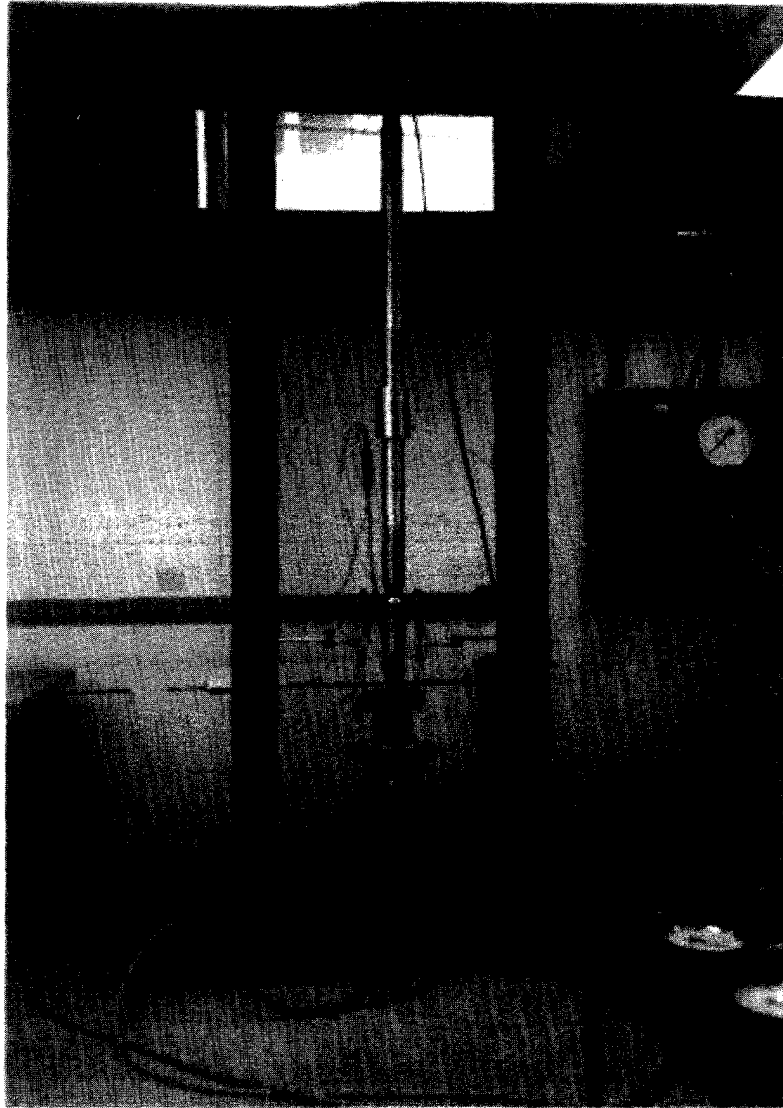


Figure 25a. Schematic of the Calibration Frame for the MDMP.





**Figure 25b. Photograph of the Calibration Frame for the MDMP.**

**Table 9. Middle Load Cell Calibration Results.**

Test	Calibration $\frac{V_{out}}{V_{in}}$ lb	Coefficient of Determination	Remarks
Factory Calibration	$6.3654 \times 10^{-8}$	0.99999	Without outer sleeve
Calibration Before Test	$6.0946 \times 10^{-8}$	0.99998	Model Pile Assembled
Recalibration After Test Trial #1	$7.9535 \times 10^{-8}$	0.98848	Model Pile Assembled 0-53.4 kN
Recalibration After Test Trial #1	$6.2198 \times 10^{-8}$	0.99563	Model Pile Assembled 0-20.9 kN
Recalibration After Test Trial #2	$7.5772 \times 10^{-8}$	0.98476	Model Pile Assembled 0-53.4 kN
Recalibration After Test Trial #2	$5.9933 \times 10^{-8}$	0.98349	Model Pile Assembled 0-20.9 kN
Recalibration After Test	$6.7737 \times 10^{-8}$	0.99998	Without outer sleeve

**Table 10. Bottom Load Cell Calibration Results.**

Test	Calibration $\frac{V_{out}}{V_{in}}$ lb	Coefficient of Determination	Remarks
Factory Calibration	$6.2911 \times 10^{-8}$	0.99996	Without outer sleeve
Calibration Before Test	$5.9639 \times 10^{-8}$	0.99998	Model Pile Assembled

Since the three MDMP load cells will be monitored during driving using the Pile-Driving Analyzer (PDA), a calibration factor for the PDA was determined. The PDA calibration factor is a function of the static calibration. A multiplication factor of 0.288 is used to transform the static calibration for use as a PDA calibration factor. This multiplication factor, also called a Pile Dynamics Inc. (PDI) factor, is based on excitation voltage and the internal circuitry of the PDA (based on correspondence with Pile Dynamics, Inc.). The modulus of elasticity used for stainless steel is  $2.05 \times 10^5$  MPa ( $29.7 \times 10^6$  psi) as provided by the manufacturer of the load cells. Based on the above, the PDA calibration factor is related to the static calibration factor by the following relationship and is summarized in Table 11:

$$\text{General Factor} = \frac{\epsilon V_{in}}{m V_{out}} = \frac{\text{lb} \cdot V_{in}}{m V_{out}} \cdot \frac{1}{AE}$$

$$\text{PDA Calibration Factor} = \frac{\mu \epsilon}{V} = \frac{\mu \epsilon V_{in}}{m V_{out}} \cdot 0.288$$

**Table 11. Dynamic Calibration Results of the MDMP Load Cells.**

Load Cell	Serial Number	Channel on PDA	Static Calibration $\frac{V_{out}}{lb \cdot V_{in}}$	General Factor $\frac{\mu\mathcal{E}V_{in}}{mV_{out}}$	PDA Calibration Factor $\frac{\mu\mathcal{E}}{V}$
Top	D10T-02	F1	$5.1127 \times 10^{-8}$	894.4	257.59
Middle	D10T-01	F3	$6.0946 \times 10^{-8}$	750.3	216.08
Bottom	D10T-03	F2	$5.9639 \times 10^{-8}$	766.8	220.83

### 3.6.3 Pore Pressure Transducer Calibration

The pore pressure cell is composed of a pressure transducer connected to the porous stones via ducts. Figure 26 is a schematic of the pressure instrument calibration layout. A custom-made cylindrical calibration chamber was placed over the pore pressure cell. The cables, DAS, and all other devices that were used in the field testing program were also used in the calibration process. The chamber utilizes O-rings to form a seal that maintains a vacuum during the de-airing process and withstands pressurization during the calibrating process. The porous stones and internal channels were filled with glycerin and de-aired water mixture. A vacuum was applied to the chamber to ensure de-airing and complete saturation. A proportional integration differentiation (PID) circuit was then used to apply pressure to the fluid in the calibration chamber. An additional accurately calibrated pressure transducer was placed in line between the PID and the pressure chamber to measure the actual pressure applied to the fluid in the chamber. This additional pressure transducer was used to record the reference pressure on which the calibration factors were based.

In order to simulate field conditions, three different pressure application procedures were used. The pressure was increased and decreased at a constant rate (for four or five cycles) during all the procedures. These procedures were:

1. Opening the system to the atmosphere and holding for a short duration after each ramp up and down sequence.
2. Opening the system to the atmosphere before and after the entire ramp up and down sequence without any pauses between ramps.
3. Holding the pressure steady after each ramp up and opening the system to the atmosphere after each ramp down.

Procedures 1 and 2 both simulate driving conditions because the pressure application is rapid and the transducer can measure the pressure only if the response time is quick. Procedure 3 represents the period after driving when the pressure changes are slower and the response time of the system is not as important a factor. The different pressure application procedures did not affect the performance of the pore pressure transducer.

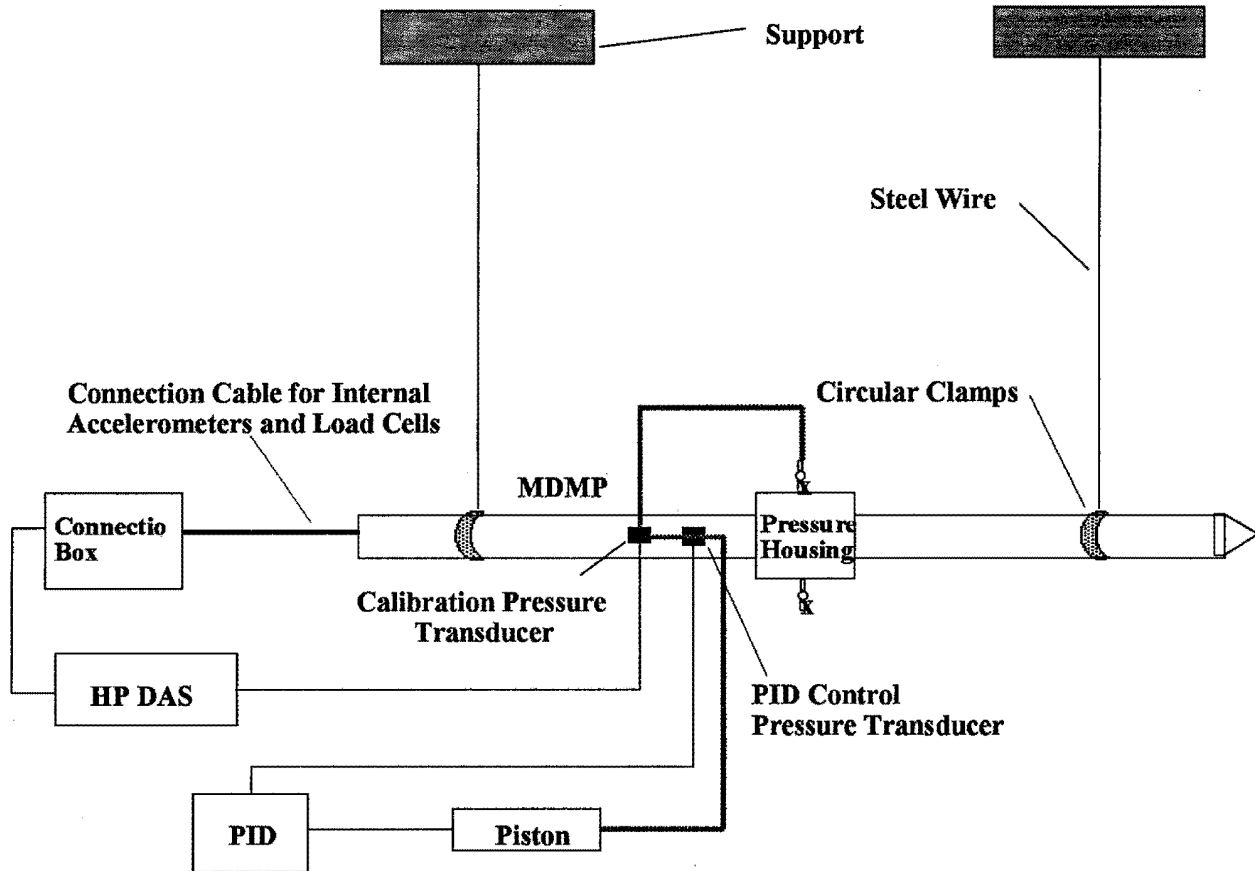


**Figure 26. Pressure Instrumentation Calibration Setup.**

The pore pressure cell was calibrated three times before the testing program at Newbury using each pressure application procedure. After the completion of the testing program, the calibration of the pore pressure cell was checked twice using the third pressure application procedure. Table 12 summarizes the pore pressure transducer calibration results of the various calibration procedures. An average of all five calibration factors were used in the test result data reduction ( $7.0652 \frac{\text{psi}}{\text{Volt}}$ ).

### **3.6.4 Total Pressure Cell Calibration**

The total pressure cell was calibrated along with the pore pressure cell using the same pressure application procedures previously outlined in section 3.6.3. The pressure application procedure was an important factor when calibrating the total pressure cell as the response time of the cell was affected by the O-rings. As a result, procedures 1 and 2 were not adequate as not enough response time was provided after each loading ramp. Table 13 summarizes the results of the various calibrations of the total pressure cell. The calibration factor for test #3 ( $64527.16 \frac{\text{psi}}{\text{Volt}}$ )

was used in the data reduction. The total pressure cell was damaged during the testing program and the calibration could not be checked after testing.

**Table 12. Pore Pressure Transducer Calibration Results.**

Test	Procedure	Calibration $\frac{\text{psi}}{\text{Volt}}$	Zero Pressure Voltage (volts)	Coefficient of Determination	Remarks
Test #1	#1	7.0209	1.5120	0.99998	Before Testing Program
Test #2	#2	7.0687	1.4786	0.99999	Before Testing Program
Test #3	#3	7.0838	1.5218	0.99999	Before Testing Program
Test #4	#3	7.0849	1.5623	0.99997	After Testing Program
Test #5	#3	7.0678	1.5510	0.99998	After Testing Program

**Table 13. Total Pressure Cell Calibration Results.**

Test	Procedure	Calibration $\frac{\text{psi}}{\text{Volt}}$	Zero Pressure Voltage (volts)	Coefficient of Determination	Remarks
Test #1	#1	67114.9912	0.0004323	0.9997	Before Testing Program
Test #2	#2	65261.119	0.0004187	0.9972	Before Testing Program
Test #3	#3	64527.1586	0.0005621	0.9999	Before Testing Program

### **3.6.5 Displacement Transducer Calibration**

The assembled MDMP was suspended from the reaction frame using the same setup used to calibrate the load cells. Two displacement transducers were aligned 180° apart to measure the movement of the hydraulic ram. With the slip joint in the fully extended position, the ram was advanced approximately 5 cm to close the slip joint. The displacements monitored by the two displacement transducers (that measured the ram movement) were averaged together to determine the movement of the slip joint. The calibration constant determined for the DC-LVDT displacement transducer obtained via this procedure is  $0.097735 \text{ in}/V_{\text{out}}$ .

### **3.6.6 Accelerometer Response During Dynamic Loading**

The MDMP was not calibrated under dynamic loading. The actual calibration of the accelerometers was performed by Pile Dynamics, Inc., of Cleveland, Ohio. The response of the MDMP instrumentation under dynamic loading was examined using a custom-designed support

system that was fabricated for this purpose by George Saliby, a graduate research assistant at UMass-Lowell. Figures 27a and b are a schematic and photograph of the configuration used for the support of the MDMP and associated loading equipment. Four supports were constructed out of steel wiring and circular clamps. These supports were fixed to a ceiling beam.

The MDMP was oriented horizontally and placed within two of the supports in order to simulate a completely free pile (i.e., without frictional or end-bearing resistance). The responses of the three accelerometers and load cells within the MDMP were tested in this system. The two remaining supports were clamped to a steel ram that was used as a hammer. Different rams, which varied in weight (based on lengths between 15.2 and 61.0 cm (6 to 24 in)), were machined from a 76.2-mm- (3-in-) diameter solid steel cylinder. Alternatively, a 5-lb (22.2-N) sledgehammer was used to impact the top of the MDMP. A 12.7-mm- (1/2-in-) thick piece of plywood and/or a 3.175-mm- (1/8-in-) thick piece of plastic were used for pile cushions. In some cases, drill rods were connected to the top of the MDMP. An additional strain gauge and accelerometer from the Pile-Driving Analyzer (PDA) system were attached to these drill rod segments to measure force and acceleration applied to the rods. The output from the three MDMP accelerometers and strain gauges, and the additional drill rod strain gauge and accelerometer, was recorded and routed to the PDA via a connection box.

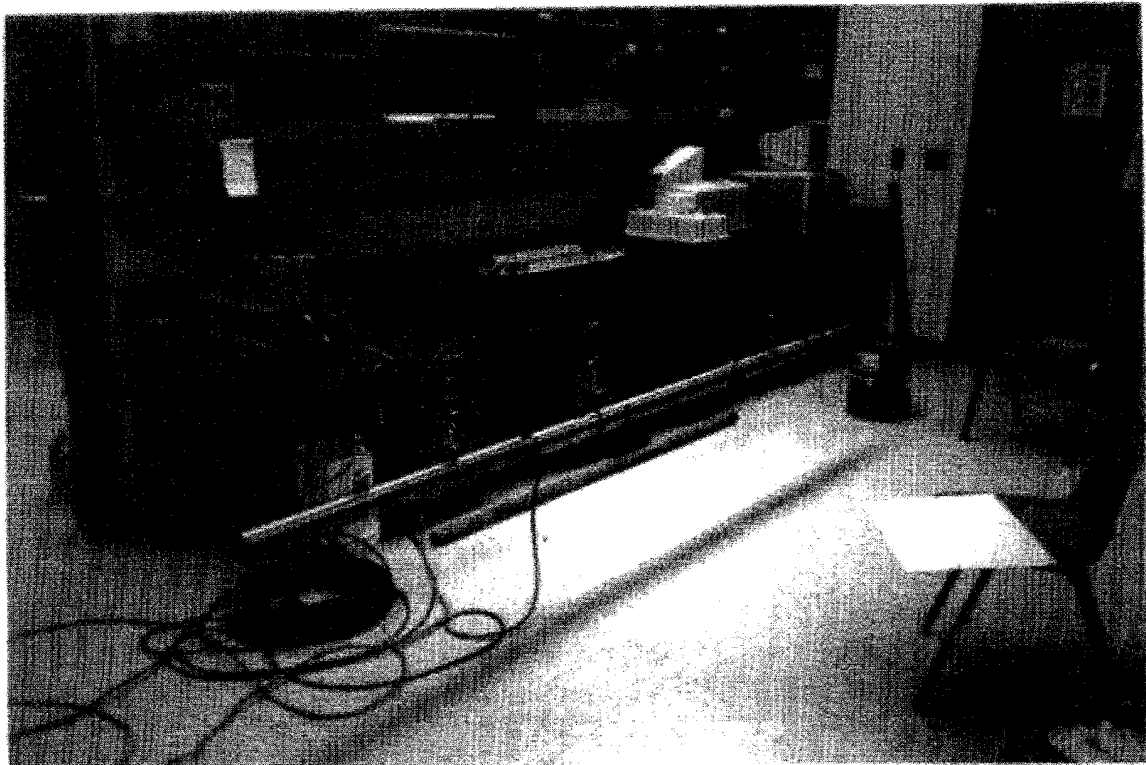


**Figure 27a. Photograph of the Dynamic Instrumentation Testing Setup.**

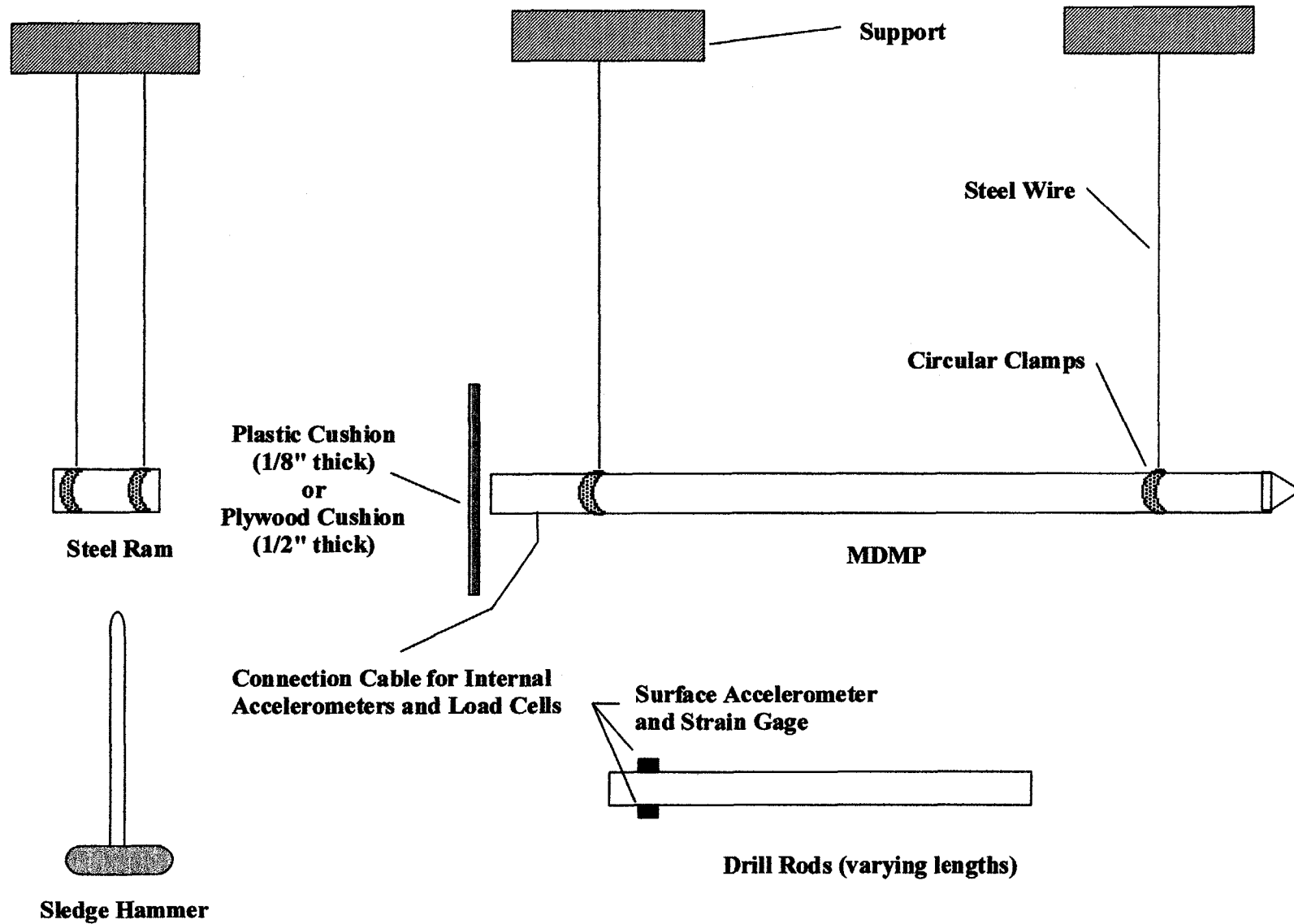


Figure 27b. Schematic of the Dynamic Instrumentation Testing Setup.





## CHAPTER 4. MDMP PERIPHERAL TEST ACCESSORIES

### 4.1 Overview of Peripheral Test Accessories

The MDMP requires peripheral systems to conduct the various testing procedures. Two Data Acquisition Systems (DAS) measure the response of the instrumentation during the different stages of testing. A loading frame provides the reaction for both compression and extension static load tests. A hydraulic system applies the loads for these static load tests. A drill rig, equipped with a drop hammer, is used to install the MDMP.

Three basic test procedures are conducted with the model pile during the pile history. During installation, the pile is driven with a standard SPT hammer (0.623 kN (140 lb)) or Casing hammer (1.33 kN (300 lb)). The pile is monitored during driving utilizing the Pile-Driving Analyzer (PDA). After driving, the soil/pile response is measured with time. During the initial period after installation, the response is measured (using a Hewlett Packard (HP) DAS) at a sampling rate of approximately 3 to 4 Hz over a period of about 2 h. Thereafter, the frequency is decreased as the soil/pile system approaches an equilibrium state. Several static load tests, both in compression and tension, are conducted periodically on the model pile to determine the gain of capacity with time. Additional tests such as dynamic restrikes at the end of the test sequence and/or rapid load/unload cycling to determine the ultimate capacity may also be performed.

All of these responses are measured by the various MDMP sensors using an elaborate DAS composed of an HP DAS, PDA, connection box, and cables. Depending on the test procedure, some sensors are monitored while others are not. A schematic of the DAS with the other related components of the model pile is shown in Figure 28. The figure is color-coded to enable easy identification of the various cables and associated connections. Table 14 provides a list of the components as numbered in Figure 28.

**Table 14. List of Components as Shown in Figure 28.**

Component Number	Description	Type of Connector
#1	Piezoelectric receptacle on the PDA	19-pin connector (MS3101A22-14P)
#2	Piezoresistive receptacle on the PDA	19-pin connector (MS3101A22-14P)
#3	Connection for dynamic gauges (piezoelectric) to PDA	19-pin connector (MS3106A22-14S)
#4	Connection for dynamic gauges (piezoelectric) to PDA	19-pin connector (MS3102A22-14P)
#5	Connection for dynamic gauges (piezoresistive) to PDA	19-pin connector (MS3106A22-14S)
#6	Connection for dynamic gauges (piezoresistive) to PDA	19-pin connector (MS3102A22-14P)
#7	Connection for output signals to HP DAS	48 pin connector (MS3106A36-10S)
#8	Connection for output signals to HP DAS	48 pin connector (MS3102A36-10P)
#9	Connection for dynamic gauges to connection box	19-pin connector (MS3102A22-14S)
#10	Connection for surface sensors to connection box	19-pin connector (MS3102A22-14S)
#11	Connection for connection box to MDMP main cable	Amphenol 50-pin connector
#12	Connection for MDMP main cable to connection box	Amphenol 50-pin connector
#13	Branch line connection for surface measurements	19-pin connector (MS3101A22-14P)
#14	Connection to the multiplexer in the HP DAS	HP terminal block connection

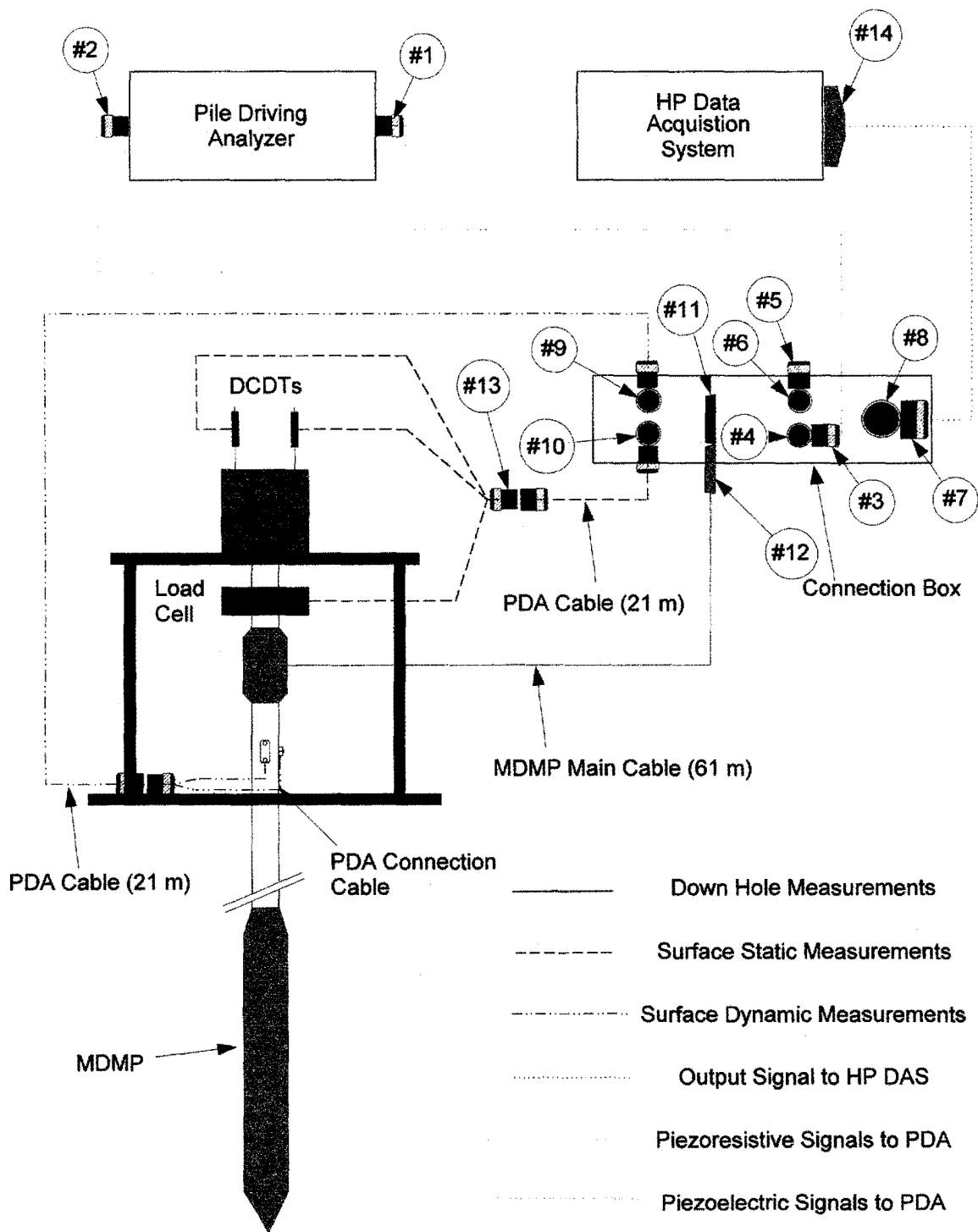


**Figure 28. Schematic of the MDMP Data Acquisition System.**

## 4.2 Hewlett Packard Data Acquisition System

The Hewlett Packard Data Acquisition System (HP DAS) is used throughout the testing sequence. The HP DAS is required to trigger and store data from nine channels at 4 Hz. The data are recorded to hard drive and floppy disk periodically to ensure data recovery. The HP DAS consists of two components: the HP 75000 Series B cage VXI Bus DAS and an IBM-compatible 486 PC. The HP 75000 Series is composed of a mainframe HP E1301A with several modular components. Figure 29 is a photograph of the HP DAS system.



**Figure 29. Hewlett Packard Data Acquisition System (HP DAS).**

The mainframe has a front-panel keyboard and display. Modules are installed in the mainframe that control the different DAS functions to include module-to-module synchronization. The modules installed in the mainframe HP E1301A are: a 5½-Digit Multimeter (HP E1326B), a 16-Channel Relay Multiplexer Module (HP E1345A), and a 4-Channel D/A Converter Module (HP E1328A). The 5½-Digit Multimeter can be used as stand-alone or combined with multiplexers to form a scanning multimeter. The multimeter measurement functions include: DC Voltage, root mean squared (RMS) AC Voltage, 2-Wire Resistance, 4-Wire Resistance, Temperature, and Strain. The 16-Channel Relay Multiplexer switches up to 16 channels, where each channel has High (H), Low (L), and Guard (G) connections. Field wiring is connected to a terminal block that plugs into the Multiplexer. The 4-Channel D/A Converter Module provides four independent 16-bit digital-to-analog converter channels. Two operating modes are available — calibrated or non-calibrated — with typical output voltage ranges of  $\pm 10.922$  V DC or  $\pm 12$  V DC and typical output current ranges of  $\pm 21.84$  mA DC or  $\pm 24$  mA DC (HP User's Manuals).

The software program HP VEE was used to trigger the scanning multimeter, set the number of channels to be monitored and the sampling frequency, display real-time data to the screen, and store the data with a time stamp to a hard drive. HP VEE is a Windows-based iconic programming language that was installed on an IBM-compatible 486 PC operating at 33 MHz (Helsel, 1994).

The HP DAS records nine signals during static loading and three signals during dynamic loading. These signals are routed to the HP DAS from the connection box, which supplies the excitation voltage. Table 15 presents all the instruments in the overall MDMP system with respect to the data collection mode (dynamic vs. static). During static loading, the signals from the static surface instruments and all MDMP sensors are recorded, except for the MDMP accelerometers. During driving, the signals from the pore pressure transducer, total lateral pressure transducer, and slip joint LVDT are recorded.

**Table 15. MDMP Data Acquisition and Instrumentation Configuration.**

Instrument	Location	Static	Dynamic	
		HP Channel Number	HP Channel Number	PDA Channel Number
Lebow 25-Ton	Surface	0	-	-
DCDT		1	-	-
DCDT		2	-	-
Strain Gauge		-	-	1
Accelerometer		-	-	2
Top Load Cell	MDMP	3	-	3
Top Accelerometer		-	-	4
Middle Load Cell		4	-	5
Middle Accelerometer		-	-	6
Bottom Load Cell		5	-	7
Bottom Accelerometer		-	-	8
Total Pressure Cell		6	6	-
Pore Pressure Transducer		7	7	-
Slip Joint DC-LVDT		8	8	-

Note: "-" indicates that the data acquisition system does not record signals.

### 4.3 Pile-Driving Analyzer

The Pile-Driving Analyzer (PDA) is a signal conditioning and data acquisition system developed by Pile Dynamics, Inc. The PDA monitors pile driving in order to estimate pile capacity and determine pile stresses during installation. The PDA used in this research consists of a 486 SLC 25-MHz processor with 8 Mb RAM and a 240-Mb hard disk. The PDA has eight channels, thereby having the capability of monitor eight sensors and four strain gauges, 2 piezoelectric accelerometers, and 2 piezoresistive accelerometers. The system has a built-in automatic balancing of all signal conditioning. The maximum sampling rate is 20,000 Hz and records 1029 data points on each channel. For model pile testing, this high sample rate is needed to accurately record the sharp rise of the hammer impact, similar to the one developed during standard

penetration testing (SPT). The recorded force and velocity data can be further analyzed with software such as the case method and case pile wave analysis program (CAPWAP) to predict soil behavior and estimate static pile capacity.

Figure 30 is a photograph of the PDA system. The PDA collects the dynamic instrumentation signals from the three MDMP load cells and accelerometers and the surface strain gauge and accelerometer during driving only. These eight signals are routed to the PDA from the connection box when the three load cell switches on the connection box are set to the dynamic position (see Table 15).



**Figure 30. File-Driving Analyzer (PDA) Data Acquisition System.**

An alternative data collection procedure can be employed during driving if another PDA is used to collect the surface measurements. With a second PDA, two strain gauge and two accelerometer signals can be attached to the drill rods at the surface and monitored without the use of the connection box. The first PDA can be used as previously described with only the three strain gauge and accelerometer signals within the MDMP routed through the connection box and recorded by the PDA. This alternative provides a more reliable measurement of force and velocity readings (and, therefore, energy) at the pile top (drill rods).

## **4.4 Connection Box**

### **4.4.1 General**

The connection box serves as the nerve center for the entire MDMP DAS. The connection box was designed and fabricated by Gary Howe, Civil Engineering Laboratory Director at the UMass-Lowell. All the cables from the MDMP and the surface instruments are routed through this box before being connected to the respective DAS (either HP or PDA), as shown in Figure 28. This connection box accepts the input signals from the various sensors, supplies the excitation voltages, and routes output signals to the correct DAS. The fundamental design requirements of the connection box were: (1) to allow instantaneous switching from dynamic to static readings (e.g., at the end of driving) and (2) to simplify the data acquisition process by centralizing all of the cables and connections in one place so that repairs could be made relatively easily in the field if problems were encountered. Wire diagrams of the connection box are presented in Appendix F.

### **4.4.2 Power Supply Requirement**

The connection box supplies a total of four different direct current (DC) excitation voltages (+5, +15, -15, and +18 V) via a dual DC external power supply. The pressure transducer for the pore pressure measurements requires a constant current. A circuit board provided by the manufacturer supplies a constant 4-mA current and is capable of amplifying the output signal. This circuit board requires a constant voltage supply of +18 V. The DC-LVDT displacement transducer requires an excitation voltage of  $\pm 15$  V DC. The lateral pressure cell requires an excitation voltage of 5 V DC. The connection box internal circuitry supplies all the required excitation voltages through a connection to an external power supply.

### **4.4.3 Input**

A schematic of the back faceplate of the connection box is shown in Figure 31. The connection box accepts three different input cables. These three cables are connected to the left side of the back faceplate. One cable contains all of the MDMP instrumentation wires (down hole input), while the other two cables carry the dynamic and static ground-surface instrumentation wires. Refer to Section 4.5 for details on the various cables. Included in the connection box requirements was the incorporation of the available PDA cables. In order to do so, socket receptacle connections were fabricated. These receptacles are push-on connections that allow the cables to be pulled out if a sudden jerking motion occurs, rather than having the wires severed.

### **4.4.4 Output**

Three different output cables route the input signals to the appropriate DAS, depending on the data collection mode (either static or dynamic). The three different output connections are shown on the right side of the back faceplate in Figure 31. The static output connection carries the signals measured during static testing to the HP DAS. The dynamic output is split into two connections, depending on the type of accelerometers. The output from the two piezoelectric accelerometers and their associated strain gauges in the MDMP load cells (top and middle) is

routed to the piezoelectric receptacles of the PDA. The output from the piezoresistive accelerometer and associated strain gauge in the tip load cell of the MDMP and the piezoresistive accelerometer and strain gauge at the surface is routed to the piezoresistive receptacle of the PDA.

The output signals are wired directly from the input cable to the HP DAS. The accelerometers from the model pile are also wired in the connection box for direct attachment to the PDA. Using the connection box, other instrumentation, such as thermometer and an inclinometer can easily be added in the future.

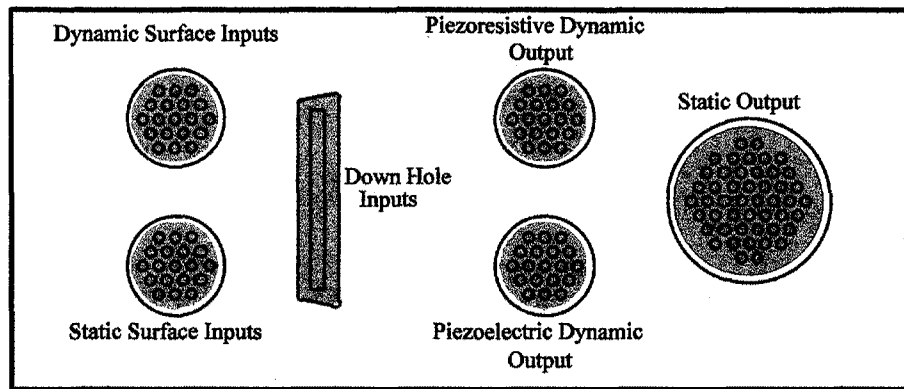


**Figure 31. Connection Box, Back Faceplate.**

#### **4.4.5 Operation**

The front faceplate of the connection box is shown in Figure 32. Three switches in the front faceplate enable the data collection from the three MDMP load cells to toggle between dynamic and static modes. When the three switches are placed in the dynamic position during driving, the PDA supplies the excitation voltage and records the output strain and acceleration signals from the three MDMP load cells and the surface strain gauge/accelerometer pair. The HP DAS records the displacement of the slip joint LVDT, pore pressure, and total lateral pressure during driving.

During static loading, the three switches are placed in the static position. The connection box supplies the excitation voltage, while the strain signals from the strain gauges within the three MDMP load cells are recorded by the HP DAS. In addition, the connection box supplies the excitation voltages for the three additional MDMP instruments (pore pressure transducer, lateral pressure transducer, and slip joint LVDT) and the three surface instruments (load cell and two DCDTs), while the HP DAS records the signals. The accelerometer signals are meaningless during static loading and are not recorded.

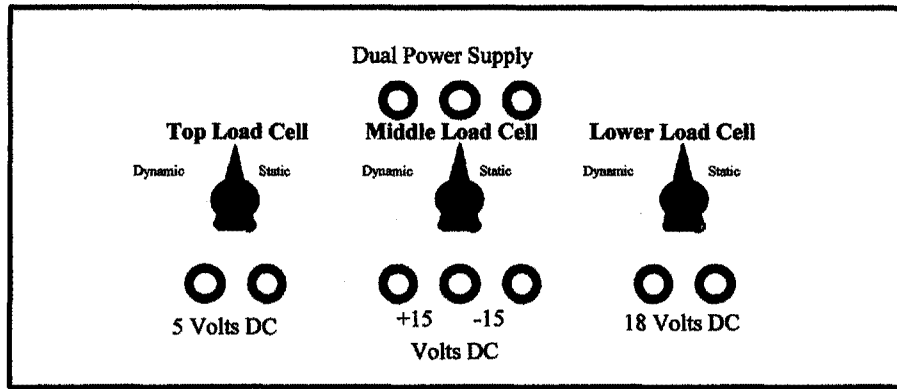


**Figure 32. Connection Box, Front Faceplate.**

## 4.5 Cables and Connections

### 4.5.1 General

Six cables are used in the overall MDMP DAS. Three cables collect the data from the surface instruments and MDMP instruments. Three additional cables are used for output to the PDA or HP DAS. The pin connections for the different cables are presented in Appendix F. The following sections present a description of the cables and connections.

### 4.5.2 Input Cables

A 61-m (200-ft) main cable is used for all the wiring from the various MDMP measuring devices. A total of nine instrument signals from the three load cells, three internal accelerometers, slip joint LVDT, pore pressure transducer, and lateral pressure transducer are transferred via this cable. This cable is the brown line in Figure 28 and is referred to as the "down hole measurements" cable. The MDMP end of the cable is sealed with a watertight connection (MINO-44#20-CCP connector). The other end of the cable has an Amphenol 50-pin connector (#12 in Figure 28). This 50-pin connection connects to the #11 slot in the connection box.

Surface measurements are recorded by two separate cables. The "surface static measurement" cable is a 21-m (70-ft) PDA cable that combines the surface load cell (Lebow load cell) and the two surface DCDT wires at connection #13. This combined cable is the blue line in Figure 28 and connects to slot #10 in the connection box. The other surface cable is referred to as the "surface dynamic measurements" cable (red line in Figure 28). This is another 21-m (70-ft) PDA cable that combines one strain transducer and one piezoresistive accelerometer to the connection box in slot #9.

### 4.5.3 Output Cables

There are three output cables that route the various input signals to the HP DAS and PDA. Two output cables convey the dynamic signals to the PDA. These two cables are designated either as



piezoresistive (yellow line) or piezoelectric (green line). Refer to Section 3.4.2 for details on the difference between the two accelerometer types. These cables are specially manufactured for the PDA. The piezoresistive signal connection (#5) is routed from the connection box (slot #6) to the piezoresistive receptacle on the PDA (#2). This cable carries the signals from the tip load cell (strain gauge and accelerometer pair) in the MDMP and the surface strain gauge and accelerometer pair to the PDA. The piezoelectric signal connection (#3) is routed from the connection box (slot #4) to the piezoelectric receptacle on the PDA (#1). This cable carries the signals from the upper and middle load cells (strain gauge and accelerometer pair) in the MDMP to the PDA. All cables are compatible with the PDA, utilizing connector part numbers MS3101A22-14P and MS3106A22-14S.

A 3-m (10-ft) long output signal cable from the connection box to the HP DAS (purple line) was custom-made at UMass Lowell to record all signals other than the dynamic strain and acceleration signals. A 48-pin contact connection (part no. MS3106A36-10S) (#7) connects to slot #8 on the connection box. The other end of the cable is a terminal block connection manufactured by HP (#14) that connects to the multiplexer in the HP DAS. During static loading, this cable routes signals from the surface static measurements (Lebow load cell and two DCDTs at the surface) and down hole measurements (three strain-gauged load cells, slip joint LVDT, pore pressure transducer, and total lateral pressure transducer from the MDMP) to the HP. During driving, this cable carries signals from the LVDT slip joint, pore pressure, and total lateral pressure.

## **4.6 Static Loading System**

### **4.6.1 Overview**

The loading system provides tension and compression loads (and their reaction) for the MDMP static load tests. The static load tests are performed in order to measure the soil/pile interaction. When assessing gain of capacity with time, multiple load tests are conducted with the following requirements: (1) in order to assess the initial capacity, the first load test needs to be conducted as soon as possible after the MDMP installation is completed; and (2) as the gain of capacity of small piles is achieved during a short period (e.g., about 7 days for the MDMP), the load test needs to be of the “fast” load test type, not allowing creep or changes in stress to take place during the load test period. These requirements are accomplished with a pre-assembled portable load frame and hydraulic piston. The reaction is supplied from pre-installed ground anchors as detailed below.

### **4.6.2 Loading Frame**

Figures 33a and b are a schematic and photograph of the static loading system, including the load frame, load application system, reaction system, and surface measurements. There are two steel plates made of type 4130 plate steel, each 25.4 mm (1 in) thick. The lower plate has five through holes, one in the center for the model pile to pass through and four in the corners for threaded support rods to be attached to the top plate. The top plate has several through holes as well. Like the bottom plate, it has a center hole for the pile to pass through and four holes for

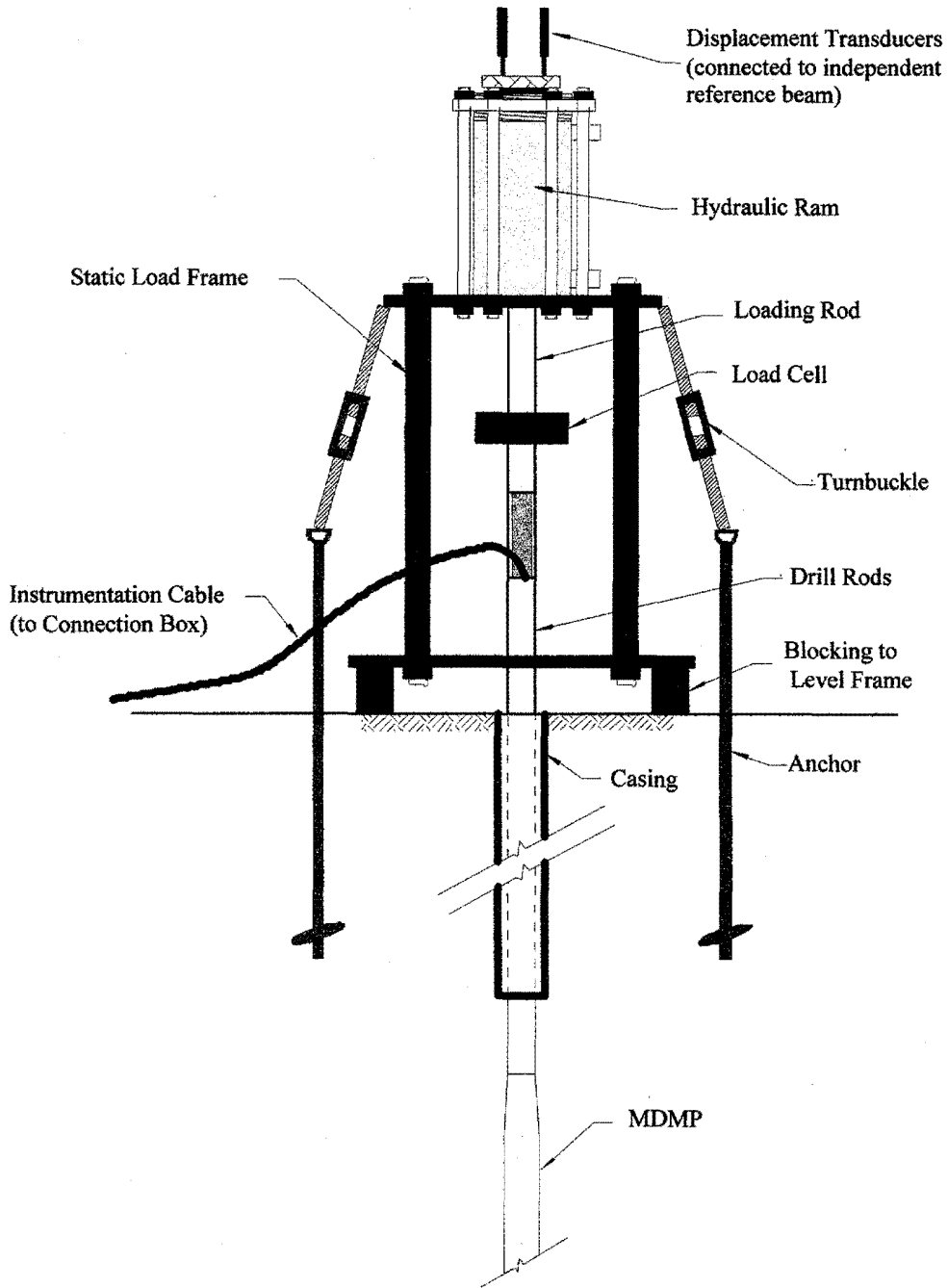


**Figure 33a. Schematic of the MDMP Static Load Frame.**

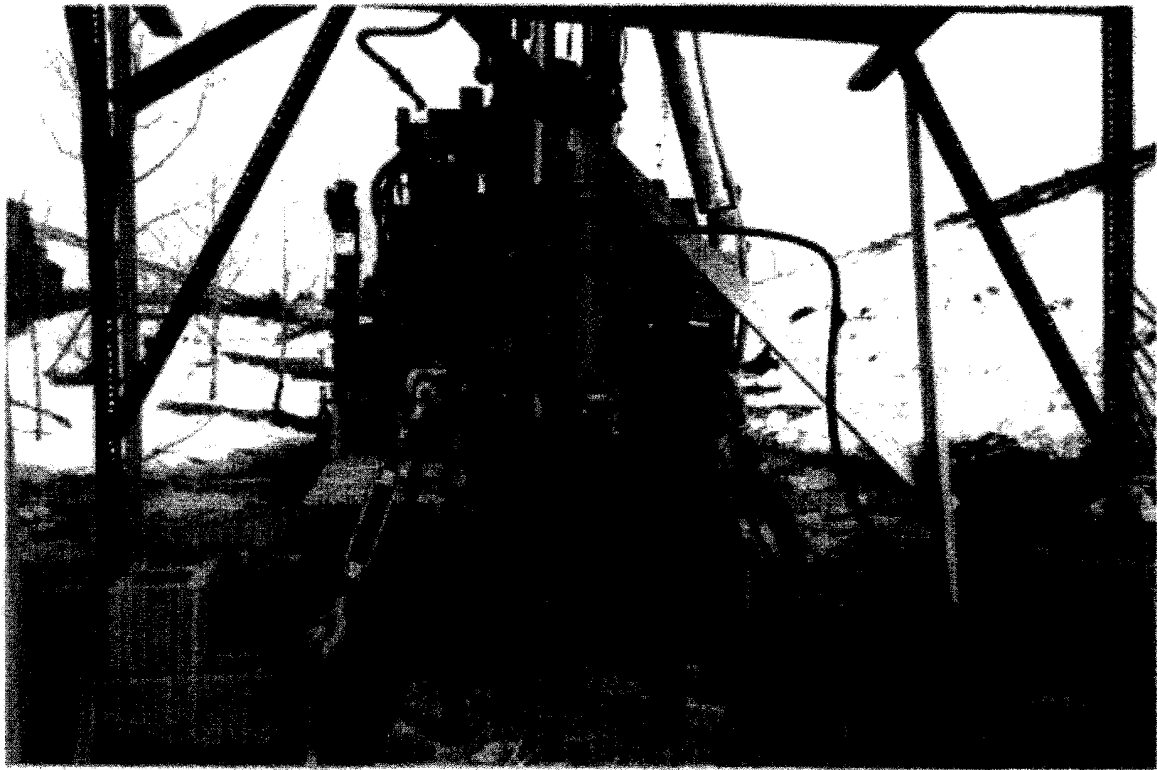


**Figure 33b. Photograph of the MDMP Static Load Frame.**

the threaded support rods. In addition, six holes are used to attach the double-acting ram to the top plate and four holes in the corners are used to attach the load frame to the anchor system. The threaded support rods used to connect the bottom and top plates are 91.44-cm- (36-in-) long, 38.1-mm- (1.5-in-) all-thread rod with hex nuts to secure both ends. The four threaded support rods slide into four steel tubes (sleeves), 41.275-mm (1.625-in) I.D. x 6.35-mm (0.25-in) wall thickness x 76.2 cm (30 in) long, that separate the top and bottom plates. A threaded disk screws onto the top of the hydraulic ram. The disk has six threaded holes that match up with the six holes on the top plate of the loading plate. Six 25.4-mm- (1.0-in-) threaded rods connect the disk to the top plate to secure the hydraulic ram. The machine drawing of load frame components is presented in Appendix C with the shop drawing of the MDMP.

The frame is designed to resist both upward loading (tension) and downward loading (compression). A loading rod is used to transfer loads from the hydraulic ram to the drill rods. The hydraulic ram is bolted to the loading frame. The loading rod bolts to the top of the ram, passes through the ram, and screws into the load cell and/or drill rods below. For tension loading, the ram pushes up on the bolted loading rod. The reaction load to this upward ram movement is transferred downward to the loading frame and ultimately the ground anchors provide the reaction load. For compression loading, the ram is extended prior to loading. The ram pulls downward on the bolted plate and transfers the load to the drill rods. The reaction load to this downward ram movement is transferred from the ram to the frame that is attached to ground anchors with turnbuckles. Four ground anchors, type 816 Chance 20.32-cm (8-in) No-Wrench Anchor, resist the upward load. The maximum load for the 25.4-mm (1-in) diameter rod

of each anchor is 160 kN (36,000 lb). The soil at the Newbury Site appears to be type 1 or 2, which correlates to an anchor capacity of 142 kN (32,000 lb) (Chance, 1992).

#### **4.6.3 Hydraulic Loading System**

A double-acting hollow-plunger hydraulic cylinder (Enerpac RRH-10010) is used to apply the load to the model pile. The ram has a capacity of 890 kN (100 tons) when advanced, 602 kN (67.7 tons) when retracted, and 254 mm (10 in) of travel. A two-speed electric high-pressure hydraulics pump (Power Team PE214S) supplies the hydraulic pressure for the hydraulic cylinder. The hydraulic pump has three functions: advance, hold, and return. The hydraulic pump does not have a control to regulate the speed of the hydraulic cylinder. To control the speed of the cylinder, a flow control valve (Parker F600S) is placed in line with a maximum operating pressure of 34.5 MPa (5000 psi). The valve controls the flow of the hydraulic fluid in one direction and allows free flow in the opposite direction. The valve has different color bands that are used as a reference scale for quick adjustment. For fine adjustment, the first three full turns control at low flow and the next three full turns open the needle valve to full flow. Two of these valves are used to control the hydraulic cylinder in both directions so compression and extension static load tests are possible at a controlled displacement rate.

#### **4.7 Driving System**

A typical drop hammer and cathead is being used to drive the MDMP. The rated energy of the driving system is approximately 475 J (350 ft·lb) (based on a ram weight of 0.623 kN (140 lb) and an average stroke of 0.762 m (2.5 ft)). Figure 21 is a schematic showing a typical drill rig drop hammer used in SPT exploration. The drill hole is advanced by conventional methods (e.g., standard wash and drive drilling). A 10.16-cm- (4-in-) diameter casing is then driven to the top of the testing zone. The hole is cleaned out and the MDMP is then attached to the drill rods and inserted to the top of the test zone. The MDMP is driven approximately 3.05 m (10 ft) (MDMP length) below the top of the testing zone.

## **CHAPTER 5. MDMP TESTS AT THE NEWBURY, MA SITE**

### **5.1 Site Overview and Location**

The first field deployment of the MDMP was conducted at a site located in Newbury, MA during March 1996. Refer to Figure 34 for the site locus. The original construction of a multiple-span, reinforced-concrete bridge along Route 1 was completed in 1935. This bridge was demolished during the summer of 1996 and will be replaced by a new bridge currently being constructed at the site. The new bridge is being built to accommodate an extension of the Commuter Rail from Ipswich, MA and a new Commuter Rail station.

The test location was chosen as the first test site for the MDMP because it contained a 9- to 12-m- (30- to 40- ft-) thick clay deposit close to the ground surface. This clay is ideal for assessing the pile capacity gain and pore pressure dissipation with time. In addition to the MDMP testing, full-scale instrumented piles will be tested at the site during future research phases. Both test and production piles for the new bridge will be conducted at the same location as well.

This chapter provides information regarding the subsurface soils at the site, predicted MDMP behavior prior to installation, and a description of the testing procedure and schedule. The test results are presented in Chapter 6, with analyses in Chapter 7.

### **5.2 Previous Subsurface Exploration Program Studies**

Previous subsurface studies were conducted in the 1930's for the original bridge and again in 1988 and 1992 for the new bridge. Supplemental borings were performed in 1996 during the construction phase of the new replacement bridge. The 1930's study included six borings. A study for the initial evaluation for the foundation of the replacement bridge was completed in 1988. During this study, six borings were completed and eight undisturbed samples were collected and tested. Additional subsurface testing was conducted in 1992, including 20 borings and 8 test pits (GZA GeoEnvironmental, 1993).

### **5.3 UMass-Lowell Subsurface Exploration Program**

The UMass-Lowell conducted several borings (designated as NB1, NB2, NB4, and B5) to determine the soil profile and properties within the immediate vicinity of the proposed model pile test location. The boring designation NB2 was also used for the first MDMP test. The boring designation NB3 was used for the second MDMP test at the same location as boring NB2. Figure 35 shows the location of the borings and the MDMP tests. A detailed subsurface investigation, with soil properties, will be presented by Chen (1997). The following sections outline the extent of the investigation and the major features related to the MDMP testing.

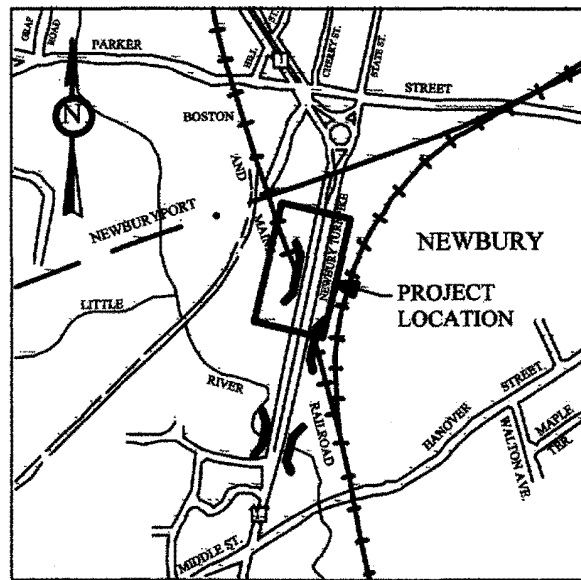
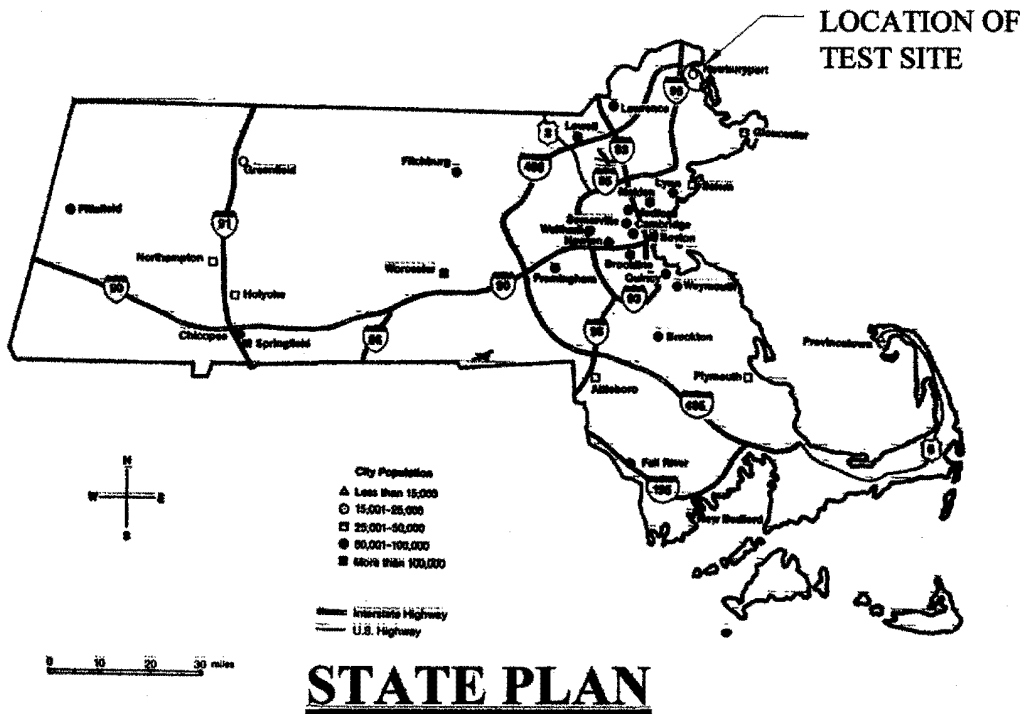


**Figure 34. Newbury Site Locus Plan.**

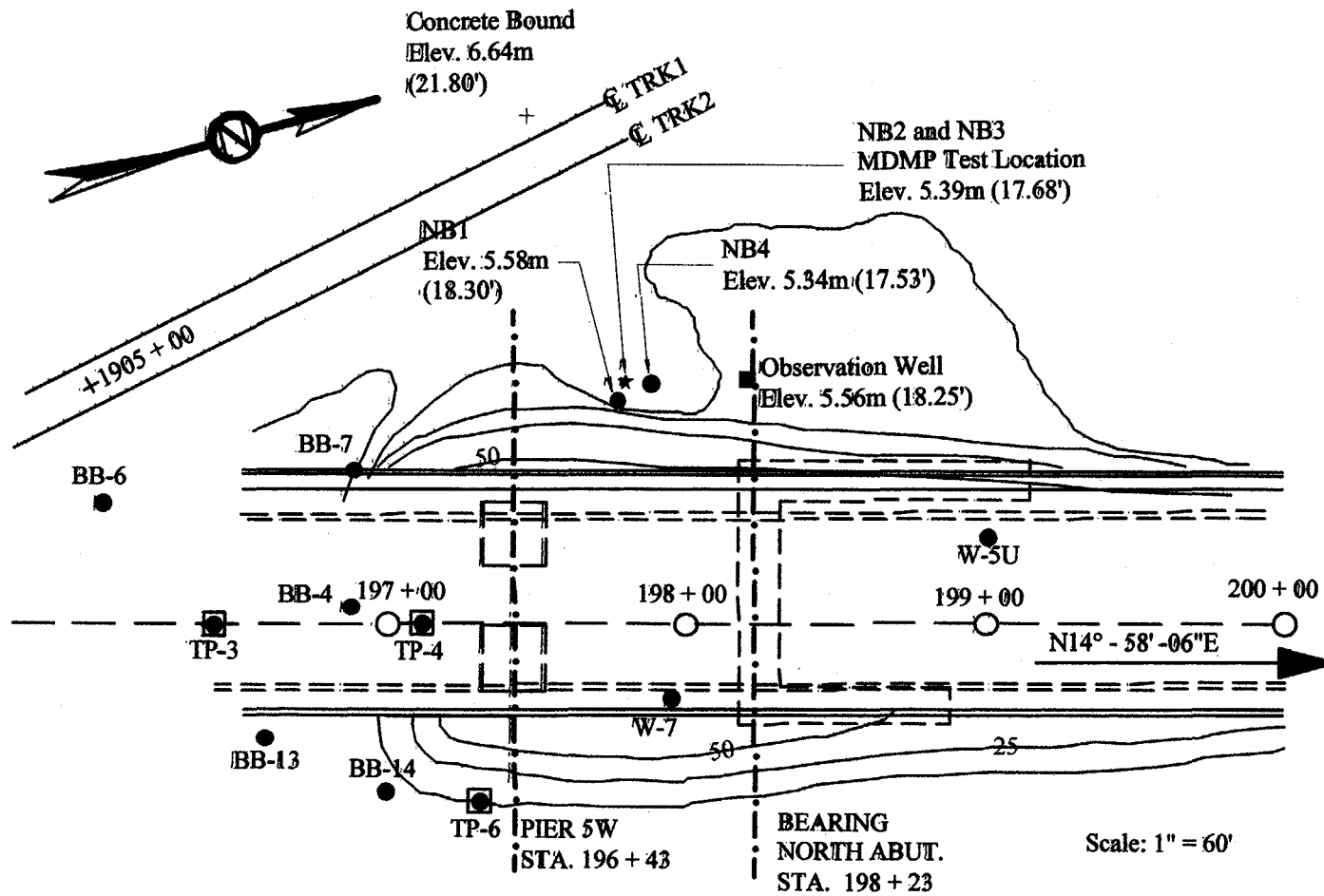


Figure 35. Newbury MDMP Site Plan.

### **5.3.1 Sampling and Field Testing**

Test boring NB1 was completed by New Hampshire Boring, Inc. of Londonderry, New Hampshire on September 25 and 26, 1995. The boring was conducted to evaluate the stratigraphy at the site and to obtain geotechnical properties of the clay deposit for correlations with the model pile tests. The boring was located approximately 12.2 m (40 ft) west of the existing northern bridge abutment in a position that will remain accessible after the completion of the entire project. The boring was initially advanced using a hollow-stem auger to a depth of approximately 3.05 m (10 ft) to the top of the clay. The auger was removed and 10.16-cm (4-in) I.D. casing was subsequently driven to a depth of 5.49 m (18 ft) below ground surface. The boring was then advanced using open-hole drilling techniques to the bottom of the clay layer at a depth of 16.46 m (54 ft) below ground surface. A 10.16-cm (4-in) I.D. casing was installed to stabilize the open hole as drilling continued until refusal was encountered at a depth of 31.09 m (102 ft) below ground surface. Split-spoon samples (S-1 through S-14) were taken at generally 1.52-m (5-ft) intervals within the fill layer and again within the stratified sand/silt/clay and till layers below the clay. Undisturbed tube sampling (T-1 through T-6) was performed within the clay deposit. In all, a total of 14 split-spoon and 5 undisturbed soil samples were successfully obtained. Table 16 provides a summary of the obtained samples with depth for NB1. Upon completion of the boring, an observation well was installed to a depth of 4.42 m (14.5 ft) below ground surface.

Test boring NB4 was completed by New Hampshire Boring, Inc. from March 11 through March 18, 1996 during the MDMP testing program. This boring was necessary to determine the depth and quality of the bedrock, to install a piezometer, and to gather more undisturbed samples. The boring was initially advanced using a hollow-stem auger to a depth of approximately 3.05 m (10 ft), corresponding to the top of the clay. The auger was then removed and 10.16-cm (4-in) I.D. casing was subsequently driven to a depth of 4.27 m (14 ft) below ground surface. Wash and drive techniques were used to advance the boring to the top of the bedrock at a depth of 30.5 m (100 ft) below ground surface. Split-spoon samples (B-1, S-1 through S-15) were taken at generally 1.52-m (5-ft) intervals within the fill layer and again within the stratified sand/silt/clay and till layers below the clay. Undisturbed tube sampling (B-2, T-1 through T-3) was performed within the clay deposit. In all, a total of 15 split-spoon and 3 undisturbed soil samples were successfully obtained. Table 17 provides a summary of the obtained soil samples with depth for NB4. Upon the completion of the boring, a Vibrating Wire piezometer and an observation well were installed to a depth of 10.24 m (33.6 ft) and 7.92 m (26 ft) below ground surface, respectively.

Test boring NB5 was completed by New Hampshire Boring, Inc., between September 3 and 4, 1996 in order to gather additional undisturbed samples in the clay layer. A 10.16-cm (4-in) I.D. casing was installed to 2.74 m (9 ft) below the ground surface. The boring was advanced using an open-hole drilling technique to a depth of 14.94 m (49 ft) below ground surface where casing was installed at the end of the first day. Undisturbed tube sampling (T-1 through T-6A) was performed within the clay deposit and interbedded sand/silt/clay deposit. In all, six undisturbed soil samples were successfully obtained. Table 18 provides a summary of the obtained soil samples with depth for NB5.



**Table 16. Sampling Performed at Boring NB1.**

Sample	Depth m (ft)	Recovery cm (inches)	Blow Count	SPT N	Remarks
SS-1	0-0.6 (0-2)	55.9 (22)	9-55- 47-45	102	
SS-2	1.52-1.83 (5-6)	15.2 (6)	44- Refusal	R	Refusal at 5'8"
SS-3	3.05-3.66 (10-12)	61.0 (24)	4-8-14- 21	22	Torvane-2.2tsf,1.0tsf,0.95tsf P.Penetro.-4.5tsf,3.25tsf,3.25tsf
T-1	4.57-5.18 (15-17)	58.4 (23)	N/A	N/A	Torvane-0.88tsf,0.6tsf P.Penetro.-2.8tsf,2.2tsf
FV-1	6.71-7.01 (22-23)	N/A	N/A	N/A	
T-2	7.62-8.23 (25-27)	55.9 (22)	N/A	N/A	Torvane-0.1tsf P.Penetro.-0.4tsf
FV-2	9.75-10.06 (32-33)	N/A	N/A	N/A	
T-3	10.67-11.28 (35-37)	58.4 (23)	N/A	N/A	Piston advanced Torvane-0.036tsf
FV-3	12.80-13.11 (42-43)	N/A	N/A	N/A	
T-4	13.72-14.33 (45-47)	30.5 (12)	N/A	N/A	Piston advanced
T-5	15.24-15.85 (50-52)	no recovery	N/A	N/A	Piston advanced
SS-4	15.54-16.15 (51-53)	58.4 (23)	5-1- WOR	WOR	Blow Count Suspect
SS-5	16.76-17.37 (55-57)	25.4 (10)	4-4-4-4	8	Not 30" drop
SS-6	18.29-18.90 (60-62)	43.2 (17)	6-6-10- 11	16	Torvane-0.12tsf,0.14tsf
T-6	18.90-19.51 (62-64)	25.4 (10)	N/A	N/A	Piston advanced
SS-7	19.81-20.42 (65-67)	41.9 (16.5)	6-9-13- 20	22	
SS-8	21.34-21.95 (70-72)	61.0 (24)	3-2-12- 24	14	Torvane-0.15tsf,0.24tsf
SS-9	22.86-23.47 (75-77)	40.6 (16)	9-8-13- 12	21	Torvane-0.22tsf,0.24tsf,0.12tsf P.Pentro.-0.5tsf,0.25tsf
SS-10	24.38-24.99 (80-82)	38.1 (15)	11-13- 14-13	27	
SS-11	24.99-25.60 (82-84)	43.2 (17)	6-9-13- 14	22	Continuous Sampling
SS-12	25.60-26.21 (84-86)	61.0 (24)	7-9-11- 12	20	Continuous Sampling
SS-13	27.43-28.04 (90-92)	22.9 (9)	11-22- 17-12	39	
SS-14	28.96-29.87 (95-98)	27.9 (11)	17-22-25- 31-33	N/A	3" split-spoon sampler

**Table 17. Sampling Performed at Boring NB4.**

Sample	Depth m (ft)	Recovery cm (inches)	Blow Count	SPT N	Remarks
B-1	1.52-1.83 (5-6)	N/A	20 for 1"	R	Refusal
SS-1	2.13-2.74 (7-9)	22.9 (9)	7-8-8-9	16	
SS-2	2.74-3.35 (9-11)	40.6 (16)	2-6-14- 22	20	
B-2	3.35-3.66 (11-12)	15.2 (6)	N/A	N/A	Unsuccessful Shelby Tube
T-1	4.27-4.88 (14-16)	22.9 (9)	N/A	N/A	Piston advanced
T-2	7.01-7.62 (23-25)	62.2 (24.5)	N/A	N/A	Piston advanced
T-3	10.06-10.67 (33-35)	62.2 (24.5)	N/A	N/A	Piston advanced
SS-3	11.89-12.50 (39-41)	61.0 (24)	WOR	WOR	
SS-4	13.41-14.02 (44-46)	61.0 (24)	WOR	WOR	
SS-5	14.94-15.54 (49-51)	53.3 (21)	W-5-8-5	13	
SS-6	16.46-17.07 (54-56)	53.3 (21)	7-6-4-4	10	
SS-7	17.98-18.59 (59-61)	61.0 (24)	1-1-2-5	3	
SS-8	19.51-20.12 (64-66)	35.6 (14)	3-4-9-9	13	
SS-9	21.03-21.64 (69-71)	61.0 (24)	9-8-6-7	14	
SS-10	22.86-23.47 (75-77)	45.7 (18)	3-2-1-1	3	
SS-11	24.08-24.69 (79-81)	61.0 (24)	1-2-9-9	11	
SS-12	25.91-26.52 (85-87)	61.0 (24)	32-38- 37-29	75	
SS-13	27.13-27.74 (89-91)	5.1 (2)	54-60- 57	117	
SS-14	28.65-29.26 (94-96)	2.5 (1)	26-44- 47-28	91	
SS-15	30.18-30.48 (99-100)	12.7 (5)	37-55	R	55 Blows for 3"
R-1	31.39-32.61 (103-107)	116.8 (46)	N/A	N/A	% Recovery 95.8% RQD 81.25%
R-2	32.61-33.53 (107-110)	88.9 (35)	N/A	N/A	% Recovery 92.1% RQD 89.5%

**Table 18. Sampling Performed at Boring NB5.**

Sample	Depth m (ft)	Recovery cm (inches)	Blow Count	SPT N	Remarks
T-1	2.74-3.35 (9-11)	50.8 (20)	N/A	N/A	Push
T-2	4.27-4.88 (14-16)	61.0 (24)	N/A	N/A	Push
T-3	5.79-6.40 (19-21)	63.5 (25)	N/A	N/A	Push
T-4	8.84-9.45 (29-31)	63.5 (25)	N/A	N/A	Push
T-5	11.89-12.50 (39-41)	0	N/A	N/A	No Recovery
T-5A	12.50-13.11 (41-43)	63.5 (25)	N/A	N/A	Push
T-6	14.94-15.54 (49-51)	0	N/A	N/A	No Recovery
T-6A	15.54-16.15 (51-53)	63.5 (25)	N/A	N/A	Push

In addition, samples were recovered during the installation of the MDMP on March 6, 1996. Table 19 provides a summary of the obtained soil samples with depth for NB2.

**Table 19. Sampling Performed at Boring NB2.**

Sample	Depth m (ft)	Recovery cm (inches)	Blow Count	SPT N	Remarks
SS-1	4.27-4.88 (14-16)	43.2 (17)	7-9-11- 16	20	
SS-2	4.88-5.49 (16-18)	61.0 (24)	12-10- 9-10	19	Continuous Sampling

Standard penetration testing (SPT) was performed during split-spoon sampling to evaluate the resistance of the soil. SPT testing was conducted according to ASTM D 1586-84 using a 3.49-cm (1.375-in) I.D. split-spoon sampler typically driven 60.96 cm (24 in) with a 63.56-kg (140-lb) hammer falling from a height of 76.2 cm (30 in). Field strength index testing using the pocket penetrometer and the torvane devices were performed on selected split-spoon and undisturbed soil samples obtained from the clay layer.

The pocket penetrometer is a device that provides a quick measure of the unconfined compressive strength of a clay by failing the clay in a "punching" mode under normal stresses. The unconfined compressive strength is theoretically twice the undrained shear strength. The torvane device provides a rough estimate of the undrained shear strength of a clay by failing the clay in a rotational "shearing" mode. In all, a total of six torvane and four pocket penetrometer tests were completed in the field. In addition, three field vane shear tests (FV-1 through FV-3) were performed in the upper portion of the clay stratum.

### **5.3.2 Groundwater Monitoring**

Several monitoring wells were observed by the UMass-Lowell to determine the groundwater elevation. An existing well with a 50.8-mm (2-in) PVC riser was located at the site (marked as "Observation Well" on Figure 35). This well was monitored until its apparent destruction during the construction of the replacement bridge. The monitoring well installed in NB1 was constructed with a 50.8-mm (2-in) PVC wellscreen attached to a solid PVC riser. The well is 4.42 m (14.5 ft) deep with a 3.05-m- (10-ft-) long PVC wellscreen, measured from the bottom upwards. The annular area above the screen between the well and the soil was sealed with bentonite. At NB4, a vibrating wire piezometer was installed to a depth of 10.24 m (33.6 ft) with approximately 0.305 m (1 ft) of sand placed above and below the piezometer. Bentonite pellets were used to seal the sand zone above and below the piezometer. The monitoring well in NB4 was installed to a depth of 7.92 m (26 ft) with 1.22 m (4 ft) of 50.8-mm- (2-in-) diameter PVC wellscreen and 6.71-m- (22-ft-) PVC riser. Bentonite pellets were used to seal above and below the wellscreen to ensure that the pore water pressure in the clay is measured. A roadbox set in cement was used as a cover to protect each well. The locations of the monitoring wells are shown in Figure 35.

### **5.4 Typical Subsurface Stratigraphy**

Figure 36 presents the soil stratigraphy at the model pile test location. This stratigraphy is based on borings NB1, NB2, NB4, NB5, and other borings performed in the vicinity during previous subsurface studies. Figure 37 presents a soil profile based on four borings along the center line of the proposed construction. Referring to Figures 36 and 37, the general soil profile at the model pile test location (from ground surface downward) consists of the following soil strata: 2.44 m (8 ft) of granular fill composed of very dense, brown sand and gravel intermixed with frequent concrete fragments, overlying a thin layer (approximately 0.3 m (1 ft)) of highly compressible organic silt and peat. Below the fill and organics is an approximately 13.72-m- (45-ft-) thick deposit of a marine clay, known as Boston Blue Clay. The clay consists of approximately 2.74 m (9 ft) of medium stiff to very stiff, over-consolidated layer (crust), over 6.10 m (20 ft) of very soft to soft, plastic, normally to slightly over consolidated clay and 4.88 m (16 ft) of soft, plastic, normally consolidated clay. An interbedded deposit of silt, fine sand, and silty clay approximately 2.90 m (9.5 ft) thick underlies the clay. Below this interbedded deposit is a layer of silty sand approximately 2.44 m (8 ft) thick. Another interbedded deposit of silt, fine sand, and silty clay approximately 2.29 m (7.5 ft) thick underlies the silty sand. Below this interbedded deposit is a layer approximately 2.44 m (8 ft) thick of medium dense to dense, fine to medium sand. Underlying the fine to medium sand is a dense glacial till consisting of medium dense to dense, fine to coarse sand and gravel, with traces of silt and rock fragments. Based on the subsurface information within the vicinity of the model pile test location, mylonitic, basalt bedrock underlies the glacial till.

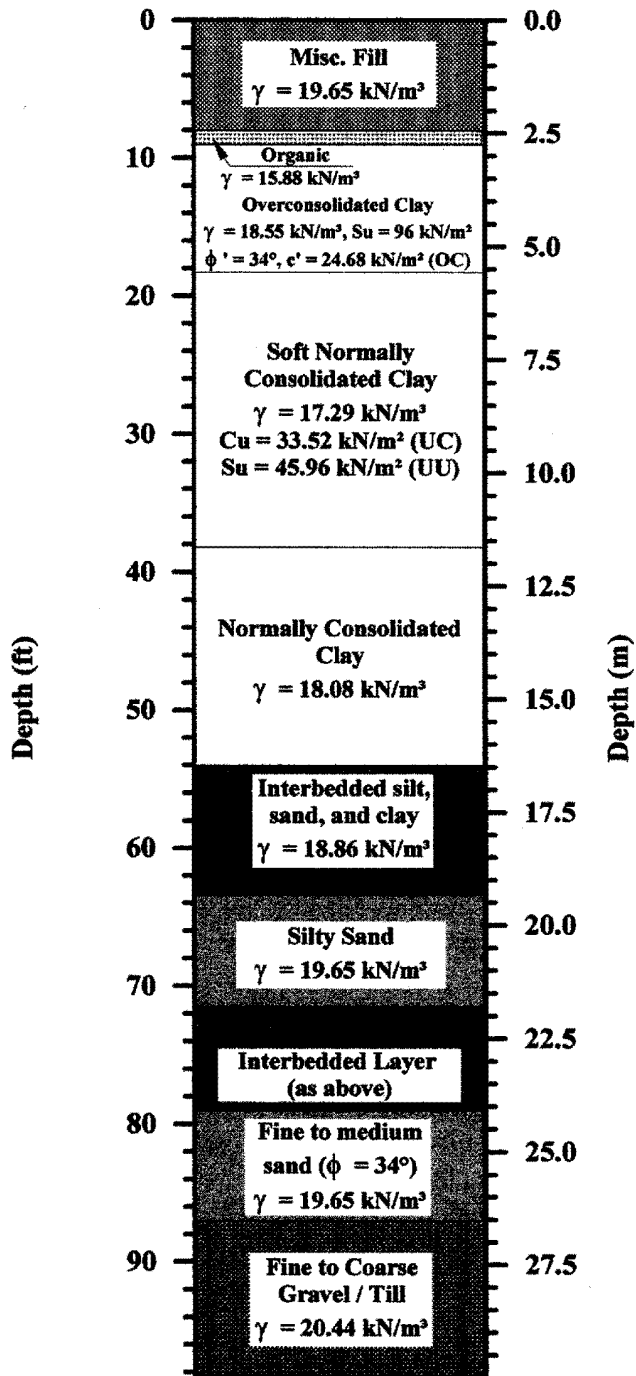


**Figure 36. Representative Soil Stratigraphy at the Newbury MDMP Test Site (Chen, 1997).**

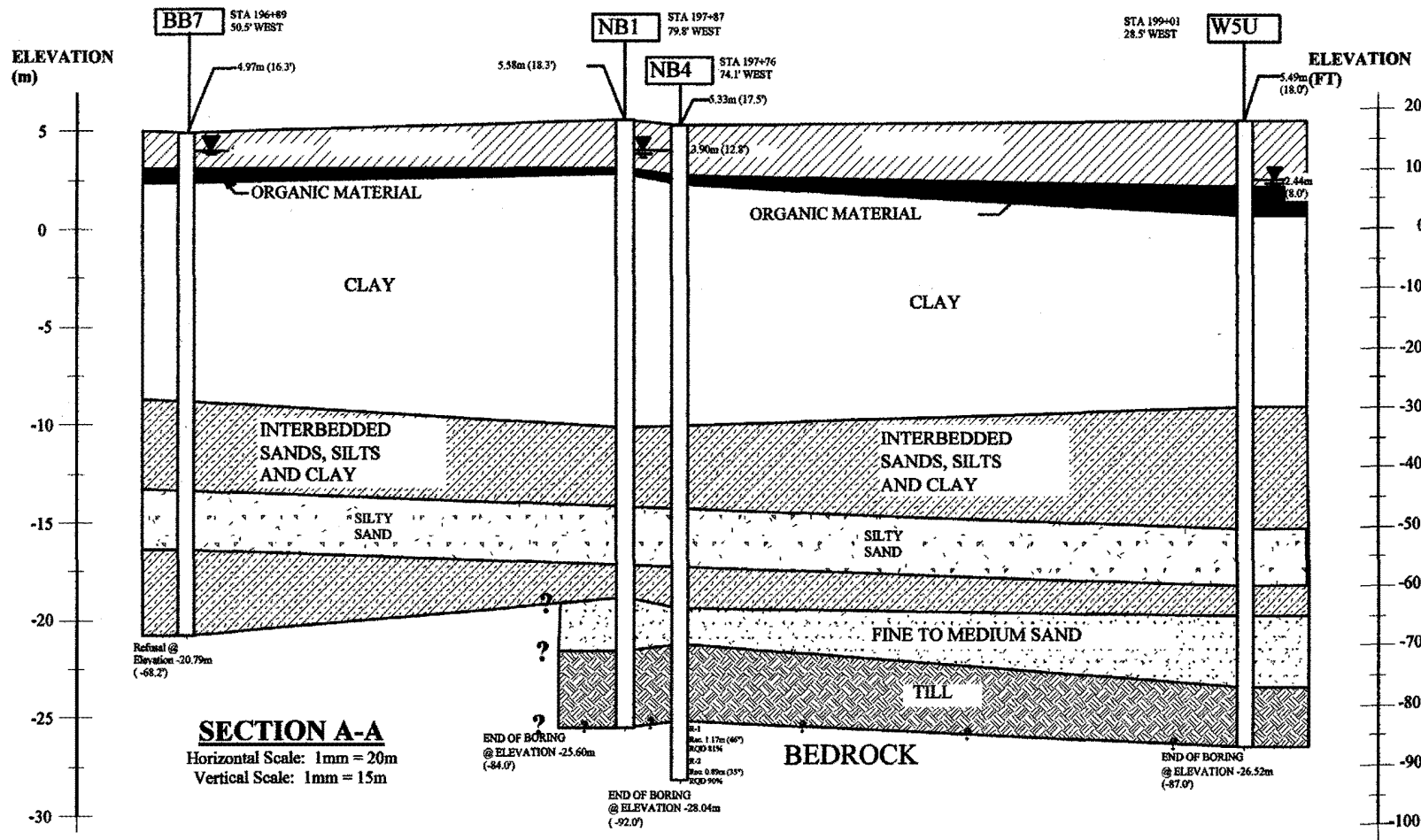
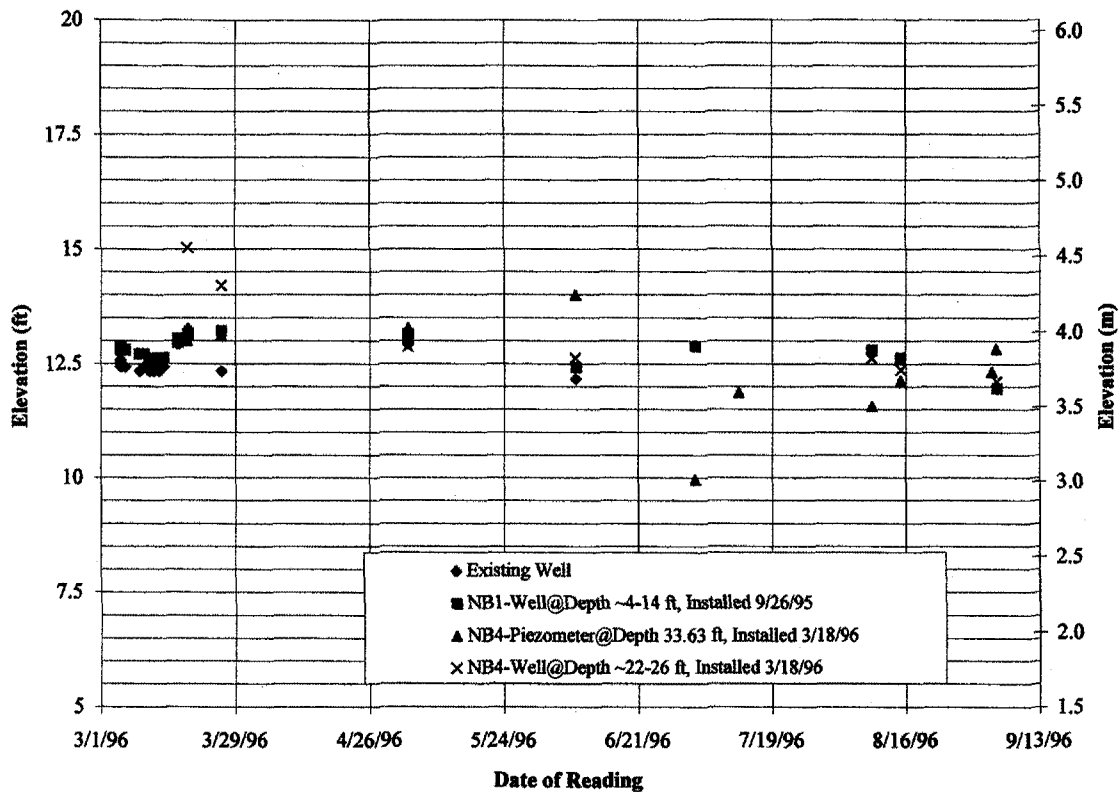


Figure 37. Soil Profile of the Newbury Test Site (North-South).

Groundwater was periodically measured in the monitoring wells near the MDMP test area for the time period between March 5, 1996 and September 4, 1996. Additional measurements carried out at the site will be presented in subsequent reports. Based on these groundwater measurements, a relationship of groundwater elevation versus time is presented in Figure 38.



**Figure 38. Groundwater Elevations at the Newbury Test Site.**

### 5.5 Engineering Properties of the Clay at the Newbury Test Site

Laboratory and field tests are being conducted and analyzed by Yu Lin Chen at the UMass-Lowell and will be presented in subsequent reports. The aim of this study is to determine the soil properties at the Newbury test site. Table 20 presents the preliminary test results of natural water content, Atterberg Limits, unit weight, shear strength based on various methods, sensitivity, and Over Consolidation Ratio (OCR) for the clay layers at the Newbury site. Figure 39 presents the profile of the maximum past pressure with depth in the clay layer. Figure 40 presents a profile of calculated and measured undrained shear strength with depth for the clay layer.

The calculated values are based on preliminary results of Direct Simple Shear (DSS) tests that were performed on samples at depths of 9.37 m (30.75 ft) and 13.03 m (42.75 ft) by Don De Groot of UMass-Amherst. Based on the obtained test results, stress history and normalized soil engineering properties (SHANSEP) (Ladd and Foott, 1974) relationships were developed. For the sample depth of 9.37 m (30.75 ft) the recommended relationship is:

**Table 20. Summary of Soil Properties at the Newbury Site (based on the preliminary test results of Y.L. Chen).**

Soil Properties		Overconsolidated Clay Layer	Soft Normally Consolidated Clay Layer	Normally Consolidated Clay Layer
Depth	(m)	2.74-5.49	5.49-11.58	11.58-16.46
	(ft)	(9-18)	(18-38)	(38-54)
Natural Water Content (%)		21-47	39-51	22-39
Atterberg Limit (%)	PL	20.0-29.1	22.0-27.3	17.5-26.4
	LL	37.0-48.8	37.0-45.2	26.6-44.0
Unit Weight	(pcf)	116-121	107-113.5	112-119
	(kN/m <sup>3</sup> )	18.2-19.0	16.8-17.8	17.6-18.7
Shear Strength	UU Test	60-100 kPa 1253-2089 psf	15-50 kPa 313-1044 psf	15-25 kPa 313-522 psf
	UC Test	N/A	30 kPa 627 psf	N/A
	Torvane	40-210 kPa 835-4386 psf	20-25 kPa 418-522 psf	15 kPa 313 psf
	Pocket Penetrometer	130-375 kPa 2715-7832 psf	45-55 kPa 940-1149 psf	30 kPa 626 psf
Sensitivity	Field Vane Shear Test	N/A	6.87-9.4	9.3
	Lab. Vane Shear Test	N/A	1.1-1.6	2.3-4
Friction angle (°)		34	N/A	N/A
Cohesion (psi / kPa)		3.58 / 24.7	N/A	N/A
Coefficient of Consolidation $c_v$ (cm <sup>2</sup> /min)		0.066	0.06	0.072
Coefficient of Permeability $k_v$ (cm/s)		$5.5 \times 10^{-9}$	$5.0 \times 10^{-9}$	$7.0 \times 10^{-9}$
OCR		2-7	1-1.8	1

Remarks: UU Test — Unconsolidated Undrained Triaxial Test  
 UC Test — Unconfined Compression Test



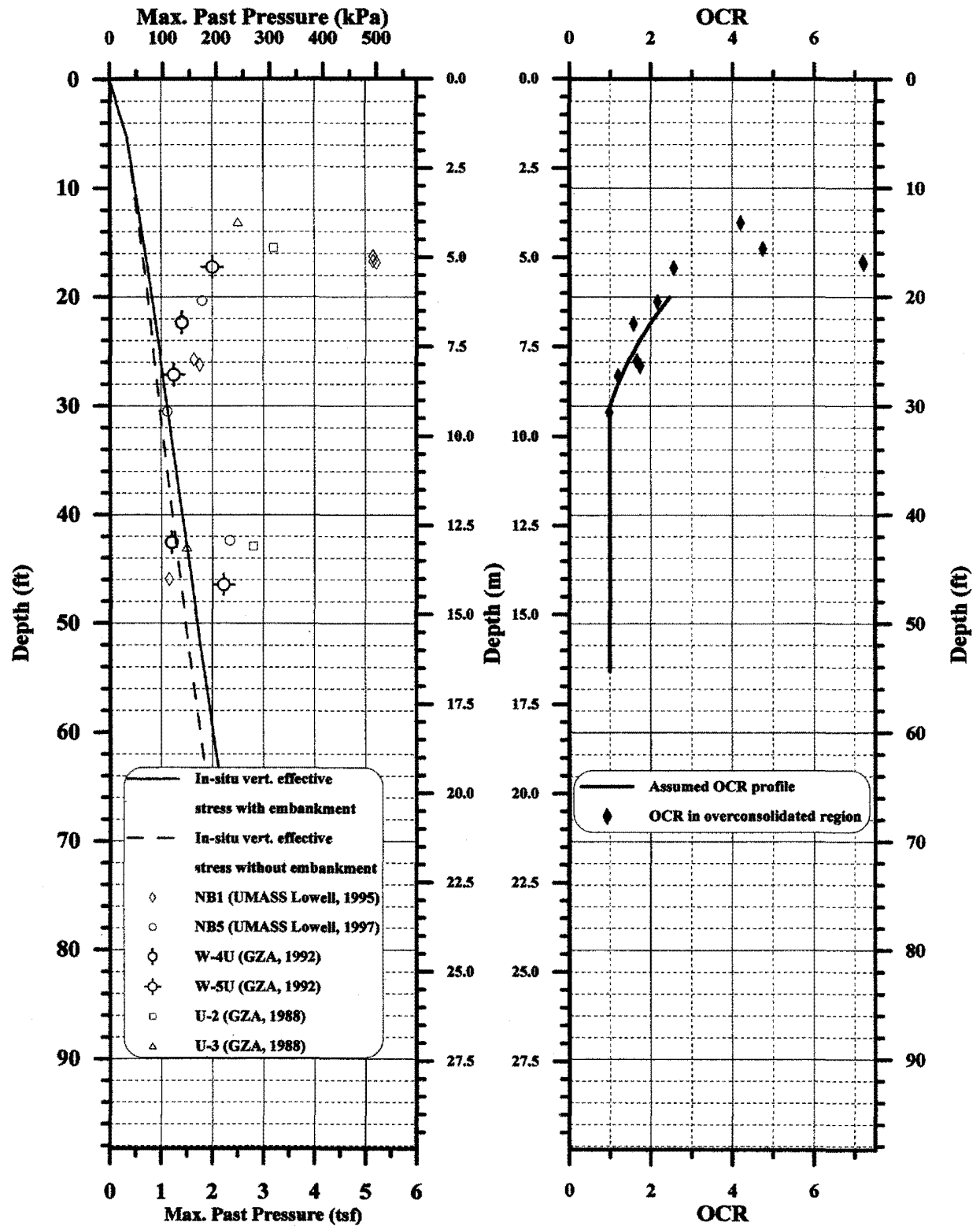


**Figure 39. Profiles of Vertical Effective Stress, Maximum Past Pressure, and OCR at the Newbury Site (Chen, 1997).**

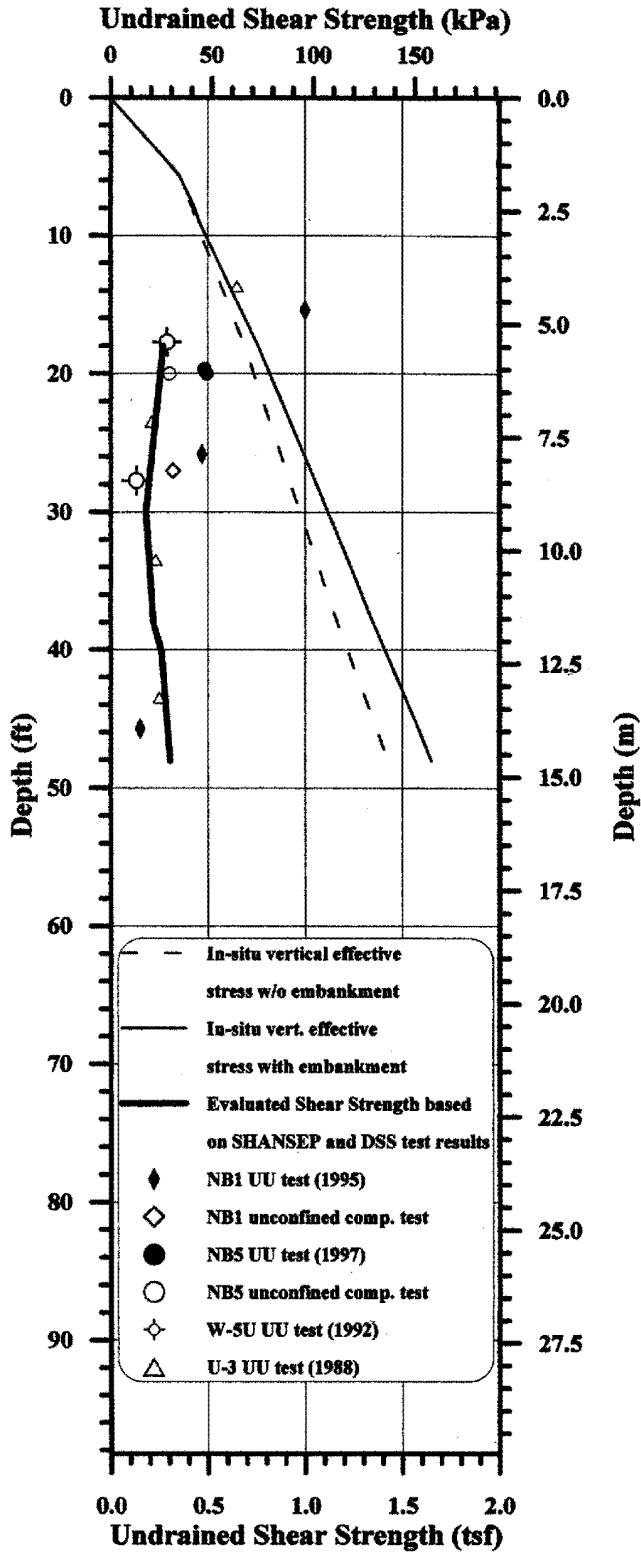


**Figure 40. Profiles of Vertical Effective Stress, and Calculated and Measured Undrained Shear Strength at the Newbury Site (Chen, 1997).**

$$\frac{S_u}{\sigma_v'} = 0.162 * OCR^{0.72} \quad (5.1)$$

For the sample at a depth of 13.03 m (42.75 ft), the recommended relationship is:

$$\frac{S_u}{\sigma_v'} = 0.184 * OCR^{0.72} \quad (5.2)$$

In both cases, the DSS tests at the Newbury Site yielded lower strength parameters than the following typical relationship used for Boston Blue Clay (BBC):

$$\frac{S_u}{\sigma_v'} = 0.20 \pm 0.01 * OCR^{0.72 \pm 0.05} \quad (5.3)$$

Using equation 5.1 as a representative relationship for the soft, normally consolidated clay layer (between depths of 5.49 m (18 ft) and 11.58 m (38 ft)) and equation 5.2 to represent the underlying normally consolidated layer (between depths of 11.58 m (38 ft) and 16.46 m (54 ft)) leads to the calculated undrained shear strength shown in Figure 40. These calculations make use of the OCR values presented in Figure 39. The calculated values in Figure 40 seem to compare well with the laboratory tests, suggesting that the DSS tests and SHANSEP relationship provide a reasonable description of the undrained shear strength of the clay layers at the Newbury test site. For the MDMP test NB2 that was conducted at a depth (to radial stress measurement) of 7.39 m (24.25 ft), the representative soil parameters are  $OCR \approx 1.7$  and  $S_u = 21.3$  kPa (30.9 psi). For the MDMP test NB3 at a depth (to radial stress measurement) of 10.45 m (34.3 ft), the representative soil parameters are  $OCR \approx 1$  and  $S_u = 19.1$  kPa (2.77 psi). Both relationships are based on equation 5.1.

## 5.6 Predicted Behavior of the Multiple Deployment Model Pile

### 5.6.1 Overview

The MDMP's expected behavior was evaluated prior to deployment to determine the range of measurements and to develop a schedule of testing. This assessment "prediction" was based on the findings and methodology presented in an earlier phase of the time-dependent pile capacity research (Paikowsky et al., 1995). The present section provides the details of this evaluation as it pertains to the magnitude of excess pore pressure, time and dissipation rate of the excess pore pressure, and capacity gain rate and time.

### 5.6.2 Estimated Increase in Pore Water Pressure Due to Driving

Figure 41 presents the initial excess pore pressure distribution for clays with an OCR range of 1 to 10 and pore measurement at a distance of 17 radii or more from the pile tip (representing the "shaft" condition along the pile). The data in Figure 41 suggests that the ratio of average initial excess pore pressure to vertical effective stress for a large variety of clays (79 cases) can be estimated to be:

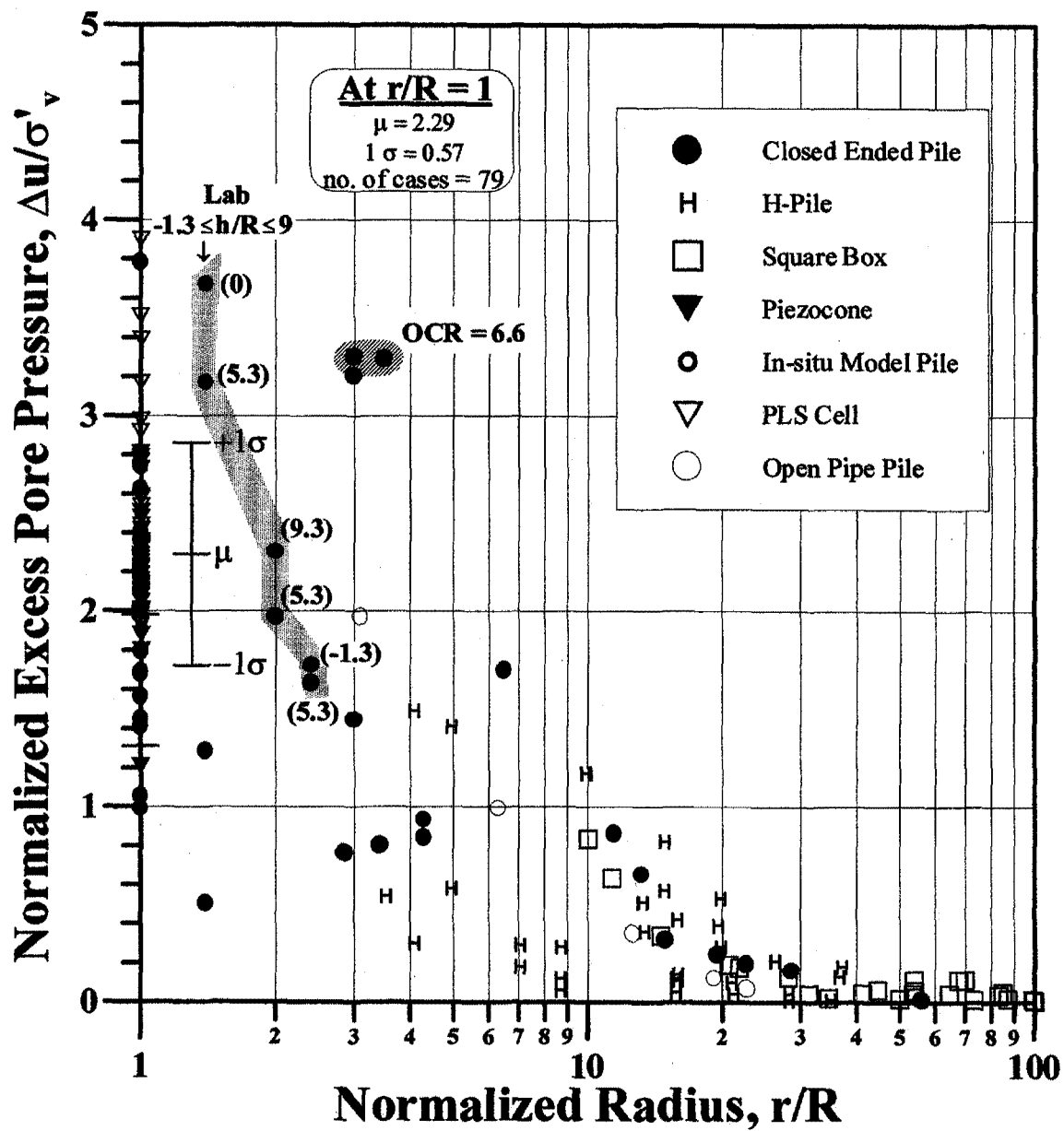


**Figure 41. Initial Excess Pore Pressure Distribution (only readings for  $1 < OCR < 10$  included) (Paikowsky et al., 1995).**

$$\frac{\Delta u_i}{\sigma_v} = 2.29 \pm 0.57 \quad (1 \text{ S.D.}) \quad (5.4)$$

The effect of OCR on the ratio of initial excess pressure can be estimated through the relationship presented in Figure 42.

$$\frac{\Delta u_i}{\sigma_v} = 1.90 + 0.154(\text{OCR}) \quad (5.5)$$

Based on the MDMP installation depths to the pressure transducer and total pressure cell of 7.39 and 10.45 m (24.25 and 34.30 ft), the total and hydrostatic pressures at these depths are 146.85 and 205.21 kPa (21.30 and 29.76 psi) and 57.02 and 87.43 kPa (8.27 and 12.68 psi), respectively. These values lead to a vertical effective stress of 89.83 and 117.78 kPa (13.03 and 17.08 psi) for depth to pressure instruments of 7.39 and 10.45 m (24.25 and 34.30 ft), respectively. Considering equation 5.4, the expected magnitude of the initial pore pressure is 205.71 and 269.72 kPa (29.83 and 39.12 psi). Based on laboratory tests and equation 5.5, the soil at a depth of 7.39 m (24.25 ft) has an  $\text{OCR} \approx 2$  (corresponds to  $\Delta u/\sigma_v' = 2.21$ ), while the soil at a depth of 10.45 m (34.3 ft) has an  $\text{OCR} \approx 1$  (corresponds to  $\Delta u/\sigma_v' = 2.05$ ). Considering equation 5.5, the expected magnitude of the initial pore pressure is 198.34 and 241.92 kPa (28.77 and 35.09 psi).

### 5.6.3 Estimated Time for Excess Pore Water Pressure Dissipation

The MDMP is designed to capture the pore pressure increase due to penetration and the subsequent dissipation of the excess pore pressures. From the data compiled and analyzed by Paikowsky et al., 1995, the rate of pore pressure dissipation can be used to estimate the time required for the excess pore pressure to dissipate. The method presents normalized excess pore pressure relative to the initial excess pore pressure after penetration. When plotted on a semi-log plot, the best fit line from 20% to 80% dissipation represents the linear portion of the curve. The equation of the line is:

$$\frac{\Delta u}{\Delta u_i} = -H_{ut} \log_{10}(t) \quad (5.6)$$

where:  $\Delta u$  = excess pore pressure at any time "t"

$\Delta u_i$  = initial excess pore pressure

$H_{ut}$  = horizontal pore pressure dissipation parameter

t = time after pile driving (seconds)

Utilizing data from the test in Boston Blue Clay, the horizontal pore pressure dissipation parameter,  $H_{ut}$ , is  $0.498 \pm 0.067$ . To reference the rate to time scale, the time at 50% dissipation,  $t_{50}$ , for BBC is  $1.57 \text{ h} \pm 0.334 \text{ h}$ . This data was normalized to a pile with a radius of the PLS cell (equal to 19.177 mm). To correct the time of 50% dissipation to the size of the MDMP with a radius of 38.1 mm, the following equation is used:

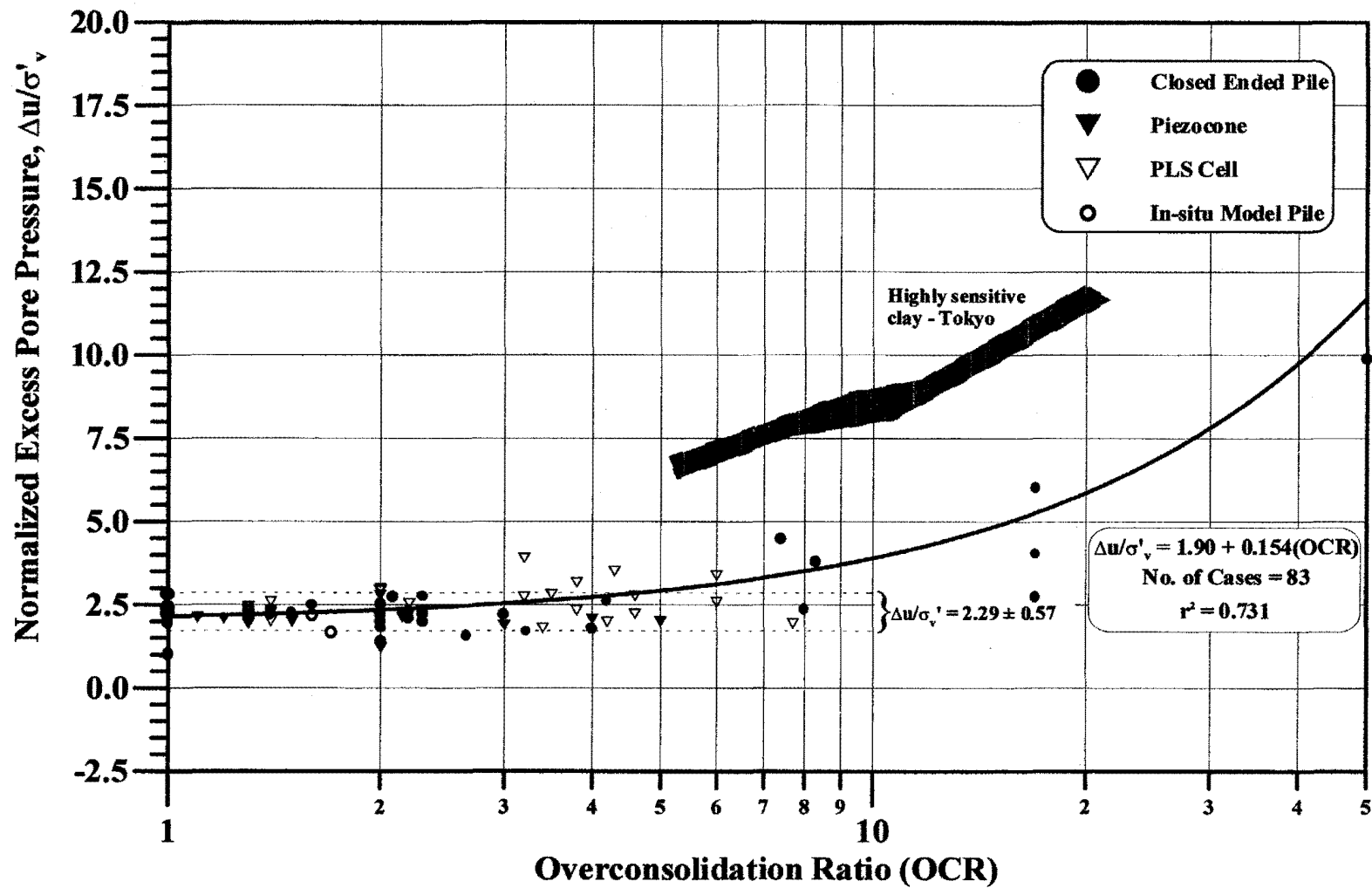


Figure 42. Effects of OCR on  $\Delta u/\sigma'_v$  Along the Shaft ( $h/r \geq 17$ ) for  $r/R = 1$  (Paikowsky et al., 1995).

$$\frac{t_1}{t_2} = \left( \frac{r_1}{r_2} \right)^2 \quad (5.7)$$

where:  $t_1$  = elapsed time since driving adjusted to a standardized pile size  
 $t_2$  = actual time since driving for a known pile  
 $r_1$  = radius of standardized pile  
 $r_2$  = radius of a known pile

Substituting the geometrical relationships of the PLS cell and the MDMP into equation 5.7 leads to:

$$t_{\text{PLS}} = \left( \frac{r_{\text{PLS}}}{r_{\text{MDMP}}} \right)^2 t_{\text{MDMP}} = \left( \frac{19.177 \text{ mm}}{38.1 \text{ mm}} \right)^2 t_{\text{MDMP}} = (0.253)t_{\text{MDMP}} \quad (5.8)$$

The adjusted time to 50% dissipation of the excess pore pressure around the MDMP is therefore  $t_{50} = 6.21 \pm 1.32$  h. Using the range of  $t_{50}$  and the average dissipation rate of  $H_{\text{ut}} = 0.498$  leads to the estimated range of dissipation time presented in Figure 43. According to the obtained relations, 80% of the excess pore pressure will dissipate after about 25 h, with a possible range (based on 1 S.D.) between 18 and 35 h.

#### 5.6.4 Estimated Time for Capacity Gain

In order to assess the rate of capacity gain, Paikowsky et al. (1995) obtained the relationship between the ratio of the pile capacity to the maximum capacity over time. These relationships allow the prediction of the pile capacity gain with time using a process similar to that used for the prediction of the pore pressure dissipation with time.

The estimation of the time required for the MDMP capacity gain is based on the following relationship between the rate of gain and the normalized capacity:

$$\frac{R_{s(t)}}{R_{s \text{ max}}} = C_{\text{gt}} \log_{10}(t) \quad (5.9)$$

where:  $R_{s(t)}$  = pile shaft capacity at any time "t" after driving  
 $R_{s \text{ max}}$  = maximum pile shaft capacity  
 $C_{\text{gt}}$  = parameter representing the rate at which the pile gains capacity  
 $t$  = time after pile driving (hours)

The data on which  $C_{\text{gt}}$  is based requires the measurement of capacity with time after driving, which is difficult to obtain. The correct relationship of equation 5.9 should be based on the skin friction at a zone along the pile for which the assumption of radial consolidation is valid. While these values are measured by the MDMP, they were not readily available for many cases.

Therefore, the  $C_{\text{gt}}$  parameter evaluation was carried out in the following ways:

- (1) Based on data related to the total pile capacity:  $C_{\text{gt}} = 0.389 \pm 0.119$  (1 S.D.) (for 15 cases).
- (2) Based on data related to the friction along the pile:  $C_{\text{gt}} = 0.356 \pm 0.088$  (1 S.D.) (for 17 cases).

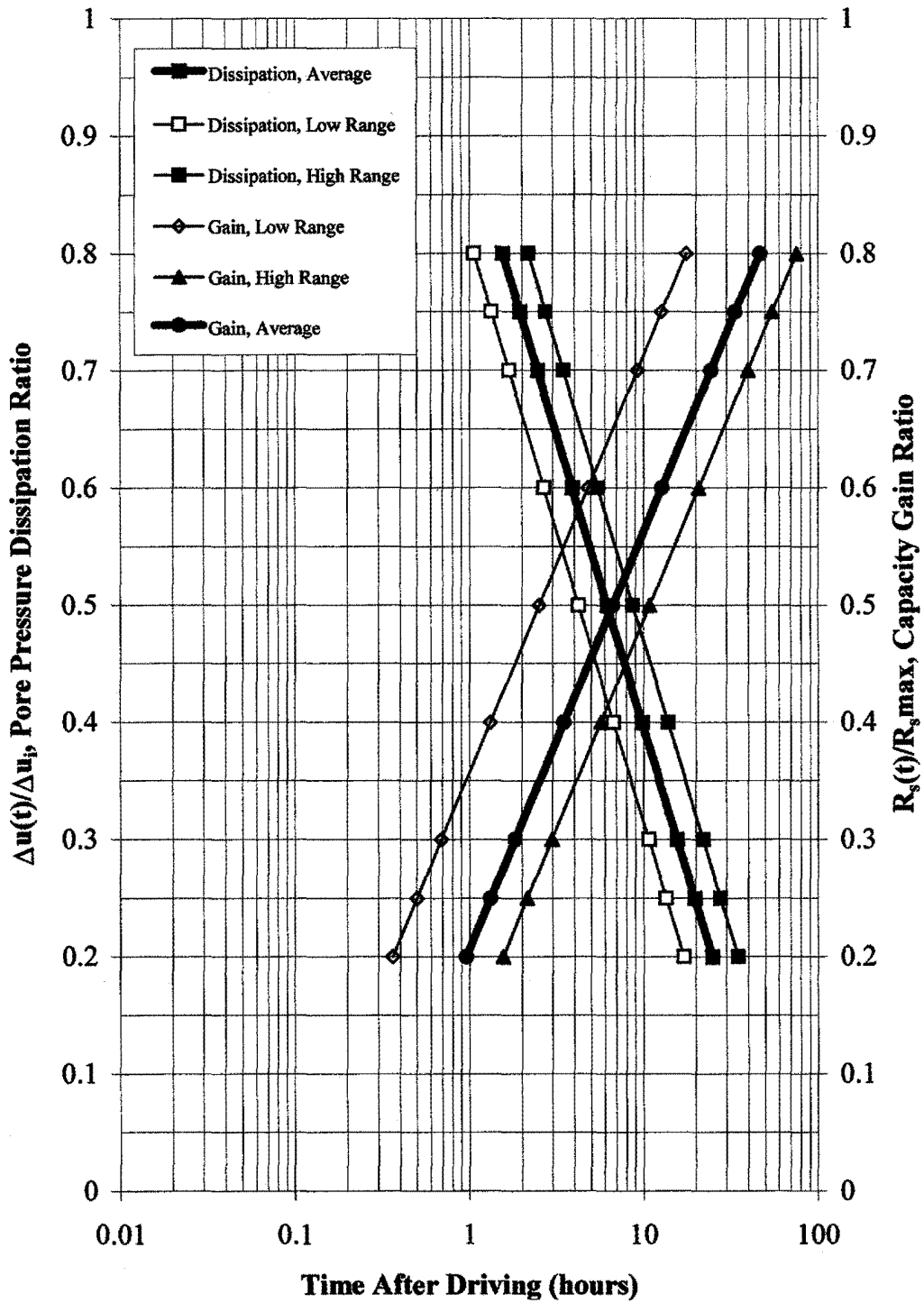


**Figure 43. Predicted Pore Pressure Dissipation and Capacity Gain for the MDMP at the Newbury Site.**



The values used for evaluation of the MDMP are based on the average from all data where  $C_{gt} = 0.367 \pm 0.096$  (for 39 cases).

In order to align the dissipation rate to a specific time, the time to 75% capacity gain was used by Paikowsky et al. (1995). This time was found to be:

- (1) Based on data related to the total pile capacity:  $t_{75} = 385.0 \pm 226.3$  h (1 S.D.) (for five cases).
- (2) Based on data related to the friction along the pile:  $t_{75} = 539.5 \pm 336.2$  h (1 S.D.) (for 12 cases).

The values used for evaluation of the MDMP are based on the data when measurements of friction along the shaft of the pile were analyzed, where  $t_{75} = 539.5 \pm 336.2$  h (for 12 cases). These times are all related to a 30.48-cm- (12-in-) diameter pile. Equation 5.7 can be used to adjust  $t_{75}$  to the MDMP size as shown in equation 5.10:

$$t_{30.48 \text{ cm}} = \left( \frac{r_{30.48 \text{ cm}}}{r_{\text{MDMP}}} \right)^2 t_{\text{MDMP}} = \left( \frac{152.4 \text{ mm}}{38.1 \text{ mm}} \right)^2 t_{\text{MDMP}} = (16)t_{\text{MDMP}} \quad (5.10)$$

The resulting value of  $t_{75} = 33.7 \pm 21.0$  (1 S.D.) hs was used to develop Figure 43.

The relationship shown in Figure 43 is based on  $C_{gt} = 0.356$  and  $t_{75} = 33.7 \pm 21.0$  h (1 S.D.). This suggests that 80% of the MDMP maximum frictional capacity will be obtained about 47 h after driving, with a possible range of 17.6 to 75.6 h.

## 5.7 MDMP Testing Procedure

### 5.7.1 Overview

The MDMP testing program was conducted during March 1996. The tests were conducted at the locations marked as NB2 and NB3 (adjacent to the location of boring NB1) as shown in Figure 35. The drilling, installation, and removal of the MDMP were carried out with the assistance of New Hampshire Boring, Inc., of Londonderry, New Hampshire.

Personnel and Data Acquisition Systems were housed in a tent supplied by the Army Research Labs in Natick, MA. A kerosene heater was used to keep the equipment above freezing temperatures. Power was supplied via two portable generators. Major weather variations took place during the testing, including 0.61 m (2 ft) of snow in the first week of testing, followed by rapid snow melt. Figure 44 presents three photographs depicting the general layout of the site. Figure 44a shows the site as equipment was delivered and the DAS was assembled in the tent. Figure 44b was taken during a snowstorm while the drill rig was in place over NB4. The blue structure attached to the drill rig was temporary protection around the static load frame during MDMP test NB2. Figure 44c shows the static load frame with the independent reference beam.

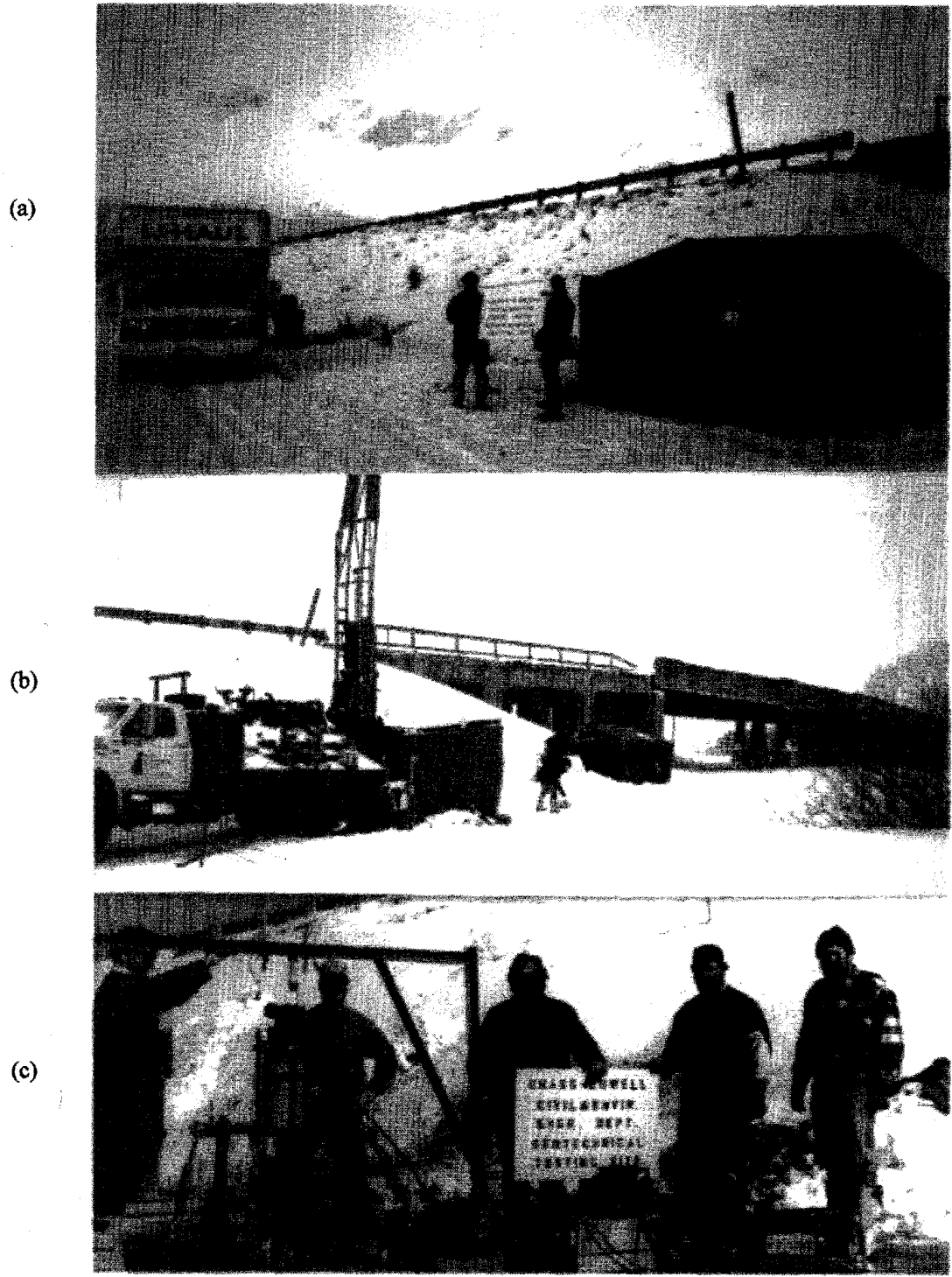


**Figure 44. Site Layout During MDMP Tests at the Newbury Site: (a) Initial Setup, (b) During Snowstorm, and (c) Static Load Test.**

The purpose of the testing program was to measure the excess pore pressure dissipation, the gain of capacity with time, and soil and pile responses during installation and removal. The tests at the Newbury site were conducted in the soft to medium normally consolidated clay, representing easy driving conditions. Although the MDMP was designed to be advanced to any desired depth using drill rods, the test hole was cased to the bottom of the drill rods, ensuring that soil friction did not develop along the rods. Figure 45 shows the steps of a typical MDMP installation and testing performed at the Newbury site.

### **5.7.2 General Test Plan**

The first step involved drilling a vertical 10.16-cm- (4-in-) diameter cased hole through the fill region to approximately 3.05 m (10 ft) below the ground surface. Next, four helix anchors for the static load test frame were installed. Due to existing concrete outwash in the fill, it was necessary to pre-auger holes, place the four anchors, and then backfill with ready-mix concrete to secure the anchors. Drilling was then continued through the stiff upper clay. Split-spoon samples were gathered in the stiff clay as drilling proceeded to determine the transition zone from the stiff yellow desiccated overconsolidated clay to the soft to medium blue clay. The transition was identified approximately 5.49 m (18 ft) below the ground surface. The casing was then driven and washed out to a depth of 6.25 m (20.5 ft) below the ground surface.

The 61-m (200-ft) instrumentation cable was threaded through the drill rods. The rods were attached to the MDMP and lowered into the cased hole. The top of the drill rod was instrumented with strain gauges and accelerometers as part of the dynamic measurements. The borehole was completely filled with water and the MDMP was held in place in order to stabilize the temperature of the instrumentation and check the data acquisition system.

The MDMP was then driven with a 0.623-kN (140-lb) safety hammer (see Figure 46a). The PDA was used to measure the force and velocity in the rods at the surface and inside the MDMP during driving. The initial hammer stroke was 15.2 cm (6 in) and was increased to 30.5 cm (12 in) and then again to 45.7 cm (18 in) after inspection of the stresses measured by the PDA. The driving stresses were kept between approximately 138 and 207 MPa (20 and 30 ksi) to avoid damage to the MDMP sensors. Driving continued until the entire instrumented section of the MDMP was driven deep enough into the clay and the top of the drill rods reached the level required to attach the pile to the static load frame. Monitoring of the MDMP during driving was accomplished with an additional Pile-Driving Analyzer on loan from the Federal Highway Administration.

A 222.4-kN (50,000-lb) load cell was attached between the drill rod string and the drill rig connection. Two displacement transducers were fixed to a reference beam and positioned to measure the vertical movement at the top of the drill rod string. The initial static load test was completed with the drill rig applying the loading force at a slow rate.

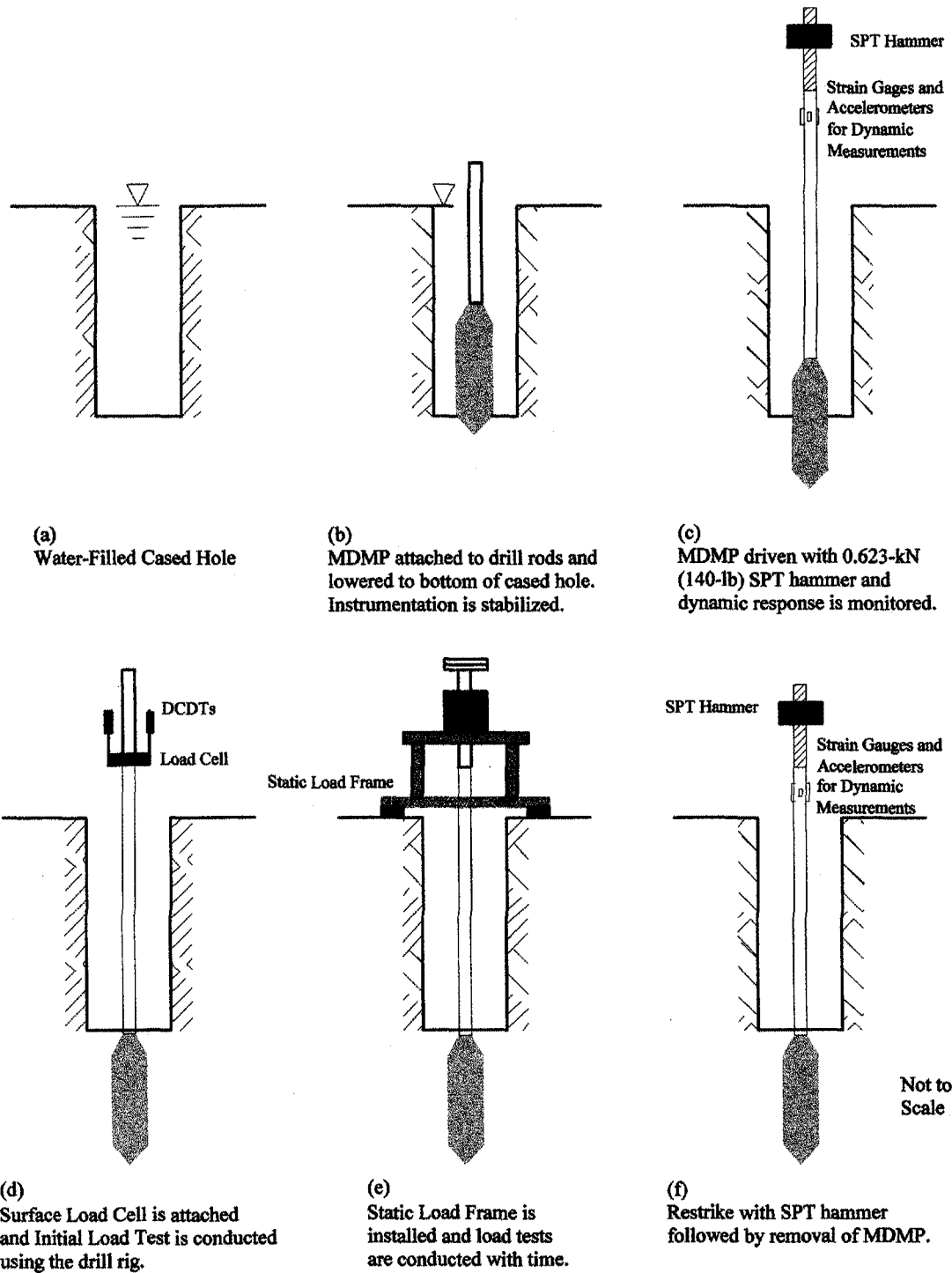


**Figure 45. Steps for Installation and Testing of the MDMP at the Newbury Site.**

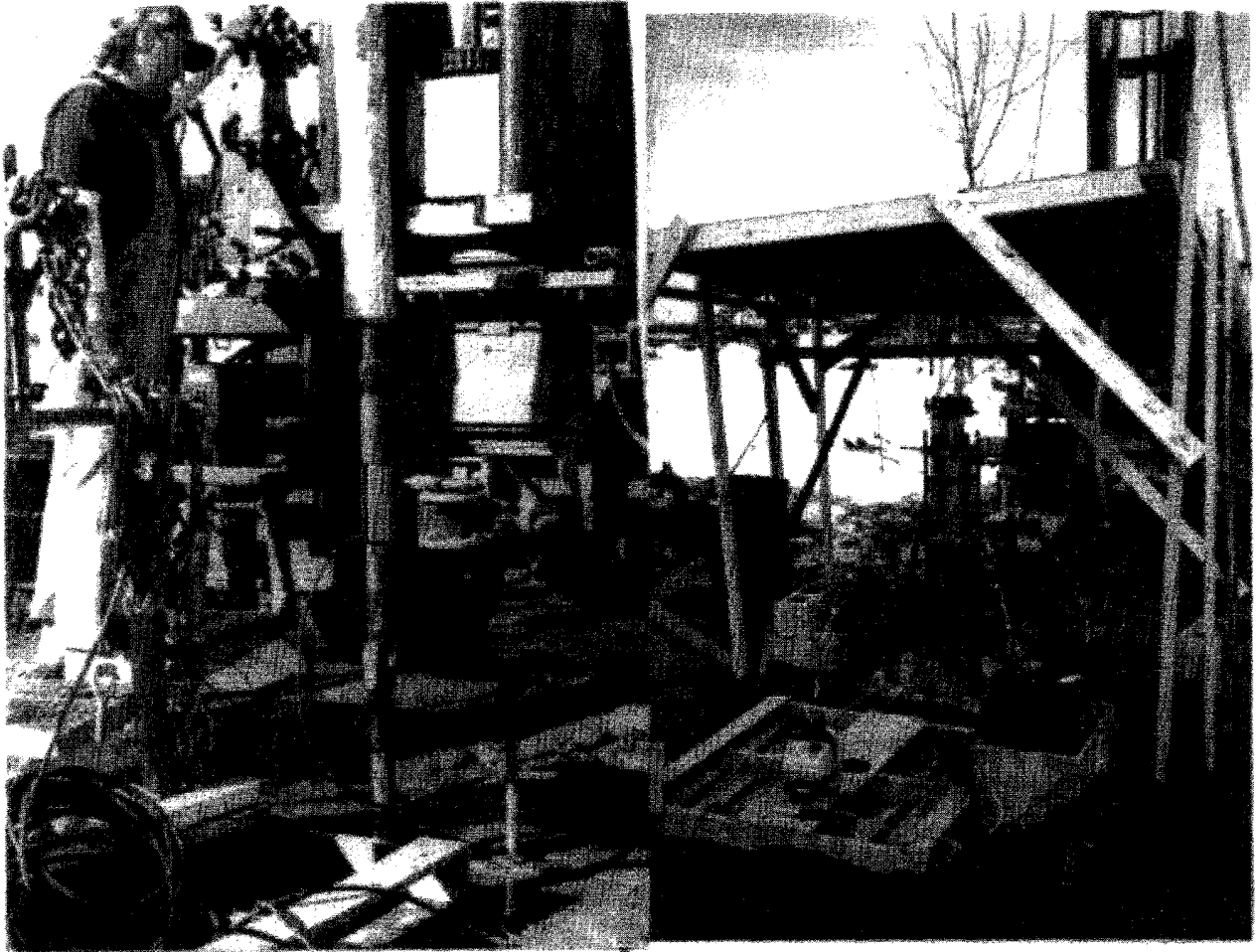
The assembled static load frame was lifted in place, screwed to the anchors, and attached to the MDMP (see Figures 46a and b). Several static load tests were conducted with increasing time intervals between tests. Each load test was performed in tension at a near constant load rate for a predetermined amount of displacement (usually 12.5 mm). The intervals between static load tests were determined as the test progressed to assess the gain of capacity with pore pressure dissipation. A final load test was performed when the excess pore pressure due to installation had dissipated. The final load test consisted of a series of rapid cyclic loading and unloading cycles to determine the pile capacity independent of the strain rate. Before the removal of the MDMP, the pile was driven again (restrike) and dynamic measurements were recorded with two PDAs.

For both MDMP tests NB2 and NB3, measurements of force, displacement, total lateral pressure, and pore pressure were recorded continuously by the HP DAS after the pile had been successfully driven. During driving and restrikes, two PDAs were used to monitor the three internal load cells and accelerometers, and the additional strain gauges and accelerometers at the top of the drill rods. The total lateral pressure and pore pressure were also recorded by the HP DAS during driving and restrikes.

### ***5.7.3 Testing Procedure for the MDMP During Test NB2***

On March 6, 1996, the first of two model pile tests was conducted at the Newbury site. A borehole was washed and cased to a depth of 6.25 m (20.5 ft) below ground surface. The MDMP was inserted into the cased hole and came to rest so that the tip was 6.50 m (21.34 ft) below the ground surface. The PDA gauges were attached and the MDMP was allowed to stabilize for 1 h and 5 min. A safety hammer was used to install the MDMP with an increasing stroke of 15.2, 30.5, and 45.7 cm (6, 12, and 18 in). During driving, the pile penetrated a total of 2.57 m (8.42 ft) in 8.78 min. The initial load test using the drill rig started at 25.23 min after the start of driving. The pile was pushed 53.1 mm (2.09 in) to ensure that the slip joint was completely closed, and then pulled in two steps for a total 133.9 mm (5.27 in) until the slip joint was completely open. At the end of the tension load test, the slip joint immediately collapsed under the self-weight of the pile when the pile was disconnected from the drill rig. Forty minutes after the start of driving, the MDMP was pushed approximately 15.2 cm (6 in) to allow proper attachment with the hydraulic ram and static load frame. At this point, the static load frame was moved into place and the pile was connected. During the connection process, some unrecorded displacement may have taken place. Once the static load frame was properly attached, the MDMP tip was at a depth of 9.31 m (30.56 ft) below ground surface.

For approximately the next 6 days, the MDMP was continuously monitored using the HP DAS. Eleven static tension load tests were performed using the static load frame. Table 21 shows the time, displacement, and rate of movement for all tests. Following load test #11, the final load test was performed 137.7 h after the start of installation. The final load test consisted of a series of alternating compression tests to failure, followed by tension tests to decrease the load at the top of the pile to approximately zero. Table 22 shows the time, duration, delay between each movement, displacement, and average displacement rate of all of the tests in the final load test sequence.



(a)

(b)

**Figure 46. (a) MDMP Being Driven and (b) Static Load Frame Assembled.**

**Table 21. The MDMP Static Load Tests During Test NB2.**

Testing Stage	Type of Test	Time After Start of Driving (hours)	Displacement (mm (inches))	Duration of Displacement (seconds)	Average Displacement Rate (mm/second)
Initial Load Test	Compression	0.4206	53.09 (2.09)	26.70	1.988
	Tension	0.4396	70.36 (2.77)	67.28	1.0458
	Tension	0.4686	63.50 (2.50)	61.90	1.0258
Load Test #1	Tension	1.7246	18.80 (0.74)	31.70	0.5931
	Tension	1.7658	17.27 (0.68)	28.62	0.6034
Load Test #2	Tension	3.0054	17.78 (0.70)	30.38	0.5853
Load Test #3	Tension	5.6973	18.80 (0.74)	34.11	0.5512
Load Test #4	Tension	9.0117	17.53 (0.69)	30.70	0.5710
Load Test #5	Tension	14.6632	13.21 (0.52)	23.29	0.5672
Load Test #6	Tension	20.6594	15.24 (0.60)	27.97	0.5449
Load Test #7	Tension	27.6417	13.21 (0.52)	24.01	0.5502
Load Test #8	Tension	37.7386	10.92 (0.43)	19.73	0.5535
Load Test #9	Tension	46.5802	11.94 (0.47)	20.52	0.5819
Load Test #10	Tension	90.8731	13.97 (0.55)	24.98	0.5592
Load Test #11	Tension	118.6351	5.59 (0.22)	9.36	0.5972
Final Load Test	Cyclic	137.709	see Table 22		

**Table 22. The MDMP Final Loading Sequence During Test NB2.**

Type of Movement	Time at Start of Movement (hours)	Duration Of Movement (seconds)	Delay Before Next Movement (seconds)	Displacement (mm (inches))	Average Displacement Rate (mm/second)
Push	137.709	772.92	76.68	80.47 (3.168)	0.1041
Pull	137.945	17.64	56.88	0.3556 (0.014)	0.02016
Push	137.9657	223.2	7.2	18.97 (0.747)	0.08499
Pull	138.0297	11.16	366.84	1.201 (0.0473)	0.1076
Push	138.1347	299.88	3.6	20.35 (0.801)	0.06786
Pull	138.219	5.4	361.44	0.8509 (0.0335)	0.1576
Push	138.3209	336.96	3.6	21.39 (0.842)	0.06348
Pull	138.4155	11.88	443.88	0.5232 (0.0206)	0.04404
Push	138.5421	268.20	2.52	14.76 (0.581)	0.05503
Pull	138.6173	18.00		0.4623 (0.0182)	0.02568

Following the final sequence of static load tests, a restrrike test was performed. The pile was driven 40.64 cm (16 in) using a 45.7-cm (18-in) stroke. The pile was then removed from the borehole utilizing the safety hammer to "bump up" the MDMP and drill rods to break soil resistance. A cake of clay was observed around the pile equal to the I.D. of the casing. When the clay cake was removed, the porous stones were missing. However, the soil did not appear to have entered the ducts that connect the porous stone cavity to the pressure transducer.

During the installation of the pile, damage occurred to the load cell at the tip of the MDMP. This was evident by the increasing load measured during the entire time the pile was in place. After examining the load cell, one of the strain gauges was found to be damaged. The total pressure cell was also damaged at some point during the test, most likely during the removal of the MDMP.

#### **5.7.4 Testing Procedure for the MDMP During Test NB3**

On March 13, 1996, the second of the two model pile tests was conducted at the Newbury Site. The same borehole used in the first test was washed and cased to a depth of 9.30 m (30.5 ft) below ground surface. The MDMP was inserted into the cased hole with its tip resting at 9.58 m (31.42 ft) below the ground surface. The PDA gauges were attached and the MDMP was allowed to stabilize for 1 h and 42 min. A safety hammer was used to install the MDMP using a stroke of 45.7 cm (18 in). During driving, the pile penetrated a total of 2.23 m (7.33 ft) in 5 min. Six additional blows were required to set the pile to the final depth for attachment to the static load frame. The initial load test, utilizing the drill rig, started 21.52 min after the start of driving. The pile was pushed 97.5 mm (3.84 in) to ensure that the slip joint was completely closed. At this point, the static load frame was installed and the pile was connected to the hydraulic ram. The connection process was changed to limit displacement that occurred during the first testing sequence. The new connection procedure involved attaching the loading rod to the drill rod string and then moving the ram up enough to bolt the loading rod to the ram. Unfortunately, there was slack between the loading rod and the hydraulic ram because of problems encountered in leveling the static load frame. This may have caused the erroneous displacement measurement observed during load test #1. Another factor that may have affected this reading is that the two DCDTs at the pile head may not have been properly secured to the reference beam. After load test #1 was completed, the MDMP tip was at a depth of 12.3 m (40.42 ft) below ground surface.

For approximately the next 5 days, the MDMP was continuously monitored using the HP DAS. Nine static tension load tests were performed using the static load frame. Table 23 shows the time, displacement, and rate of movement for all nine static load tests. Following load test #9, the final load test was performed 119.4 h after the start of installation. The final load test consisted of a series of alternating compression tests to failure, followed by tension tests to decrease the load at the top of the pile to approximately zero. Table 24 shows the time, duration, delay between each movement, displacement, and average displacement rate of all of the tests in the final load test sequence.

After the entire sequence of static load tests, a restrrike test was performed on the MDMP with the 0.623-kN (140-lb) safety hammer. The pile was driven 1.22 m (4 ft) using a 45.7-cm (18-in) stroke. The pile was then removed from the borehole utilizing the safety hammer to "bump up" the MDMP and drill rods to break soil resistance. A cake of clay was observed around the pile equal to the I.D. of the casing.

The porous stones did not fall out this time since thicker stones (10.2 mm) were used during the second test. The stones were approximately 5.1 mm thick in the first test. The lower load cell and total pressure cell did not function properly during any part of the second test.



**Table 23. The MDMP Static Load Tests During Test NB3.**

Testing Stage	Type of Test	Time After Start of Driving (hours)	Displacement (mm (inches))	Duration of Displacement (seconds)	Average Displacement Rate (mm/second)
Initial Load Test	Compression	0.3587	97.49(3.84)	30.48	3.20
Load Test #1	Tension	0.9991			
Load Test #2	Tension	2.7551	11.48(0.452)	20.54	0.559
Load Test #3	Tension	7.4190	9.66(0.380)	17.24	0.560
Load Test #4	Tension	14.8429	9.40(0.370)	33.50	0.281
Load Test #5	Tension	25.7109	10.31(0.406)	15.70	0.657
Load Test #6	Tension	42.0963	9.54(0.376)	17.74	0.538
Load Test #7	Tension	52.3560	9.25(0.364)	36.47	0.254
Load Test #8	Tension	73.9952	10.92(0.430)	20.49	0.533
Load Test #9	Tension	94.9156	9.07(0.357)	15.48	0.586
Final Load Test	Cyclic	119.3636	See Table 24		

**Table 24. The MDMP Final Loading Sequence During Test NB3.**

Type of Movement	Time at Start of Movement (hours)	Duration of Movement (seconds)	Delay Before Next Movement (seconds)	Displacement (mm (inches))	Average Displacement Rate (mm/seconds)
Push	119.3636	728.64	0	76.78 (3.023)	0.1054
Pull	119.566	11.52	358.20	0.676 (0.0266)	0.0587
Push	119.6687	255.96	4.68	20.12 (0.792)	0.0786
Pull	119.7411	6.12	856.44	0.932 (0.0367)	0.152
Push	119.9807	118.08	2.16	12.42 (0.489)	0.105
Pull	120.0141	12.6	261.72	1.095 (0.0431)	0.0869
Push	120.0903	123.84	6.84	17.45 (0.687)	0.141
Pull	120.1266	10.08		1.270 (0.050)	0.126



## CHAPTER 6. NEWBURY SITE TEST RESULTS

### 6.1 Pore Pressure Measurements

#### 6.1.1 Overview

The pore pressure measurements were recorded throughout the entire tests. The data were assembled into a spreadsheet and a calibration factor of 48.7146 kPa/V (7.0652 psi/V) was applied to the raw data (see Appendix D for the pressure gauge calibration). The zero voltages of 1.600216 and 1.539500 V were determined in the field before the pile driving of tests NB2 and NB3, respectively. Initial measurements were taken while the pile was standing in the water-filled borehole and the accuracy of the measurement was determined based on the known head. The temperature was below freezing during both installation periods. The glycerin/water mixture was effective and the liquid did not freeze.

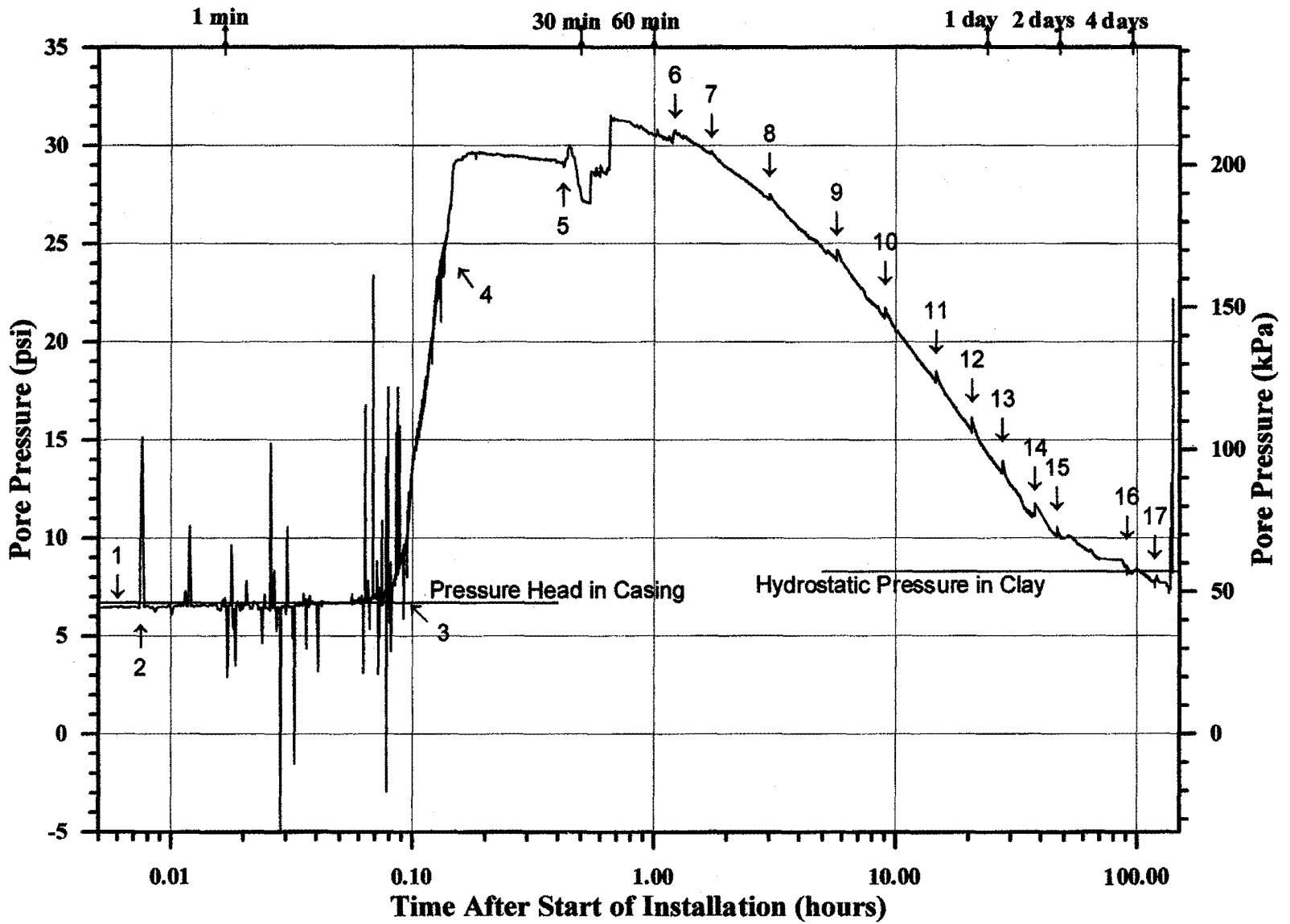
#### 6.1.2 Pore Pressure Results for the MDMP Test NB2

The measured pore pressure is presented in Figures 47 and 48, versus logarithmic and linear time scales, respectively. Table 25 provides the codes identifying the events during the test as marked in the figures. Figure 47 shows that before driving, while the pile is standing in the cased water-filled borehole, the measured pressure is 44.54 kPa (6.46 psi). Based on 4.70 m (15.41 ft) of head, the expected pressure is 46.06 kPa (6.68 psi). This difference in pressures corresponds to a 3.3% or approximately 150-mm (6-in) head and may be due to a falling head as water drained from the borehole. From Figure 48, it is apparent that the excess pore pressure has almost completely dissipated by the end of the test (approximately 90 h after the start of installation). The measured pore pressure at the end of the dissipation period was 51.02 kPa (7.4 psi). As indicated in Figure 38, the groundwater table at the site varies possibly due to a gradient toward the surrounding lower wetlands. The range of hydrostatic pressure at the site during the monitoring period of March 5 to March 26, 1996 was 55.92 kPa (8.11 psi) to 58.68 kPa (8.51 psi) (3.76 m (12.33 ft) to 4.04 m (13.25 ft) National Geodetic Vertical Datum (NGVD)). The average groundwater elevation for that period is 3.87 m (12.69 ft) NGVD, resulting in an expected hydrostatic pressure at the end of the test of 57.02 kPa (8.27 psi).

**Table 25. Legend of Events for Pore Pressure Build-Up and Dissipation With Time for Model Pile Test NB2 (see Table 21 for a time schedule).**

1	Model Pile is in cased borehole	11	Load Test #5, using the Static Load Frame
2	Start of Driving	12	Load Test #6, using the Static Load Frame
3	Pore Pressure Cell penetrates soil	13	Load Test #7, using the Static Load Frame
4	End of Driving	14	Load Test #8, using the Static Load Frame
5	Initial Load Test using the Drill Rig	15	Load Test #9, using the Static Load Frame
6	Model Pile attached to the Static Load Frame	16	Load Test #10, using the Static Load Frame
7	Load Test #1, using the Static Load Frame	17	Load Test #11, using the Static Load Frame
8	Load Test #2, using the Static Load Frame	18	Final Load Test, using the Static Load Frame
9	Load Test #3, using the Static Load Frame	19	Restrike and Removal of Model Pile
10	Load Test #4, using the Static Load Frame		

Figure 47. Pore Pressure Build-Up and Dissipation With Time for Model Pile Test NB2.



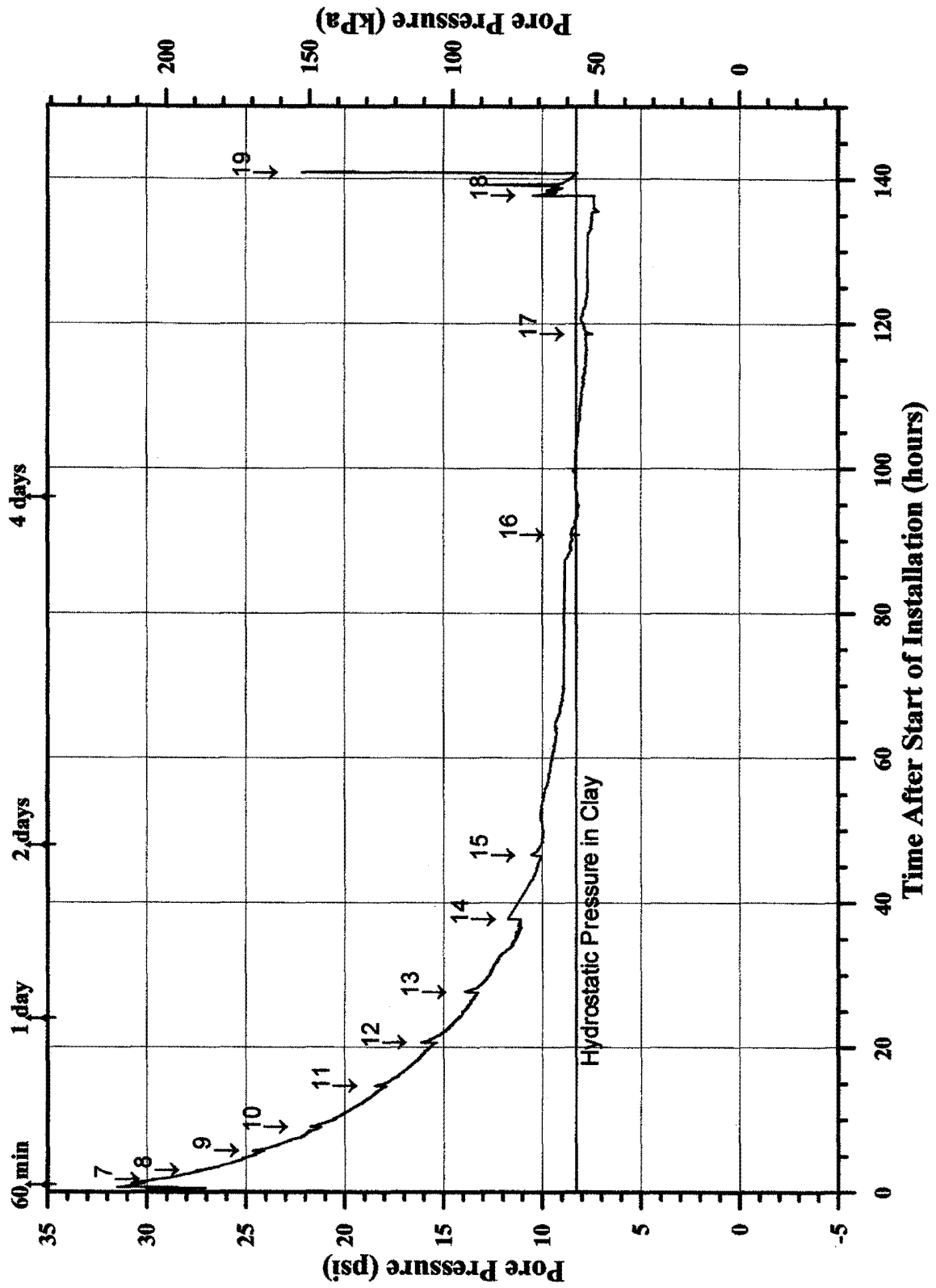


Figure 48. Pore Pressure Build-Up and Dissipation With Time for Model Pile Test NB2.

The maximum pore pressure following the completion of driving was 201.3 kPa (29.2 psi). After the initial load test, the pile was pushed approximately 150 mm (6 in) to allow proper connection to the static load frame. As a result, the pore pressure increased to 217.3 kPa (31.5 psi).

### 6.1.3 Pore Pressure Results for the MDMP Test NB3

The pile was removed at the conclusion of test sequence NB2 and the porous stones were missing. The MDMP was transported back to UMass-Lowell Geotechnical Laboratories, where the porous stones were replaced on March 12, 1996. The pore pressure element had been de-aired overnight and the MDMP was installed the following day (March 13, 1996). A zero voltage reading of 1.539500 V was taken before the pile was lowered into the water-filled borehole. The measured pore pressure is presented in Figures 49 and 50, versus logarithmic and linear time scales, respectively. Table 26 provides the codes identifying the events during the test as marked on the figures. From Figure 49, the measured pressure while the MDMP was stabilizing in the water-filled case hole was 80.71 kPa (11.706 psi). Based on 7.77 m (25.49 ft) of head, the calculated pressure was 76.19 kPa (11.05 psi), which corresponded to a 5.9% difference in pressure. Again, these are based on the assumption that the borehole was completely filled. At the end of the test, as shown in Figure 50, the excess pore pressure dissipation appears to be complete. The measured pore pressure at the end of the test is 92.46 kPa (13.41 psi). The range of hydrostatic pressure at the site during the monitoring period of March 5 to March 26, 1996 was 86.33 kPa (12.52 psi) to 89.08 kPa (12.92 psi) (3.76 m (12.33 ft) to 4.04 m (13.25 ft) National Geodetic Vertical Datum (NGVD)). The average groundwater elevation for this period was 3.87 m (12.69 ft) NGVD, resulting in an expected hydrostatic pressure at the end of the test of 87.43 kPa (12.68 psi), which corresponded to a 5.8% difference relative to the measured value.

The maximum pore pressure measured following driving was 224.0 kPa (32.49 psi).

**Table 26. Legend of Events for Pore Pressure Build-Up and Dissipation With Time for Model Pile Test NB3 (see Table 23 for a time schedule).**

1	Model Pile is in cased borehole	10	Load Test #3, using the Static Load Frame
2	Start of Driving	11	Load Test #4, using the Static Load Frame
3	Pore Pressure Cell penetrates soil	12	Load Test #5, using the Static Load Frame
4	Pause in Driving	13	Load Test #6, using the Static Load Frame
5	End of Driving	14	Load Test #7, using the Static Load Frame
6	Model Pile detached from the Drill Rig	15	Load Test #8, using the Static Load Frame
7	Initial Load Test using the Drill Rig	16	Load Test #9, using the Static Load Frame
8	Load Test #1, using the Static Load Frame	17	Final Load Test, using the Static Load Frame
9	Load Test #2, using the Static Load Frame	18	Restrike and Removal of Model Pile

### 6.1.4 Common Pore Pressure Behavior of the Two Tests

Figures 47 and 48, as related to NB2, show that from Load Test #1 (event 7) to Load Test #9 (event 15), an increase in pore pressure resulted from each load test, while Load Tests #10 (event 16, about 91 h after driving) and #11 (event 17) resulted in a decrease in pore pressure. Figures

Figure 49. Pore Pressure Build-Up and Dissipation With Time for Model Pile Test NB3.

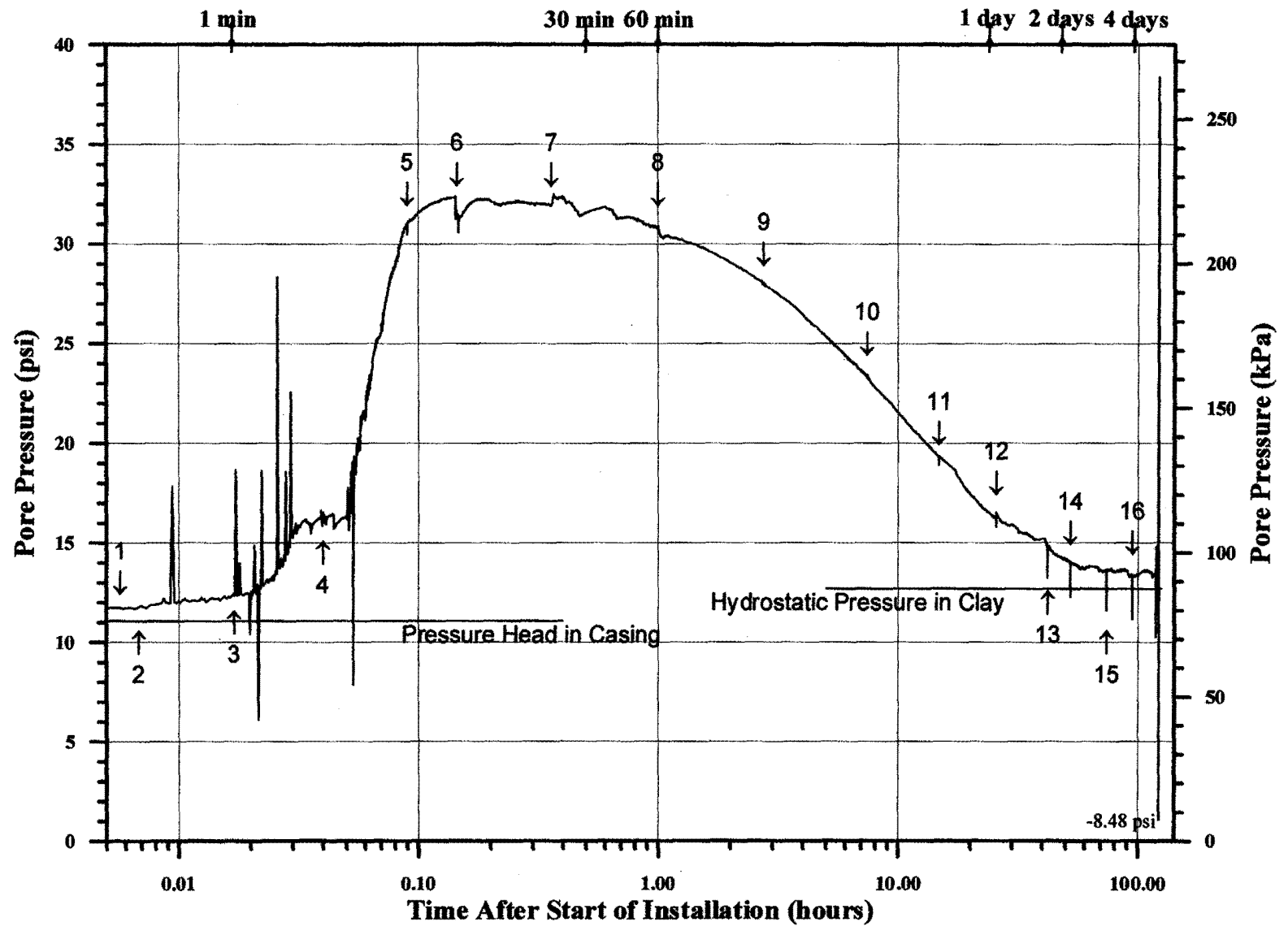
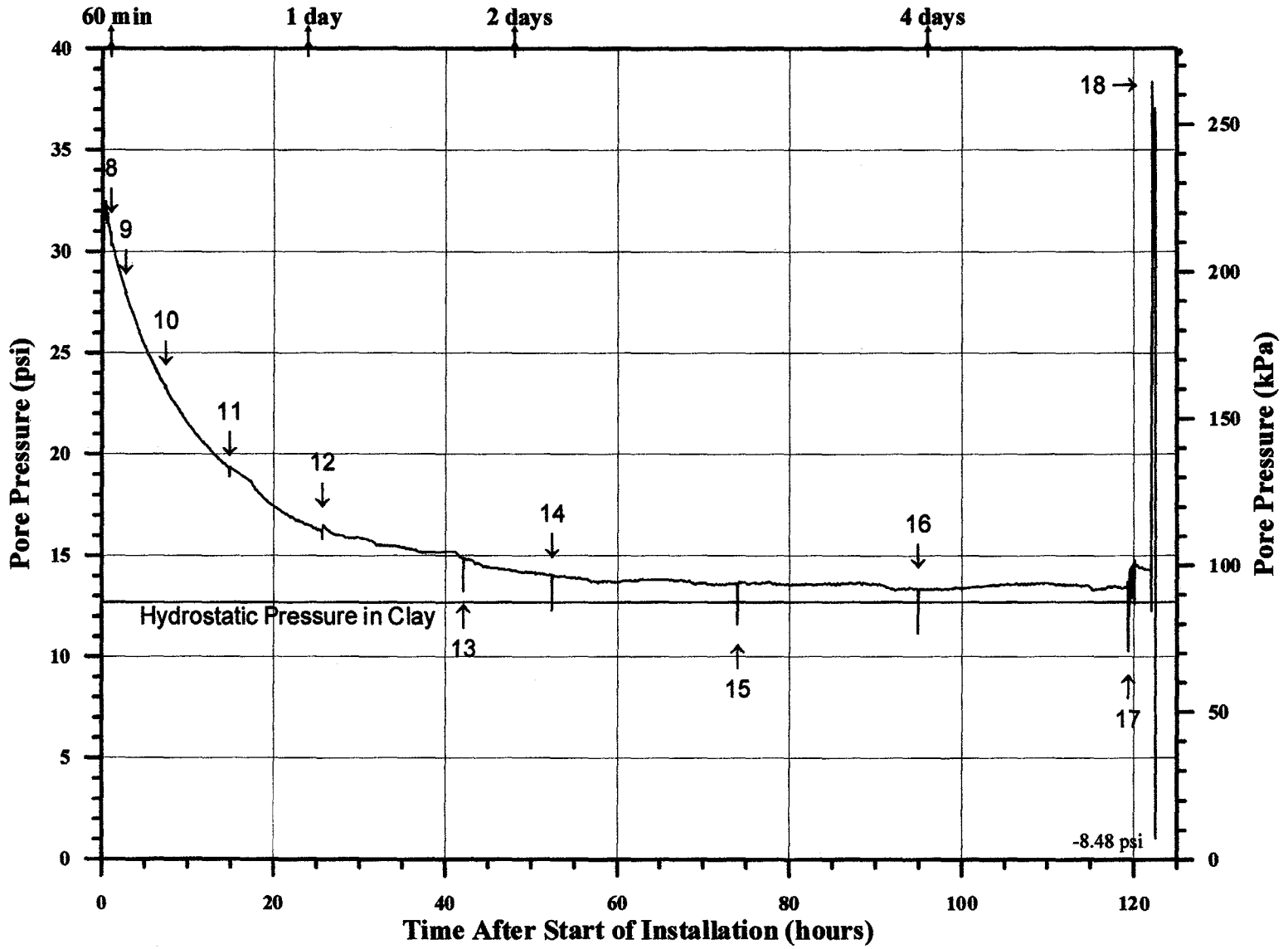


Figure 50. Pore Pressure Build-Up and Dissipation With Time  
Model Pile Test NB3.





49 and 50, as related to NB3, show that the later load tests, Load Test #4 (event 11, about 15 h after driving) to Load Test #9 (event 16), indicate a sudden decrease in the pore water pressure due to each static load test. This could be caused by the different soil properties — NB2 was tested in medium to soft clay, while NB3 was tested in soft clay. The change in behavior during one set of testing (e.g., NB2) indicates the variation of soil properties with time. Initial remolding after driving leaves the soil in a normally consolidated state and, hence, results in a positive pore pressure during shear. With time, the pore pressure dissipates and the soil consolidates, thus becoming overconsolidated. As a result, subsequent shearing results in dilation and reduction in pore water pressure.

In all cases, visual inspection suggests that the pore pressure dissipation rate is not affected by the sudden short-duration pore pressure changes that resulted from the static load tests. Since all the pore pressure changes during the static loading of the MDMP test NB2 are relatively small, their possible effect on the capacity gain process does not seem to be pronounced. The effect of the load testing on the soil's shear strength is not entirely clear. On one hand, the cyclic loading with time may contribute to increased soil strength; on the other hand, the aforementioned pore pressure behavior and changes with time suggest that the tests themselves have a very limited effect on the entire capacity gain process. In cases where the pore pressure decreased during a static load test, the behavior was similar and the pore pressure increased back to the pre-load test pore pressure level within a very short time. The effect of the static testing on the excess pore pressure and capacity can be further examined through MDMP test NB2, where the pile was pushed 15.24 cm (6 in) and the pore pressure increase was significant (see Figure 47, event 6). The rate of pore pressure dissipation does not appear to be affected by the change (slope of the line on a log time scale), but the actual time required to allow for the additional pore pressure dissipation has increased the total time required for the initial dissipation of the excess pore pressure due to driving.

During driving of the MDMP, sharp spikes were recorded by the pore pressure transducer (see Figures 47 and 49). These spikes are caused by the stress wave traveling through the pile as a result of the hammer impact. The smaller magnitude of these spikes compared to the stress wave is due to the fact that the pressure transducer measures only the effect of the driving on the glycerin/water mixture and is not directly exposed to the stress wave. Also, an important observation from the driving is that even though there are sharp spikes in the recorded data, the average response corresponds well to the actual pressure at each elevation. Before the pore pressure cell penetrates the soil, the majority of the data appears to measure the actual water pressure of the standing head of water in the borehole.

## **6.2 Radial Stress Measurements**

### **6.2.1 Total Stress**

The total radial stress cell presented difficulties due to complications caused by cold weather and snow (temperature was below freezing). A zero voltage of -0.000812 V, was taken along with the pore pressure zero voltage. The calibration constant used in the data reduction was 64527.16 psi/V (see Appendix D). The total radial stress cell utilizes O-rings to maintain a watertight

environment. During the period when the zero voltage was obtained, the MDMP was subjected to a prolonged period (approximately 48 h) of below-freezing temperatures. Changing properties of the O-ring and possible freezing of internal moisture appears to have led to an erroneous zero voltage. This is evident when observing Figures 51a and 52a. Using the above-zero reading, the initial total pressure measured while the pile was standing in the water-filled borehole is -51.71 kPa (-7.5 psi). This value is meaningless as it should be equal to the water head in the casing and, hence, the pore pressure measurement. The data were adjusted in Figures 51b and 52b so that the measured radial stress was equal to the pressure head in the casing by shifting the curve up 98.39 kPa (14.27 psi). The negative pressures measured before the driving of the MDMP can be explained by a temperature increase. The higher temperature in the water relative to the air caused an elongation of the aluminum dogbone on which the strain gauges are mounted. This elongation resulted in tension in the strain gauges or a measurement of increased negative stresses (compression stresses are positive). An additional correction was made in Figures 51b and 52b at 0.182 h after the start of the test to adjust for a sharp increase of 52.4 kPa (7.6 psi). The data from 0.182 h to the end of the test was shifted down to compensate for the sharp increase. This correction may not be valid since the actual cause of the sudden stress change is unknown and the original measurements may very well correspond to the correct pressure. The change may be a result of the cell overcoming the added resistance (stick) of the O-rings due to a temperature increase and thawing of the ice, allowing the realignment of the moving components combined with an actual increase in total pressure. After the sudden increase (jump), the total radial pressure measurements appeared to be consistent with a few sudden large changes. In spite of the adjustments presented in Figures 51b and 52b, the recorded data in Figures 51 and 52, from about 11 min after the start of installation, are valid. At the end of the test, the total radial stress cell was examined and one strain gauge was found to be loose. During attempts to refasten the strain gauge, the total radial stress cell was damaged beyond immediate repair. MDMP test NB3 was conducted without a functioning total radial stress cell.

From Figure 51a, the unadjusted total radial stress remained at a near constant pressure of -41.4 to -55.2 kPa (-6 to -8 psi) until the pressure cell penetrated the soil. Sharp increases due to driving stresses of up to 76 kPa (11 psi) were measured during this time period. After initial adjustment, the radial stress averaged 44.8 to 58.6 kPa (6.5 to 8.5 psi) before the cell penetrated soil. Once the cell penetrated the soil, the total radial stress increased by 186 kPa (27 psi) during driving. At about 0.182 h after the start of installation, the total radial stress suddenly increased by 52.4 kPa (7.6 psi). After this sudden change, the measured total radial stress decreased similar to the pore pressure dissipation, with the exception that the magnitude of the decrease was only about 86.2 kPa (12.5 psi), while the pore pressure dissipated 141.3 kPa (20.5 psi) over the same period (from peak radial stress to Load Test #8, event 14). Figure 52a shows that the total radial stress began to increase 46 h after installation and from 72 to 136 h, the total radial stress was near constant.

Concentrating on the underlying radial stress behavior, using the data from Figures 52a and 53a, some observations are:

Figure 51a. Total Radial Stress,  $\sigma_r$  With Time, MDMMP Test NB2.

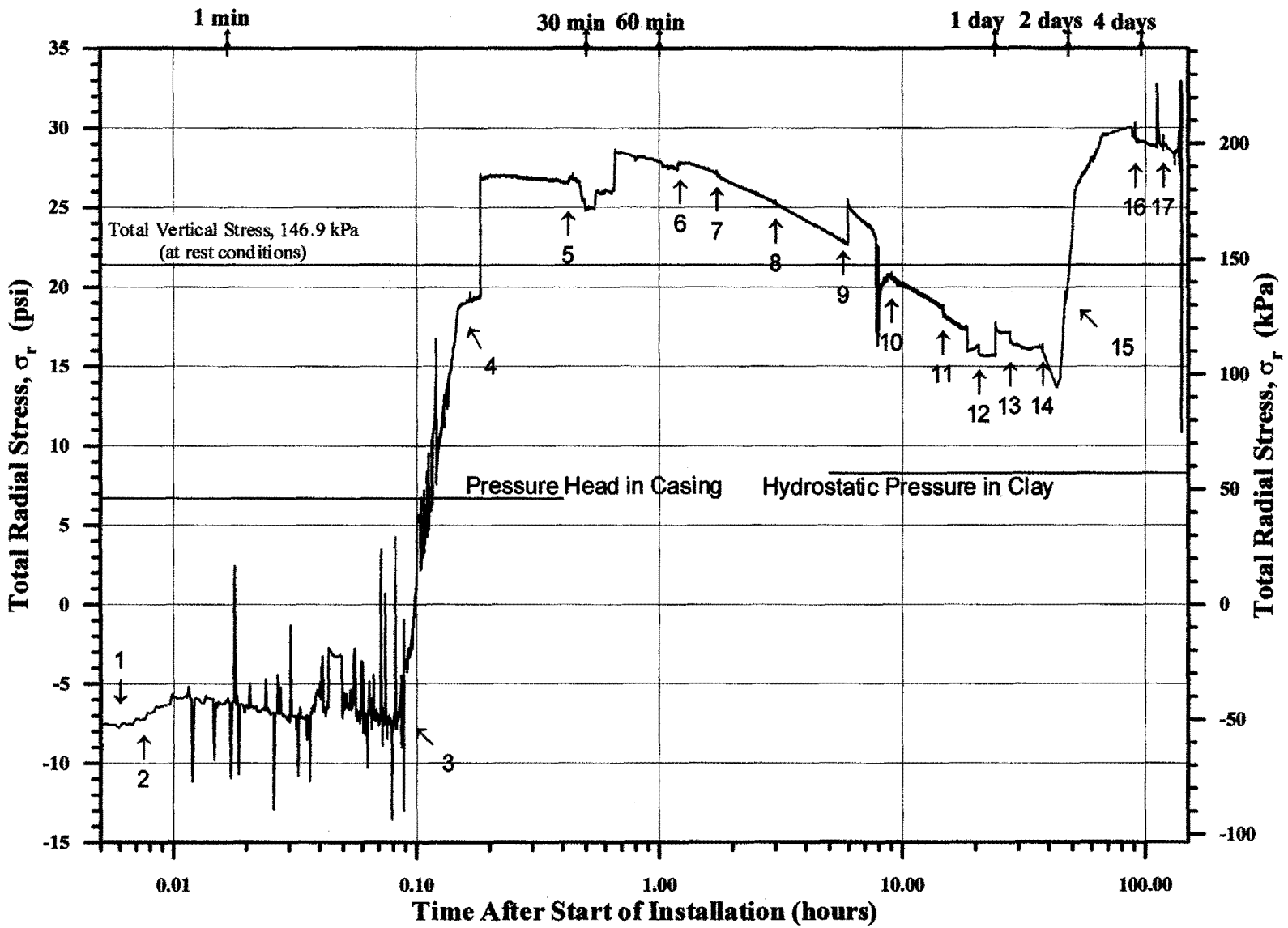


Figure 51b. Total Radial Stress,  $\sigma_r$  With Time, MDMIP Test NB2  
 (including a possible adjustment).

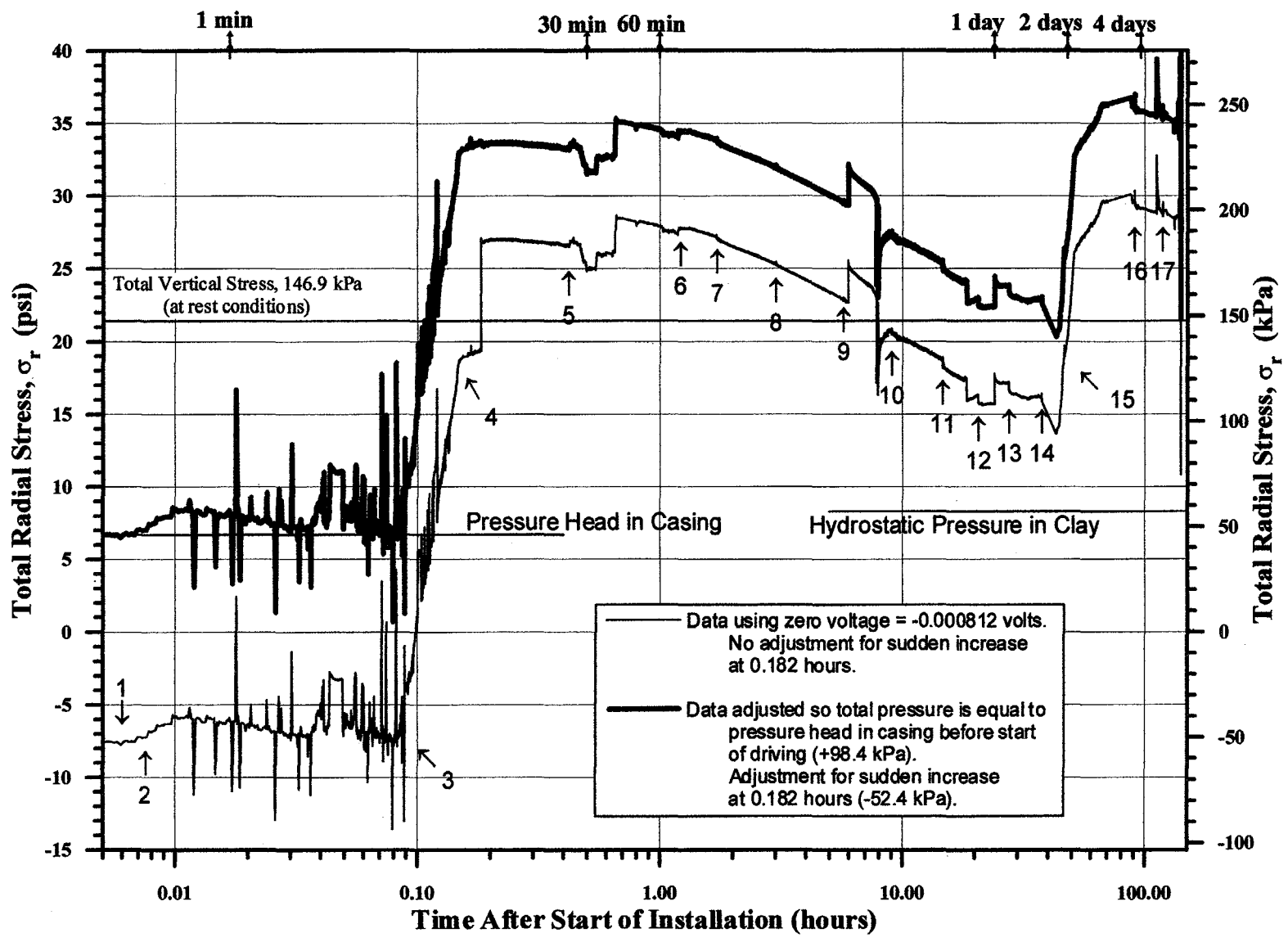


Figure S2a. Total Radial Stress,  $\sigma_r$  With Time, MDMP Test NB2.

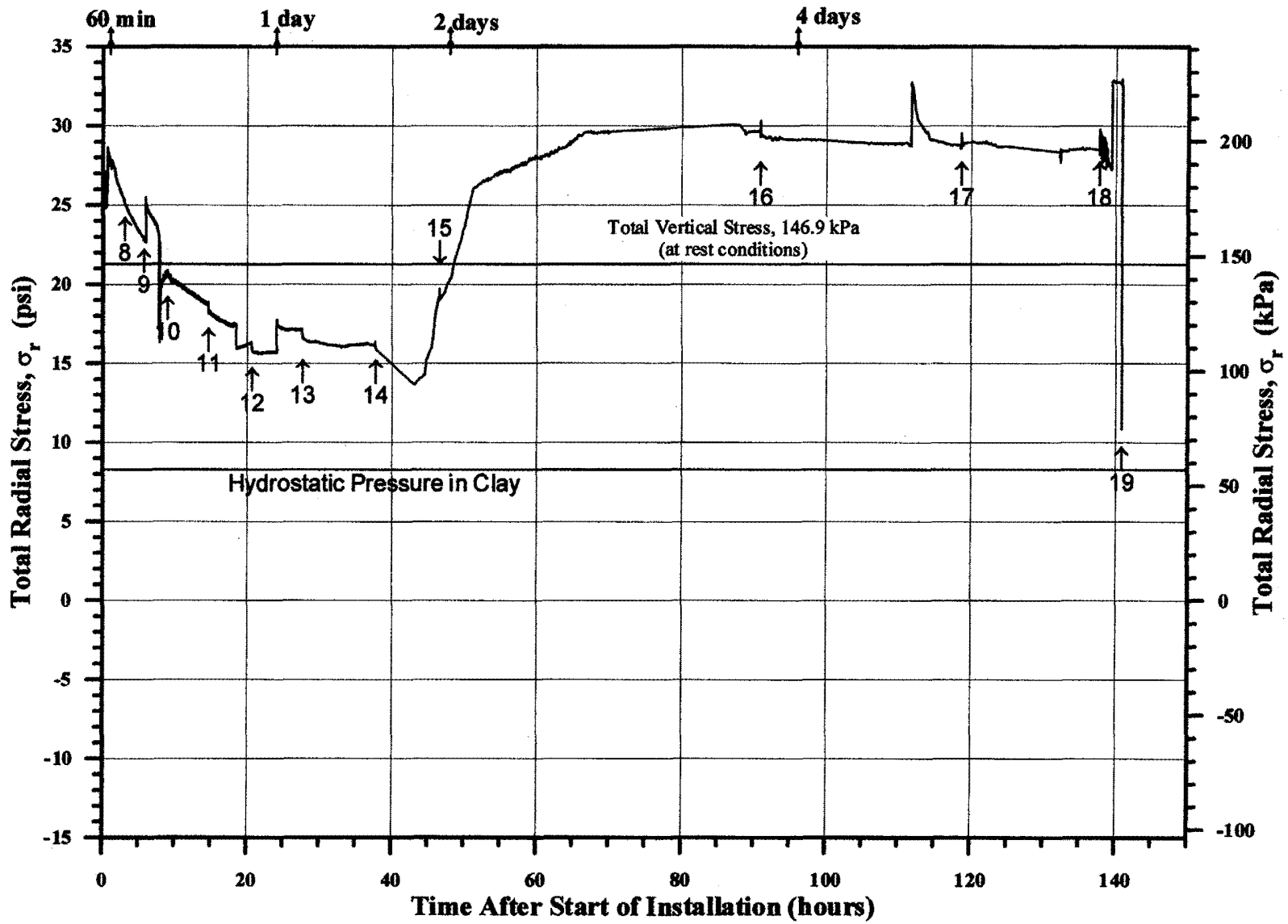
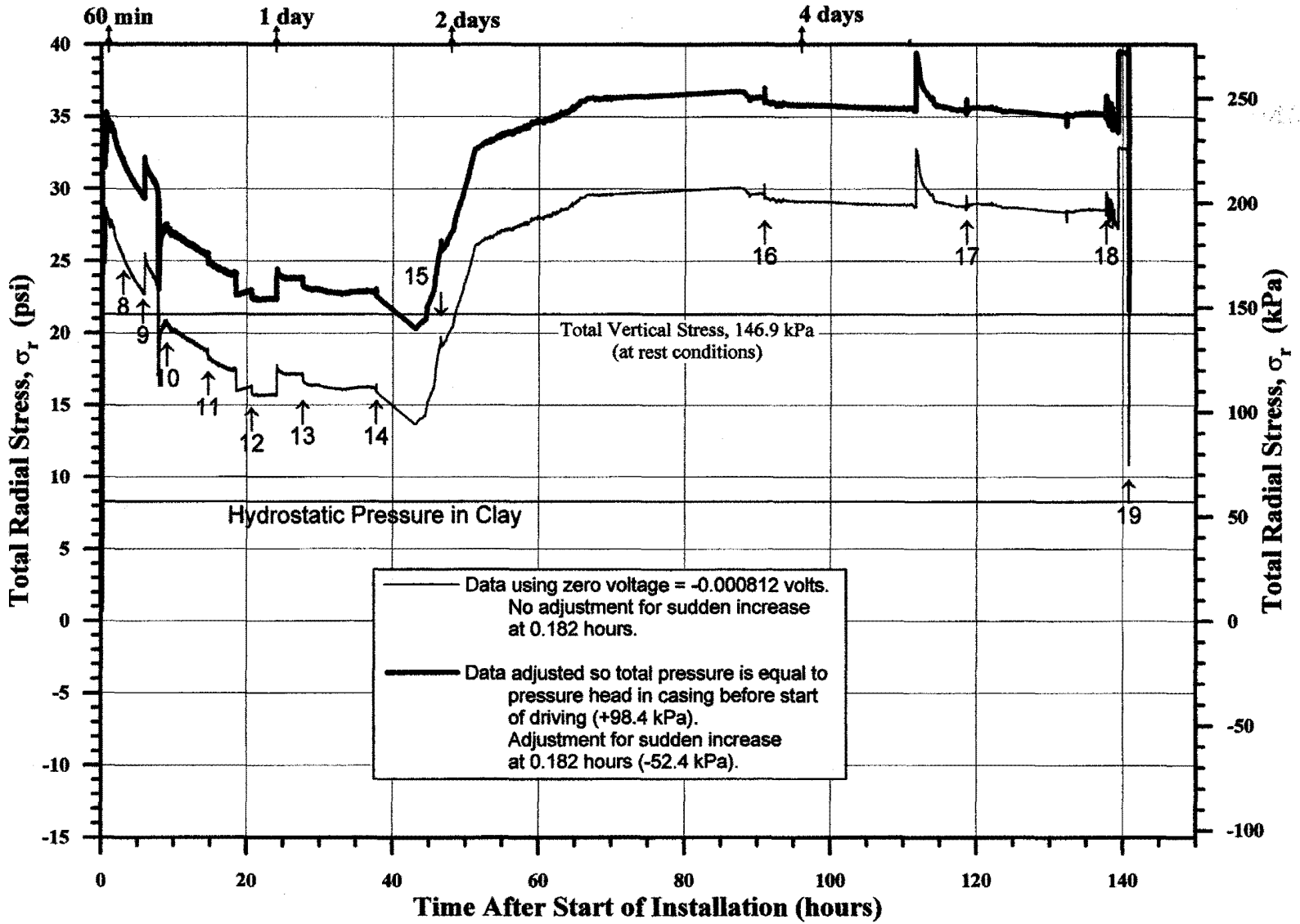


Figure 52b. Total Radial Stress,  $\sigma_r$ , With Time, MDMP Test NB2  
 (including a possible adjustment).



1. Excluding questionable measurements up to a few minutes after the end of driving, a total pressure of about 200 kPa (29.0 psi) was developed normal to the pile shaft. This pressure is about 1.36 times the total vertical stress at rest at the same depth and about 2.1 times the estimated radial stress at rest at the same depth (assuming  $K_o=0.65$ ) (Kulhawy and Mayne, 1990).
2. For about 37 h following the end of the MDMP installation (to approximately event 14), the total stress decreased at approximately a constant rate on a logarithmic time scale (see Figure 51a). This rate of decrease is approximately 3.45 kPa/h (0.50 psi/h) compared to the pore pressure dissipation rate of approximately 3.72 kPa/h (0.54 psi/h) over the same period. In absolute numbers, the pore pressure decreased by 134.5 kPa (19.5 psi) and the total pressure decreased by 86.2 kPa (12.5 psi).
3. The end of the total pressure decrease is associated with the completion of 90% of the radial consolidation process. At this point, the radial increase at a high rate of about 10.1 kPa/h (1.46 psi/h) was followed by a slower increase of about 1.6 kPa/h (0.23 psi/h).
4. At about 67 h after the end of installation, the total stress arrived at a level of about 200 kPa (29 psi) at which it remained approximately constant until the end of the test. This stress is about 3.4 kPa (0.5 psi) higher than the maximum total stress after installation.

The exact phenomenon is not clear and requires an in-depth theoretical evaluation along with additional experimental verification. Preliminary qualitative evaluation of the total radial pressure measurements of full-scale pile testing at the Newbury site (driven on February 23, 1997) suggests a similar behavior to that obtained for the model pile. This behavior indicates an initial reduction of the total pressure, possibly due to radial stress redistribution around the pile, most likely when the soil was remolded to a fluidized state immediately following the pile penetration. Changes throughout the consolidation process changed the nature of the soil/pile interaction, allowing for an increase in stress. Although not well understood at this stage, this phenomenon explains (as well as verifies) other observations of the pile capacity gain with time.

### **6.2.2 Effective Stress**

The effective stresses during MDMP test NB2 are shown in Figures 53a and 54a versus logarithmic time scale and in Figures 53b and 54b versus linear time scale. Figures 53a and b and 54a and b were obtained by subtracting the pore pressure of Figures 47 and 48 from the total radial stress of Figures 51a and b and 52a and b, respectively. Both adjusted and unadjusted total radial stress measurements were used for calculating the effective stresses presented in Figures 53b and 54b.

Figure 53a. Effective Radial Stress,  $\sigma_r$  ' With Time, MDMP Test NB2.

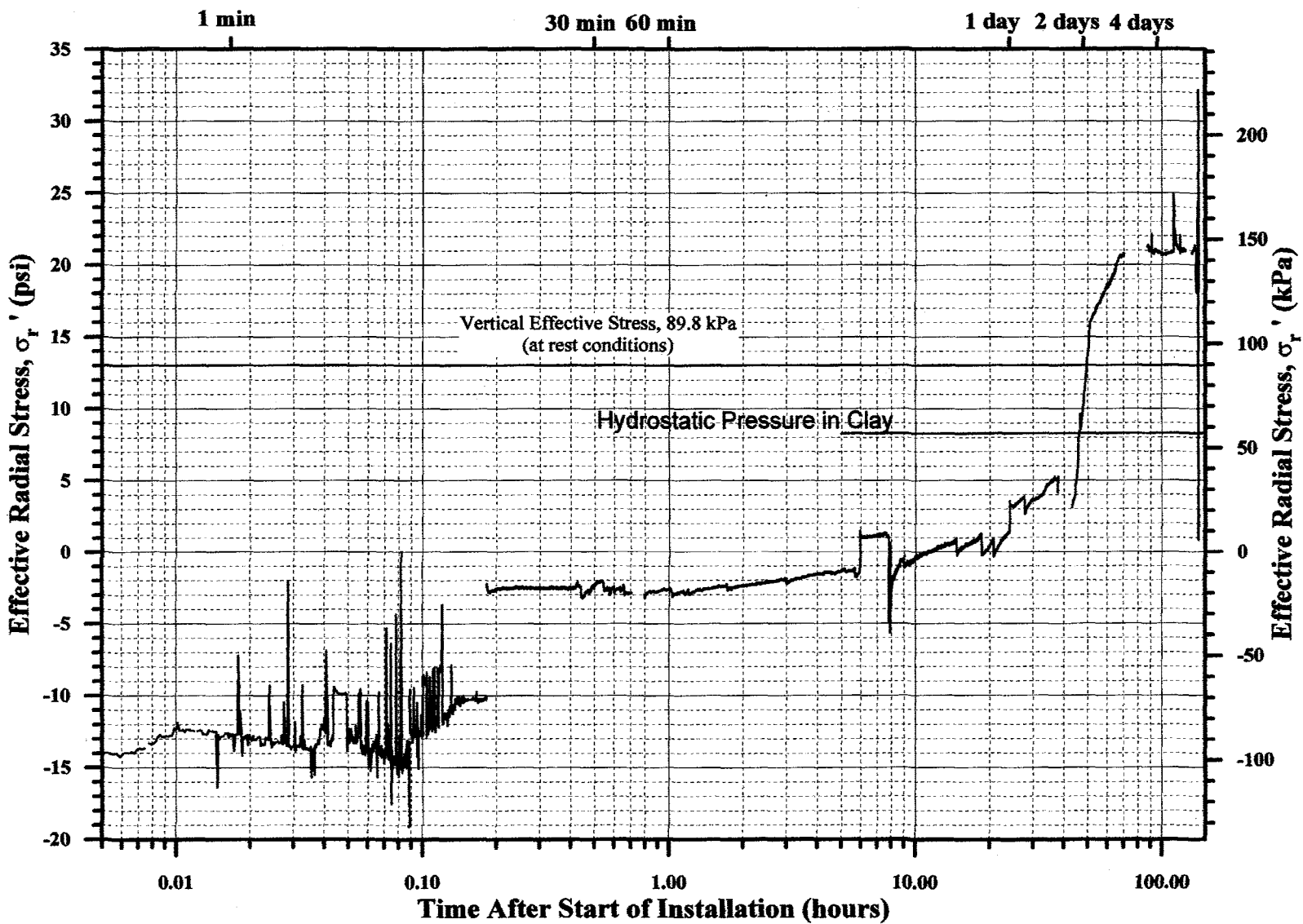




Figure 53b. Effective Radial Stress,  $\sigma_r$  ' With Time, MDMP Test NB2 (including radial stress measurement adjustment).

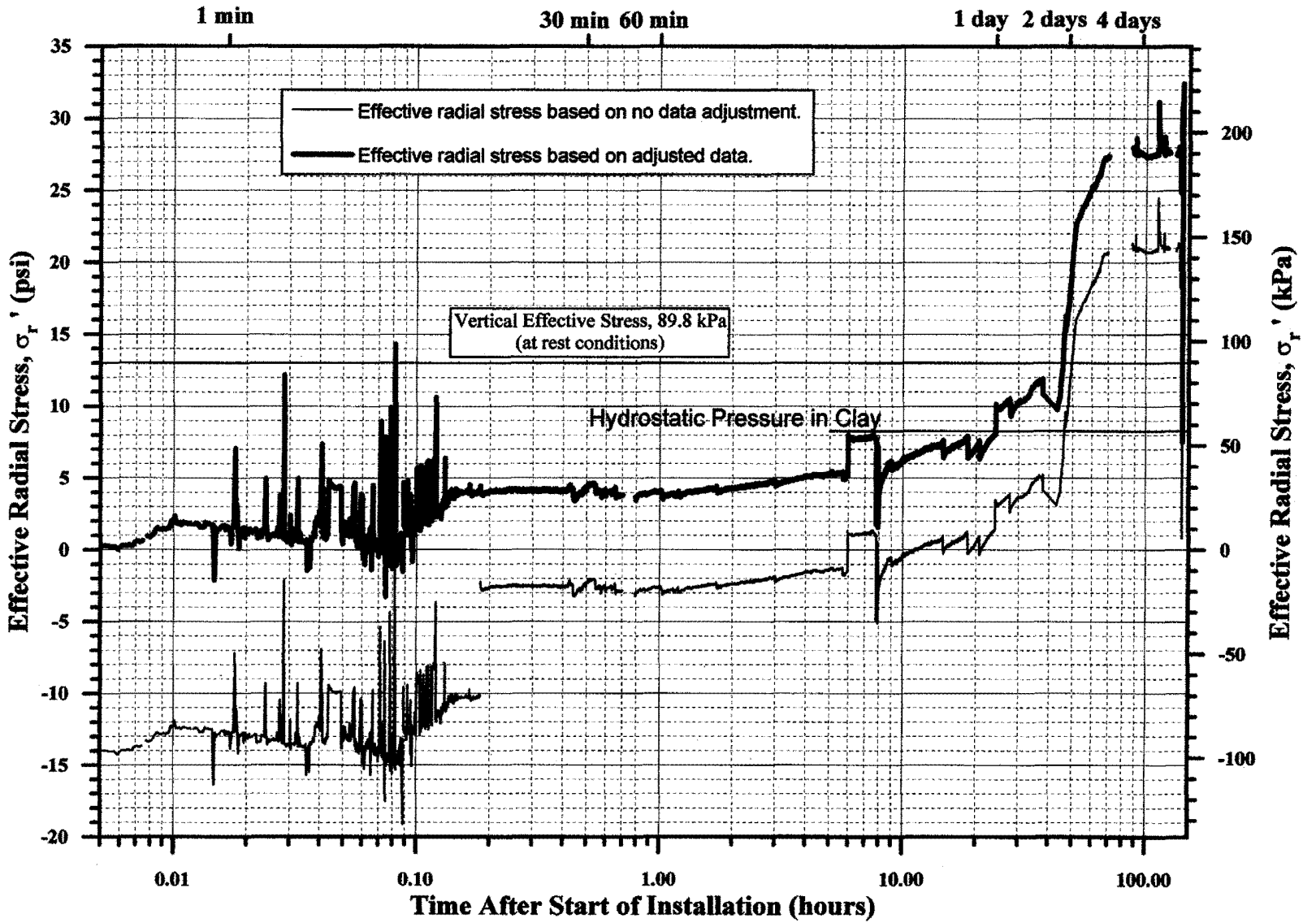


Figure 54a. Effective Radial Stress,  $\sigma_r$ , ' With Time, MDMP Test NB2.

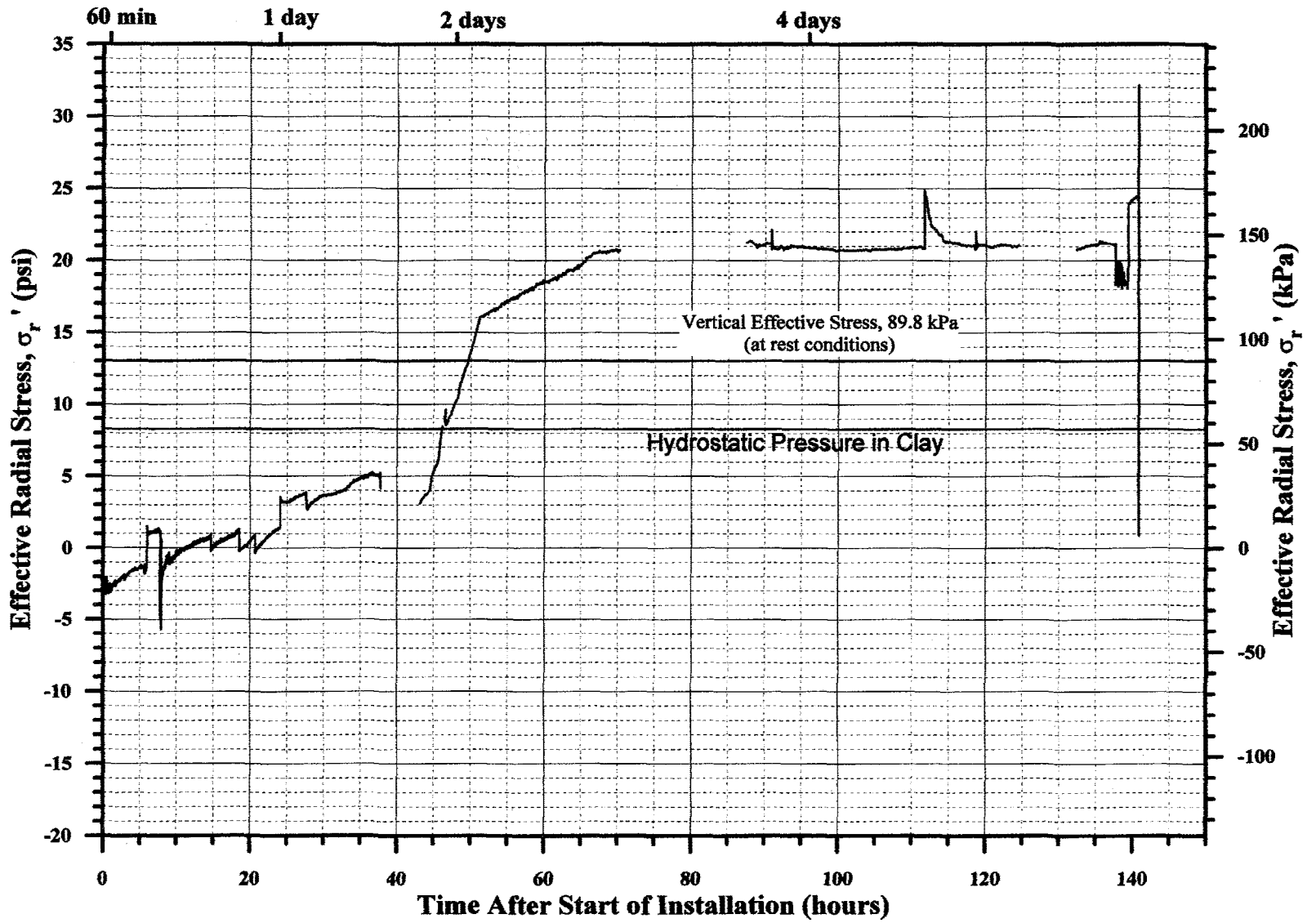
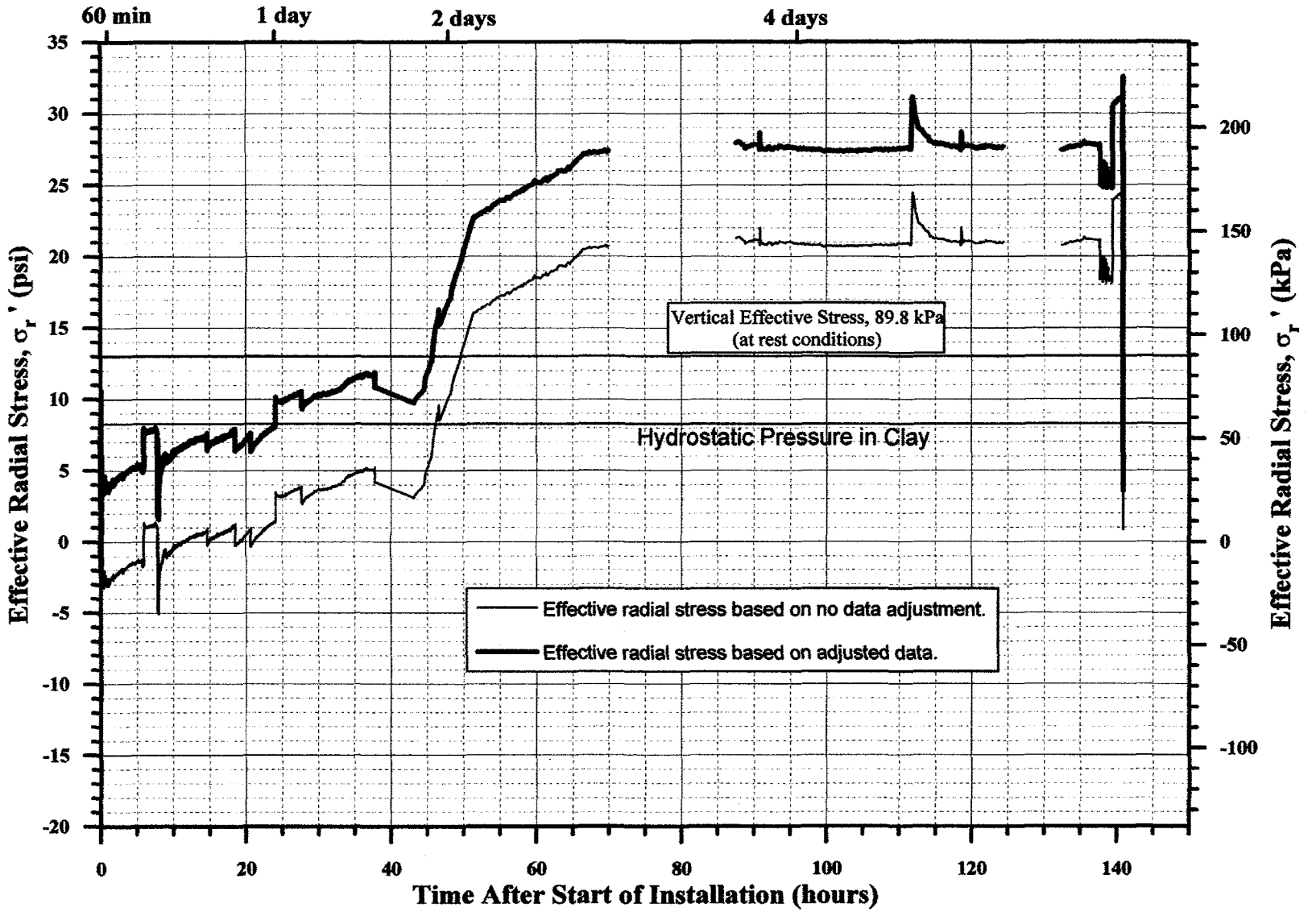


Figure 54b. Effective Radial Stress,  $\sigma_r$ , ' With Time, MDMP Test NB2  
(including radial stress measurement adjustment).



Figures 53a and b include sharp spikes in the effective stresses during driving, as a result of the impact stress waves on both the pore pressure and total radial stress measurements. Following the completion of driving (approximately 0.15 h after the start of installation), the effective stress appeared to increase at a slow constant rate of approximately 1.52 kPa/h (0.22 psi/h) for the first 37 h after installation. This slow rate represents the difference between the fast pore pressure decrease of approximately 141.3 kPa (20.5 psi) and the total radial pressure decrease of approximately 86.8 kPa (12.6 psi) over the same period. From 44 h to 70 h after the start of installation, the effective stresses rapidly increased by 121.4 kPa (17.6 psi) as a result of a sharp increase of 111.0 kPa (16.1 psi) in the total radial stress, while the pore pressure only decreased by 10.3 kPa (1.5 psi). After about 70 h after the start of installation, the effective stress leveled off to a constant value ranging from 144.8 kPa (21 psi) for unadjusted data to 191.0 kPa (27.7 psi) for adjusted data. This is approximately 1.6 to 2.1 times the vertical effective stress at that depth prior to the pile installation. Since the accuracy of the total radial stress measurement is unknown, the actual magnitude of the effective stress may be somehow different from that shown, but the data correctly represent the underlying mechanism. The discontinuities in the graph are due to lost data as a result of power failures.

The following observations can be made regarding the radial effective stress history as presented in Figure 54a:

1. Due to questionable total pressure measurements prior to and during driving to about 11 min after the end of driving, the calculated radial effective stresses during this period are considered irrelevant.
2. Until an extended period after the end of driving, the radial effective stresses remained very low, practically zero. This is possibly due to the very high initial pore pressure that developed around the pile at the end of driving. It remained so even while the pore pressure dissipated because the total pressure decreased as well during this period of time.
3. Following the end of the primary consolidation at approximately 40 h after the pile installation, the radial effective stresses increased at a fast rate and stabilized about 27 h later at a steady level of approximately 144.8 kPa (21 psi).
4. The final radial effective stress that was achieved was approximately 1.6 times the vertical effective stress and 2.5 times the estimated horizontal effective stress as evaluated at a depth of 7.39 m (24.25 ft) under at-rest conditions.

## **6.3 Load Transfer Along the Friction Sleeve**

### **6.3.1 General Considerations — Initial Reading**

The load cells in the model pile were subjected to low temperatures (sub-freezing) prior to driving, dynamic impact forces during installation, and restrike and large tension forces in the

pull-out removal process. During the first installation of the MDMP, the recorded dynamic forces at the pile tip were large enough to overload the bottom load cell.

Initial readings (zero voltages) were taken while the pile was standing in the water-filled borehole. By taking the initial readings at that time, the weight of the pile acting on the load cells was practically removed from further measurements, except for variations in the pile assembly. For the MDMP test NB2, the surface load cell was not attached and for the MDMP test NB3, the surface load cell and, possibly, some sections of the drill rods were not attached at the time when the initial readings (voltage) were recorded. The initial readings for the top load cell were -0.001064 and -0.001328 V for MDMP tests NB2 and NB3, respectively. The initial readings for the middle load cell were 0.0017997 and 0.001776 V for MDMP tests NB2 and NB3, respectively. The initial reading for the bottom load cell during MDMP test NB2 was 0.001984 V. Using the initial (zero) voltages recorded before the MDMP installation (while the pile was standing in the cased borehole), the calculated values of loads throughout the testing appeared to be of the correct order of magnitude, indicating that the load cells were not damaged during driving. This fact reaffirms the obtained measurements.

An examination of the initial readings was conducted, followed by small adjustments that are summarized in Table 27 and presented in Figure 55. The following is a discussion outlining the rationale of these adjustments. When completing the installation of the MDMP test NB2, the loads measured by the top and middle load cells were -0.5515 kN (-123.98 lb) and 0.1239 kN (27.86 lb), respectively. These measurements are presented in Figure 55a, along with the recorded forces during the initial load test on the MDMP test NB2. The unadjusted reading resulted in a top load cell reading consistently lower than the middle load cell. Therefore, the initial readings were adjusted to ensure that the top load cell measured a larger magnitude of load during both tension and compression static load tests. The adjustment was based on the assumption that at the end of driving, prior to external load application, the friction along the pile was very small. As a result, the load measured by each load cell prior to the initial load test was assumed to be the initial (zero) reading. Based on this procedure, each load cell was adjusted by the constant load specified in Table 27. Figure 55b presents the result of this adjustment for the initial load test for MDMP test NB2. The small adjustment in this case resulted in more reasonable load measurements for the two load cells, while accounting for the pile, drill rods, and surface load cell dead weight. As a result of these adjustments, the friction along the sleeve was decreased by constant values of 0.4206 kN (94.55 lb) for MDMP test NB2 and 0.05898 kN (13.26 lb) for MDMP test NB3. These adjustments corresponded to 7.05% of the peak friction measured during MDMP test NB2 and 1.25% of the peak friction measured during MDMP test NB3. Since the load cells were designed to measure static loads of 89 kN (10 tons) with 2.5 times overload, the adjusted loads represented about 0.5% of the full-scale measurement.

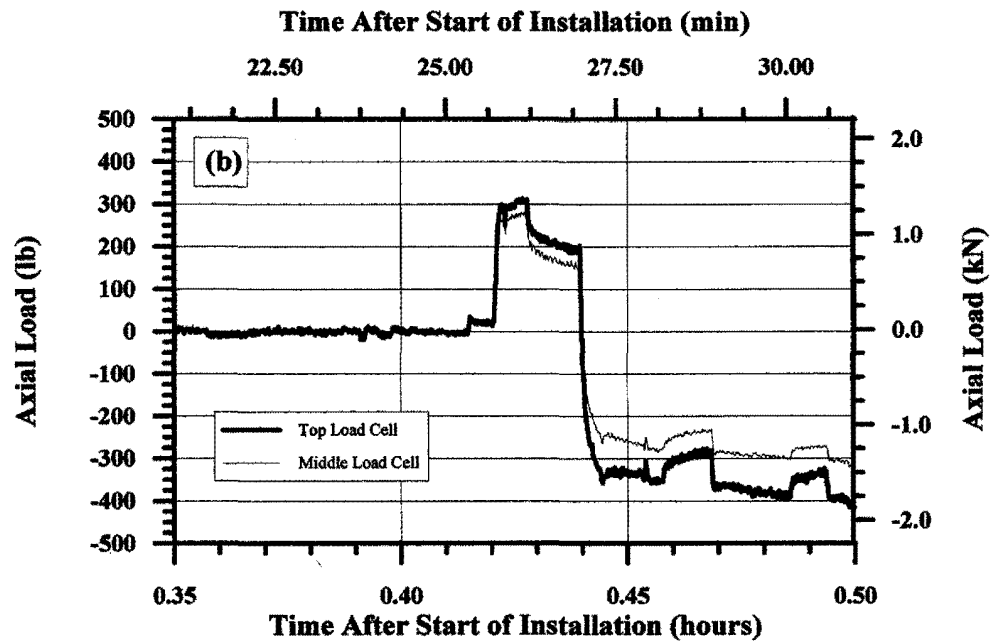
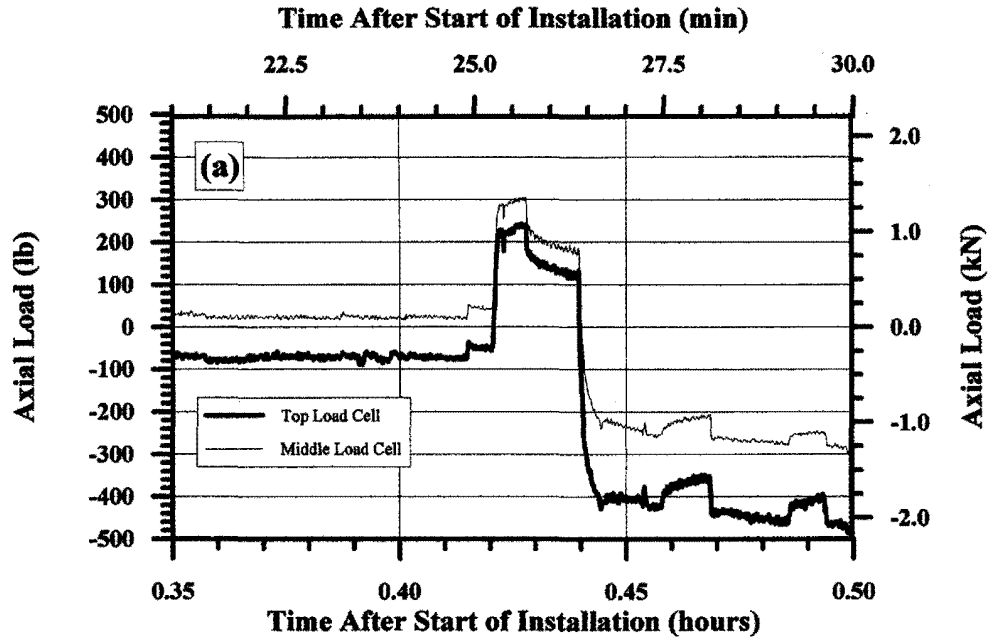


**Figure 55. Force Measurements in Top and Middle MDMP Load Cells for Test NB2: (a) Unadjusted records based on initial readings before driving and (b) Adjusted records based on zero loads assumed prior to the initial load test.**

**Table 27. Initial Adjustments to Internal Load Cell Measurements.**

MDMP Test	Internal Load Cell	Initial Zero Voltage	Load Adjustment (kN)	Load Adjustment (lb)
NB2	Top	-0.001064	0.3042	68.4
	Middle	0.001780	-0.1165	-26.2
	Bottom	0.001984	0.2255	50.7
NB3	Top	-0.001328	-0.6623	-148.9
	Middle	0.001776	-0.7215	-162.2

Possible factors that required the adjustment included a shift in the zero voltage as well as loading after driving due to effects of heave, suction forces, movement at the slip joint, residual stresses, disturbance when disconnecting the MDMP from the drill rig, and mounting the surface load cell. The zeroing of both load cells after the end of driving suggested that the calculated friction at that time was zero as well. In reality, however, some friction must have existed along the side of the pile during and following installation. Since high excess pore pressure was generated during driving, the effective stress in the soil decreased and the friction along the pile became very small, theoretically approaching zero as the effective stress approached zero. However, as the pile's weight was being balanced by the force under and along the pile, some friction existed at all times. It is clear that the initial frictional forces were very small and became considerably insignificant when the side friction increased with time. To examine the magnitude of the initial friction along the sleeve and to justify the aforementioned adjustment procedure, some observations that support this approach are discussed below.

(1) Pile resistance during driving.

A consistent and almost unchanged energy was delivered to the pile throughout the driving. During the last 1.28 m (4.2 ft) of penetration of the MDMP test NB2, the delivered energy (based on dynamic measurements) was approximately 0.079 J (0.058 k-ft), associated with an almost constant rate of penetration of about 10.5 blows/10 cm (9.6 blows/0.3 ft). The energy measured at the top and middle load cell locations (to be presented in section 6.6) suggested that only a small portion of the total delivered energy was lost over this section. The above observations should also be reviewed in light of the difficulties associated with obtaining the presented data (i.e., the small geometrical dimensions and short penetration distance). The above observations despite their limitations, suggest that when assuming the tip resistance to be constant throughout the entire penetration depth, the friction along the pile must have been extremely small. Other possibilities would be difficult to explain, such as: (1) a large amount of energy and/or a smaller rate of penetration would have been observed with deeper penetration, and (2) a larger energy loss would have been recorded along the friction sleeve.

(2) Immediately following the initial load test.

Immediately following the MDMP installation of test NB2, the initial load test was conducted with the drill rig. During this load test, the pile was first pushed downward approximately 50 mm (2 in) and then pulled until the slip joint was completely open (approximately 127 mm (5 in)) in order to allow for compression static tests with time. When disconnected from the rig, the pile

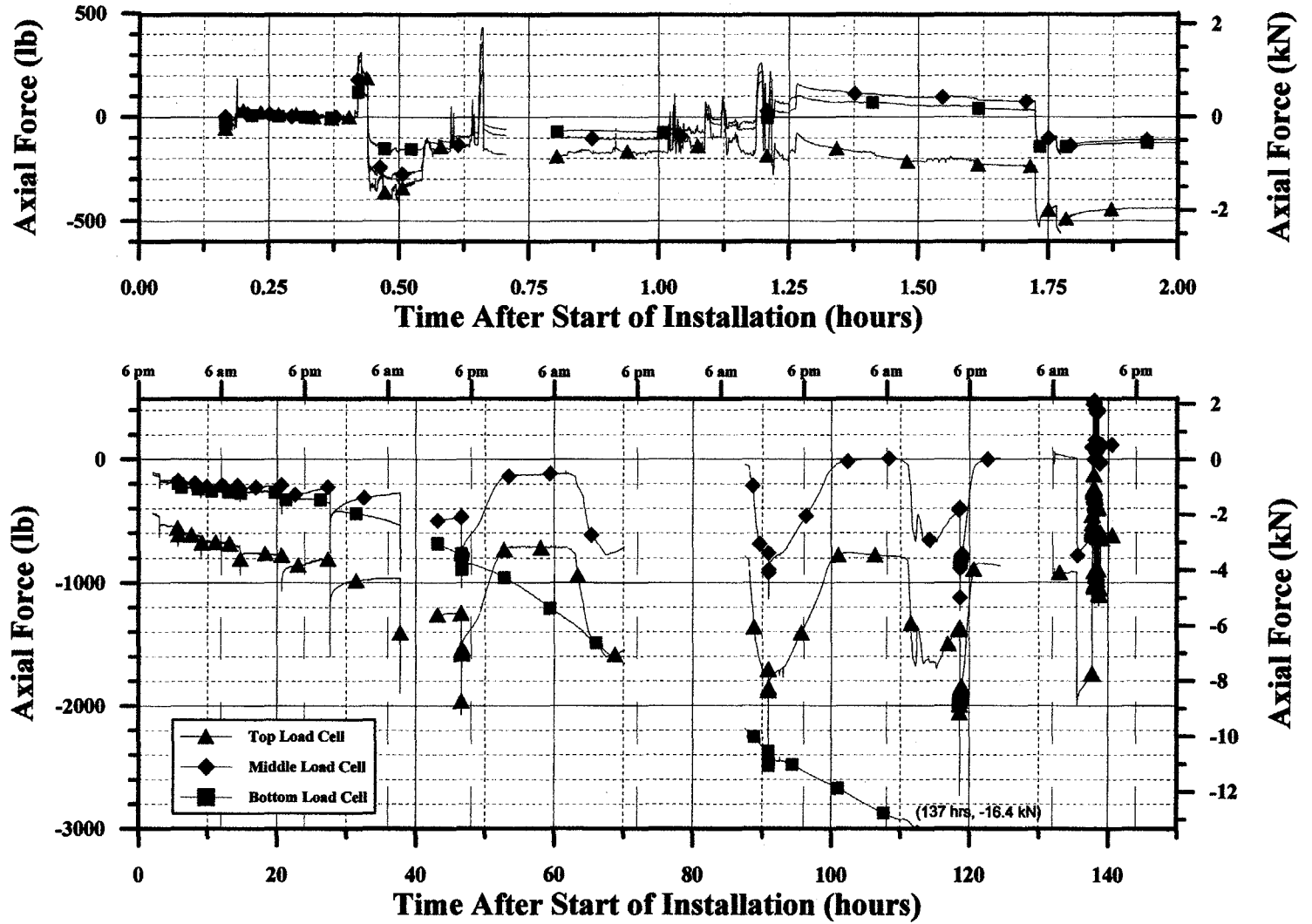
fell back down, indicating that the friction along the side of the pile was not sufficient to support the buoyant weight of the pile (the drill rods and the surface load cell totaled 1.02 kN (230 lb)). When the pile fell down, the slip joint also closed and further motion was stopped due to tip resistance. No measurements of displacement were recorded during the sudden fall resulting from the disconnection of the rods from the drill rig. Visual observations indicate that the pile fell to a depth approximately equal to the depth it had been at when the initial compression test ended. This would lead one to believe that: (1) the friction along the pile was indeed small in comparison to tip resistance, and (2) this friction must have been smaller than the aforementioned weight.

### **6.3.2 Model Pile Test NB2**

The average zero voltages for the internal load cells were determined based on readings obtained during the period between 0.3483 to 0.4146 h after the start of installation. The average zero voltages used for the top, middle, and bottom load cells were -0.001081, 0.001808, and 0.001999 V respectively. Figure 56 presents the loads recorded with the three MDMP load cells throughout the entire testing sequence of 140.8 h. A detailed (exploded) view of the readings during the initial 2 h is provided as well. From the data in Figure 56, it is apparent that the bottom load cell provided questionable data after about 10 h, suggesting that it did not work properly. Up to 46.6 h after the start of installation, each tension load test was followed by some decrease in measured forces. After 46.6 h, the measured loads increased and decreased while the loading system was held stationary. This fluctuation in the measured load may be attributed to the daily change in temperature. From approximately 8 to 9 a.m., the top and middle load cells saw an increase in tension, while in the evening, the two load cells saw an increase in compression (middle of day and middle of night exhibited constant loads). This effect was possible due to two reasons: (1) the hydraulic fluid in the loading system changed its volume as a result of the temperature changes, and (2) the drill rods changed their length due to the temperature changes. Since the loading system consisted of a double-acting ram with fluid on both sides of a loading ring, any change in pressure due to temperature change would be equal, thus there would not be daily load changes (this was possible since both sides of the ram were at equal pressures at the end of each static load test and then needle valves were closed to maintain equal pressure, assuming both volumes were equal). The change in length of the drill rods due to a 15°C (27°F) temperature change was 0.54 mm (assuming 3 m of drill rod were exposed to the temperature change). A length change of 0.54 mm would correspond to a force of 29.8 kN (6,700 lb) if both ends were fixed. Since the daily load change was up to 4.4 kN (1,000 lb), the pile must have moved relative to the soil to mobilize the frictional capacity of the pile. The measured daily load change of 4.4 kN (1,000 lb) was approximately equal to the measured load during the final cyclic load test before the slip joint closed. This is reasonable because the slip joint was extended during the periods of load fluctuation (assumed to be due to temperature variation) and no load transfer would have been measured below the slip joint.



Figure 56. Internal Load Measurements, MDMMP Test NB2.



During the attachment of the static load frame to the pile head (1.01 to 1.3 h after the start of installation), the internal load cell measurements recorded some disturbance (shown in the highlighted region of figure 57). The load transfer along the friction sleeve could not realistically undergo an increase from 0.28 kN (62 lb) to 1.38 kN (312 lb) within a period of about 15 min. The changes could therefore be attributed to the disturbance that occurred during the attachment of the static load frame. An assumption was made that the load transfer along the friction sleeve would not have changed if not for the disturbance. As a result, the measured load in each internal load cell was adjusted to the pre-disturbance level. The middle load cell was adjusted by decreasing the force by 0.796 kN (179 lb) and the top load cell was adjusted by increasing the force by 0.316 kN (71 lb). This adjustment remained constant throughout the duration of the testing sequence. It should be noted that the decrease in both forces at 1.72 h and 1.77 h after the start of installation took place due to static load test #1 (event 7 on Figures 47, 48, and 51).

Details of the static load tests carried out during model pile test NB2, including the initial load test using the drill rig and the following 11 tension load test results, are shown in Appendix G. The top graph presents the load displacement relationship, including the individual measured load cell loads, as well as the difference between them, which represents the friction along the friction sleeve. The rates of displacement and load increase are provided in the additional two graphs.

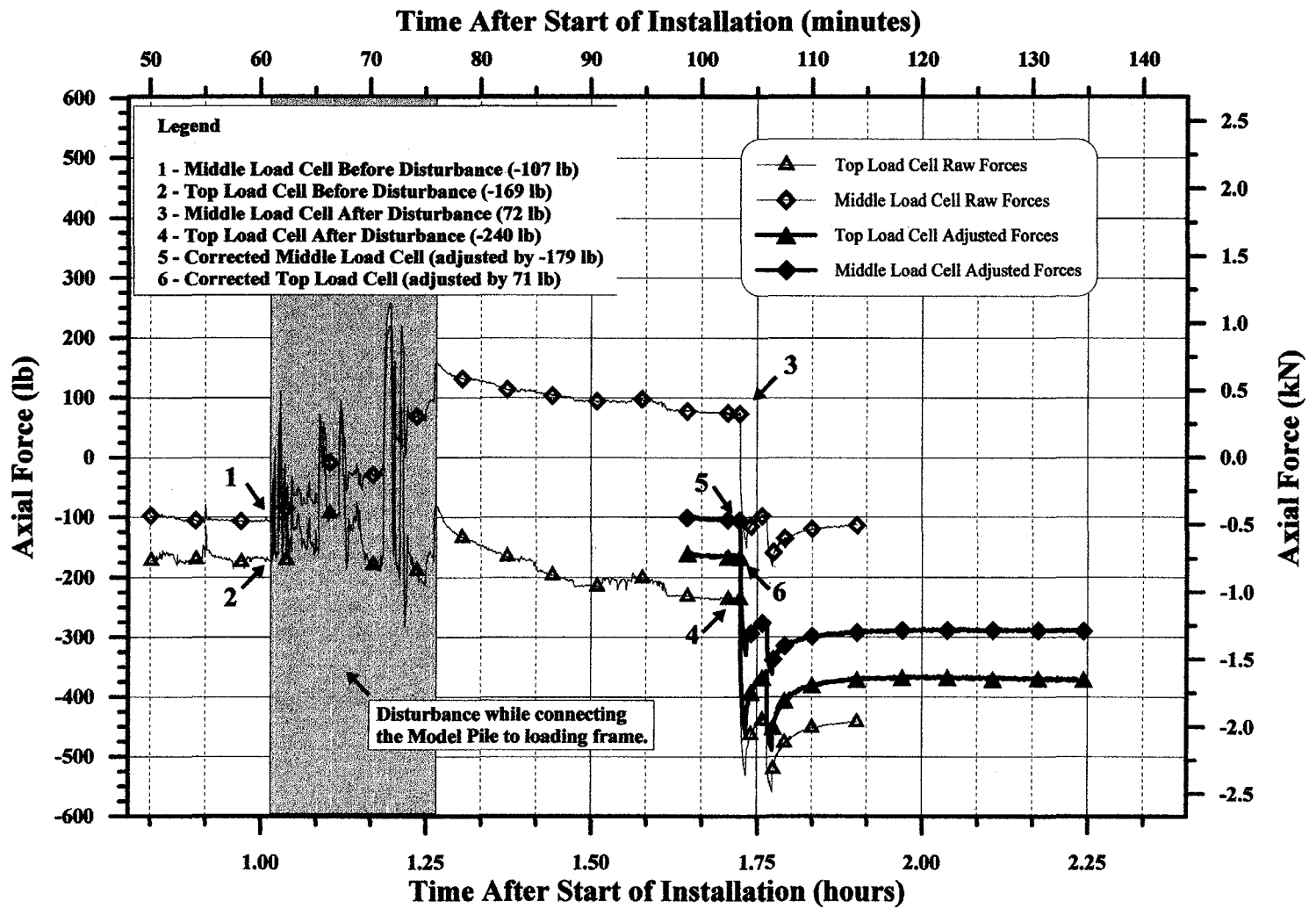
For each static load test, the detailed frictional force during the initial displacement of 6.35 mm (0.25 in) is presented in Figure 58. The initial load test (utilizing the drill rig), both in compression and tension, are also presented in Figure 58. A substantial increase in the friction forces along the friction sleeve was observed as the load test sequence proceeded. The degree of consolidation,  $U$ , is also indicated in Figure 58, on the load test legend, suggesting a close relationship between the consolidation process and the increase in frictional capacity.

The load displacement relationship presented in Figure 58 suggests a soil behavior variation with time. Initially, almost a perfect “plastic” behavior was observed up to load test #5 (associated with 59% consolidation). At this stage, a clear peak followed by a residual strength behavior was observed, indicating the progress in the consolidation process. Due to the limitations of the DAS, the peak values are not well defined. Under the assumption that the soil shears along the pile surface, the shear (frictional) stresses can be calculated using the area of the frictional sleeve of 2000 cm<sup>2</sup>. The calculated shear stresses are presented in Figure 59. At an approximately 80% consolidation ratio, only 50% of the capacity gain had occurred. At the peak shear strength, the shear stresses were approximately equal to the shear strength of the soil at this depth (see Figure 53). This observation coincided with the fact that upon pile removal, the MDMP shaft was surrounded by a clay layer, suggesting that the shear took place in the soil away from the pile shaft.

### **6.3.3 Model Pile Test NB3**

The average zero voltages for the internal load cells were determined based on readings obtained during the period between 0.3353 and 0.3557 h after the start of installation. The average zero voltages used for the top and middle load cells were -0.001290 and 0.001825 V, respectively.

Figure 57. Adjustments to Internal Load Measurements, MIDMP Test NB2.



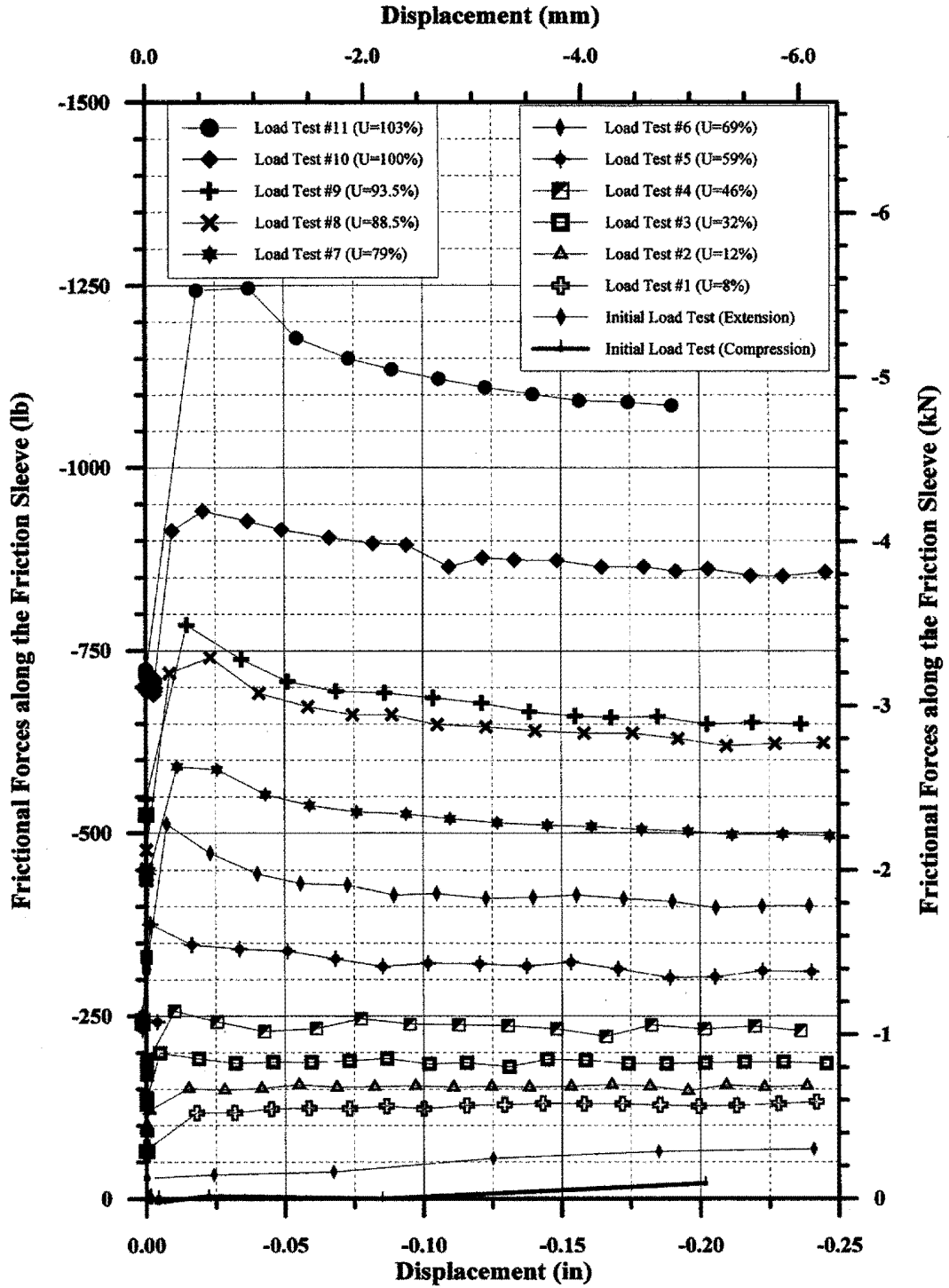


Figure 58. Frictional Forces Along the Friction Sleeve for MDMP Test NB2.

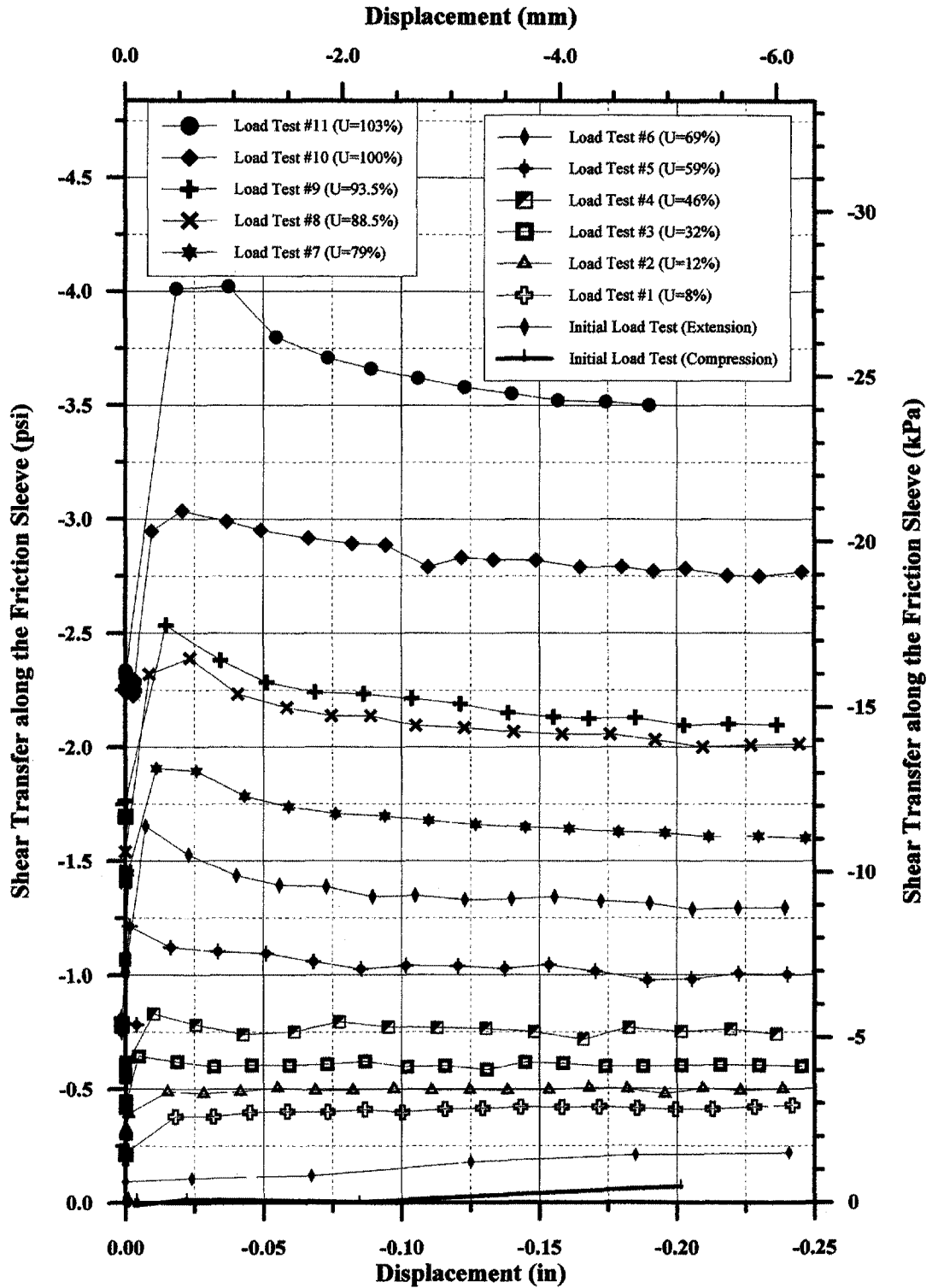


Figure 59. Shear Transfer Along the Friction Sleeve for MDMP Test NB2.

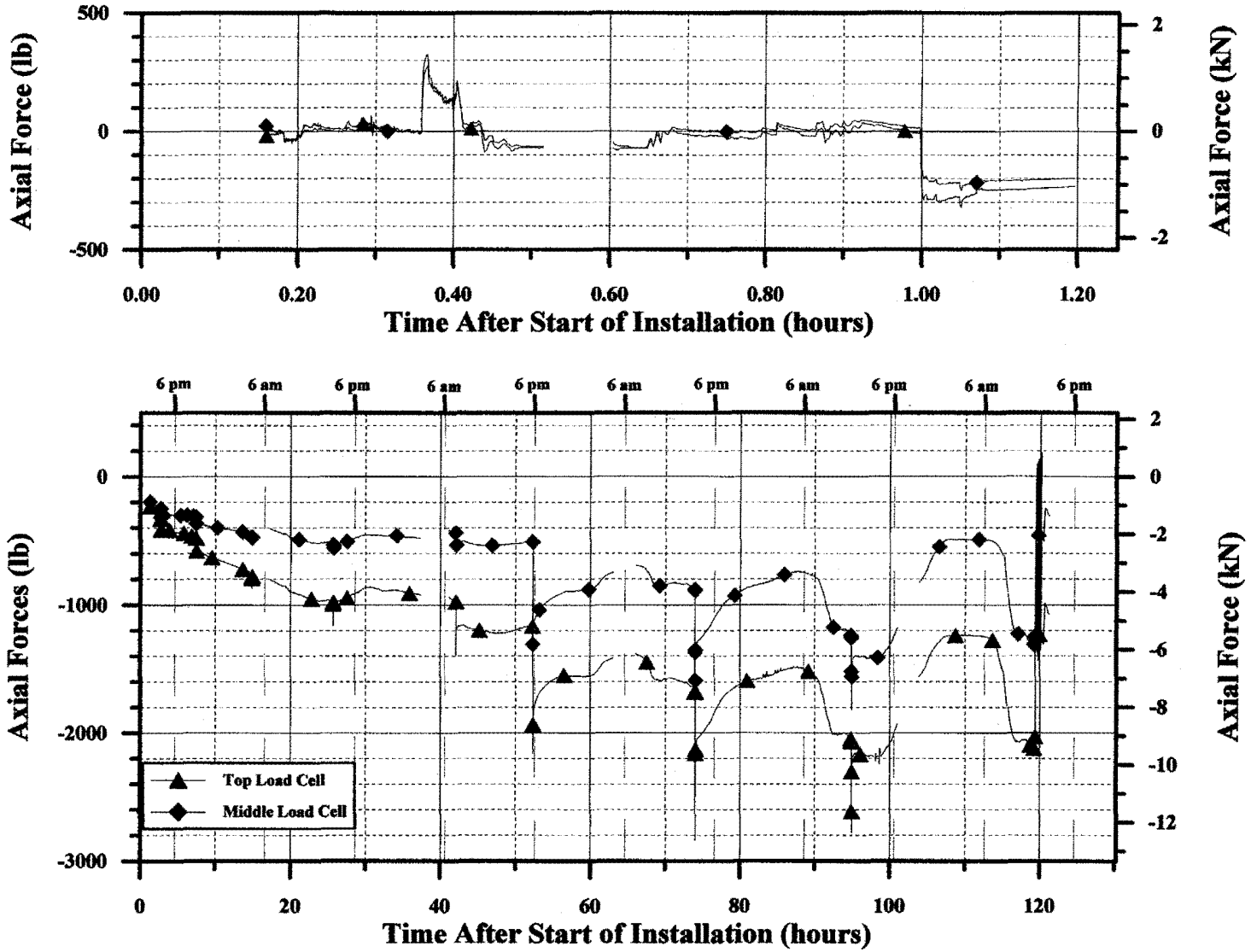
Figure 60 presents the loads recorded by the two load cells above and below the friction sleeve throughout the entire testing sequence of 122 h. A detailed (exploded) view of the readings during the initial 1.25 h is provided as well. Similar to the behavior observed during the MDMP test NB2, some load build-up took place without any externally imposed displacement. The friction mobilization appeared to be the result of displacement caused by the change in temperature during a 24-h period. From approximately 8 to 9 a.m., an increase in tension was measured by both top and middle load cells. At about 4 p.m., a more gradual reduction in measured tension was recorded. This effect was seen 40 h after the start of installation. Based on an average change in temperature of 15°C (27°F) during a 24-h period, the displacement caused by the temperature change would be 0.54 mm (assuming 3 m of drill rod exposed to the temperature change). During the attachment of the static load frame to the model pile in the NB3 testing sequence, less disturbance was created relative to that observed during the MDMP test NB2. As a result, the forces along the friction sleeve had remained unchanged and no adjustment was required for the NB3 testing sequence.

Details of the static load tests carried out during model pile test NB3, including the initial load test using the drill rig and the following nine tension load test results, are shown in Appendix H. The top graph presents the load displacement relationship, including the individual measured load cell loads, as well as the difference between them, which represents the friction along the friction sleeve. The rates of displacement and load increase are provided in the additional two graphs.

For each static load test, the detailed frictional force during the initial displacement of 6.35 mm (0.25 in) is presented in Figure 61. The initial load test (utilizing the drill rig), performed in compression, is also presented in Figure 61. A substantial increase in the friction forces along the friction sleeve was observed as the load test sequence proceeded. The degree of consolidation,  $U$ , is also indicated in Figure 61, on the load test legend, suggesting a close relationship between the consolidation process and the increase in the frictional capacity.

The load displacement relationship presented in Figure 61 suggested a soil behavior variation with time. Initially, almost a perfect “plastic” behavior was observed up to load test #4 (associated with 67% consolidation). At this stage, a clear peak, followed by a residual strength behavior, was observed, indicating the progress in the consolidation process. Due to the limitations of the DAS, the peak values were not well defined. Under the assumption that the soil shears along the pile surface, the shear stresses can be calculated using the area of the friction sleeve (2,000 cm<sup>2</sup>). The calculated shear stresses are presented in Figure 62. At an approximately 80% consolidation ratio, only 50% of the capacity gain had occurred. At the peak shear strength, the shear stresses were approximately equal to the shear strength of the soil at this depth (see Figure 53). This observation coincided with the fact that upon pile removal, the MDMP shaft was surrounded by a clay layer, suggesting that the shear took place in the soil away from the pile shaft.

Figure 60. Internal Load Measurements, MDMP Test NB3.



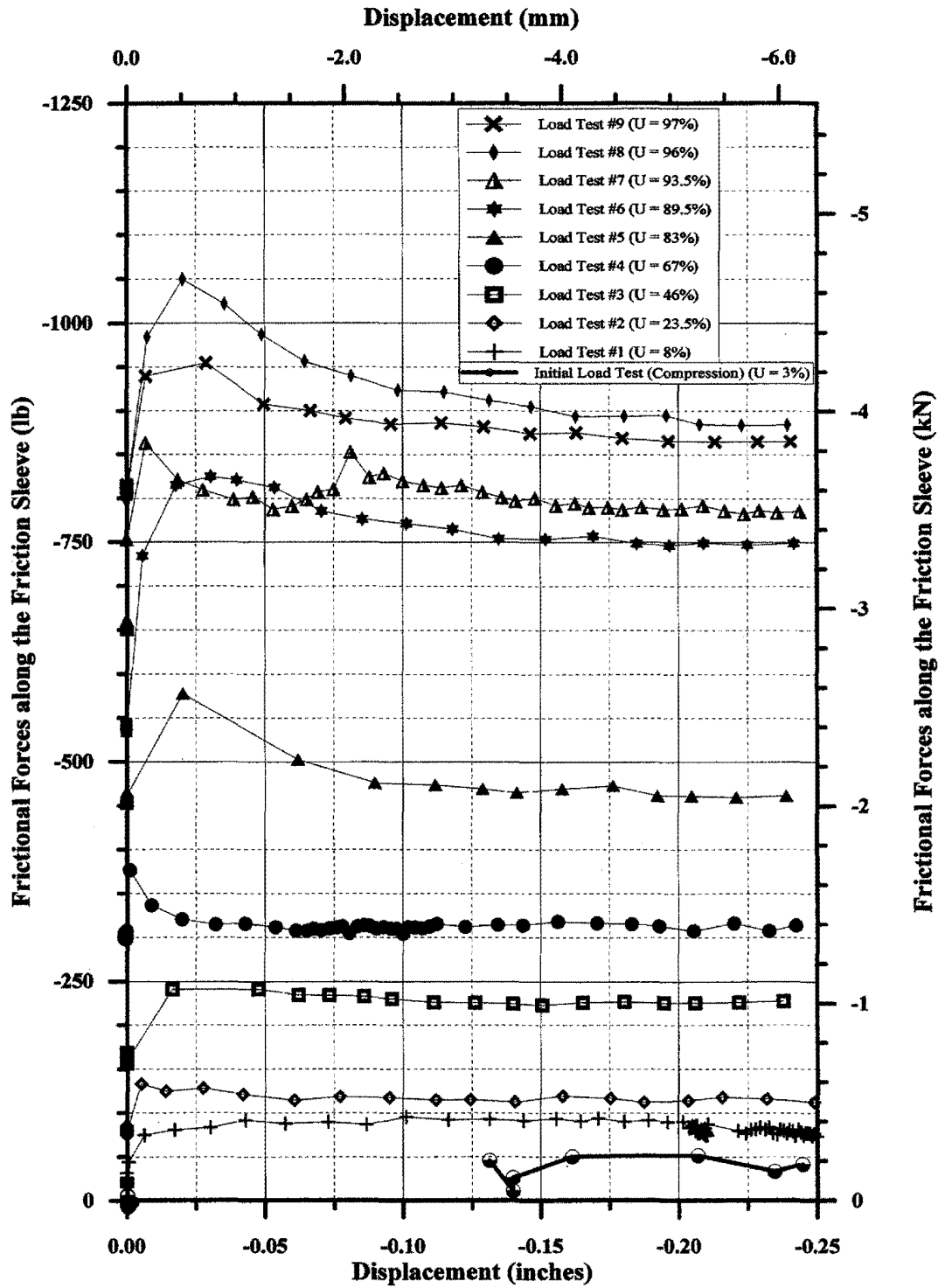


**Figure 61. Frictional Forces Along the Friction Sleeve for MDMP Test NB3.**



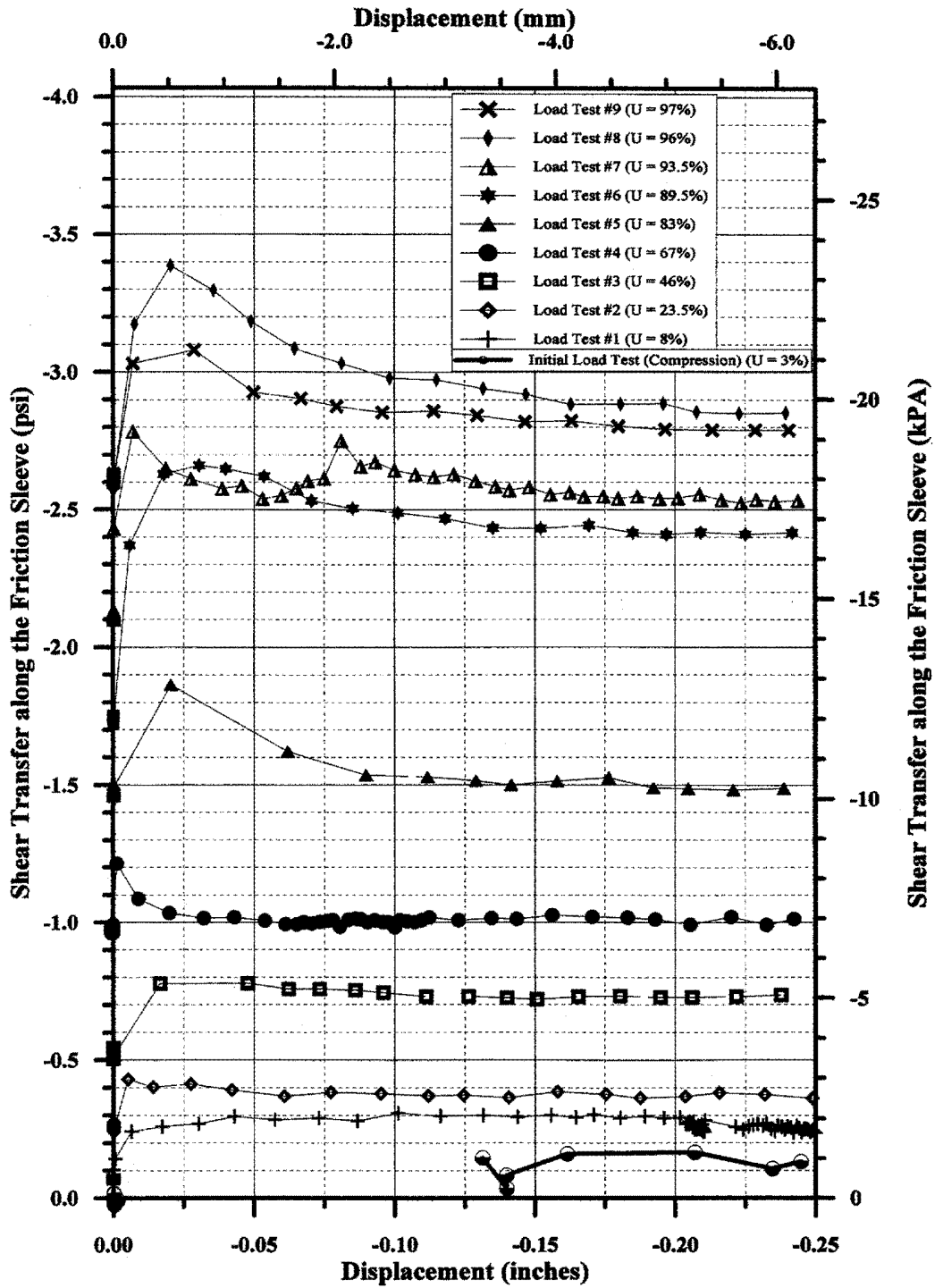


Figure 62. Shear Transfer Along the Friction Sleeve for MDMP Test NB3.

## 6.4 Surface Load Cell Measurements

### 6.4.1 General

During the static load tests, a 222-kN (50-kip) Lebow load cell was placed at the surface on top of the drill rods above the MDMP. This load cell was used as a force back-up measurement in case the internal load cells failed during testing. The load cell measurements can be utilized in a way similar to that in the traditional static load test performed on full-scale piles. During compression or tension tests, one would expect the surface load cell to record a force equal to or larger than that recorded by the internal load cells. However, during both model pile tests, the internal load cells continued to measure larger forces than the surface load cell. These records are presented and discussed in the following sections. During the MDMP test NB2, a large force, possibly due to heave, was measured during the initial static load test and is presented in the next section.

### 6.4.2 Heave Measurements During Model Pile Test NB2

As soon as the MDMP installation was completed, the initial load test was set up. This entailed attaching a 222-kN (50-kip) load cell at the top of the drill string and positioning displacement transducers on an independent reference beam to measure the movement of the pile top. The drill rig was reattached to the pile (above the load cell) and at approximately 23 min after the start of installation, the load cell and the displacement transducers were in place recording data. Figure 63 presents the obtained data, showing that from 23.54 min after the start of installation, the surface load cell recorded an increasing compressive load without any apparent movement of the pile top (follow the displacement record in the lower graph of Figure 63). These data indicated an upward pile motion against the stable platform of the drill rig. It is also important to note that during the time that the surface load cell was being loaded without any pile head movement, the forces measured by the internal load cells were not changing. A logical explanation is that the whole soil mass around the pile was moving upward with the pile due to heave. During periods of recorded pile top movement (shown in the gray shaded areas), the measured surface load appeared to consist of superimposed forces due to both shear and heave. This is especially evident during the second movement, where the pile was pulled in tension. During this period, the surface load cell measured an increase in tension force (decrease in total force) of 2.38 kN (535 lb) and then a decrease in tension force (increase in total force). While this occurred, load measurements recorded by the internal load cells showed steady forces following the shear, an expected behavior in a normally consolidated soil (no distinct peak). This indicates that heave of the soil surrounding the pile results in a push upward, thus increasing the compressive force measured by the surface load cell.

Figure 64 was obtained by subtracting the load recorded by the surface load cell prior to the initial load test, 7.17 kN (1612 lb) from the data presented in Figure 63. The forces measured by the surface load cell can then be compared to the internal load cell readings. At the onset of the displacement, with a small amount of movement, large changes in loads were recorded in the surface and internal load cells. After the initial sharp increase in load, the surface load cell appeared to gain additional compressive load at a faster rate than the internal load, suggesting

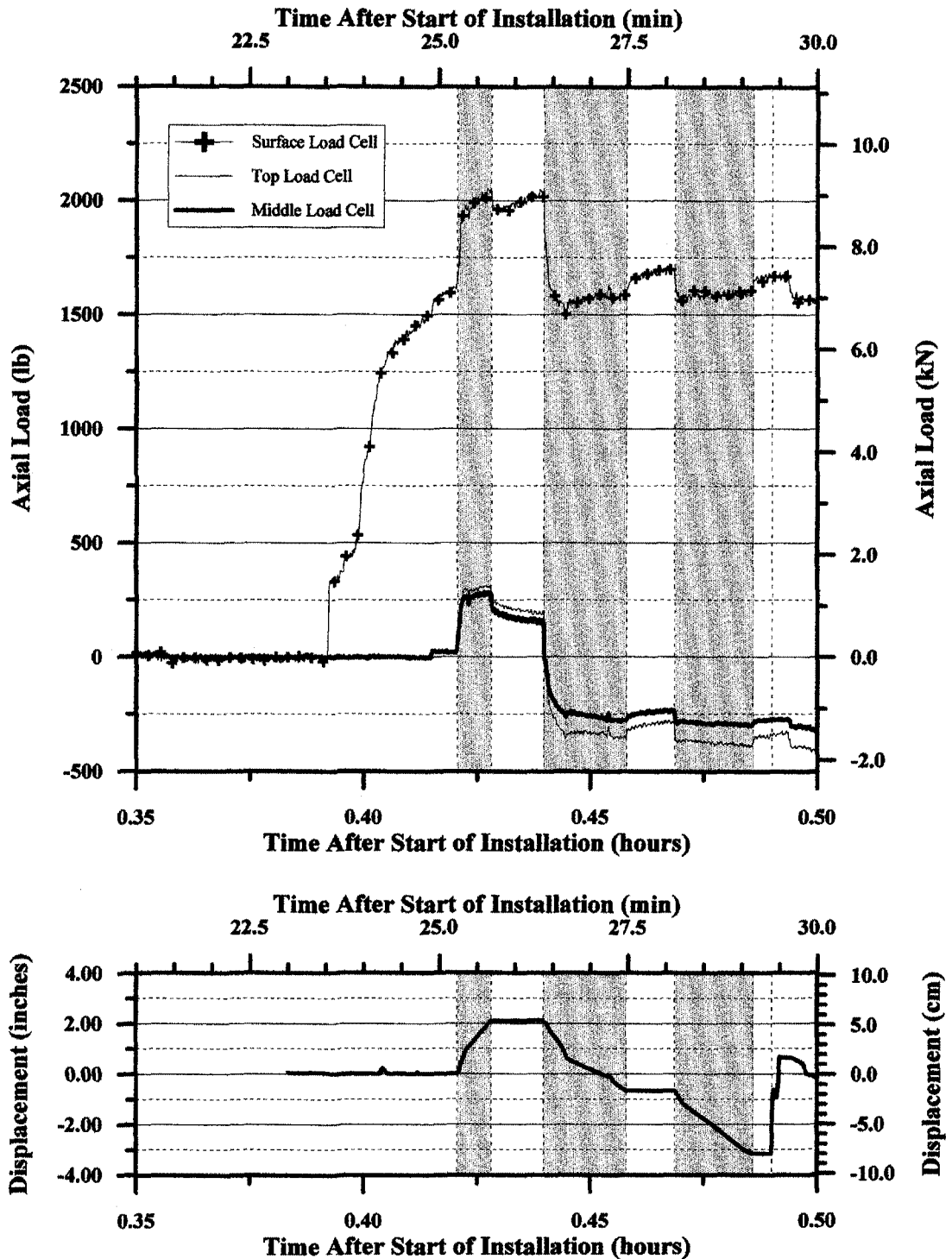


**Figure 63. Force and Displacement Measurements Following the MDMP Installation of Test NB2, Including Heave Effect and Initial Load Test.**

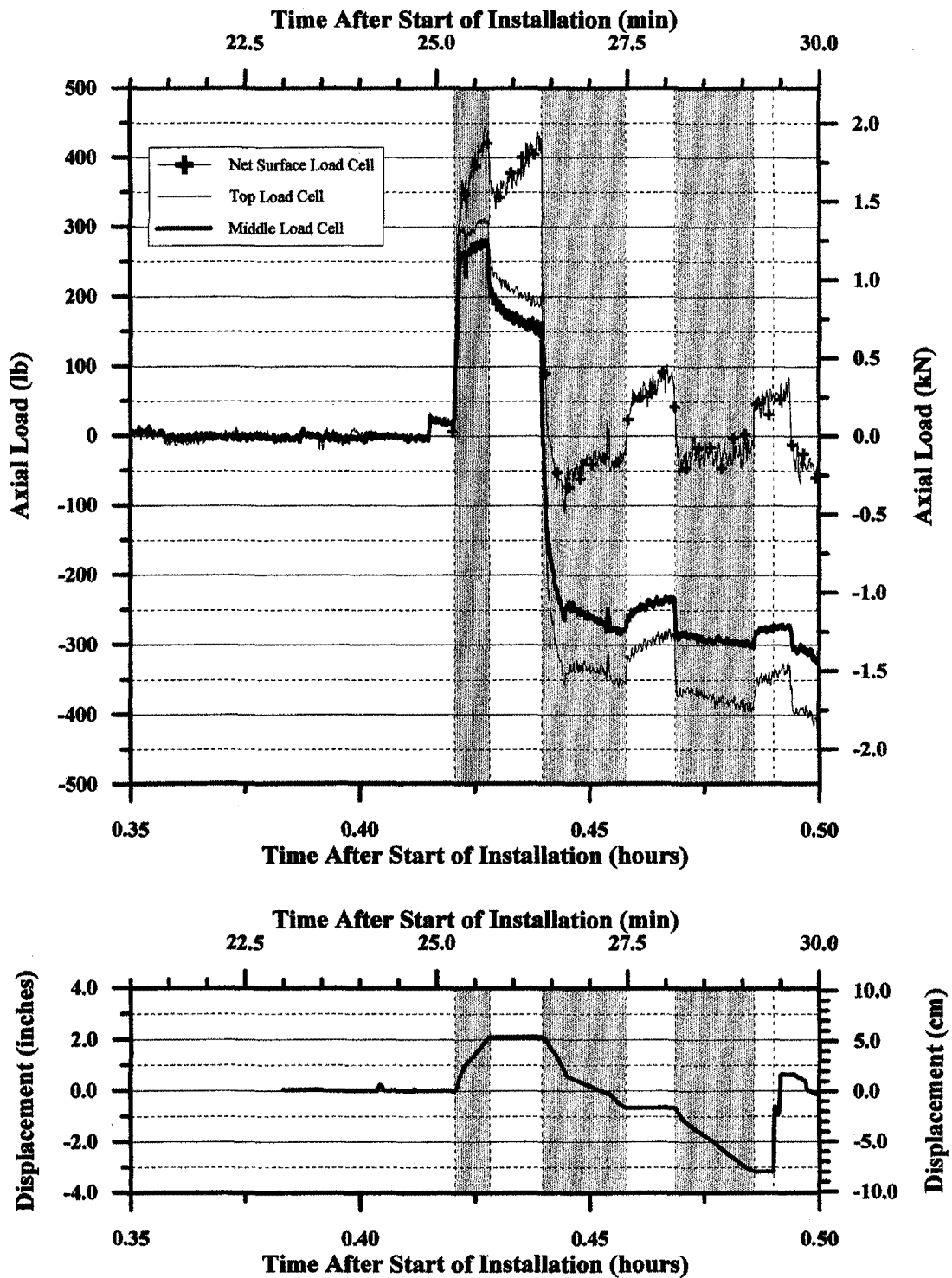


**Figure 64. Force and Displacement Measurements Following the MDMP Installation of Test NB2, Adjusted for Heave Prior to the Initial Load Test.**

further heave action. After the displacement was stopped, the internal load cells exhibited load relaxation while the surface load cell continued to gain compressive load. This behavior further indicated that the pile and the soil were moving upward together. Even when the pile was forced to move relative to the soil along the interface, the heave continued to take place.

### **6.4.3 Comparison of Surface and Internal Load Cell Measurements**

Figures 65 and 66 present the measurements of all the MDMP internal load cells and the surface load cell. The data suggest that the surface load cell recorded similar trends to the ones recorded by the internal load cells. As noted earlier in sections 6.3.2 and 6.3.3, the measured load changed without any apparent displacement. The assumption that temperature variation was the cause for the load changes was also supported by the fact that the surface load cell measured load changes at the same time as the internal load cells. During MDMP test NB2, the surface load cell moved into contact with the static load frame at approximately 135 h after the start of installation (Figure 65), causing the surface load cell to measure an increased load of 62.31 kN (14,008 lb). All these changes took place without any controlled movement of the hydraulic ram.

During a compression test, it is expected that the surface load cell would record an equal or larger compressive load compared to the loads recorded by the internal load cells. Also, it is expected that the tension forces measured by the surface load cell would be equal to or greater than the internal load cells. The data of Figures 65 and 66 indicated that the surface load cell did not always record a greater tension or compression load than that recorded by the internal load cells. This can be a result of the testing procedure, in which the valves to the hydraulic pump were closed at the end of the load test to prevent further ram movement. As the soil/pile system equilibrated, a decrease in tension forces was measured in most cases. Locked-in stresses continued to be measured by the internal load cells during the period between the load tests. During the tension load test, the pile elongated and then, as the tension forces decreased in the pile (due to equilibration), the pile shortened and the locked-in stresses continued to act. These locked-in stresses along the pile may be the reason why the load measured by the surface load cell did not match up to the loads measured by the internal load cells.

## **6.5 Static-Cyclic Loading**

### **6.5.1 Final Load Testing Sequence**

The final load tests were conducted following the excess pore pressure dissipation (see Figures 48 and 50 for event nos. 18 and 17, respectively). Figures 67 and 68 describe the sequences of the loading conducted during the last stage of testing for NB2 and NB3, respectively. Each figure includes the axial load (at all three locations), axial displacements (top of rods at the surface and the slip joint), and pore pressure with time throughout the final load testing sequence.

Initially, the MDMP was pushed downward 70 mm (2.75 in) to ensure that the slip joint had been completely closed. Figures 67 and 68 indicate that the slip joint was closed after 50.8 mm (2 in) of movement as measured at the top of the drill rods. After this point (the intersection of the slip joint and the surface displacement measurements), all the measured forces increased due to the

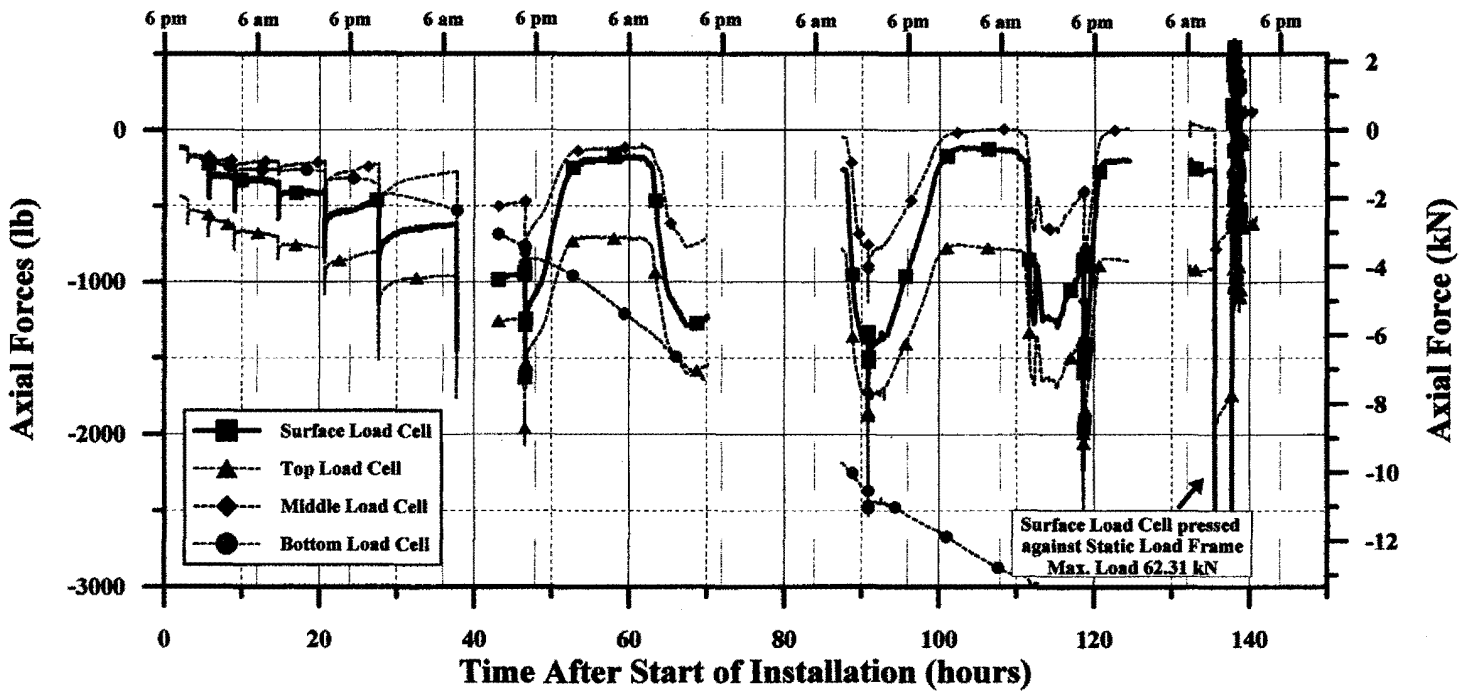
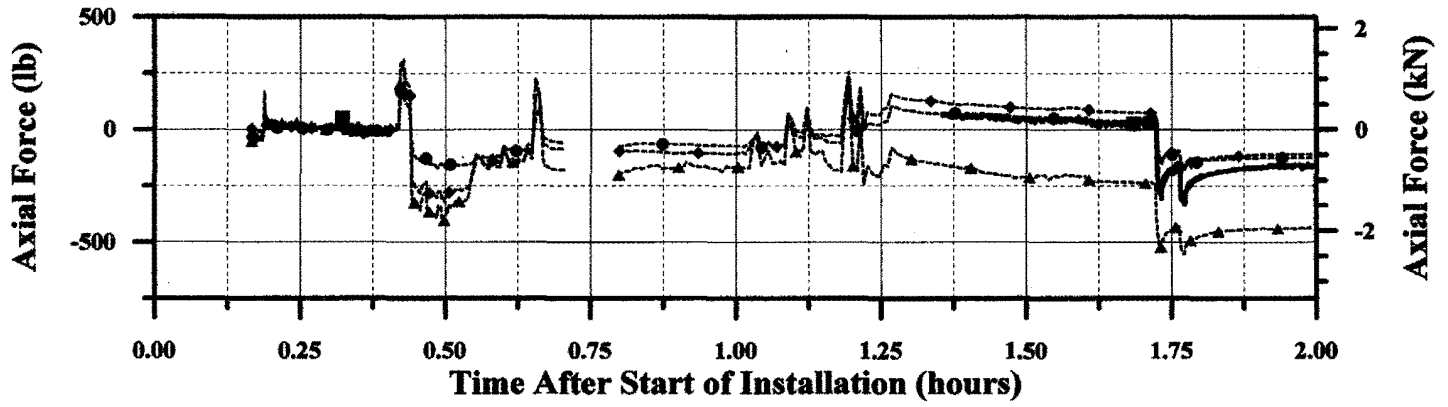


Figure 65. Comparison Between the Surface and the Internal Load Cell Measurements for MDMP Test NB2.

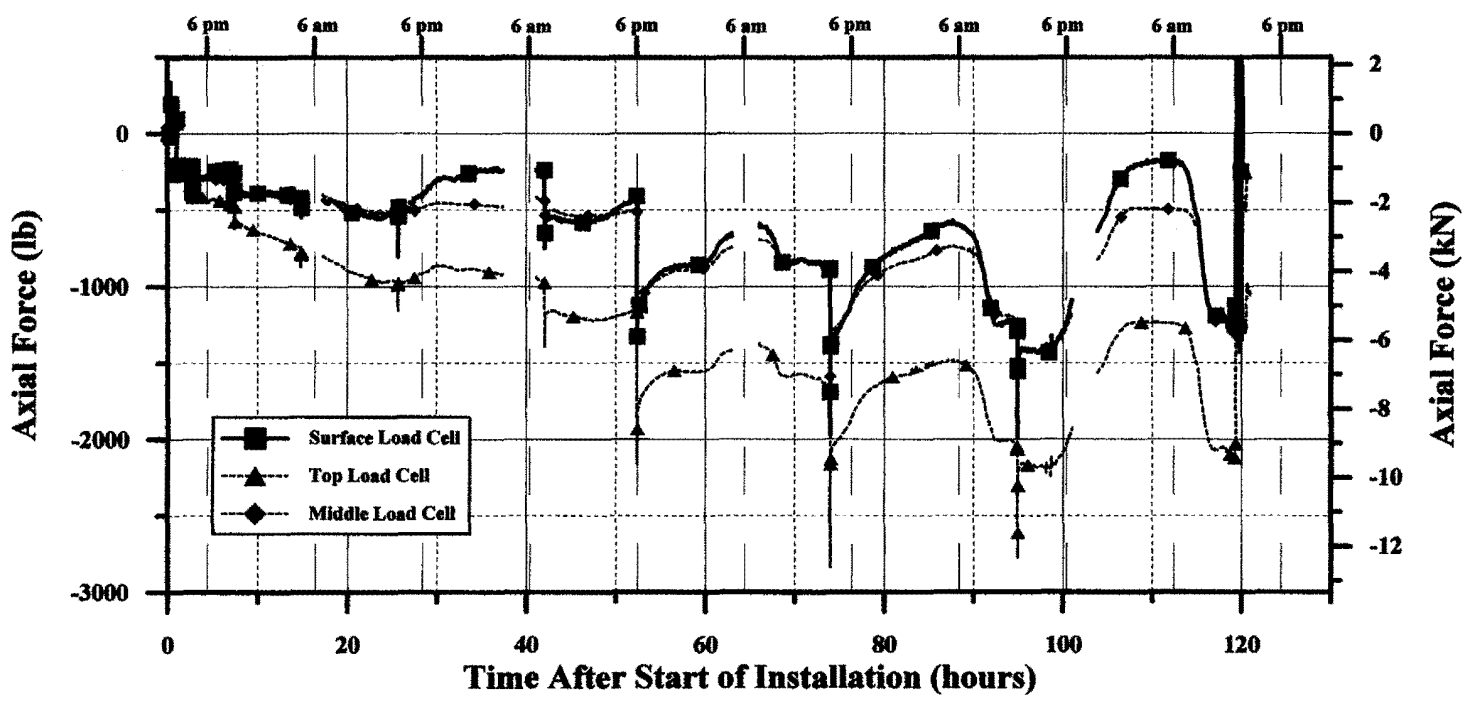
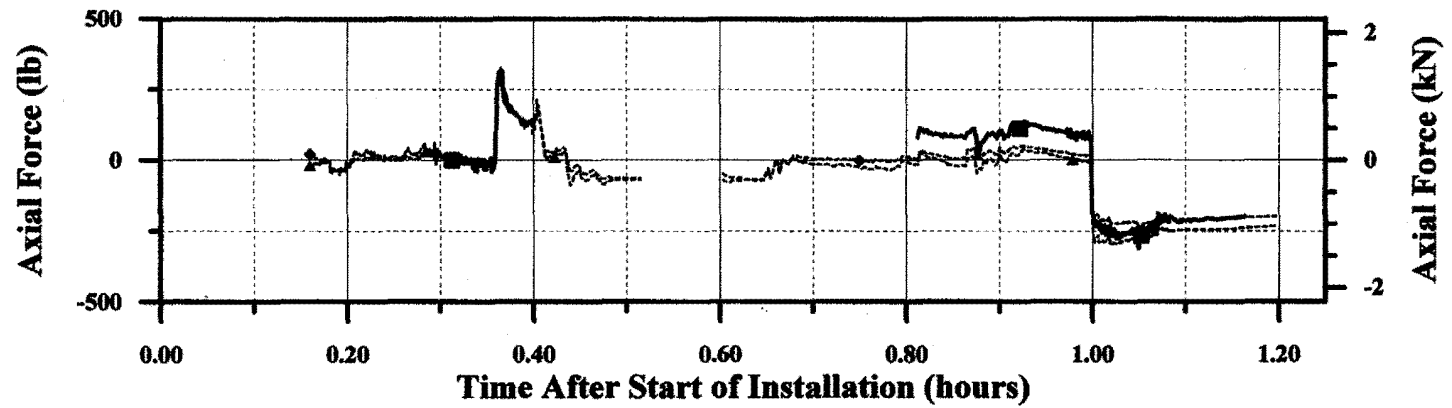
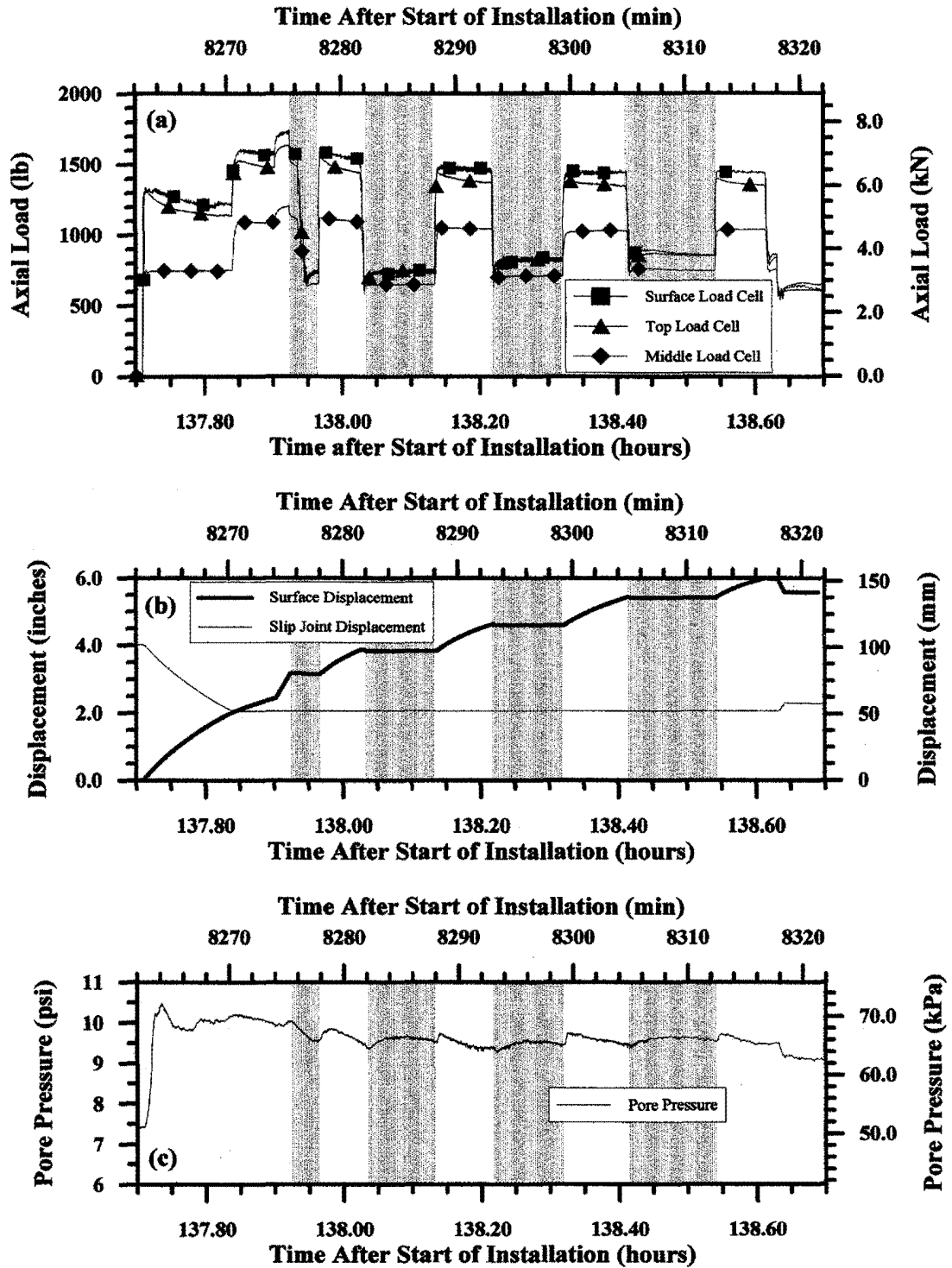
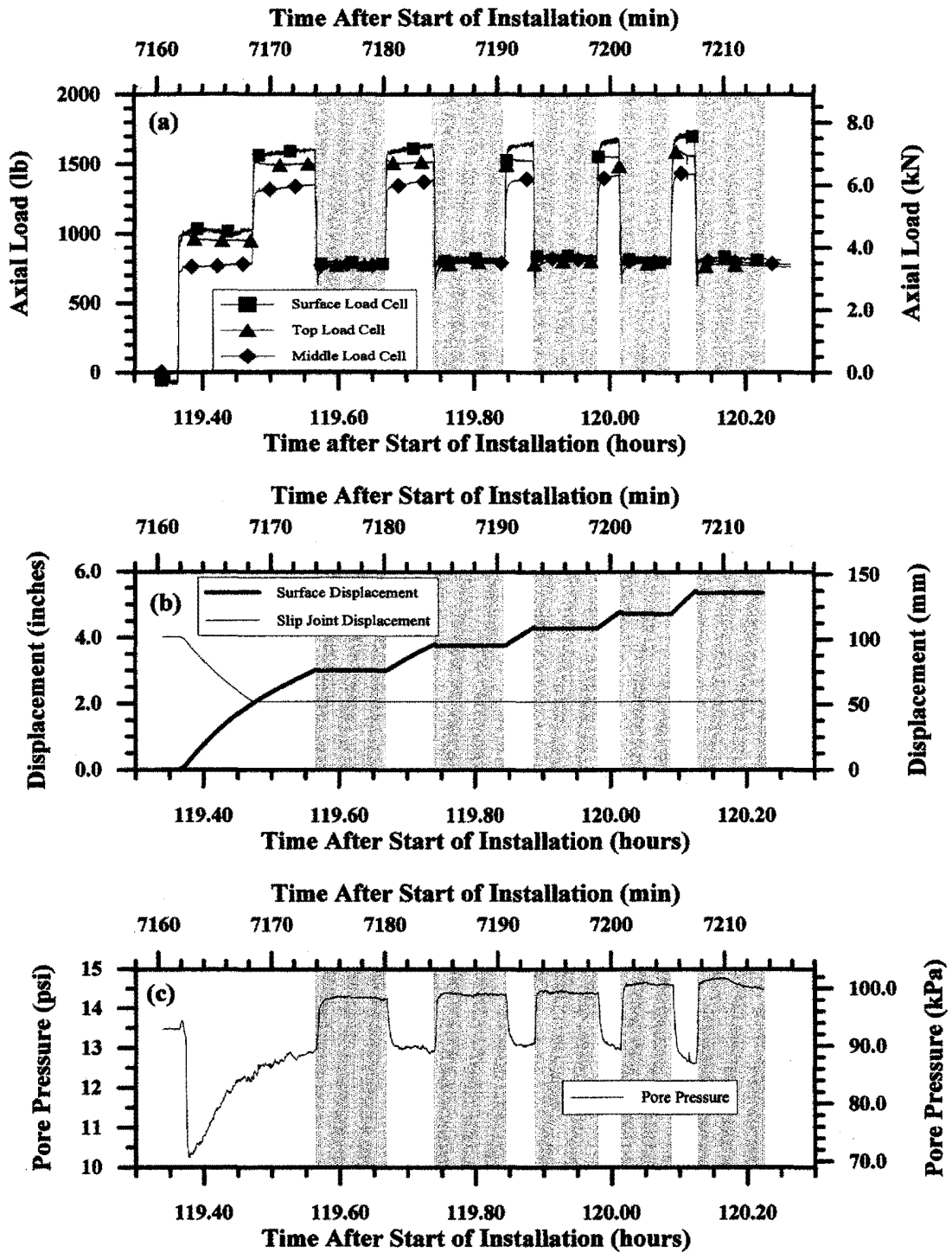


Figure 66. Comparison between the Surface and the Internal Load Cell Measurements for MDMIP Test NB3.



**Figure 67. Static-Cyclic Load Test Results for MDMP Test NB2:**  
**(a) Load cell measurements versus time, (b) Displacement measurements versus time, and (c) Pore pressure measurements versus time.**





**Figure 68. Static-Cyclic Load Test Results for MDMP Test NB3:**  
**(a) Load cell measurements versus time, (b) Displacement measurements versus time, and (c) Pore pressure measurements versus time.**

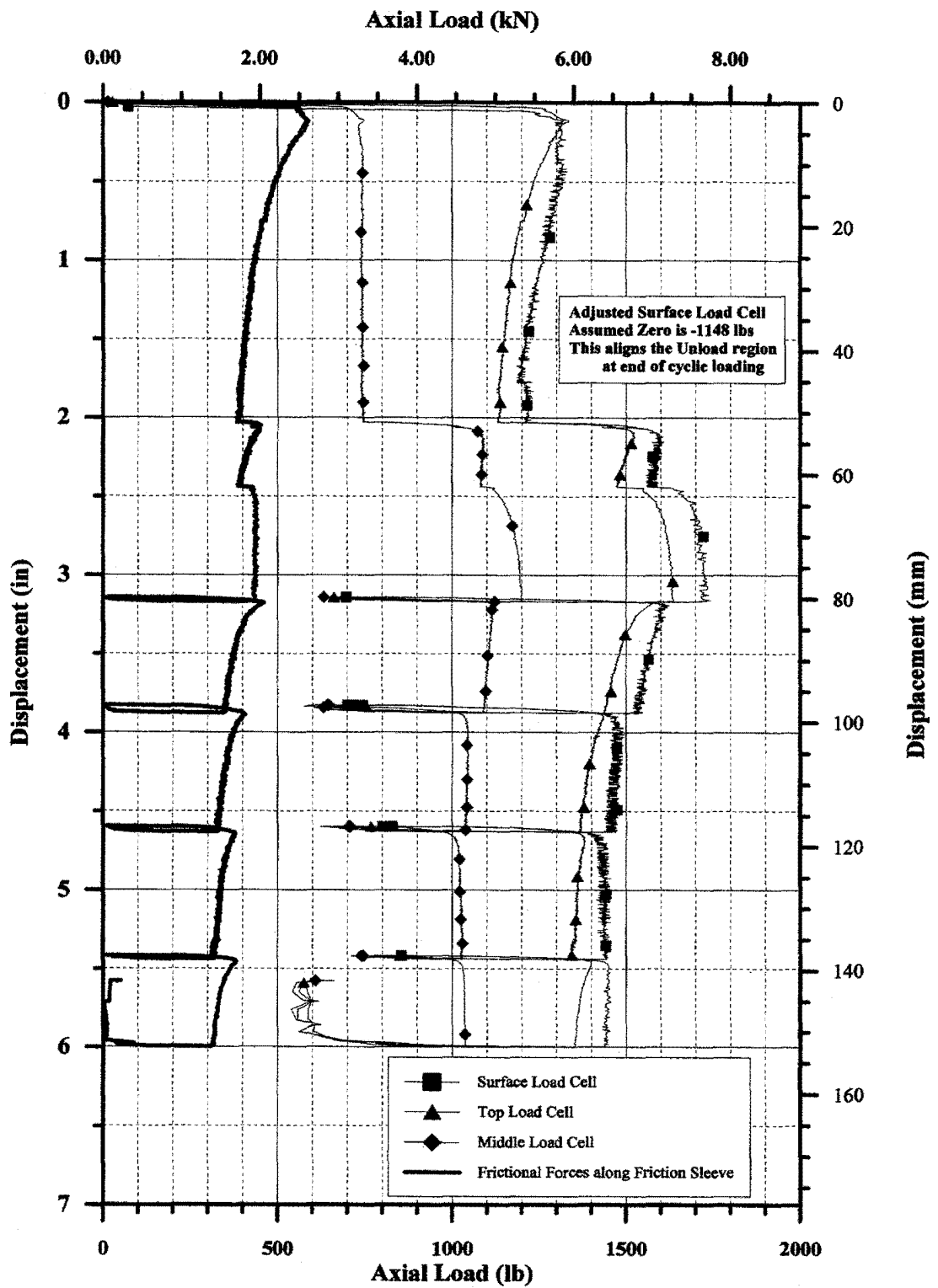
additional mobilized resistance at the tip and skin below the slip joint. After the initial downward push, the pile was pulled a short distance of about 0.76 mm (0.03 in) to unload the built-up loads. The pile was then cyclically loaded by pushing down 12.7 mm to 19.1 mm (0.5 to 0.75 in), followed by a short unloading, returning to the initial loading state. The pile was allowed to rest for 2 to 7 min between each unloading to allow the pore pressure to stabilize. This sequence of testing was in accordance with a new static cyclic load testing procedure currently under investigation. The shaded areas in Figures 67 and 68 represent the time at which the pile was held with no displacement.

### **6.5.2 Model Pile Test NB2**

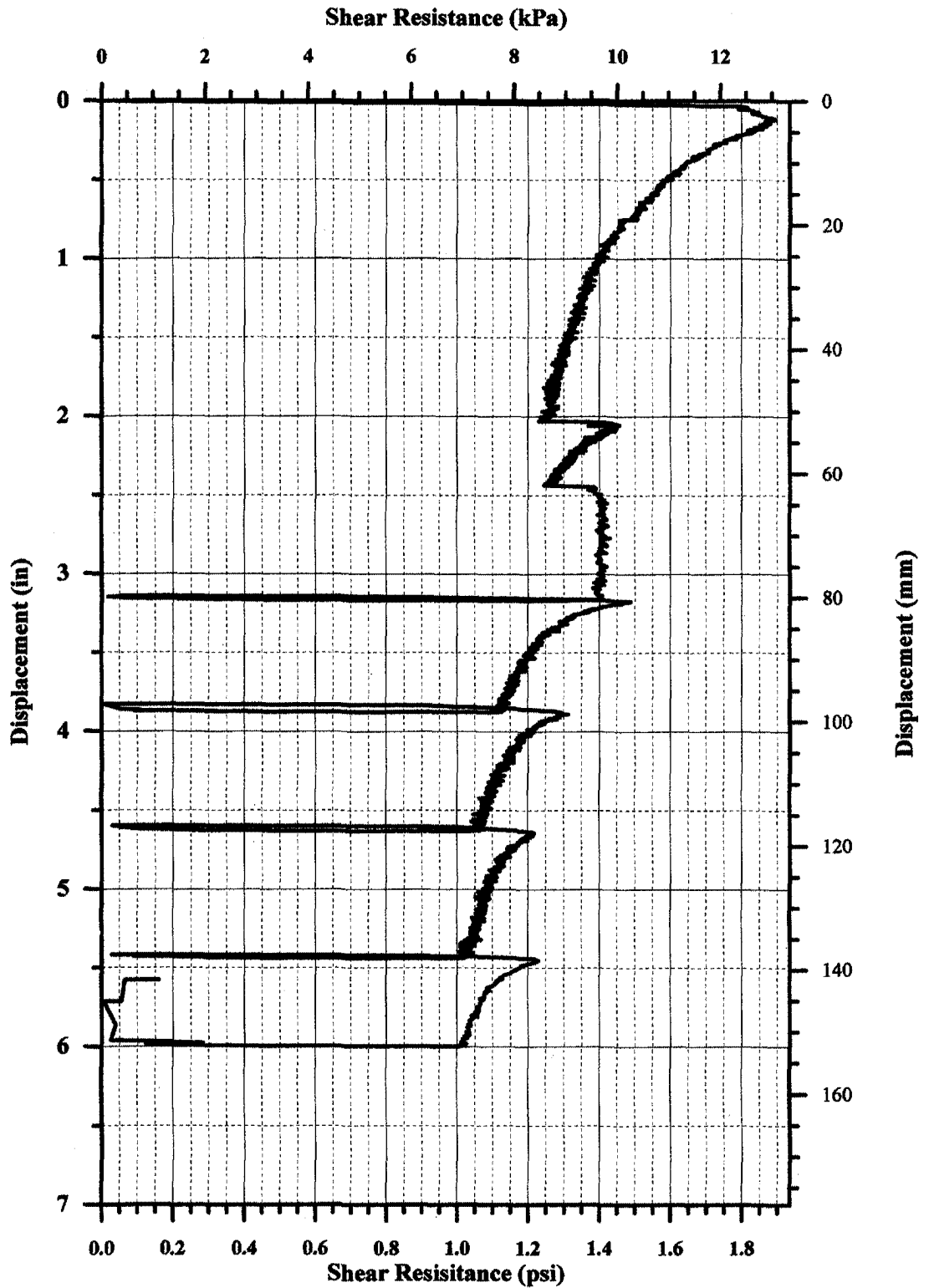
As a result of the load testing sequence throughout the MDMP test NB2, the surface load cell had been displaced the maximum possible distance and was compressed against the static load frame. As such, the load recorded before the start of the final load test was erroneous. To correct this error: (1) the load recorded by the internal top and middle load cells prior to the start of the final load test was assumed to be zero, and (2) the surface load measurement was assumed to be the same as that of the internal load cells at the end of the cyclic test. At this stage, due to the unloading, both internal load cells recorded approximately the same readings. The last assumption neglected to consider the weight of the pile allowing the comparison between the surface load measurements and the internal load measurements.

Figure 69a presents the details of the load-displacement relationships for all load cells recorded during the final load testing sequence. The obtained relationships between the individual load cell measurements seem to be reasonable (i.e., the surface load cell measurement is greater than that measured by the top load cell, which is greater than that measured by the middle) as a result of the above outlined adjustment procedure. Figure 69a also includes the force difference between the top and middle load cells, which represents the net force acting along the friction sleeve. Figure 69b contains an enlarged presentation of the force acting on the friction sleeve during the testing sequence. Within an initial displacement of about 1 mm, the frictional force is mobilized. A distinct peak shear strength of 13.07 kPa (1.90 psi) is followed by a strain softening. The shear stress was calculated assuming that the shear was taking place along the soil/shaft interface. It was evident, however, at the end of the testing (when the MDMP was retrieved) that as a thick layer of clay was attached to the pile, the shear took place in the soil some distance away from the pile. At the end of 50.8 mm of displacement, the residual shear strength was 8.61 kPa (1.25 psi). The pore pressure response to the cyclic load test is shown in Figure 67c. For reasons that are not clear, there was a positive pore pressure response in spite of a clear overconsolidated soil response as described above.

At a penetration distance of about 51 mm, the slip joint gap was closed and the lower portion of the pile became engaged in resistance to the loading. A large force increase was recorded at that point in all load cells (Figure 69a), with a small increase in the friction force along the friction sleeve. An additional small increase in all forces took place at a penetration distance of 62.2 mm (2.45 in), apparently due to a sharp increase in the displacement rate as can be seen in Figure 67b at approximately 8274.2 min after start of installation.



**Figure 69a. Load-Displacement Relationship for Static-Cyclic Final Load Test for MDMP Test NB2.**



**Figure 69b. Shear Resistance-Displacement Relationship Along the Friction Sleeve During Static-Cyclic Final Load Test for MDMP Test NB2.**

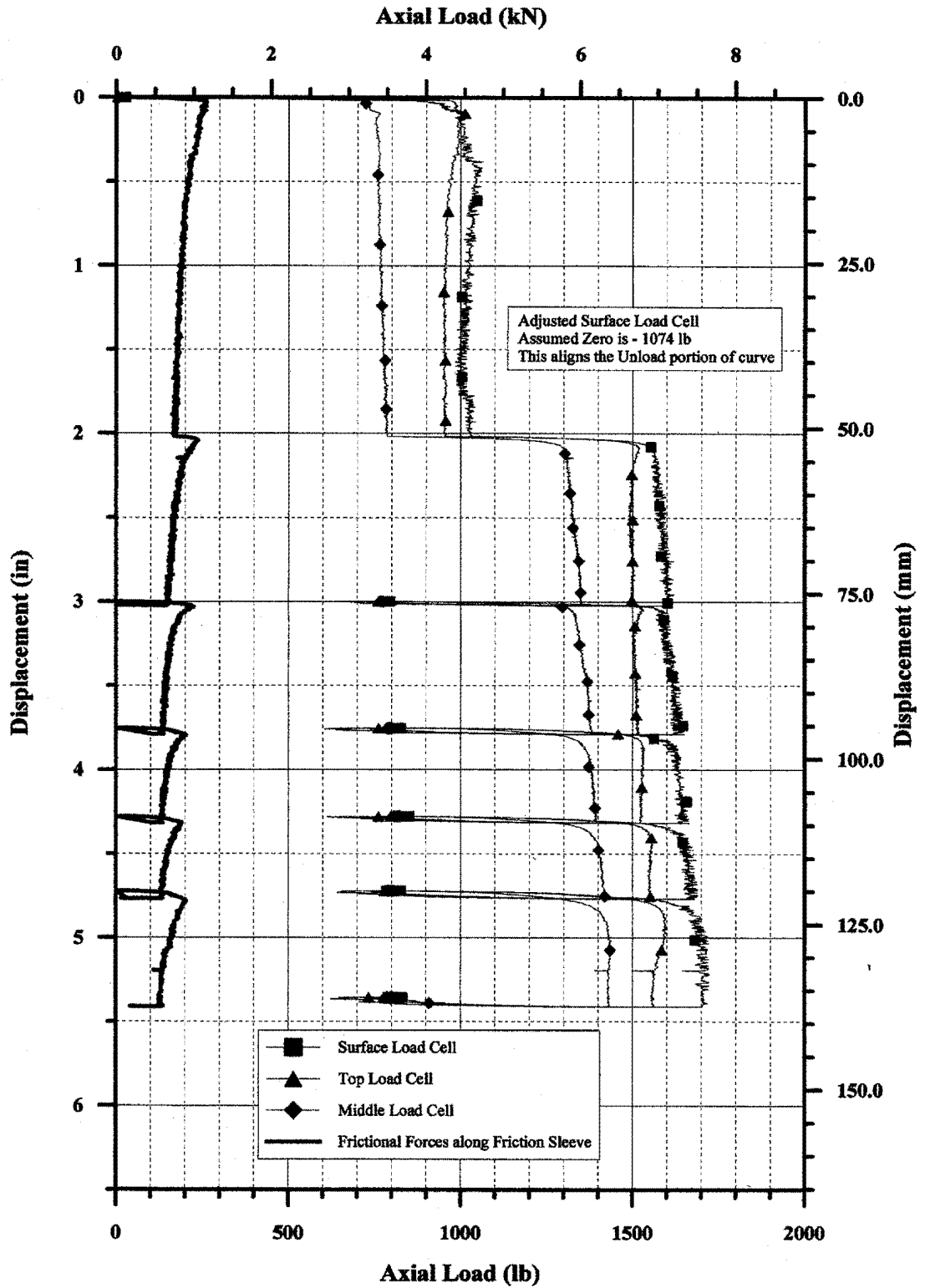
Following the initial penetration of 80 mm, a sequence of four unload-reload cycles were carried out. Each unloading was obtained through a very short upward motion between 0.46 and 1.20 mm and hence cannot be clearly seen in Figure 67b. The reloading has a distinctive peak, with a clear frictional degradation that continues to take place with the continuation of penetration. This degradation seems to be following approximately the same trend that was recorded for the first loading, suggesting that within a penetration distance of approximately 153 mm, the frictional stress decreased from a peak of 13.07 kPa (1.90 psi) to a residual stress of 7.04 kPa (1.02 psi). This continued slow degradation seems to be in line with interfacial and shear test results carried out on clay by Lemos (1986) and Bishop (1971), respectively. During this period, the pore pressure was maintained approximately constant, with a general trend of a slow decrease with time (Figure 67c).

### **6.5.3 Model Pile Test NB3**

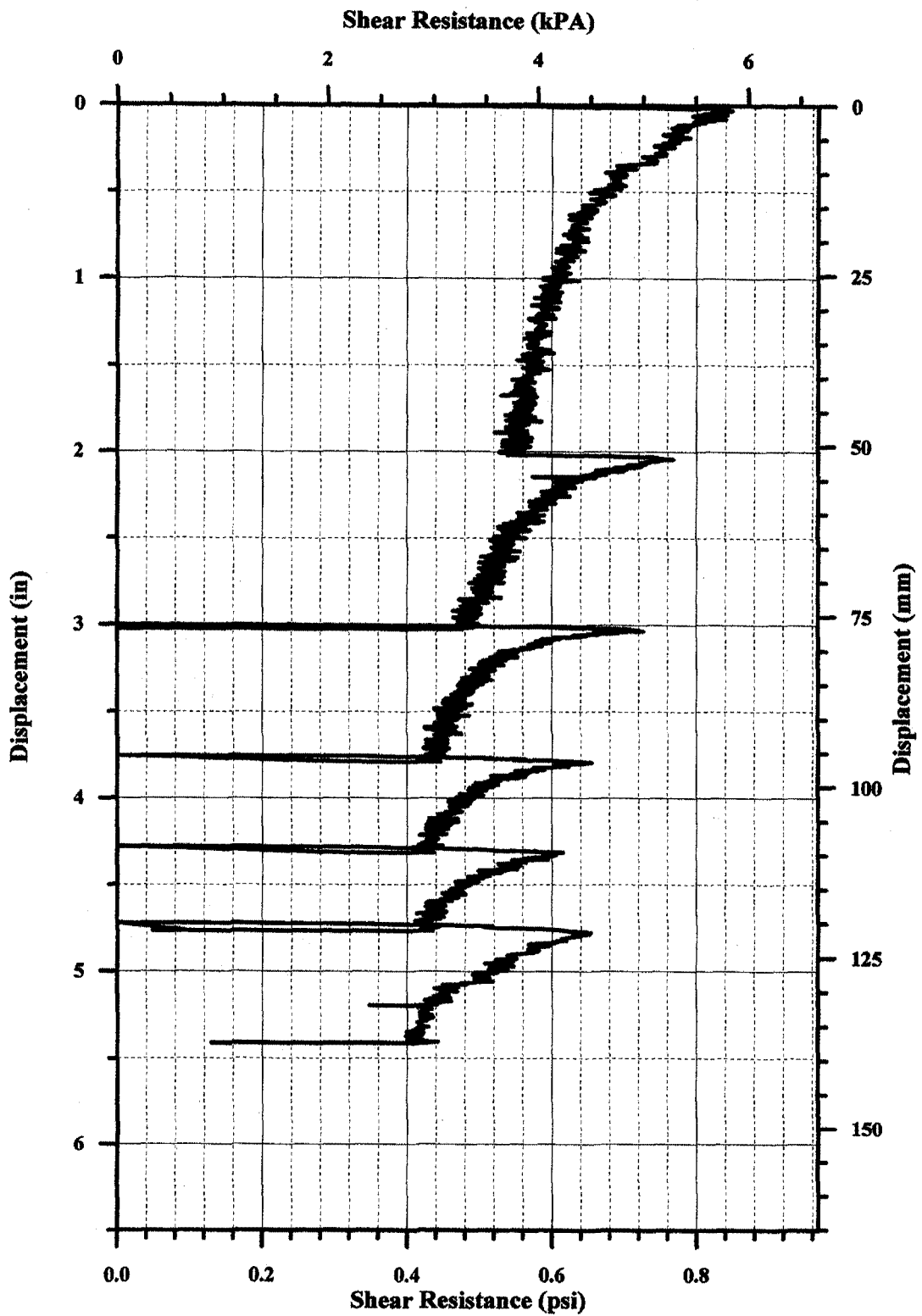
To analyze the data from the final loading sequence for the MDMP test NB3: (1) the load recorded by the internal top and middle load cells prior to the start of the final load test was assumed to be zero, and (2) the surface load measurement was assumed to be the same as that of the internal load cells at the end of the cyclic test and during periods of no displacement. At these stages, both internal load cells recorded approximately the same readings. The last assumption neglects to consider the weight of the pile allowing the comparison between the surface load measurements and the internal load measurements.

Figure 70a presents the details of the load-displacement relationships for all load cells recorded during the final load testing sequence. The obtained relationships between the individual load cell measurements seem to be reasonable (i.e., the surface load cell measurement is greater than the top load cell, which is greater than the middle) as a result of the above outlined adjustment procedure. Figure 70a also includes the force difference between the top and middle load cells, which represents the force acting along the friction sleeve. Figure 70b contains an enlarged presentation of the force acting on the friction sleeve during the testing sequence. Within an initial displacement of about 1 mm, the frictional force is mobilized. A distinct peak shear strength of 5.85 kPa (0.85 psi) is followed by a strain softening. The shear stress was calculated assuming that the shear was taking place along the soil/shaft interface. It was evident, however, at the end of the testing (when the MDMP was retrieved) that as a thick layer of clay was attached to the pile, the shear took place in the soil some distance away from the pile. At the end of 51 mm of displacement, the residual shear strength was 3.64 kPa (0.53 psi). The pore pressure response to the cyclic load test is shown in Figure 68c. For reasons that are not clear, there was a positive pore pressure response in spite of a clear overconsolidated soil response as described above.

At a penetration distance of about 51 mm, as the slip joint gap was closed, the lower portion of the pile engaged and contributed to the measured resistance as a result of the loading. A large force increase was recorded at that point in all load cells (Figure 70a), with a small increase in the friction force along the friction sleeve.



**Figure 70a. Load-Displacement Relationship for Static-Cyclic Final Load Test for MDMP Test NB3.**



**Figure 70b. Shear Resistance-Displacement Relationship Along the Friction Sleeve During Static-Cyclic Final Load Test for MDMP Test NB3.**

Following the initial penetration of 77 mm, a sequence of four unload-reload cycles were carried out. Each unloading was obtained through a very short upward motion between 0.67 to 1.27 mm and hence cannot be clearly seen in Figure 68b. The reloading has a distinctive peak, with a clear frictional degradation that continues to take place with the continuation of penetration. This degradation seems to be following approximately the same trend that was recorded for the first loading, suggesting that within a penetration distance of approximately 137 mm, the frictional stress decreased from a peak of 5.85 kPa (0.85 psi) to a residual stress of 2.92 kPa (0.42 psi). This continued slow degradation seems to be in line with interfacial and shear test results carried out on clay by Lemos (1986) and Bishop (1971), respectively. During this period, the pore pressure was maintained approximately constant, with a general trend of a slow decrease with time (Figure 68c).

## **6.6 Dynamic Measurements**

### **6.6.1 Driving System and Dynamic Measurements**

The top of the drill rod string was instrumented (Surface Measurement) with strain gauges and accelerometers as part of a dynamic measurement system manufactured by Pile Dynamics, Inc. of Cleveland Ohio. A Pile-Driving Analyzer (PDA) (model PAK) monitored the gauges during the MDMP installation and a subsequent restrike following the completion of the pore pressure dissipation. In addition, the internal load cells and accelerometers (at the top and middle load cell locations) were monitored with additional PDA provided by Carl Ealy, a Geotechnical Research Engineer from FHWA. The force wave was measured using the MDMP internal load cells mounted in the model pile and designed for static load application. Reusable gauges manufactured by Pile Dynamics, Inc., specifically designed for dynamic applications, were bolted to the drill rods to monitor the impact force at the pile top. The acceleration of the pile was recorded by three accelerometers that were mounted internally inside each load cell and externally with up to four accelerometers bolted on the drill rods. Of the three accelerometers inside the MDMP, two were of the piezoelectric type and were mounted inside the top and bottom load cells, while the accelerometer mounted inside the middle load cell was a piezoresistive type.

The driving system consisted of a 0.623-kN (140-lb) safety hammer normally used for Standard Penetration Tests (SPT). The operator of the drill rig controlled the hammer drop by visual inspection. During the installation of the MDMP Test NB2, the stroke of the hammer was initially limited to 0.152 m (6 in) to ensure that dynamic stresses would not harm the instruments inside the MDMP. Since all instrumentation continued to record data within the assigned limits, the stroke was subsequently increased to 0.305 m (12 in) and then to 0.457 m (18 in). The compressive stresses, recorded by the PDA during the driving sequences, did not exceed 90% of the yield strength ( $0.9f_y$ ) of steel in order to avoid overstressing the pile.

The number of blows required to drive the pile a predetermined amount was visually observed and recorded during driving. The force and acceleration data were recorded with the two PDAs at a frequency of 20,000 Hz (one test was at 5,000 Hz). The recorded blows from each PDA were synchronized by using the time stamp for each PDA. Several indiscriminate blows were recorded



## (2) Typical Dynamic Measurements.

Typical dynamic measurement data obtained via the PDA along the MDMP during driving of NB2 are shown in Figures 72 and 73. Figures 72 and 73 present the force and velocity signals recorded at the top of the drill rods (denoted as surface measurement) and the internal load cells inside the pile above and below the friction sleeve (denoted as top load cell and middle load cell) and at the pile tip (denoted as bottom load cell) for two blows. Note that the data related to blow 21 in Figures 72a and b corresponded to the same impact denoted as blow 20 in Figures 72c and d. In the same way the data related to blow 221 in Figures 73a and b correspond to the same blow denoted as blow 241 in Figures 73c and d. The different notations are a result of the use of two different acquisition (PDA) systems as previously described (section 4.3). Blows 21/20 and 221/241 were recorded at penetration depths of approximately 6.74/0.183 m (22.1/0.6 ft) and 8.69/2.44 m (28.5/8.0 ft) as related to the ground surface and the bottom of the cased borehole, respectively.

The data in Figures 72a and 73a were related to the surface measurements for a time period of 25 ms, while Figures 72b and 73b depict the same data over a 5-ms period detailing the impact wave and its reflections during the travel time down to the tip and back. The data in Figures 72a and b and 73a and b indicated the following:

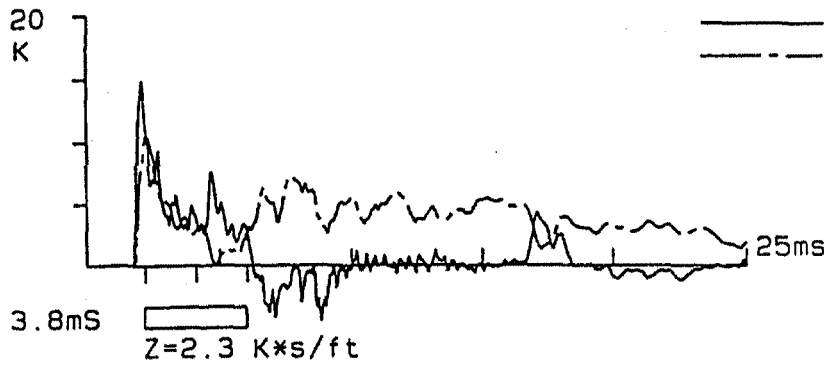
1. **Surface Force** - The force at the top of the rods seemed to undergo sharp fluctuations. Examining the individual force records led to the conclusion that F3 was the main contributor to the variations, while the force records of F4 contained smaller variations. Three possible reasons could be connected to these fluctuations: (1) the vibrations of the strain transducers themselves — the small diameter of the drill rod (in comparison with a full-scale pile) made the attachment of the force transducers difficult and, as a result, the transducers can vibrate during driving; (2) the rods were made of sections of mechanical tubing with screw sections welded to each end — the large increase in the impedance of the rods at each connection resulted in a force reflection that was recorded as an increased force at the surface measurement; and (3) the differences between F3 and F4 suggested the existence of an uneven impact at the pile top — if the transducers were mounted close to the impact (in this case, 0.305 m below the top drill rods and approximately 1.25 m from the impact), then the records would reflect the uneven stress distribution in the pile. A better understanding of the source of the presented records could be obtained through the examination of the surface force records obtained during the MDMP driving of NB3. During this driving, two sets of surface gauges were attached to the drill rods, allowing a better assessment of the fluctuation source in the force measurements. The data and relevant discussion are presented in section 6.6.4 and Figures 77a through f. At approximately 2.5 ms after the peak force had been recorded, an increase in the force was measured. This positive increase was associated with the reflection of the traveling wave from the rod/pile connection at a distance of 7.01 m (23 ft) from the surface measurement.

UNIVERSITY MASS-LOWELL  
Newbury Model Pile Test

PDI PILE DRIVING ANALYZER® v4.04

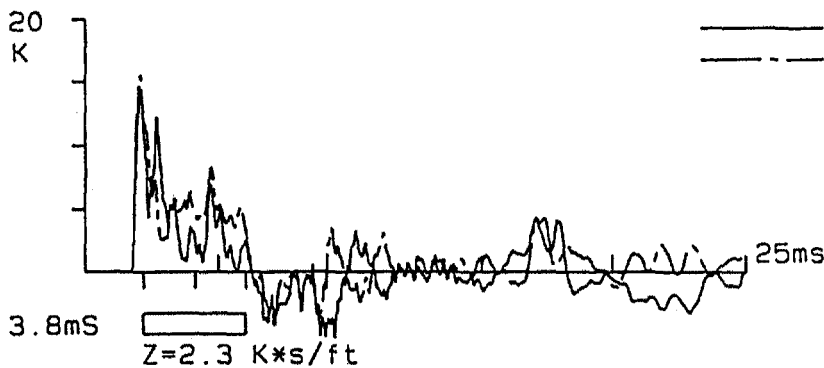
NB2R00IN 06-Mar-96

Surface Measurement



BN	21
EMX	0.04 Kip-ft
FMX	15.0 Kips
VMX	4.6 ft/s
DMX	0.55 inch
DFN	0.55 inch
FT1	11.8 Kips
VT1	4.6 ft/s
RTL	11.1 Kips
RMX	2.7 Kips
LE	32.40 ft
AR	1.29 in2
EM	30000 Ksi
SP	0.492 K/ft3
WS	16810 ft/s

Surface Measurement



BN	21
EMX	0.04 Kip-ft
FMX	15.0 Kips
VMX	4.6 ft/s
DMX	0.55 inch
DFN	0.55 inch
FT1	11.8 Kips
VT1	4.6 ft/s
RTL	11.1 Kips
RMX	2.7 Kips
LE	32.40 ft
AR	1.29 in2
EM	30000 Ksi
SP	0.492 K/ft3
WS	16810 ft/s

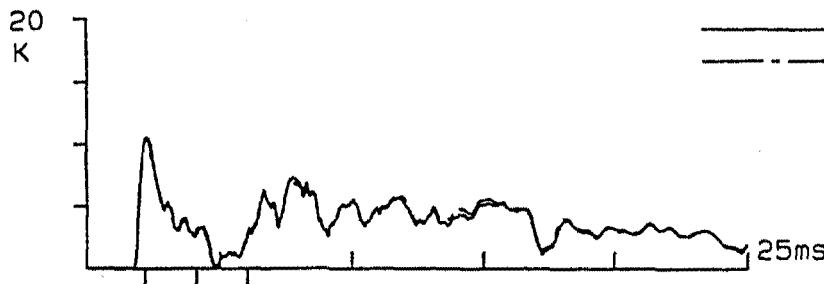


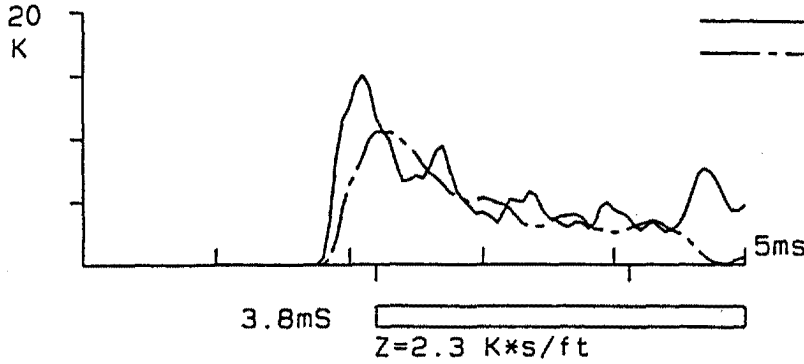
**Figure 72a. PDA Dynamic Measurements During the Installation of MDMP Test NB2: Surface Force and Velocity Records Over 25 ms.**

UNIVERSITY MASS-LOWELL  
Newbury Model Pile Test

PDI PILE DRIVING ANALYZER® v4.04

NB2R00IN 06-Mar-96

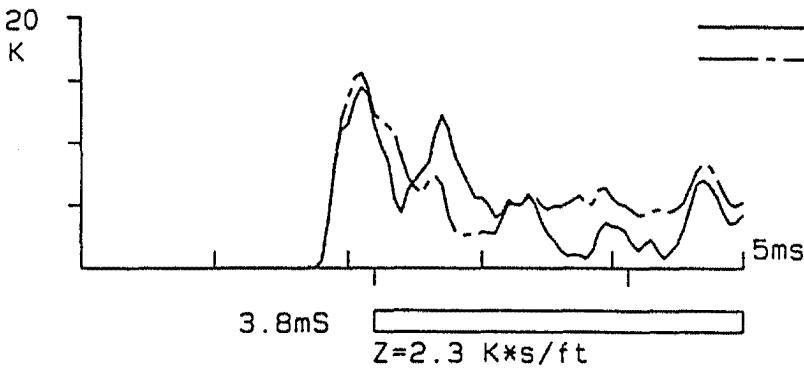
Surface Measurement



BN	21
EMX	0.04 Kip-ft
FMX	15.0 Kips
VMX	4.6 ft/s
DMX	0.55 inch
DFN	0.55 inch
FT1	11.8 Kips
VT1	4.6 ft/s
RTL	11.1 Kips
RMX	2.7 Kips

LE	32.40 ft
AR	1.29 in2
EM	30000 Ksi
SP	0.492 K/ft3
WS	16810 ft/s

Surface Measurement



BN	21
EMX	0.04 Kip-ft
FMX	15.0 Kips
VMX	4.6 ft/s
DMX	0.55 inch
DFN	0.55 inch
FT1	11.8 Kips
VT1	4.6 ft/s
RTL	11.1 Kips
RMX	2.7 Kips

LE	32.40 ft
AR	1.29 in2
EM	30000 Ksi
SP	0.492 K/ft3
WS	16810 ft/s

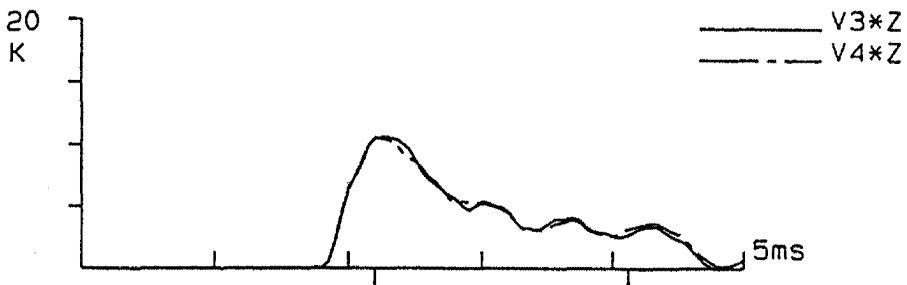


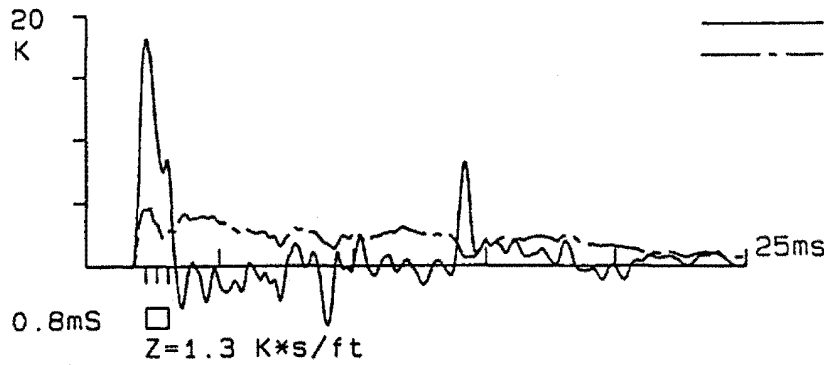
**Figure 72b. PDA Dynamic Measurements During the Installation of MDMP Test NB2: Surface Force and Velocity Records Over 5 ms.**

UNIVERSITY MASS-LOWELL  
Newbury Model Pile Test

PDI PILE DRIVING ANALYZER® v4.04

NB2MPIN 06-Mar-96

Top Load Cell

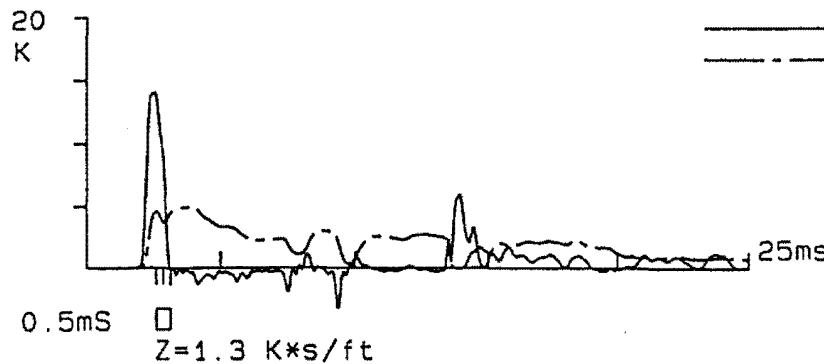


BN	20
EMX	0.04 Kip-ft
FMX	18.0 Kips
VMX	3.5 ft/s
DMX	0.52 inch
DFN	0.52 inch
FT1	18.0 Kips
VT1	3.4 ft/s
RTL	14.0 Kips
RMX	14.0 Kips
LE	7.10 ft
AR	0.74 in2
EM	30000 Ksi
SP	0.492 K/ft3
WS	16810 ft/s

Newbury Model Pile Test

NB2MPIN 06-Mar-96

Middle Load Cell

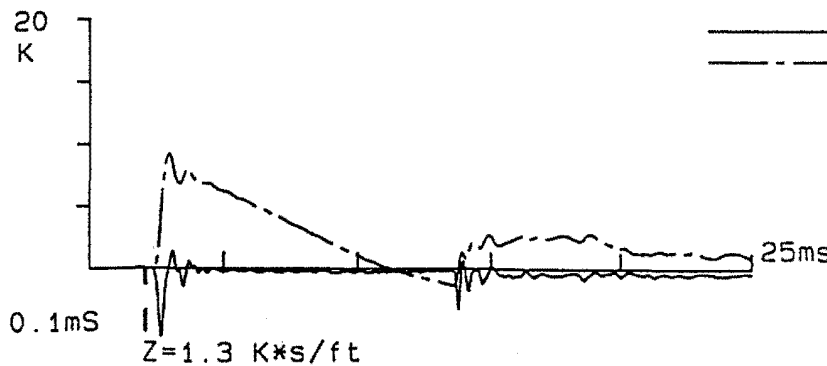


BN	20
EMX	0.03 Kip-ft
FMX	14.1 Kips
VMX	3.8 ft/s
DMX	0.49 inch
DFN	0.49 inch
FT1	13.9 Kips
VT1	3.5 ft/s
RTL	6.9 Kips
RMX	6.9 Kips
LE	4.70 ft
AR	0.74 in2
EM	30000 Ksi
SP	0.492 K/ft3
WS	16810 ft/s

Newbury Model Pile Test

NB2MPIN 06-Mar-96

Bottom Load Cell



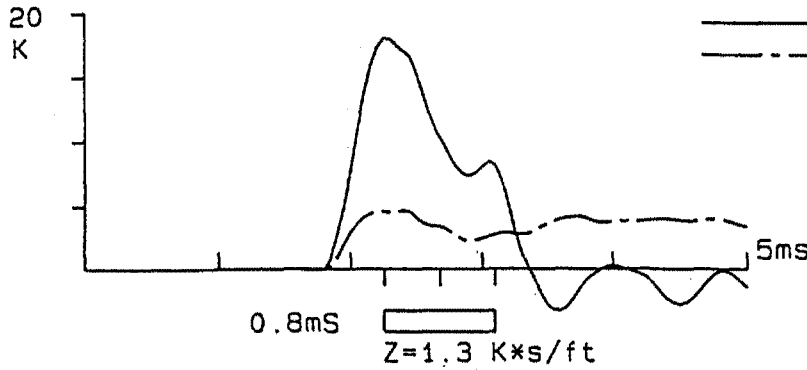
BN	20
EMX	0.00 Kip-ft
FMX	1.5 Kips
VMX	7.1 ft/s
DMX	0.59 inch
DFN	0.59 inch
FT1	0.1 Kips
VT1	0.0 ft/s
RTL	0.0 Kips
RMX	1.7 Kips
LE	1.00 ft
AR	0.74 in2
EM	30000 Ksi
SP	0.492 K/ft3
WS	16810 ft/s

**Figure 72c. PDA Dynamic Measurements During the Installation of MDMP Test NB2: Internal Force and Velocity Records Over 25 ms.**

UNIVERSITY MASS-LOWELL  
Newbury Model Pile Test

PDI PILE DRIVING ANALYZER® v4.04

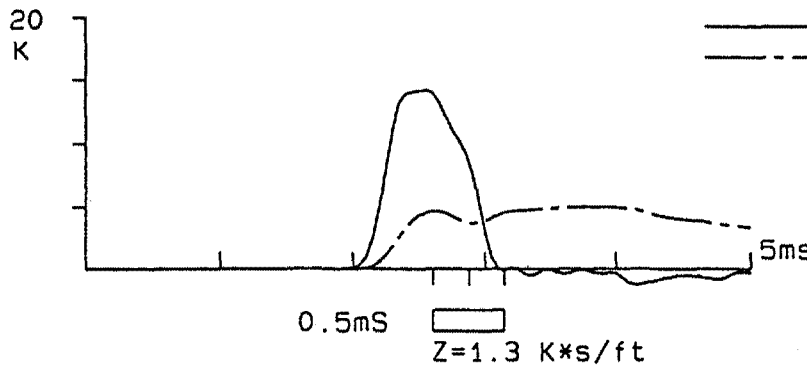
NB2MPIN 06-Mar-96  
Top Load Cell



BN	20
EMX	0.04 Kip-ft
FMX	18.0 Kips
VMX	3.5 ft/s
DMX	0.52 inch
DFN	0.52 inch
FT1	18.0 Kips
VT1	3.4 ft/s
RTL	14.0 Kips
RMX	14.0 Kips
LE	7.10 ft
AR	0.74 in2
EM	30000 Ksi
SP	0.492 K/ft3
WS	16810 ft/s

Newbury Model Pile Test

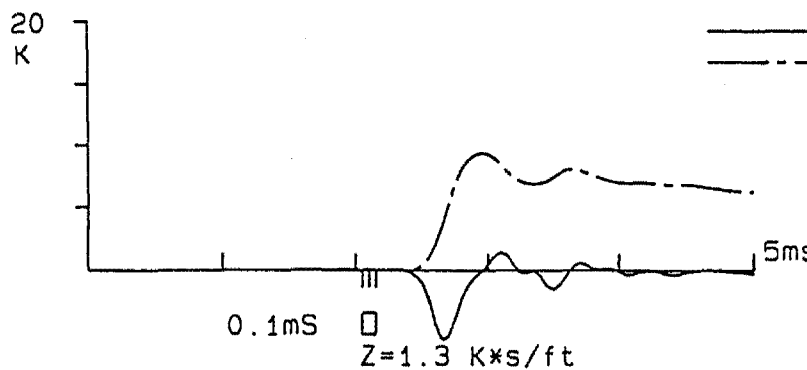
NB2MPIN 06-Mar-96  
Middle Load Cell



BN	20
EMX	0.03 Kip-ft
FMX	14.1 Kips
VMX	3.8 ft/s
DMX	0.49 inch
DFN	0.49 inch
FT1	13.9 Kips
VT1	3.5 ft/s
RTL	6.9 Kips
RMX	6.9 Kips
LE	4.70 ft
AR	0.74 in2
EM	30000 Ksi
SP	0.492 K/ft3
WS	16810 ft/s

Newbury Model Pile Test

NB2MPIN 06-Mar-96  
Bottom Load Cell



BN	20
EMX	0.00 Kip-ft
FMX	1.5 Kips
VMX	7.1 ft/s
DMX	0.59 inch
DFN	0.59 inch
FT1	0.1 Kips
VT1	0.0 ft/s
RTL	0.0 Kips
RMX	1.7 Kips
LE	1.00 ft
AR	0.74 in2
EM	30000 Ksi
SP	0.492 K/ft3
WS	16810 ft/s

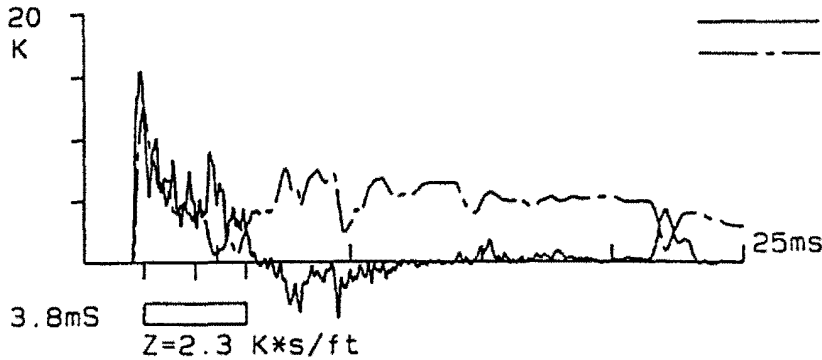
**Figure 72d. PDA Dynamic Measurements During the Installation of MDMP Test NB2: Internal Force and Velocity Records Over 5 ms.**

UNIVERSITY MASS-LOWELL  
Newbury Model Pile Test

POI PILE DRIVING ANALYZER® v4.04

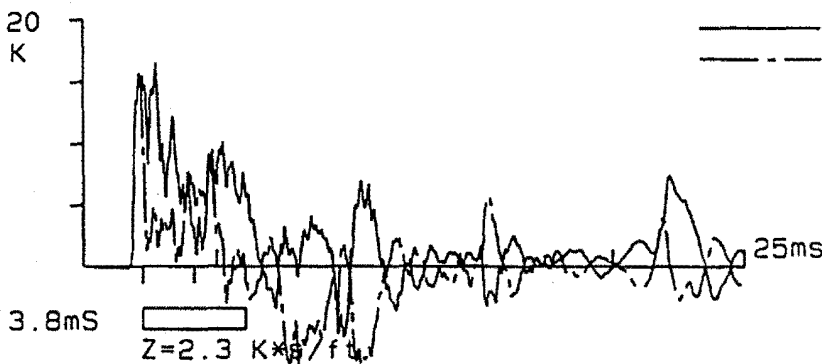
NB2RODIN 06-Mar-96

Surface Measurement



BN	221
EMX	0.06 Kip-ft
FMX	15.5 Kips
VMX	5.5 ft/s
DMX	0.72 inch
DFN	0.72 inch
FT1	12.9 Kips
VT1	5.5 ft/s
RTL	12.5 Kips
RMX	3.3 Kips
LE	32.40 ft
AR	1.29 in <sup>2</sup>
EM	30000 Ksi
SP	0.492 K/ft <sup>3</sup>
WS	16810 ft/s

Surface Measurement



BN	221
EMX	0.06 Kip-ft
FMX	15.5 Kips
VMX	5.5 ft/s
DMX	0.72 inch
DFN	0.72 inch
FT1	12.9 Kips
VT1	5.5 ft/s
RTL	12.5 Kips
RMX	3.3 Kips
LE	32.40 ft
AR	1.29 in <sup>2</sup>
EM	30000 Ksi
SP	0.492 K/ft <sup>3</sup>
WS	16810 ft/s

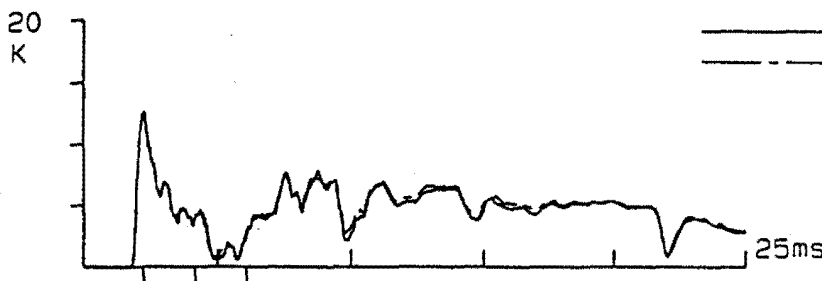


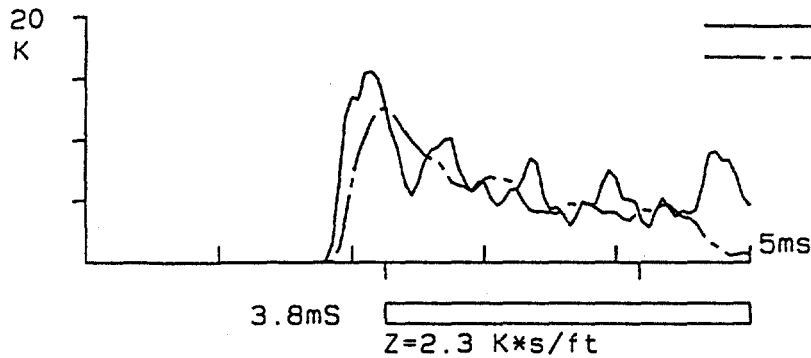
**Figure 73a. PDA Dynamic Measurements During the Installation of MDMP Test NB2: Surface Force and Velocity Records Over 25 ms.**

UNIVERSITY MASS-LOWELL  
Newbury Model Pile Test

POI PILE DRIVING ANALYZER® v4.04

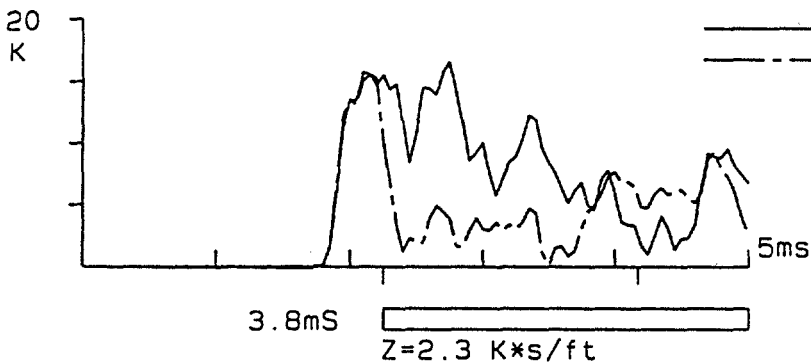
NB2RODIN 06-Mar-96

Surface Measurement



BN	221
EMX	0.06 Kip-ft
FMX	15.5 Kips
VMX	5.5 ft/s
DMX	0.72 inch
DFN	0.72 inch
FT1	12.9 Kips
VT1	5.5 ft/s
RTL	12.5 Kips
RMX	3.3 Kips
LE	32.40 ft
AR	1.29 in <sup>2</sup>
EM	30000 Ksi
SP	0.492 K/ft <sup>3</sup>
WS	16810 ft/s

Surface Measurement



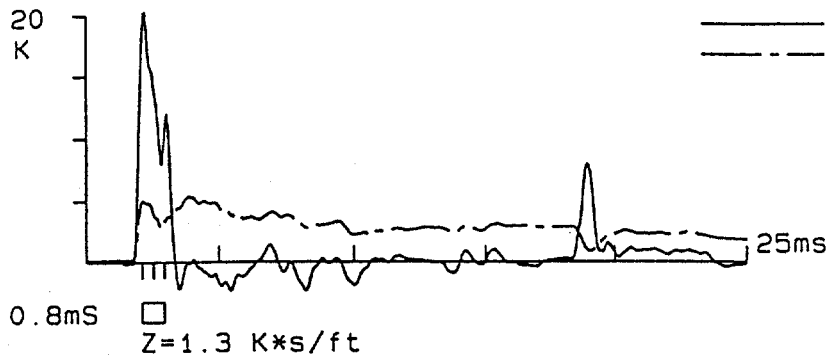
BN	221
EMX	0.06 Kip-ft
FMX	15.5 Kips
VMX	5.5 ft/s
DMX	0.72 inch
DFN	0.72 inch
FT1	12.9 Kips
VT1	5.5 ft/s
RTL	12.5 Kips
RMX	3.3 Kips
LE	32.40 ft
AR	1.29 in <sup>2</sup>
EM	30000 Ksi
SP	0.492 K/ft <sup>3</sup>
WS	16810 ft/s



**Figure 73b. PDA Dynamic Measurements During the Installation of MDMP Test NB2: Surface Force and Velocity Records Over 5 ms.**

UNIVERSITY MASS-LOWELL  
Newbury Model Pile Test

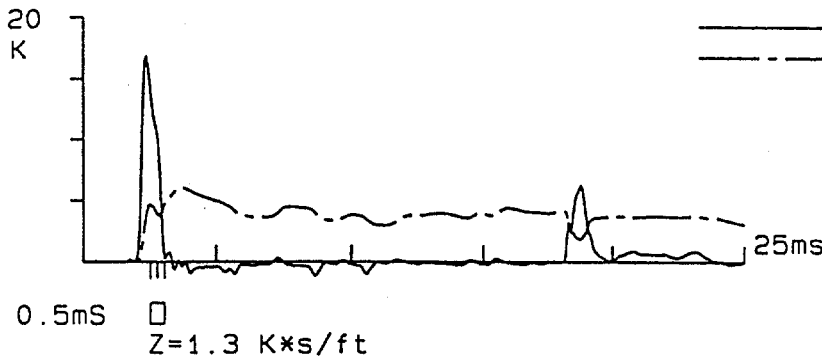
PDI PILE DRIVING ANALYZER® v4.04  
NB2MPIN 06-Mar-96  
Top Load Cell



BN	241
EMX	0.06 Kip-ft
FMX	20.3 Kips
VMX	4.1 ft/s
DMX	0.75 inch
DFN	0.75 inch
FT1	19.1 Kips
VT1	3.8 ft/s
RTL	16.1 Kips
RMX	16.1 Kips
LE	7.10 ft
AR	0.74 in2
EM	30000 Ksi
SP	0.492 K/ft3
WS	16810 ft/s

Newbury Model Pile Test

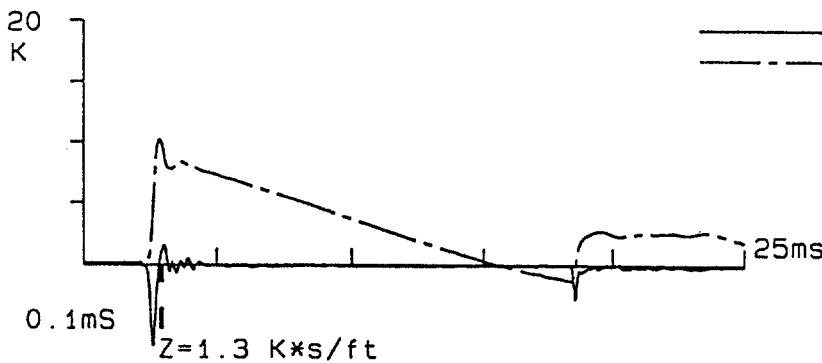
NB2MPIN 06-Mar-96  
Middle Load Cell



BN	241
EMX	0.04 Kip-ft
FMX	16.9 Kips
VMX	4.6 ft/s
DMX	1.06 inch
DFN	1.06 inch
FT1	14.2 Kips
VT1	3.6 ft/s
RTL	7.2 Kips
RMX	7.2 Kips
LE	4.70 ft
AR	0.74 in2
EM	30000 Ksi
SP	0.492 K/ft3
WS	16810 ft/s

Newbury Model Pile Test

NB2MPIN 06-Mar-96  
Bottom Load Cell



BN	241
EMX	0.00 Kip-ft
FMX	1.6 Kips
VMX	7.8 ft/s
DMX	0.78 inch
DFN	0.78 inch
FT1	0.6 Kips
VT1	7.8 ft/s
RTL	1.4 Kips
RMX	2.0 Kips
LE	1.00 ft
AR	0.74 in2
EM	30000 Ksi
SP	0.492 K/ft3
WS	16810 ft/s

**Figure 73c. PDA Dynamic Measurements During the Installation of MDMP Test NB2: Internal Force and Velocity Records Over 25 ms.**

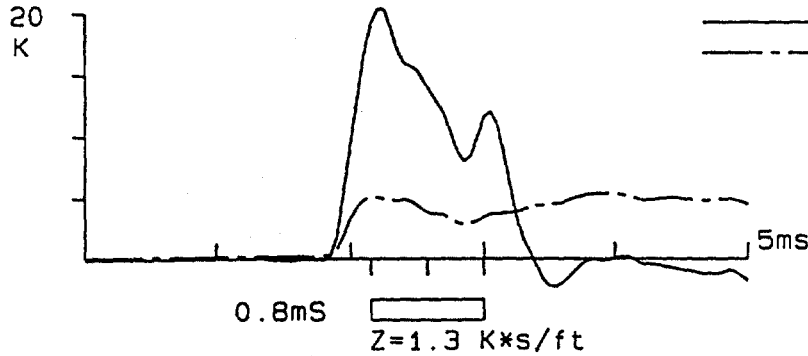


UNIVERSITY MASS-LOWELL  
Newbury Model Pile Test

PDI PILE DRIVING ANALYZER® v4.04

NB2MPIN 06-Mar-96

Top Load Cell

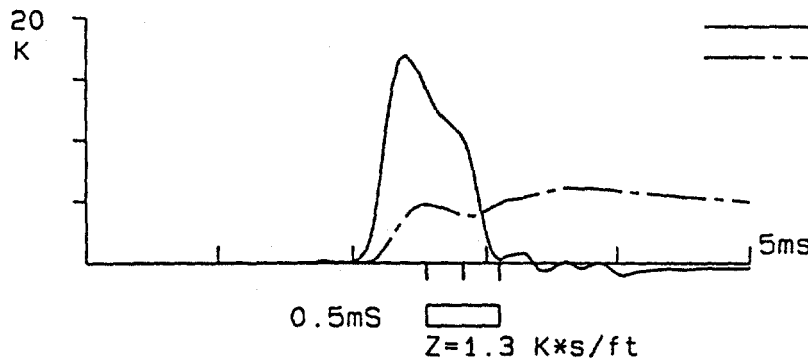


BN	241
EMX	0.06 Kip-ft
FMX	20.3 Kips
VMX	4.1 ft/s
DMX	0.75 inch
DFN	0.75 inch
FT1	19.1 Kips
VT1	3.8 ft/s
RTL	16.1 Kips
RMX	16.1 Kips
LE	7.10 ft
AR	0.74 in2
EM	30000 Ksi
SP	0.492 K/ft3
WS	16810 ft/s

Newbury Model Pile Test

NB2MPIN 06-Mar-96

Middle Load Cell

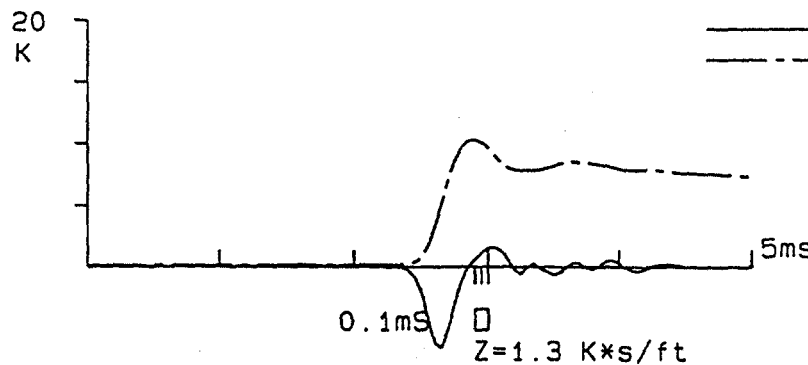


BN	241
EMX	0.04 Kip-ft
FMX	16.9 Kips
VMX	4.6 ft/s
DMX	1.06 inch
DFN	1.06 inch
FT1	14.2 Kips
VT1	3.6 ft/s
RTL	7.2 Kips
RMX	7.2 Kips
LE	4.70 ft
AR	0.74 in2
EM	30000 Ksi
SP	0.492 K/ft3
WS	16810 ft/s

Newbury Model Pile Test

NB2MPIN 06-Mar-96

Bottom Load Cell



BN	241
EMX	0.00 Kip-ft
FMX	1.6 Kips
VMX	7.8 ft/s
DMX	0.78 inch
DFN	0.78 inch
FT1	0.6 Kips
VT1	7.8 ft/s
RTL	1.4 Kips
RMX	2.0 Kips
LE	1.00 ft
AR	0.74 in2
EM	30000 Ksi
SP	0.492 K/ft3
WS	16810 ft/s

**Figure 73d. PDA Dynamic Measurements During the Installation of MDMP Test NB2: Internal Force and Velocity Records Over 5 ms.**

2. **Surface Velocity** - The velocity record at the top of the drill rods was multiplied by the rod's impedance and presented in force units for comparison to force measurements. In general, the velocity followed the force signal due to the input hammer blow. The ratio of proportionality between the two peaks (velocity\*impedance/force) ranged from 0.76 to 0.89. This ratio was reasonable under the anticipated uneven stress distribution resulting from the SPT hammer blow. The smoother shape of the velocity curve and the nice match between the two independent records suggested that the record was valid as the acceleration record would not be affected by the aforementioned factors affecting the force record. The only factor from those previously mentioned that affected the velocity record was the impedance variations along the rods. In the case of an increase in impedance, a decrease in the velocity was recorded. The increase in the velocity at about 7 ms to an elevated level of approximately 0.610 to 0.914 m/sec (2 to 3 ft/sec) suggested that the pile continued to move at some constant velocity (approximately) over a lengthy period of time. The evaluation of this record could be done through integration of the velocity over time. This record provided the pile displacement and could be compared to the observed driving records. Moreover, with continuous motion of easy driving, the maximum displacement (denoted as DMX) should be equal to the final displacement (denoted DFN). The record for blow 21/20 (Figure 72) indicated that, indeed,  $DMX=DFN=13.97$  mm (0.55 in). This compared well with the observed displacement of eight blows per 91.44 mm (3.6 in), which translated to an average of 11.43 mm (0.45 in) per blow. This is not so for blow 221/241 (Figure 73), where the displacement obtained from the velocity record ( $DMX=DFN=18.3$  mm (0.72 in)) differed from the penetration resistance of 10 blows per 91.44 mm (3.6 in), which translated to an average of 9.14 mm (0.36 in) per blow. It should be emphasized that for acceleration records over a long period, double integration (in order to obtain displacement) is prone to increasing inaccuracy. Small DC voltage in the acceleration record will be integrated to a triangular-shaped velocity added to the actual record. Integration of this component will result in a second order increase at the displacement record, all as a function of time.

The data in Figures 72c and 73c were related to the internal measurements for a time period of 25 ms, while Figures 72d and 73d depict the same data over a 5-ms period to show the details of the impact wave traveling down through the pile. The data in Figures 72c and d and 73c and d indicate the following:

1. **Internal Forces** - The internal forces were recorded using the existing built-in large load cells. These load cells were designed for measuring static loads and were not configured for quick response. In spite of this fact, the obtained records seemed to be adequate and reliable. The records for blow 21/20 (presented in Figure 72c and d) suggested that the wave arrived to the top load cell was about 1.2 times the magnitude of the wave recorded at the surface and was of a similar shape. The ratio between the surface load cell and the top load cell force measurement for blow 221/241 was 1.3. Both records reflected the influence of the impedance increase when the rods were

record is presented in Chapter 7, where it is shown to match the expected analysis. The peak wave passing through the middle load cell was reduced by about 17.3 and 15.1 kN (3.9 and 3.4 kips) for blows 21/20 and 221/241, respectively. This reduction was equal to the friction force acting on the sleeve and will be discussed further in Chapter 7. The discontinuity of the internal force records was a result of the MDMP slip joint. The impact was transferred to the lower section, which separated because it was incapable of transferring the reflected wave coming from the tip.

The records referring to the bottom load cell related to the gauges installed in the segment about 1.2 m (3.8 ft) below the slip joint and about 178 mm (7 in) from the tip of the pile. Both records (referring to blows 21 and 221 in Figure 72 and 73) showed consistent behavior. A negative force was recorded with a downward velocity. The impact at the slip joint sent a compressive wave down the lower section of the pile. This compressive stress, under easy driving conditions, should be reflected as a tensile stress upwards. Therefore, the expected records should have consisted of compressive and tensile waves, differing from the presented records. It is unclear as to why the recorded wave shape is in its present form. One possibility is an uncommon electronic problem known to exist with the electrical strain gauges system (Rausche, 1997).

2. **Internal Velocities** - Overall, the acceleration records at all locations seemed to provide consistent and reliable velocity signals. The data in Figures 72a and b and 73a and b suggested that both accelerometers mounted at the surface worked well throughout the driving, independently providing a velocity record that matched very well with each other. The overall good performance of the accelerometers suggested that: (1) the installation of only one accelerometer at each internal load cell was justified, and (2) the single velocity signals at each elevation within the pile were reliable.

The constant velocity throughout the record suggested a continuous pile movement at a steady velocity. The velocity records for blow 21 (Figure 72c and d) showed that the top and middle accelerometer records translated to 13.2 and 12.4 mm (0.52 and 0.49 in) of displacement, respectively. These measurements compared well to the 14.0-mm (0.55-in) movement recorded at the surface and the average of 11.4 mm (0.45 in) per blow during the driving. The velocity records for blow 221 (Figure 73c and d) showed that the top and middle accelerometer records translated to 19.1 and 26.9 mm (0.75 and 1.06 in) of displacement, respectively. These measurements compared well with the 18.3-mm (0.72-in) movement recorded at the surface, but did not compare well with the average of 9.1 mm (0.36 in) per blow during driving. The displacement of the tip element for blows 21 and 221 was 15.0 and 19.8 mm (0.59 and 0.78 in), which seemed reasonable considering the fact that the lower segment could separate from that above. The velocity record for the bottom segment indicated deceleration at a constant rate, resulting in a constant reduction in the velocity record. This seemed to be the result of the lower segment separating at the slip joint and traveling against the surrounding soil.

### **6.6.3 MDMP Restrike During Model Pile Test NB2**

#### **(1) Assembly and Recorded Data.**

The MDMP installation as described in the previous section was conducted on March 6, 1996 at 6 p.m. Following the completion of the pore pressure dissipation and the static load tests (including the cyclic loading (see section 6.5)), a dynamic restrike was conducted on March 12, 1996 at 2:50 p.m.

The pile assembly and gauge locations were identical to that of the initial installation as outlined in the previous section. Figure 74 shows the relative position of the MDMP before and after the restrike.

During the restrike, 120 blows were recorded by the surface gauges and 119 blows were recorded by the PDA monitoring the internal instruments. The difference between the time stamps of the two PDAs was 283 s. The pile was driven 0.406 m (1.3 ft). The number of blows required to penetrate each 76.2 mm (3 in) were recorded during the restrike. A total of 117 blows were recorded as part of the manual blow counting procedure, 3 less than the number recorded by the PDA. The total penetration during the restrike was solely determined from the pile-driving log. In addition to the outline of the pile installation and observed driving resistance, Figure 74 contains the measured energy at the top of the pile during the driving (surface measurement). The measured energy allowed a better assessment of the observed blow count with the possible use of a simplified direct relationship between the energy level and the blow count. The analyses of the pile capacity based on the dynamic measurements will be presented in Chapter 7.

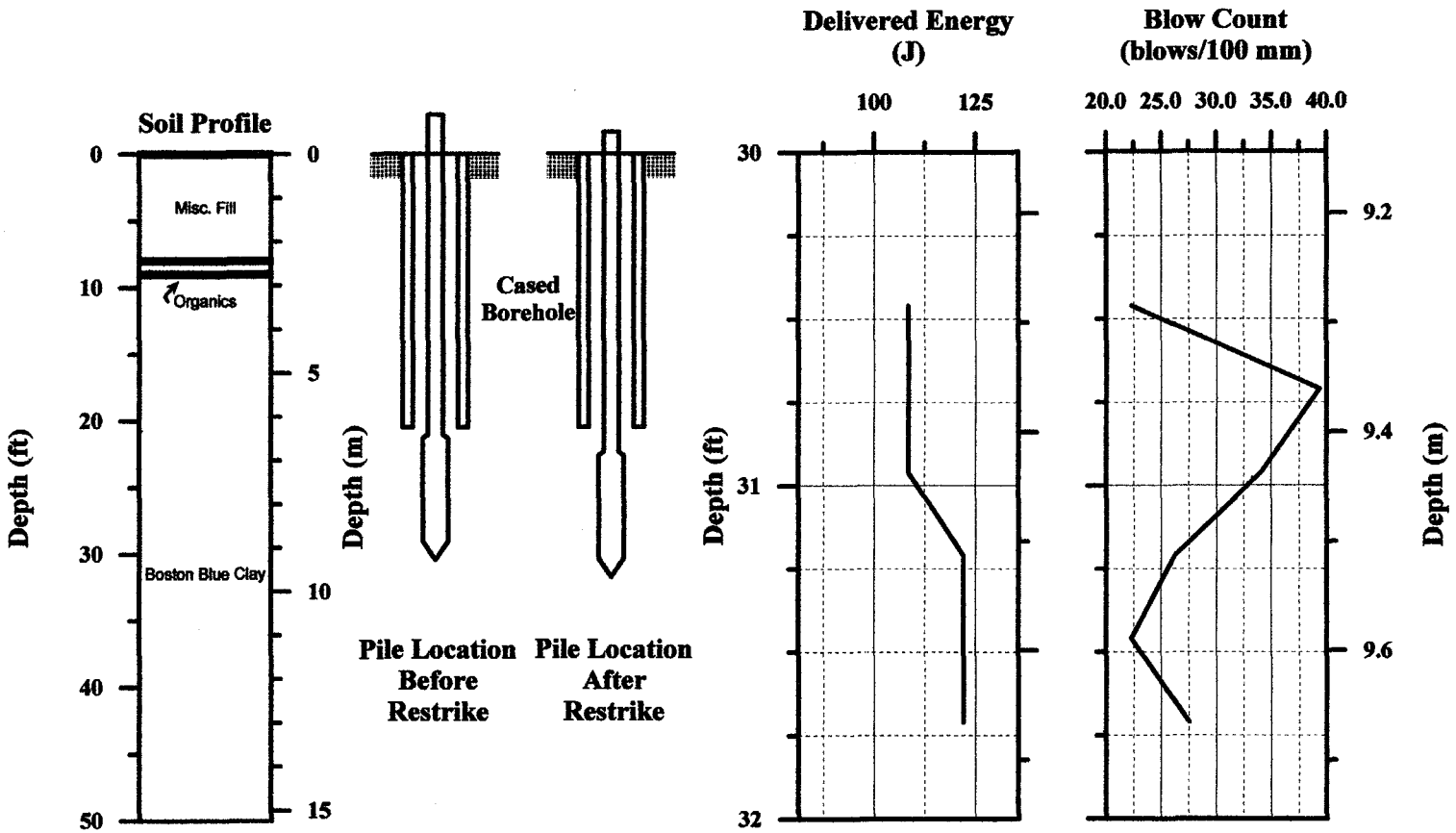
#### **(2) Typical Dynamic Measurements.**

Typical dynamic measurement data obtained via the PDA along the MDMP during the restrike of NB2 are shown in Figure 75. Figure 75 presents the force and velocity signals recorded at the top of the drill rods (denoted as surface measurement) and the internal load cells inside the pile above and below the friction sleeve (denoted as top load cell and middle load cell) and at the pile tip (denoted as bottom load cell) for blow 1. Blow 1 was also analyzed using CAPWAP analysis and the results are included in Chapter 7.

The data in Figure 75a were related to the surface measurements for a time period of 50 ms while Figure 75b depicts the same data over a 20 ms period detailing the impact wave and its reflections during travel time down to the tip and back. The energy measured in blow 1 was about double than that recorded during the initial driving of NB2 and about 33% higher than that at the end of driving. The data in Figure 75a and b indicated the following:

1. Surface Force - Similar to the force recorded during installation, at approximately 2.5 ms after the peak force was recorded, an increase in the force was measured. This positive increase was associated with the reflection of the traveling wave from the rod/pile connection at a distance of 7.01 m (23 ft) from the surface measurement.

**Figure 74. Blow Count and Energy Delivered Versus Penetration Depth for the Restrike of MIDMP Test NB2.**

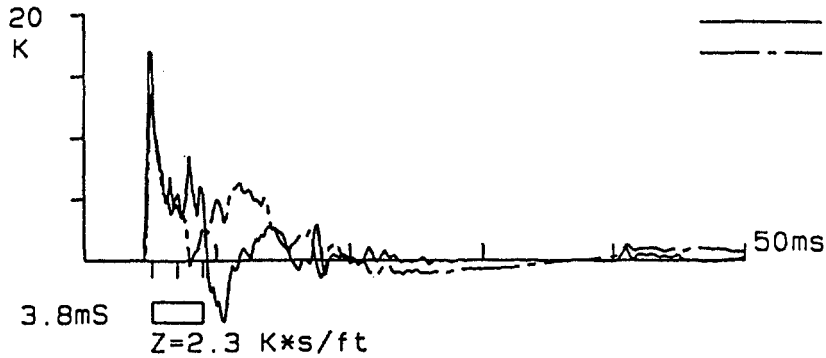


UNIVERSITY MASS-LOWELL  
Newbury Model Pile Test

PDI PILE DRIVING ANALYZER® v4.04

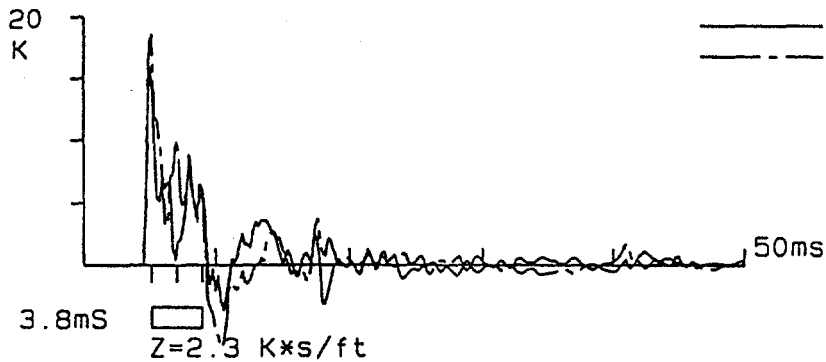
NB2RODRE 12-Mar-96

Surface Measurement



BN	1
EMX	0.08 Kip-ft
FMX	16.9 Kips
VMX	6.0 ft/s
DMX	0.35 inch
DFN	0.32 inch
FT1	16.8 Kips
VT1	6.0 ft/s
RTL	16.9 Kips
RMX	5.8 Kips
LE	32.40 ft
AR	1.29 in2
EM	30000 Ksi
SP	0.492 K/ft3
WS	16810 ft/s

Surface Measurement



BN	1
EMX	0.08 Kip-ft
FMX	16.9 Kips
VMX	6.0 ft/s
DMX	0.35 inch
DFN	0.32 inch
FT1	16.8 Kips
VT1	6.0 ft/s
RTL	16.9 Kips
RMX	5.8 Kips
LE	32.40 ft
AR	1.29 in2
EM	30000 Ksi
SP	0.492 K/ft3
WS	16810 ft/s

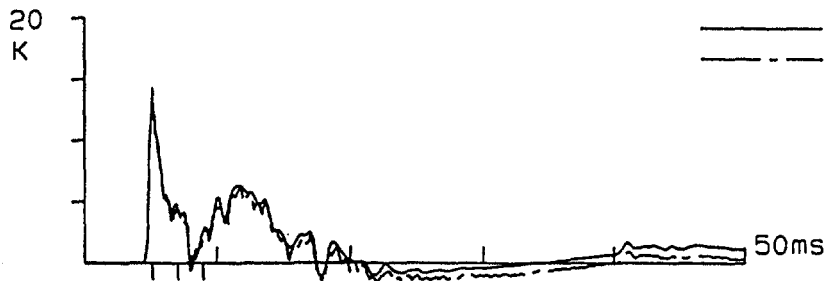


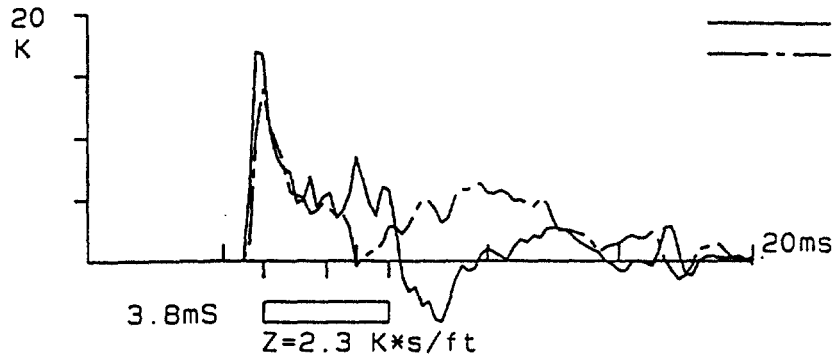
**Figure 75a. PDA Dynamic Measurements During the Restrike of MDMP Test NB2: Surface Force and Velocity Records Over 50 ms.**

UNIVERSITY MASS-LOWELL  
Newbury Model Pile Test

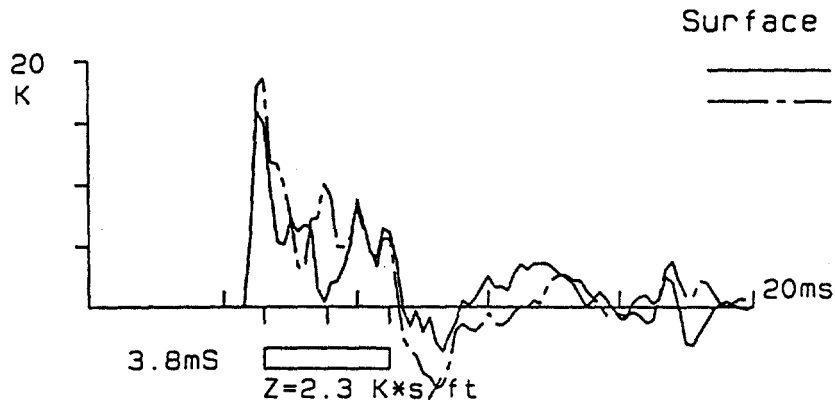
POI PILE DRIVING ANALYZER® v4.04

NB2R0DRE 12-Mar-96

Surface Measurement



BN	1
EMX	0.08 Kip-ft
FMX	16.9 Kips
VMX	6.0 ft/s
DMX	0.35 inch
DFN	0.32 inch
FT1	16.8 Kips
VT1	6.0 ft/s
RTL	16.9 Kips
RMX	5.8 Kips
LE	32.40 ft
AR	1.29 in2
EM	30000 Ksi
SP	0.492 K/ft3
WS	16810 ft/s



Surface Measurement

BN	1
EMX	0.08 Kip-ft
FMX	16.9 Kips
VMX	6.0 ft/s
DMX	0.35 inch
DFN	0.32 inch
FT1	16.8 Kips
VT1	6.0 ft/s
RTL	16.9 Kips
RMX	5.8 Kips
LE	32.40 ft
AR	1.29 in2
EM	30000 Ksi
SP	0.492 K/ft3
WS	16810 ft/s

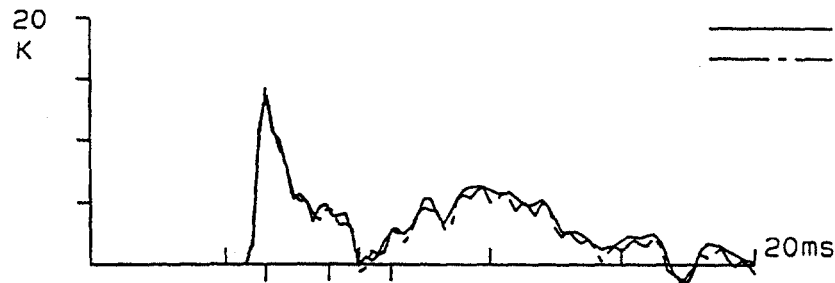


Figure 75b. PDA Dynamic Measurements During the Restrike of MDMP Test NB2:  
Surface Force and Velocity Records Over 20 ms.

UNIVERSITY MASS-LOWELL

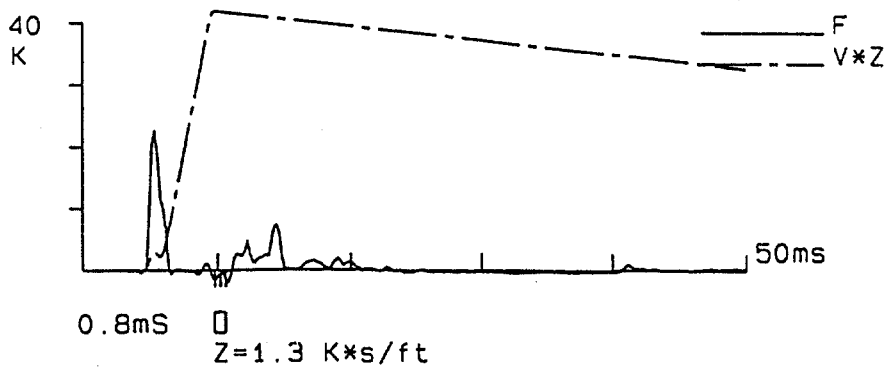
POI PILE DRIVING ANALYZER® v4.04

Newbury Model Pile Test

NB2MPRE 12-Mar-96

PDA OP: LJH

Top Load Cell



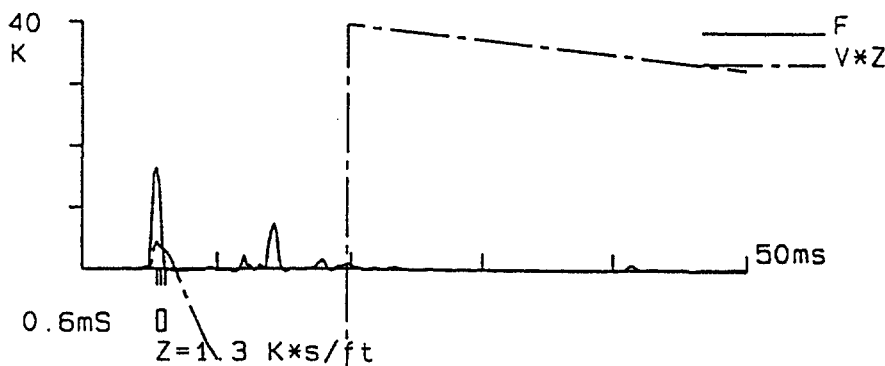
BN	1
EMX	0.52 Kip-ft
FMX	22.6 Kips
VMX	31.8 ft/s
DMX	30.78 inch
DFN	30.78 inch
FT1	-1.7 Kips
VT1	31.8 ft/s
RTL	-1.5 Kips
RMX	4.6 Kips
LE	7.10 ft
AR	0.74 in <sup>2</sup>
EM	30000 Ksi
SP	0.492 K/ft <sup>3</sup>
WS	16810 ft/s

Newbury Model Pile Test

NB2MPRE 12-Mar-96

PDA OP: LJH

Middle Load Cell



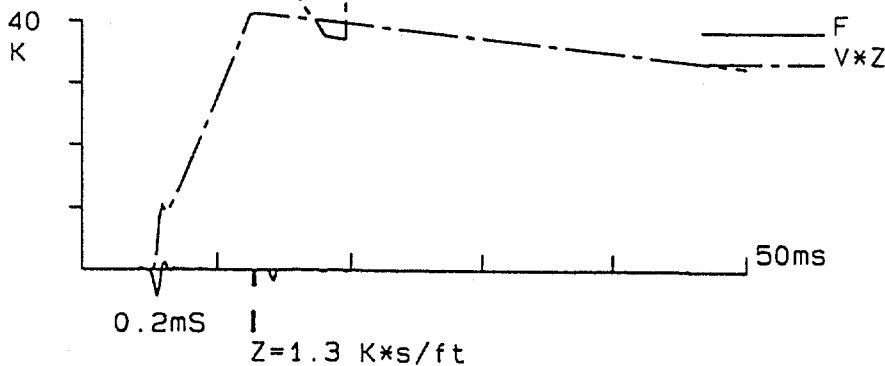
BN	1
EMX	0.08 Kip-ft
FMX	16.5 Kips
VMX	30.0 ft/s
DMX	27.61 inch
DFN	27.61 inch
FT1	16.5 Kips
VT1	3.5 ft/s
RTL	8.8 Kips
RMX	8.8 Kips
LE	4.70 ft
AR	0.74 in <sup>2</sup>
EM	30000 Ksi
SP	0.492 K/ft <sup>3</sup>
WS	16810 ft/s

Newbury Model Pile Test

NB2MPRE 12-Mar-96

PDA OP: LJH

Bottom Load Cell



BN	1
EMX	0.00 Kip-ft
FMX	1.3 Kips
VMX	31.4 ft/s
DMX	30.78 inch
DFN	30.78 inch
FT1	0.0 Kips
VT1	31.4 ft/s
RTL	0.0 Kips
RMX	0.1 Kips
LE	1.00 ft
AR	0.74 in <sup>2</sup>
EM	30000 Ksi
SP	0.492 K/ft <sup>3</sup>
WS	16810 ft/s

**Figure 75c. PDA Dynamic Measurements During the Restrike of MDMP Test NB2: Internal Force and Velocity Records Over 50 ms.**



UNIVERSITY MASS-LOWELL

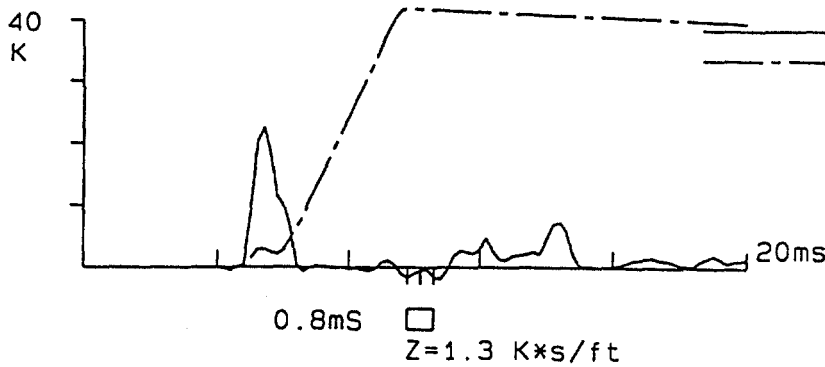
Newbury Model Pile Test

PDA OP: LJH

POI PILE DRIVING ANALYZER® v4.04

NB2MPRE 12-Mar-96

Top Load Cell



BN	1
EMX	0.52 Kip-ft
FMX	22.6 Kips
VMX	31.8 ft/s
DMX	30.78 inch
DFN	30.78 inch
FT1	-1.7 Kips
VT1	31.8 ft/s
RTL	-1.5 Kips
RMX	4.6 Kips
LE	7.10 ft
AR	0.74 in2
EM	30000 Ksi
SP	0.492 K/ft3
WS	16810 ft/s

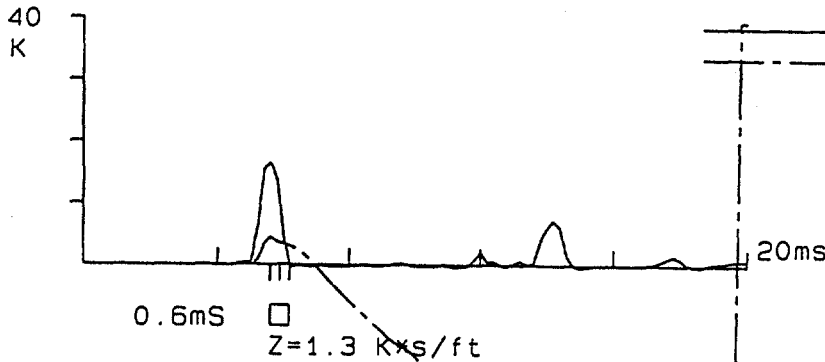
Newbury Model Pile Test

PDA OP: LJH

NB2MPRE

12-Mar-96

Middle Load Cell



BN	1
EMX	0.08 Kip-ft
FMX	16.5 Kips
VMX	30.0 ft/s
DMX	27.61 inch
DFN	27.61 inch
FT1	16.5 Kips
VT1	3.5 ft/s
RTL	8.8 Kips
RMX	8.8 Kips
LE	4.70 ft
AR	0.74 in2
EM	30000 Ksi
SP	0.492 K/ft3
WS	16810 ft/s

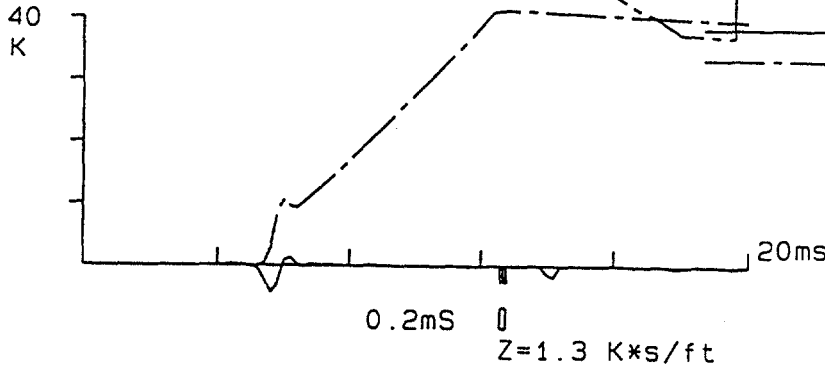
Newbury Model Pile Test

PDA OP: LJH

NB2MPRE

12-Mar-96

Bottom Load Cell



BN	1
EMX	0.00 Kip-ft
FMX	1.3 Kips
VMX	31.4 ft/s
DMX	30.78 inch
DFN	30.78 inch
FT1	0.0 Kips
VT1	31.4 ft/s
RTL	0.0 Kips
RMX	0.1 Kips
LE	1.00 ft
AR	0.74 in2
EM	30000 Ksi
SP	0.492 K/ft3
WS	16810 ft/s

Figure 75d. PDA Dynamic Measurements During the Restrike of MDMP Test NB2: Internal Force and Velocity Records Over 20 ms.

2. **Surface Velocity** - The velocity record at the top of the drill rods behaved much the same as during the installation. Unlike the easy driving encountered during initial driving, the velocity record did not increase to an elevated level. DMX (maximum pile top displacement) was 8.9 mm (0.35 in), while DFN (final pile top displacement) was 8.1 mm (0.32 in) compared to the average set of 4.5 mm (0.176 in) per blow. This could be the result of the difference in the pile behavior between each individual blow and the average set for a number of blows as shown in Figure 74 and detailed in the driving log in Appendix I.

The data in Figure 75c were related to the internal measurements for a time period of 50 ms, while Figure 75d depicts the same data over a 20-ms period detailing the impact wave traveling down through the pile. The data in Figure 75c and d indicated the following:

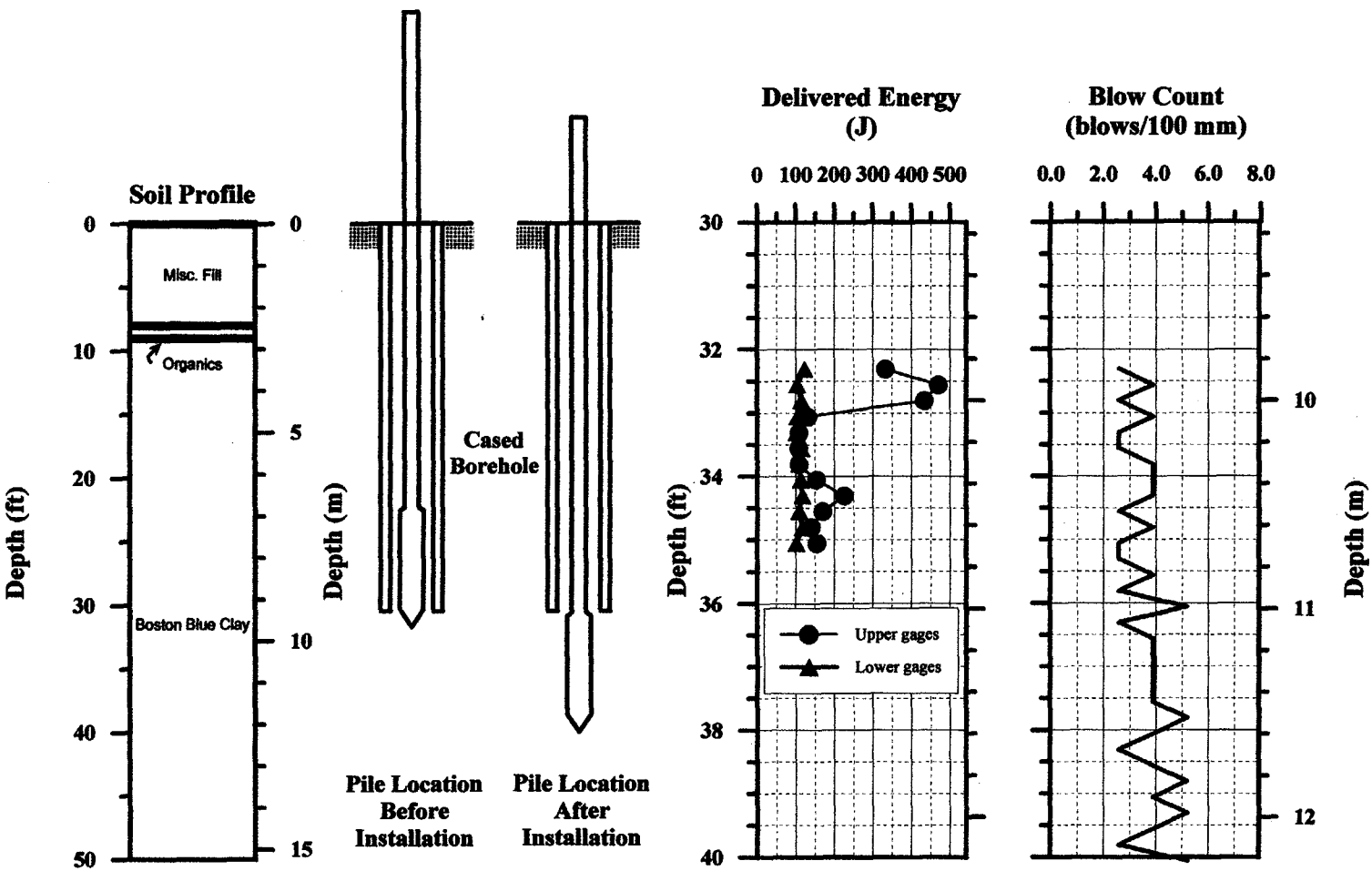
1. **Internal Forces** - The internal forces records seemed to be adequate and reliable as also shown during installation. The records for blow 1 (presented in Figure 75) suggested that the wave arriving at the top load cell was about 1.34 times the magnitude of the wave recorded at the surface and was of a similar shape. The record reflected the influence of the impedance increase at the point where the rods were connected to the instrumented pile. Evaluation of this increase over the penetration record is presented in Chapter 7, where it is shown to match the expected analysis. The peak wave passing through the middle load cell was reduced by about 27.1 kN (6.1 kips) for blow 1. This reduction was equal to the dynamic friction force acting on the sleeve and will be discussed further in Chapter 7. The bottom load cell records were consistent with the behavior described in the previous section.
2. **Internal Velocities** - The data suggested that the accelerometers mounted in the pile did not properly record the motion, since in all three locations shown in Figures 75c and d the accelerometers seemed to reach the saturation level and, therefore, the calculated velocity is not reliable. Additional investigation of the data (e.g., acceleration records) was not carried out and is believed to be of limited use.

#### **6.6.4 Installation During Model Pile Test NB3**

##### **(1) Assembly and Recorded Data.**

The assembled pile consisted of the 2.87-m (9.4-ft) instrumented section with seven 1.52-m (5-ft) and two 0.61-m (2-ft) drill rod sections. The total length of the pile during installation was 14.8 m (48.4 ft). The gauges were located 0.3 m (1 ft), 0.91 m (3 ft), 12.6 m (41.3 ft), and 13.3 m (43.7 ft) from the top of the assembled pile. The pile was placed in a 9.3-m (30.5-ft) cased borehole and held in place after it had penetrated 0.37 m (1.23 ft) under its own weight (including the weight of the drill rods). The pile would have continued to penetrate if not physically held in place for approximately 1.5 h. When disconnected from the drill rig following this period, the pile did not appear to penetrate any farther. Figure 76 shows the relative position of the pile before and after installation.

Figure 76. Blow Count and Energy Delivered Versus Penetration Depth for the Installation of MDMP Test NB3.



The dynamic records for the first 30 blows were recorded with the gauges attached to the pile top (surface measurements). Only the first 30 blows were recorded by the PDA due to limited storage space in that particular PDA (860 blows in the buffer) and the oversight of leaving the data recorded earlier during MDMP test NB2. The surface measurements included two sets of gauges attached to the drill rods, each with a different type of accelerometer — piezoelectric and piezoresistive. The PDA monitoring the internal instruments recorded 100 blows. The difference between the time stamps of the two PDAs was 283 s. The pile was driven 2.54 m (8.33 ft). Ninety blows were recorded for a total penetration of 2.44 m (8.0 ft). Discounting the random blows recorded by the PDA measuring the internal gauges, the blow count appeared to be reasonable. The error in the total penetration length was 101.6 mm (4 in). This error could be attributed to the incorrect marking of the 76.2-mm (3-in) increments on the drill rods or a missed increment during driving. In addition to outlining the pile installation and the observed driving resistance, Figure 76 contains the measured energy at the top of the pile during the driving (surface measurement). The measured energy allowed better assessment of the observed blow count, with the possible use of a simplified direct relationship between the energy level and the blow count. The analyses of the pile capacity based on the dynamic measurements will be presented in Chapter 7.

## (2) Typical Dynamic Measurements.

Typical dynamic measurement data obtained via the PDA along the MDMP during driving of NB3 are shown in Figure 77. Figure 77 presents the force and velocity signals recorded at two places at the top of the drill rods (denoted as surface measurement ELE and surface measurement RES) and the internal load cells inside the pile above and below the friction sleeve (denoted as top load cell and middle load cell) and at the pile tip (denoted as bottom load cell) for one blow. Note that the data related to blow 16 in Figures 72a through d corresponded to the same blow denoted as blow 26 in Figures 72e and f. Blow 16/26 corresponded to a penetration depth of approximately 10.13/0.83 m (33.23/2.73 ft) as related to the ground surface and bottom of the cased borehole, respectively.

The data in Figures 77a and c were related to the surface measurements for a time period of 25 ms, while Figures 77b and d depict the same data over a 5-ms period detailing the impact wave and its reflections during the travel time down to the tip and back. The data in Figures 77a through d indicated the following:

1. Surface Force - During the installation of NB3, two sets of force transducers and accelerometers (a total of four force transducers and four accelerometers) were mounted at the top of the pile. The records denoted as F1 and F2 referred to the force transducers mounted 0.3048 m (1 ft) below the top of the drill rods (approximately 1.25 m from the impact) in an arrangement similar to the one used for the NB2 installation. The records for these transducers, as shown in Figures 77a and b, were very similar in nature to those obtained in MDMP test NB2 (see Figures 72a and b). The records denoted as F3 and F4, shown in Figure 77c and d, referred to measurements 0.91 m (3 ft) below the top of the drill rods (approximately 1.86 m

UNIVERSITY MASS-LOWELL  
Newbury Model Pile Test

PDI PILE DRIVING ANALYZER<sup>®</sup>

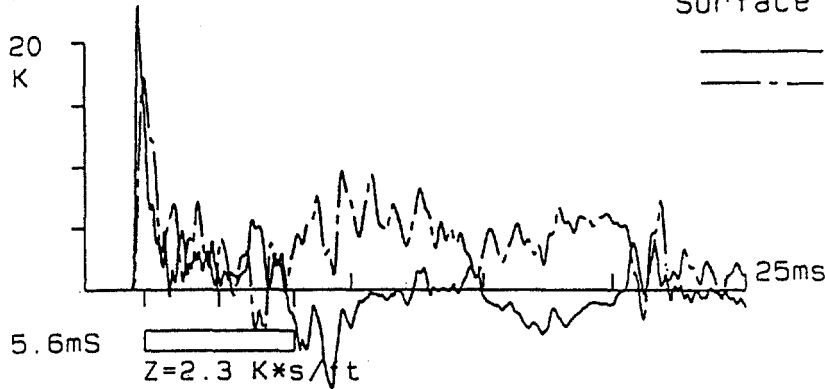
NB3RODIN 13-Mar-96

Surface Measurement ELE

BN 16

——— F  
- - - - V\*Z

EMX	0.06	Kip-ft
FMX	23.0	Kips
VMX	7.5	ft/s
DMX	0.60	inch
DFN	0.60	inch
FT1	14.9	Kips
VT1	7.5	ft/s
RTL	13.1	Kips
RMX	2.5	Kips



LE	47.40	ft
AR	1.29	in <sup>2</sup>
EM	30000	Ks <sup>1</sup>
SP	0.492	K/ft <sup>3</sup>
WS	16810	ft/s

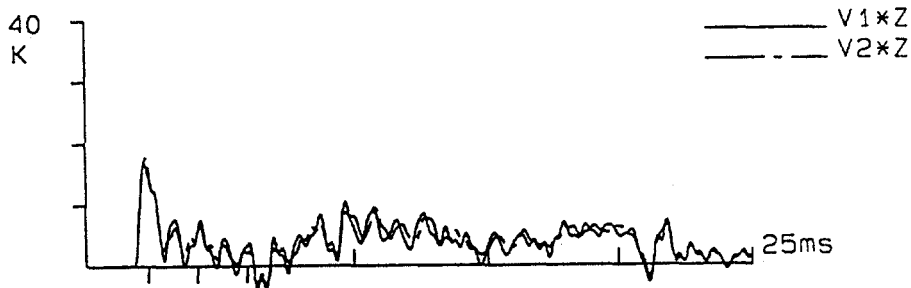
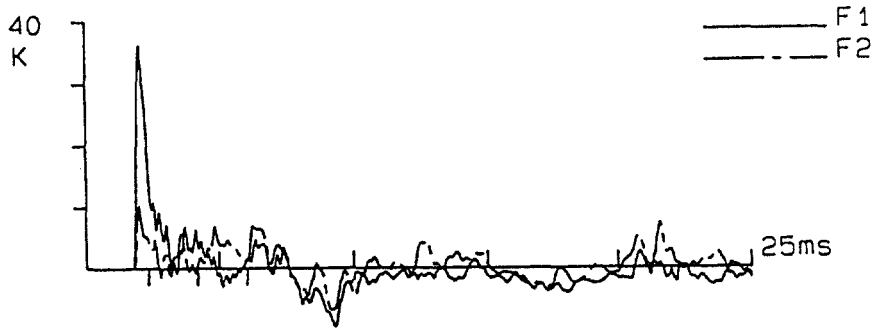


**Figure 77a. PDA Dynamic Measurements During the Installation of MDMP Test NB3: Surface Force and Velocity Records Over 25 ms (at the upper location).**

UNIVERSITY MASS-LOWELL

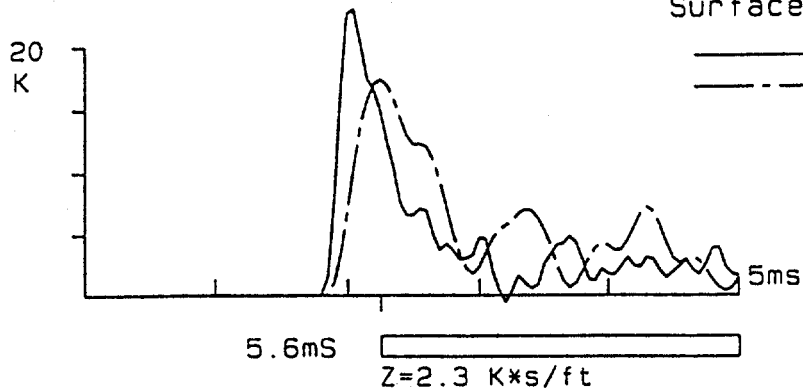
Newbury Model Pile Test

PDI PILE DRIVING ANALYZER<sup>®</sup> v4.04

NB3RODIN 13-Mar-96

Surface Measurement ELE

BN 16



EMX	0.06 Kip-ft
FMX	23.0 Kips
VMX	7.5 ft/s
DMX	0.60 inch
DFN	0.60 inch
FT1	14.9 Kips
VT1	7.5 ft/s
RTL	13.1 Kips
RMX	2.5 Kips

LE	47.40 ft
AR	1.29 in <sup>2</sup>
EM	30000 Ks <sup>1</sup>
SP	0.492 K/ft <sup>3</sup>
WS	16810 ft/s

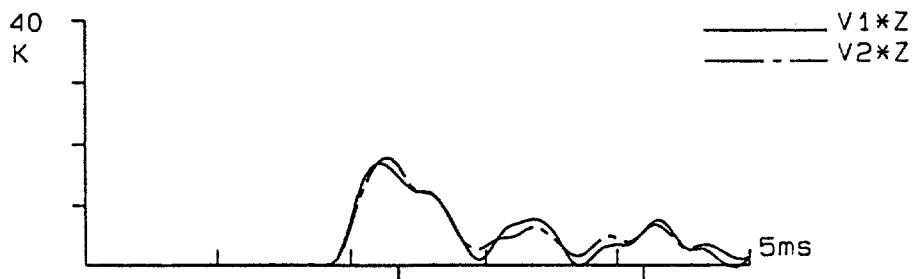
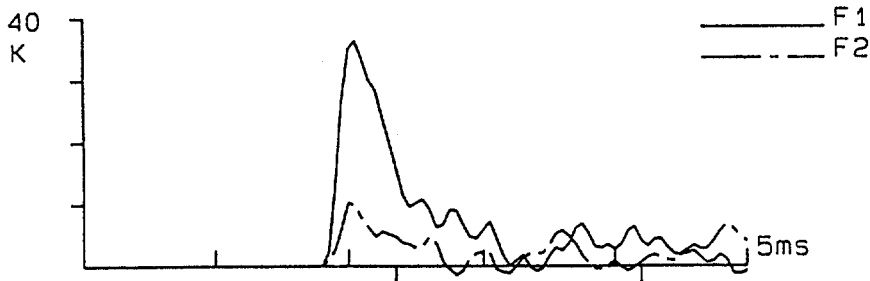


**Figure 77b. PDA Dynamic Measurements During the Installation of MDMP Test NB3: Surface Force and Velocity Records Over 5 ms (at the upper location).**

UNIVERSITY MASS-LOWELL  
Newbury Model Pile Test

PDI PILE DRIVING ANALYZER<sup>®</sup> v4.0a

NB3RODIN 13-Mar-96

Surface Measurement RES

BN	16
EMX	0.07 Kip-ft
FMX	16.7 Kips
VMX	6.0 ft/s
DMX	0.68 inch
DFN	0.68 inch
FT1	13.0 Kips
VT1	6.0 ft/s
RTL	10.1 Kips
RMX	3.5 Kips
LE	45.40 ft
AR	1.29 in <sup>2</sup>
EM	30000 Ksi
SP	0.492 K/ft <sup>3</sup>
WS	16810 ft/s

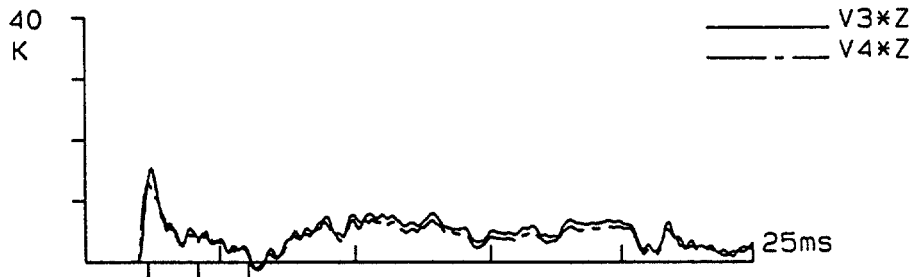
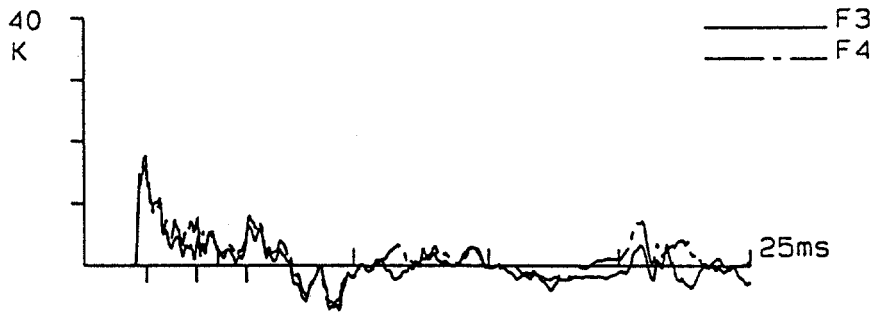
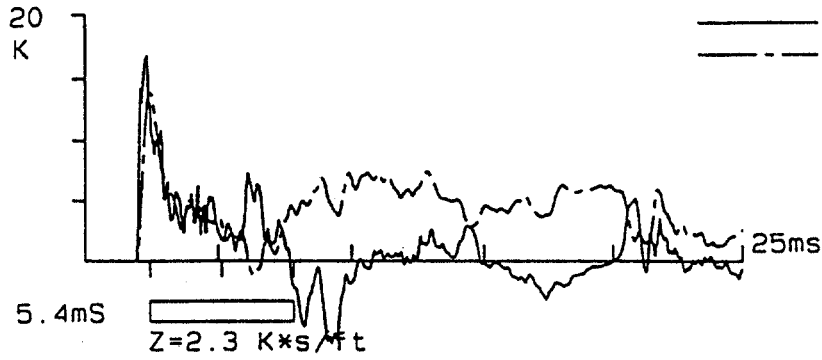
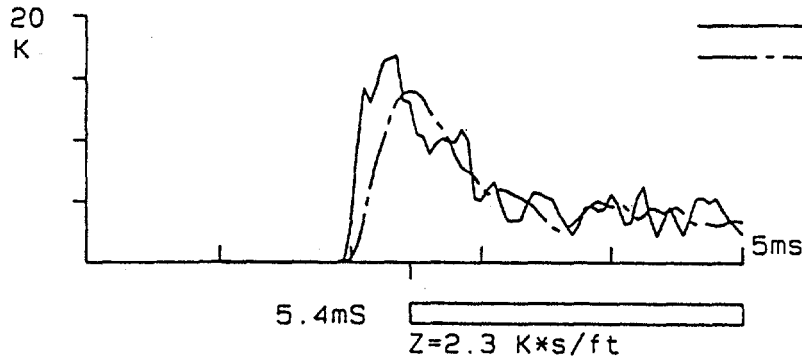


**Figure 77c. PDA Dynamic Measurements During the Installation of MDMP Test NB3: Surface Force and Velocity Records Over 25 ms (at the lower location).**

UNIVERSITY MASS-LOWELL  
Newbury Model Pile Test

PDI PILE DRIVING ANALYZER<sup>®</sup> v4.04

NB3RODIN 13-Mär-96  
Surface Measurement RES



BN	16
EMX	0.07 Kip-ft
FMX	16.7 Kips
VMX	6.0 ft/s
DMX	0.68 inch
DFN	0.68 inch
FT1	13.0 Kips
VT1	6.0 ft/s
RTL	10.1 Kips
RMX	3.5 Kips
LE	45.40 ft
AR	1.29 in2
EM	30000 Ksi
SP	0.492 K/ft3
WS	16810 ft/s

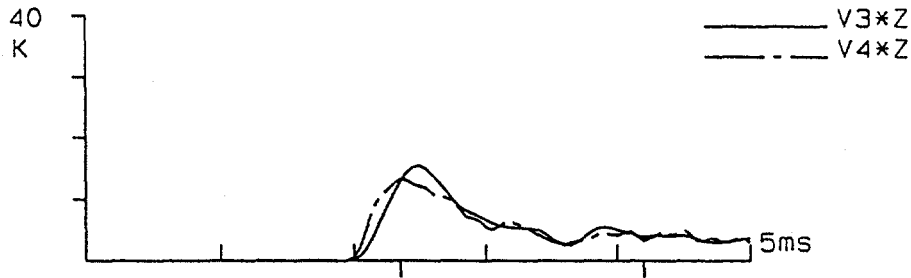
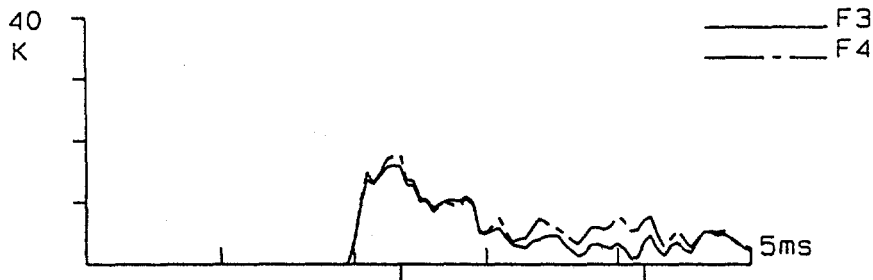
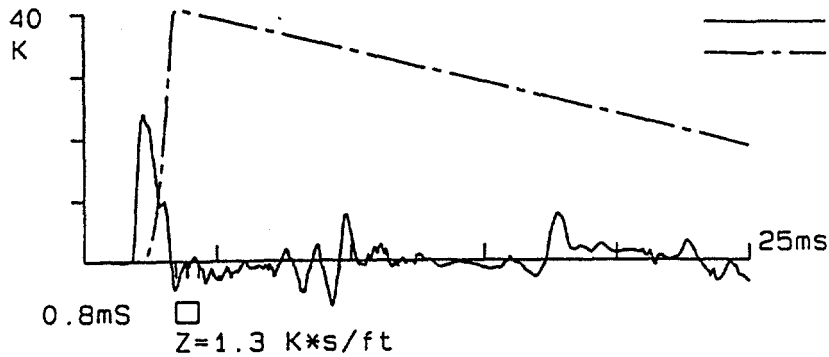


**Figure 77d. PDA Dynamic Measurements During the Installation of MDMP Test NB3: Surface Force and Velocity Records Over 5 ms (at the lower location).**



UNIVERSITY MASS-LOWELL  
Newbury Model Pile Test

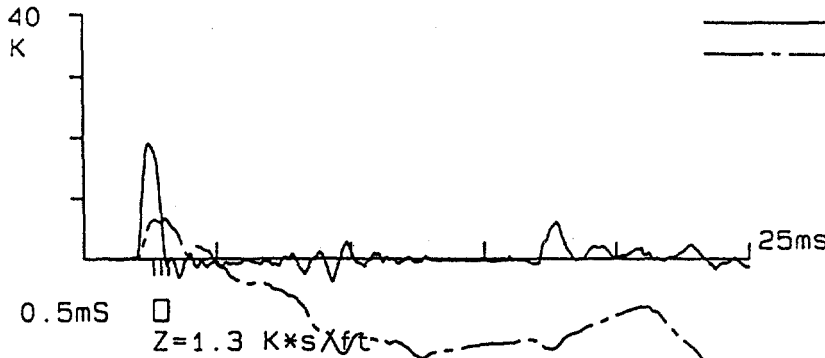
POI PILE DRIVING ANALYZER® v4.04  
NB3MPIN 13-Mar-96  
Top Load Cell



BN	26
EMX	0.07 Kip-ft
FMX	24.0 Kips
VMX	31.0 ft/s
DMX	7.55 inch
DFN	7.55 inch
FT1	-4.4 Kips
VT1	31.0 ft/s
RTL	-1.9 Kips
RMX	5.5 Kips
LE	7.10 ft
AR	0.74 in2
EM	30000 Ksi
SP	0.492 K/ft3
WS	16810 ft/s

Newbury Model Pile Test

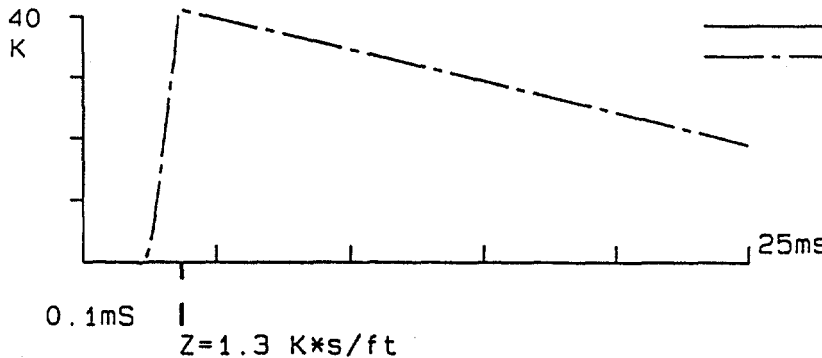
NB3MPIN 13-Mar-96  
Middle Load Cell



BN	26
EMX	0.08 Kip-ft
FMX	19.1 Kips
VMX	5.1 ft/s
DMX	0.09 inch
DFN	-3.66 inch
FT1	17.9 Kips
VT1	4.9 ft/s
RTL	8.7 Kips
RMX	8.7 Kips
LE	4.70 ft
AR	0.74 in2
EM	30000 Ksi
SP	0.492 K/ft3
WS	16810 ft/s

Newbury Model Pile Test

NB3MPIN 13-Mar-96  
Bottom Load Cell

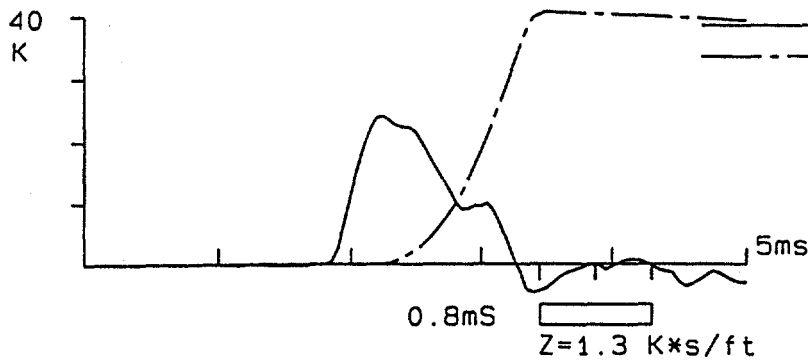


BN	26
EMX	0.00 Kip-ft
FMX	0.0 Kips
VMX	31.3 ft/s
DMX	7.64 inch
DFN	7.64 inch
FT1	0.0 Kips
VT1	31.3 ft/s
RTL	0.0 Kips
RMX	0.0 Kips
LE	1.00 ft
AR	0.74 in2
EM	30000 Ksi
SP	0.492 K/ft3
WS	16810 ft/s

**Figure 77e. PDA Dynamic Measurements During the Installation of MDMP Test NB3: Internal Force and Velocity Records Over 25 ms.**

UNIVERSITY MASS-LOWELL  
Newbury Model Pile Test

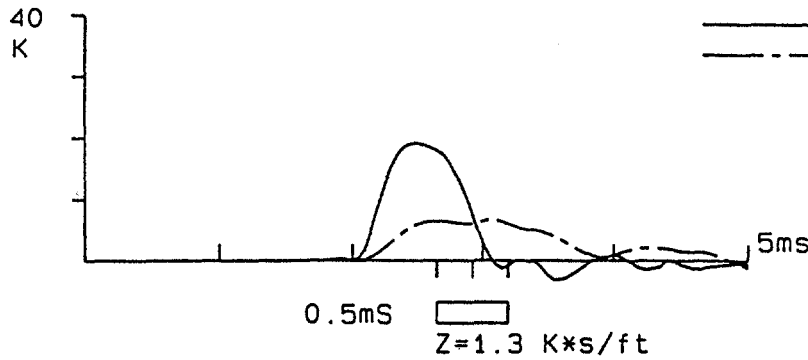
PDI PILE DRIVING ANALYZER® v4.04  
NB3MPIN 13-Mar-96  
Top Load Cell



BN	26
EMX	0.07 Kip-ft
FMX	24.0 Kips
VMX	31.0 ft/s
DMX	7.55 inch
DFN	7.55 inch
FT1	-4.4 Kips
VT1	31.0 ft/s
RTL	-1.9 Kips
RMX	5.5 Kips
LE	7.10 ft
AR	0.74 in2
EM	30000 Ksi
SP	0.492 K/ft3
WS	16810 ft/s

Newbury Model Pile Test

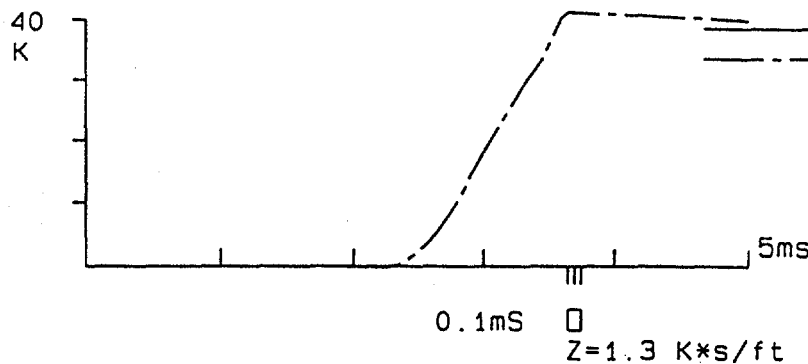
NB3MPIN 13-Mar-96  
Middle Load Cell



BN	26
EMX	0.08 Kip-ft
FMX	19.1 Kips
VMX	5.1 ft/s
DMX	0.09 inch
DFN	-3.66 inch
FT1	17.9 Kips
VT1	4.9 ft/s
RTL	8.7 Kips
RMX	8.7 Kips
LE	4.70 ft
AR	0.74 in2
EM	30000 Ksi
SP	0.492 K/ft3
WS	16810 ft/s

Newbury Model Pile Test

NB3MPIN 13-Mar-96  
Bottom Load Cell



BN	26
EMX	0.00 Kip-ft
FMX	0.0 Kips
VMX	31.3 ft/s
DMX	7.64 inch
DFN	7.64 inch
FT1	0.0 Kips
VT1	31.3 ft/s
RTL	0.0 Kips
RMX	0.0 Kips
LE	1.00 ft
AR	0.74 in2
EM	30000 Ksi
SP	0.492 K/ft3
WS	16810 ft/s

**Figure 77f. PDA Dynamic Measurements During the Installation of MDMP Test NB3: Internal Force and Velocity Records Over 5 ms.**

below the impact), meaning 0.610 m (2 ft) below F1 and F2. Although the average recorded force indicated some fluctuation (see force and velocity records combined), the individual records suggested that both F3 and F4 measured a similar record. As a result, it can be concluded that due to changes in impedance in the rods, compressive force reflections were measured at the pile top. However, due to unevenly distributed stresses during impact, gauges that were mounted only 0.3048 m (1 ft) below the top of the rods suffered from extreme variations and resulted in highly fluctuated forces. Although 0.305 m (1 ft) below the top of the rods seemed to be a more than safe distance (compared to full-scale pile operation in which the gauges are mounted three pile diameters below the impact), the dynamic measurements on a small-scale pile were difficult and required increased distance to ensure quality data that were not affected by uneven impacts.

2. **Surface Velocity** - The velocity records at the top of the drill rods appeared to be of the same basic shape as those observed in the driving of test NB2 (see section 6.6.2). The increased velocity at about 8 ms, to an elevated level of approximately 0.610 to 0.914 m/sec (2 to 3 ft/sec), suggested that the pile continued to move at some constant velocity (approximately) over a lengthy period of time. As shown before, during easy driving, the record for blow 16 (Figure 77e and f) indicated that, indeed,  $DMX=DFN=15.24$  mm (0.60 in). This was in comparison with the observed displacement of three blows per 76.2 mm (3.0 in), which translated to an average of 25.4 mm (1.0 in) per blow.

The data in Figure 77e were related to the internal measurements for a time period of 25 ms, while Figure 77f depicts the same data over a 5-ms period detailing the impact wave and its reflections during the travel time down to the tip and back. The data in Figures 77e and f indicated the following:

1. **Internal Forces** - The internal forces were recorded using the existing built-in large load cells. The records for blow 16 (presented in Figures 77e and f) suggested that the wave arriving at the top load cell was about 1.04 times the magnitude of the wave recorded at the surface with the upper instrumentation as shown in Figures 77a and b for the records for F1 and F2. The ratio between the surface load cell and the top load cell for blow 16 was 1.44 times the magnitude of the wave recorded at the surface with the lower instrumentation as shown in Figures 77c and d for the records for F3 and F4. Both records were affected by the impedance increase at the connection of the drilling rods and the instrumented pile. An evaluation of this increase over the penetration record is presented in Chapter 7, where it is shown to match the expected analysis.

The peak wave passing through the middle load cell was reduced by about 21.8 kN (4.9 kips). This reduction was equal to the dynamic friction force acting on the sleeve and will be discussed further in Chapter 7. The discontinuity of the internal records was a result of the MDMP slip joint. The impact was transferred to the lower section that separated; it was incapable of transferring the reflected wave coming from the tip.

No force data were recorded by the bottom load cell due to difficulties following MDMP test NB2.

2. Internal Velocities - The accelerometer records were questionable during the initial installation of NB3. The data in Figures 77e and f suggested that the accelerometers mounted at the top and bottom locations reached saturation and thus were not reliable. The middle accelerometer appeared to respond properly, but the large negative final displacement of DFN = -93.0 mm (-3.66 in) suggested that its reliability beyond about 2.5 ms (see Figure 77e) was questionable, most likely due to drift at the DC level.

### **6.6.5 Restrike During Model Pile Test NB3**

#### **(1) Assembly and Recorded Data.**

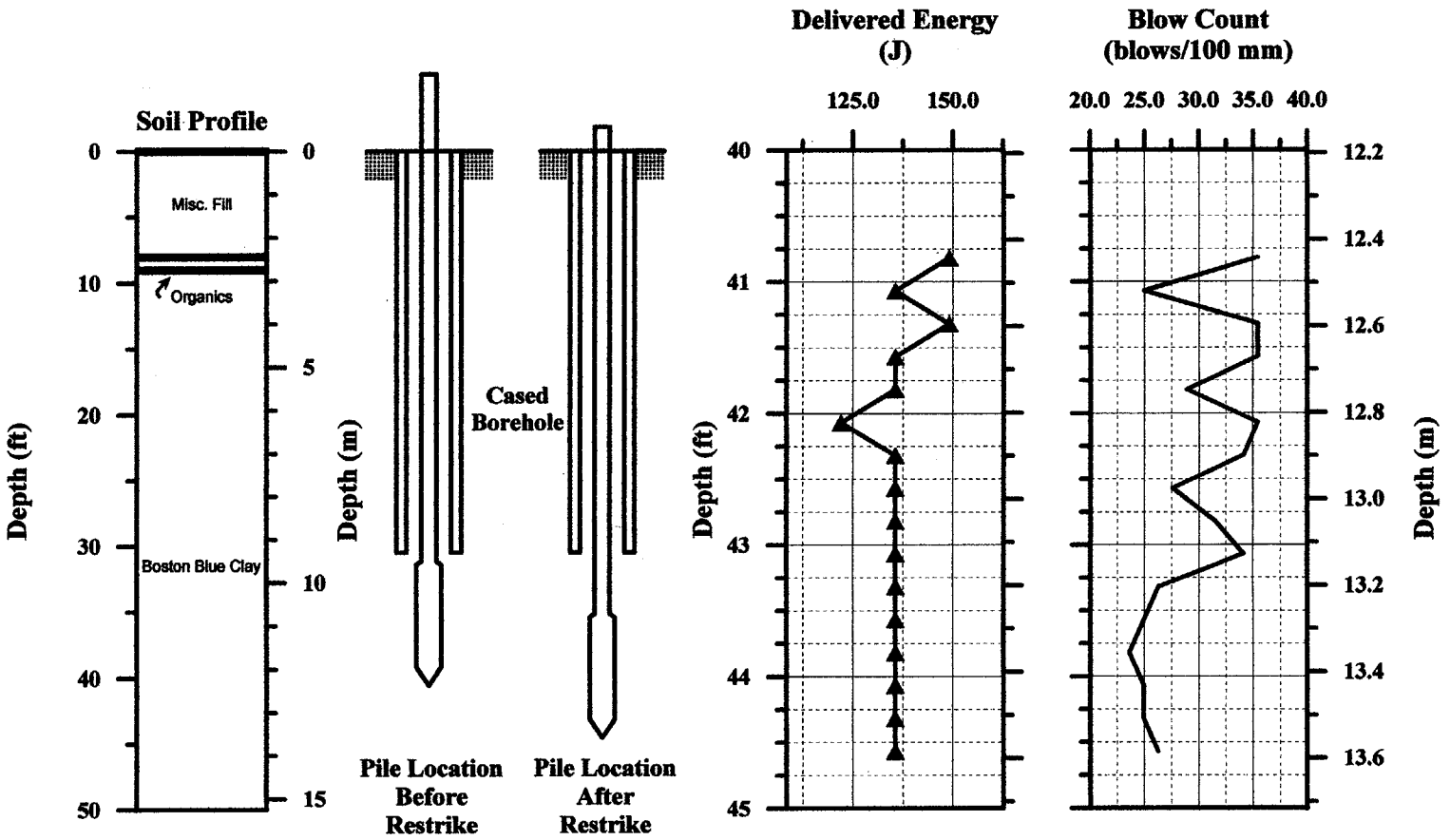
The assembled pile consisted of the 2.87-m (9.4-ft) instrumented section with seven 1.52-m (5-ft) and one 0.61-m (2-ft) drill rod sections. The total length of the pile during installation was 14.1 m (46.4 ft). The gauges were located 0.3 m (1 ft), 12.0 m (39.3 ft), and 12.7 m (41.7 ft) from the top of the assembled pile. Following the completion of the dissipation process and static load tests (including the cyclic loading (see section 6.5)), a dynamic restrike was conducted on March 18, 1996 at 3:38 p.m. Figure 78 shows the relative position of the pile before and after the restrike.

During the restrike, 359 blows were recorded by the surface gauges and 351 blows were recorded by the PDA monitoring the internal instruments. The difference between the time stamps of the two PDAs was 289 s. The pile was driven 1.22 m (4.0 ft). The number of blows needed to penetrate 76.2 mm (3 in) were recorded during the restrike. A total of 361 blows were recorded as part of the blow-counting procedure, 2 more than recorded by the PDA. The total penetration during the restrike was determined solely from the pile-driving log. In addition to the outline of the pile installation and observed driving resistance, Figure 78 contains the measured energy at the top of the pile during the driving (surface measurement). The measured energy allowed better assessment of the observed blow count with the possible use of a simplified direct relationship between the energy level and the blow count. The analyses of the pile capacity based on the dynamic measurements will be presented in Chapter 7.

#### **(2) Typical Dynamic Measurements.**

Typical dynamic measurement data obtained via the PDA along the MDMP during restrike of NB3 are shown in Figure 79. Figure 79 presents the force and velocity signals recorded at the top of the drill rods (denoted as surface measurement) and the internal load cells inside the pile above and below the friction sleeve (denoted as top load cell and middle load cell) and at the pile tip (denoted as bottom load cell) for blow 2. Blow 2 was analyzed using CAPWAP analysis and the results are presented in Chapter 7.

**Figure 78. Blow Count and Energy Delivered Versus Penetration Depth for the Restrike of MDMP Test NB3.**

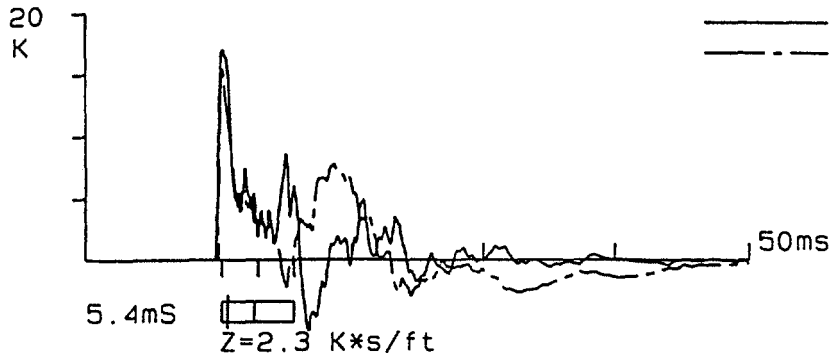


UNIVERSITY MASS-LOWELL  
Newbury Model Pile Test

PDI PILE DRIVING ANALYZER® v4.04

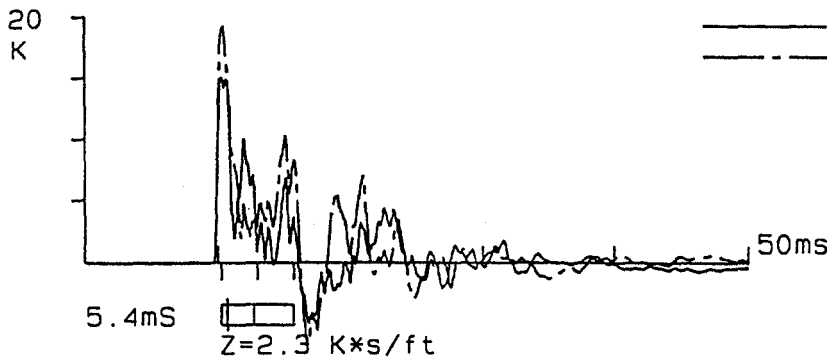
NB3RODRE 18-Mar-96

Surface Measurement



BN 2	
EMX	0.10 Kip-ft
FMX	17.1 Kips
VMX	6.8 ft/s
DMX	0.28 inch
DFN	0.11 inch
FT1	17.1 Kips
VT1	6.8 ft/s
RTL	18.7 Kips
RMX	7.4 Kips
LE	45.40 ft
AR	1.29 in2
EM	30000 Ksi
SP	0.492 K/ft3
WS	16810 ft/s

Surface Measurement



BN 2	
EMX	0.10 Kip-ft
FMX	17.1 Kips
VMX	6.8 ft/s
DMX	0.28 inch
DFN	0.11 inch
FT1	17.1 Kips
VT1	6.8 ft/s
RTL	18.7 Kips
RMX	7.4 Kips
LE	45.40 ft
AR	1.29 in2
EM	30000 Ksi
SP	0.492 K/ft3
WS	16810 ft/s

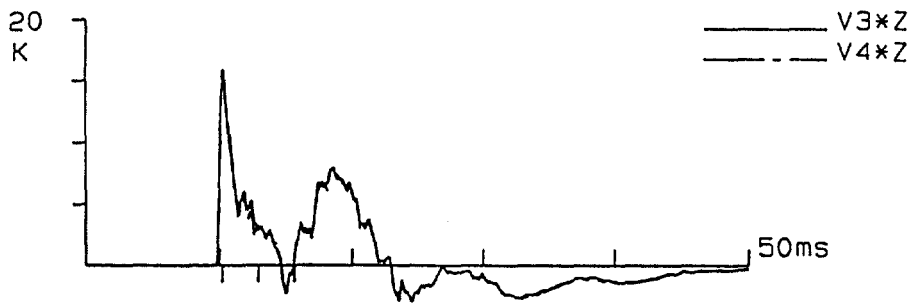


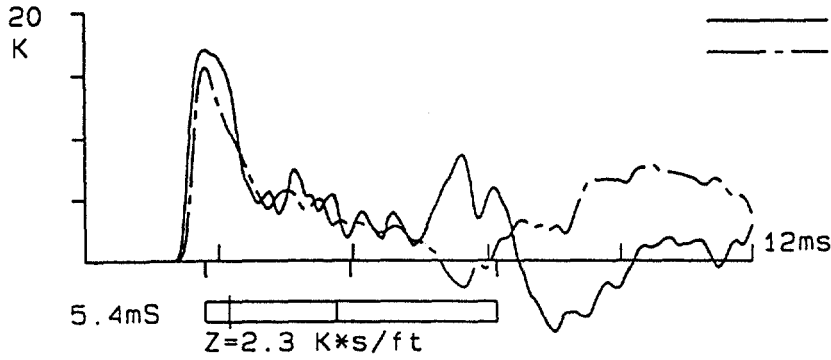
**Figure 79a. PDA Dynamic Measurements During the Restrike of MDMP Test NB3: Surface Force and Velocity Records Over 50 ms.**

UNIVERSITY MASS-LOWELL  
Newbury Model Pile Test

PDI PILE DRIVING ANALYZER® v4.04

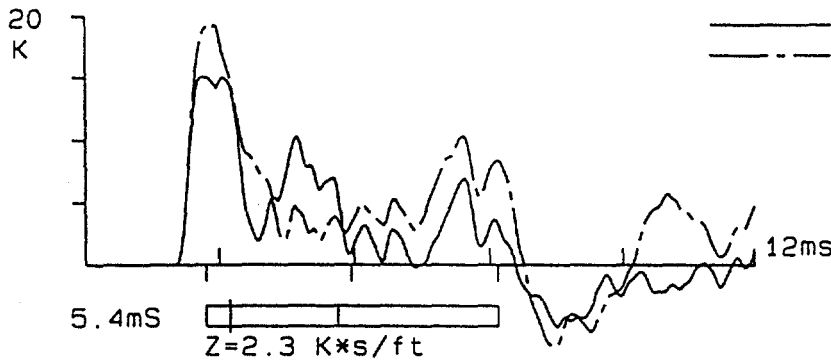
NB3RODRE 18-Mar-96

Surface Measurement



BN	2
EMX	0.10 Kip-ft
FMX	17.1 Kips
VMX	6.8 ft/s
DMX	0.28 inch
DFN	0.11 inch
FT1	17.1 Kips
VT1	6.8 ft/s
RTL	18.7 Kips
RMX	7.4 Kips
LE	45.40 ft
AR	1.29 in2
EM	30000 Ksi
SP	0.492 K/ft3
WS	16810 ft/s

Surface Measurement



BN	2
EMX	0.10 Kip-ft
FMX	17.1 Kips
VMX	6.8 ft/s
DMX	0.28 inch
DFN	0.11 inch
FT1	17.1 Kips
VT1	6.8 ft/s
RTL	18.7 Kips
RMX	7.4 Kips
LE	45.40 ft
AR	1.29 in2
EM	30000 Ksi
SP	0.492 K/ft3
WS	16810 ft/s

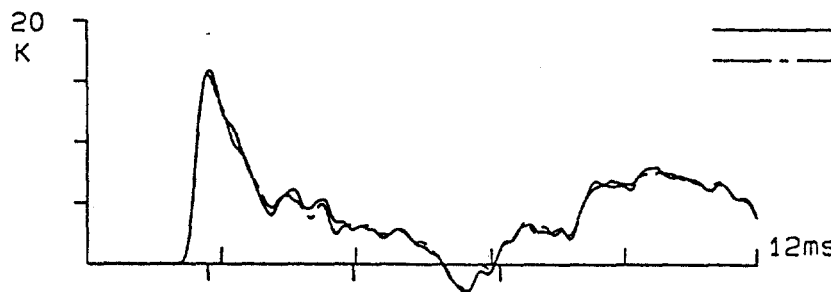
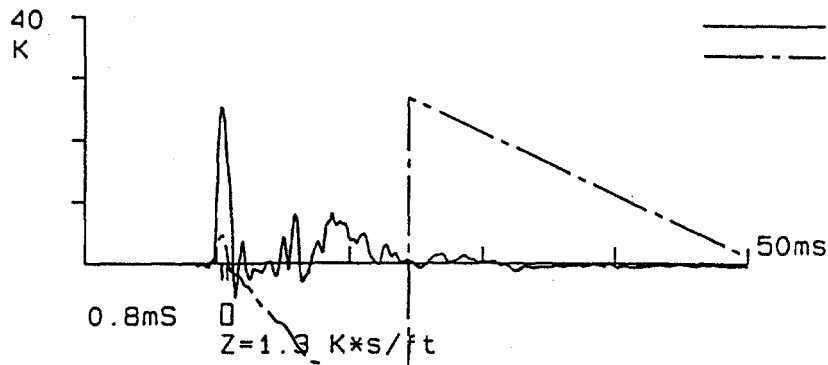


**Figure 79b. PDA Dynamic Measurements During the Restrike of MDMP Test NB3: Surface Force and Velocity Records Over 12 ms.**

UNIVERSITY MASS-LOWELL  
 Newbury Model Pile Test  
 PDA OP: LJH

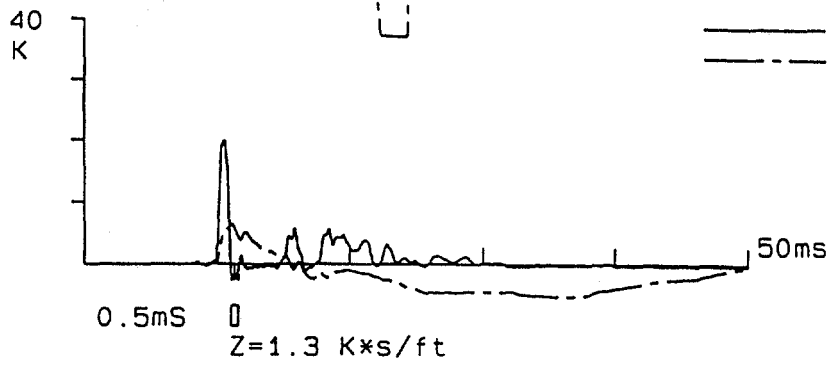
POI PILE DRIVING ANALYZER® v4.04  
 NB3MPRES 18-Mar-96  
 Top Load Cell



BN	2
EMX	0.07 Kip-ft
FMX	25.2 Kips
VMX	20.2 ft/s
DMX	1.03 inch
DFN	1.03 inch
FT1	25.2 Kips
VT1	3.5 ft/s
RTL	15.4 Kips
RMX	15.4 Kips
LE	7.10 ft
AR	0.74 in2
EM	30000 Ksi
SP	0.492 K/ft3
WS	16810 ft/s

Newbury Model Pile Test  
 PDA OP: LJH

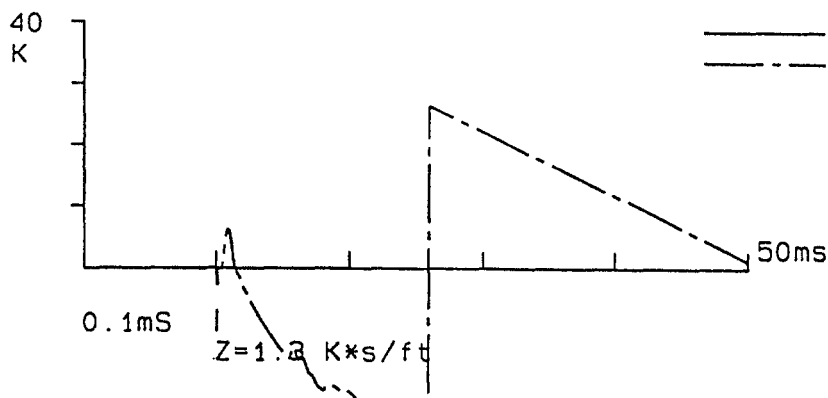
NB3MPRES 18-Mar-96  
 Middle Load Cell



BN	2
EMX	0.05 Kip-ft
FMX	20.0 Kips
VMX	5.0 ft/s
DMX	0.16 inch
DFN	-0.86 inch
FT1	-2.5 Kips
VT1	5.0 ft/s
RTL	-0.4 Kips
RMX	5.9 Kips
LE	4.70 ft
AR	0.74 in2
EM	30000 Ksi
SP	0.492 K/ft3
WS	16810 ft/s

Newbury Model Pile Test  
 PDA OP: LJH

NB3MPRES 18-Mar-96  
 Bottom Load Cell



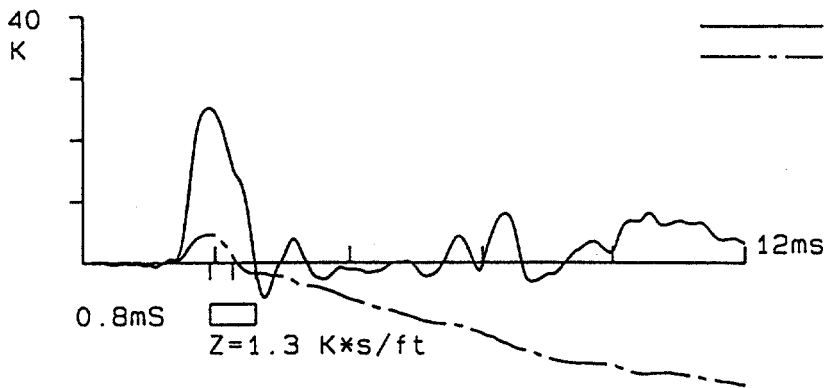
BN	2
EMX	0.00 Kip-ft
FMX	0.0 Kips
VMX	20.0 ft/s
DMX	0.10 inch
DFN	0.10 inch
FT1	0.0 Kips
VT1	0.1 ft/s
RTL	0.0 Kips
RMX	1.3 Kips
LE	1.00 ft
AR	0.74 in2
EM	30000 Ksi
SP	0.492 K/ft3
WS	16810 ft/s

**Figure 79c. PDA Dynamic Measurements During the Restrike of MDMP Test NB3: Internal Force and Velocity Records Over 50 ms.**



UNIVERSITY MASS-LOWELL  
 Newbury Model Pile Test  
 PDA OP: LJH

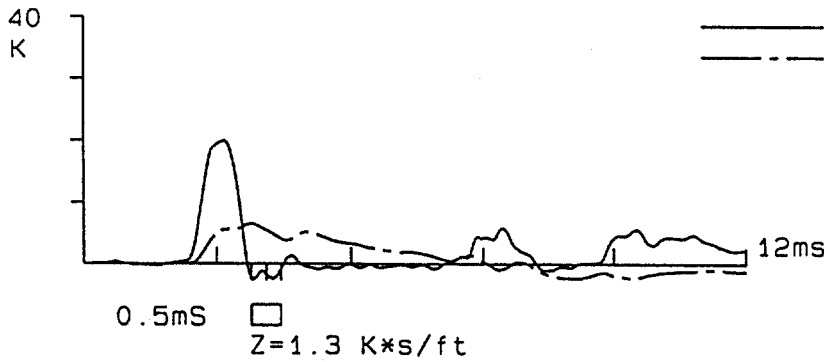
PDI PILE DRIVING ANALYZER® v4.04  
 NB3MPRES 18-Mar-96  
 Top Load Cell



BN	2
EMX	0.07 Kip-ft
FMX	25.2 Kips
VMX	20.2 ft/s
DMX	1.03 inch
DFN	1.03 inch
FT1	25.2 Kips
VT1	3.5 ft/s
RTL	15.4 Kips
RMX	15.4 Kips
LE	7.10 ft
AR	0.74 in2
EM	30000 Ksi
SP	0.492 K/ft3
WS	16810 ft/s

Newbury Model Pile Test  
 PDA OP: LJH

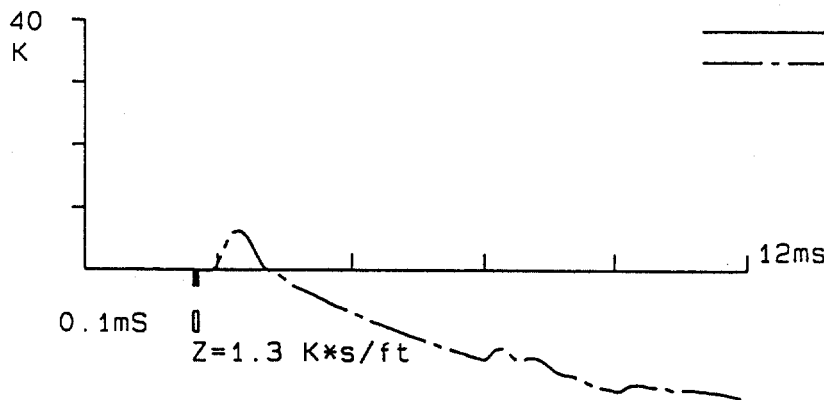
NB3MPRES 18-Mar-96  
 Middle Load Cell



BN	2
EMX	0.05 Kip-ft
FMX	20.0 Kips
VMX	5.0 ft/s
DMX	0.16 inch
DFN	-0.86 inch
FT1	-2.5 Kips
VT1	5.0 ft/s
RTL	-0.4 Kips
RMX	5.9 Kips
LE	4.70 ft
AR	0.74 in2
EM	30000 Ksi
SP	0.492 K/ft3
WS	16810 ft/s

Newbury Model Pile Test  
 PDA OP: LJH

NB3MPRES 18-Mar-96  
 Bottom Load Cell



BN	2
EMX	0.00 Kip-ft
FMX	0.0 Kips
VMX	20.0 ft/s
DMX	0.10 inch
DFN	0.10 inch
FT1	0.0 Kips
VT1	0.1 ft/s
RTL	0.0 Kips
RMX	1.3 Kips
LE	1.00 ft
AR	0.74 in2
EM	30000 Ksi
SP	0.492 K/ft3
WS	16810 ft/s

**Figure 79d. PDA Dynamic Measurements During the Restrike of MDMP Test NB3: Internal Force and Velocity Records Over 12 ms.**

The data in Figure 79a were related to the surface measurements for a time period of 50 ms, while Figure 79b depicts the same data over a 12-ms period detailing the impact wave and its reflections during the travel time down to the tip and back. The data in Figures 79a and b indicated the following:

1. **Surface Force** - The force at the top of the rods seemed to undergo sharp fluctuations. The causes of these fluctuations are discussed in sections 6.2.2 and 6.4.4.
2. **Surface Velocity** - The velocity record at the top of the drill rods was multiplied by the rods' impedance and was presented in force units for comparison to the force measurements. In general, the velocity followed the force signal during the input hammer blow. The average ratio of proportionality between the two peaks (velocity\*impedance/force) was 0.89. This ratio was reasonable under the anticipated uneven stress distribution resulting from the SPT hammer blow.

The data in Figure 79c were related to the surface measurements for a time period of 50 ms, while Figure 79d depicts the same data over a 12-ms period, detailing the impact wave and its reflections during the travel time down to the tip and back. The data in Figures 79c and d indicated the following:

1. **Internal Forces** - The internal forces were recorded and seemed to be adequate and reliable. The records for blow 2 (presented in Figure 79) suggested that the wave arriving at the top load cell was about 1.47 times the magnitude of the wave recorded at the surface and was of a similar shape. The record reflected the influence of the impedance increase when the rods were connected to the instrumented pile. An evaluation of this increase over the penetration record is presented in Chapter 7, where it is shown to match the expected analysis. The peak wave passing through the middle load cell was reduced by about 23.1 kN (5.2 kips). This reduction was equal to the dynamic friction force acting on the sleeve and will be discussed further in Chapter 7.
2. **Internal Velocities** - The accelerometers were questionable during the initial restrike of NB3. The data in Figures 79c and d suggested that the accelerometers mounted at the top and bottom locations reached saturation and thus were not reliable. The middle accelerometer appeared to respond properly, but the large negative final displacement of DFN=-21.8 mm (-0.86 in) suggested that the records were not reliable either.

#### **6.6.6 Force Measurements**

The two surface force transducers bolted to the drill rods at 180° across from each other recorded different forces for the same blow. Since the gauges were on opposite sides of the pile, the cause of the different force measurements was eccentric impact, i.e., the hammer was not striking the guide rod evenly at a plane perpendicular to the direction of the traveling wave. The force signals inside the MDMP were measured using a single axial load cell a long distance from the

impact. As a result, the internal load cells were not capable of identifying uneven stress distribution in the pile wall. The safety hammer was not inspected to confirm the cause of the uneven force measurements. The force measurements for gauges bolted to the drill rods were averaged together to yield an average force that was used for all subsequent analyses. Figures 72, 73, 75, 77, and 79 all indicate the existence of uneven contact stresses during the impact.

Figures 80 through 83 present the maximum (peak) forces recorded for each blow at three gauge positions: surface measurement, and top and middle load cell locations. In general, the peak forces recorded at the surface and middle load cell locations were of the same magnitude, while higher forces were measured at the top load cell location. An important observation from these figures was that the gauges in the MDMP recorded consistent data. Table 28 presents the average peak forces recorded at each location during each stage of driving. The standard deviation decreased after the first test because during the NB2 installation, the appropriate stroke was investigated and was maintained in subsequent driving. Initially, a 0.152-m (6-in) stroke was examined and subsequently increased to 0.305 m (12 in) and then to 0.457 m (18 in). The remaining tests were conducted with a 0.457-m (18-in) stroke.

**Table 28. Average Peak Forces Measured at Three Locations in the MDMP.**

Test	Surface Measurements			Top Load Cell Location			Middle Load Cell Location		
	# Blows	F <sub>max</sub> (kN)	Std Dev.	# Blows	F <sub>max</sub> (kN)	Std Dev.	# Blows	F <sub>max</sub> (kN)	Std Dev.
<b>NB2 Installation</b>	252	69.74	6.85	213	88.03	10.08	213	70.35	8.51
<b>NB2 Restrike</b>	120	77.73	4.83	119	107.5	6.63	119	80.71	4.90
<b>NB3 Installation</b>	30	104.4	9.74	30	104.6	4.38	30	84.05	3.92
<b>upper/lower*</b>	30	83.49	3.32						
<b>NB3 Restrike</b>	355	81.99	3.63	349	109.8	5.44	349	86.66	4.61

\*The force transducers are identified according to their relative position at the surface.

### 6.6.7 Velocity Measurements

The average velocity measured during each of the tests are shown in Table 29. Figures 84 through 87 show that the measurements at the surface location were consistent and yielded average proportionality ratios of 0.76, 0.78, 0.79, and 0.89 for NB2 installation, NB2 restrike, NB3 installation (piezoresistive gauge), and NB3 restrike, respectively. The velocity records from the top load cell location were inconsistent and many times the signal appeared to be saturated. This indicated that the connection of the accelerometer to its mount and/or the mount to the load cell wall was not secure or possibly that the accelerometer was broken. Based on the fact that the accelerometer did record sporadic data, the connection of the accelerometer to the pile seemed to be the reason for the difficulties. Similar irregularities appeared in the velocity measurements at the middle load cell location, but were far less frequent. The average value presented in Table 29 for the middle load cell location only included velocities between 0.305 and 2.44 m/s (1 and 9 ft/s).

Figure 80. Maximum Dynamic Forces Measured During Installation of MDMP Test NB2.

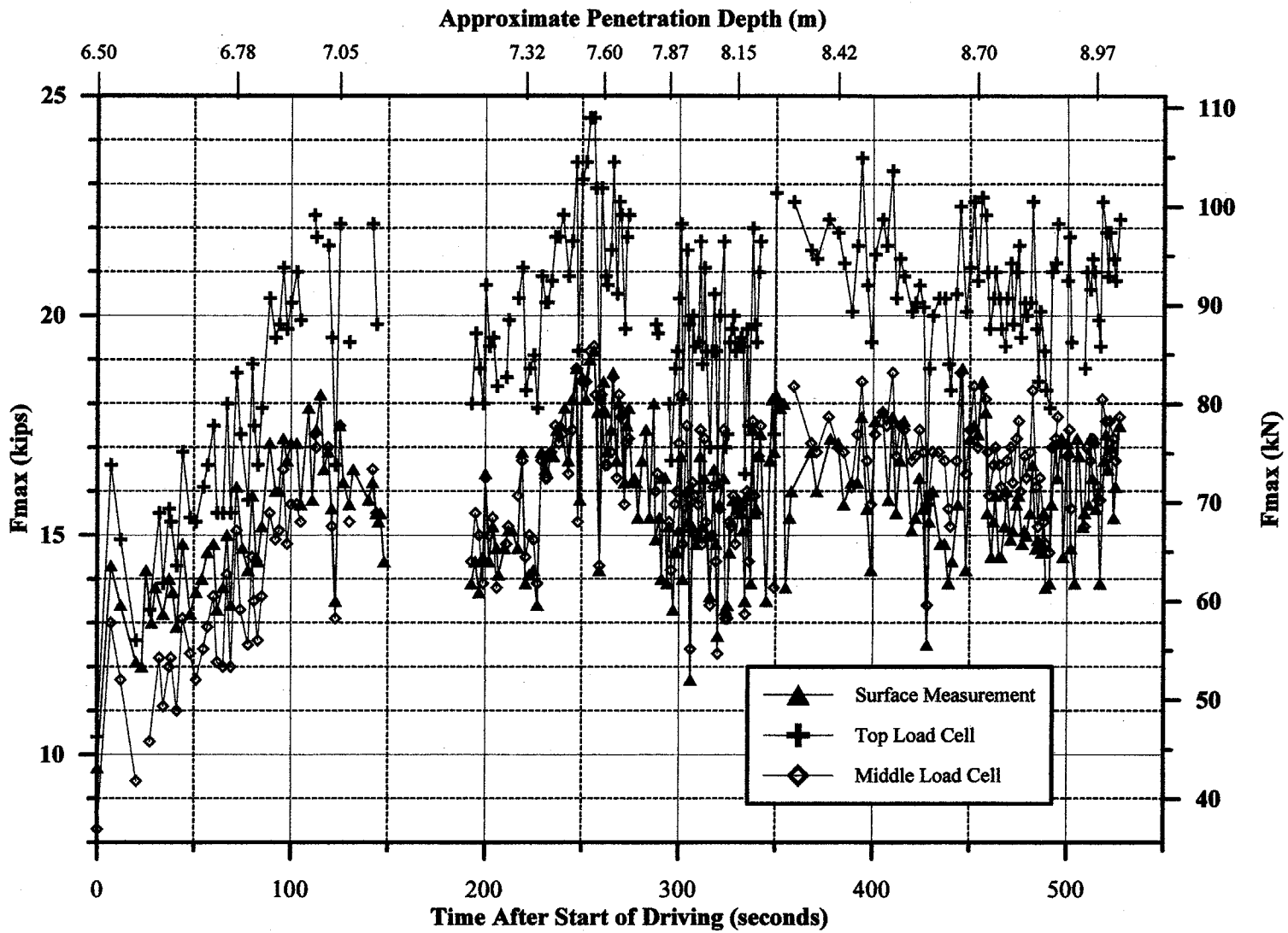


Figure 81. Maximum Dynamic Forces Measured During Restrike of the MDMP Test NB2.

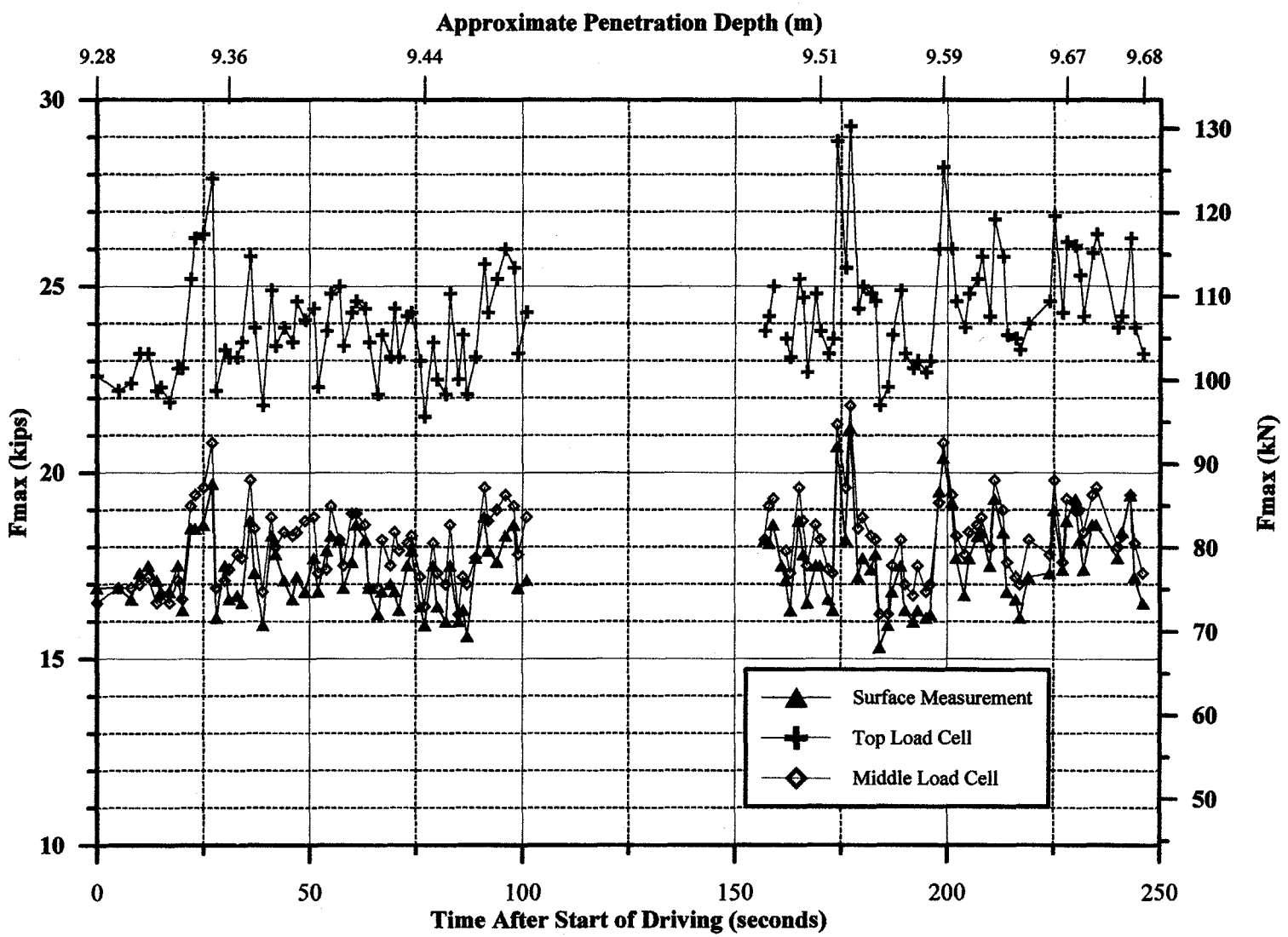


Figure 82. Maximum Dynamic Forces Measured During Installation of MDMP Test NB3.

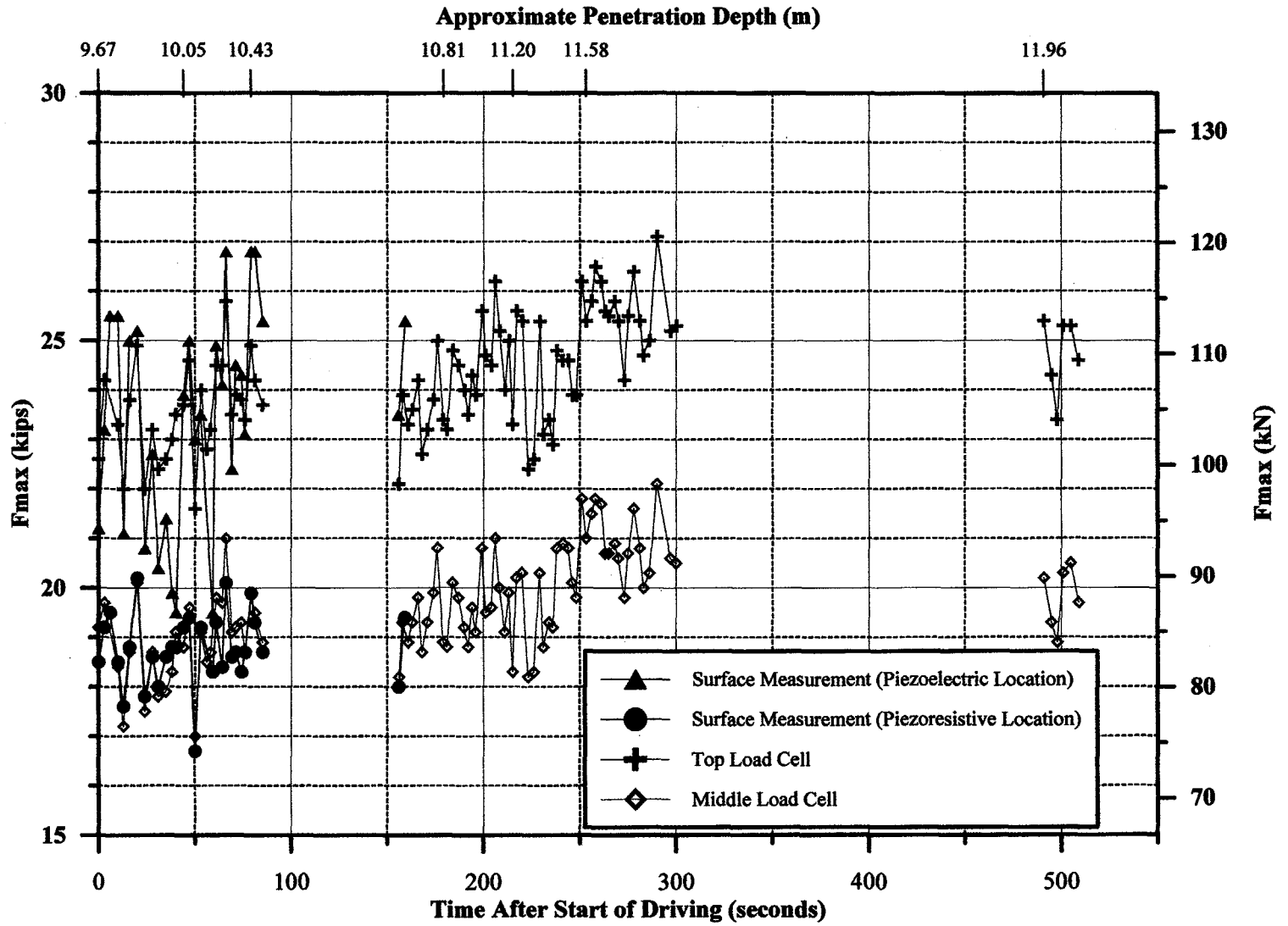
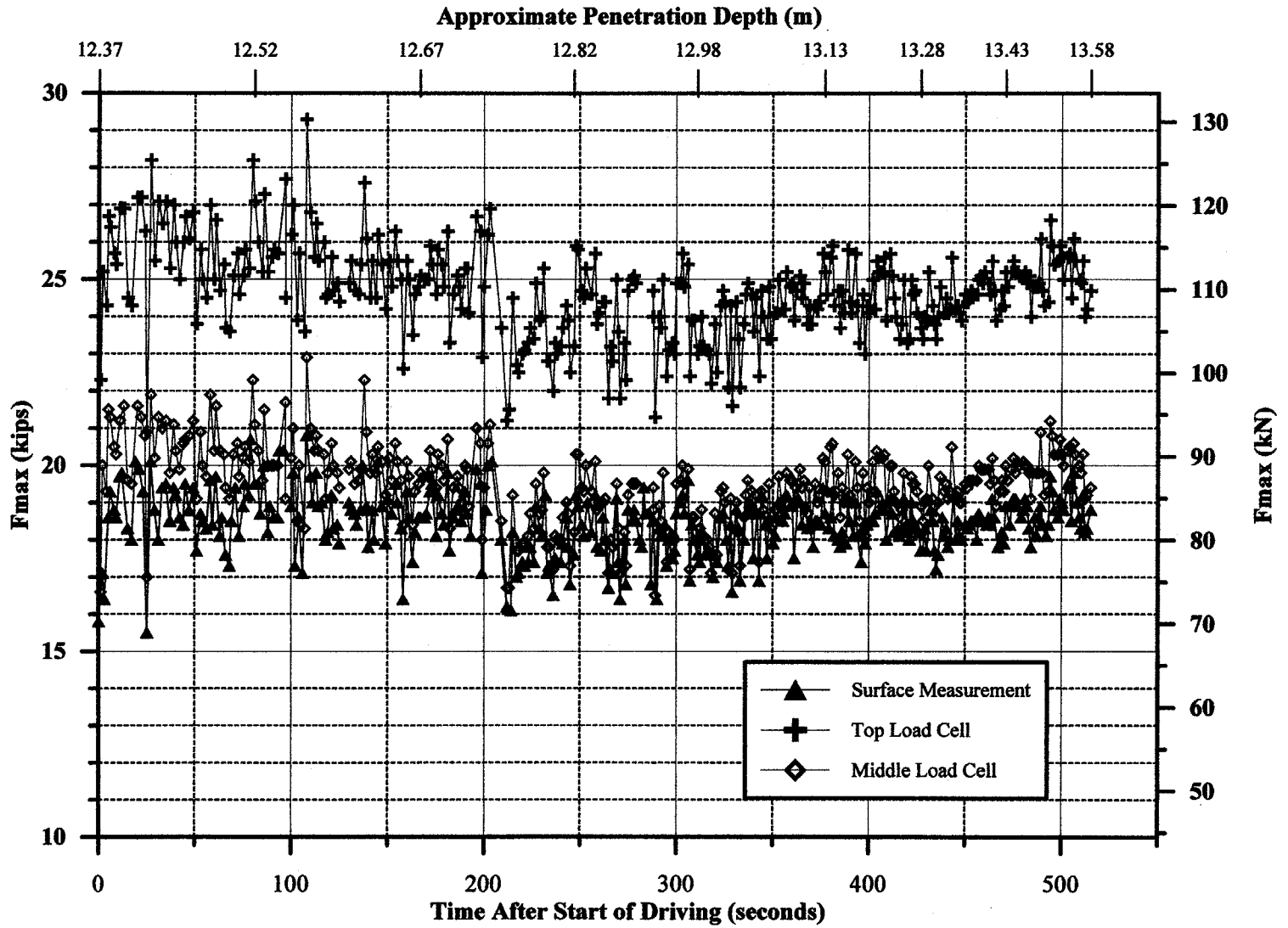
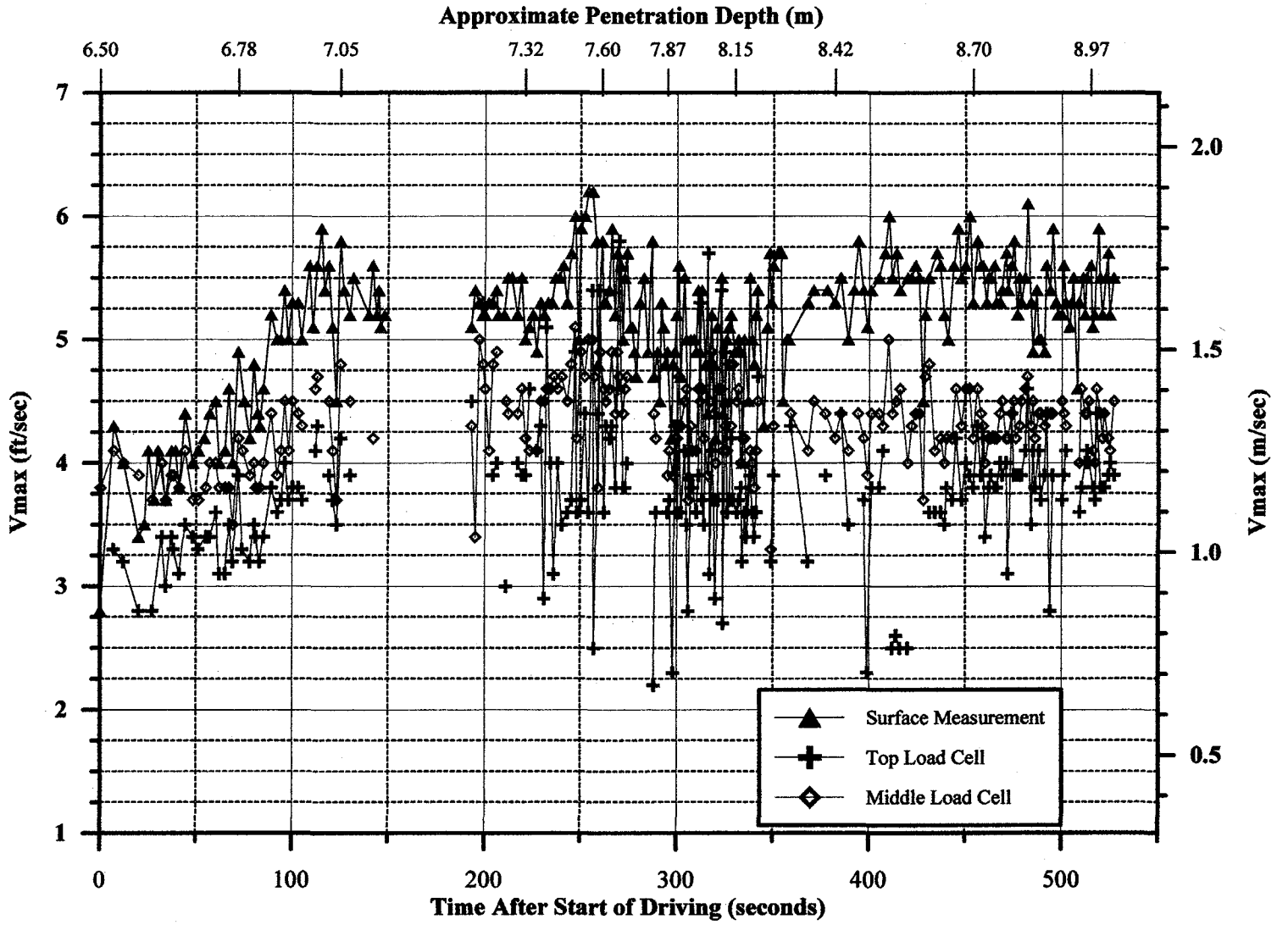


Figure 83. Maximum Dynamic Forces Measured During Restrike of MDMP Test NB3.



**Figure 84. Maximum Dynamic Velocities Measured During Installation of MDMP Test NB2.**





**Figure 85. Maximum Dynamic Velocities Measured During Restrike of MDMP Test NB2.**

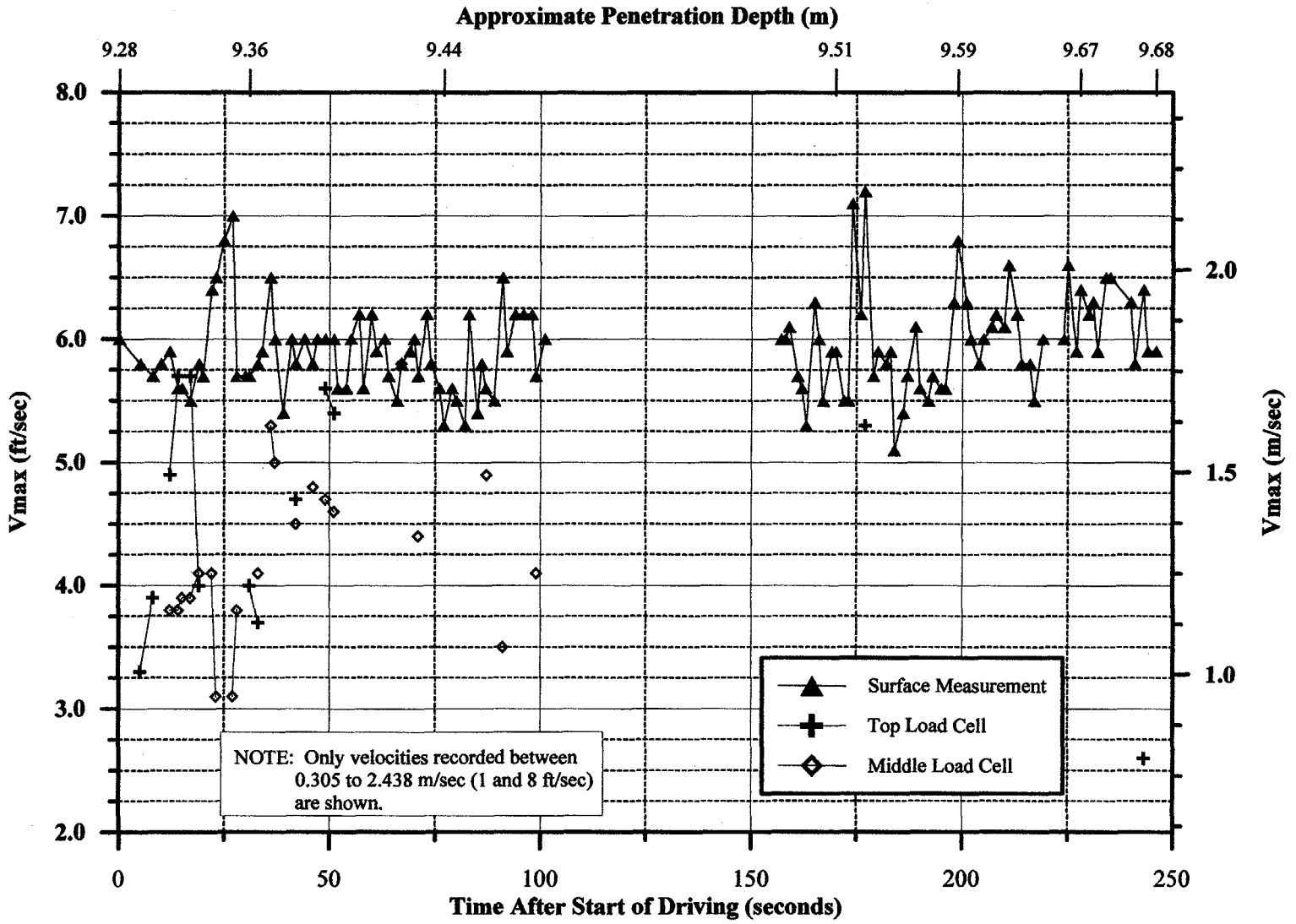


Figure 86. Maximum Dynamic Velocities Measured During Installation of MDMP Test NB3.

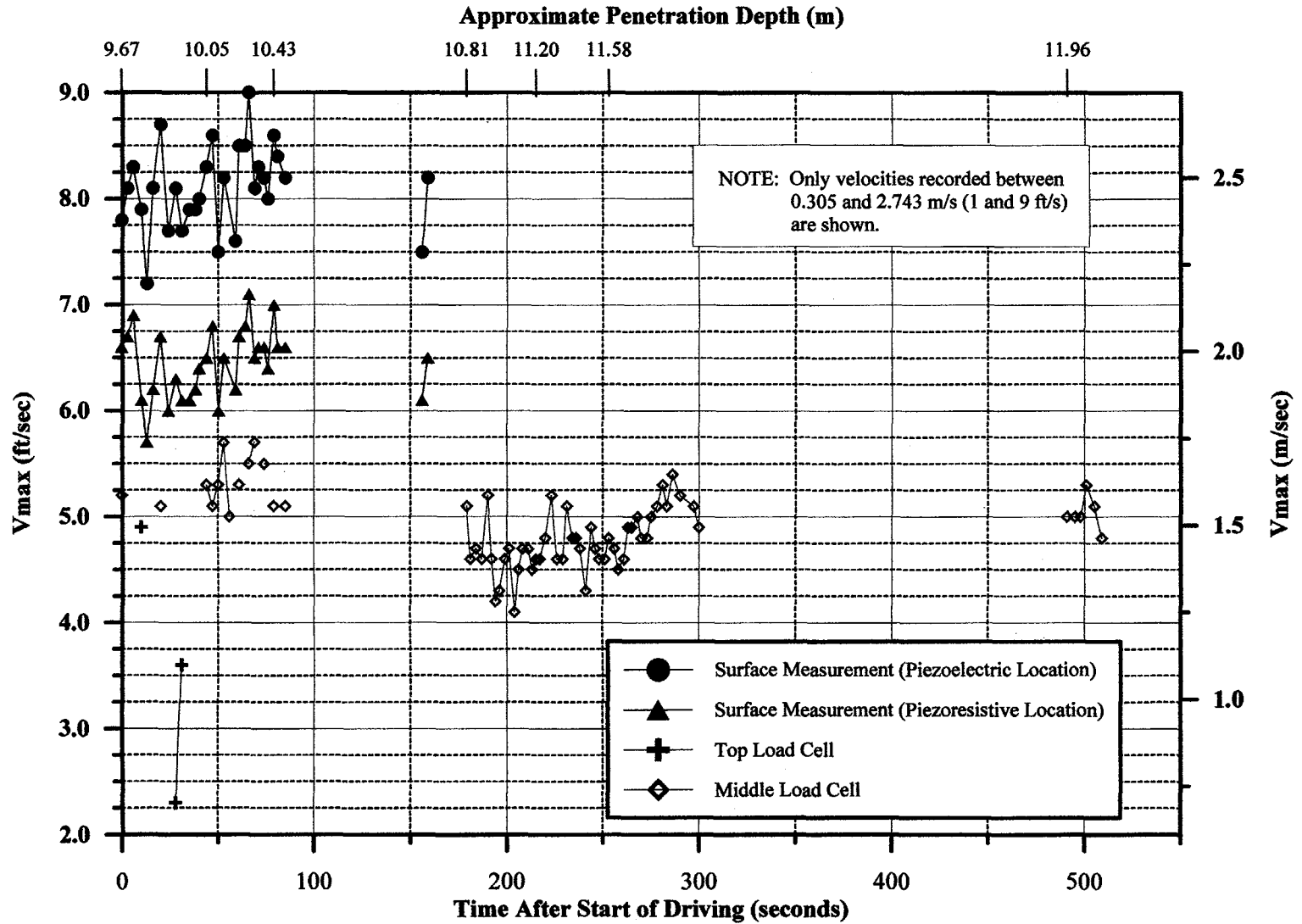
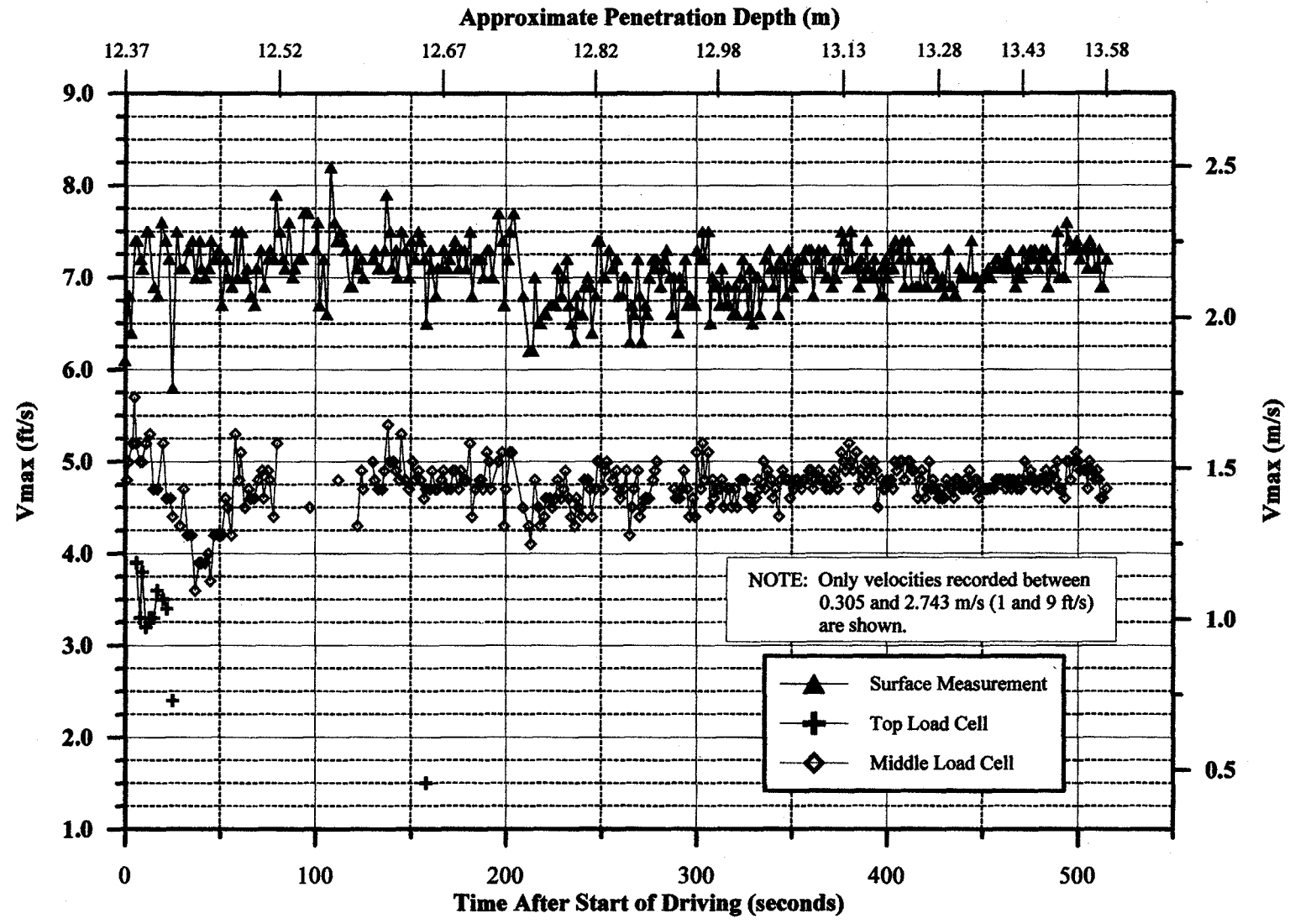


Figure 87. Maximum Dynamic Velocities Measured During Restrike of MDMP Test NB3.



**Table 29. Average Peak Velocity Measured at Three Locations in the MDMP.**

Test	Surface Measurements			Top Load Cell Location			Middle Load Cell Location		
	# Blows	V <sub>max</sub> (m/sec)	Std Dev.	# Blows	V <sub>max</sub> (m/sec)	Std Dev.	# Blows	V <sub>max</sub> (m/sec)	Std Dev.
<b>NB2 Installation</b>	252	1.57	0.16	200	1.17	0.24	213	1.31	0.10
<b>NB2 Restrike</b>	120	1.81	0.12	N/A	N/A	N/A	30	1.620	0.55
<b>NB3 Installation</b>	30	2.47	0.12	N/A	N/A	N/A	13	1.62	0.07
<b>upper/lower*</b>	30	1.97	0.10						
<b>NB3 Restrike</b>	355	2.16	0.09	N/A	N/A	N/A	326	1.45	0.08

- \*Notes: 1. During NB3 installation, both types of accelerometers were utilized at the surface and average values only include the first 30 blows.  
 2. Values for the Middle Load Cell include data only for the range of 0.305 to 2.743 m/s (1 to 9 ft/s).  
 3. Accelerometer at Top Load Cell location did not work properly.

## CHAPTER 7. ANALYSIS OF THE MDMP TEST RESULTS

### 7.1 Normalized Pore Pressure Dissipation

#### 7.1.1 MDMP Test NB2

The maximum (peak) pore pressure measured during MDMP test NB2 was observed following the final downward displacement associated with the alignment of the static load frame at 39.72 min after the start of installation (see Figure 47). This maximum pore pressure of 217.33 kPa (31.52 psi) was used as the initial pore pressure, denoted by  $u_i$ . By subtracting the hydrostatic pore pressure of 58.12 kPa (8.43 psi), the initial excess pore pressure ( $\Delta u_i$ ) was 159.21 kPa (23.09 psi). For the analysis of normalized pore pressure, the time associated with the end of driving was considered to be that of the aforementioned adjustment since it was accompanied by a significant gain of pore pressure. From this assigned end of driving to the end of the test, the excess pore pressure record was normalized by the maximum initial pore pressure ( $\frac{\Delta u}{\Delta u_i}$ ). Figure

88 shows the normalized excess pore pressure versus time after driving. The consolidation ratio of the soil at the point of measurement was the difference between 1 and the normalized excess pore pressure ratio:

$$u_z = \left( 1 - \frac{\Delta u}{\Delta u_i} \right) \quad (7.1)$$

The normalized excess pore pressure continued below the zero line (i.e., beyond 100% consolidation) because the actual measured pore pressure at the end of the test was below the average hydrostatic water pressure at the site. These values could be corrected to ensure that the final pore pressure would not decrease below the hydrostatic level; however, it was chosen not to do so in order to reflect the actual accuracy of the field measurements. From 80% to 20% normalized excess pore pressure (20% to 80% consolidation), the slope of the best-fit line on the log-normal scale represented the rate of radial consolidation,  $H_{ur}$ , and was 0.6047. The time at 50% dissipation,  $t_{50}$ , was 9.854 h (35476 s). When adjusted to the PLS cell radius (19.177 mm),  $t_{50(pls)}$  was 2.493 h (8975 s). The time adjustment (see section 5.6) allowed the comparison of the absolute time of any dissipation process to another, regardless of the pile size. As previous data analysis used the PLS cell as its standard (Paikowsky et al., 1995), the current measurements were adjusted to the same size as well.

#### 7.1.2 MDMP Test NB3

The maximum (peak) pore pressure during model pile test NB3 was 224.02 kPa (32.49 psi). This maximum pore pressure was used as the initial pore pressure value ( $u_i$ ) in the normalization process. The maximum/initial excess pore pressure was, therefore, obtained by subtracting the hydrostatic pressure of 88.53 kPa (12.84 psi) from the initial excess pore pressure, resulting in a  $\Delta u_i$  of 135.49 kPa (19.65 psi). Figure 89 shows the normalized excess pore pressure versus time after driving, from the end of driving to the end of the test. The normalized excess pore pressure at the end of the test was above zero as the final measured pore pressure was above the average hydrostatic pore pressure calculated for that depth. From 80% to 20% normalized excess pore

Figure 88. Normalized Excess Pore Pressure and Shear Transfer Gain, Model Pile Test NB2.

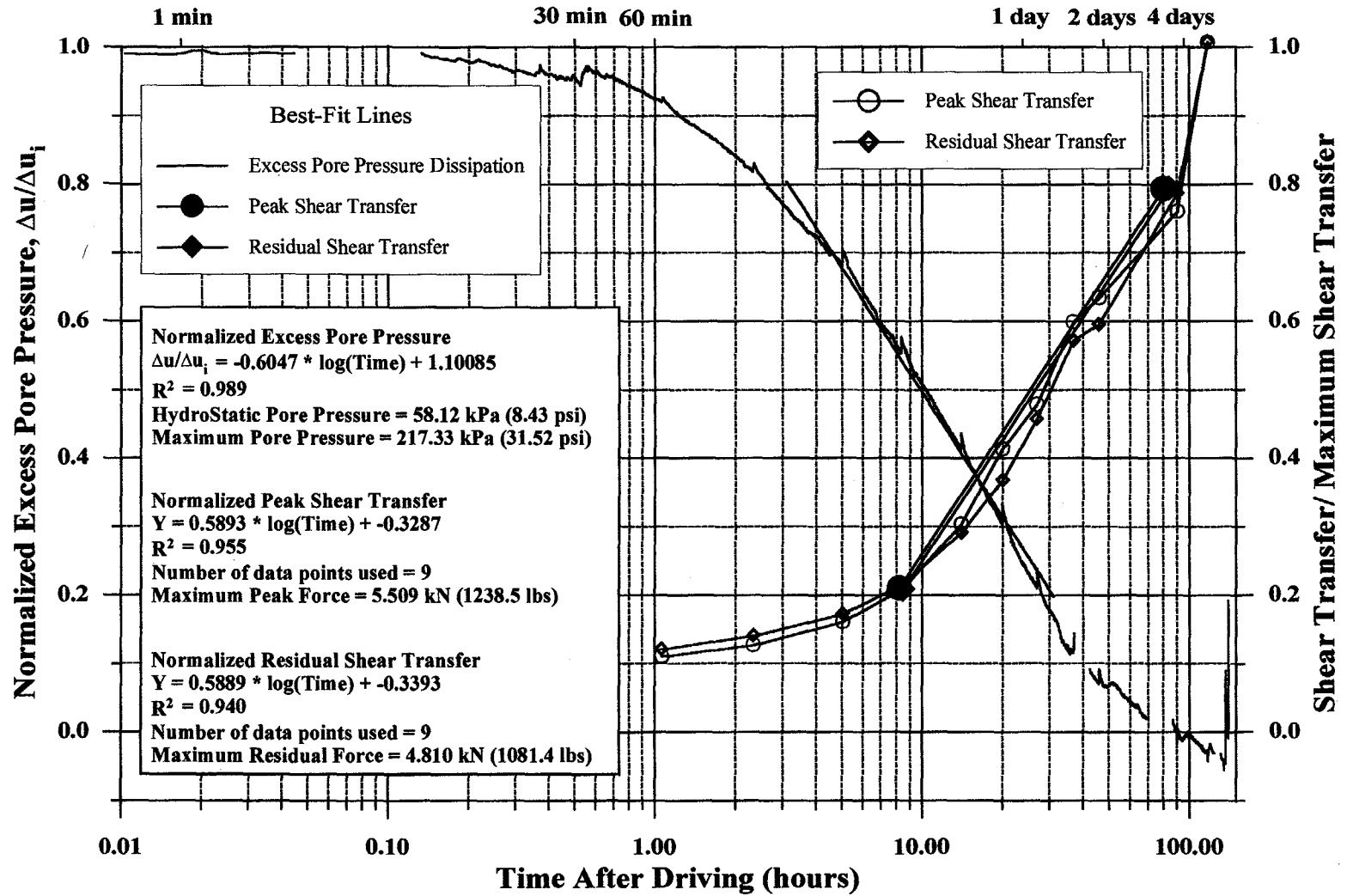
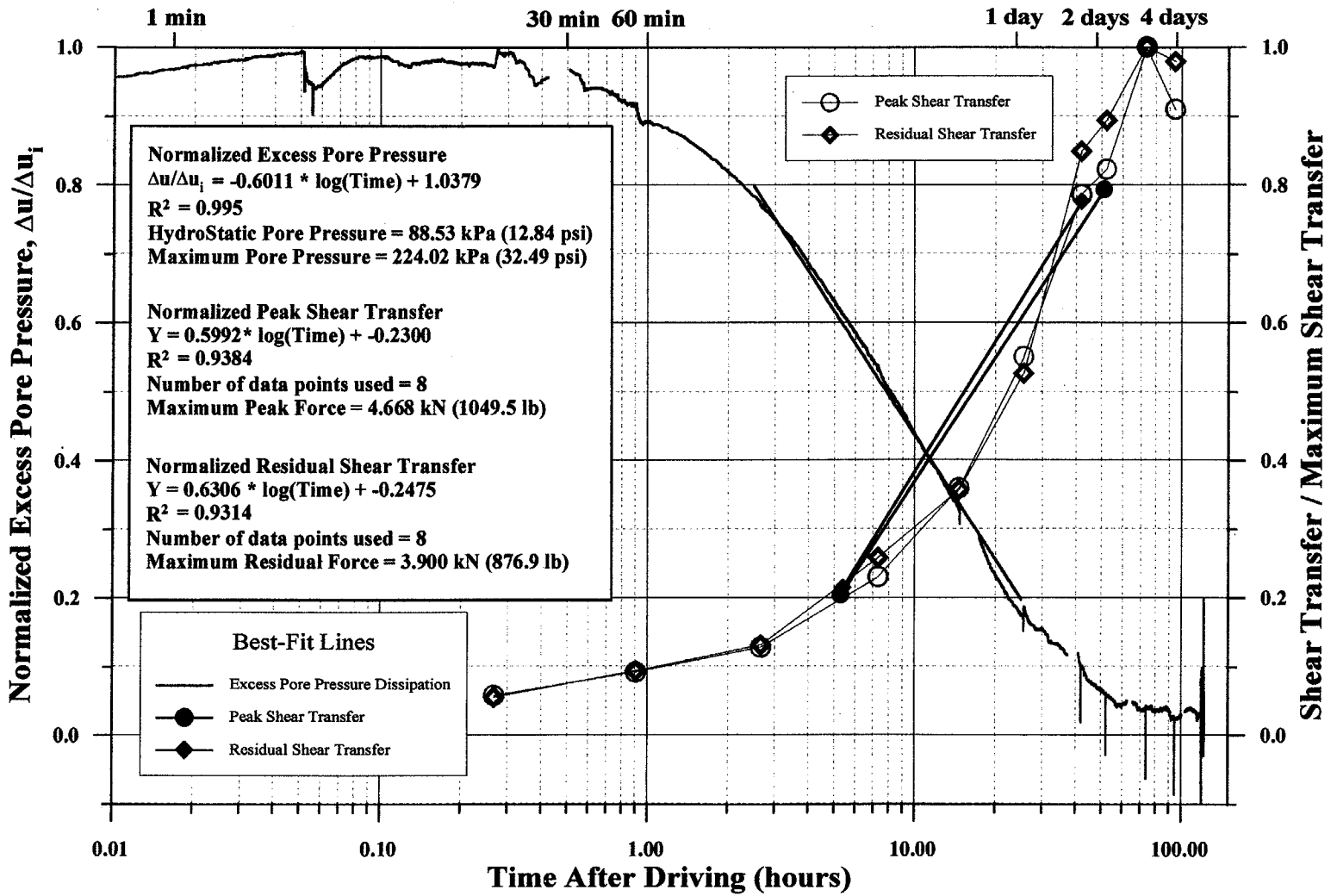


Figure 89. Normalized Excess Pore Pressure and Shear Transfer Gain, Model Pile Test NB3.



pressure (equivalent to 20% to 80% consolidation), the slope of the best-fit line on the log-normal scale,  $H_{ur}$ , was 0.6011. The time at 50% dissipation,  $t_{50}$ , was 7.849 h (28256 s). When adjusted to the PLS cell radius (19.177 mm),  $t_{50(pls)}$  was 1.986 h (7149 s).

### 7.1.3 Comparison With Other Test Results

Paikowsky et al. (1995) found, based on a database analysis, that the rate of pore pressure dissipation,  $H_{ur}$ , was  $0.466 \pm 0.089$  (33 cases) for normally consolidated soil and  $0.498 \pm 0.067$  (12 cases) for normally consolidated Boston Blue Clay (BBC). The complete range of  $H_{ur}$  values for normally consolidated soils was from 0.325 to 0.763, with a narrower range of 0.351 to 0.584 for the normally consolidated BBC. Table 30 summarizes the results of the excess pore pressure dissipation during the Newbury Testing as compared to the study presented by Paikowsky et al. (1995).

**Table 30. Summary of Excess Pore Pressure Dissipation Parameters and Their Comparison to a Large Data Set.**

Site	Hydrostatic Pore Pressure (kPa)	Initial Excess Pore Pressure, $\Delta u_i$ (kPa)	Vertical* Effective Stress, $\sigma_v'$ (kPa)	$\Delta u_i/\sigma_v'$ *	$H_{ur}$	$t_{50(pls)}$ (hours)
NB2	58.1	159.2	80.46/90.98	1.98/1.74	0.6047	2.493
NB3	88.5	135.5	103.37/119.30	1.31/1.14	0.6011	1.986
Average	N/A	N/A	N/A		0.6030	2.240
Data from Paikowsky et al. (1995)						
All Soils NC	N/A	N/A	N/A	$\Delta u_i/\sigma_v' = 2.29 \pm 0.57$ (1 S.D.) for OCR $\leq 10$	0.466 $\pm 0.089$	1.796 $\pm 1.018$
All Soils OC	N/A	N/A	N/A		0.968 $\pm 0.602$	0.922 $\pm 1.174$
BBC NC	N/A	N/A	N/A		0.498 $\pm 0.067$	1.571 $\pm 0.334$
BBC OC	N/A	N/A	N/A		0.614 $\pm 0.110$	0.293 $\pm 0.261$
BBC NC Saugus Site	N/A	N/A	N/A		0.492 $\pm 0.072$	1.597 $\pm 0.356$

\*Related to vertical effective stresses without and with embankment influence, respectively.

The rate of pore pressure dissipation in both tests was practically identical, with an average  $H_{ur}$  of 0.603. This value falls within the range of recorded values for all normally consolidated soils (from 0.325 to 0.763), but indicated a faster dissipation than the mean value of  $H_{ur} = 0.466 \pm 0.089$  (33 cases). The measured rate was also about 20% higher than the mean value found for BBC at the Saugus, MA site ( $H_{ur} = 0.492 \pm 0.072$ ).

The above measurements and ranges suggest that: (1) the use of an average  $H_{ur}$  value from a large data set provided a reasonably good initial estimation of the dissipation rate, but a site-specific investigation was required for an accurate evaluation, and (2) the normally consolidated BBC contained a larger variation of soil composition and/or deposition sequence, which affected the radial consolidation process. Preliminary investigation of the soils at the Newbury site



by John Chen at UMass-Lowell) suggested that the clay at the testing location contained a larger proportion of silt content than the typical BBC clay.

The time required to achieve 50% dissipation ( $t_{50}$ ) normalized to the PLS cell radius (19.177 mm) was  $1.796 \pm 1.02$  h ( $6466 \pm 3665$  s) for all normally consolidated soils and  $1.57 \pm 0.334$  h ( $5655 \pm 1202$  s) for normally consolidated BBC. The actual range of  $t_{50}$  values for 27 normally consolidated soils was found by Paikowsky et al. (1995) to be 0.655 h (2359 s) to 6.03 h (21722 s) and 1.08 h (3878 s) to 2.21 h (7958 s) for normally consolidated BBC. The average  $t_{50}$  for the MDMP tests at the Newbury site normalized to the PLS cell radius is 2.24 h (8062 s). This value fell within the range for all non-consolidated (NC) soils, but indicated a longer time before 50% dissipation was completed at the Newbury site, compared to the previously measured dissipation times in BBC.

The above measurements and ranges suggested that, as with the  $H_{ut}$  parameter, using the average  $t_{50}$  from the large data set provided a reasonably good initial estimation of the time to 50% dissipation, but a site-specific investigation was required for an accurate evaluation. Based on the large variability of the  $t_{50}$  parameter, a range should be used when predicting the dissipation time.

Table 31 presents a typical time range for a 0.3048-m (1-ft) diameter pile to reach various amounts of dissipation. From these analyses, the combined effect of the two parameters,  $H_{ut}$  and  $t_{50}$ , could be examined. Even though the dissipation rate was faster at the Newbury site, the time to 80% dissipation was about the same as for the Saugus site and all NC soils based on the longer time required for 50% consolidation.

**Table 31. Evaluated Pore Pressure Dissipation Time (Adjusted to the PLS Diameter) Based on the Newbury Test Results Compared With a Large Data Set.**

Site	Parameter		Time to % Dissipation (hours)		
	$H_{ut}$	$t_{50}$ (hours)	20%	50%	80%
Newbury, MA	0.603	2.24	45.0	141.5	444.8
Saugus, MA <sup>†</sup>	0.492	1.60	24.8	100.9	410.6
All Soils NC <sup>†</sup>	0.466	1.80	25.8	113.4	499.4

<sup>†</sup>Data from Paikowsky et al. (1995)

## 7.2 Normalized Capacity Gain

### 7.2.1 MDMP Test NB2

The shear transfer measured along the friction sleeve during the static load tests was normalized to the maximum measured shear transfer and presented in Figure 88 along with the normalized pore pressure readings. Both peak and residual shear transfer values from each static load test were included in the normalized shear transfer relations. Utilizing the data between the load transfer ratios of 0.1 to 1.0, the rate of capacity gain ( $C_{gt}$ ) for both peak values and residual values was 0.589. The time to 75% gain of capacity,  $t_{75}$ , was 67.7 h for peak values and 70.7 h for residual values. Following the standard normalization used by Paikowsky et al. (1995),  $t_{75}$  was adjusted to a 152.4-mm (6-in) radius pile. The  $t_{75(152.4 \text{ mm})}$  was 1083.2 h for peak values and 1131.2 h for residual values.

### 7.2.2 MDMP Test NB3

The shear transfer measured along the friction sleeve during the static load tests was normalized to the maximum measured shear transfer and presented in Figure 89 along with the normalized pore pressure readings. Both peak and residual shear transfer values from each static load test were included in the normalized shear transfer relations. Utilizing the data between the load transfer ratios of 0.1 to 1.0, the rate of capacity gain ( $C_{gt}$ ) was 0.599 for peak values and 0.631 for residual values. The time to 75% gain of capacity,  $t_{75}$ , was 43.2 h for peak values and 38.2 h for residual values. Following the standard normalization used by Paikowsky et al. (1995), the  $t_{75}$  was adjusted to a 152.4-mm- (6-in-) radius pile. The  $t_{75(152.4 \text{ mm})}$  was 691.2 h for peak values and 610.9 h for residual values.

### 7.2.3 Comparison With Other Test Results

Based on the analysis of data set compiled at UMass-Lowell, Paikowsky et al. (1995) found that the expected  $C_{gt}$  from 39 cases was 0.367, with a standard deviation of 0.096. The time to 75% gain in capacity was  $370.7 \pm 338.7$  h when normalized to a 152.4-mm (6-in) pile radius. Table 32 summarizes the gain in capacity behavior based on the Newbury MDMP test results, along with the data presented by Paikowsky et al. (1995) for other locations.

**Table 32. Summary of Gain of Capacity Parameters and Their Comparison to a Large Data Set.**

Site	$C_{gt}$ (peak)	$C_{gt}$ (residual)	$t_{75(152.4 \text{ mm})}$ (peak) (hours)	$t_{75(152.4 \text{ mm})}$ (residual) (hours)		
NB2	0.589	0.589	1083.2	1131.2		
NB3	0.599	0.631	691.2	610.9		
Average	0.594	0.610	887.2	871.1		
Data from Paikowsky et al. (1995)						
	No. of Cases	$C_{gt}$	Std. Dev.	No. of Cases	$t_{75(152.4 \text{ mm})}$ (hours)	Std. Dev.
All Data	39	0.367	0.096	23	370.7	338.7
Shaft Capacity	17	0.356	0.088	12	539.5	336.2

The average  $C_{gt}$  for the Newbury site was 0.594 for peak values and 0.610 for residual values. The  $C_{gt}$  values were consistent for the two MDMP tests at the Newbury site and were much higher than those determined by Paikowsky et al. (1995) based on other test results. This difference may be explained by one or more of the following reasons:

- (1) The multiple load tests in each of the MDMP loading sequences followed the capacity gain process very accurately, revealing a significant delay in the capacity gain process (see Figures 88 and 89), followed by a sharp increase. Most of the cases used by Paikowsky et al. (1995) did not contain such detailed data and, hence, large time intervals between load tests resulted in a significantly more moderate slope of the capacity gain process. For example, when connecting the initial normalized capacity

values to the final ones, the  $C_{gt}$  for peak values of NB2 and NB3 were 0.44 and 0.33, respectively.

- (2) Based on knowledge acquired from other studies, the MDMP was designed such that the pore pressure measurements were situated away from both ends of the pile. This location ensured "true" radial dissipation/consolidation at the point of measurement and, hence, significantly longer dissipation time compared to cases in which other effects took place, allowing possible vertical dissipation.
- (3) The number of case histories for which capacity was monitored with time is limited. In many of those cases, the final load test may not necessarily have represented the end of consolidation and/or the maximum capacity (as may be the case for test NB2). Obtaining a  $t_{75}$  based on normalization to the maximum load (not maximum capacity) would result in a time shorter than the one actually required for the entire capacity gain process. Even the concept of using  $t_{75}$  when monitoring capacity gain was developed as a result of a lack of data in the initial stages of capacity gain, along with the possible failure to complete the process (Paikowsky et al., 1995).
- (4) The influence of the multiple load testing on the interfacial shear strength was unclear when combined with all aspects of penetration, pore pressure build-up, radial stress changes, etc. It was, however, known that multiple shear of the same material contributed to its strength. In other words, the testing procedure of the phenomena itself affected the test results and, hence, resulted in a higher strength that was achieved over a longer period of time.

The average  $t_{75(152.4 \text{ mm})}$  for the Newbury site was 887.2 h for peak values and 871.1 for residual values. The average value represented about a  $\pm 22\%$  difference from the actual measurements, which seemed to be a very large variation within the same layer. Several possible explanations are: (1) The MDMP test NB2 was not completed and the final measured capacity did not necessarily represent the maximum shear transfer that actually existed. When using this value in the normalization process, naturally the obtained  $t_{75}$  was smaller than the actual, along with a decrease in the  $C_{gt}$  parameter. (2) A large variation in the soil was detected in the subsurface exploration study. Its influence on the radial consolidation process has yet to be assessed.

Table 33 presents the differences between the data collected at the Newbury site and the data presented by Paikowsky et al. (1995). The  $C_{gt}$  parameter found at the Newbury site was 1.6 times higher than values determined from the data set. The  $t_{75}$  obtained at the Newbury site was also larger than the one obtained at other locations, resulting in an overall longer capacity gain time even though the capacity gain was faster. This fact becomes apparent when examining Table 33; at 50% pore pressure dissipation, the pile designed with the Newbury site parameters would only gain 27.6% of the overall capacity, while the pile designed from data set parameters would gain about 50% of the capacity. Even at the 80% pore pressure dissipation, still only 57.2% of the capacity gain had taken place at the Newbury site.

**Table 33. Evaluated Gain of Capacity (Adjusted to 152.4-mm Radius Pile) Based on the Newbury Test Results Compared With a Large Data Set.**

Site	Parameters		Time to % Capacity			% Capacity Gain at	
	$C_{gt}$	$t_{75(152.4\text{ mm})}$ (hours)	20% (hours)	50% (hours)	80% (hours)	50% Pore Pressure Dissipation	80% Pore Pressure Dissipation
Newbury	0.594 (peak)	887.2 (peak)	105.2	336.6	1077.0	27.6%	57.2%
All Data	0.367	370.7	11.8	77.2	507.3	56.1% <sup>†</sup>	79.8% <sup>†</sup>
Shaft Capacity	0.356	539.5	15.4	107.1	745.5	50.9% <sup>†</sup>	73.8% <sup>†</sup>

<sup>†</sup>Based on times for All Soils NC in Table 31.

### 7.3 Comparison Between Predicted and Measured Values

#### 7.3.1 Overview

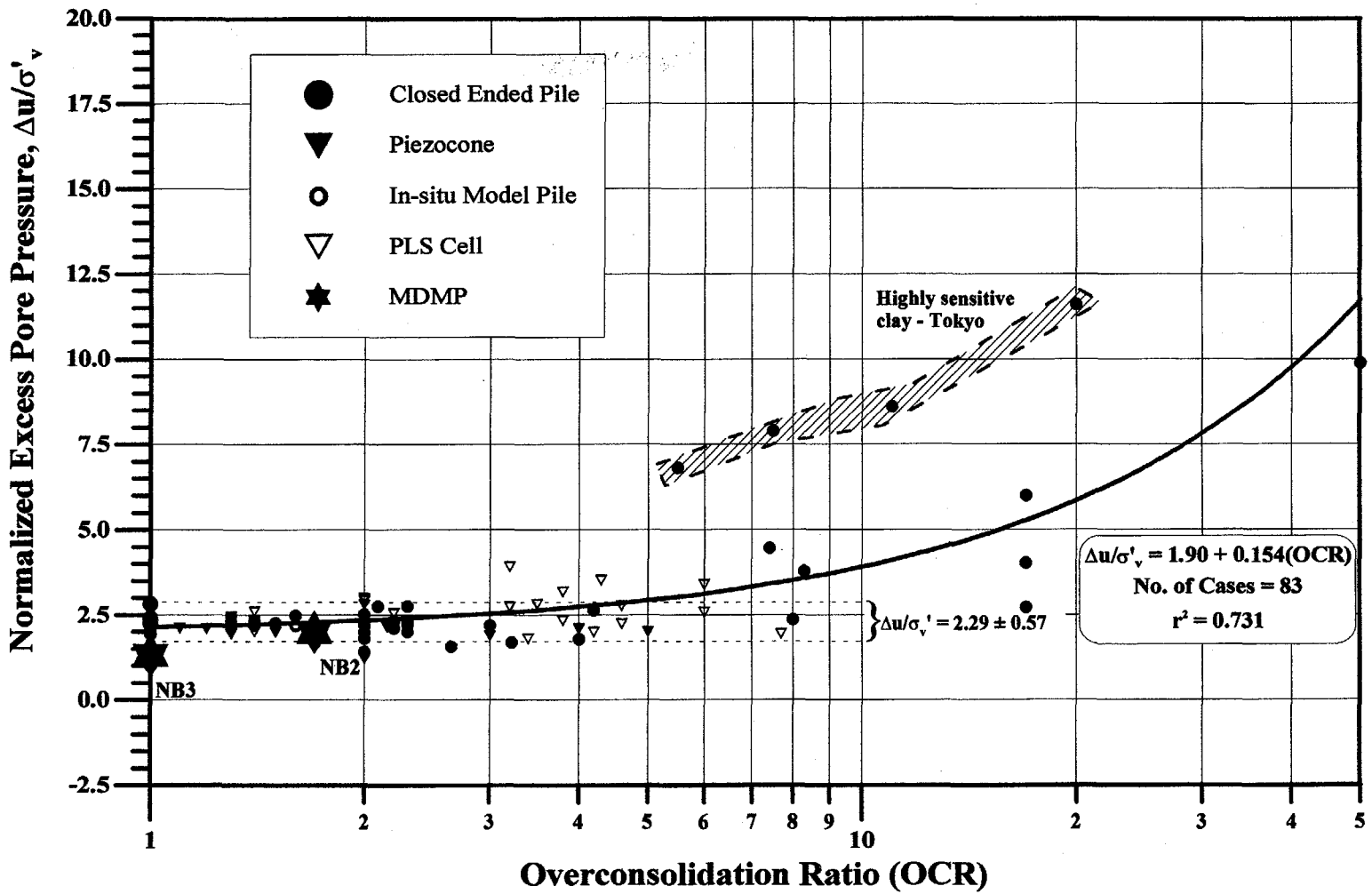
Section 5.6 outlined the predicted measurements of the MDMP based on the data presented by Paikowsky et al. (1995). The following sections present a comparison between the measured and the predicted values and the associated observations and conclusions. Since sections 7.1 and 7.2 showed some similar comparisons, references will be made to those sections when appropriate.

#### 7.3.2 Pore Water Pressure Increase Due to Driving

As presented earlier, the pore water pressure increased markedly from hydrostatic pressure to an elevated level due to the effects of driving. Referring to Table 30, the pore water pressure increased a total of 159.2 kPa and 135.5 kPa for MDMP tests NB2 and NB3, respectively. When normalized with the vertical effective stress without considering the additional stresses caused by the embankment located near the test site, the normalized excess pore pressure was 1.98 and 1.31 for MDMP tests NB2 and NB3, respectively. These values had been added to the data set compiled by Paikowsky et al. (1995) and are presented in Figures 90 and 91. When considering the possible effects of the embankment, the normalized excess pore pressure decreased to 1.74 and 1.14 for MDMP tests NB2 and NB3, respectively. The normalized excess pore pressure obtained from MDMP test NB2 was lower than the mean, however, within 1 standard deviation of the data presented by Paikowsky et al. (1995). The data for MDMP test NB3 was also lower than the mean, however, outside the 1 standard deviation range. Therefore, both measurements of the initial excess pore pressure ( $\Delta u_i$ ) seemed lower than those anticipated. This observation was confirmed by  $u_3$  measurements of CPT tests showing  $\Delta u_3/\sigma_v'$  values of about 2.3 at approximate elevations of -3.05 and -9.14 m (-10 and -30 ft) (Paikowsky and Chen, 1998). These observations suggest two possibilities: (1) incomplete saturation of the MDMP pore pressure system (air in porous stones) and/or (2) insufficient frequency of data collection not able to record the initial peaks in the pore pressure measurements.



Figure 91. Effects of OCR on  $\Delta u/\sigma'_v$  along the shaft ( $h/r \geq 17$ ) for  $r/R=1$  with MDMP data included (based on Paikowsky et al., 1995).



### 7.3.3 Excess Pore Pressure Dissipation and Capacity Gain

Figure 92 presents the range of originally predicted pore pressure dissipation,  $\Delta u(t)/\Delta u_i$ , and capacity gain ratio,  $R_s(t)/R_{smax}$ , based on data presented by Paikowsky et al. (1995). Figure 92 also depicts for the same ratios, the actual measured relationships for both tests NB2 and NB3. From this graphical representation, the observations presented earlier in section 7.2.3 became obvious. The pore pressure dissipation rate was faster than the predicted range as was evident by an increased negative slope of the measured pore pressure lines for both tests NB2 and NB3. The relationships in Figure 92 were based on the measurements described in Chapter 6 and the rates described earlier. If the aforementioned assumption was correct and  $\Delta u_i$  should have been higher as suggested by the CPT tests, then the dissipation relationship would have started earlier, hence, better matching the predicted dissipation zone.

The capacity gain rate in Figure 92 was faster than the predicted range as shown by an increased positive slope of the measured capacity gain lines for both tests. Also, at approximately 50% dissipation, only about 25% to 30% of the capacity gain had occurred, whereas the predicted ranges indicated that at approximately 50% pore dissipation, about 50% of the capacity gain would have occurred. The practical completion of the process however, was closer to the predicted values, relating the decrease in the excess pore pressure to 20% of the initial excess pressure build-up, and to the capacity increase to the level of 80% of the maximum capacity.

Figure 93 presents the effect of pile radius on the time for 50% excess pore pressure dissipation ( $t_{50}$ ) for clays with an OCR of 1 to 2. The values of  $t_{50}$  for MDMP tests NB2 and NB3, respectively, were 35476 s and 28256 s. Both of these values fell within the range previously presented by Paikowsky et al. (1995), indicating that  $t_{50}$  may be estimated from data presented in Figure 93 and further validates the normalization procedure as presented in section 5.6.3. If, however, the actual initial pore pressure was higher and earlier (based on the CPT), then  $t_{50}$  would have decreased and better matched the data presented in Figure 93.

## 7.4 Radial Consolidation

The radial coefficient of consolidation,  $c_h$ , can be evaluated from the dissipation tests. The pore pressure filter element location was positioned to ensure radial dissipation and, hence, the radial (horizontal, cylindrical) consolidation equation was being used:

$$c_h = \frac{T_{50(h)}r^2}{t_{50}} \quad (7.2)$$

for which  $T_{50(h)}$  is the time factor associated with 50% radial consolidation,  $r$  is the piles radius, and  $t_{50}$  is the time for 50% excess pore pressure dissipation. According to Levadoux and Baligh (1986),  $T_{50(h)}$  was 33 and, hence, the coefficients of horizontal consolidation were as follows:

- NB2 @ 24.25 ft,  $t_{50} = 591$  min,  $c_h = 0.0135$  cm<sup>2</sup>/s
- NB3 @ 34.33 ft,  $t_{50} = 471$  min,  $c_h = 0.0170$  cm<sup>2</sup>/s

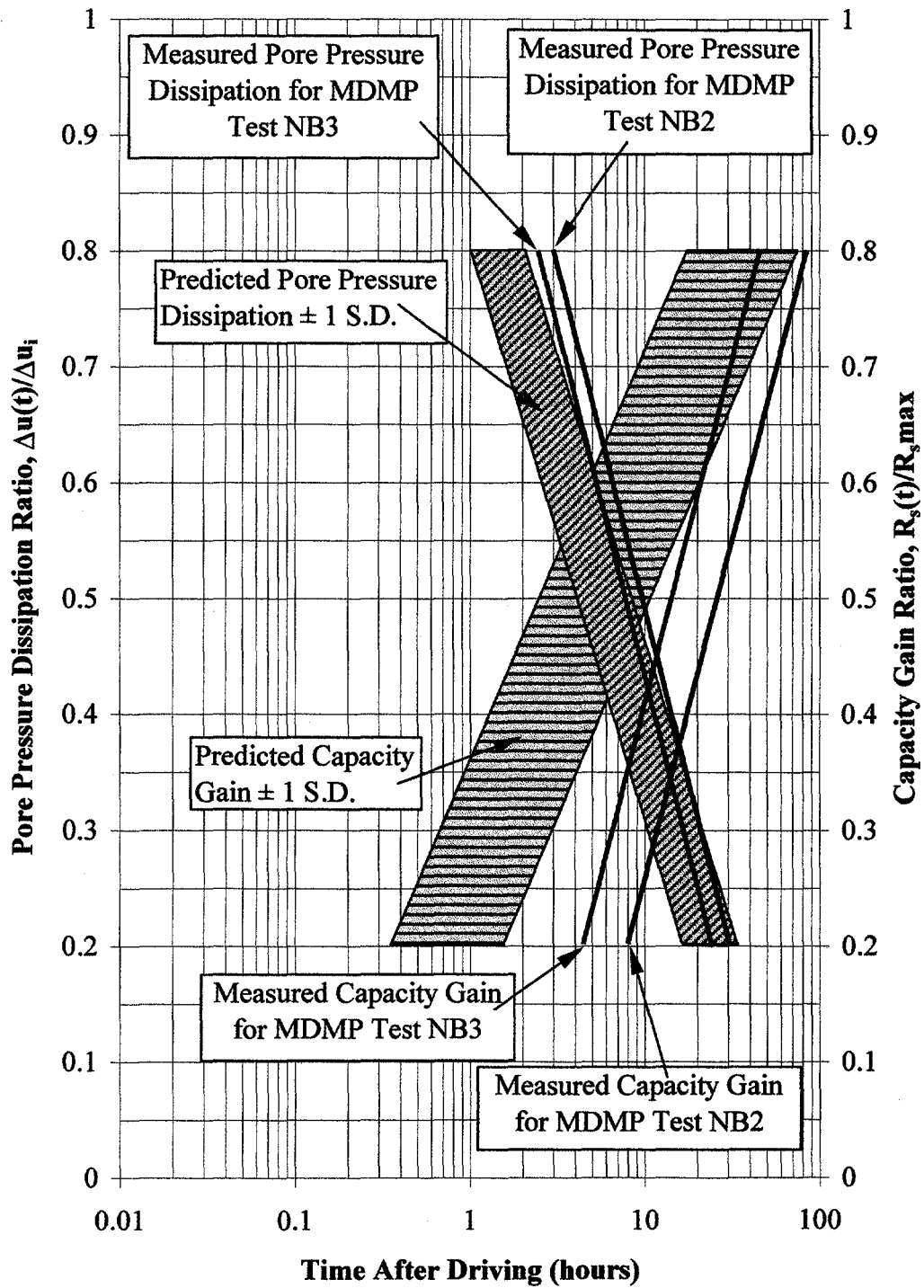


**Figure 92. Measured Pore Pressure Dissipation and Capacity Gain for MDMP Tests at the Newbury Site With Predicted Ranges.**



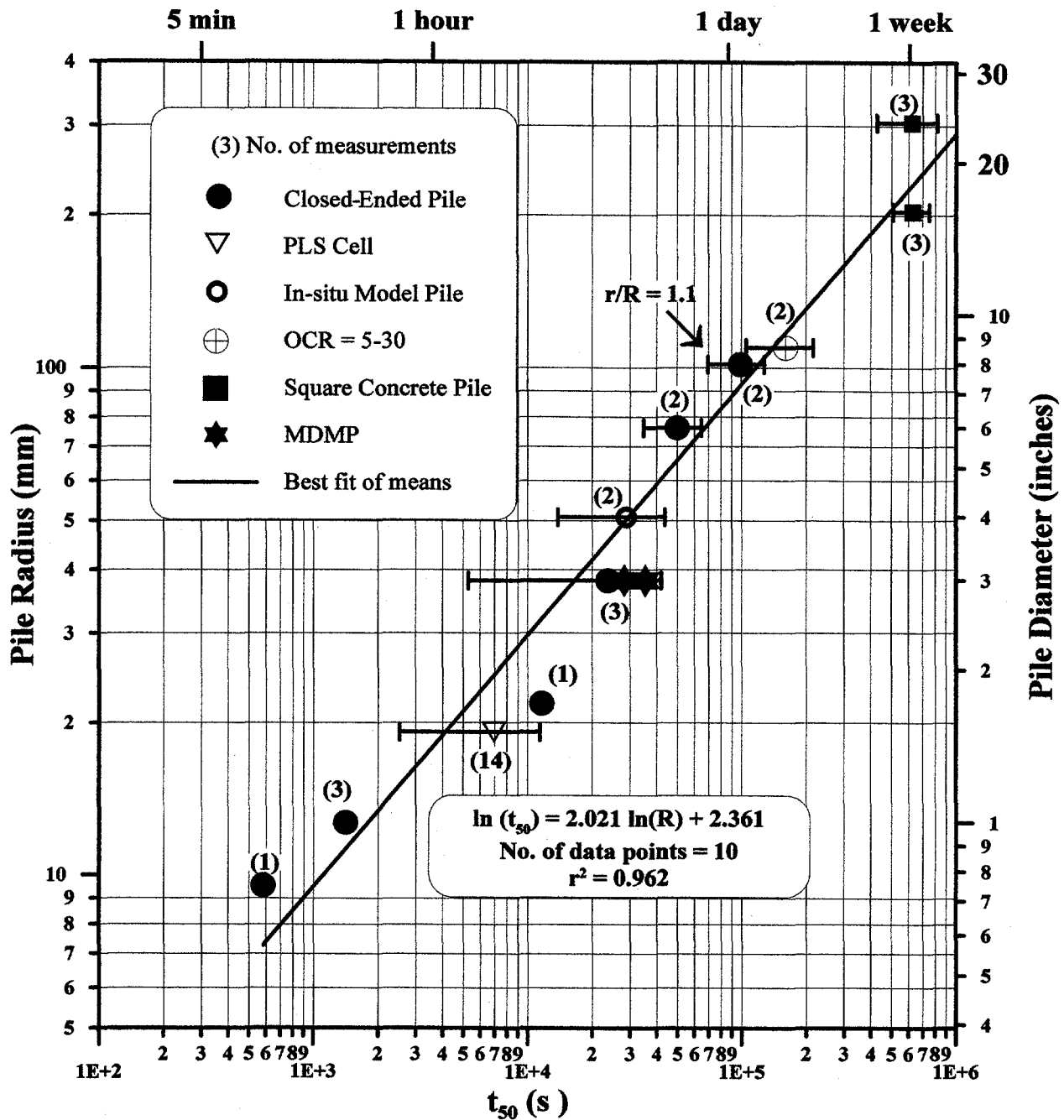


**Figure 93. Effect of Pile Radius on  $t_{50}$  (Time for 50% Excess Pore Pressure Dissipation) for NC Clays (OCR=1-2), Including MDMP Data (based on Paikowsky et al., 1995).**

These values were about half of the  $c_h$  values calculated from the CPT dissipation tests. For the three CPT tests around 10 to 10.7 m (33 to 35 ft) penetration,  $c_h = 0.034 \text{ cm}^2/\text{s}$ . For the two CPT tests around 13 m (43 ft) penetration, the  $c_h$  varied between 0.07 and 0.16  $\text{cm}^2/\text{s}$  (see Paikowsky and Chen, 1998). The difference between the coefficients of consolidation obtained from the CPT and the MDMP was most likely the result of the variation in the initial pore pressure measurements that markedly affected the determined  $t_{50}$ .

## 7.5 Time-Dependent Radial Stresses

The total radial stress decreased for 35 h after the end of driving. At that time, a dramatic increase of about 110 kPa (16 psi) took place where the radial stresses became approximately constant at about 200 kPa (29 psi). A thorough analysis was required to explain the phenomenon in detail; however, a possible interpretation was offered. When the pile was installed, the penetration was accompanied by large soil displacements, remolding, and shear, resulting in a substantial build-up of pore water pressure and significant changes in radial stresses. The clay at this stage was in a complete liquid-plastic state, with total pressures approximately equal to that of the pore water pressure, and with a possible zone of water around the pile's shaft. These pressures resulted in about zero radial effective stresses and a negligible interfacial friction. The described initial stage was well depicted in Figure 94a, which outlined the pore pressure, total stresses, and resulting effective stresses on a logarithmic time scale. In the "classical" one-dimensional consolidation process, this initial stage would have been followed-up by pore pressure dissipation accompanied by an equal increase in the effective stresses. The presented data in Figure 94a and b clearly showed a different process in which both the pore pressure and the total stress decreased with time. The decrease in the total stresses could be explained by redistribution of stresses around the pile following the driving. The total stresses, as a result of external loading, remained constant in a one-dimensional consolidation condition. In the pile penetration process, the loading due to penetration was fast, creating an immediate increase in stresses in an area surrounding the pile, extending to a point within the far field in which no change in the stresses was noticed. This zone did not remain stable, however, and as a result, changes took place in which the high stresses first developed next to the pile wall and transferred outwards, redistributing the load to soil further away from the pile wall. This process of radial soil pressure redistribution continued in parallel to the pore pressure dissipation at a rate somewhat lower than that of the pore water pressure dissipation. As a result, the radial effective stresses increased at a very gradual rate (of approximately 1.5 kPa/h on a semi-log scale) for the first 35 h after driving. The gradual increase of the radial effective stresses from approximately 0 kPa at the end of driving to approximately 56 kPa at 35 h after driving was probably accompanied by the disappearance of the water film around the pile, the change of the soil state from plastic liquid to plastic solid, and the increase of the contact between the soil and the pile wall. At that time (about 35 h after driving), a sudden increase in the total stresses (and accordingly in the effective stresses) took place. While the previous process might explain the events, the actual increase might have been triggered by a load test that was carried out at the time, accompanied by the transformation of the shear zone from interfacial shear to internal shear within the soil some distance away from the shaft.

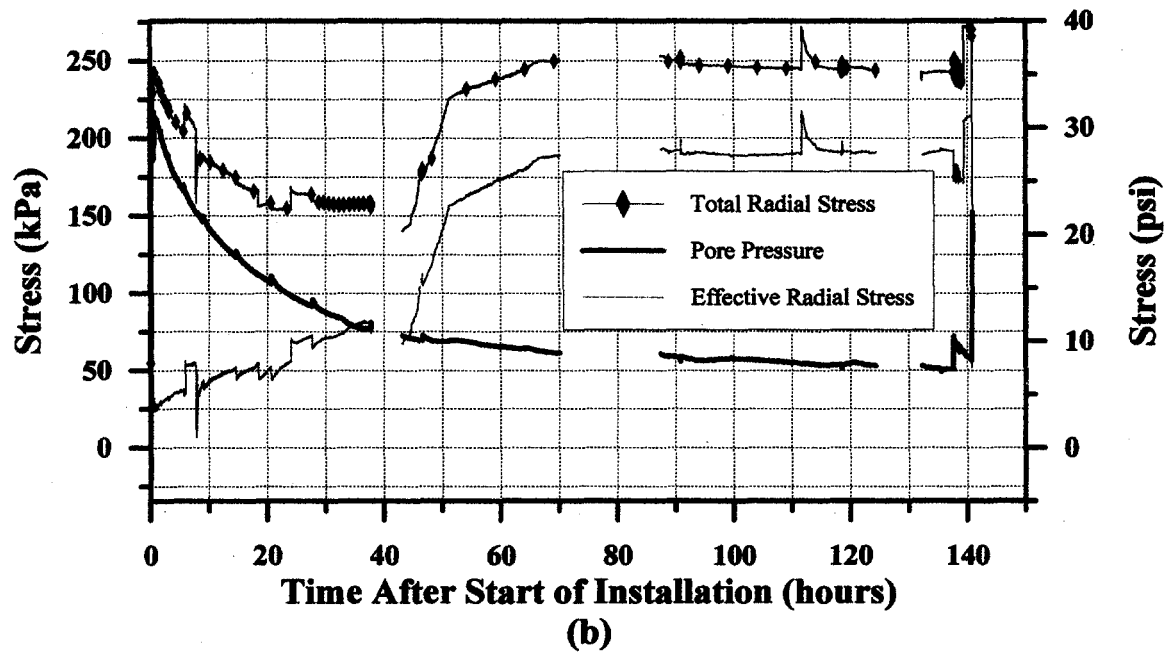
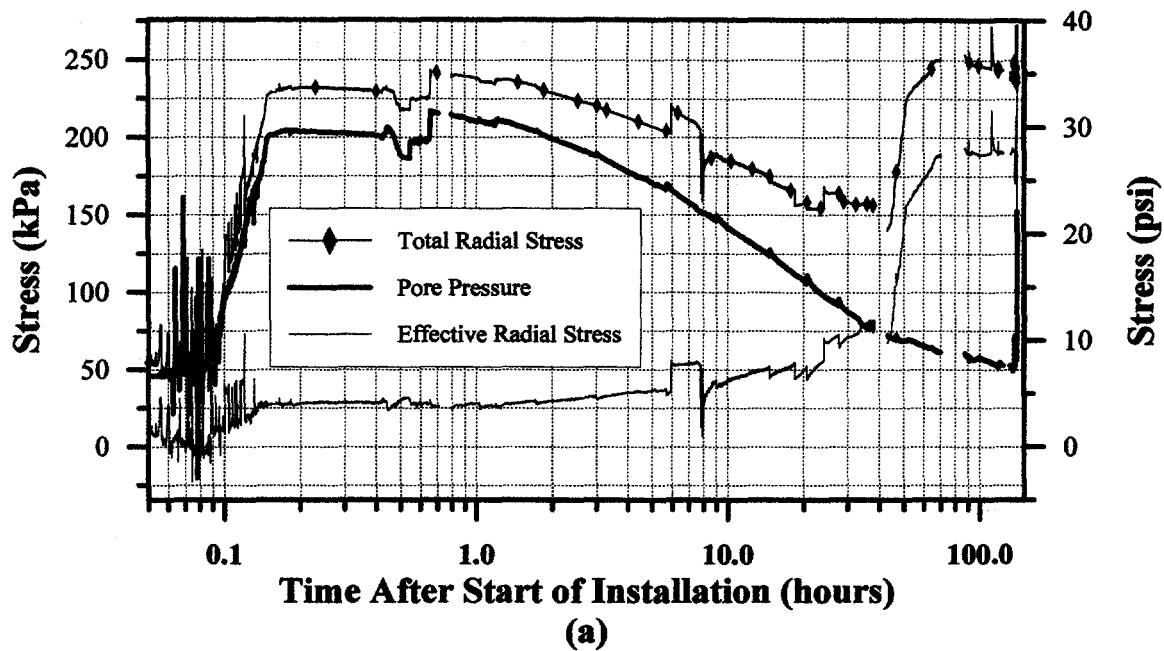


**Figure 94. Changes in Pore Pressure, and Total and Effective Radial Stresses: (a) Log Time Scale and (b) Linear Time Scale.**

## 7.6 The Relationship Between Pore Pressure Dissipation, Frictional Capacity Gain, and Radial Stresses

Figure 95 presents a summary of the different parameters affecting the shear resistance along the MDMP. The absolute frictional resistance increased with time, starting with values close to zero at the end of driving to about 25 kPa (3.5 psi) approximately 5 days later. The increase of the frictional resistance was consistently accompanied by an increase in the radial effective stresses. This rough observation suggests that for frictional material, the ratio between the shear resistance and the normal stress remained approximately constant. Such relationships are seen in the lower part of Figure 95, presenting the ratio between the frictional force to the radial effective stress.

When examining the relationships presented in Figure 95, it is important to note that the shear measured along the frictional sleeve did not necessarily take place along the pile/soil interface. As a matter of fact, when the MDMP was pulled out of the ground, a layer of clay (with a diameter equal to the internal casing diameter) was attached to the pile, clearly indicating that shear was taking place away from the interface. Correcting for such observations would result in lower frictional stresses along the sleeve at a later time after installation and approximately constant frictional resistance from about 35 to 45 h after penetration. The timing was closely associated to the period for which a large increase in total and effective stresses was observed.

## 7.7 Observed Heave

Figure 63 indicated a sharply increased surface load cell force measurement following the driving of model pile test NB2. This increase was attributed to the pile/soil upward movement (i.e., heave) as no displacement was measured at the surface load cell location. This behavior, on a smaller magnitude, repeated itself whenever there was a stop in the pile motion as shown in the white areas of Figure 63. The initial heave load of 7.17 kN (1612 lb) was subtracted from the measurements and the net measured forces were presented in Figure 64. The data in Figure 64 suggested that when the top motion was stopped (no change in top displacement with time, e.g., from about 25.5 to 26.5 min after the start of installation), the internal MDMP load cell measurements gradually decreased, whereas the surface load cell recorded an increase in force. Details of the measurements are presented in Figure 65. This behavior may be interpreted in the following ways: (1) The increase in the load was due to heave, in which the pile moved upwards, and (2) the pile moved together with a mass of soil around it. As the load cells inside the pile did not record an increase in load, the only possibility was shear in the soil some distance away from the pile. These observations were further supported by measurements conducted during the pushing period in which the surface load cell continued to measure the heave effect, while the internal load cell measurements reflected shear that took place due to loading.

No heave effects were observed during MDMP test NB3. The differences between the tests may be explained through the variation in the soil conditions with depth. The soil in which NB2 was driven was stiffer and the driving resistance was about 10 blows per 100 mm. During installation of MDMP test NB3, the pile was penetrating under its own weight prior to driving and was held in place while the hammer was attached. The driving resistance for NB3 was about four blows per 100 mm at the end of driving.

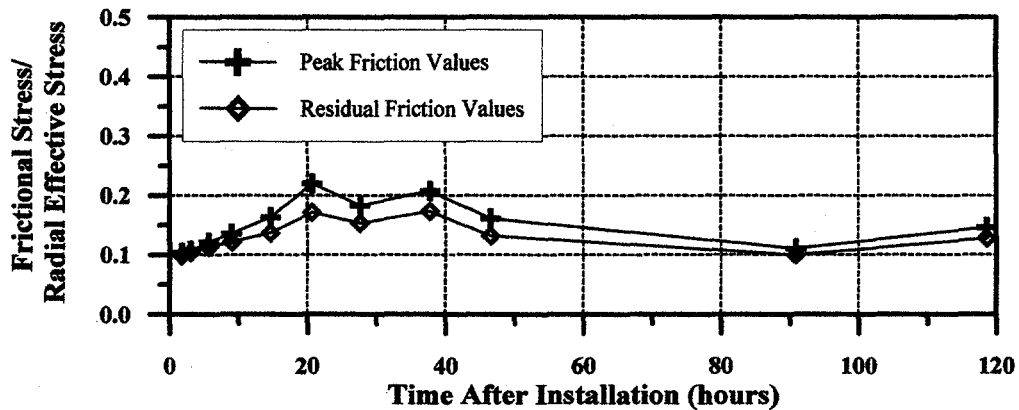
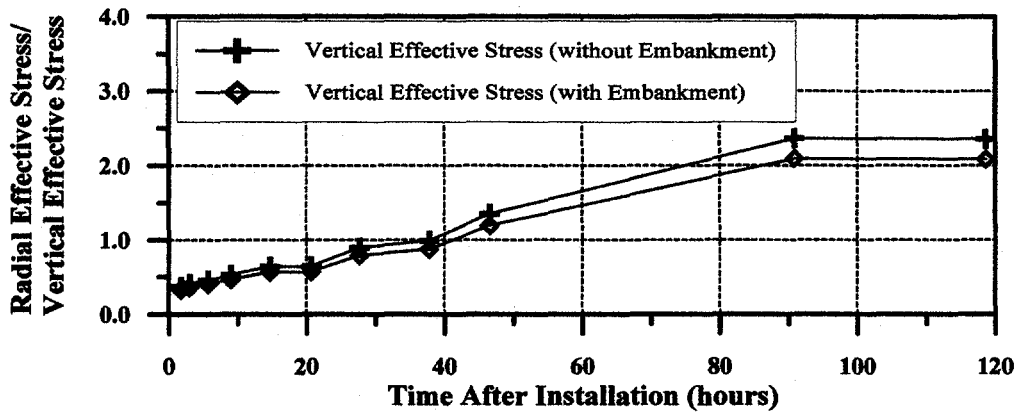
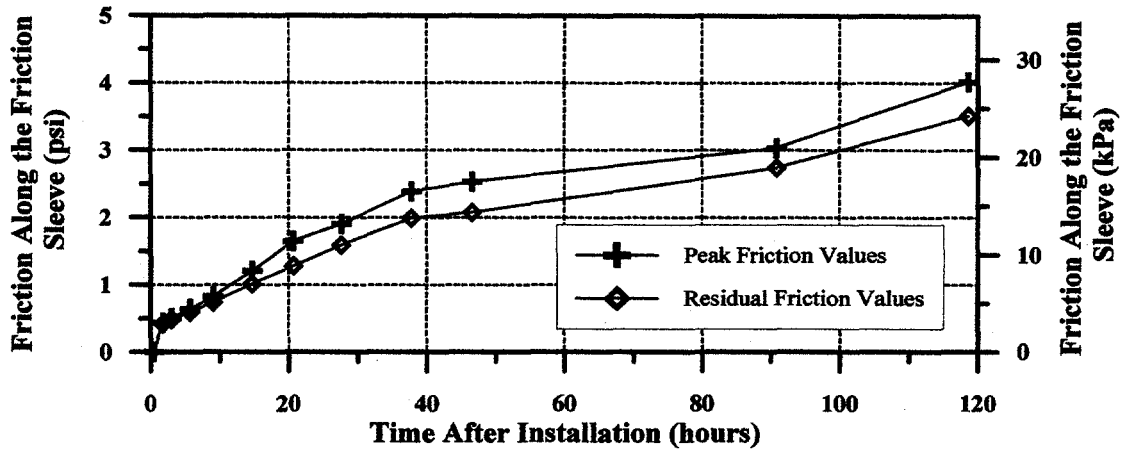


Figure 95. Relationships Between Shaft Friction, Radial Stress, and Vertical Stress for MDMP Test NB2.

## 7.8 Static-Cyclic Load Tests

A slow (pseudo-static) cyclic load test was performed following the completion of the excess pore pressure dissipation process. All static load tests that were conducted during the dissipation process were performed as tension tests by pulling the MDMP upwards. The final load test, including the static-cyclic load tests, was performed as a compression test by pushing the pile downward. The displacement versus the loads recorded in all load cells and the net load on the friction sleeve are presented in Figures 96 and 97 for MDMP tests NB2 and NB3, respectively. The displacements presented in Figures 96 and 97 refer to measurements at the surface. The MDMP was at a fully extended slip joint position at the end of the tension test series. As such, the final load tests began by pushing the pile down until the slip joint was completely closed (a distance of approximately 50.8 mm (2 in)) and then the cyclic load test was carried out over an additional 25.4 mm (1 in) of penetration. During the movement along the initial 50.8 mm (2 in), before the slip joint was closed, the lower portion of the pile was not loaded and the measured loads reflected the friction developed along the upper part of the pile (1625.6 mm (64 in) long). After about 50.8 mm (2 in) of displacement (see Figures 96 and 97), the lower portion of the pile (1143 mm (45 in) long) was engaged and the measured loads reflected the friction along the entire pile and the tip resistance.

The shear transfer recorded during the final load test of MDMP test NB2 was described in Tables 34 and 35. Table 34 details the discrete load-displacement relationships at the various stages and Table 35 presents average values. Tables 36 and 37 describe the respective information for the final load test for NB3. The observed behavior in Figures 96 and 97 was reasonable and is discussed in detail in section 6.5. The absolute measured values, however, were in sharp contrast to the forces measured in the sequential pull-out tests presented in Figures 58 and 61. The peak forces along the friction sleeve in the final pull-out tests were approximately 5.65 kN (1270 lb) and 5.43 kN (1220 lb) for MDMP tests NB2 and NB3, respectively, whereas for the push tests, these forces were 2.61 kN (588 lb) and 1.17 kN (263 lb). No clear explanation exists and although the reversal of the shear direction may be a reason for some degradation, it cannot explain this large reduction.

**Table 34. Shear Transfer Recorded During NB2 Final Load Test.**

Event	Displacement (mm/in)	Force Along the Friction Sleeve (kN/lb)
Peak After Initial Push	3.0 / 0.12	2.61 / 588
Before Slip Joint Is Compressed	51.5 / 2.03	1.72 / 387
After Slip Joint Is Compressed	52.7 / 2.08	1.98 / 446
At End of Initial Push	79.7 / 3.14	1.94 / 437
Peak After 2 <sup>nd</sup> Push	80.6 / 3.17	2.05 / 461
At End of 2 <sup>nd</sup> Push	98.4 / 3.88	1.54 / 347
Peak After 3 <sup>rd</sup> Push	98.8 / 3.89	1.81 / 407
At End of 3 <sup>rd</sup> Push	117.6 / 4.63	1.45 / 325
Peak After 4 <sup>th</sup> Push	117.8 / 4.64	1.68 / 378
At End of 4 <sup>th</sup> Push	138.0 / 5.44	1.41 / 317
Peak After 5 <sup>th</sup> Push	138.6 / 5.46	1.69 / 381
At End of 5 <sup>th</sup> Push	152.1 / 5.99	1.41 / 317

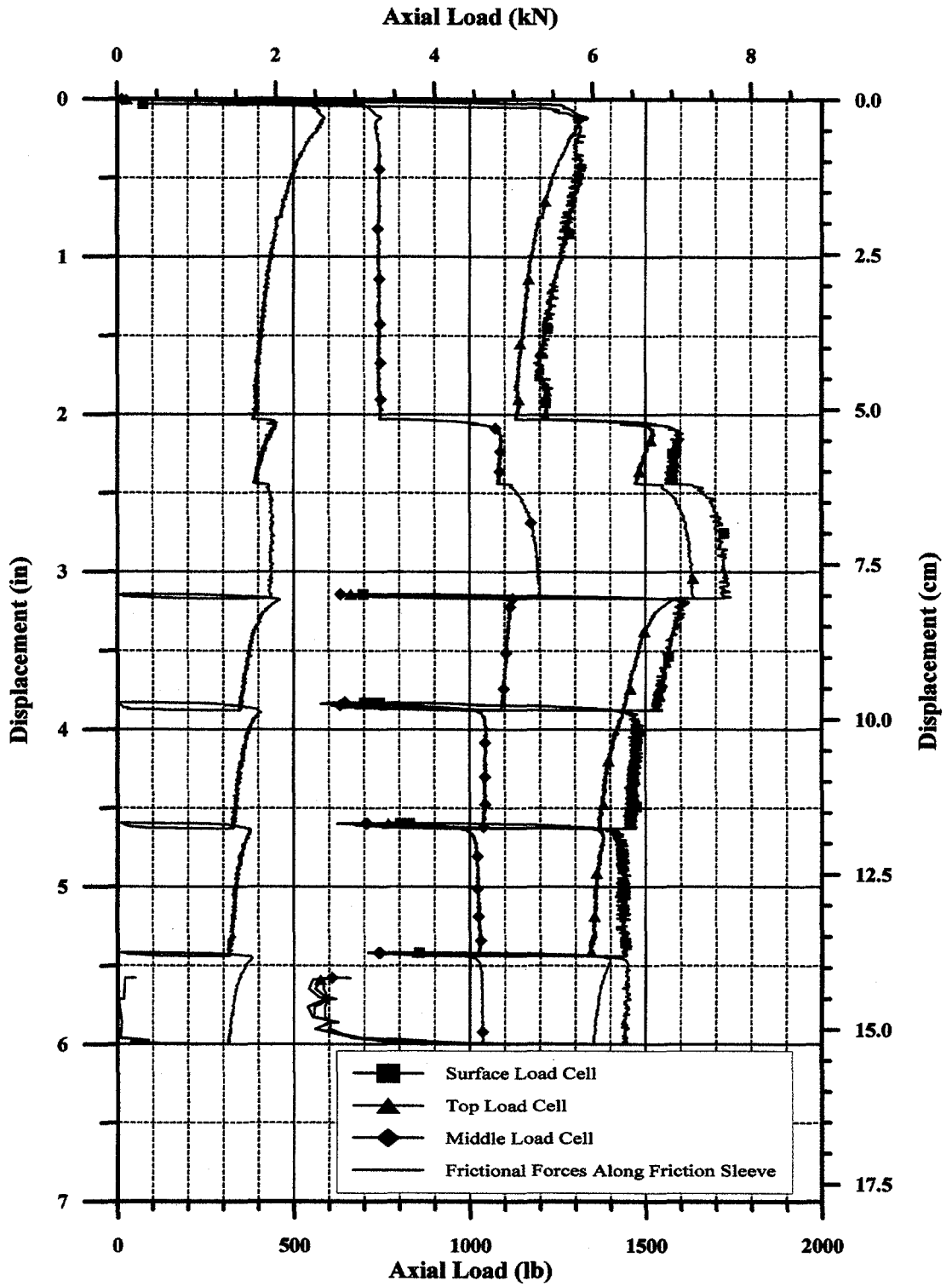


Figure 96. Final Load Test for MDMP Test NB2.

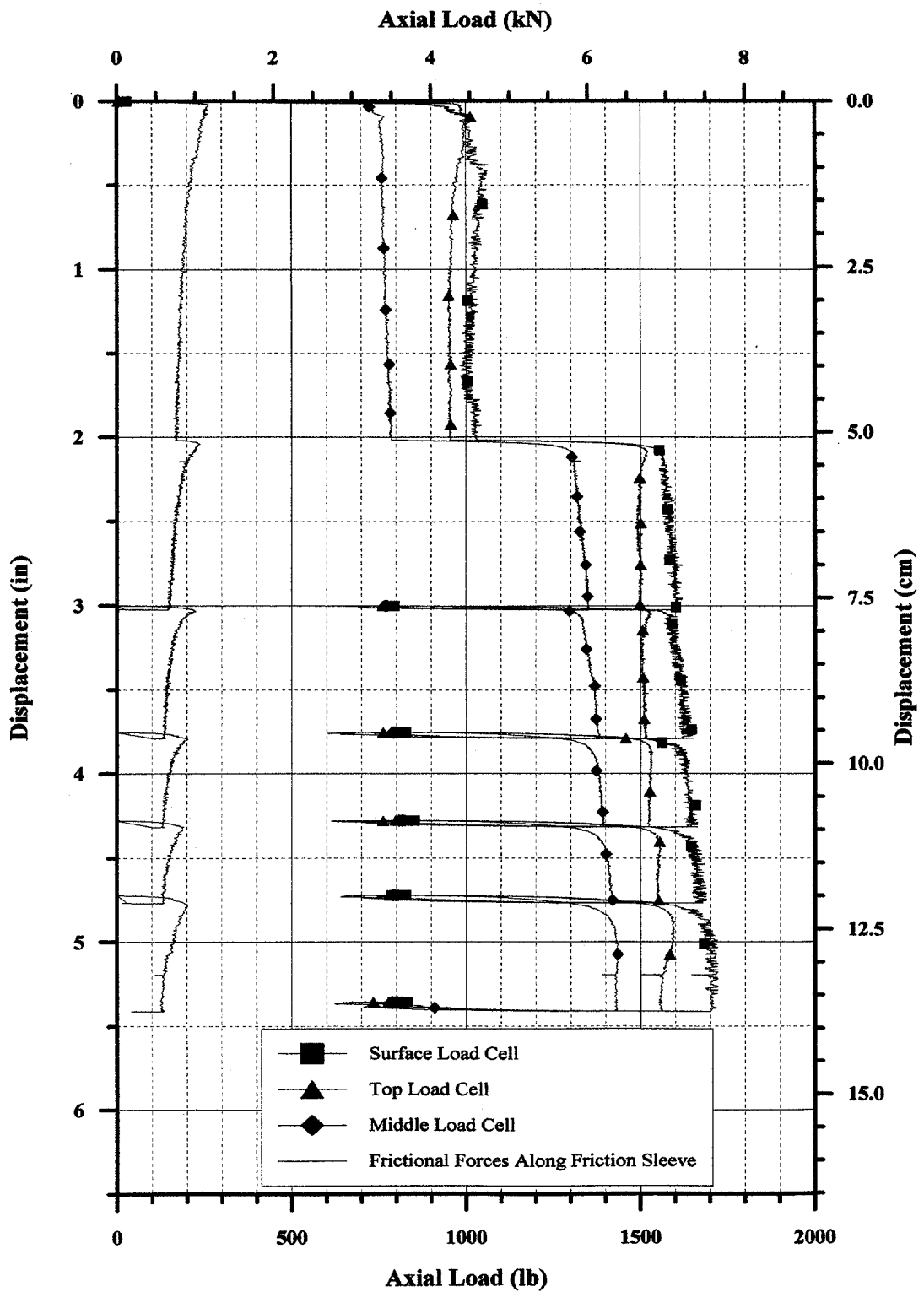


Figure 97. Final Load Test for MDMP Test NB3.



**Table 35. Average Shear Transfer Recorded During NB2 Final Load Test.**

Case	Residual Force (kN/lb)		Peak Force (kN/lb)	
	average	std. dev.	average	std. dev.
All Events	1.58 / 355	0.21 / 48	1.97 / 443	0.35 / 78
Without Slip Joint	1.55 / 348	0.23 / 51	1.97 / 443	0.39 / 88
Excluding First Loading	1.45 / 326	0.06 / 14	1.81 / 407	0.17 / 39

**Table 36. Shear Transfer Recorded During NB3 Final Load Test.**

Event	Displacement (mm/in)	Force Along the Friction Sleeve (kN/lb)
Peak After Initial Push	0.8 / 0.03	1.17 / 263
Before Slip Joint Is Compressed	50.9 / 2.00	0.73 / 164
After Slip Joint Is Compressed	51.9 / 2.04	1.06 / 238
At End of Initial Push	76.8 / 3.03	0.64 / 144
Peak After 2 <sup>nd</sup> Push	77.1 / 3.03	1.00 / 225
At End of 2 <sup>nd</sup> Push	96.3 / 3.79	0.62 / 138
Peak After 3 <sup>rd</sup> Push	96.4 / 3.80	0.90 / 203
At End of 3 <sup>rd</sup> Push	109.6 / 4.31	0.58 / 129
Peak After 4 <sup>th</sup> Push	109.9 / 4.33	0.84 / 188
At End of 4 <sup>th</sup> Push	121.1 / 4.77	0.60 / 135
Peak After 5 <sup>th</sup> Push	121.4 / 4.78	0.90 / 203
At End of 5 <sup>th</sup> Push	137.1 / 5.40	0.58 / 131

**Table 37. Average Shear Transfer Recorded During NB3 Final Load Test.**

Case	Residual Force (kN/lb)		Peak Force (kN/lb)	
	average	std. dev.	average	std. dev.
All Events	0.62 / 140	0.06 / 13	0.98 / 220	0.12 / 28
Without Slip Joint	0.60 / 136	0.03 / 6	0.96 / 216	0.13 / 29
Excluding First Loading	0.59 / 133	0.02 / 4	0.91 / 205	0.07 / 15

## 7.9 Shaft Resistance and Design Parameters

Figures 98 and 99 present the shear transfer along the friction sleeve for MDMP tests NB2 and NB3, respectively. Both figures present the build-up of the shear transfer with time, assuming that the actual shear took place along the pile surface (see sections 6.3.2 and 6.3.3 for details). Figures 100 and 101 present the variation of the peak and residual shear transfer as a function of the degree of consolidation for MDMP tests NB2 and NB3, respectively. Figure 102 presents the evaluated undrained shear strength of the subsurface based on various field and laboratory tests as presented by Paikowsky and Chen (1998). The data in Figure 102 suggested that the undrained shear strength of the clay reasonably ranged between the values proposed by the SHANSEP parameters based on DSS tests and those obtained from the CPT. Using these values, the undrained shear strength at the elevation of NB2 (-2.0 m) ranged between 23.0 kPa (0.24 tsf) and 33.5 kPa (0.35 tsf), and at the elevation of NB3 (-5.1 m) ranged between 19.2 kPa (0.20 tsf) and 37.3 kPa (0.39 tsf). The average representative value for tests NB2 and NB3 was identical and equal to 28.2 kPa (0.30 tsf). This representative undrained shear strength was used for normalizing the shear transfer measured along the shaft as shown on the left vertical axes in Figures 100 and 101. The obtained ratio was typically denoted by  $\alpha$ , used in the design

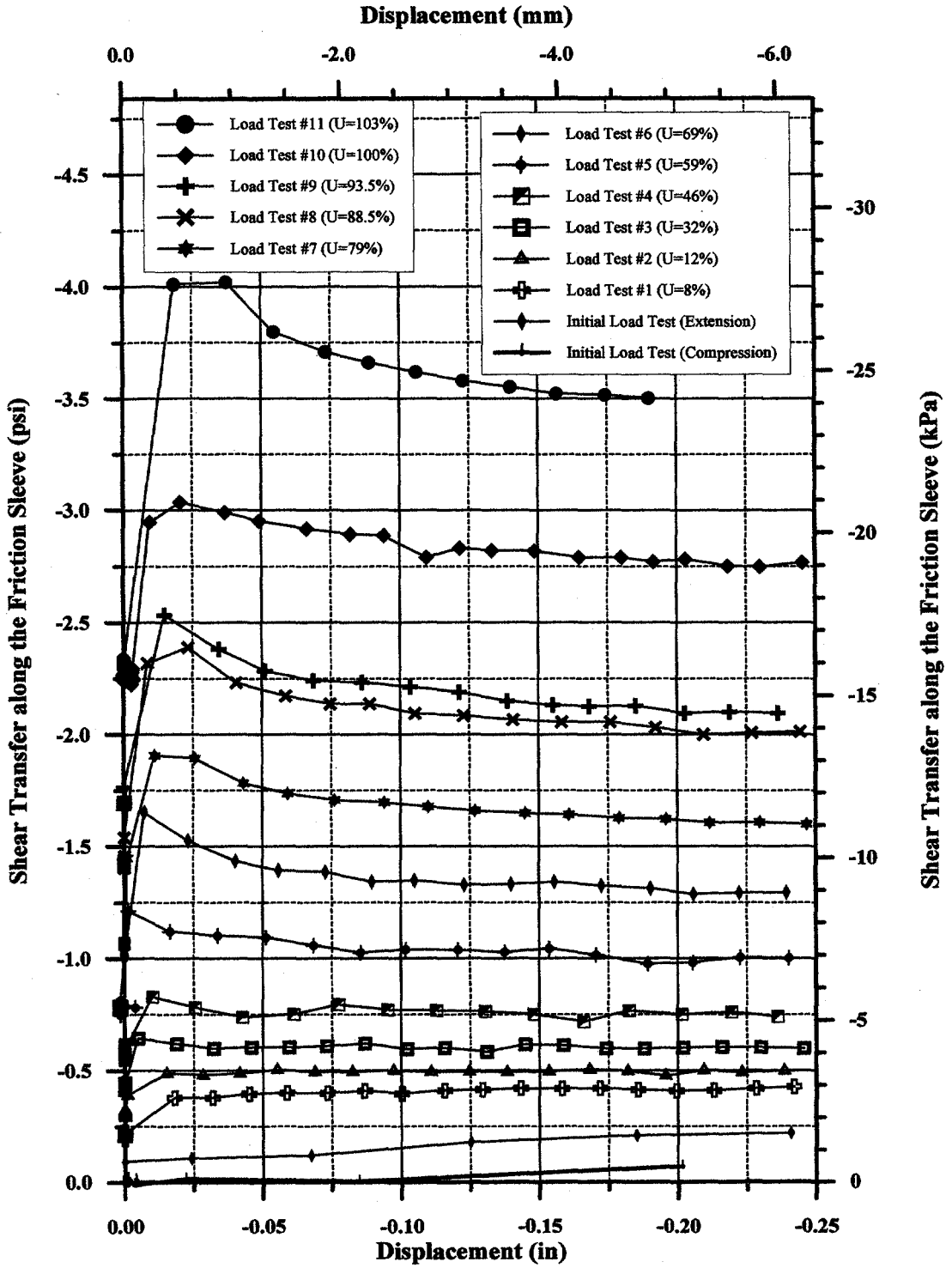


Figure 98. Shear Transfer Along the Friction Sleeve for MDMP Test NB2.

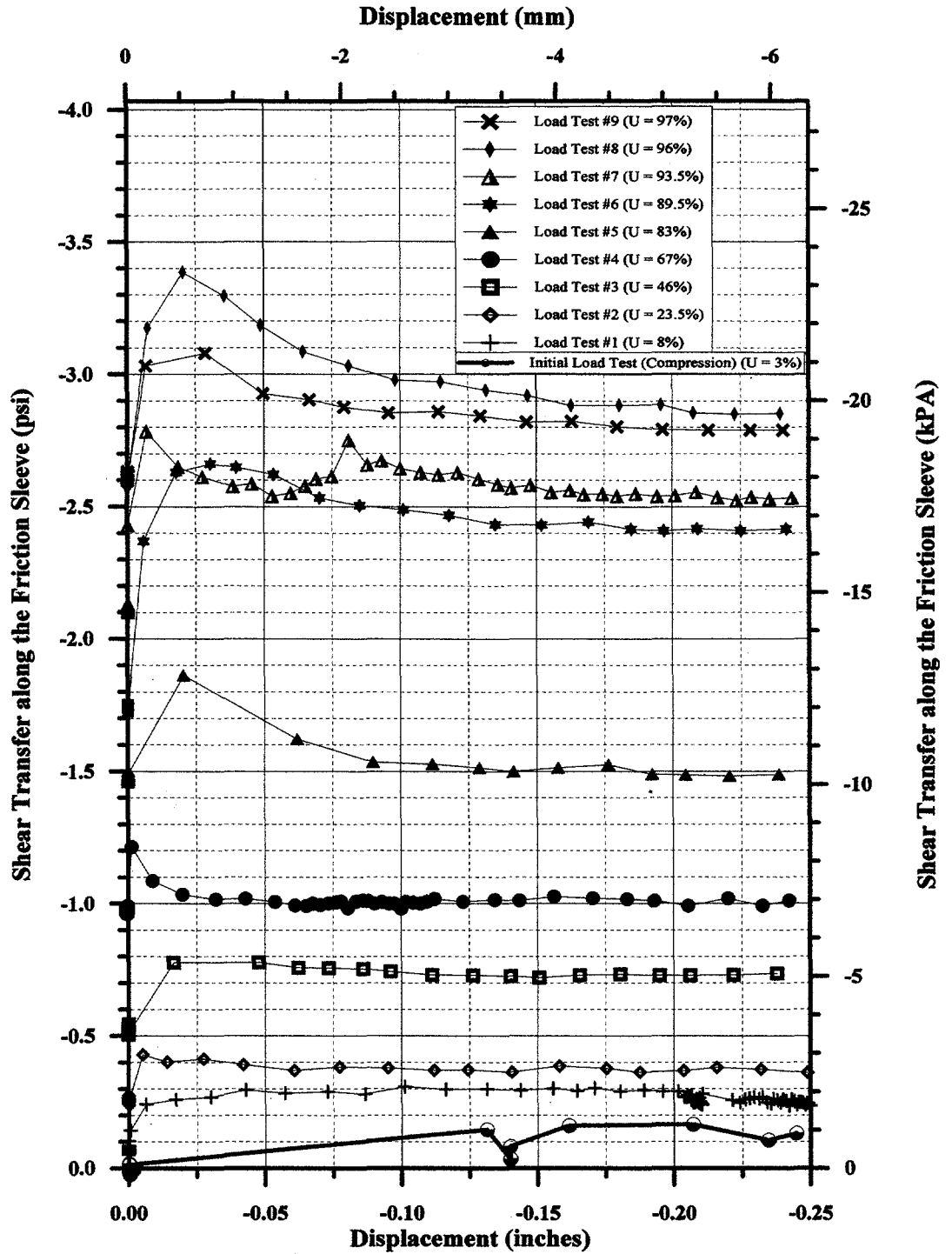
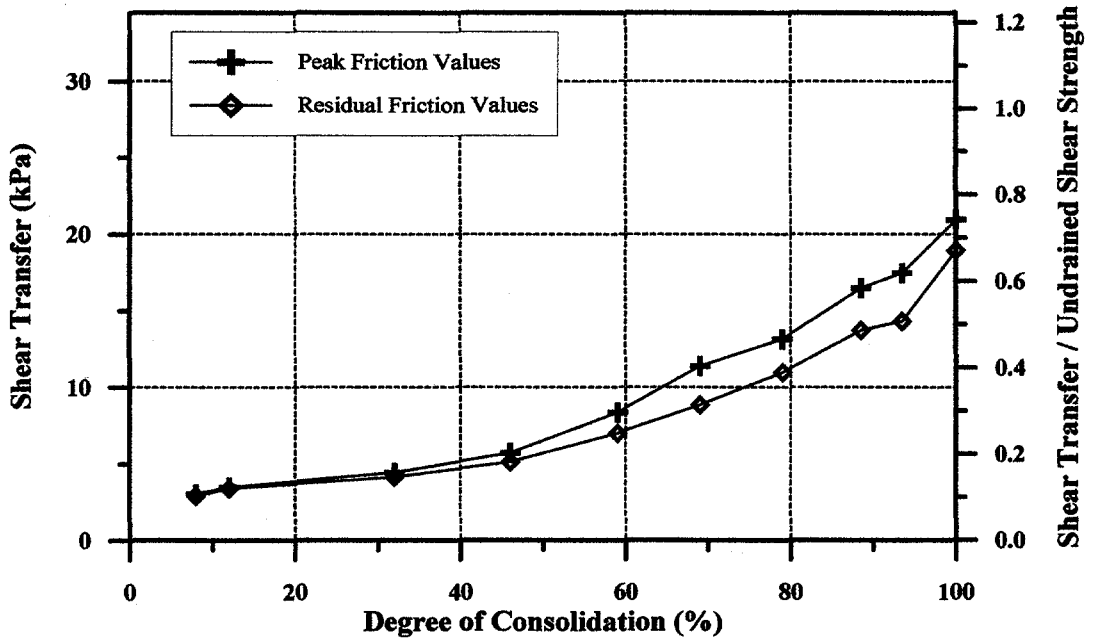
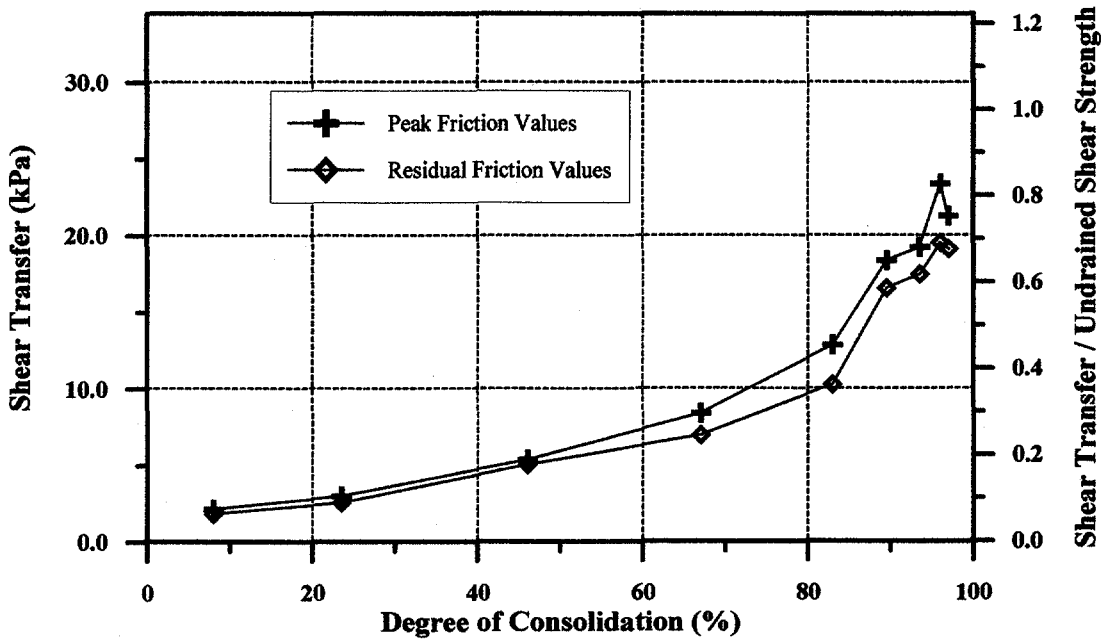


Figure 99. Shear Transfer Along the Friction Sleeve for MDMP Test NB3.



**Figure 100. Shear Transfer Along the Friction Sleeve as a Function of the Degree Consolidation for MDMP Test NB2.**



**Figure 101. Shear Transfer Along the Friction Sleeve as a Function of the Degree Consolidation for MDMP Test NB3.**

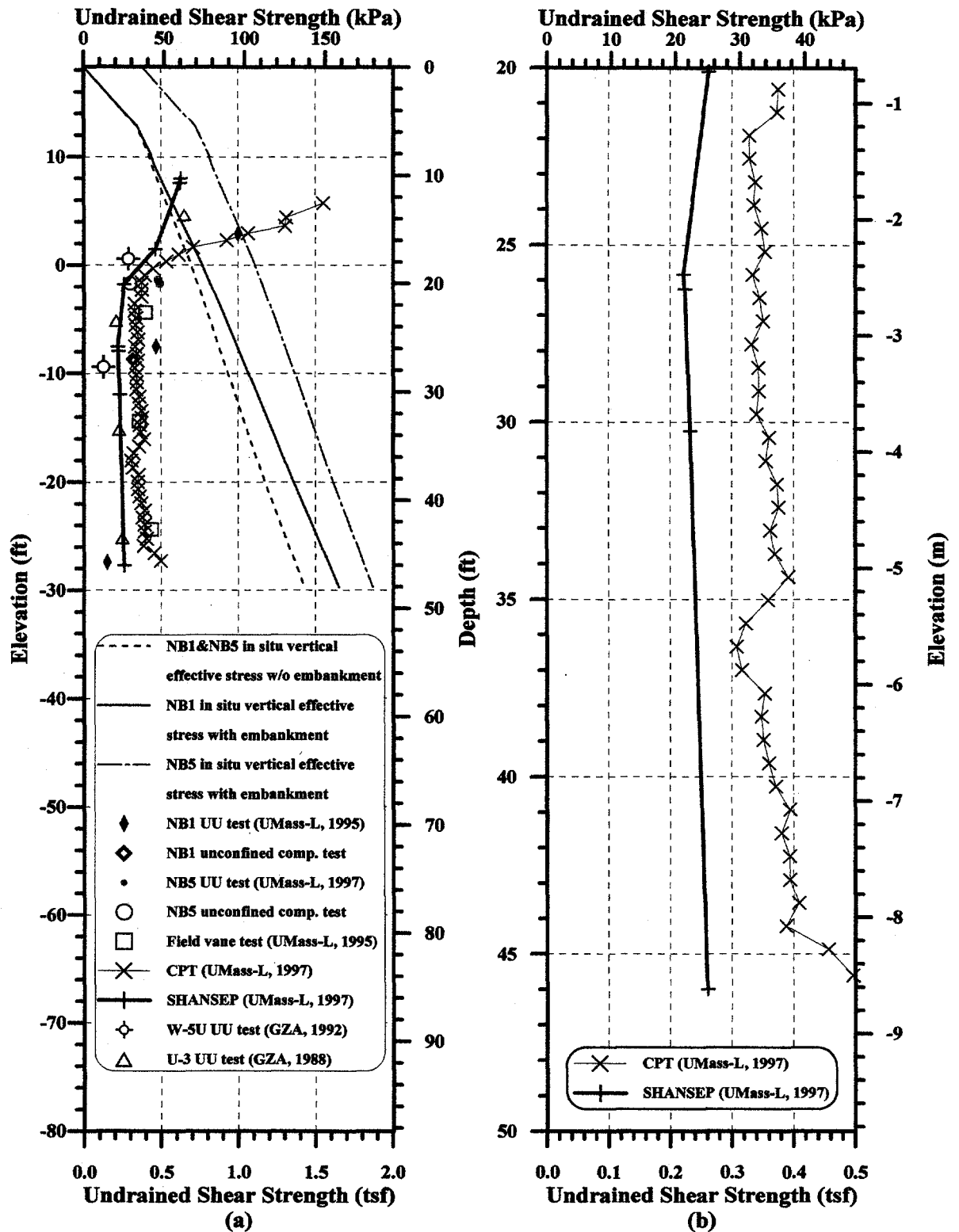


**Figure 102. Undrained Shear Strength of the BBC at the Newbury Test Site:**  
**(a) Variation With Depth Along With Results of Different Testing and**  
**(b) Details of CPT and SHANSEP Parameters Between the Depths of 6.1 and 13.7 m (20 to 45 ft)**  
 (based on Paikowsky and Chen, 1998).

procedure known as the  $\alpha$  method (Bowles, 1988 after Tomlinson, 1971) and was presented on the right vertical axis in Figures 100 and 101. The maximum obtained ratio of approximately 0.8 generally agreed well with the reduction of the peak adhesion factor ( $\alpha_p$ ) when considering high embedded length over diameter ratio (Tomlinson, 1986). Tomlinson suggested the use of  $\alpha_p = 1.0$  for a  $C_v/\sigma_v'$  of 0.2 to 0.35 and a reduction factor of 0.7 for an embedded length over width ratio greater than 120 (equivalent to 9.1 m (30 ft) of penetration for the MDMP).

## 7.10 Dynamic Measurements Interpretation

### 7.10.1 Measured Signals and Wave Mechanics

Section 6.6 presents the dynamic measurements during the various stages of testing. The wave shapes are discussed in great detail, pointing out the variation between the behavior of a homogeneous uniform pile to that of a non-uniform pile. The present section provides the analysis that explains these measurements, in particular, the fact that the lower load cells measured dynamic forces higher than the surface load cells.

Figure 103 presents the make-up of the MDMP segments during the driving of tests NB2 and NB3. As all segments were made of steel, it was assumed that no variation in the modulus of elasticity existed between one segment and the other. As such, the relative variations in the impedance could be taken as the relative variations in the cross-sections. Two distinctive cross-sectional zones existed along the pile — one made mostly of the drilling rods and the other from the rods/MDMP connection to the upper point of measurement inside the MDMP. Table 38 summarizes the weighted areas of each of the sections for the two tests.

**Table 38. Variations in the Cross-Section / Impedance Between the Drilling Rods and the MDMP.**

Test	Weighted Cross-Sectional Area (in <sup>2</sup> / cm <sup>2</sup> )	
	Drill Rods	MDMP
NB2 Installation	1.46 / 9.45	3.75 / 24.2
NB2 Restrike	1.46 / 9.45	3.75 / 24.2
NB3 Installation <sup>1</sup>	1.49 / 9.60	3.75 / 24.2
NB3 Installation <sup>2</sup>	1.48 / 9.52	3.75 / 24.2
NB3 Restrike	1.48 / 9.52	3.75 / 24.2

Notes: <sup>1</sup>Upper location.

<sup>2</sup>Lower location.

Figure 104 presents a simplified view of the model pile make-up during driving and the influence of the variation in impedance on the traveling force and velocity waves.

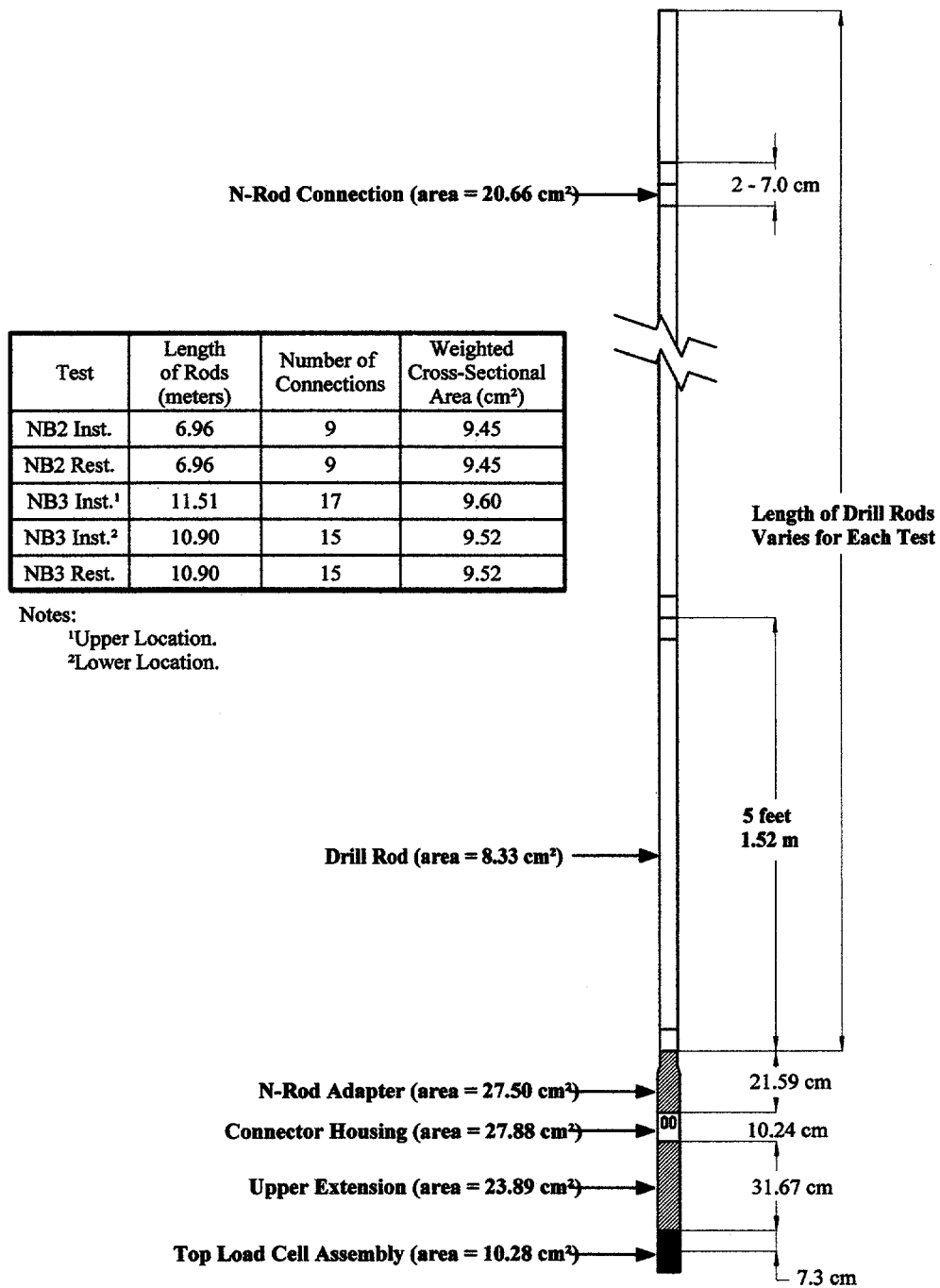
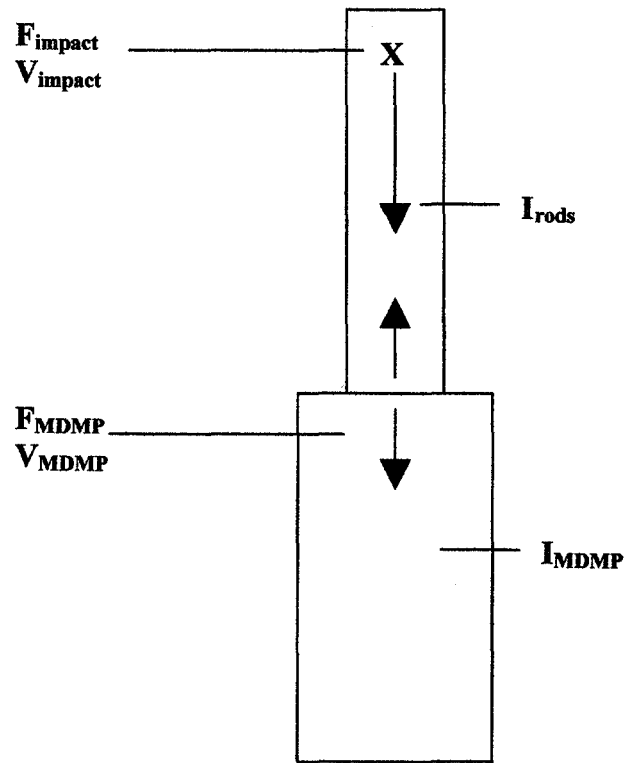


**Figure 103. Details of the Various Segments That Made Up the MDMP (from the point of surface measurements to the upper inner load cell).**



$$F_{\text{MDMP}} = F_{\text{Impact}} \cdot \frac{2 \cdot I_{\text{MDMP}}}{I_{\text{rods}} + I_{\text{MDMP}}} \quad (7.3)$$

$$V_{\text{MDMP}} = V_{\text{Impact}} \cdot \frac{2 \cdot I_{\text{rods}}}{I_{\text{rods}} + I_{\text{MDMP}}} \quad (7.4)$$

**Figure 104. The Relationship Between the Pile Impedance and Measured Signals**  
(modified after Rausche, 1981).



Substituting the weighted axial cross-sections of Table 38 in equations 7.3 and 7.4 yield the following:

$$\frac{F_{\text{MDMP}}}{F_{\text{Impact}}} = 1.44 \quad (7.5)$$

$$\frac{V_{\text{MDMP}}}{V_{\text{Impact}}} = 0.56 \quad (7.6)$$

The above ratios can be compared to the values provided in sections 6.6.6 and 6.6.7 for force and velocity measurements, respectively. Using the average measured values presented in Table 28, the ratios of  $F_{\text{MDMP}}$  to  $F_{\text{impact}}$  were 1.26 and 1.38 for NB2 and 1.25 and 1.34 for NB3 (installation and restrike, respectively). These values matched the simplified calculated ratio of equation 7.5 relatively well and explained the higher impact forces measured inside the pile compared to those measured at the top of the rods. Using the average measured values presented in Table 29, the ratio of  $V_{\text{MDMP}}$  to  $V_{\text{impact}}$  was 0.75 for NB2 during installation. Again, this ratio compared reasonably well with the simplified ratio obtained from equation 7.6.

The measurements obtained by the internal load cells allowed the assessment of the resisting dynamic forces that acted on the pile during driving. Assuming the frictional force to be concentrated and plastic in nature (activated at once as a response to the motion), the following relationship was valid:

$$\text{Force}_{\text{top}} - \text{Force}_{\text{middle}} = 0.5 \text{ Resisting Force} \quad (7.7)$$

Where  $\text{Force}_{\text{top}}$  and  $\text{Force}_{\text{middle}}$  refer to the measured forces above and below the friction sleeve, respectively. The resisting force on the friction sleeve was, therefore, twice the difference between the simultaneously measured forces at both ends of the friction sleeve. As the force provided in Table 28 reflected the maximum forces, they were not the simultaneously measured forces, but they correctly indicated the magnitudes. Using the values from Table 28 suggested that the dynamic resistance forces along the sleeve varied from about 38 kN during installation to about 52 kN during restrike. These forces were substantially higher than the maximum static forces measured along the friction sleeve (approximately 5.3 kN) and indicated the influence of the dynamic resisting force due to the high-velocity penetration taking place during driving.

### ***7.10.2 Capacity Based on the Energy Approach***

The pile capacity was determined using the Energy Approach method (Paikowsky et al., 1994). This simplified method was proven to provide accurate long-term pile capacity based on the dynamic measurements taken during installation. This method utilized the energy delivered to the pile ( $E$ ) and the maximum displacement ( $D_{\text{max}}$ ) as determined from the PDA readings, along with the permanent displacement or set ( $S$ ) as determined from the driving record (blow count). The calculated resistance was:

$$R_u = \frac{E}{\left( S + \frac{D_{\text{max}} - S}{2} \right)} \quad (7.8)$$

The evaluation of MDMP capacity using equation 7.8 is presented in Table 39. The parameters used for the end of driving capacities for NB2 reflected average values for the last 305 mm (12 in) of driving. For the end of the driving capacity of NB3, the first 30 blows were averaged together because the blow count remained constant throughout the installation. The parameters used for the restrike capacities reflected average values for the first five blows.

**Table 39. Energy Approach Capacity Predictions for the MDMP.**

Test	End of Driving (kN / kips)	Beginning of Restrike (kN / kips)
NB2	6.41 / 1.44	17.79 / 4.00
NB3	4.58 / 1.03	26.87 / 6.04

A comparison between the Energy Approach and the Case method capacities is presented in section 7.10.4 (Figures 117 through 125) in which the variation of the capacity with depth is presented as well.

### **7.10.3 Capacity Based on CAPWAP Analysis**

#### **(1) General.**

CAPWAP (Case Pile Wave Analysis Program) (CAPWAP Manual, 1996) solved the wave equation through an iterative process and prescribed measured boundary conditions (e.g., velocity at the top). By varying the resisting forces acting on the pile, a match was obtained between a calculated and a measured additional boundary condition (e.g., force at the top). The static component of the resistance that provided the satisfactory match was assumed to be the static bearing capacity of the pile.

An accurate modeling of the pile was required for the CAPWAP analysis. Since the model pile included a slip joint that was free to open up a space of up to 5 cm (2 in), the modeled pile length depended on the status of the slip joint (open or closed) and the nature of the traveling wave (compression or tension). At any point in time, the slip joint could be closed, partially opened, or completely opened. When the slip joint was closed, a compression wave traveling down was able to travel through the joint, but a returning tension wave coming from the pile tip would be able to travel through the joint as long as the resistance to the slip joint motion was equal to or higher than the magnitude of the traveling wave. In reality, the slip joint would continuously be opening and closing, depending on the magnitude of the traveling waves and the final condition of the slip joint between one impact and the next.

Additional difficulty associated with the CAPWAP modeling of the MDMP was due to the multiple units comprising the MDMP. The one-dimensional wave equation formulation was based on a uniform slender body. Multiple variations in the cross-section had two effects: (1) they created multiple reflections and (2) if the connections between the units were not completely tight, the wave speed was reduced.

During a calibration test for which all the connections were tight, a wave speed of 4,954 m/s (16,254 ft/s) was measured. Small strain reflection tests using a Pile Integrity Tester (PIT) device (PIT Manual, 1993) have resulted in an average wave speed of 5,016 m/s (16,458 ft/s) through one connection. Wave speeds as low as 4,246 m/s (13,931 ft/s) were measured through a connection not properly tightened. These measured velocities were lower compared to the typical wave speed traveling through steel of 5,124 m/s (16,810 ft/s).

All of the above creates major difficulties when modeling the MDMP. Therefore, the CAPWAP analyses were focused on: (1) the restrrike data — as CAPWAP results tended to reflect the resistance at the time of measurement, analysis of the records at the beginning of the restrrike would potentially be able to determine the long-term capacity; (2) using small-sized pile elements when discretizing the MDMP — such modeling enabled better accommodation for section variability; and (3) examining different combinations when modeling the possible slack at the slip joint (Table 40 presents the cross-sectional areas and the associated lengths used when modeling the MDMP in the CAPWAP analyses).

**Table 40. Cross-Sectional Areas for CAPWAP Modeling of the MDMP.**

MDMP Section	Outside Diameter (mm)	Inside Diameter (mm)	Wall Thickness (mm)	Area (cm <sup>2</sup> )	Length (mm)
Drill Rods	60.33	50.77	4.78	8.33	Varies
N-Rod Connections	60.33	31.75	14.29	20.66	60.96
N-Rod Adapter	76.20	48.01	14.10	27.50	215.90
Connector Housing	76.20	47.50	14.35	27.88	102.36
Upper Extension	76.20	52.58	11.81	23.89	312.67
Load Cell (10-ton)	N/A	44.45	N/A	10.28	146.00
Coupling	76.20	53.85	11.18	22.83	257.40
Transducer Housing	76.20	N/A	N/A	34.84	59.94
Upper Slip Joint	76.20	57.20	9.50	19.91	204.01
Lower Slip Joint	76.20	N/A	N/A	19.83	102.13
Lower Extension	76.20	N/A	6.35	13.94	820.42
Tip	76.20	N/A	N/A	45.6-0	101.60

(2) Model Pile Test NB2.

Figure 105 presents the force and velocity (multiplied by the impedance and presented in force units) records for blow 1 of the restrrike. Three CAPWAP analyses were performed for this case:

- (1) Pile length of 9.88 m (32.4 ft) as a continuous pile.
- (2) Pile length of 9.88 m (32.4 ft) with a compression slack of 0.381 mm (0.015 in), 25% effectiveness and a 50.8-mm (2-in) tension slack.
- (3) Pile length of 8.72 m (28.6 ft) assuming that the slip joint was practically the end of the pile.

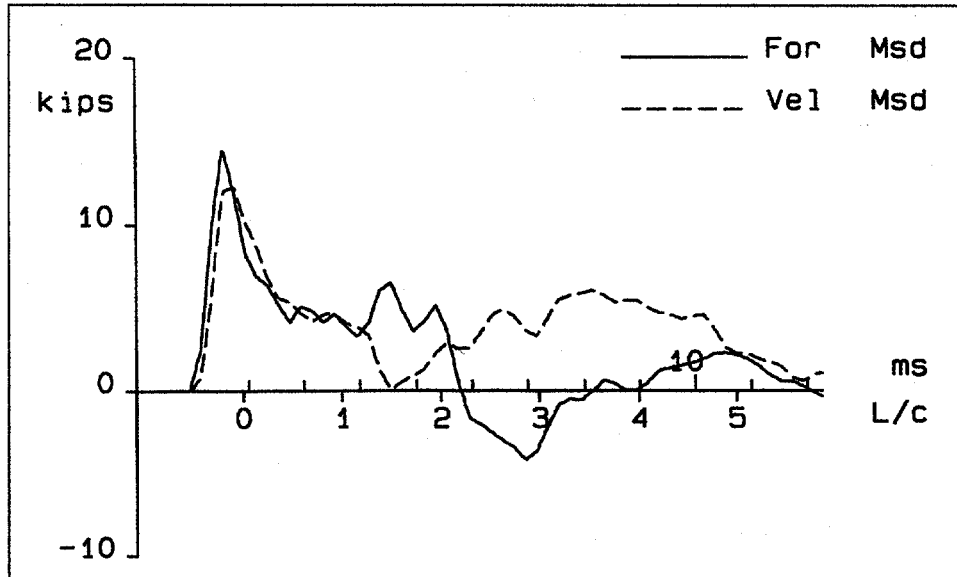


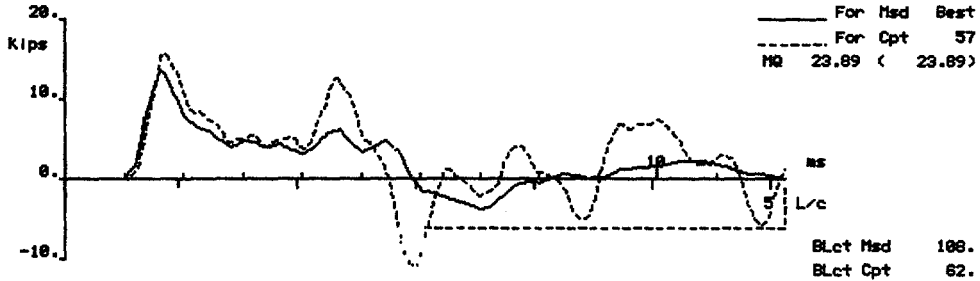
**Figure 105. Surface Force and Velocity Records of the MDMP Test NB2 Restrike, Blow 1.**

Figures 106, through 108 present the drill rods and pile geometry modeling, along with the associated best match between the calculated and measured forces for the above cases (1), (2), and (3), respectively. Tables 41 through 43 detail the input and output parameters associated with Figures 106, through 108, respectively. A wave speed of 4,938 m/s (16,200 ft/s) was used in these analyses based on a trial-and-error process for the best match over a time period of approximately 1.5 L/c (length/wave speed) (before the embedded section reflection arrived at the top measurement point). Segments of about 15.24 cm (6 in) long were used in all three analyses. CAPWAP analysis of case (1) (refer to Figure 106 and Table 41) resulted in a capacity of 5.3 kN (1.2 kips) with practically no tip resistance. CAPWAP analysis of case (2) (refer to Figure 107 and Table 42) resulted in a capacity of 9.3 kN (2.1 kips), including a 1.3-kN (0.3-kip) tip resistance. CAPWAP analysis of case (3) (refer to Figure 108 and Table 43) resulted in a capacity of 4.4 kN (1.0 kips) with practically no tip resistance.

In spite of the large differences between the modeling conditions and the obtained capacities, similar wave matches were obtained for all cases. A reasonably good agreement existed between the measured and calculated force waves along a time equivalent to about 1 L/c. Most of this length was associated with the stress wave traveling through the drill rods. A consistently poor match existed between 1.5 L/c and 2 L/c, the range that represented the wave reflections from the pile tip. These results suggested that the complex waves that developed due to the large variation in the cross-sections (when moving from the drilling rod to the pile) were difficult to model.

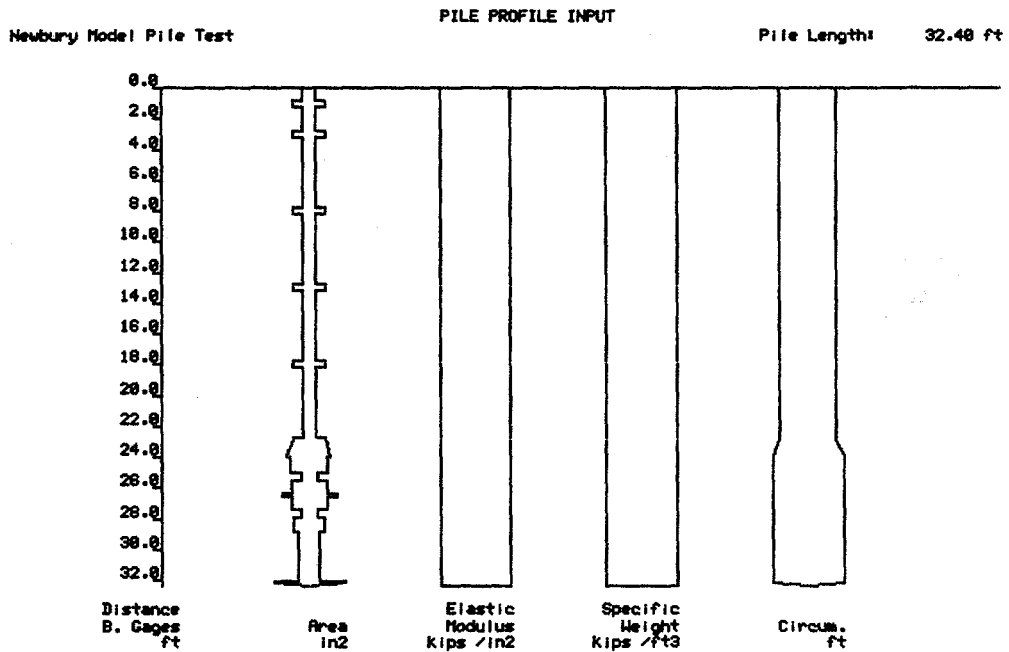
In order to assess the "proper" modeling, the calculated force and measured force (previously presented in Figures 75c and d) associated with the top, middle, and bottom load cells of the three analyzed CAPWAP cases are presented in Figures 109 through 111. The internal measurements were compared to the modeled analyses only upon completion of the top matching process and, hence, did not affect the traditional CAPWAP matching process. Figures 109 through 111 suggest that cases (1) and (2) (for which the full MDMP length was modeled)

JS/JT	SS/ST	OS/OT	UN/UC	CS/CT	LS/LT	PI/PL	SK/ST	MS/MT	RS/RT	RU/OP
0.117	0.231	0.041	1.000	0.020	-1.000	0.010	0.000	0.00	1.2	1.2
0.265	20.330	0.044	0.000	0.020	0.000	0.000	0.000	0.00	0.0	0.0
max dtoe		0.233	toe segment weight			0.005				
								PNat	RUto	REss
								1.	OFF	0.



Segment	1	2	3	4	5	6	7	8	9	10
Curr. Rs	0.1	0.1	0.1	0.1	0.1	0.1	0.1	0.1	0.1	0.0

(a) Best Match Between Measured and Calculated Force at Top.



(b) Drill Rods and Pile Geometry Modeling.

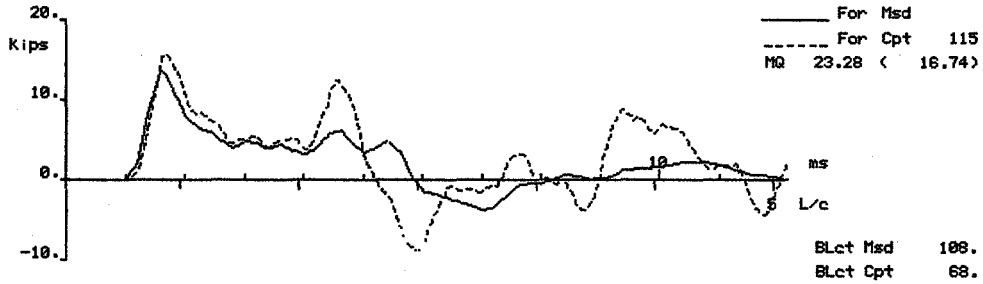
**Figure 106. Test NB2 Restrike CAPWAP Modeling of MDMP Case (1): (a) Best Match Between Measured and Calculated Force at Top and (b) Drill Rods and Pile Geometry Modeling.**



JS/JT	SS/ST	QS/QT	UN/UC	CS/CT	LS/LT	PI/PL	SK/BT	MS/MT	RS/RT	RU/OP
0.095	0.121	0.040	0.500	0.035	-1.000	0.010	0.000	0.00	1.8	2.1
0.169	1.296	0.052	0.000	0.020	0.000	0.000	0.000	0.00	0.3	0.0

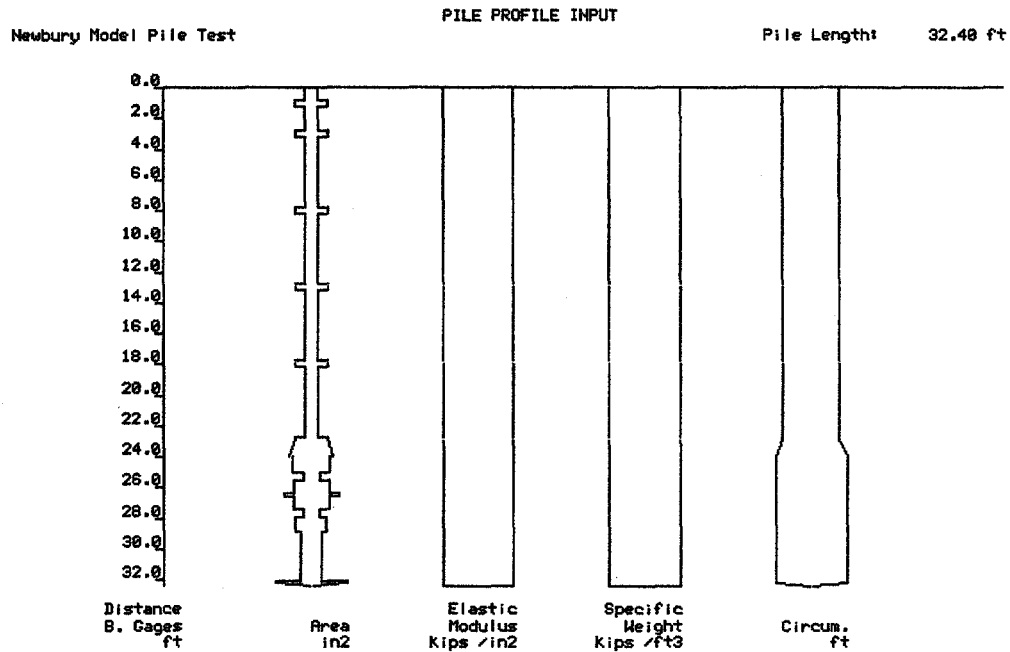
max dtoe 0.217      toe segment weight 0.005

ANat 1.      AAuto OFF      REss 0.



Segment	1	2	3	4	5	6	7	8	9	10
Curr. Rs	0.2	0.2	0.2	0.2	0.2	0.2	0.2	0.2	0.2	0.3

(a) Best Match Between Measured and Calculated Force at Top.



(b) Drill Rods and Pile Geometry Modeling.

**Figure 107. Test NB2 Restrike CAPWAP Modeling of MDMP Case (2): (a) Best Match Between Measured and Calculated Force at Top and (b) Drill Rods and Pile Geometry Modeling.**

**Table 42. CAPWAP Results of Test NB2 Restrike, Case (2), Assuming a 9.88-m (32.4-ft) Model Pile With Slip Joint Modeling.**

Newbury Model Pile Test  
 File: NB2 Restrike      Blow: 1      Data: Surface Measurement  
                                  Operator: LJH                                   CAPWAP(R) Ver. 1997-1

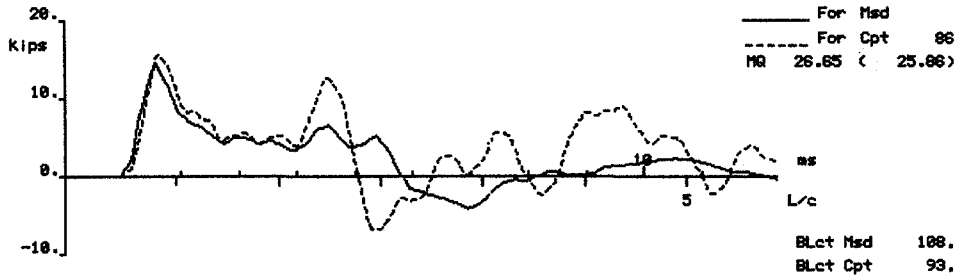
**CAPWAP FINAL RESULTS**

Total CAPWAP Capacity:      2.1; along Shaft      1.8; at Toe      .3 kips

Soil Sgmt No.	Dist. Below Gages ft	Depth Below Grade ft	Ru kips	Force in Pile at Ru kips	Sum of Ru kips	Unit Resist. w. Respect to		Smith Damping Factor s/ft	Quake inch
						Depth kips/ft	Area kips/ft <sup>2</sup>		
				2.1					
1	24.4	1.4	.2	1.9	.2	.20	.26	.121	.040
2	25.4	2.4	.2	1.7	.4	.20	.25	.121	.040
3	26.4	3.4	.2	1.5	.6	.20	.25	.121	.040
4	27.4	4.4	.2	1.3	.8	.20	.25	.121	.040
5	28.4	5.4	.2	1.1	1.0	.20	.25	.121	.039
6	29.4	6.4	.2	.9	1.2	.20	.25	.121	.039
7	30.4	7.4	.2	.7	1.4	.20	.25	.121	.039
8	31.4	8.4	.2	.5	1.6	.20	.25	.121	.039
9	32.4	9.4	.2	.3	1.8	.20	.30	.121	.040
Average Skin Values			.2			.19	.26	.121	.039
Toe			.3				6.12	1.296	.052
Soil Model Parameters/Extensions						Skin	Toe		
Case Damping Factor						.095	.169		
Unloading Quake (% of loading quake)						3	1		
Unloading Level (% of Ru)						50			

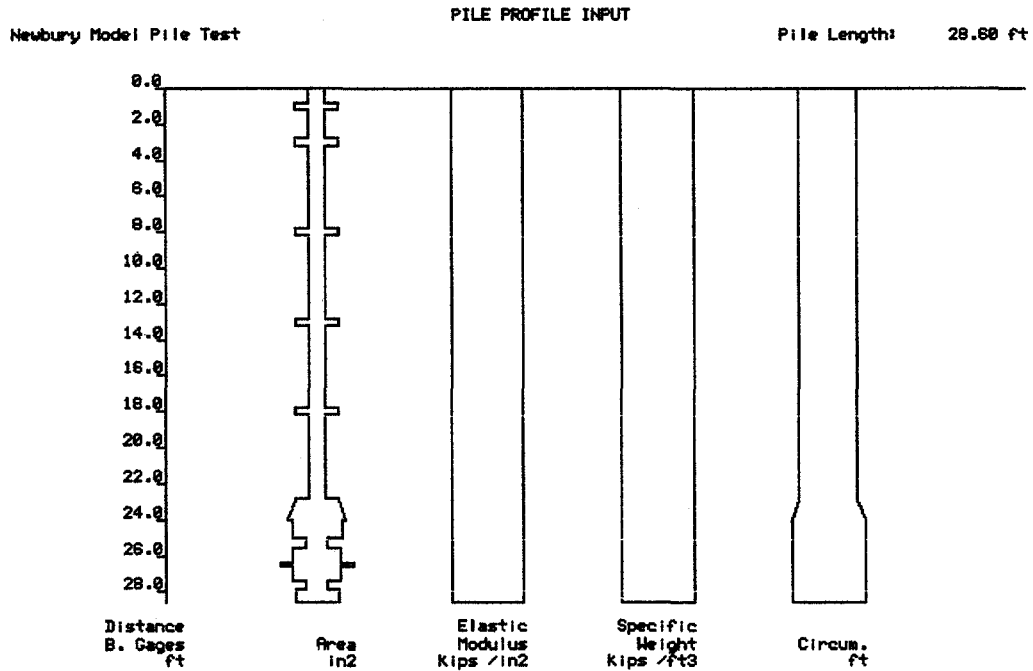


JS/JT	SS/ST	QS/QT	UN/TG	CS/CT	LS/LT	PI/PL	SK/ST	MS/MT	RS/RT	RU/OP
0.266	0.659	0.117	1.000	0.020	-1.000	0.010	0.000	0.00	1.0	1.0
0.319	73.452	0.139	0.000	0.020	0.000	0.006	0.000	0.00	0.0	0.0
	max dtoe	0.243		toe segment weight		0.005				
								ANat	AUTO	REss
								1.	OFF	0.



Segment	1	2	3	4	5	6	7
Curr. Rs	0.0	0.2	0.2	0.2	0.2	0.2	0.0

(a) Best Match Between Measured and Calculated Force at Top.



(b) Drill Rods and Pile Geometry Modeling.

**Figure 108. Test NB2 Restrike CAPWAP Modeling of MDMP Case (3): (a) Best Match Between Measured and Calculated Force at Top and (b) Drill Rods and Pile Geometry Modeling.**

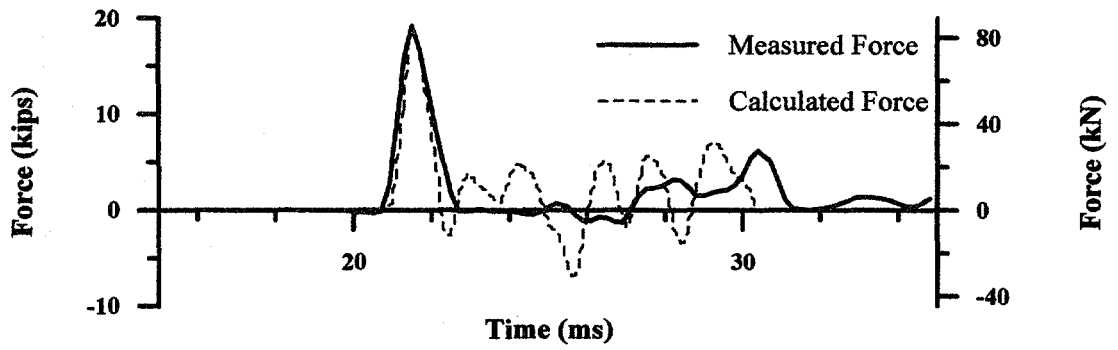
**Table 43. CAPWAP Results of Test NB2 Restrike, Case (3), Assuming a 8.72-m (28.6-ft) Model Pile With Pile Ending at Slip Joint.**

Newbury Model Pile Test  
 File: NB2 Restrike      Blow: 1      Data: Surface Measurements  
                                  Operator: LJH                                   CAPWAP (R) Ver. 1997-1

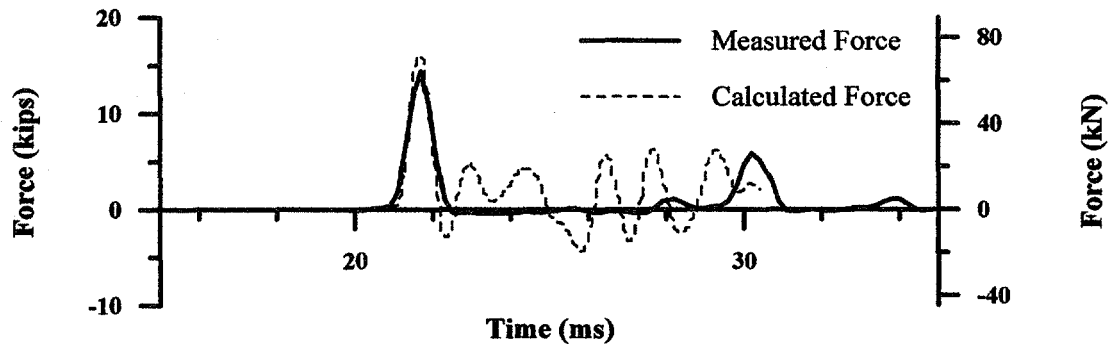
CAPWAP FINAL RESULTS

Total CAPWAP Capacity:      1.0; along Shaft      1.0; at Toe      .0 kips

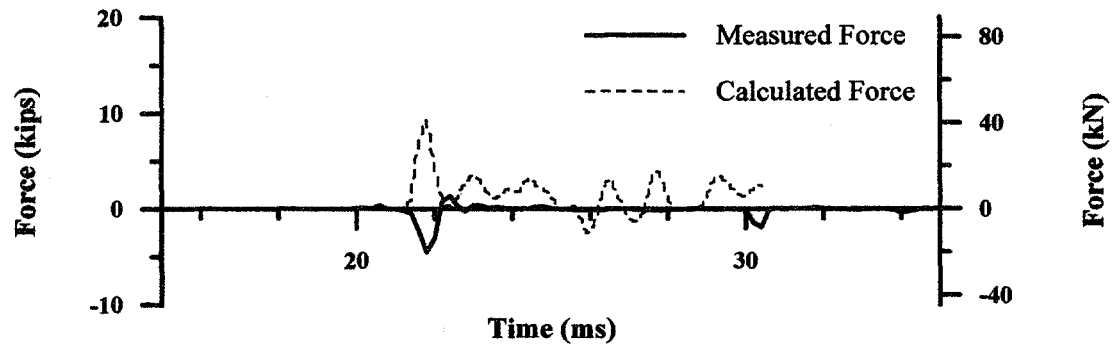
Soil Sgmnt No.	Dist. Below Gages ft	Depth Below Grade ft	Ru kips	Force in Pile at Ru kips	Sum of Ru kips	Unit Resist. w. Respect to		Smith Damping Factor s/ft	Quake inch
						Depth kips/ft	Area kips/f <sup>2</sup>		
				1.0					
1	23.6	.6	.0	1.0	.0	.00	.00	.659	.117
2	24.6	1.6	.2	.8	.2	.20	.26	.659	.116
3	25.6	2.6	.2	.6	.4	.20	.25	.659	.115
4	26.6	3.6	.2	.4	.6	.20	.25	.659	.115
5	27.6	4.6	.2	.2	.8	.20	.25	.659	.114
6	28.6	5.6	.2	.0	1.0	.20	.25	.659	.112
Average Skin Values			.2			.18	.22	.659	.114
Toe			.0				.20	73.452	.139
Soil Model Parameters/Extensions						Skin	Toe		
Case Damping Factor						.286	.319		
Unloading Quake (% of loading quake)						1	1		
Soil Plug Weight (kips)							.01		



(a) Top Load Cell

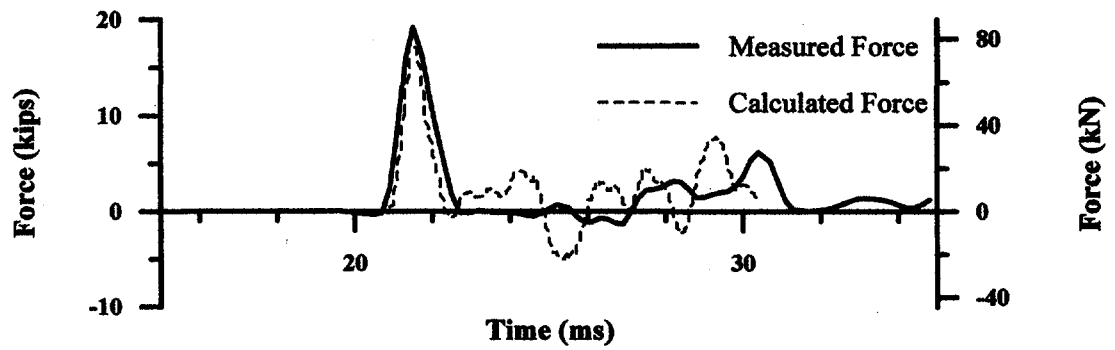


(b) Middle Load Cell

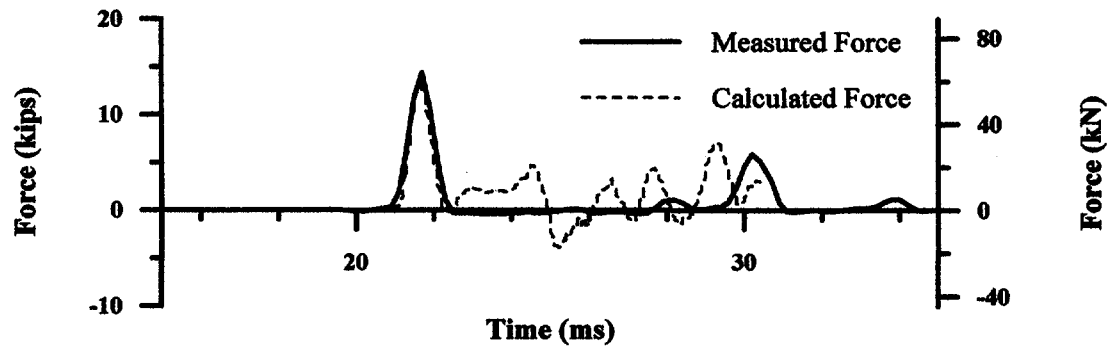


(c) Bottom Load Cell

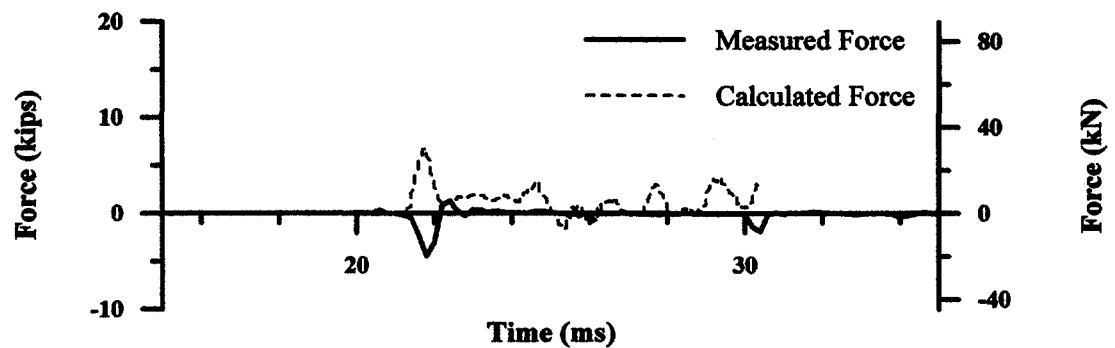
**Figure 109. Modeling of Case (1), Calculated and Measured Forces at the Internal Load Cell Locations for the MDMP Test NB2 Restrike Blow 1 (analysis based on a force match at the surface measurement location only).**



(a) Top Load Cell

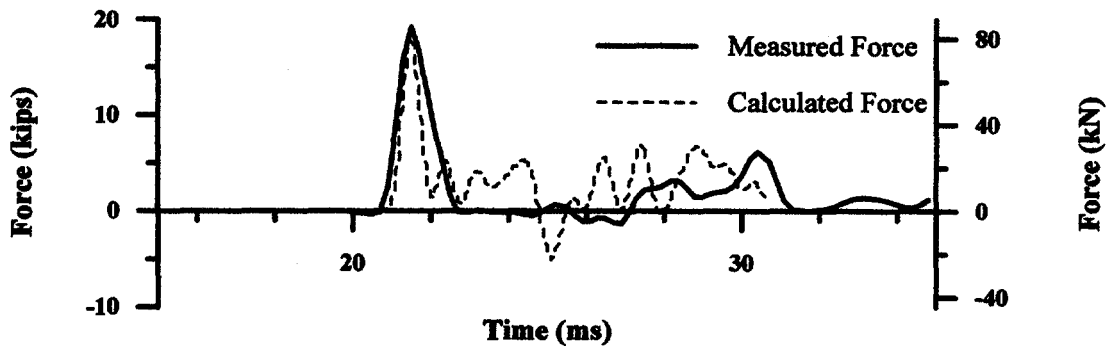


(b) Middle Load Cell

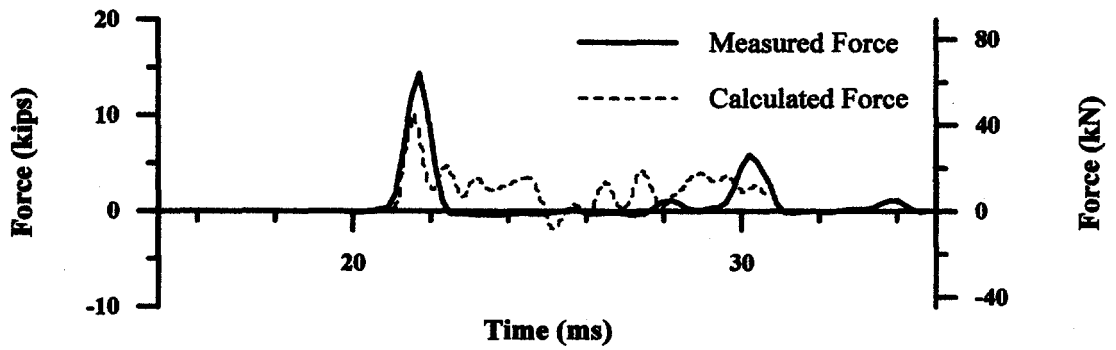


(c) Bottom Load Cell

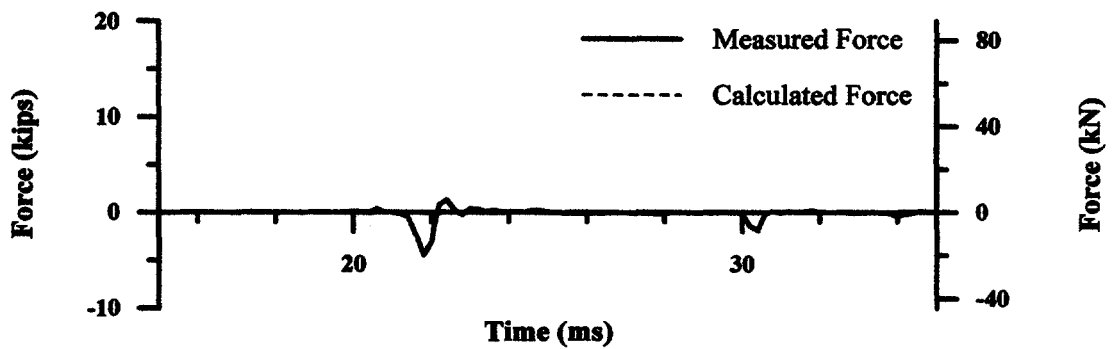
**Figure 110. Modeling of Case (2), Calculated and Measured Forces at the Internal Load Cell Locations for the MDMP Test NB2 Restrike Blow 1 (analysis based on a force match at the surface measurement location only).**



(a) Top Load Cell



(b) Middle Load Cell



(c) Bottom Load Cell

**Figure 111. Modeling of Case (3), Calculated and Measured Forces at the Internal Load Cell Locations for the MDMP Test NB2 Restrike Blow 1 (analysis based on a force match at the surface measurement location only).**

resulted in a very good match between the measured and calculated traveling wave along the pile. The good match was presented in both magnitude and time for both cases, which means that a full pile length modeling was required and the existence of a slip joint under the compressive wave had not affected the modeled behavior since both cases were similar. The less desirable match obtained for case (3) implied that the assumption of a "short" pile (ending at the slip joint) was not valid. A poor match existed for all cases at the time beyond the major traveling wave. This could be a result of four major factors:

- (1) The measurements of small dynamic forces with the large internal load cells were limited in their response and accuracy. The measured forces may have reflected this condition and, hence, did not show the smaller peaks.
- (2) A larger damping was required in the CAPWAP modeling of the soil. Such an increased damping coefficient would result in a "smoother" wave shape.
- (3) The modeled segment, although it was very short, it was larger than the one required to model accurately the measured motion.
- (4) The adopted modeling of the slip joint (case 2) did not correctly reflect the actual physical phenomenon and, hence, did not result in zones of no loading as indicated by the measured records.

(3) Model Pile Test NB3.

Figure 112 presents the force and velocity records for blow 2 of the restrrike. Two CAPWAP analyses were performed for this case:

- (1) Pile length of 13.84 m (45.4 ft) with a 50.8-mm (2-in) tension slack.
- (2) Pile length of 12.68 m (41.6 ft), assuming the slip joint is practically the end of the pile.

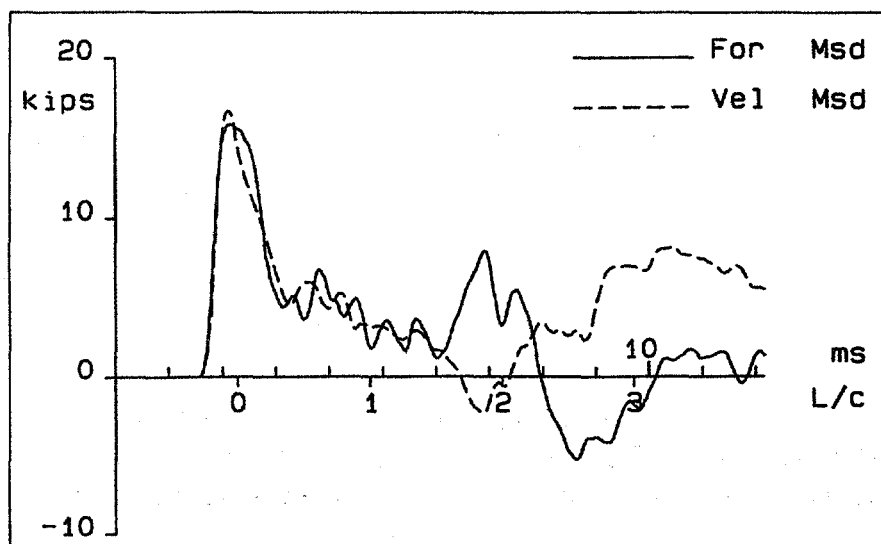


Figure 112. Surface Force and Velocity Records for MDMP Test NB3 Restrike, Blow 2.

Figures 113 and 114 present the drill rods and pile geometry modeling, along with the associated best match between the calculated and measured forces for the above cases (1) and (2), respectively. Tables 44 and 45 detail the input and output parameters associated with Figures 113 and 114, respectively. A wave speed of 4,758 m/s (15,610 ft/s) was used in these analyses, based on a trial-and-error process for the best match over a time period of approximately 1.5 L/c (before the embedded section reflection arrived at the top measurement point). Segments of about 10.16 cm (4 in) long were used in all three analyses. The CAPWAP analysis of case (1) (refer to Figure 113 and Table 44) resulted in a capacity of 5.3 kN (1.2 kips), including a 0.4-kN (0.1-kip) tip resistance. The CAPWAP analysis of case (2) (refer to Figure 114 and Table 45) resulted in a capacity of 8.0 kN (1.8 kips), including a 1.3-kN (0.3-kip) tip resistance.

In order to assess the "proper" modeling, the calculated force and measured force (previously presented in Figures 79c and d) associated with the top and middle load cells of the two analyzed cases are presented in Figures 115 and 116. The internal measurements were compared to the modeled analyses only upon completion of the top matching process and thus did not influence the CAPWAP matching process that was conducted for the measurements at the top of the drilling rods (surface). Figures 115 and 116 reinforce the conclusions previously presented in the analyses of test NB2, restrike blow 1. In summary, the modeling that included the entire pile length provided a good prediction of the stress wave in the pile based on the measurements at the top. However, a variation between the measured and calculated forces beyond the major traveling wave remained questionable and the aforementioned possibilities (see section 7.10.3 part (2) discussion for the NB2 CAPWAP results) remained valid.

#### **7.10.4 Capacity Based on the Case Method**

##### **(1) General.**

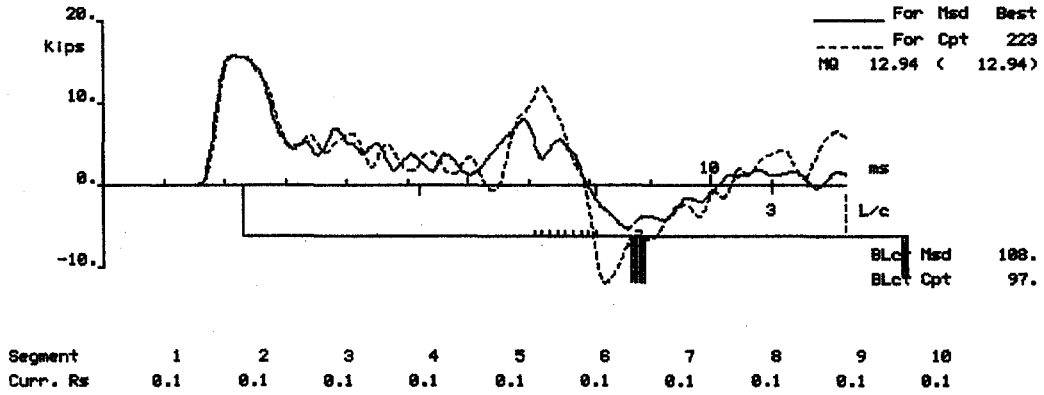
The Case method (see Goble et al., 1970 and Rausche et al., 1972) is a simple field procedure used by the PDA to estimate pile capacities (for a complete review, see Paikowsky et al., 1994). Analysis by the Case method is based on the assumption of a uniform elastic pile, ideal plastic soil behavior, and a simplified wave propagation formulation. Force and velocity measurements taken at the pile top and a correlation between the soil at the pile's tip and a damping parameter are used.

##### **(2) The Case Method Equation.**

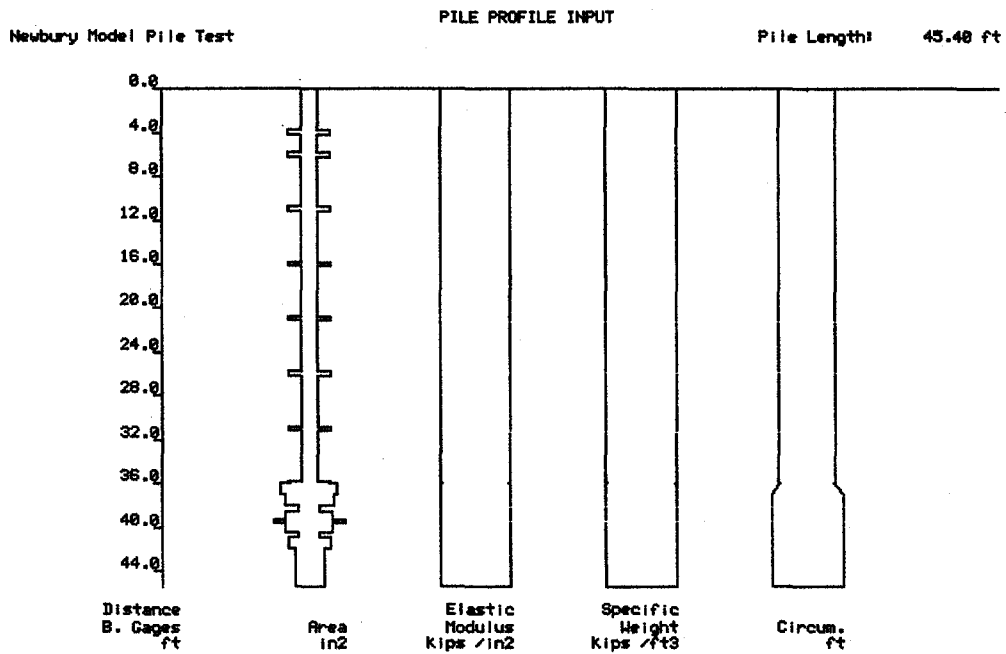
The Case method calculates the total soil resistance (RTL) activated during pile driving, using the following equation:

$$RTL = \frac{[F(T1) + F(T1 + \frac{2L}{C})]}{2} + [v(T1) - v(T1 + \frac{2L}{C})] * \frac{MC}{2L} \quad (7.9)$$

JS/JT	SS/ST	QS/QT	UN/UG	CS/CT	LS/LT	PI/PL	SK/BT	MS/MT	RS/RT	RU/OP	
0.050	0.110	0.090	1.000	0.120	-1.000	0.030	0.105	0.00	1.1	1.2	
0.173	4.299	0.100	0.100	0.200	0.070	0.003	0.020	10.00	0.1	0.0	
max dtoc		0.218	toe segment weight			0.003			RNat	RUTO	REss
									1.	OFF	0.



(a) Best Match Between Measured and Calculated Force at Top.



(b) Drill Rods and Pile Geometry Modeling.

**Figure 113. Test NB3 Restrike CAPWAP Modeling of MDMP Case (1): (a) Best Match Between Measured and Calculated Force at Top and (b) Drill Rods and Pile Geometry Modeling.**



**Table 44. CAPWAP Results of Test NB3 Restrike, Case (1), Assuming a 13.84-m (45.4-ft) Model Pile With Slip Joint Modeling.**

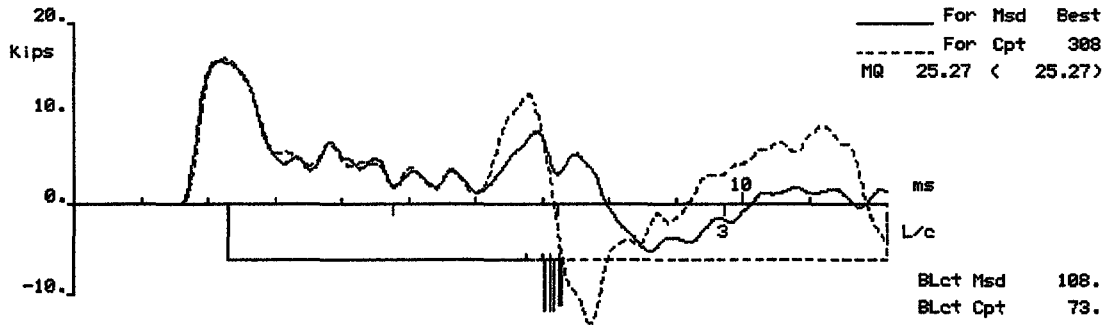
Newbury Model Pile Test, Project: NB3  
 File: NB3RODRE Blow: 2 Data: Surface Measurements  
 Operator: LJH CAPWAP(R) Ver. 1997-1

**CAPWAP FINAL RESULTS**

Total CAPWAP Capacity: 1.2; along Shaft 1.1; at Toe .1 kips

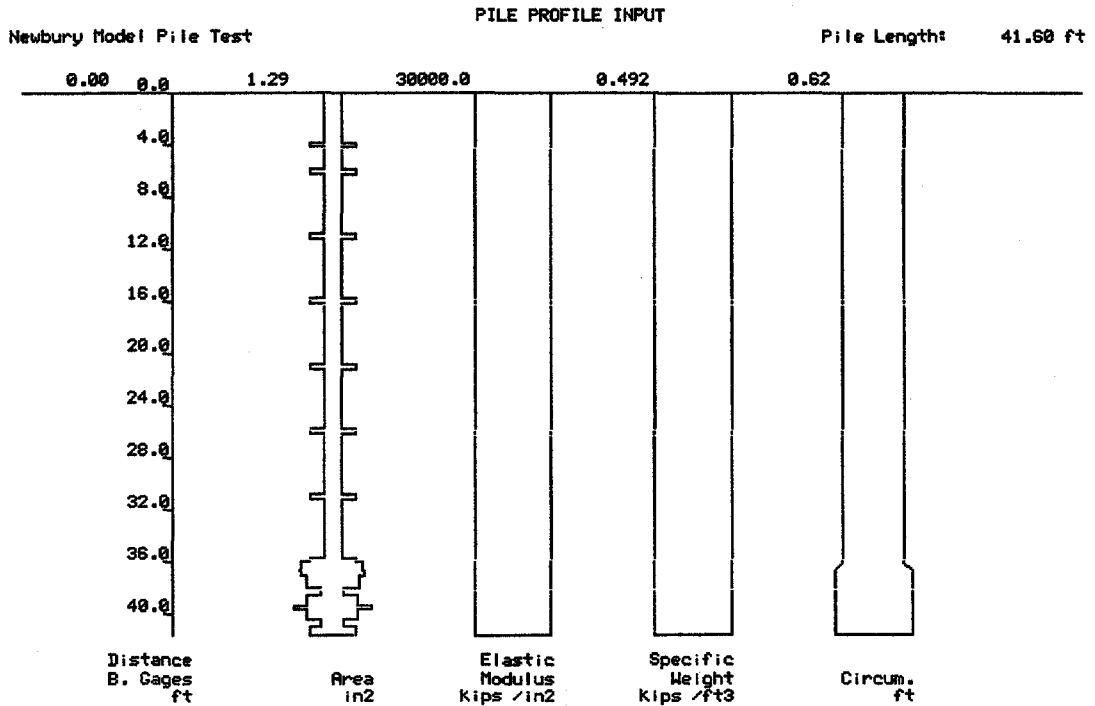
Soil Sgmt No.	Dist. Below Gages ft	Depth Below Grade ft	Ru kips	Force in Pile at Ru kips	Sum of Ru kips	Unit Resist. w. Respect to		Smith Damping Factor s/ft	Quake inch
						Depth kips/ft	Area kips/f <sup>2</sup>		
1	37.4	1.4	.1	1.2	.1	.13	.17	.109	.090
2	38.4	2.4	.1	1.0	.3	.13	.16	.109	.089
3	39.4	3.4	.1	.9	.4	.13	.16	.109	.088
4	40.4	4.4	.1	.7	.5	.13	.16	.109	.087
5	41.4	5.4	.1	.6	.6	.13	.16	.109	.086
6	42.4	6.4	.1	.5	.8	.13	.16	.109	.085
7	43.4	7.4	.1	.4	.9	.13	.16	.109	.083
8	44.4	8.4	.1	.2	1.0	.13	.16	.109	.081
9	45.4	9.4	.1	.1	1.1	.13	.16	.109	.080
Average Skin Values			.1			.12	.16	.109	.086
Toe			.1				2.06	4.269	.200
Soil Model Parameters/Extensions						Skin	Toe		
Case Damping Factor						.050	.173		
Unloading Quake (% of loading quake)						12	20		
Reloading Level (% of Ru)						-100	7		
Resistance Gap (included in Toe Quake) (inch)							.100		
Soil Plug Weight (kips)							.00		
Soil Support Dashpot						.105	.031		
Soil Support Mass (kips)						.08	10.00		

JS/JT	SS/ST	QS/QT	UN/TG	CS/CT	LS/LT	PI/PL	SK/BT	MS/MT	RS/RT	RU/OP
0.066	0.110	0.020	1.000	0.100	-1.000	0.030	0.105	0.08	1.5	1.8
0.303	2.500	0.010	0.010	0.020	0.070	0.011	0.200	1.00	0.3	0.0
	max dtoe	0.182	toe segment weight			0.004				
								ANat	AUTO	REss
								1.	OFF	0.



Segment	1	2	3	4	5	6
Curr. Rs	0.3	0.3	0.3	0.3	0.3	0.3

(a) Best Match Between Measured and Calculated Force at Top.



(b) Drill Rods and Pile Geometry Modeling.

**Figure 114. Test NB3 Restrike CAPWAP Modeling of MDMP Case (2): (a) Best Match Between Measured and Calculated Force at Top and (b) Drill Rods and Pile Geometry Modeling.**

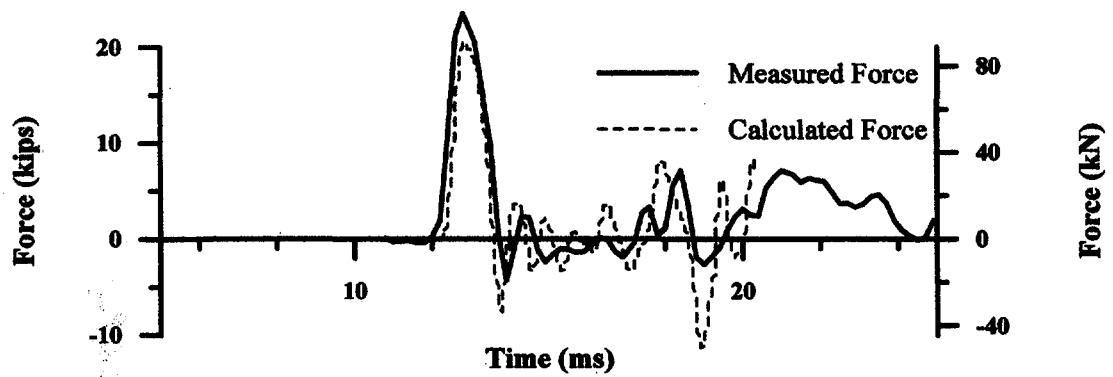
**Table 45. CAPWAP Results of Test NB3 Restrike, Case (2), Assuming a 12.68-m (41.6-ft) Model Pile With Pile Ending at the Slip Joint.**

Newbury Model Pile Test, Project: NB3  
 File: NB3RODRE Blow: 2 Data: Surface Measurements  
 Operator: LJH CAPWAP(R) Ver. 1997-1

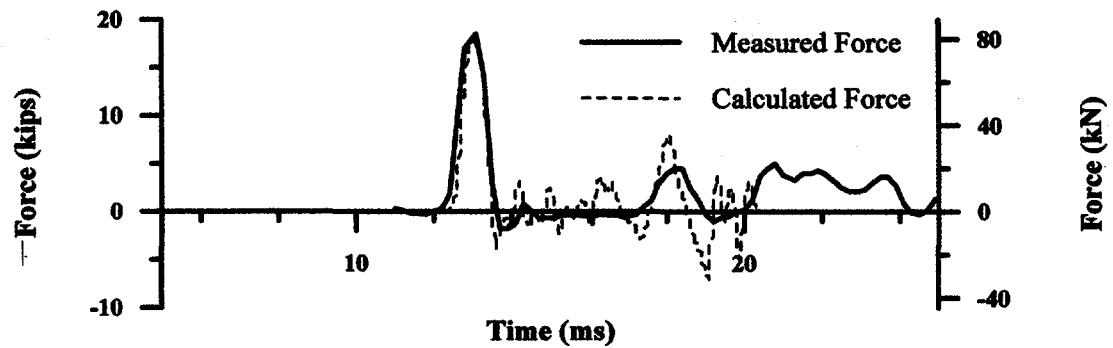
CAPWAP FINAL RESULTS

Total CAPWAP Capacity: 1.8; along Shaft 1.5; at Toe .3 kips

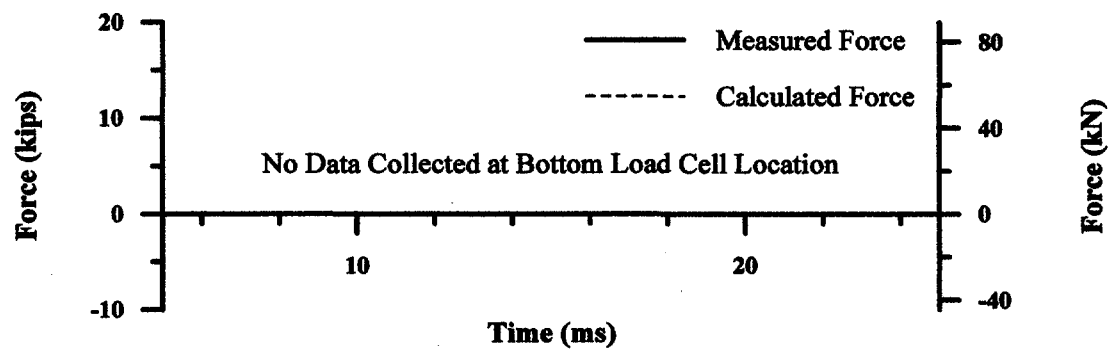
Soil Sgmt No.	Dist. Below Gages ft	Depth Below Grade ft	Ru kips	Force in Pile at Ru kips	Sum of Ru kips	Unit Resist. w. Respect to		Smith Damping Factor s/ft	Quake inch
						Depth kips/ft	Area kips/f <sup>2</sup>		
1	37.6	1.6	.3	1.5	.3	.30	.38	.109	.020
2	38.6	2.6	.3	1.2	.6	.30	.38	.109	.020
3	39.6	3.6	.3	.9	.9	.30	.38	.109	.020
4	40.6	4.6	.3	.6	1.2	.30	.38	.109	.018
5	41.6	5.6	.3	.3	1.5	.30	.38	.109	.009
Average Skin Values			.3			.27	.38	.109	.017
Toe			.3				6.15	2.488	.020
Soil Model Parameters/Extensions						Skin	Toe		
Case Damping Factor						.066	.303		
Unloading Quake (% of loading quake)						10	1		
Reloading Level (% of Ru)						-100	7		
Resistance Gap (included in Toe Quake) (inch)							.010		
Soil Plug Weight (kips)							.01		
Soil Support Dashpot						.105	.444		
Soil Support Mass (kips)						.08	1.00		



(a) Top Load Cell

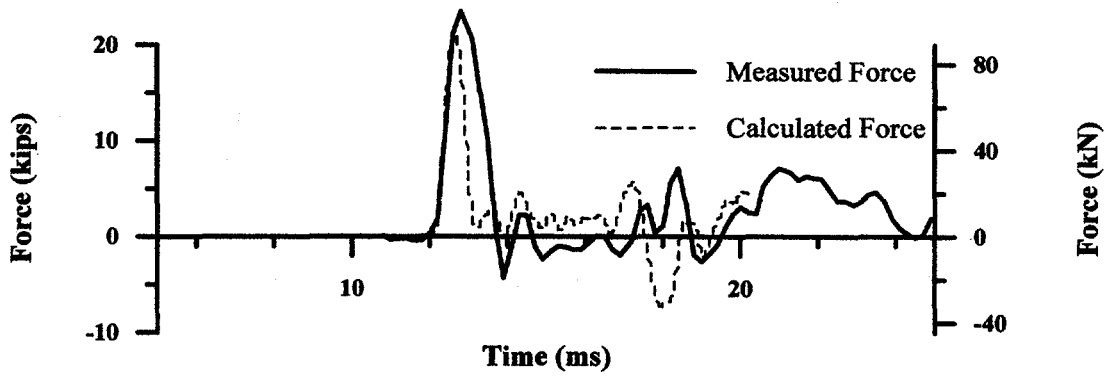


(b) Middle Load Cell

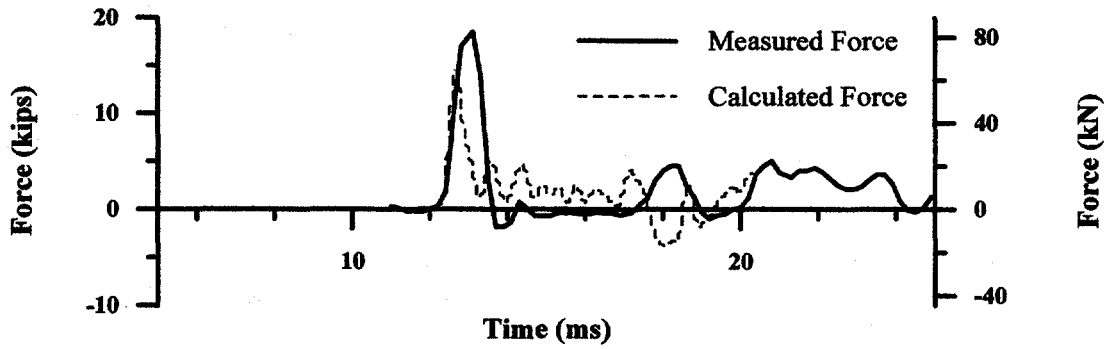


(c) Bottom Load Cell

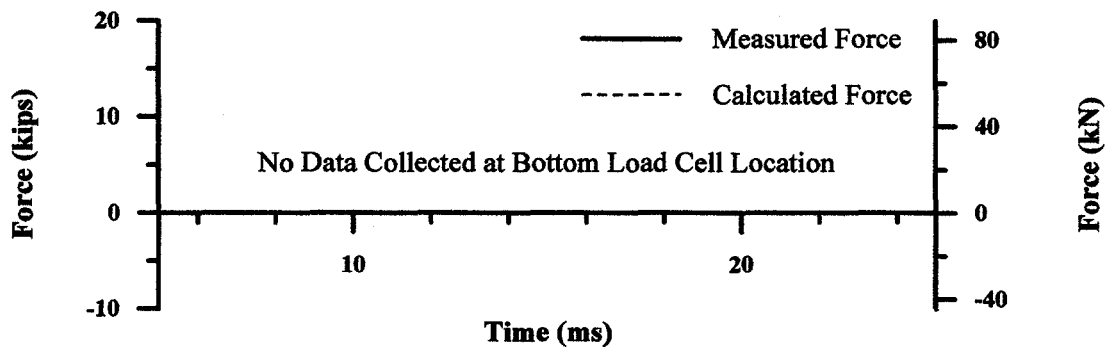
**Figure 115. Modeling of Case (1), Calculated and Measured Forces at the Internal Load Cell Locations for the MDMP Test NB3 Restrike Blow 2 (analysis based on a force match at the surface measurement location only).**



(a) Top Load Cell



(b) Middle Load Cell



(c) Bottom Load Cell

**Figure 116. Modeling of Case (2), Calculated and Measured Forces at the Internal Load Cell Locations for the MDMP Test NB3 Restrike Blow 2 (analysis based on a force match at the surface measurement location only).**

where:	F(T1)	=	measured force at the time T1
	F(T1+2L/C)	=	measured force at the time T1 plus 2L/C
	v(T1)	=	measured velocity at the time T1
	v(T1+2L/C)	=	measured velocity at the time T1 plus 2L/C
	L, M	=	length and mass of the pile, respectively
	C	=	speed of wave propagation in the pile.

Different variations of the Case method have been developed taking T1 as the time of impact or modified to include a time delay constant allowing higher RTL values to be obtained. The time T1 is defined, in equation form, as:

$$T1 = TP + \delta \quad (7.10)$$

where:	TP	=	time of the impact peak
	$\delta$	=	time delay.

In most cases,  $\delta = 0$ . However, the time delay is required in soils capable of large deformations before achieving full resistance. A time delay is also used in situations where the hammer impact is uneven (PDA Manual, 1996). Several factors that influence the pile-soil system must be considered when the total predicted resistance is evaluated. These factors include time-dependent soil strength changes and refusal driving when the soil's resistance is not fully mobilized under a single hammer blow.

The total resistance calculated is a combination of the static resistance (S), which is displacement dependent, and the dynamic resistance (D), which is velocity dependent. Therefore, the total resistance (Goble et al., 1975) is:

$$RTL = S + D \quad (7.11)$$

The dynamic resistance D is considered to be viscous in nature, hence, it is a function of the velocity at the pile toe ( $V_{toe}$ ) and a damping constant (J) where:

$$D = J * V_{toe} \quad (7.12)$$

By applying the wave propagation theory, the pile toe velocity can be calculated as a function of the velocity at the pile top:

$$V_{toe} = 2V_{top} - \frac{L}{MC}RTL \quad (7.13)$$

where:	L	=	pile length
	M	=	pile mass
	C	=	wave speed of the pile material
	RTL	=	total resistance
	$V_{top}$	=	velocity at pile top.

$V_{top}$  is taken as the pile top velocity at the time T1.

According to Goble et al. (1975), remolding effects cause the majority of the damping resistance to be concentrated near the pile tip. Consequently, the damping constant is determined according to the soil type at the pile tip. In most cases, the damping constant (J) is proportional to the pile properties (EA/C), and is, therefore, represented by a dimensionless coefficient ( $J_c$ ) using the following

equation:

$$J = J_c \frac{EA}{C} \quad (7.14)$$

where:  $J_c$  = dimensionless Case damping coefficient  
 $E$  = elastic modulus of the pile material  
 $A$  = pile cross-sectional area  
 $C$  = wave speed of the pile material.

Recommended  $J_c$  values are provided according to soil type (PDA Manual, 1996). These values keep changing over the years as a result of improvements to the PDA and continued research in this area. Paikowsky and Chernauskas (1996) had clearly demonstrated that the use of viscous damping parameters for pile-penetration modeling was in lieu of soil inertia that was not accounted for in the pile-penetration formulation. As such, Paikowsky and Chernauskas have shown a better correlation between viscous damping parameters and the combination of pile size and blow count rather than soil type.

### (3) The Maximum Resistance Method (RMX).

Several variations of the Case method have evolved for the analysis of different driving situations and soil types. The variations are similar in that they all begin with the initial total resistance prediction (RTL) of equation (7.9). Five distinct methods employ the predicted RTL: the Damping Factor Method, the Maximum Resistance Method, the Minimum Resistance Method, the Unloading Method, and the Automatic Method. A brief review of the method most commonly used (the Maximum Resistance Method) follows. By substituting equation (7.13) into equation (7.12), and this, in turn, into equation (7.11) (expressed as the static pile resistance component, RSP), one obtains the standard Case Method equation:

$$RSP = RTL - J \frac{MC}{L} * V_{toe} \quad (7.15)$$

The Maximum Resistance Method uses the RSP equation with  $2L/C$  as a fixed quantity. The time  $T1$  used in the RSP equation is varied between the impact time (TP) and  $TP + 30$  ms to find the corresponding maximum RSP value, denoted as RMX.

The evaluation of the MDMP capacity using equation 7.15 as RMX is presented in Figures 117 through 124, along with the Energy Approach method capacity (see section 7.10.2 and equation 7.8). The Case method capacity was determined using the pile properties of the drill rods and was based on the measurements obtained at the surface. Three different damping factors were examined, investigating the sensitivity of the calculated static capacity to the variations in the damping coefficient. Figures 117 and 118 present the capacity determined for the MDMP test NB2 installation and restrike data, assuming the wave reflection from the pile tip (pile length was 9.88 m) as in cases (1) and (2). Figures 119 and 120 present the capacity determined for MDMP test NB2 for installation and restrike data, assuming that the wave reflection was related to the slip joint (pile length was 8.72 m) as in case (3). Figures 121 and 122 present the capacity determined for MDMP test NB2 for installation and restrike data, assuming the wave reflection

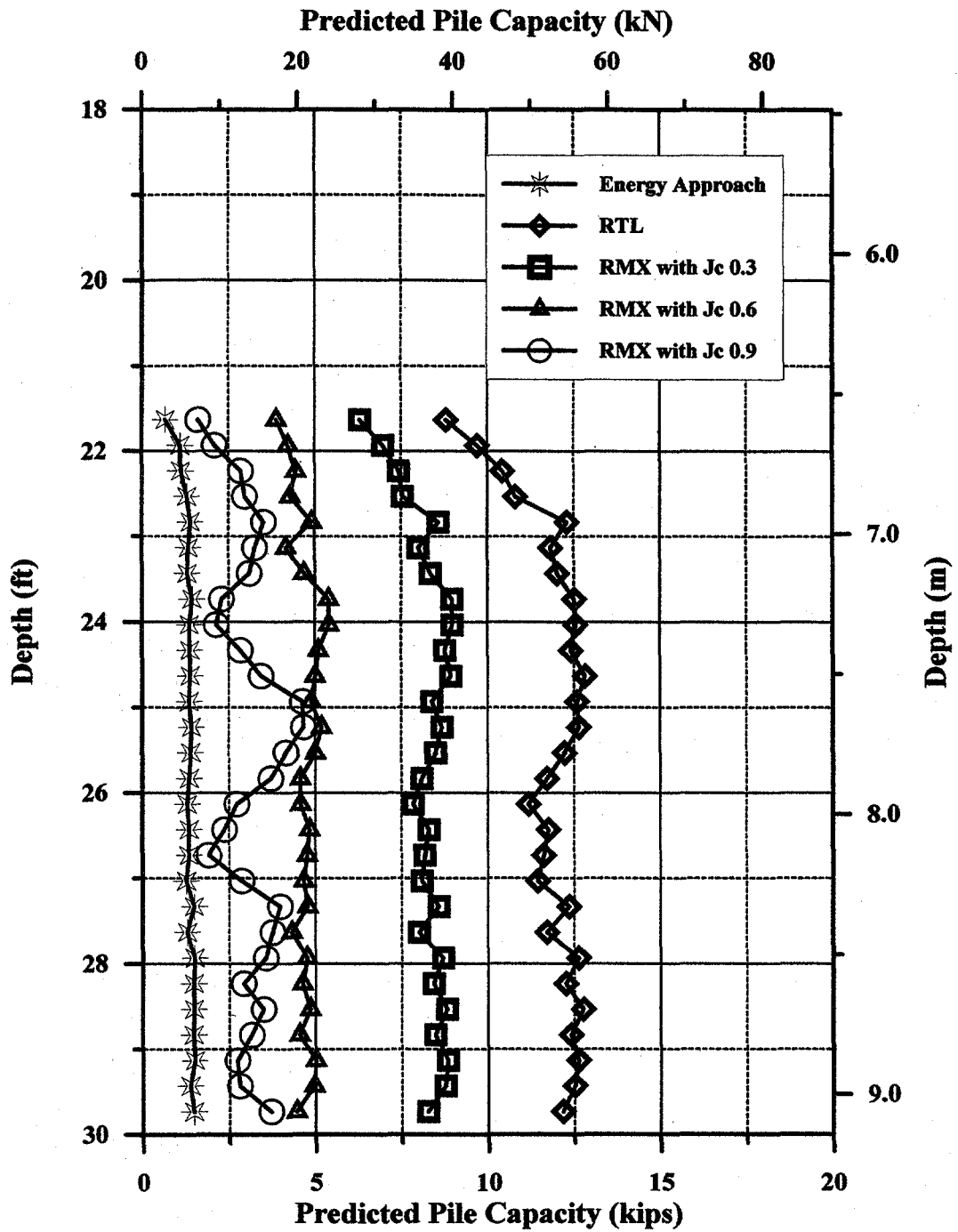


**Figure 117. Predicted Pile Capacity for the Installation of MDMP Test NB2 (Cases 1 and 2) Based on the Energy Approach Method and the Case Method With Varying  $J_c$  Values (assuming pile length is 9.88 m (32.4 ft)).**



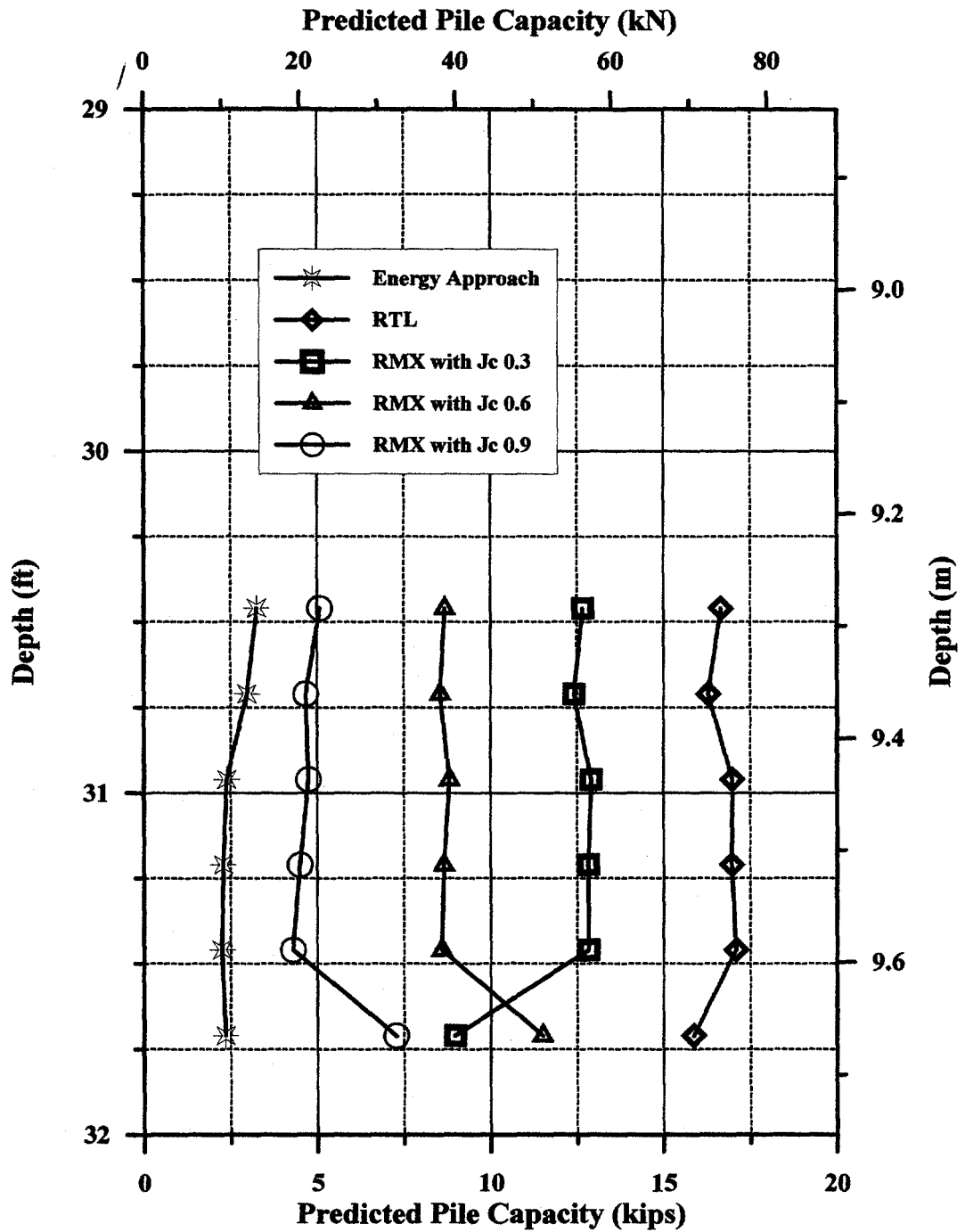


**Figure 118. Predicted Pile Capacity for the Restrike of MDMP Test NB2 (Cases 1 and 2) Based on the Energy Approach Method and the Case Method With Varying  $J_c$  Values (assuming pile length is 9.88 m (32.4 ft)).**

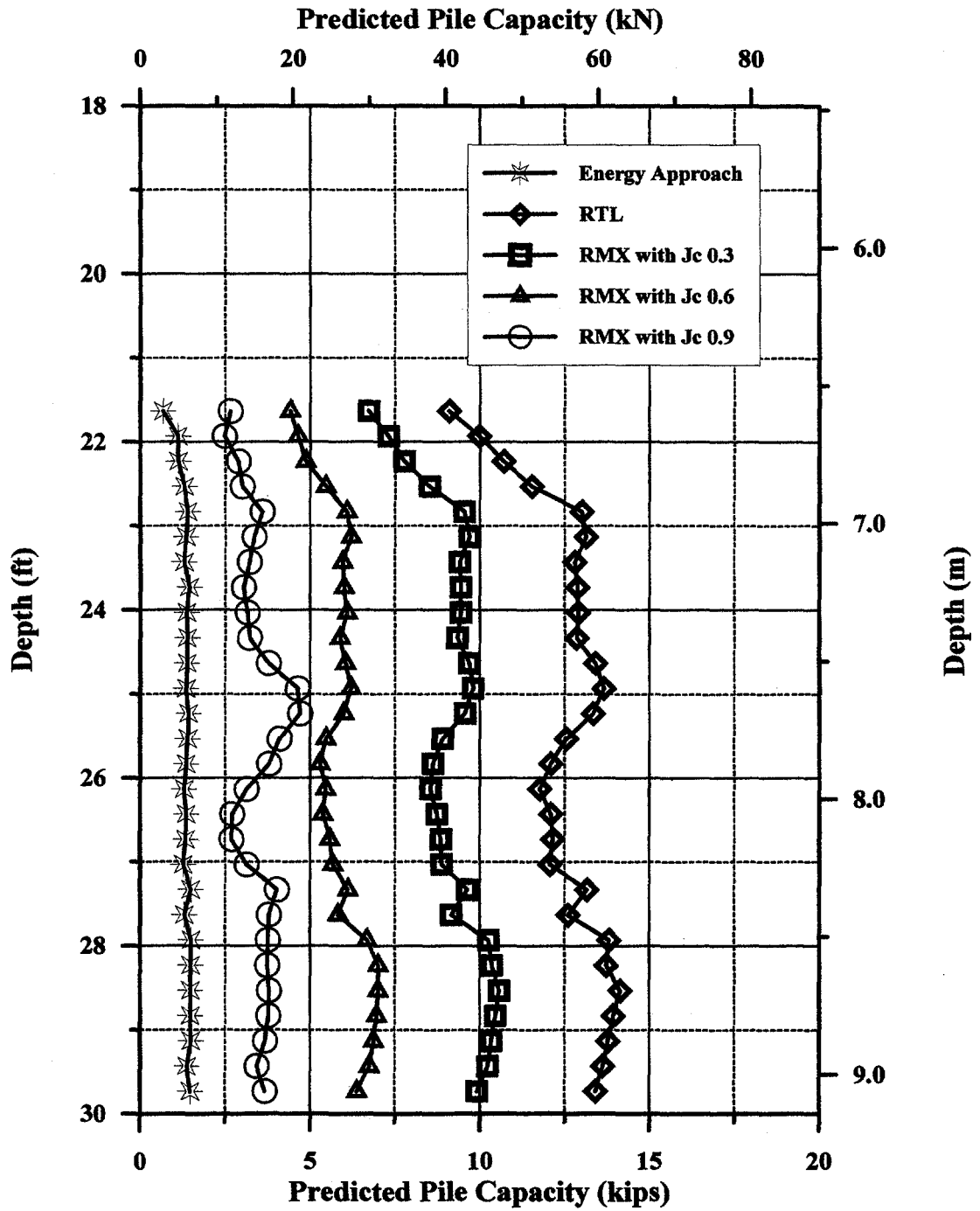


**Figure 119. Predicted Pile Capacity for the Installation of MDMP Test NB2 (Case 3) Based on the Energy Approach Method and the Case Method With Varying  $J_c$  Values (assuming pile length is 8.72 m (28.6 ft)).**

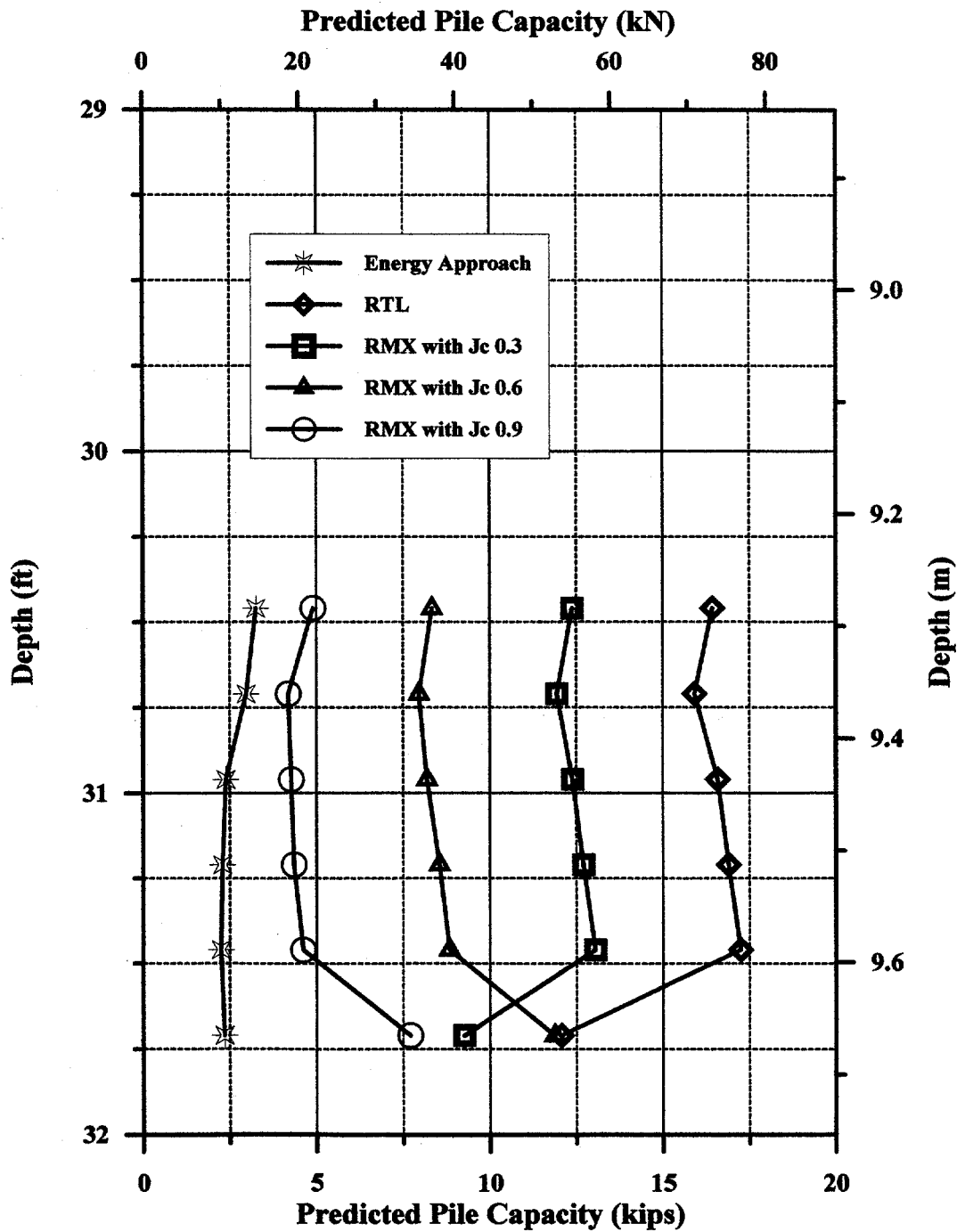


**Figure 120. Predicted Pile Capacity for the Restrike of MDMP Test NB2 (Case 3) Based on the Energy Approach Method and the Case Method With Varying  $J_c$  Values (assuming pile length is 8.72 m (28.6 ft)).**

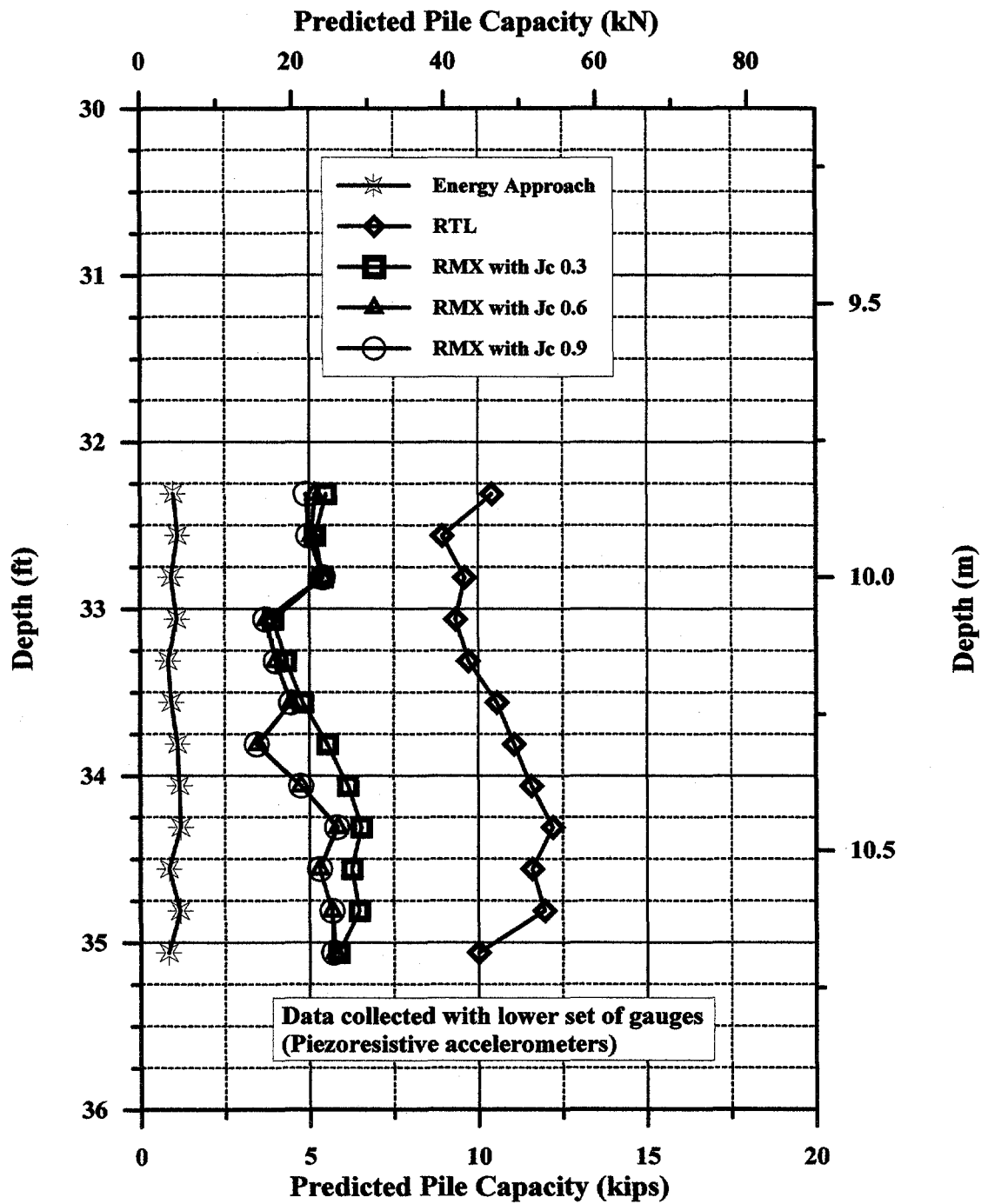


**Figure 121. Predicted Pile Capacity for the Installation of MDMP Test NB3 (Case 1) Based on the Energy Approach Method and the Case Method With Varying  $J_c$  Values (assuming pile length is 13.84 m (45.4 ft)).**

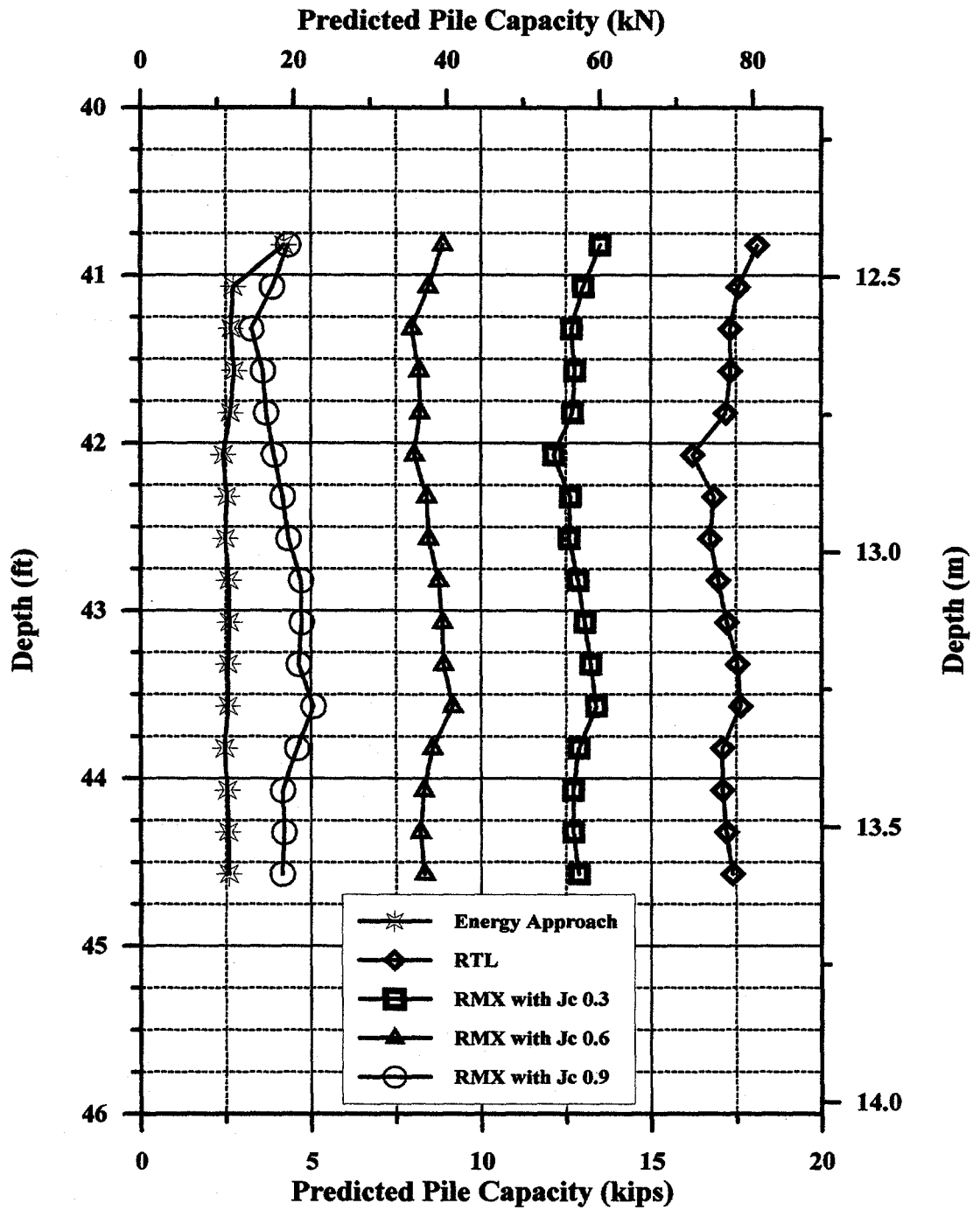
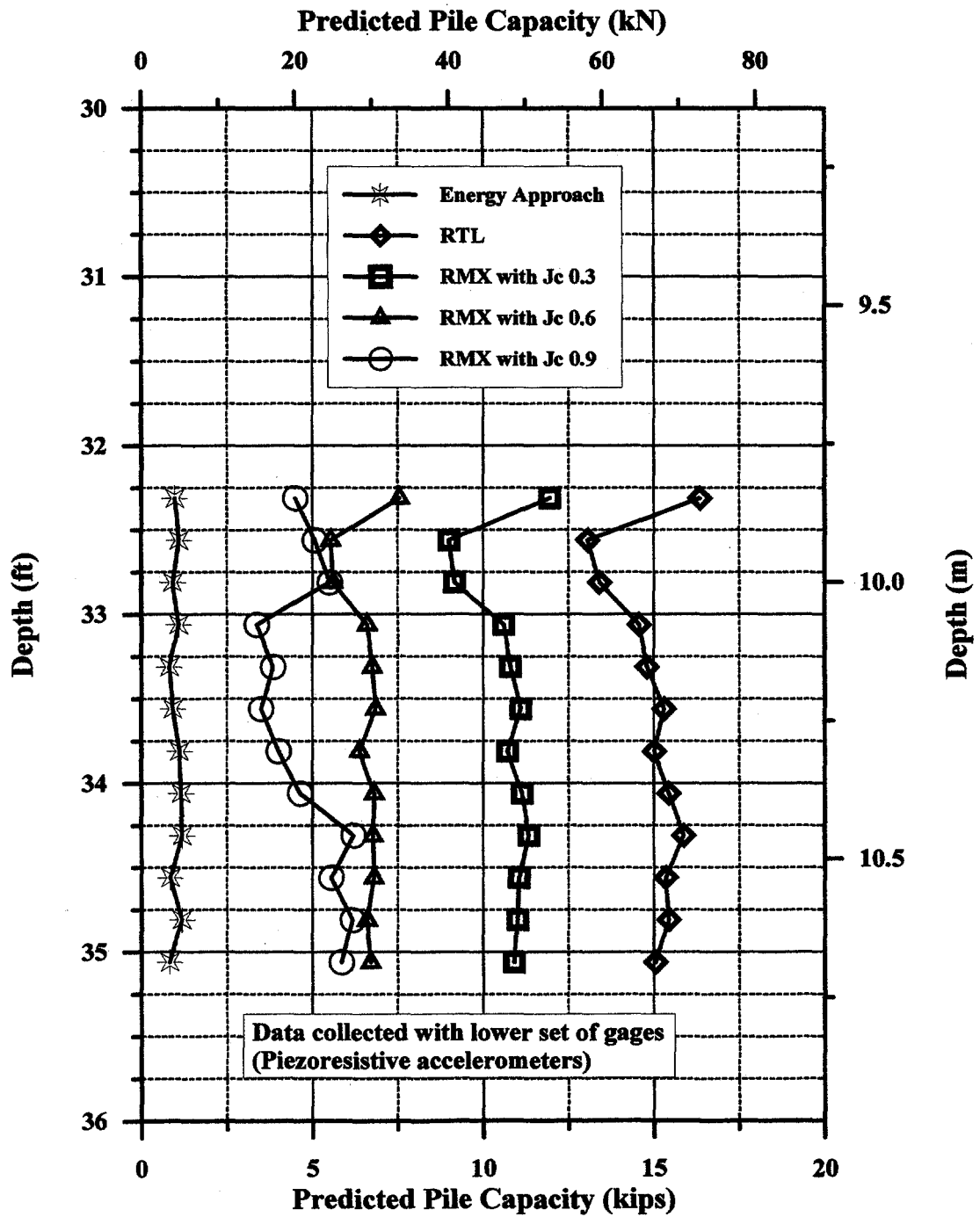
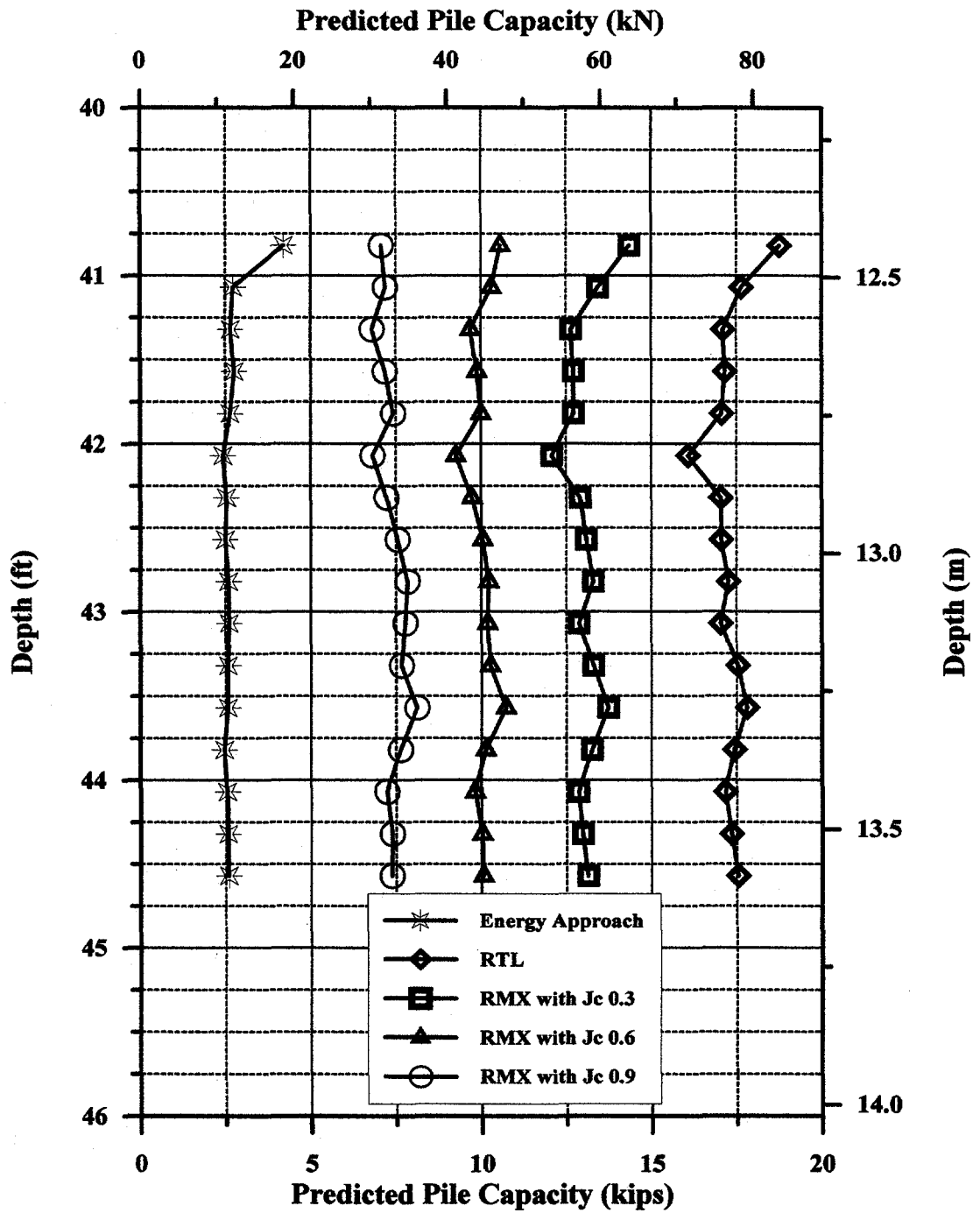


Figure 122. Predicted Pile Capacity for the Restrike of MDMP Test NB3 (Case 1) Based on the Energy Approach Method and the Case Method With Varying  $J_c$  Values (assuming pile length is 13.84 m (45.4 ft)).



**Figure 123. Predicted Pile Capacity for the Installation of MDMP Test NB3 (Case 2) Based on the Energy Approach Method and the Case Method With Varying  $J_c$  Values (assuming pile length is 12.68 m (41.6 ft)).**



**Figure 124. Predicted Pile Capacity for the Restrike of MDMP Test NB3 (Case 2) Based on the Energy Approach Method and the Case Method With Varying  $J_c$  Values (assuming pile length is 12.68 m (41.6 ft)).**

from the pile tip (pile length was 13.84 m) as in case (1). Figures 123 and 124 present the capacity determined for MDMP test NB2 for installation and restrike data, assuming that the wave reflection was related to the slip joint (pile length was 12.68 m) as in case (2).

All analyses consistently presented the Energy Approach predictions as being the lowest, whereas the total resistance (RTL) of the Case method was roughly 5 to 10 times the values predicted by the Energy Approach. Since the Energy Approach was based on a simplified elastoplastic soil resistance relationship without referring to dynamic losses, it consistently presented higher resistance values. The fact that the Case method's various calculations were so much higher suggested that the different values of force and velocity used in its evaluation (in particular, those related to the time  $T1+2L/C$ , see equation (7.9)) were strongly affected by the MDMP geometry and, hence, not applicable to the Case method formulation. The high velocities measured during driving explained the large variations in the static resistance values when changing the damping coefficients. The small variation of resistance with depth reasonably reflected the small variation in resistance expected to take place in a clay layer over a small penetration depth. This is in sharp contrast to the variations that existed between the methods, or the variations that existed as a result of the changes in the damping coefficient.

#### **7.11 Comparison Between the Static Capacity and the Analyses Based on Dynamic Measurements**

The complexity of the MDMP testing in regards to time and methods resulted in a variety of static resistances, which raised difficulties for obtaining a single representative value. Table 46 summarizes the different resistances encountered during the final pull-out and compression tests. The discrepancy between the sleeve frictional resistances during pull-out and compression tests were discussed earlier (see section 7.8). A reasonable assessment was provided based on the surface load cell readings during the final compression tests of MDMP tests NB2 and NB3 for 7.15 kN (1.61 kips) and 7.01 kN (1.58 kips), respectively. Using an average of 7.09 kN (1.59 kips) provided a lower estimation for the total capacity. A higher end estimation of the static capacity could be obtained from the surface load cell measurements in the final pull-out tests for 9.91 kN (2.23 kips) and 8.85 kN (1.99 kips) for MDMP tests NB2 and NB3, respectively. Using an average of these values, 9.36 kN (2.11 kips) provided a higher estimation of the total capacity. A reasonable range for the MDMP static capacity for both tests was, therefore, 7.09 kN (1.59 kips) to 9.36 kN (2.11 kips).

The above range was compared to the prediction of the various dynamic analyses in Figures 125 and 126 for MDMP tests NB2 and NB3, respectively. The following methods and conditions were chosen for the dynamic analyses:

- (1) Energy Approach Method for end of driving records (EOD). As the Energy Approach method was developed for the driving condition, its use for restrike measurements was not recommended.
- (2) CAPWAP analysis results for restrike measurements using the full-length pile modeling (case 1).
- (3) Case method (RMX) value using a high damping factor of  $J_c = 0.9$  and records from EOD and restrike.



**Table 46. Summary of the MDMP Final Static Capacities During the Tension (Pull-Out) and Compression Load Tests.**

Test	Last Pull-Out Test				Compression Test			
	Surface Load Cell	Top Load Cell	Middle Load Cell	Friction Sleeve	Surface Load Cell	Top Load Cell	Middle Load Cell	Friction Sleeve
	kN / kips	kN / kips	kN / kips	kN / kips	kN / kips	kN / kips	kN / kips	kN / kips
NB2 (LT11)	9.91 / 2.23	11.83 / 2.66	6.28 / 1.41	5.55 / 1.25				
NB2 after initial displacement (slip joint open)					5.92 / 1.33	5.94 / 1.34	3.33 / 0.75	2.62 / 0.59
NB2 after slip joint closed					7.15 / 1.61	6.79 / 1.53	4.87 / 1.09	2.01 / 0.45
NB2 maximum at any time					7.75 / 1.74	7.28 / 1.64	5.36 / 1.20	2.62 / 0.59
NB3 (LT9)	8.85 / 1.99	12.35 / 2.78	8.10 / 1.82	4.25 / 0.96				
NB3 (LT8)	8.77 / 1.97	12.63 / 2.84	8.09 / 1.82	4.67 / 1.05				
NB3 after initial displacement (slip joint open)					4.61 / 1.04	4.52 / 1.02	3.41 / 0.77	1.17 / 0.26
NB3 after slip joint closed					7.01 / 1.58	6.76 / 1.52	5.91 / 1.33	1.06 / 0.24
NB3 maximum at any time					7.66 / 1.72	7.11 / 1.60	6.40 / 1.44	1.17 / 0.26

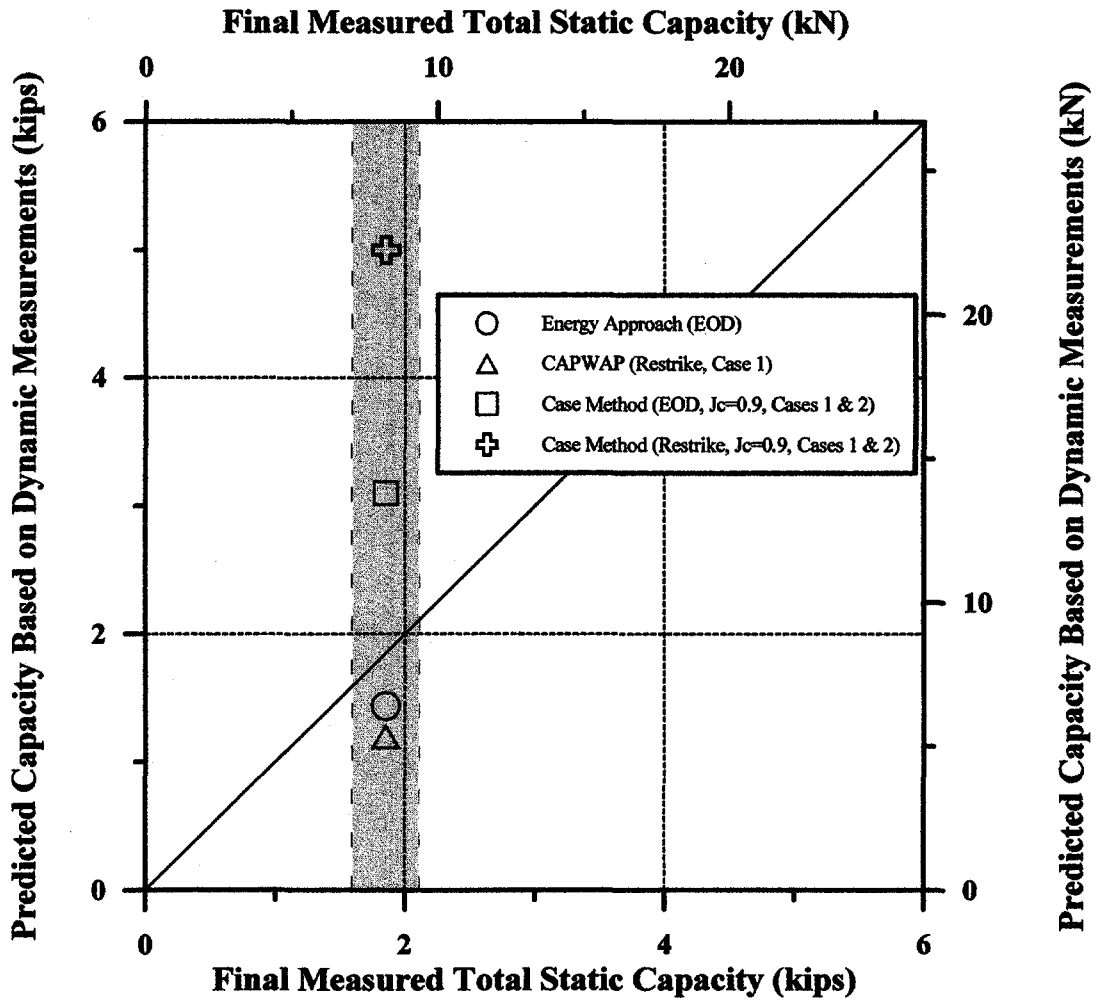


**Figure 125. Comparison Between the Measured Static Capacity for MDMP Test NB2 and Predictions Based on the Dynamic Measurements Utilizing Various Methods of Analysis.**

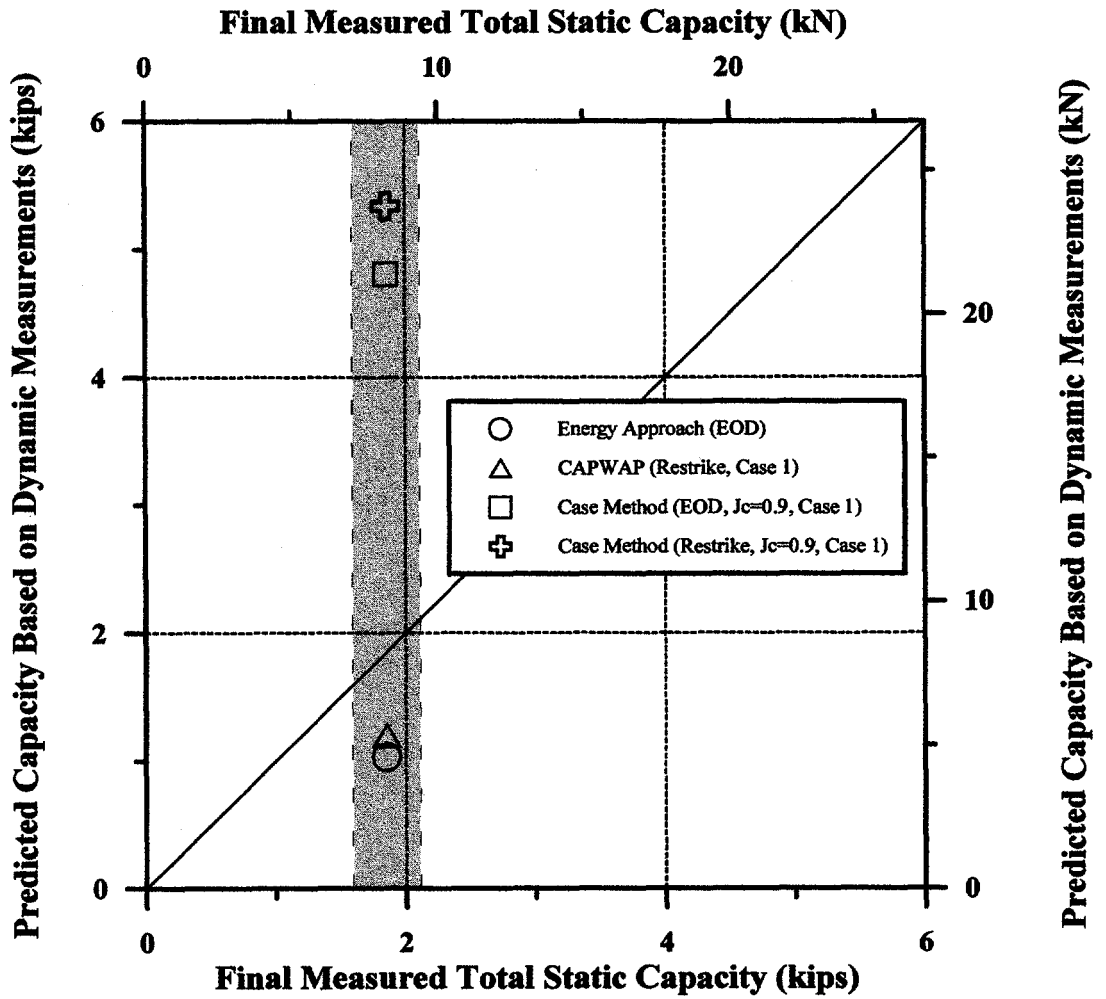


**Figure 126. Comparison Between the Measured Static Capacity for MDMP Test NB3 and Predictions Based on the Dynamic Measurements Utilizing Various Methods of Analysis.**

The obtained results suggested that the Energy Approach method for the EOD records and CAPWAP for the restrike records provided the best predictions for the long-term measured capacities. Both methods underpredicted the measured capacities by approximately 29% and 40% for NB2 and NB3, respectively (referring to the average of the static capacity zone). The Case method predictions for both EOD and restrike were substantially higher than the measured capacity. This observation was most likely associated with the incompatibility of the method with the make-up of the MDMP due to its influence on the values used in the Case method analysis.

## CHAPTER 8. SUMMARY CONCLUSIONS AND RECOMMENDATIONS

### 8.1 Summary

#### 8.1.1 The MDMP Configuration and Specifications

The Multiple Deployment Model Pile (MDMP) is an in situ soil testing device composed of a series of modular sensors that can be assembled in various desired configurations. The MDMP can be either pushed or driven to the required testing depth, typically beyond the bottom of a cased borehole. The model pile is capable of measuring axial loads, pore water pressure, total radial stresses, local displacement, and pile acceleration. A typical configuration of the modular MDMP is shown in Figure 127. The MDMP instrumentation includes three load cells, three accelerometers, a displacement transducer, a pore pressure transducer, and a total pressure cell. The friction sleeve between the top and middle load cells is 83.5 cm (32.9 in) long and constitutes a surface area of 2000 cm<sup>2</sup> (310 in<sup>2</sup>). Table 47 summarizes the ranges of the MDMP instrumentation.

#### 8.1.2 The Newbury Site Testing

The first field deployment of the MDMP was at a site located in Newbury, Massachusetts during March 1996. The test location was chosen because it contained a 9- to 12-m- (30- to 40-ft-) thick clay deposit close to the ground surface, allowing to assess the pile capacity gain and pore pressure dissipation with time. Additional full-scale instrumented pile testing was also carried out at the same location.

**Table 47. Summary of the MDMP Instrumentation Ranges.**

Component	Location	Type	Installation Condition	Range
Accelerometers	Top of Rods	Piezoresistive	N/A	0-2000 g's
	Top Load Cell	Piezoelectric	N/A	0-2000 g's
	Middle Load Cell	Piezoresistive	N/A	0-2000 g's
	Bottom Load Cell	Piezoelectric	N/A	0-2000 g's
Load Cells	Top, Middle, and Bottom Load Cells	Electric Strain Gauges	Soft/Medium Soil	89 kN
			Hard/Stiff Soil	445 kN
			Dynamic	2.5 times static cap.
Pore Pressure Transducer	Transducer Housing	Electric Strain Gauges	All	1070 kPa
Total Pressure Cell	Transducer Housing	Electric Strain Gauges	All	1214 kPa
Slip Joint	Slip Joint	LV-DCDT	All	5 cm
Loading Frame	N/A	N/A	All	445 kN

On March 6, 1996, the first of two model pile tests was conducted at the Newbury Site. The pile was driven about 9.33 m (30.6 ft) below ground surface, with the pressure cell and friction sleeve at a depth of 7.39 m (24.25 ft). An initial load test was performed in compression, followed by 11 load tests with time performed in tension. A final static-cyclic load test in compression was performed about 138 h after pile installation.

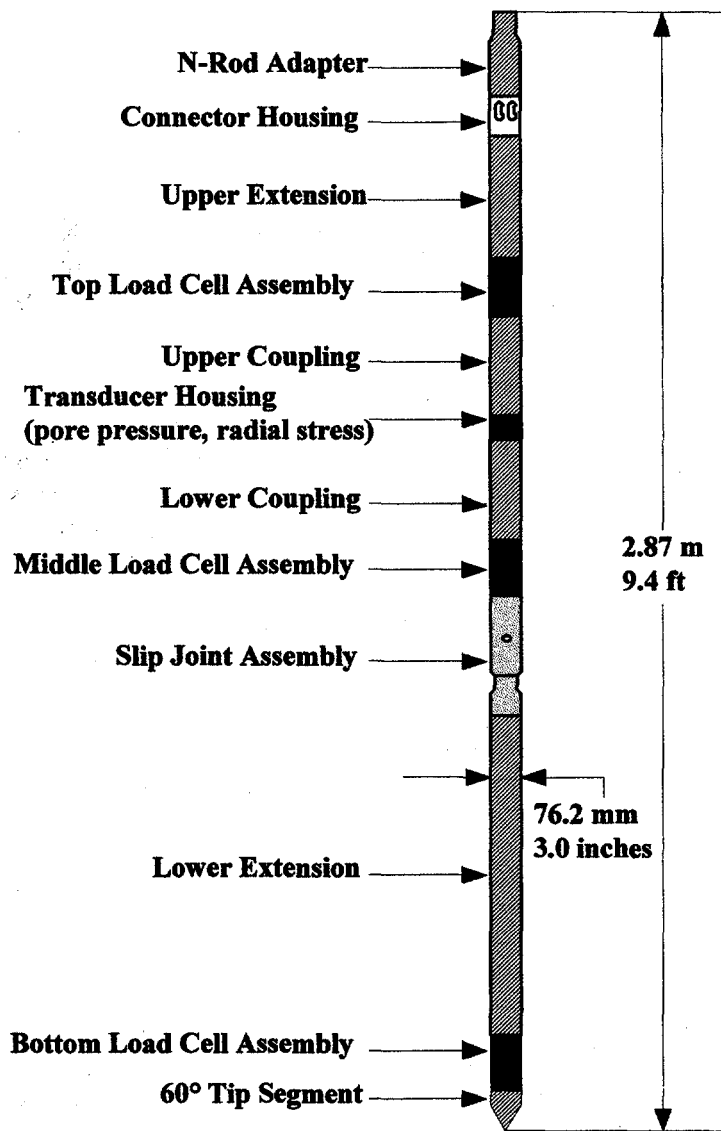


**Figure 127. Typical Configuration of the Modular MDMP.**

On March 13, 1996, the second of the two model pile tests was conducted at the Newbury Site. The pile was driven about 12.31 m (40.4 ft) below ground surface, with the pressure cell and friction sleeve at a depth of 10.46 m (34.33 ft). An initial load test was performed in compression, followed by nine load tests with time performed in tension. A final static-cyclic load test in compression was performed about 120 h after pile installation.

In both tests, the MDMP was monitored with the Pile Driving Analyzer (PDA) during installation and a restrike following the static load tests. When the pile was extracted (after the completion of each testing series), it was surrounded by a soil cake conforming to the 101.6-mm

(4-in) casing, indicating that the shear in the soil had taken place some distance away from the pile wall.

### 8.1.3 Test Results

#### (1) Pore Pressure Dissipation.

The hydrostatic pressure was established to be 57.02 kPa and 87.43 kPa for the NB2 and NB3 testing depths, respectively. The initial (peak) and final measured pore water pressures during test NB2 were 217.3 kPa and 51.02 kPa, respectively. The initial and final measured pore water pressures during test NB3 were 224.0 kPa and 92.46 kPa, respectively. Using the methodology presented by Paikowsky et al. (1995), the rate of pore pressure dissipation,  $H_{ut}$ , was found to be 0.6047 and 0.6011 for NB2 and NB3, respectively. The time at 50% dissipation,  $t_{50}$ , for NB2 was 9.854 h (35476 s) and for NB3, it was 7.849 h (28256 s). When adjusted to the PLS Cell radius (19.177 mm),  $t_{50(pls)}$  was 2.493 h (8975 s) and 1.986 h (7149 s) for NB2 and NB3, respectively.

#### (2) Capacity Gain.

A compression load test was carried out 25 min after the installation of MDMP test NB2 in which a skin resistance of 0.16 kN (35 lb) was measured along the frictional sleeve (equivalent to a shear stress of 0.78 kPa (0.11 psi)). The final pull-out test (11<sup>th</sup> in the sequence) was conducted 118.6 h after the end of installation in which a skin resistance of 5.54 kN (1246.5 lb) was measured along the frictional sleeve (equivalent to a shear stress of 27.72 kPa (4.02 psi)).

A compression load test was carried out 21.5 min after the installation of MDMP test NB3 in which a skin resistance of 0.23 kN (51 lb) was measured along the frictional sleeve (equivalent to a shear stress of 1.13 kPa (0.16 psi)). The final pull-out test (9<sup>th</sup> in the sequence) was conducted 94.9 h after the end of installation in which a skin resistance of 4.67 kN (1,050 lb) was measured along the frictional sleeve (equivalent to a shear stress of 23.35 kPa (3.39 psi)).

Using the methodology presented by Paikowsky et al. (1995), the rate of capacity gain ( $C_{gt}$ ) for both peak values and residual values measured during NB2 was 0.589. MDMP test NB3 resulted in a rate of capacity gain ( $C_{gt}$ ) of 0.599 for peak values and 0.631 for residual values. The time to 75% gain of capacity,  $t_{75}$ , for NB2 was 67.7 h for peak values and 70.7 h for residual values, and for NB3,  $t_{75}$  was 43.2 h for peak values and 38.2 h for residual values. Following the standard normalization used by Paikowsky et al. (1995),  $t_{75}$  was adjusted to a 152.4-mm (6-in) radius pile. The  $t_{75(152.4\text{ mm})}$  was 1083.2 h for peak values and 1131.2 h for residual values, and 691.2 h for peak values and 610.9 h for residual values for NB2 and NB3, respectively.

#### (3) Radial Consolidation.

The coefficients of horizontal consolidation,  $c_h$ , were 0.0135 cm<sup>2</sup>/s and 0.0170 cm<sup>2</sup>/s for NB2 and NB3, respectively.

#### (4) Radial Stresses.

The total radial stresses were measured to be similar to the magnitude of the pore pressures at the end of the MDMP installation (200 kPa for NB2). The total radial stresses then gradually decreased at a rate somewhat lower than the pore pressure dissipation, which resulted in a slow increase in the effective radial stresses. This increase was at a rate of 1.52 kPa/h beginning about 1 h after the end of the driving, and reached about 36 kPa 37 h later. At that point, the total radial stress was about equal to the total vertical stress. At the same time, the consolidation process was at about 90% and a sharp increase was observed in the radial total and effective stresses. The radial stresses seemed to stabilize about 67 h after the end of the MDMP NB2 installation and remained about constant thereafter, affected only by the load testing.

#### (5) Static - Cyclic Load Tests.

A test consisting of a large displacement (about 50 mm) downward, following by a static-cyclic full-mobilization load test completed the final testing of MDMP tests NB2 and NB3. The frictional behavior presented degradation with the displacement and repetitive behavior in the loading-unloading cycle of the testing. The peak forces along the friction sleeve in the push tests were 2.61 kN (588 lb) and 1.17 kN (263 lb).

#### (6) Dynamic Analysis.

Multiple dynamic measurements were carried out at the top of the drilling rods and inside the MDMP. The analysis of the measurements, while allowing insight for the behavior, encountered some difficulties due to the complexity of the pile geometry.

## 8.2 Conclusions

### 8.2.1 General Conclusions

1. The MDMP was successfully analyzed, specified, constructed, calibrated, and tested.
2. The dynamic monitoring during installation and subsequently following static loading provided the capability of examining the relationship between the dynamic resistance and the static components during driving and with time.
3. The ability to monitor the pile capacity gain with time, along with the controlling mechanisms (pore pressure and radial stress variations), provided significant insight into pile analysis, design, and testing.
4. The MDMP provided direct measurement of soil/structure interaction and served, therefore, as an ideal in situ tool that enabled direct correlation between the measured strength/capacity values and design parameters. Extrapolation of the measurements allowed for full-scale pile capacity time-dependent evaluation.



### **8.2.2 Major Conclusions**

1. The capacity gain with time was found to be an extreme phenomenon in which the soil resistance changed from about zero (fluidized soil) to a significant portion of its natural shear strength. The capacity gain was related to the variation of skin friction with time. This, in turn, was found to depend on the radial effective stresses. In contrast to common knowledge and one-dimensional consolidation theories, as a result of a total radial stress decrease after installation, the radial effective stresses were found not to increase at the same rate as the pore pressure dissipation. These observations suggested redistribution of total stresses around the pile after driving, resulting in a delay in the capacity gain beyond the direct relationship to pore pressure dissipation.
2. The exact analysis of pore pressure dissipation rates and time called for accurate and reliable initial pore pressure measurements. These were difficult to achieve and required careful examination of the obtained data. However, their influence on the time required for the completion of the processes (pore pressure dissipation and capacity gain) was limited.
3. The load-displacement measurements provided direct soil/structure interaction monitoring with time, which allowed both design parameters and modeling relationships.
4. The use of dynamic measurements along with the MDMP installation provided insight into pile behavior and the dynamic measurement capabilities. The geometrical complications of the MDMP restricted the effective use of the dynamic methods of analysis and further development was required in this area.

### **8.2.3 Detailed Conclusions**

1. The initial (peak) pore pressure measurements were found to be 20% to 47% lower than the  $u_3$  measurements obtained in the CPT testing (Paikowsky and Chen, 1998). As the CPT measurements closely matched the expected values presented by Paikowsky et al. (1995), it is believed that a modification is required that addresses the combination of filter saturation and that data acquisition sampling rate. The MDMP installation method (driving) created challenges not common to steady-state penetration methods (e.g., CPT).
2. The rate of pore pressure dissipation in both tests was practically identical to an average  $H_{ut}$  of 0.603. This value falls within the range of recorded values for all normally consolidated soils (from 0.325 to 0.763), but indicates a faster dissipation than the mean value of  $H_{ut}=0.466\pm 0.089$  (33 cases). The measured rate was also about 20% higher than the mean value found for BBC at the Saugus, MA site of  $H_{ut}=0.492\pm 0.072$ . The analyzed rates of pore pressure dissipation and time related to the process were affected by the initial pore pressure readings. The obtained results were very good, in particular, the final process predictions were affected only in a

limited way by the initial pore pressure readings. These observations suggest that: (1) site-specific testing is recommended and (2) the above modification to the control of the initial pore pressure readings is important.

3. The radial consolidation values were about half of the  $c_h$  values calculated from the CPT dissipation tests. The difference between the coefficients of consolidation obtained from the CPT and the MDMP was most likely the result of the variation in the initial pore pressure measurements that markedly affected the determined  $t_{50}$ .
4. The rate of capacity gain denoted by the parameter,  $C_{gt}$  was found at the Newbury site to be 1.6 times higher than values determined from the data base. The  $t_{75}$  obtained at the Newbury site was also larger than the ones obtained at other locations, resulting in an overall longer capacity gain time even though the capacity gain was faster. A possible reason for this was that rarely (if at all) were any of the capacity gain rates in the database based on a complete monitoring of the skin friction from a very short time after installation to the end of consolidation.
5. A reasonable match was obtained between the predicted capacity at the end of driving based on the Energy Approach, the CAPWAP prediction at the time of restrike, and the final static capacity. The high dynamic resistance during driving and the low static resistance afterwards indicated the significance of the soil inertia and viscosity in resisting pile penetration.

### 8.3 Recommendations

1. Following the initial testing described in this research, the MDMP requires "fine-tuning," including: (1) an improved saturation procedure; (2) rebuilding and testing of the total soil pressure cell; (3) restoration and recalibration of strain-gauged load cells; (4) examination of calibration in light of temperature changes; (5) remachining of parts in the load test assembly, allowing easier frame mounting at the end of driving; (6) examination of lower load cell and accelerometer circuitry as a result of a reverse signal; and (7) building new drilling rods for deeper penetration testing.
2. Further investigation is required to determine the influence of the testing procedures and frequency on the final shear strength, e.g., conducting only one test at the end of the consolidation period versus multiple tests during the consolidation process.
3. Further investigation is required to determine the extent and the influence of the shear zone at the end of the consolidation process. The investigation of this zone can provide insight into the mechanism taking place around loaded piles and the accuracy of the assumed shear stresses.
4. Further investigation is required to be better understand the redistribution of the radial stresses around the pile as they control the effective stresses and the actual rate of capacity gain.

## REFERENCES

- American Society for Testing and Materials, (D3441-86), 1994, "Standard Test Method for Deep, Quasi-Static, Cone and Friction-Cone Penetration Tests of Soil," *Annual Book of ASTM Standards*, Vol. 4.08, Philadelphia, pp. 338-343.
- API, 1984, "API Recommended Practices for Planning, Designing, and Constructing Fixed Offshore Platforms," 15/e, American Petroleum Institute, API RP2A, pp. 115.
- Azzouz, A.S., 1985a, "The Piezocone Penetrometer," Lecture 6, MIT Special Summer Course 1.60S, MIT Department of Civil Engineering, August.
- Azzouz, A.S., 1985b, "The Piezo-Lateral Stress (PLS) Cell," Lecture 9, Part 2, MIT Special Summer Course 1.60S, MIT Department of Civil Engineering, August.
- Azzouz, A.S., and Lutz, D.G., 1986, "Shaft Behavior of a Model Pile in Plastic Empire Clays," *Journal of Geotechnical Engineering*, ASCE, Vol. 112, No. 4, pp. 389-406.
- Azzouz, A.S., and Morrison, M.J., 1988, "Field Measurements on Model Pile in Two Clay Deposits," *Journal of Geotechnical Engineering*, Vol. 114, No. 1, January, pp. 104-121.
- Baligh, M.M. and Levadoux, J.N., 1980, "Pore Pressure Dissipation After Cone Penetration," MIT, Boston, Report MITSG 80-13.
- Bhushan, K., 1982, "Discussion: New Design Correlations for Piles in Sands," *Journal of Geotechnical Engineering Division*, ASCE, GT 11, Nov., pp. 1508-1510.
- Bishop, A.W., 1971, "Shear Strength Parameters for Undisturbed and Remoulded Soil Specimens," *Stress-Strain Behavior of Soils*, Proceedings of the Roscoe Memorial Symposium, Cambridge University, G.T. Foulis & Co. Ltd.
- Bogard, J.D., and Matlock, H., 1990a, "Application of Model Pile Tests to Axial Pile Design," Paper presented at the 22nd Annual Offshore Technology Conference, Houston, Texas, May 7-10.
- Bogard, J.D., and Matlock, H., 1990b, "In-Situ Pile Segment Model Experiments at Empire, Louisiana," Paper presented at the 22nd Annual Offshore Technology Conference, Houston, Texas, May 7-10.
- Bogard, J.D., and Matlock, H., 1990c, "In-Situ Pile Segment Model Experiments at Harvey, Louisiana," Paper presented at the 22nd Annual Offshore Technology Conference, Houston, Texas, May 7-10.
- Bogard, J.D., Matlock, H., Audibert, J.M.E., and Bamford, S.R., 1985, "Three Years' Experience With Model Pile Segment Tool Tests," Paper presented at the 17th Annual Offshore Technology Conference, Houston, Texas, May 6-9.

Bond A.J., and Jardine, R.J., 1991, "Effects of Installing Displacement Piles in a High OCR Clay," *Geotechnique*, Vol. 41, No. 3, pp. 341-363.

Bond A.J., and Jardine, R.J., 1995, "Shaft Capacity of Displacement Piles in a High OCR Clay," *Geotechnique*, Vol. 45, No. 1, pp. 3-23.

Bond A.J., Jardine, R.J., and Dalton, J.C.P., 1991, "Design and Performance of the Imperial College Instrumented Pile," *Geotechnical Testing Journal*, Vol. 14, No. 4, pp. 413-424.

Bowles, J.E., 1988, *Foundation Analysis and Design*, 4th ed., McGraw-Hill, Inc., New York.

*CAPWAP Manual*, 1996, Goble Rausche Likins and Associates, Inc., Cleveland Ohio.

Chance Company, 1992, Bulletin 04-9202, 210 North Allen, Centralia, MO 065240.

Chen, B.S., and Mayne, P.W., 1994, *Profiling the Overconsolidation Ratio of Clays by Piezocone Tests*, National Science Foundation, Report No. GIT-CEECEO-94-1, August.

Chen, Y.L., 1997, "Field and Laboratory Study of the Physical Characteristics and Engineering Parameters of Subsurface at the Newbury Test Site," thesis submitted in partial fulfillment of the requirements of the degree of Master of Science in Civil and Environmental Engineering, University of Massachusetts-Lowell, see also Paikowsky and Chen, 1998.

Coop, M.R., and Wroth, C.P., 1989, "Field Studies of an Instrumented Model Pile in Clay," *Geotechnique*, Vol. 39, No. 4, pp. 679-696.

de Ruiter, J., 1975, "The Use of In-Situ Testing for North Sea Soil Studies," Offshore Europe Conference, Aberdeen.

de Ruiter, J., 1982, "The Static Cone Penetration Test, State-of-the-Art Report," *Proceedings of the Second European Symposium on Penetration Testing*, Amsterdam, May.

de Ruiter, J. and Beringer, F., 1979, Pile Foundations for Large North Sea Structures, *Marine Geotechnology*, 3, No. 3, pp. 267-314.

Goble, G., Likins, G., and Rausche, F., (1970), *Dynamic Studies on the Bearing Capacity of Piles, Phase III*, Report No. 48, Division of Solid Mechanics, Structures and Mechanical Design, Case Western Reserve University.

Goble, G., Likins, G., and Rausche, F., (1975), *Bearing Capacity of Piles From Dynamic Measurements*, Final Report, Ohio Department of Transportation, OHIO-DOT-05-75.

Goble, G., Rausche, F., and Likins, G., (1995), *GRLWEAP Manual*, Cleveland, OH.

Grosch, J.J., and Reese, S.C., 1980, "Field Tests of Small-Scale Pile Segments in a Soft Clay Deposit Under Repeated Axial Loading," Paper Presented at the 12th Annual Offshore Technology Conference, Houston, TX, May 5-8.

GZA GeoEnvironmental, 1993, *Geotechnical Engineering Report, Reconstruction of Bridge N-10-15, U.S. Route 1*, Newbury, Massachusetts, File No. 12982.

Helsel, Robert, 1994, *Cutting Your Test Development Time With HP VEE*, PTR Prentice Hall, Englewood Cliffs, New Jersey.

Hewlett Packard, 1990, *HP 75000 Series B/C, 5½-Digit Multimeter HP E1326B/E1411B User's Manual*, Manual Number: E1326-90003.

Hewlett Packard, 1991, *HP 75000 Series B, Mainframes HP E1300A and E1301A User's Manual*, Manual Number: E1300-90005.

Hewlett Packard, 1993, *HP 75000 Series B, 16-Channel Relay Multiplexer Module HP E1343A/44A/45A/47A User's Manual*, Manual Number: E1345-90003.

Hewlett Packard, 1994, *HP 75000 Series B/C, 4-Channel D/A Converter Module HP E1328A User's Manual*, Manual Number: E1328-90003.

Jardine, R.J., Bond, A.J., and Lehane, B.M., 1992, "Field Experiments With Instrumented Piles in Sand and Clay," *Piling — European Practices and Worldwide Trends*, Proceedings of a conference organized by the Institution of Civil Engineers, London, April 7-9.

Karlsrud, K., and Haugen, T., 1981, "Cyclic Loading of Piles and Pile Anchors, Field Model Tests at Haga," Contract Research Report, Norwegian Geotechnical Institute (NGI), Feb 5.

Karlsrud, K., and Haugen, T., 1985a, "Axial Static Capacity of Steel Model Piles in Overconsolidated Clay," Paper presented at the 11th International Conference on Soil Mechanics and Foundation Engineering, San Francisco.

Karlsrud, K., and Haugen, T., 1985b, "Behavior of Piles in Clay Under Cyclic Axial Loading + Results of Field Model Tests," Paper presented at the 4th International Conference on Behavior of Offshore Structures, Delft.

Kulhawy, F.H., and Mayne, P.W., 1990, *Manual on Estimating Soil Properties for Foundation Design*, Electric Power Research Institute, EPRI EL-6800, Project 1493-6 Final Report.

Kurup, P.U., 1993, "Calibration Chamber Studies of Miniature Piezocone Penetration Tests in Cohesive Soil Specimens," Doctor of Philosophy dissertation, Louisiana State University.

Ladd and Foott, 1974, "New Design Procedure for Stability of Soft Clays," ASCE, *Journal of Geotechnical Engineering Division*, July.

Lehane, B.M., 1992, "Experimental Investigations of Pile Behavior Using Instrumented Field Piles," thesis submitted to the University of London in partial fulfillment of the requirements for the degree of Doctor of Philosophy in the Faculty of Engineering.

Lehane, B.M., and Jardine, R.J., 1994, "Displacement-Pile Behavior in a Soft Marine Clay," *Canadian Geotechnical Journal*, Vol. 31, pp. 181-191.

Lemos, L., 1986, "The Effect of Rate on Residual Strength of Soil," thesis submitted to the Imperial College of Science and Technology at the University of London in partial fulfillment of the requirements for the degree of Doctor of Philosophy, January.

McClelland, B., 1972, "Design of Deep Penetration Piles for Ocean Structures," 9th Terzaghi Lecture, October 18, 1972.

Meyerhoff, G., 1951, "The Ultimate Bearing Capacity of Foundations," *Geotechnique*, Vol. 2, No. 4, pp. 301-331.

Meyerhoff, G., 1976, "Bearing Capacity and Settlement of Pile Foundations," *Journal of Geotechnical Engineering Division*, ASCE, Vol. 102, GT3, March, pp. 195-228 (Terzaghi Lecture).

Morrison, M.J., 1984, "In Situ Measurements on a Model Pile in Clay," thesis presented in partial fulfillment of the requirements for the degree of Doctor of Philosophy in Civil Engineering, Massachusetts Institute of Technology.

Mynampaty, R.N., 1993, "Pore Pressure Build-Up and Dissipation Around Piles Penetrating in Clay," thesis submitted in partial fulfillment of the requirements of the degree of Master of Science, University of Massachusetts-Lowell.

Paikowsky, S.G., Baligh, M.M., and Whitman, R.V., 1989, "A New Look at the Phenomenon of Offshore Pile Plugging," *Marine Geotechnique*, 8(3):213-230.

Paikowsky, S.G., and Chen, Y.L., 1998, *Field and Laboratory Study of the Physical Characteristic and Engineering Parameters of the Subsurface at the Newbury Bridge Site*, Research Report submitted to the Massachusetts Highway Department, Geotechnical Section, Boston.

Paikowsky, S.G., LaBelle, V.A., and Mynampaty, R.N., 1995, *Static and Dynamic Time Dependent Pile Behavior*, Research Report submitted to the Massachusetts Highway Department, Geotechnical Section, Boston.

Paikowsky, S.G., Player, C.M., and Connors, P.J., 1995b, "A Dual Interface Apparatus for Testing Unrestricted Friction of Soil Along Solid Surfaces," *Geotechnical Testing Journal*, GTJODJ, Vol. 18, No. 2, pp. 168-193.

Paikowsky, S.G., Regan, J.E., and McDonnell, J.J., 1994, *A Simplified Field Method for Capacity Evaluation of Driven Piles*, Report No. FHWA-RD-94-042, Federal Highway Administration, Research and Development, Turner-Fairbank Highway Research Center, McLean, VA.

Patent Number: 5,259,240, 1993, "Device for In Situ Testing of Soils That Includes a Vent Valve Adapted to Close at a Predetermined Depth During Installation," inventors: Raines, R.D., Boggess, R.L., Lamb, W.C., and Templeton, J.S.

*PDA Manual*, 1995, Pile Dynamics, Inc., Model PAK, Cleveland OH.

P.I.T. Manual, 1993, Pile Dynamics, Inc., Cleveland OH.

Price, G., and Wardle, I.F., 1982, "A Comparison Between Cone Penetration Test Results and the Performance of Small-Diameter Instrumented Piles in Stiff Clay," *Proceedings of the Second European Symposium on Penetration Testing*, Amsterdam, May 24-27, pp. 775-780.

Rausche, F., 1981, "A Short Introduction to Continuous and Discrete Wave Mechanics," technical notes prepared for the second seminar on the Dynamics of Pile Driving, Boulder, Colorado, March 24-25.

Rausche, F., 1995, Personal communication.

Rausche, F., Moses, F., and Goble, G.G., 1972, "Soil Resistance Predictions From Pile Dynamics," ASCE, *Journal of Soil Mechanics and Foundations*, Vol. 98, No. SM9, Sept 1972, pp. 917-937.

Schaap, L.H.J., and Zuiberg, H.M., 1982, "Mechanical and Electrical Aspects of the Cone Penetrometer Tip," *Proceedings of the Second European Symposium on Penetration Testing* Amsterdam, May 24-27, pp. 841-851.

Smith, E.A.L., 1960, "Pile Driving Analysis by the Wave Equation," *Journal of Soil Mechanics and Foundations*, ASCE, pp. 35-61.

Tomlinson, M., 1971, "Some Effects of Pile Driving on Skin Friction," *Proceedings — Conference on Behaviour of Piles*, ICE, London, pp. 107-114.

Tomlinson, M.J., 1986, *Foundation Design and Construction*, Longman Scientific & Technical, Essex, England.

Toolan, F.E., and Coutts, J.S., 1980, "The Application of Laboratory and In Situ Design of Deep Foundations," *Offshore Site Investigations*, ed. D.A. Arduis, G. Trotman, London, pp. 231-246.

Toolan, F., and Fox, D., 1977, "Geotechnical Planning of Pile Foundations for Platforms," *Proceedings of the Institution of Civil Engineers*, London.

Van Berg, A.P., 1982, "Latest Developments in Static Cone Penetration Testing Equipment (On Land — Offshore)," *Proceedings of the Penetration Testing*, Amsterdam.

Vesic, A., 1975, "Principles of Pile Foundation Design," *OTC of Engineering*, Duke University, 48 pp. + figures.

Vesic, A., 1977, *Design of Pile Foundations*, NCHP Washington, D.C., 68 pp.

Vijaya, V., and Focht, J., 1972, "A New Offshore Technology Conferen

Wissa, A.Z.E., Martin, R.T., and Garlanger, J.E., 1975, "The Piezometer Probe," *Proceedings of ASCE Specialty Conference on In Situ Measurement of Soil Properties*, Raleigh, N.C. 536-545.